



**School of Architecture, Planning and Landscape**

**Assessment of Thermal and Visual Micro-climate of a Traditional  
Commercial Street in a Hot Arid Climate**

**Mohamed Mahgoub**

Bsc, Msc

**PhD Thesis**

NewcastleUniversity  
Newcastle Upon Tyne, UK

June 2015

## **Title page**

**Thesis Title:** Assessment of Thermal and Visual Micro-climate of a  
Traditional Commercial Street in a Hot Arid Climate

**Full name:** Mohamed Hussein Kamel Elnabawy Mahgoub

**Qualification:** Doctor of Philosophy

**School:** School of Architecture, Planning and Landscape

**Submission Date:** April 2015

## ABSTRACT

In the hot arid contexts, the impact of urban climate is often associated with negative effects on outdoor thermal comfort and an increase in the urban heat island (UHI) effect.

The primary aim of this research is to investigate the outdoor thermal performance of traditional commercial urban streets located in the hot arid context of Cairo in Egypt. A number of methods were used including field measurements and social surveys. Consequently, urban air flows, temperature and daylight simulations to assess existing and possible improvement scenarios to extend pedestrian thermal and visual comfort were tested. The field measurements were conducted in order to first assess the UHI intensity in the urban street, and to investigate the effectiveness of the traditional design solutions in ensuring comfortable outdoor conditions based on human-biometeorological assessment methods. Validation of results was carried out by comparing measured and simulated results of thermal conditions in the commercial spine

ENVI-met is a three dimensional microclimatic model based on computational fluid dynamics (CFD) models and is designed to simulate surface-air interactions in urban environments. It was used to calculate the mean radiant temperature and obtaining the microclimatic maps with problematic areas concerning the pedestrian's thermal comfort for the existing urban configurations.

Outdoor thermal comfort was assessed based on a thermal sensation survey and the physiological equivalent temperature (PET), with a comfort range of (24°C - 32°C).

To improve outdoor thermal conditions at pedestrian level seven different shading scenarios addressing the form and the opening of shading devices were simulated using CFD Fluent, based on two dependant variables including air temperature distribution and wind velocity. The daylight analysis software (DIVA) was used to evaluate the solar access for the tested cases. The findings show that typology and the opening locations are one of the paramount factors in providing a temperature reduction in the urban scale. As the air temperature was reduced by (2.3°C) for the best case compared to the base leading to a lower PET for the best case recording 32.9°C against 35°C for the base case.

## Related Published Work

- Elnabawi M, Hamza N, Dudek S. [Outdoor thermal comfort in the old Fatimid city, Cairo, Egypt](#). In: *International Conference on “Changing Cities”: Spatial, morphological, formal & socio-economic dimensions*. 2013, Skiathos Island, Greece.
- Elnabawi M, Hamza N, Dudek S. [Microclimatic Investigation of Two Different Urban Forms in Cairo, Egypt: Measurements and Model Simulations](#). In: *Building Simulation 2013 Conference - Towards Sustainable & Green Built Environment*. 2013, Cairo, Egypt.
- Elnabawi M, Hamza N, Dudek S. [Use And Evaluation of The Envi-met Model for Two Different Urban Forms in Cairo, Egypt: Measurements and Model Simulations](#). In: *13th International Conference of the International Building Performance Simulation Association*. 2013, Chambéry, France.
- Elnabawi M, Hamza N, Dudek S. [Numerical Modelling Evaluation for the Microclimate of an Outdoor Urban Form in Cairo, Egypt](#). HBRC Journal (2014), <http://dx.doi.org/10.1016/j.hbrcj.2014.03.004>



## ACKNOWLEDGMENT

Having the opportunity to complete a doctorate was a professional, family and personal experience. In this sense, it could not have been accomplished without the guidance of my committee members, help from friends, and support from my family. Because of them, my graduate experience has been one that I will cherish forever.

Firstly, I would like to gratefully acknowledge the effort of both my supervisors, who contributed to this work in various ways. Dr. Neveen Hamza has been an endless source of motivation and advice, and I have learnt a great deal of experience throughout the progress of this research from her. I wish to thank her not only for reading and correcting errors in earlier drafts, but also for the valuable suggestions on my entire work, and especially for all the effort she exerted during the submission period of this thesis. Dr. Steven Dudek, a person with the highest academic and personal qualities, was always ready not only to discuss and confront my ideas, but also to offer guidance, support and advice on arguably any theme and concern. Doubtlessly, I could not have survived the period of my study without their patient support.

I am also grateful to my colleagues at Newcastle University, Dr. Mansour Helmy, Dr. Ali Sedki and Mabrouk Al-Sheliby, for their support throughout the work, and special thanks to Dr. Mohamed Al Hajj who was ready to do everything I needed and offered everything I asked.

My gratitude extends to my friends, without whom the completion of this project could not have been accomplished: Sameh Elghazzawy, Hisham Elmasry, Ahmed Hegab, Ather Abdelbaky, Jenna and Sarah. I cannot thank them adequately enough for all their love, help and support; their role throughout this period cannot be expressed in words.

Finally, a more personal note, I have no way to express my thanks to my adorable grandmother, for her love, warmth and incredible support. Lastly, I would like to dedicate this thesis to my parents, Professor Hussein Elnabawi and Naglaa. Their unconditional love and motivation spurred me on. I owe a great deal to my mother for her sympathy and care; her phone calls from Egypt have relieved hard times and have produced motivation and enthusiasm. As for my father, I wish to sincerely thank him for continuous encouragement, help and advice throughout this study. They have shown

great understanding, patience and support during the course of my PhD study, without which I could not have approached my aim. I hope that I am able to repay them some of their favours and to fulfill my obligations towards them. Special thanks go to my brothers, Kareem and Shadi, and two month niece Camillia, all my family, who gave me every possible support and help.

*To Dina F. Barakat*

## Table of Contents

ABSTRACT .....	iii
Related Published Work .....	iv
ACKNOWLEDGMENT .....	v
Tables of Contents.....	xivii
LIST OF TABLES.....	xiv
LIST OF FIGURES.....	xvii
<b>Chapter One .....</b>	<b>1</b>
1. Introduction .....	1
1.1 Introduction .....	2
1.2 The conceptual framework.....	2
1.2.1 Problem statement.....	2
1.3 Research aim and objectives .....	12
1.4 Hypothesis and Research questions .....	12
1.5 Scope and limitations .....	13
1.6 Significance of the study.....	14
1.7 Research Methodology.....	16
1.8 Research context.....	19
1.8.1 The geographical setting of the research.....	19
1.8.2 Climate characteristic.....	20
1.8.3 Cairo and Al-Muizz urban development.....	23
1.9 The physical pattern development of Al-Muizz.....	27
1.9.1 The first Muslim settlements.....	27
1.9.2 Fatimids (969 – 1171AD) .....	27
1.9.3 Ayubbids (1171 – 1252AD).....	27
1.9.4 Mamluks (1252 – 1517AD).....	28

1.9.5	Ottomans (1517 – 1805AD, including the French expedition in 1798AD) .....	28
1.9.6	The Present.....	28
1.9.7	Open/Built Structure .....	31
1.9.8	The exterior shaping for the elements among Al-Muizz Street .....	31
1.9.9	Space development.....	32
1.10	Research design.....	34
1.11	Research Structure .....	34
<b>Chapter Two.....</b>		<b>38</b>
2.	Review of Urbanization, Climate Change and Thermal Comfort.....	38
2.1	Introduction.....	39
2.2	Urbanization and climate .....	39
2.2.1	Nature of the urban atmosphere .....	40
2.3	Urban Heat Island (UHI).....	44
2.3.1	Air Temperature UHI.....	47
2.3.2	Surface Temperature UHI .....	47
2.4	Urbanization and global warming.....	48
2.4.1	Energy Consumption.....	49
2.4.2	Air Quality and Greenhouse Gases .....	50
2.4.3	Human Health and Comfort .....	51
2.4.4	Water Thermal Quality .....	52
2.5	UHI and climate change in Cairo, Egypt .....	53
2.5.1	Climate change and energy consumption in Egypt.....	55
2.5.2	Urbanization process and thermal comfort .....	56
2.6	Traditional and contemporary climate responsive strategies .....	57
2.6.1	Street Orientation .....	58
2.6.2	The Urban Fabric .....	58
2.7	Conclusion.....	60

**Chapter Three..... 62**

3. Review of Microclimate and Outdoor thermal comfort..... 62

3.1 Introduction..... 63

3.2 Scales of urban climate ..... 63

3.3 Street canyon design and urban microclimate ..... 66

3.4 The surface energy balance (SEB) of an urban canyon ..... 67

3.4.1 Energy budget applications for an urban canyon..... 70

3.4.2 Air and surface temperature ..... 75

3.4.3 Urban canyon air flow..... 77

3.4.4 Solar access ..... 80

3.4.5 Vegetation..... 82

3.4.6 Shading consideration in the hot, arid climate ..... 84

3.4.7 Thermal properties of materials ..... 86

3.5 Outdoor thermal comfort..... 88

3.5.1 The heat balance (physiological approach)..... 89

3.5.2 Variables influencing thermal comfort ..... 92

3.5.3 Psychological approach..... 94

3.6 Indices for assessing heat stress ..... 98

3.6.1 Rational indices (steady state assessment)..... 100

3.6.2 Empirical indices (non-steady state assessment) ..... 101

3.7 The mean radiant temperature..... 104

3.8 Outdoor thermal comfort applications ..... 107

3.9 Recent research of outdoor thermal comfort..... 110

3.10 Conclusion..... 117

**Chapter Four..... 119**

4. Methodology and Operational Framework ..... 119

4.1 Introduction..... 120

4.2	Research Methodology Framework .....	120
4.3	Primary data collection (Phase One).....	122
4.4	Field measurements (Phase Two) .....	124
4.4.1	First field measurements .....	124
4.4.2	Second field measurements.....	125
4.4.3	The portable weather station adjustments .....	125
4.5	Questionnaire Surveys (Phase Three) .....	128
4.5.1	Field survey timing and structure.....	129
4.5.2	Metabolic rate (met) and clothing level (clo).....	131
4.6	Micro-urban performance simulations (Phase Four) .....	132
4.6.1	Numerical Models predicting urban microclimate .....	134
4.6.2	The numerical model ENVI-met 3.1.....	136
4.6.3	The numerical model CFD code Fluent 13.0.....	138
4.6.4	Solar access analysis .....	150
4.6.5	Pre-simulation procedures.....	150
4.6.6	Reliability of data.....	151
4.7	Conclusion.....	152
<b>Chapter Five.....</b>		<b>153</b>
5.	The Field Measurements .....	153
5.1	Introduction.....	154
5.2	Cairo climate analysis .....	154
5.3	Current conditions of air temperature in Al-Muizz Street .....	156
5.3.1	The microclimate in the canyon.....	158
5.4	Measuring Sites.....	159
5.5	Result Analysis....	161
5.5.1	Air Temperature.....	162
5.5.2	Wind speed.....	165

5.5.3	Relative Humidity .....	168
5.5.4	Mean Radiant Temperature.....	171
5.6	Thermal comfort analysis (PET).....	176
5.7	Validation of ENVI-met model: computed and measurement comparison ...	180
5.7.1	Results analysis .....	182
5.8	ENVI-met microclimatic map.....	185
5.9	Conclusions.....	189
<b>Chapter Six.....</b>		<b>193</b>
6.	Outdoor Thermal Comfort Analysis .....	193
6.1	Introduction.....	194
6.2	Anthropometric profile of subjects and observations .....	194
6.3	Thermal Sensation.....	197
6.3.1	Thermal acceptable range .....	198
6.4	Thermal adaptation mechanism .....	199
6.4.1	Psychological adaptation experience factor .....	200
6.4.2	Psychological adaptation and the expectation factor .....	202
6.4.3	Perceived control factors for psychological adaptation .....	207
6.4.4	Behavioural adaptation.....	209
6.5	The thermal sensation votes (TSV) difference within Al-Muizz's two locations.....	211
6.6	Correlation between predicted thermal comfort and subjective thermal sensation.....	214
6.7	Non-environmental variables.....	215
6.7.1	Frequency of visitation.....	217
6.7.2	Personal variables.....	217
6.8	Conclusion.....	218
<b>Chapter Seven .....</b>		<b>220</b>
7.	The Comparative Numerical Assessment .....	220

7.1	Introduction.....	221
7.2	Shading performance and CFD.....	222
7.3	CFD simulation settings.....	223
7.3.1	Computational domain dimension.....	224
7.3.2	Horizontal homogeneity of the atmospheric boundary layer (ABL) profile through the computational domain.....	226
7.3.3	Computational mesh.....	230
7.3.4	Mesh independence test.....	232
7.4	CFD simulation validation.....	233
7.4.1	CFD simulation: model validation.....	233
7.4.2	The CFD model validation.....	239
7.5	Comparative study.....	241
7.5.1	CFD simulations: comparative results.....	243
7.5.2	Solar access simulation.....	264
7.6	Conclusion.....	277
<b>Chapter Eight.....</b>		<b>280</b>
8.	Conclusions and Recommendations.....	280
8.1	Introduction.....	281
8.2	The theoretical part based on the research aims and objectives.....	281
8.3	The operational framework based on the research questions.....	284
8.3.1	The case study.....	286
8.3.2	Field measurement.....	287
8.3.3	Field survey.....	289
8.3.4	Numerical modelling.....	290
8.4	Guidelines for improving the microclimate within the UCL in the hot, arid climate.....	295
8.5	Outline for possible future research.....	296
8.6	Limitations of the study.....	299



8.7 Contribution of the study .....	299
<b>References.....</b>	<b>301</b>
<b>Appendix 'A'.....</b>	<b>320</b>
Al-Muizz Street Urban Development.....	320
• Cairo urban development.....	321
• The development of Al-Muizz Street.....	323
Al-Muizz Street urban pattern type.....	326
• Al-Muizz as a World Heritage Site (WHS) .....	346
• Conclusion.....	355
<b>Appendix 'B'.....</b>	<b>358</b>
Appendix 'B1'.....	359
General structure of ENVI-met 3.1 .....	359
Appendix 'B2'.....	366
CFD model equations.....	366
<b>Appendix 'C'.....</b>	<b>369</b>
Questinnaire Survey.....	370
<b>Appendix 'D'.....</b>	<b>373</b>
Basic ENVI-met 3.1 configuration file (Renovated part).....	373
Basic ENVI-met 3.1 configuration file (Non-Renovated part) .....	376
<b>Appendix 'E'.....</b>	<b>379</b>
Solar radiation calculator.....	379

## LIST OF TABLES

### Chapter One

Table 1-1 Main climatic characteristics for the climatic zones in Egypt according to HBRC (2006) (T air: Air Temperature (°C) T op: Operative Temperature (°C)) ...	22
---	----

### Chapter Two

Table 2-1 Possible urban factors and effects on the urban environment (Oke, 1991; Shahidan, 2011).....	44
Table 2-2 Simple classification scheme of UHI types (after Oke, 1995 and Roth, 2002) (Shahidan, 2011).....	46
Table 2-3 Impacts of urban heat islands, and/or a warmer base climate, on temperature-sensitive aspects of cities in cold and hot climate regions after Roth, 2002 (from Oke, 1997b). .....	49
Table 2-4 Climatic projection in North Africa in 2080 to 2099 (source IPCC, 2007a) ..	54
Table 2-5 GCM estimates of temperature and precipitation change for Egypt. Source OECD (2004).....	54

### Chapter Three

Table 3-1 Total radiation yield of the canyon in (kwh/m) for different street directions, typical dates and street widths with flat roofs (Robins and Macdonald, 1999).....	81
Table 3-2 The albedo and thermal emissivity of typical natural and man-made material Sources: Oke (1987); Garratt (1992).....	87
Table 3-3 Proposed systems for rating heat stress and strain (heat stress indices). Source: Epstein and Moran (2006) .....	99
Table 3-4 Selected thermal comfort indices (Fanger, 1970; Givoni, 1963; Givoni, 1976; Hoppe, 1999 and Cohen et al., 2013) .....	101
Table 3-5 Summary of studies that assessed thermal sensation with different thermal indices. Modified from Cohen et al. (2013) .....	103

### Chapter Four

Table 4-1 The characteristics of Al-Muizz urban canyon studied and their immediate surroundings .....	123
Table 4-2 Davis Vantage Vue 6250 weather station data sheet .....	131

Table 4-3 Typical Insulation and Permeation Efficiency Values for Clothing Ensembles (ASHRAE, 2009).....	131
Table 4-4 Typical Metabolic Heat Generation for various activities. Source: ASHRAE (2009).....	132
Table 4-5 Comparison between CFD codes that can serve the research scope and the strongly desired features .....	135
Table 4-6 Requirements for a consistent CFD simulation (AboHela et al., 2012).....	141
Table 4-7 Davenport’s classification of effective terrain roughness .....	148
<b>Chapter Five</b>	
Table 5-1 Canyon properties at all measuring points in Fatimid Cairo, Egypt .....	160
Table 5-2 Average wind velocity (m/s) measured on 29 <sup>th</sup> June and 1 <sup>st</sup> July 2012 .....	166
Table 5-3 Measured globe temperature (°C) on 29 <sup>th</sup> June and 1 <sup>st</sup> July 2012.....	171
Table 5-4 Main input data used for ENVI-met.....	181
Table 5-5 The observed in-situ values used for calculating the TMRT estimated from the globe temperature (T <sub>g</sub> ), air temperature (T <sub>a</sub> ) and air velocity (V <sub>a</sub> ).....	185
<b>Chapter Six</b>	
Table 6-1 The gender and age distribution for the 320 questionnaires .....	196
Table 6-2 Physiology equivalent temperature (PET) at different levels of thermal sensation .....	202
Table 6-3 Thermal sensation vote * summer_winter Crosstabulation .....	204
Table 6-4 Thermal Comfort Conditions –ASHRAE Standard 55 (1992) Source: Charles (2003).....	207
Table 6-5 Contingency table of short-term thermal history .....	216
<b>Chapter Seven</b>	
Table 7-1 Requirements for a consistent CFD simulation (AboHela et al., 2012).....	224
Table 7-2 Output data simulated by DesignBuilder .....	237
Table 7-3 The air temperature assumed by DesignBuilder for the site compared to the field measurement.....	239
Table 7-4 Data table for the validation air temperature and the input surface temperature data.....	240

Table 7-5 The classification of the pedestrian-level natural ventilations in street canyons (Yuan and Ng, 2012) .....	243
Table 7-6 The vertical profiles of the mean wind velocities from the CFD simulation located at the centre line of the street .....	247
Table 7-7 The (Q) or the Volumetric Flow Rate (m <sup>3</sup> /s) through the street opening or street roof note that positive values of (Q) denote air entering (inlet) and negative values represent air leaving (outlet).....	249
Table 7-8 The vertical profiles of the air temperature conducted from the CFD simulation located at the centre line of the street .....	258
Table 7-9 Calculated globe temperature, mean radiant temperature and PET for the different case studies in addition to the inputs used in the equations ( <i><b>f<sub>db</sub></b></i> ) is the direct beam radiation from the sun, <i>z</i> is the solar angle to zenith, (s) is the solar irradiance (W/m <sup>2</sup> ) were calculated based on solar radiation calculator attached in appendix E).....	260
Table 7-10 Comparison between the different cases including the base case 3 and best case 7 .....	263
Table 7-11 The grid sensor nodes scattered within the model .....	266
Table 7-12 solar radiation and incident analysis between the different cases.....	270

## Chapter Eight

Table 8-1 Comparison between the different cases including the base case 3 and best case 7 .....	294
--	-----

## LIST OF FIGURES

### Chapter One

Figure 1-1 Al-Muizz Street runs from north to south across the middle of Medieval Cairo .....	10
Figure 1-2 The different local interventions for shadings in the non-renovated part compared to the renovated one .....	11
Figure 1-3 The overall methodology scheme .....	18
Figure 1-4 Map of Egypt and its geographic location .....	19
Figure 1-5 Classification of climatic zones in Egypt according to HBRC (2006) .....	20
Figure 1-6 Cairo development, starting from Al-Fustat to the north of the Roman fort Babylon in 641AD.....	25
Figure 1-7 The Al-Muizz street and Gate Al-Futuh in the north, and Zuweila in the south (Mortada, 2003) .....	26
Figure 1-8 Al-Muizz Street in 1908 and 2012 (source: bildindex.de).....	27
Figure 1-9 The historical development of Fatimid Cairo and its impact on the urban form (source: ETH Studio Basel) .....	30
Figure 1-10 Electronic bollards control the traffic at the entrance to Al-Muizz .....	31
Figure 1-11 The historical development of the spaces along Al-Muizz Street .....	33
Figure 1-12 The exterior shaping for the elements among Al-Muizz Street.....	33
Figure 1-13 Research design .....	37

### Chapter Two

Figure 2-1 The emissivity of a material determines how much absorbed solar energy is released or retained. ....	41
Figure 2-2 Generalized cross section of a typical urban heat island (Roth, 2001).....	45
Figure 2-3 Schematic of climatic scales and vertical layers found in urban areas .....	47
Figure 2-4 Surface and atmospheric temperatures vary over different land use areas .....	48
Figure 2-5 Increasing Power Loads with Temperature Increases .....	50
Figure 2-6 Relation between daily maximum air temperature and daily maximum ozone concentration in Connecticut and the chemical reaction that produces ozone on the right.....	51

Figure 2-7Relation between maximum air temperature and mortality in Shanghai from 1980 to 1989. ....	52
Figure 2-8Rapid urban growth in Cairo between 1984-2002 caused a significant rise in surface temperature, referred to as an urban heat island (UHI) effect.....	55
Figure 2-9 Increasing AC and fan sales in Egypt between 1996 and 2009 (CAPMAS, 2008; INCOM, 2008; Abdelhafiz, 2004).....	56
Figure 2-10Narrow, deep streets reduce radiant heat gains.....	58
Figure 2-11Urban compactness and narrow streets shaded by neighbouring walls.....	59
Figure 2-12Shading techniques across the street.....	60
<b>Chapter Three</b>	
Figure 3-1Schematic of climatic scales and vertical layers found in urban areas.....	65
Figure 3-2Schematic view of a symmetrical urban canyon and its geometric descriptors /Sky view factor (SVF) as a function of canyon aspect ratio (H/W) (on the right hand side).....	67
Figure 3-3Schematic section showing urban surface energy balance (SEB) components.....	69
Figure 3-4Daily energy balance of the urban facets of an urban canyon oriented N-S with $H/W \approx 1$ for a sunny summer day in Vancouver, $49^\circ\text{N}$ .....	71
Figure 3-5Route with the different aspect ratio (H/W) along Al-Muizz Street.....	72
Figure 3-6Different photos among different sections within Al-Muizz street showing the similar heights of both sides of the street in several parts .....	74
Figure 3-7Isotherm distribution across an E-W canyon at selected daytime hours (wind speed, wind direction and stability conditions at 1m height). ....	75
Figure 3-8Surface and air temperatures of urban canyon facets, for an E-W street of an aspect ratio $H/W = 0.96$ under summer conditions for Kyoto, Japan, $35^\circ\text{N}$ .....	76
Figure 3-9The effect of solar heating on individual surfaces may create substantial thermal flows affecting the air flow patterns.....	80
Figure 3-10Straight and parallel streets improve air flow into and within a city while the narrow and winding streets make air flow slow .....	80
Figure 3-11The damage caused to monuments and the street by the release of sub-surface water and sewage water in some areas of Al-Muizz.....	84

Figure 3-12 Old photos dated to the end of the 18th century for Al-Muizz Street show how people used their own techniques such as the movable tents to avoid direct solar radiation .....	86
Figure 3-13 The use of heavy materials, mainly stone, which has a high thermal capacity. In addition, using light painted colours in the buildings' external facades helps increase the urban reflectance.....	88
Figure 3-14 The components of the human heat balance .....	90
Figure 3-15 Schematic depictions of radiation exchanges between a pedestrian and the surrounding urban environment.....	92
Figure 3-16 Outdoor thermal comfort assessment framework .....	116
<b>Chapter Four</b>	
Figure 4-1 Research Methodology Framework .....	121
Figure 4-2 The two modelling domains and the two measurement points.....	123
Figure 4-3 Annual fan and air conditioning operation profile in Cairo with the PET comfort range.....	123
Figure 4-4 Route with the different measuring points at Al-Muizz Street.....	125
Figure 4-5 The mobile weather station setup. ....	126
Figure 4-6 The relation between the different softwares and their outputs.....	134
Figure 4-7 Flowchart illustrating the framework for the assessment of pedestrian wind comfort and safety with CFD .....	142
Figure 4-8 Flowchart outlining part C of the large flowchart in Figure 4-7.....	143
Figure 4-9 Computational domain dimensions for a flow around the model of height H. ....	145
<b>Chapter Five</b>	
Figure 5-1 Cairo monthly average meteorology based on 30 years records of WMO station no. 623660 calculated by Ecotect weather tool.....	155
Figure 5-2 The sunshine duration analysis conducted by Meteonorm 7 .....	156
Figure 5-3 The two locations of the portable weather stations within Al Muizz street, Cairo, Egypt.....	156
Figure 5-4 Average air temperature of the two mini weather stations within the UCL and the airport weather station during the week of field measurements .....	157

Figure 5-5The WMO station location to the case study .....	158
Figure 5-6The homogeneity of the climatic conditions in Cairo over a long term period (1980-2012) including the mean values of air temperature (Ta), relative humidity (RH), and wind speed (va) in June at Cairo WMO Station no.623660 at Cairo International Airport .....	159
Figure 5-7Route with the measuring points at different street geometries and at Al-Muizz Street.....	160
Figure 5-8Photographs of the nine selected measuring sites.....	161
Figure 5-9The in-situ air temperature (Ta) measured during the two summer days measurements .....	164
Figure 5-10The in-situ wind speed (va) (m/s) measured on 29th June and 1st July 2012 .....	167
Figure 5-11The deep canyon for location 8.....	168
Figure 5-12As the temperature changes during the day, the relative humidity also changes substantially .....	169
Figure 5-13Relative Humidity (RH%) at 1.2 m a.g.l. during the two summer days' measurements .....	170
Figure 5-14Mean radiant temperature (TMRT) at 1.1 m a.g.l. during the two summer days of measurement .....	174
Figure 5-15A local intervention, as the street is semi-covered by tents in some places which prevent direct solar radiation from focusing in one place for too long.....	175
Figure 5-16The excess heat is emitted from the mechanical ventilation to the urban air, which may increase the air temperature in the street.....	175
Figure 5-17The RayMan 1.2 interface showing the input parameters for calculating the PET .....	177
Figure 5-18Physiologically equivalent temperature (PET) at 1.2 m a.g.l. during the two measurement days.....	179
Figure 5-19The average patterns of the TMRT and PET for the two measurement days .....	180
Figure 5-20Correlation between PET and thermal sensation in summer 2012.....	180



Figure 5-21	The two modelling domains and the two measurement points which are the same receptors in ENVI-met .....	181
Figure 5-22	Comparison between the air temperature measured and the ENVI-met output .....	183
Figure 5-23	TMRT simulated by ENVI-met plotted against measured TMRT .....	184
Figure 5-24	The renovated part spatial pattern of the Mean Radiant Temperature (TMRT) for 1st July 2012 by ENVI-met .....	187
Figure 5-25	The non-renovated part spatial pattern of the Mean Radiant Temperature (TMRT) for 1st of July 2012 by ENVI-met .....	188
Figure 5-26	The difference mean radiant temperature (TMRT) between the shaded and non-shaded for 1st July 2012 by ENVI-met .....	189
<b>Chapter Six</b>		
Figure 6-1	Al-Muizz Street: renovated and non-renovated parts where the questionnaire was carried out.....	195
Figure 6-2	Distribution percentage of people purpose of visiting and distribution percentage of how often they visit the area of study .....	197
Figure 6-3	Percentage distributions of thermal sensation votes (TSVs) in cool and hot seasons .....	198
Figure 6-4	Thermal acceptable range for respondents in the street.....	199
Figure 6-5	Correlation between PET and thermal sensation in summer 2012 .....	201
Figure 6-6	Correlation between PET and thermal sensation in winter 2012.....	201
Figure 6-7	Percentage of preferences votes including air temperature, wind speed and sun exposes.....	205
Figure 6-8	Preferred temperature by Probit model.....	207
Figure 6-9	Percentage of users visiting the street for different reasons who felt overall thermally comfortable and uncomfortable under comfortable conditions $PET > 23^{\circ}\text{C}$ or $PET < 32^{\circ}\text{C}$ .....	209
Figure 6-10	Percentage of males and females who adopted adaptive behaviours .....	210
Figure 6-11	Clothes worn by males under different PET segments .....	211
Figure 6-12	The subjective thermal sensation votes (TSV) in the two different parts of Al-Muizz.....	212

Figure 6-13The percentage of preference votes for more shade, no-change, or more sun in the two parts of Al-Muizz.....	214
Figure 6-14Percentage distributions of the respondents' activities.....	216
Figure 6-15Adjusted correlation between TVS and physical activities under outdoor conditions.....	217

## Chapter Seven

Figure 7-1Shading canopies across the full width of pedestrian streets in different hot countries.....	222
Figure 7-2Flowchart illustrating the scenario framework for the assessment of pedestrian comfort using CFD for the case study. ....	225
Figure 7-3The iterations were terminated when the scaled residuals (Fluent Inc. 2006) did not show any further reduction with an increasing number of iterations, .....	227
Figure 7-4Computational domain dimensions and positions of the lines.....	228
Figure 7-5Velocity magnitude graph showing the horizontal homogeneity of the velocity profile.....	228
Figure 7-6TDR graph showing the horizontal homogeneity of the TDR profile .....	229
Figure 7-7TKE graph showing the horizontal homogeneity of the TKE profile .....	229
Figure 7-8The simulated street segment dimensions in CFD.....	231
Figure 7-9Mesh refinement area around the model and extended to 10m height above the model .....	232
Figure 7-10wind velocity profile captured at the centre line of the model for the three meshes.....	233
Figure 7-11The existing case study the CFD model and meshing domain .....	234
Figure 7-12The weather profile preliminary data from the WMO Station no.623660 records at Cairo International Airport.....	236
Figure 7-13The model as drawn in DesignBuilder with the name of the four simulated walls as W1, W2, W3 and W4.....	237
Figure 7-14Surface temperature for all walls .....	238
Figure 7-15DesignBuilder assumed air temperature for the study location and the field measurements .....	239

Figure 7-16	Comparison between the air temperature measured and the CFD output for the existing case on 1st July at pedestrian height of 1.4m.....	240
Figure 7-17	The alternative configurations for each case study with specific changes in the roof shape and opening locations.....	242
Figure 7-18	The vertical profiles of the mean wind velocity were measured at a point on the centre line of the street across the prevailing wind direction .....	245
Figure 7-19	The vertical profiles of the mean wind velocities from the CFD simulation located at the centre line of the street (from 0m on the ground level to 7m on the roof level).....	246
Figure 7-20	The total volume flow rate (m <sup>3</sup> /s) for each case.....	250
Figure 7-21	The vertical wind speed contours at the centre line of the model on the left hand side and the horizontal wind speed contours at 1.4m above the ground level on the right hand side.....	253
Figure 7-22	Calculated air change rate per hour (ACH) for the different ventilation configurations for reference wind speed U <sub>10</sub> = 5m/s.....	255
Figure 7-23	Flow rate percentages across the roof and side openings .....	255
Figure 7-24	The simulated vertical profiles of the air temperature located at the centre line of the street (from 0m on the ground level to 7m on the top roof level) .....	256
Figure 7-25	The inverse correlation between the air temperature distribution underneath the different roof shapes and the ambient wind speed at the pedestrian level.....	258
Figure 7-26	The estimated PET and T <sub>mrt</sub> for the seven cases .....	261
Figure 7-27	The grid sensor nodes scattered within the model .....	265
Figure 7-28	The grid sensor nodes scattered within the model .....	266
Figure 7-29	The solar incident analysis for all cases for the summer and winter, and annually, excluding case 1 as it is a fully exposed without any shading roofs.....	271
Figure 7-30	DIVA Radiation Map –annual grid based simulation output for the seven case studies .....	276
Figure 7-31	The base case, as used by ancient town planners in Al-Muizz Street to provide both shading and daylight.....	276

# 1

---

*“Climatic determinism has been widely accepted in architecture as well as in cultural geography, although in the latter it has recently found rather less favour. One need not deny the importance of climate to question its determining role in the creation of built form... In architecture the climatic determinist view, still rather commonly held, states that primitive man is concerned primarily with shelter, and consequently the imperatives of climate determine form” (Rapoport, 1969, p. 18)*

## **Chapter One**

---

### **1. Introduction**

---

#### Key Concepts

---

- 1.1. Introduction
- 1.2. Research design
- 1.3. Research aim
- 1.4. Hypothesis and research questions
- 1.5. Scope and limitations
- 1.6. Significance of the study
- 1.7. Research methodology
- 1.8. Research context
- 1.9. The physical pattern development
- 1.10. Research structure

## **1.1 Introduction**

The thesis aims to investigate the outdoor thermal performance of traditional commercial urban streets in the hot arid context of Cairo in Egypt, to find ways of extending the thermal comfort of pedestrians. This enables spending more time outdoors, with potential health improvements, less dependency on energy consumption indoors, and positive economic contributions to the local economy (Oke, 1988; Gehl and Gemozoe, 2001; Johansson, 2006b; Marques de Almeida, 2006; Pearlmutter et al., 2011; Makaremi et al., 2012). The strategic importance of the street as a case study is attributable to its function where the street network of an urban entity has, from a design point of view, a structural role and accounts for the main support for mobility, urban activity, and social life. It even reflects cultural specificities, particularly in traditional commercial streets (Moughtin, 2003) which have always played a central role in the social life of cities. They have always served three vital functions since they act as meeting places, market places, and spaces for connection (Gehl and Gemozoe, 2001).

This chapter is divided into five core sections, starting with the conceptual framework by discussing the rationale behind the argument, and the research aim, hypotheses, objectives, questions, limitations, propositions and significance of the study. Accordingly, section 1.7 outlines the research methodology, followed by the research context overview, such as the geographical and climatic characteristics, in addition to the historical background of the case study in sections 1.8 and 1.9, and then the research structure is outlined and the thesis overview are summarized in section 1.10.

## **1.2 The conceptual framework**

### **1.2.1 Problem statement**

According to Intergovernmental Panel on Climate Change (IPCC, 2007), global air temperatures are expected to rise by 0.2°C per decade over the next century. Furthermore, there will be an increased risk of more intense, more frequent and longer lasting heat waves. The European heat wave of 2003 is an example of the type of extreme heat event lasting from several days to over a week that is likely to become more common in a warmer future climate. For regions with hot or arid climates, the

scenario will be worse as the consequences include increased occurrence of heat stress and other heat-related diseases. Moreover, human performance of both mental and physical tasks diminishes at uncomfortably high temperatures, while deaths and illness caused by air pollution tend to increase during extremely warm weather (Harlan et al., 2006). In addition to global warming, cities are particularly in danger since it is often warmer than in surrounding rural areas during hot fine weather, especially at night. This phenomenon is referred to as the 'Urban Heat Island' (UHI) (Landsberg, 1981; Oke, 1973, 1978, 1988, 1999; Santamouris et al., 2001; Streutker, 2003; Tran, 2006; Gartland, 2008), which is caused as a result of accelerated urbanization and rapid changes to the outdoor environment in different ways (Roth, 2002). For example, this includes the fraction of urban land covered by buildings, distances between buildings, and the average height of buildings (Givoni, 1998). These parameters affect the urban microclimate in terms of solar radiation and reflection, wind speed and direction, and any inappropriate combination of these parameters which can contribute to the harshness of the environment (Shishegar, 2013), such as building a large portion of landscape consisting of rough building blocks and impervious pavements combined with a lack of green and blue areas. Therefore, the urban planning regulations, which include the instructions that lead the city development in terms of building constructions, urban forms, urban spaces, parks, street, etc., have a great impact on the microclimate in urban areas (Johansson and Yehia, 2010). In order to reduce negative climatic impacts in cities, those involved in urban development, planning, and design must begin to incorporate climate knowledge into planning strategies and create links between microclimate, thermal comfort, design, and urban planning regulations. However, the integration of the climate dimension in the design process is still missing as a result of poor interdisciplinary work (Oke, 2006; Yow 2007; Fahmy and Sharples 2008b), or as Eliasson (2000) earlier identified, this is the 'translation-gap' as designers and climatologists do not 'speak the same language'. Moreover, most studies have been conducted in the temperate regions of developed countries; most of the studies conducted in tropical areas have dealt with the urban rural difference known as the urban heat island (UHI), and fewer have been done on microclimate variations within cities (Johansson, 2006). Accordingly, regulations determining the urban design in arid regions

are often inspired by planning ideals from temperate climates and consequently are poorly suited to its local conditions, leading to uncomfortable outdoor environments for the planned settlements (Al-Hemaidi, 2001; Baker et al., 2002; Johansson, 2006).

In the hot dry city of Fez in Morocco, Johansson (2006b) reported that the current regulations' main objective is to provide daylight for buildings. This may be acceptable during the winter period when solar elevations are low and passive heating of buildings is desired. However, during the long, warm summer, when there is a need for solar protection, this results in a very poor microclimate at street level. In Saudi Arabia, it was found that the current urban design regulations encouraging dispersed urban design planning led to an unfavourable microclimate around buildings, as the provision of shade is totally lacking (Al-Hemaidi, 2001; Eben Saleh, 2001). Furthermore, Yehia (2012) reported the shortcomings of the current planning regulations regarding the outdoor thermal comfort at street level in the hot dry summers of Damascus city in Syria. The existing planning regulations similar to Saudi Arabia encouraged a dispersed urban form leaving large surface areas of the buildings and streets exposed to solar radiation without any requirements for shading for pedestrians, such as shading devices, arcades and projecting upper floors or shading trees.

In terms of socio-economic consequences, the microclimate conditions remarkably influence people's outdoor behaviour and usage of public spaces (Zacharias, 2001; Thorsson et al., 2004a; Knez and Thorsson, 2008). The number and intensity of such activities may be affected by the level of the discomfort experienced by pedestrians when they are directly exposed to the climatic conditions (Thorsson, 2007), whether they are explicitly aware of it or not. For instance, on a typical summer day in an arid city, the thermal conditions may be unpleasant so people tend to spend time outdoors only when necessary; that is, in performing essential tasks such as travelling to work or shopping. Meanwhile, optional activities and social activities, such as strolling, meeting people in public open spaces, children's play and so forth will diminish (Gehl 2001), bringing about a negative effect on outdoor commercial activities, such as café and restaurants, open-air markets, cultural events.

As a result of this connection between physical conditions and human behaviour, a poor urban climate may also increase people's isolation, and reduce quality of life by reliance on air-conditioned buildings and vehicles, resulting in higher energy consumption and less vivid cities (Gehl and Gemzoe, 2001; Johansson, 2006b; Marques de Almeida, 2006; Aljawabra and Nikolopoulou, 2010; Pearlmutter et al., 2011; Makaremi et al., 2012). However, there is a significant lack of information on thermal comfort conditions in outdoor spaces, which in effect will assist the design and planning of such spaces (Nikolopoulou and Lykoudis, 2006; Panagopoulos, 2008; Fahmy and Sharples 2008b).

Thermal comfort as a term has been defined in numerous ways. Fanger's (1970) definition links thermal comfort and the rate of energy gains and losses by the human body, describing the state of comfort when all heat flows to and from the body in equilibrium. In this definition, Fanger's (1970) studies were mainly based on the rational model, which accounts for environmental conditions and physiological regulation of body temperature within a limited range. According to British standard BS EN ISO 7730 (2013) and ASHRAE (2009), thermal comfort is defined as "the state of mind that expresses satisfaction with the surrounding environment." This means that comfort is not a state condition, but rather a state of mind, which in turn highlights the social and psychological dimensions. Recent studies have shown that thermal sensations are different among people within the same site due to the combination of large number of factors, including mood, culture, and social factors, which affect the perception of human beings. Although this description suggests psychological influences, thermal comfort was approached from a purely physical perspective for a long time. Accordingly, the first attempts made to assess thermal perception and grade thermal stress consisted of the simply measurable physical variables like air (dry-bulb) temperature (Parsons 2003, p. 197). Later, thermal indices included wet-bulb temperature and air velocity, like the indices based on 'Effective Temperature' (Parsons 2003, pp. 198-199; Gagge et al., 1986). In 1926, Macpherson defined the following six factors affecting thermal sensation: air temperature, air speed, humidity, mean radiant temperature, metabolic rate, and clothing levels (Goldman, 1999; Berglund, 1978). Since



then, a range of other indices for thermal comfort, which included more personal parameters like clothing degree and metabolic rate, were later developed with the 'Predicted Mean Vote' (PMV) by Fanger (1970, pp. 19-43), 'Physiological Equivalent Temperature' (PET) (Höppe and Mayer, 1987; Mayer, 1993; Matzarakis et al., 1999; Höppe, 2002) and the COMFA index (Brown and Gillespie, 1995). All these indices reasonably produce near accurate predictions of occupant thermal sensation; however, their sole focus on the physiological and physical dimensions was increasingly criticized, as the climatic chamber method used to underpin these indices failed to include many subjective, social and cultural real world situations (Han, 2007). Moreover, these indices are almost exclusively designed on theoretical analyses of human exchange in mid-latitude climatic in North America and Europe, such as ASHRAE standards and the ISO (Han, 2007). Other studies in different climatic regions have refuted this hypothesis and indicated a wider range of adaptation and tolerance to local conditions. Lin (2009), for example, studied outdoor thermal perception and adaptation in a hot and humid subtropical climate of Taiwan, and reported that the thermal acceptance range for the entire year was 21.3-28.5°C PET, significantly higher than the European scale of 18-23°C PET (Lin, 2009). Another study in the Mediterranean climate of Tel Aviv found the PET values were higher by 3°C PET than the European scale and lower by 5°C PET than the lower boundary of Taiwan (Cohen et al., 2013). These results revealed that a purely physiological approach is inadequate to characterize thermal comfort conditions outdoors, and thermal adaptation, which involves behaviour adjustment (personal, environmental, technological or cultural), physiological factors (genetic adaptation or acclimatization), and psychological factors (habituation or expectation) as playing an important role in the assessment of thermal environments (Brager and de Dear 1998; Nikolopoulou et al., 2001; Nikolopoulou and Steemers, 2003; Thorsson et al., 2004; Knez et al., 2009; Lin, 2009; Yang et al., 2013). Thus, different scholars such as Nikolopoulou and Lykoudis (2006), Lin and Matzarakis (2008), Kántor et al. (2012) and Cohen et al. (2013) suggest that calibration should be carried out using local subjective comfort data conducted from field surveys to provide a broader perspective to assess thermal comfort in urban spaces.

In comparison with extensively investigated thermal comfort in indoor environments, outdoor thermal comfort and its determinants are less understood by researchers and practitioners alike. Hence, four main knowledge gaps have been identified as follows:

1. The integration of the climate dimension in the design process is missing as a result of poor interdisciplinary work. Studies have shown that integrating knowledge of the climate in urban planning among planners and urban designers is often missing (Fahmy and Sharples 2008b) particularly in areas of the Middle East (Abdulrahman and Sharples 2014). Added to this, there is a lack of suitable design assessment tools (Eliasson, 2000, Givoni et al., 2003; Oke, 2006). A tool that can provide both quantitative and qualitative understanding of the relationships between the microclimatic environment, subjective thermal assessment, and social behaviour (Givoni et al., 2003; Chen and Ng, 2012)
2. Many investigations of outdoor thermal comfort extend indoor comfort methods to the outdoors by adopting thermal indices, which rely on a steady-state energy balance model and combine physical factors into a single metric to assess comprehensive thermal comfort or thermal stress (Gagge, 1981; Givoni, 1963; Hoppe, 1999). Since these indices were originally developed for enclosed indoor spaces, their validity under outdoor conditions has been increasingly questioned, as evidence is accumulating that human thermal sensation, in fact, differs from those predicted by the indices and that the parameters of an indoor setting may not be transferable to an outdoor environment (Hoppe, 2002; Nikolopoulou et al., 2001; Spagnolo, 2003; Thorsson et al., 2004b; Cohen et al., 2013)
3. A few studies have been conducted recently in hot dry climates, but only a limited number of investigations have been done in the Middle East that focus on urban design from a microclimatic perspective (Yehia, 2012). In addition to, little discussion about the integration of modern technological solutions and traditional architectural approaches (Abdulrahman and Sharples 2014). However, the situation has begun shifting with population growth and accelerating urbanization. Hence, sustaining an acceptable quality of life for this growing population is essential for

hot arid settlements, and is largely dependent on our understanding of climate-sensitive urban design

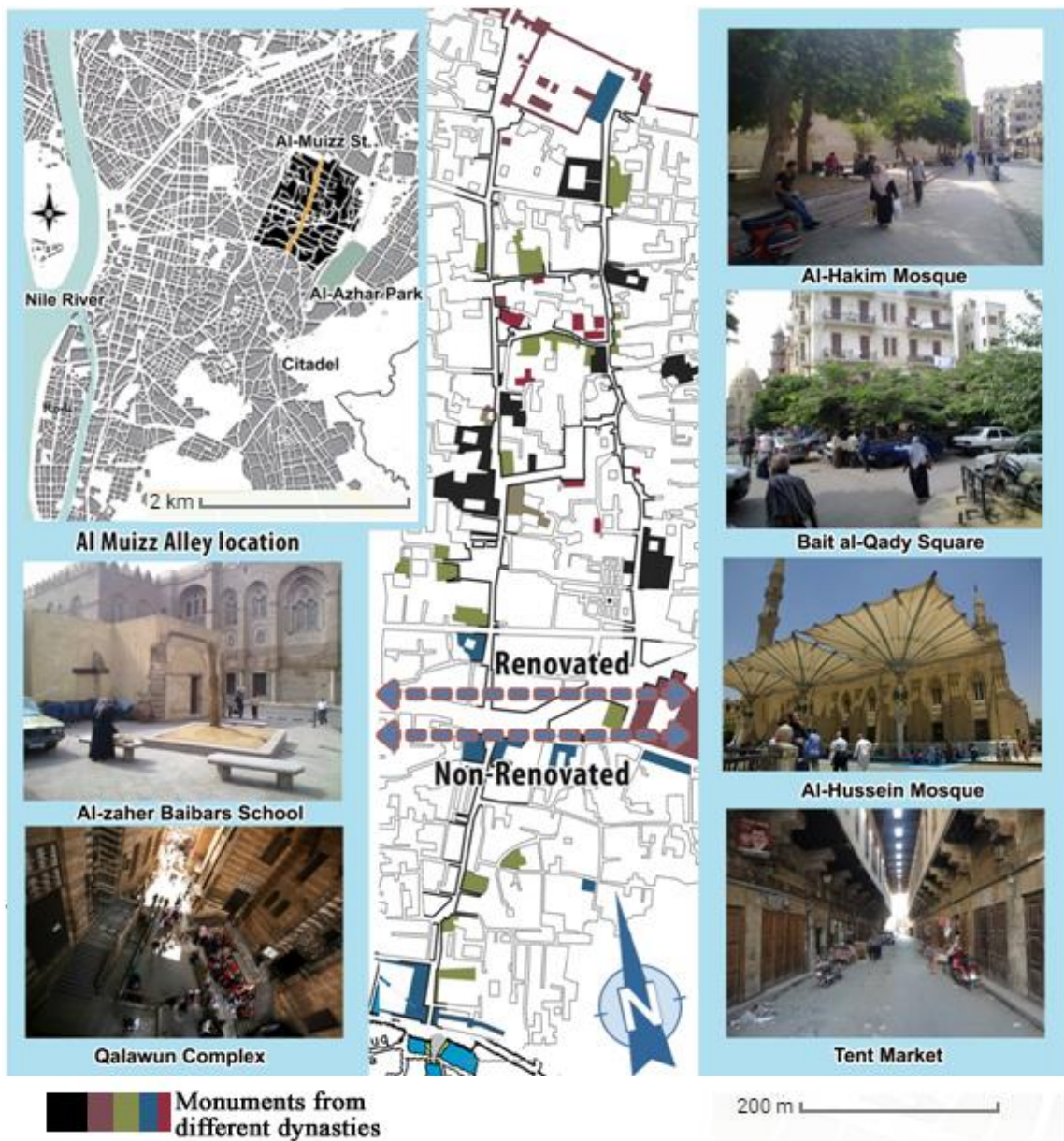
4. There is a need for a valid assessment framework which should work on at least four levels (physical, physiological, psychological, and social/behavioural), as the majority of the available studies deal with the microclimate separate between the qualitative and the quantitative approaches. Numerous researchers within the field have recently identified the psychological factors of comfort experience to be of equal importance to the technically measurable comfort indices (Auliciems, 1981; Gehl, 1987; Katzschner et al., 2002; Givoni et al., 2003; Thorsson et al., 2004; Katzschner, 2006; Nikolopoulou and Lykoudis, 2006; Walton et al., 2007; Eliasson et al., 2007).

Based on the above, the study analyzes and climatically examines the urban design on street-level thermal comfort by triangulating urban microclimatic measurements and structured interviews and urban simulations using principles of urban physics. The study highlights the importance of microclimate and thermal comfort in the planning and design processes and it provides useful insights that can mitigate the negative aspects of urban design on microclimate and thermal comfort in the hot arid climate of Cairo, Egypt.

Accordingly, Al-Muizz Street, which is one of the oldest streets in medieval Cairo (Figure 1.1), was chosen as the main case study for numerous reasons including its essential street pattern, which has been preserved and reflects a climate conscious design developed over centuries of building experience; its convoluted street system and compact urban structure limit the possibility of adopting modern large-scale developments. In addition, the area had the largest concentration of the medieval architectural treasure in the Islamic world for a period of 1,200 years (Antoniou et al., 1985), and this has helped to preserve the place to some extent from modern development. Secondly, Al-Muizz Street piloted the first large-scale pedestrianisation scheme in 2010 in Egypt. It is relevant to this thesis that pedestrianized areas encourage longer durations of use, and this therefore allows for the examination of pedestrian thermal comfort in urban streets. On top, Al-Muizz Street and its

surroundings were exposed to an extensive restoration project, to be transformed into an open-air museum, by the Egyptian government. The first half of the 1.6km (1 mile) long street was fully restored and pedestrianized in early 2010. The second half of the street is about 0.6km (0.4 mile) and has yet to undergo restoration that allows for a comparative case study between the two distinctive contexts, and their impact on use and thermal comfort in the varying urban environments.

This research argues that the restoration project has led to urban modifications and had an impact on the microclimate, which, in turn, has had an impact on the thermal comfort of the inhabitants and users of the area. This can be noticed in the changing behaviour and ways of adaptation to the microclimate of the inhabitants of both sides (the renovated and non-renovated), where the property owners of the old part still regard the pavement area as a legitimate extension to their shops and deliberately appropriate the street setting for selling and living (Rizk, 2011). Different methods of shading to avoid the intense solar radiation in hot summer time are seen in the non-renovated stretch (Figure 1.2), while in the renovated parts, the new regulation prohibited spontaneous urban shading. Therefore, life moves back into the houses, leading to a less vivid atmosphere in the renovated part (Rizk, 2011), and these changes are likely to deepen the social exclusion and contribute to the increased use of air conditioning, resulting in higher energy consumption. Subsequently, more intensive energy use through the consumption of fossil fuels brings increased pressure on the conventional energy supply and directly increases greenhouse gas emissions. In cities located in warm regions, a vicious circle arises: air conditioning units cool the interior of buildings but emit sensible and latent heat to the exterior, further worsening outdoor conditions (de Schiller and Evans 1998; Baker et al. 2002).



**Figure 1-1** Al-Muizz Street runs from north to south across the middle of what scholars refer to as Islamic, Fatimid or Medieval Cairo





**Figure 1-2** The different local interventions for shadings in the non-renovated part on the right compared to the renovated one on the left.

### 1.3 Research aim and objectives

This study aims to develop a better understanding of the relationship between outdoor thermal comfort, urban design and microclimate in order to improve the pedestrians' thermal perception within the hot arid context of Cairo. To achieve this aim, the following objectives were derived:

1. To explore the link between urbanization and the urban heat island effect phenomenon, especially in the hot arid regions and how it can be mitigated (discussed in Chapter 2).
2. To understand the effect of the urban canyon microclimate and the main surface energy balance, and how urban canyon thermal characteristics relate to thermal comfort indices (discussed in Chapter 3).
3. To triangulate measured data from various sources, findings from the literature relating to thermal comfort and the use of simulation tools to predict the performance of various shading scenarios on thermal comfort outdoors need to be linked (discussed in Chapters 5 and 6).
4. To evaluate the cooling effect of different shading patterns provided by various shading systems' designs, and to predict the optimum cooling potential by comparing Al-Muizz's current conditions and different proposed modification scenarios using the computational fluid dynamics (CFD) code Fluent 13.0. (discussed in Chapter 7).
5. To propose guidelines for improving the microclimate and outdoor thermal comfort based on a case study of Al-Muizz street in Cairo.

### 1.4 Hypothesis and Research questions

In accordance with the background to this study, the following hypotheses were investigated:

1. The first action to be taken to mitigate hot conditions outdoors in summer is to intercept direct solar radiation –the most important source of heat gain –by providing shade to both surfaces and people; this in turn will influence human outdoor thermal comfort (This hypothesis tested in chapters 5, 6 and 7)

2. The microclimatic characteristics for the outdoor urban spaces influence people's behaviour and usage of outdoor spaces. The initial results of the previous literature review demonstrates that a purely physiological approach is inadequate in characterising comfort conditions outdoors, and an understanding of the dynamic human parameter is necessary in designing spaces for public use (This hypothesis tested in chapter 6)
3. The comfort zone is different from one location to another. If the measured comfort index based on the energy balance approach is calibrated with actual or subjective thermal sensation vote, there would be a difference in the thermal acceptance ranges and the comfort zones within the hot arid region itself (This hypothesis tested in chapters 5 and 6)
4. The shading systems' can create a cooling effect and can be modified to promote wind flow in the urban canyon similar to that observed in the surrounding environment (This hypothesis tested in chapter 7).

In order to better understand the hypotheses, the study also generated the following questions to be answered:

1. Which are the main design parameters influencing the urban microclimate and outdoor thermal comfort in the hot arid climate?
2. What are the thermal comfort perception and preference of people in outdoor urban spaces? What are the impacts of thermal adaptation on human thermal sensation in outdoor spaces?
3. How can shading designs be modified to promote a significant optimum cooling effect?
4. How can an urban street bounded by the existing urban boundaries be designed to improve the microclimate and thermal comfort at street level?

## **1.5 Scope and limitations**

The research presented in this study concentrates on how urban design affects the microclimate and outdoor thermal comfort. The research focused on the effect of different shading systems' designs at street level on improving the outdoor thermal



comfort air temperature and mean radiant temperature (MRT) reduction in Al-Muizz Street, located in the old city of Cairo, Egypt. To complete the climate efficiency of the shading patterns, the impact of shading devices on daylight quality is presented in the study to assure the visual comfort underneath. Furthermore, Bodart and De Herde (2002) estimated the implementation of appropriate daylight access can reduce artificial lighting power costs from 50-80%, which in turn helps in reducing energy bills.

The study is limited to the microclimate at street level, i.e. the urban canopy layer, which is roughly the space between the ground and the rooftops. This allows for better understanding of the horizontal impact and the behaviour of cooling from different shading designs on the surrounding outdoor environment and people. Therefore, the investigations incorporated the influence of cooling impact on people's thermal perception.

This work is concerned with alleviating heat stress during the extended summer period in the hot arid region. Thermal cold stress occurs rarely in this region. Predictions from climate change scenarios in this climatic region also indicate a continuous rise in temperature reducing the importance of studies related to thermal cold stress (Jendritzky and Tinz 2009).

The study is limited to the hot arid climate of Cairo. Although some of the findings may be generalized, the conclusions of the study are not necessarily valid throughout the hot arid climate groups, since there are climatic and considerable variations between different cities in terms of size, planning principles, proximity to the sea, and topography, etc.

Air pollution and pollutant dispersion are affected by urban geometry. However, air pollution and its consequences on health are not treated here.

## **1.6 Significance of the study**

Most of the available literature on outdoor thermal comfort is carried out in temperate climates (Lenzholzer, 2010). The international comfort standards such as ASHRAE standards and the International Standard Organization (ISO) are almost

exclusively based on theoretical analyses of human heat exchange performed in mid-latitude climatic regions in North America and North Europe (Ogbonna and Harris, 2008; Djongyang et al., 2010). Only a few previous studies were found to study the outdoor thermal comfort in hot humid climates, and even fewer were found for hot arid climates (Johansson, 2007, Pearlmutter et al., 2007; Marques de Almeida, 2008; Lin et al., 2010; Cohen et al., 2013).

This study departs from previous attempts to examine outdoor thermal comfort in a hot arid street way.

Previous studies investigated the thermal performance of shading on the urban microclimate (Nakamura and Oke, 1988; Lin et al., 2010). The shading has proved to be effective in providing a better microclimate during the daytime; however, it can contribute to human discomfort during the nighttime due to the time delay in releasing long wave radiation. However, these studies ignored the effect of the different designs of these shading devices in accelerating the heat release. This research looks at changing the shading systems' with different opening locations to improve the pedestrians' thermal comfort during the nighttime. Thus, a comparative assessment is undertaken to study the effect of different shading systems' and different opening locations in the cooling effect underneath.

Previous studies have reported the unavailability of the international thermal comfort index, which can be used under different climatic zones due to the combination of a large number of factors that affect the perception of human beings. This study, therefore, diagnoses the subjects of the study through calibration between the field measurements and the field survey to define the comfort zones and acceptability limits for PET comfort index in hot arid climate of Cairo. This is very important information for urban designers aiming at a climate-conscious urban design.

This study seeks to provide a better understanding of the relationship between thermal sensation, urban open spaces and microclimate design in the hot arid climate of Cairo by linking the theoretical knowledge of urban microclimate and thermal comfort with the practical design process, which in turn provides the designers and decision

makers with a comprehensive framework for use in evaluating or predicting the effect of different designs in modifying the outdoor microclimate.

## **1.7 Research Methodology**

This study is multidisciplinary in character, as it incorporates phenomena as diverse as meteorology, urban design, urban climatology and environmental psychology. In order to capture the aim, a set of different qualitative and quantitative methodological tools were employed in three parts as follows (Figure 1.3):

### **A. Urban heat island (UHI) and microclimate investigation**

Meteorological field measurements including air temperature, wind speed, solar radiation, humidity and globe temperature within the two different parts of Al-Muizz Street were taken covering a one week pattern in summer to assess the UHI intensity in the urban street, by comparing the observed values with the readings obtained by the Cairo Airport WMO Station no.623660. Accordingly, another in-situ field measurement for nine different locations along Al-Muizz Street were observed and measured to represent the environment and map the microclimate variations within the street.

In order to cover a wide range of the urban design, an ENVI-met simulation model was used to describe the spatial pattern of mean radiant temperature along the whole street, highlighting some problematic areas concerning the UHI and the pedestrian's thermal comfort, even the comparison between restoration urban interventions and local shading interventions facilitated an interesting platform of exploration.

### **B. Human outdoor thermal comfort**

A questionnaire survey was performed simultaneous to the field measurements being taken to ascertain an immediate respondent's impression of the surrounding thermal comfort conditions, and accordingly to calibrate the boundaries of the human thermal sensation scale in the hot arid climate in comparison to other climatic zones.

### **C. Parametric analyses using numerical simulation**

In order to evaluate the effect of the different shading systems' design scenarios on the absolute reduction of the air temperature, and improvement to the outdoor thermal comfort, the computational fluid dynamic (CFD) Fluent code 13.0 was chosen to further examine the thermal comfort underneath the seven different scenarios, in addition to the existing case study for the purpose of validation. Each test scenario consisted of one specific geometrical change in the roof shape and opening locations. Later on, Diva for Rhino software was selected in order to investigate the daylight and solar access underneath these different shading scenarios.

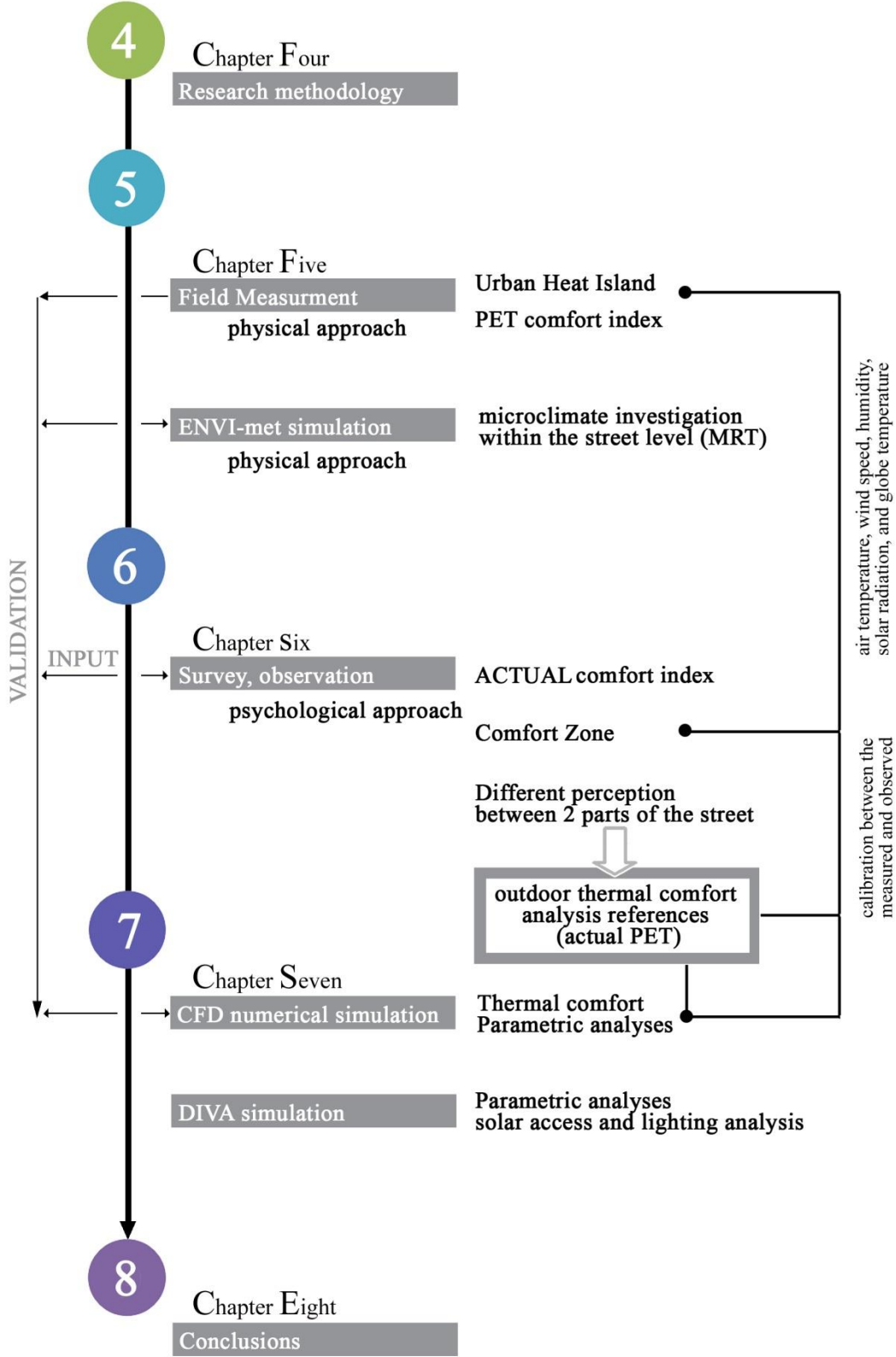


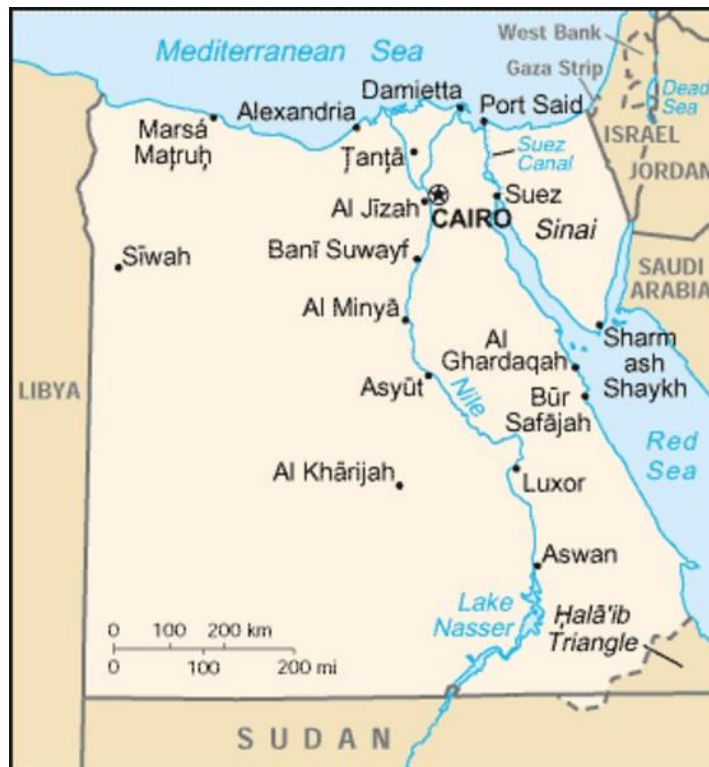
Figure 1-3 The overall methodology scheme investigating the outdoor thermal comfort

## 1.8 Research context

### 1.8.1 The geographical setting of the research

The Arab Republic of Egypt is situated approximately between longitude 25° and 35° E and latitude 22° N and 31.5° N. It occupies the north eastern corner of Africa and has the continent's only land border with Asia. Egypt's coastline has the Mediterranean Sea to the north, and its eastern coastline extends along the Red Sea. It is bordered by Libya to the west, the Gaza Strip to the east, and Sudan to the south.

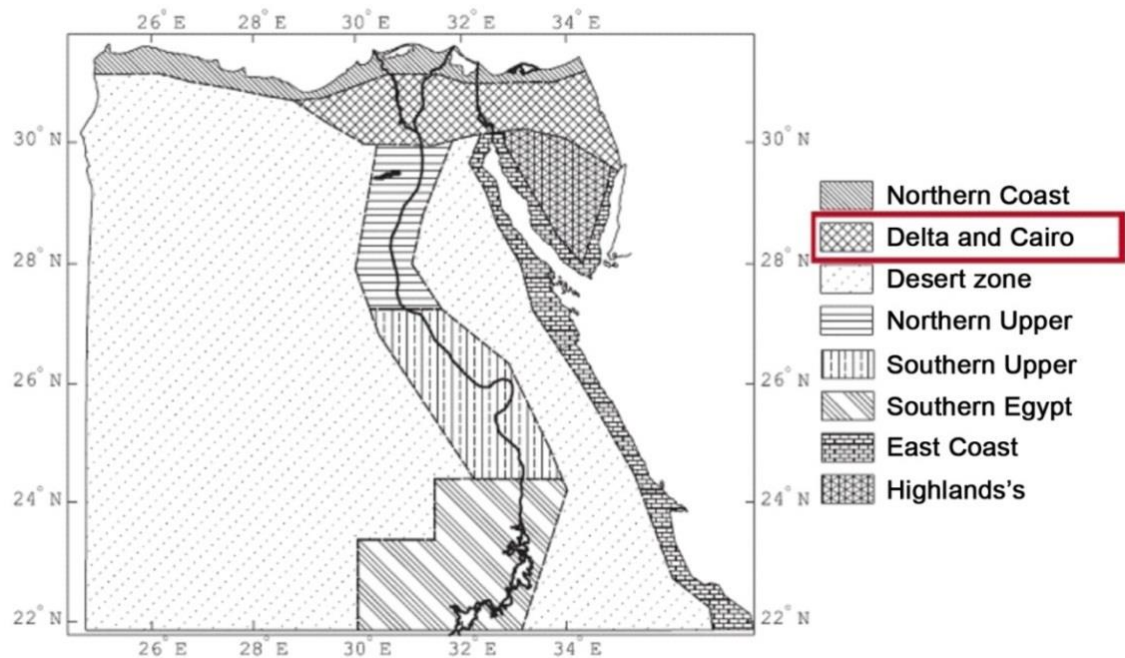
Egypt covers an area of approximately 1,001,450 km<sup>2</sup>, but the inhabited and cultivated area is less than 40,000 km<sup>2</sup>, which is about 5% of Egypt's total area. The population density in the inhabited areas is about 1,800 capita/km<sup>2</sup>. Most of these cultivated settlements are grouped along the Nile (Figure 1.4) including the capital known as Cairo. Cairo is located on latitude 26° 50' N to 30° 45' N. It is situated on the Nile at a point where the flat flood plain, constricted by desert hills to both the west and the east, begins to open out into the Nile Delta.



**Figure 1-4** Map of Egypt and its geographic location

### 1.8.2 Climate characteristic

According to Koppen and Trewartha's system of classification, Egypt lies entirely in the sub group BWh, also known as arid climate (Peel et al., 2007). The (B) symbol denotes a constantly hot, dry, subtropical desert climate, in which potential evaporation exceeds precipitation; the (W) symbol indicates that precipitation  $< 1/2$  water consumption, and (h) for the annual average temperature is greater than  $18^{\circ}\text{C}$  (Henderson and Robinson 1986). However, in 2006, the Housing and Building Research Centre (HBRC) in Egypt classified the country into eight different climatic zones within the arid climate previous classification, based on operative temperature, humidity, rainfall, wind speed, altitude, and solar radiation, as well as the physical topography of the country (Hassaan, 2011). According to the figure 1.6, the country have been classified into Northern Coast zone, Delta and Cairo zone, Northern Upper Egypt zone, Southern Upper Egypt zone, East Coast zone, Highlands zone, Desert zone, and Southern Egypt zone, and described in more detail in Table 1.1.



**Figure 1-5** Classification of climatic zones in Egypt according to HBRC (2006)

As per the Housing and Building Research Centre classification (HBRC, 2006), Cairo lies entirely under the Delta and Cairo zone where the air temperature varies from 34-35°C maximum and 22-24°C minimum during the summer months, while in winter the maximum air temperature varies from 18-21°C, and the minimum temperature varies from 9-12°C. The altitude ranges from 15-110 m above mean sea level, while the humidity level is between 32-84%. Summer time global radiation ranges from 940 to 1,050W/m<sup>2</sup>, and from 550 to 750W/m<sup>2</sup> in winter.



**Table 1-1** Main climatic characteristics for the climatic zones in Egypt according to HBRC (2006) (T<sub>air</sub>: Air Temperature (°C) T<sub>op</sub>: Operative Temperature (°C))

climatic zones	altitude	Summer Temp.		Winter Temp.		RH	global radiation
<b>Northern Coast</b>	0-100m	T <sub>air</sub>	Max.28-31 °C Min.20-24 °C	T <sub>air</sub>	Max. 17-21°C Min. 10-11°C	55-90%	Summer 890-880W/m2 Winter 500-750 W/m2
		T <sub>op</sub>	Max.33-37 °C Min.18-23 °C	T <sub>op</sub>	Max.25-26 °C Min.7-9 °C		
<b>Delta and Cairo</b>	15-110m	T <sub>air</sub>	<b>Max.34-35 °C Min.22-24 °C</b>	T <sub>air</sub>	<b>Max. 18-21°C Min. 9-12°C</b>	<b>32-84%</b>	<b>Summer 940-1050W/m2 Winter 550-750 W/m2</b>
		T <sub>op</sub>	<b>Max.37-46 °C Min.13-21 °C</b>	T <sub>op</sub>	<b>Max.25-28 °C Min.6-9 °C</b>		
<b>Northern Upper</b>	130-280m	T <sub>air</sub>	Max.36-37 °C Min.20-23 °C	T <sub>air</sub>	Max. 20-22°C Min. 6-8°C	28-83%	Summer 950-1160W/m2 Winter 610-960 W/m2
		T <sub>op</sub>	Max.40-47 °C Min.10-22 °C	T <sub>op</sub>	Max.27-31 °C Min.2-6 °C		
<b>Southern Upper</b>	200-300m	T <sub>air</sub>	Max.40-41 °C Min.24-26 °C	T <sub>air</sub>	Max. 23-24°C Min. 12-14°C	20-63%	Summer 950-1160W/m2 Winter 660-960 W/m2
		T <sub>op</sub>	Max.41-46 °C Min.16-21 °C	T <sub>op</sub>	Max.30-36 °C Min.3-9 °C		
<b>East Coast</b>	0-500m	T <sub>air</sub>	Max.36-37 °C Min.27-28 °C	T <sub>air</sub>	Max. 22-24°C Min. 12-14°C	22-60%	Summer 950-1000W/m2 Winter 670-880 W/m2
		T <sub>op</sub>	Max.39-42 °C Min.19-22 °C	T <sub>op</sub>	Max.28-31 °C Min.8-11 °C		
<b>Highlands's</b>	400-2000m	T <sub>air</sub>	Max.31-32 °C Min.16-20 °C	T <sub>air</sub>	Max. 15-18°C Min. 2- 4°C	22-58%	Summer 840-930W/m2 Winter 500-800 W/m2
		T <sub>op</sub>	Max.37-39 °C Min.12-16 °C	T <sub>op</sub>	Max.22-29 °C Min.0-5 °C		
<b>Desert zone</b>	100-500m	T <sub>air</sub>	Max.38-41 °C Min.2-27 °C	T <sub>air</sub>	Max. 22-24°C Min. 7- °C	20-60%	Summer 1030-1200 W/m2 Winter 730-1030 W/m2.
		T <sub>op</sub>	Max.42-48 °C Min.19-22 °C	T <sub>op</sub>	Max.28-31 °C Min.3-10 °C		
<b>Southern Egypt</b>	180-350m	T <sub>air</sub>	Max.40-43 °C Min.26-28 °C	T <sub>air</sub>	Max. 22-24°C Min. 12-13°C	20-60%	Summer 1100-1210W/m2 Winter 770-1050 W/m2
		T <sub>op</sub>	Max.43-48 °C Min.18-23 °C	T <sub>op</sub>	Max.29-34 °C Min.5-10 °C		

### 1.8.3 Cairo and Al-Muizz urban development<sup>1</sup>

Al-Qahira (the conquerer or the victorious), a name which passed into English as Cairo, was founded in AD969 on land adjacent to Fustat, another Islamic city established at the dawn of Islam in AD641. These cities were themselves preceded by Roman and Pharaonic settlements (Babylon and Memphis) in the same approximate location at the strategic southern apex of the Nile Delta (UN-Habitat, 2003). The city's urban design started by building the first mosque in Africa at the city centre to act as a focal point to unite the inhabitants of Egypt's new capital in prayers. Separate living quarters were assigned for the various clans in the army, and each quarter was divided from the next by a vast expanse of land to prevent internal tribal war (Rezk, 2011). This method of urban planning allowed the city of Fustat to grow rapidly, becoming an important urban centre in Egypt and later in the Islamic Empire (Antoniou, 2009). The birth of Fustat marked the beginning of Egypt's transformation, and a new Islamic society was formed that would change the country's architecture, laws and beliefs (Rezk, 2011). Al-Fustat remained relatively small for the first 100 years of its existence; this was primarily due to the fact that the Islamic empire was ruled by the Umayyad dynasty from Damascus, while Al-Fustat was too far and too small to attract attention. This situation changed with the rule of the Abbasid dynasty in 749AD and the removal of the seat of the Caliphate from Syria to Iraq (Antoniou, 2009). In Egypt, this meant the displacement of the governmental functions of the region to a newly built suburb just north of Fustat, named Al-Askar, to serve as a new urban centre (Ashmawy, 2004). Al-Askar expanded but failed to attract enough residents to compete with Fustat due to its costly real estate and limited access (Antoniou, 2009; Rezk, 2011). However, during the century or more that followed, the two communities merged so that the combined settlements of Al-Fustat and Al-Askar stretched along the axis of the Nile (Figure 1.6).

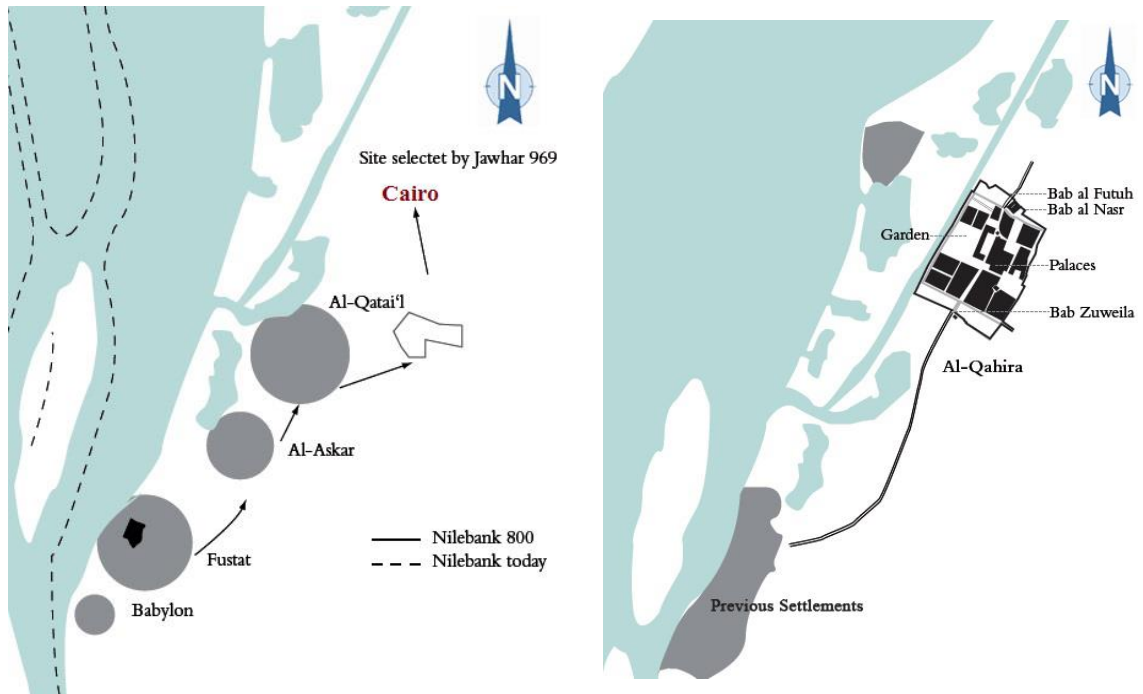
The growing decadence of the Abbasids in the late ninth century led to the increasing independence of parts of the Abbasid Empire, and Ahmed Ibn Tulun quickly seized the opportunity and proclaimed himself as the independent ruler of Egypt, founding a new

---

<sup>1</sup> A comprehensive review of Al-Muizz urban development is included in appendix 'A'

dynasty called the Tulunid dynasty (Parker et al., 2008). In 870AD, Ibn Tulun started a new town, north west of Al-Askar, called Al-Qatai, which was modelled after Samarra in Iraq. It had magnificent open spaces built for sport and tournaments, and large mosques were constructed amongst them, such as the famous Ibn Tulun mosque, which still stands (Haag, 2006). Al-Qatai had attractive markets for luxury consumer goods, and the bulk of economic activity remained in Al-Fustat. However, in 905AD, the Abbasid troops succeeded in regaining the country for the empire and destroyed most of the monuments, which had been constructed within the city of Al-Qatai, leaving Al-Fustat once again the premier city in Egypt (Antoniou, 2009; Rezk, 2011). The Abbasid rule of Egypt would not last, however, and in 969AD General Gawhar Al-Siqilli conquered Egypt for the Fatimid Caliphate, and thereby established their imperial city, Al-Qahira or Cairo (Rezk, 2011). At the time of the Fatimid invasion, the inhabited areas of the populous cities of Al-Fustat, Al-Askar, and Al-Qataie were joined together into a triple city called collectively 'Misr.' Its length, according to Maqaddassi (AD985), was about three kilometres. The site chosen for Al-Qahira or Cairo lay immediately to the north of Al-Fustat, as shown in Figure 1.6. The city is rectangular in shape, half a square mile and surrounded with fortified walls in all four directions (Figure 1.6). The main street is named after the Caliphate, Al-Muizz Street, which is probably the oldest and most stable street of Fatimid Cairo (Al-Sayyad, 1981; Rezk, 2011), and ran from north to south, connecting the gate of Bab Al-Futuh with the gate of Bab Zuwaila. These main gates were built to guard the entrance of the city, as it was built in the first place to be the residence of the Caliph and his court, his slaves and officials, and his troops; common people were not allowed in Cairo without a special permit issued by the royal house. As time went on, the population of the triple city, 'Misr' had grown and gradually moved to the immediate vicinity of the imperial stronghold. By the extinction of the Fatimid dynasty, the population overflowed into the enclosure of Cairo, causing all the cities to merge into one big city within an area no larger than 5km<sup>2</sup>, known today as Islamic Cairo (Rezk, 2011). Al-Muizz Street is still the predominant route for pedestrians, dividing the Islamic quarter into two parts. Al-Muizz is bounded in the east by Salah Salim Road and by Port Said Road in the west. The northern boundaries of

Islamic Cairo start with the 11<sup>th</sup> Century walls of Badr Al-Jamali and the southern part ends with Saliba Road (Figure 1.7).



**Figure 1-6** Cairo development, starting from Al-Fustat to the north of the Roman fort Babylon in 641AD. These Islamic cities were themselves preceded by Roman and Pharaonic settlements (Babylon and Memphis) in the same approximate location (UN-Habitat, 2003). On the right side, the city rectangular shape with Al-Muizz as the main street ran from north to south, connecting the gate of Bab Al-Futuh with the gate of Bab Zuweila. (source: <http://www.studio-basel.com/publications/books/nile-valley.html>).

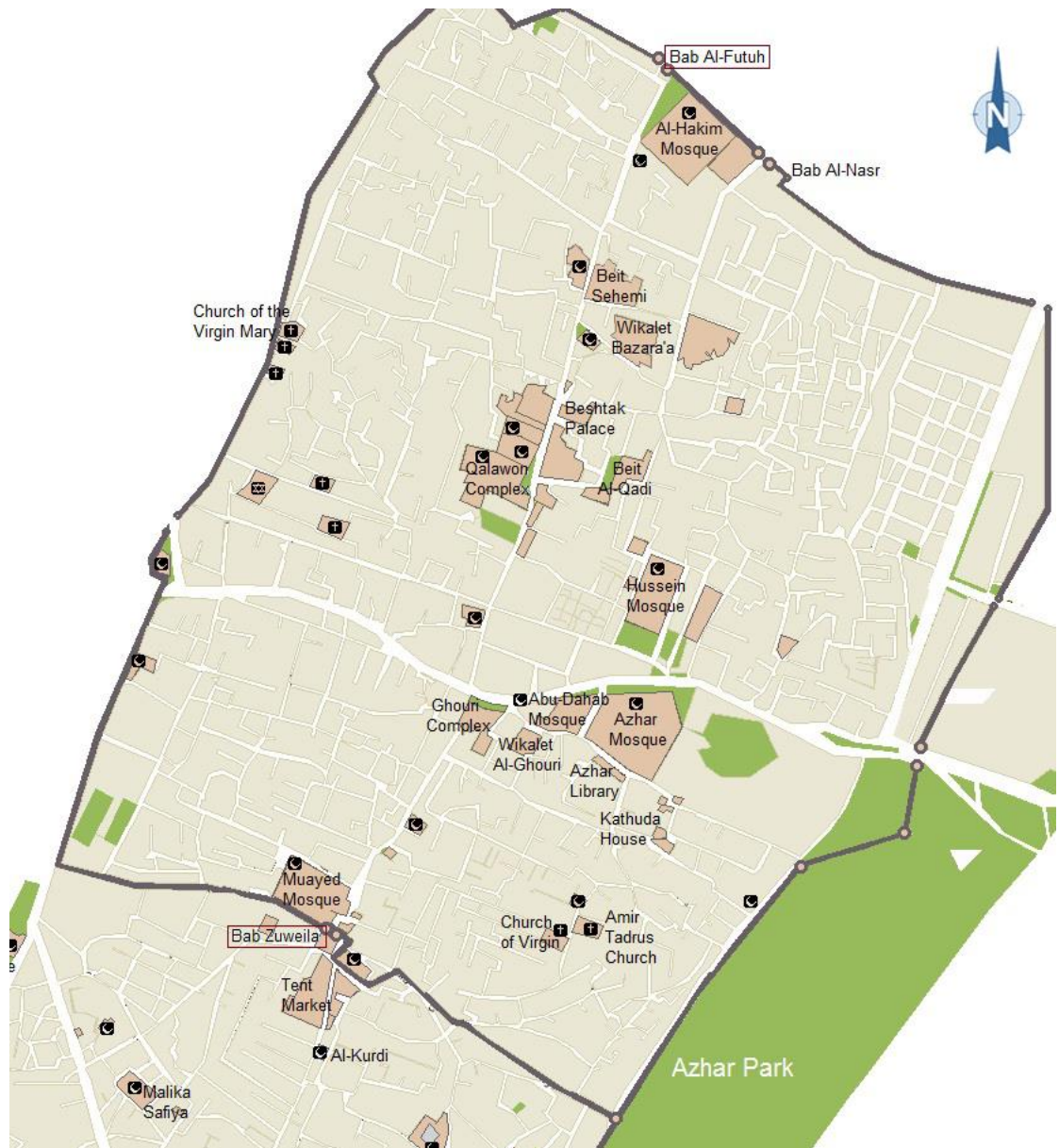


Figure 1-7 The Al-Muizz street and Gate Al-Futuh in the north, and Zuweila in the south (Mortada, 2003)

## 1.9 The physical pattern development of Al-Muizz



**Figure 1-8** Al-Muizz Street in 1908 (on the left) and 2012 (on the right) (source: bildindex.de)

### 1.9.1 The first Muslim settlements

The area was a site for a several cities started by ancient Egyptians and Romans. The city of Fustat was built close to the remains of the Babylonian fortress as the first Muslim settlement in Africa, followed by Al-Askar or Abbasids, and later Al-Qata'i of Ibn-Tulun, further north. Until 969, when Egypt was conquered by the Fatimid and the first plan for their city was developed, it was a rectangular grid with Al-Muizz as the main street for the city (Figure 1.9).

### 1.9.2 Fatimids (969 – 1171AD)

In its early years, Fatimid Cairo was built to serve the royal family and its military troops, while Al-Fustat remained as a commercial city. In 1087, Fatimid Cairo expanded outside the old wall by building new walls, and the main street (Al-Muizz) was extended from the gate of Bab-Al-Futuh in the north to the gate of Bab Zuwaila in south. The structure within the walls was almost a rectangular grid, with wide streets (Figure 1.9).

### 1.9.3 Ayubids (1171 – 1252AD)

As the Ayyubids came to power, a gigantic wall was built encircling Al-Fustat and Fatimid Cairo, and the city was opened for public use in terms of spaces and

gardens, which changed the old function and structure. The pattern developed was very dense and full of houses and new streets (Figure 1.9).

#### **1.9.4 Mamluks (1252 – 1517AD)**

During the first period of the Mamluks, which historians refer to as Bahri Mamluks, Cairo experienced great growth with new areas outside the walled city being developed. However, Al-Muizz continued in the same pattern and was developed by the Ayubids who added three new schools and the famous Qalawun hospital. Under the ruler of the Burji Mamluks, Cairo began a remarkable recovery after the plague of the Black Death<sup>2</sup> and famine<sup>3</sup>. They added some of Cairo's greatest architectural monuments, such as Al-Ghuri complex, which was the reason to start shifting the existing visual climax of the street from the area between two palaces (Figure 1.9).

#### **1.9.5 Ottomans (1517 – 1805AD, including the French expedition in 1798AD)**

During the Ottoman period, Cairo was reduced for the first time as it became a provincial capital. The walled city experienced its greatest decline during the three centuries of Turkish rule as the centre moved westward to Azbakiya. During the rule of Mohamed Ali's family, building regulations were reviewed and a re-planning of the city's streets started; new zoning was put in place, such as in Al-Muski Street, which cut through the walled city (Figure 1.9).

#### **1.9.6 The Present**

Due to the exponential expansion of Cairo, in the last few years many districts have been developed and are still growing exponentially (Figure 1.9). Because of this modernization, the urban fabric of the old city could not cope, and thus it experienced further neglect and isolation. Later, it suffered from a gradual decay for a number of reasons, among which are increased pollution, sewage problems and high population

---

<sup>2</sup> The Black Death first arrived in Egypt in 1347, and from 1347 to 1349, it wiped out one third of the Egyptian population (Article: Mamluk, pp. 750-751 *Encyclopaedia Britannica*, 15th ed., Vol. 7).

<sup>3</sup> Cairo was affected by ten major famines during Mamluk rule, in 1264, 1295-96, 1336, 1373-75, 1394-96, 1402-04, 1415-16, 1449-52, 1469-70, and 1486-87 (Sabra, 2000).



density. In the late 1990s, UNESCO recognized that Al-Muizz and its surroundings held great historical and cultural value, accordingly, in 2000, the Egyptian government proposed the huge Historic Cairo Rehabilitation Project (HCRP), aiming to protect and conserve historic Cairo with a view to developing extensive areas into an open-air museum, with the main priority given to Al-Muizz Street. In 2009, the government and UNESCO began a national campaign for the maintenance and restoration of Al-Muizz Street to regain its beauty after the completion of the development of the infrastructure facilities. The restoration started from Al Fotouh gate up to the intersection of Al-Azhar Street, at a total value of 23 million EGP. The houses and overlooking shop facades were totally renovated on both sides of the street, while buildings higher than the level of the monuments were brought down to size and painted an appropriate colour. Road surfaces were treated and fitted with benches and low-profile pavements in the spirit of the original thoroughfare, 11 new sets of electronic bollards were built around the main entrances of the street to ensure pedestrianization (Figure 1.10), and a new sewage system and piping network were built to prevent water leakage along the street. As an integral part of this project, the illuminations of this monumental area had the purpose of skillfully enhancing, through expert use of colour and light, the beauty of these architectural masterpieces.

Unfortunately, as a result of the political unrest in Egypt after the 2011 revolution, the other part of the street starting from Zuwaila Gate up to the intersection of Al-Azhar Street, has been delayed and the project duration expanded to 42 months without a fixed date. This has left behind two distinctive urban forms within the same street. Figures 1.1 and 1.2 clearly reveals the contrasts of the ambient conditions for each part of the same street, with its own urban distinctive features, regulation, materials, shadings, vegetation, and surfaces.



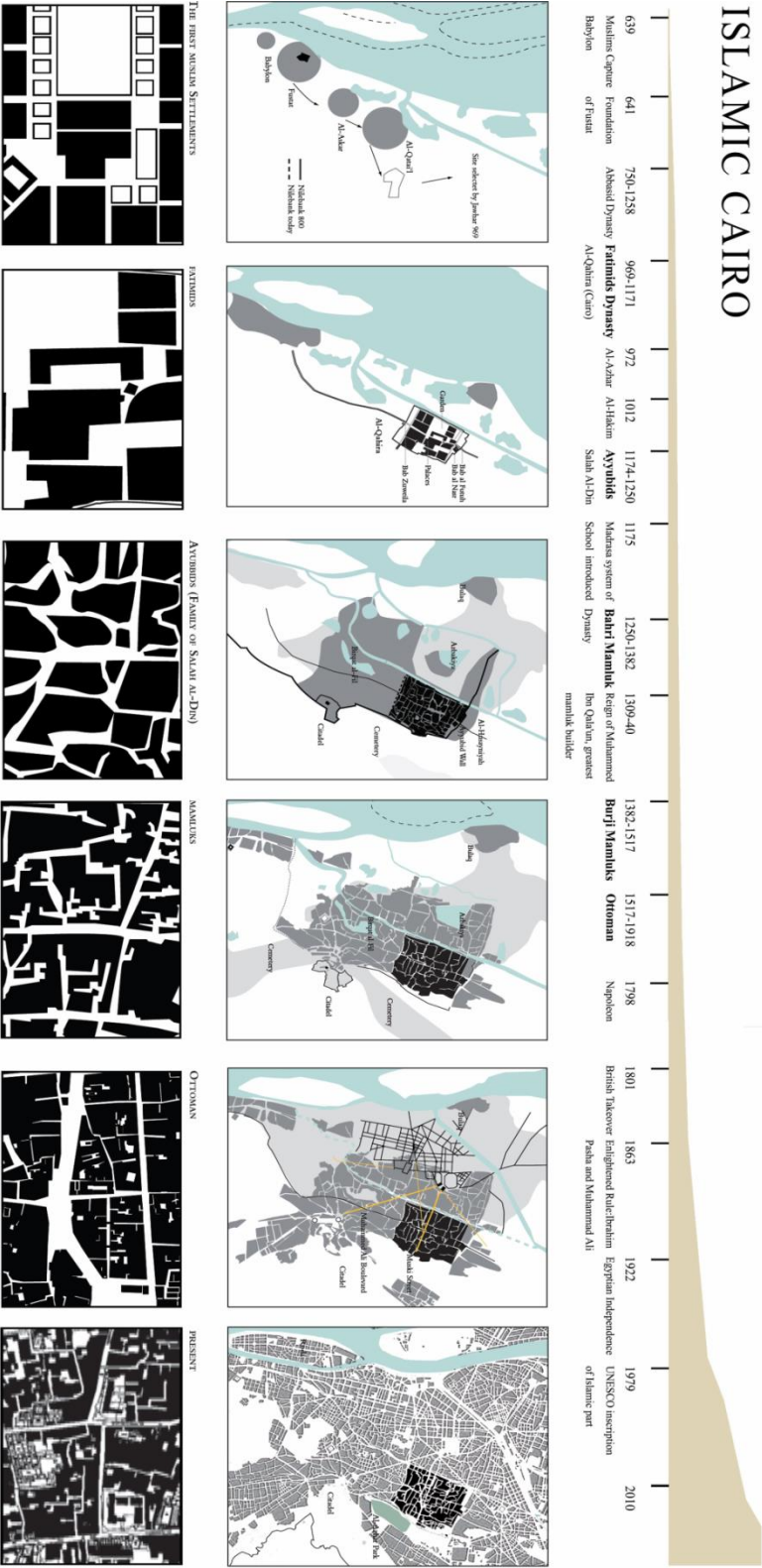


Figure 1-9 The historical development of Fatimid Cairo and its impact on the urban form (source: ETH Studio Basel)



**Figure 1-10** Electronic bollards control the traffic at the entrance to Al-Muizz

### 1.9.7 Open/Built Structure

During the Fatimid and Ayyubid rules, major spaces and buildings were usually located in the middle segment named as the area between the two palaces; it was also the widest segment along Al-Muizz Street. Then, other spaces were extended during the Bahri Mamaluk dynasty through the addition of new elements around them. The Burji Mamluks added some minor buildings and small spaces along the path at transition points. The street pattern remained with very minor changes during the Ottoman dynasty, with the exception of the decrease in the size of spaces, and later on the construction of Al-Azhar Street, which divided Al-Muizz Street into two parts. The general spaces of Al-Muizz street appears as a number of scattered spaces with an apparent hierarchy along the path and with the major space in the middle, with the key buildings nearby (Al-Sayyed, 1981) (Figure 1.11).

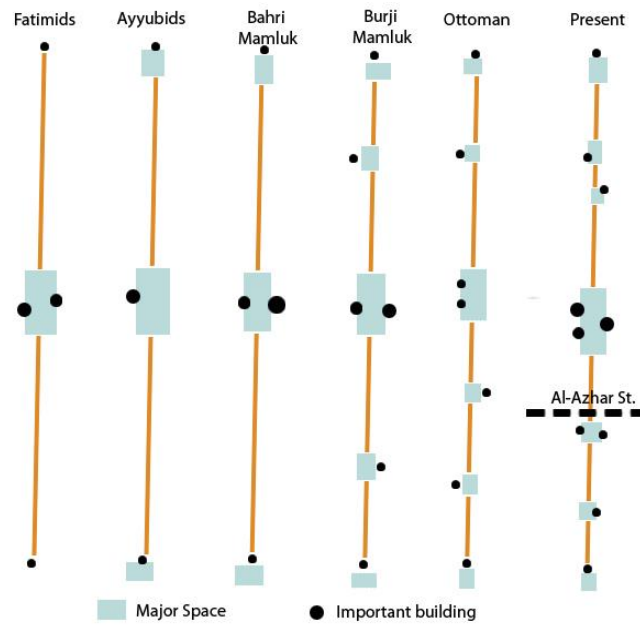
### 1.9.8 The exterior shaping for the elements among Al-Muizz Street

The most prominent building arrangements were the religious buildings, which must follow the Qibla direction for the prayers. All of the Fatimid mosques except Al-Aqmar had regular exterior facades perpendicular to the Qibla direction; this was a normal result as all the mosques were built inside the walled city before the street pattern was fully developed, and accordingly there was no restriction on their form. The facades of religious structures from the Ayyubid period followed the street centre line, as the streets were much developed during their dynasty. The Bahri Mamluk built 14 major schools where 12 of them had staggered and irregular facades; their

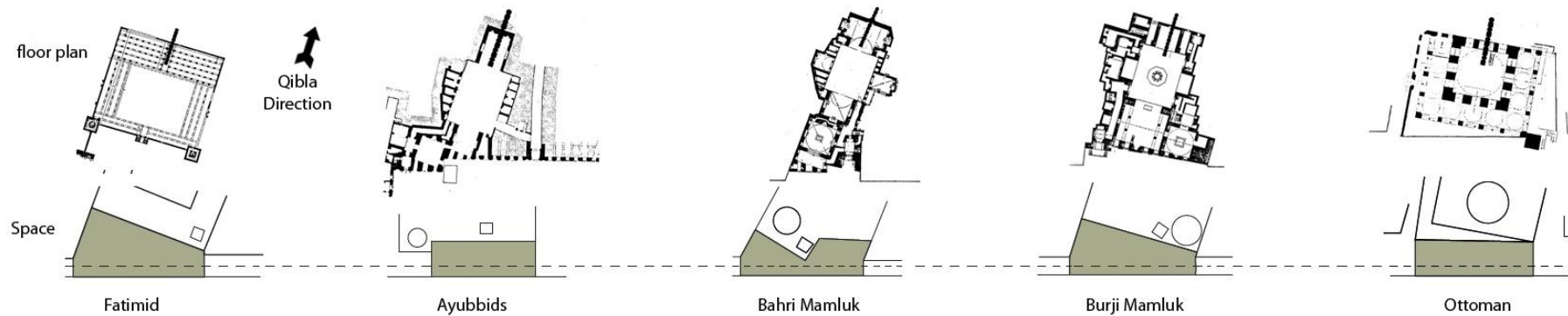
orientation was determined by both the street centre line and the Qibla direction and the irregularities in their exterior facades were skilfully adjusted to the street. Burji Mamluk exterior facades were neither parallel to the street centre line, nor perpendicular to the Qibla direction. The exterior facades were smaller due to the lack of space availability where the urban surrounding implied different amounts of inclination in each exterior facade. Most of the Turkish mosques had no regular pattern. The exterior shaping was a result of different factors such as the element location, their positioning and their size. It was how this variety of exterior architecture fitted into its urban surroundings that created the characteristic style of Islamic Cairene streets (Figure 1.12).

### **1.9.9 Space development**

The exterior shaping of Fatimid elements had a major impact on determining the spaces along Al-Muizz Street. These spaces were usually wide triangular spaces with their sides directed toward Mecca and the street alignment. Due to the rapid development during the Ayyubid period, as the city was opened to the public, the spaces became much smaller in size as buildings were constructed everywhere. The exterior parts of the new constructed spaces were usually imposed by the street alignment and the Minarets were usually located in the middle of the spaces. Bahri Mamluk spaces tended to take a monumental scale with irregular shapes of variable dimension and narrow entrances. The minarets were usually located at the intersection of two sides. Burji Mamluk spaces followed an irregular pattern as well. The minarets were located carefully with respect to the surrounding buildings and the spaces and although the scale of most Burji Mamluk elements was monumental, the overall proportions of their spaces tended to be human. The spaces developed by the Ottomans were of different sizes based on their locations. For instance, buildings constructed outside the walled city had a large space in front of them, but the elements built inside were smaller due to the lack of vacant space and thus the variety of shapes followed a somewhat consistent pattern, depending on the surrounding elements (Al-Sayyed, 1981) (Figure 1.12)



**Figure 1-11** The historical development of the spaces along Al-Muizz Street (modified from Al-Sayyed, 1981)



**Figure 1-12** The exterior shaping for the elements among Al-Muizz Street (Al-Sayyed, 1981)

## **1.10 Research design**

Polit et al. (2001, p. 167) define a research design as “the researcher’s overall strategy for answering the research question or testing the research hypothesis”. This research is a case study combining both qualitative and quantitative approaches, including a field experiment, a survey research design, and an experimental design. The thesis research design, therefore, involves three main areas, namely the conceptual, theoretical and operational framework. The conceptual framework is covered in this chapter; the theoretical framework representing the literature review is covered in chapters two and three. The operational framework reports the field measurements, the survey, the simulation validation, and the numerical simulation of the investigated case study are covered in chapters four to seven. Chapter eight presents the conclusion and recommendations for future studies (Figure 1.13).

## **1.11 Research Structure**

### **Chapter one: Introduction**

This chapter includes the conceptual framework, which focuses on the research design, methodology, and structure and concludes with the thesis overview, as outlined in Figure (1.13). It also includes an overview of the research context geography and climate sub-classification, before it examines the historical development and the main urban planning transition periods’ impact on the local scale of Al-Muizz Street as a case study based on its physical and historic characteristics.

### **Chapter Two: Review of urbanization, climate change and thermal comfort**

The chapter clarifies the influence of urbanization combined with industrialization as a main reason for causing the unfavorable urban climate and urban heat islands, and how this affects the energy consumption, air quality and greenhouse gases, human health and comfort and water quality. The chapter then reviews the effect of the UHI within the Cairo context. The chapter also illustrates a number of climatic responsive strategies, which have been developed within the traditional and contemporary architecture for the Cairo climatic zone.

**Chapter Three: Microclimate and outdoor thermal comfort**

The chapter presents an overview on the available knowledge and the state-of-the-art regarding two concepts, which are the centre of the study; the first section considers the urban canyon microclimate including the climatic scale, the main surface energy balance and urban canyon thermal characteristics. The second section deals with outdoor thermal comfort, such as human energy balance, the variables affecting people's thermal sensation, comfort indices and mean radiant temperature. It concludes with the methodological shortage in outdoor thermal comfort assessment.

**Chapter Four: The Research methodology**

This chapter describes the main research methods used in order to achieve the objective of the research. The methodology framework was divided into four phases including; the preliminary studies (phase one) discusses the primary way for gathering data such as the satellite images, climate files and building reports. Second, the field measurement (phase two) presents the in-situ measurements, the measurements dates, the instruments used and the procedures. Third, the outdoor thermal comfort survey (phase three) includes the questionnaire structure, sample, timing and procedures. In addition, so forth, the Micro-urban performance simulation including the validation and the parametric analysis.

**Chapter Five: The Field Measurements (Physical Approach)**

The chapter examines the effects of urban morphology and design on thermal comfort from a physical approach based on two types of field measurements. The first type is a one-week in-situ measurement for the main parameters as stated by ASHRAE (2009) in two different locations within Al-Muizz Street, compared against the readings obtained by the Cairo Airport WMO Station no.623660, which reveals the existence of the UHI within the case study. The second type is a comprehensive meteorological measurements carried out at nine different points along the street on two days (30<sup>th</sup> June and 1<sup>st</sup> July 2012), to investigate the street canyon geometry's parameters (height-to-width ratio (H/W)), the street orientation, and surface materials.

**Chapter Six: Outdoor Subjective Thermal Comfort**

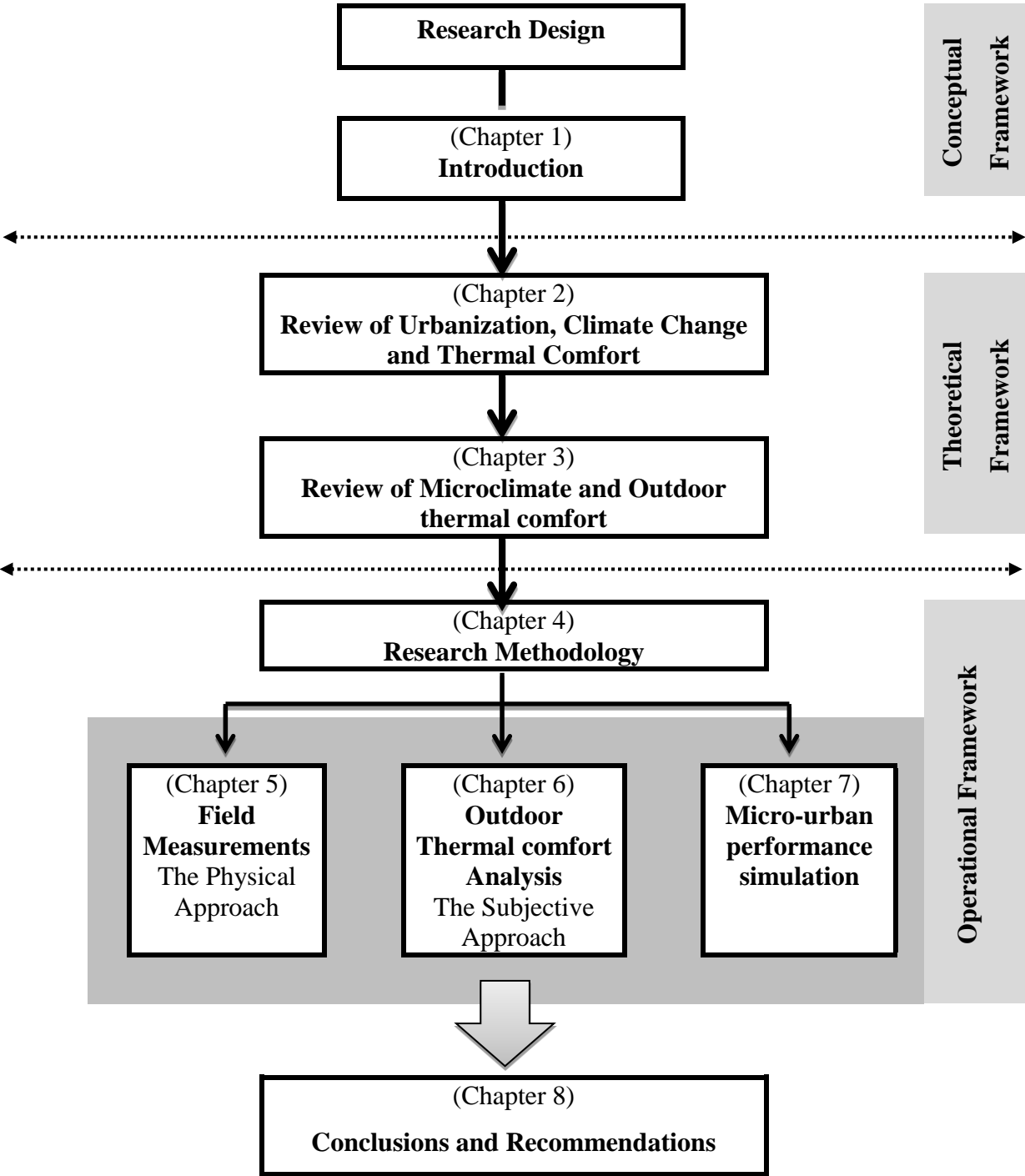
The chapter investigates users' thermal perceptions using a subjective questionnaire through applying the seven-point ASHRAE 55 thermal sensation votes

(TSV). The survey was complimented by one week of field measurements in summer and winter to examine the main climatic parameters affecting thermal comfort. Monitored data were used as data input into the RayMan model to calculate the Physiologically Equivalent Temperature (PET) as a comfort index. The relations between the calculated PET values for the investigated sites and the Thermal Sensation Vote (TSV) were correlated.

### **Chapter Seven: Micro-urban performance simulation**

The chapter focuses on evaluating the airflow rate and the heat transfer patterns during the nighttime underneath the existing tensile structure using a comparative numerical assessment. The first part is the validation study for the existing case, the second is the parametric analysis between four alternative configurations with specific changes in the roof shape and opening locations, and the third part is the daylight study for the best case and base case.

### **Chapter Eight: Conclusion and recommendations**



1-13 Research design



# 2

---

*“The climatic conditions in a man-made urban environment may differ appreciably from those in the surrounding natural or rural environs...each urban man-made element: buildings, roads, parking area, factories, etc. create around and above it a modified climate with which it interacts” (Givoni, 1989, pp1-2).*

## **Chapter Two**

---

### **2. Review of Urbanization, Climate Change and Thermal Comfort**

---

#### Key Concepts

- 2.1. Introduction
- 2.2. Urbanization and climate
- 2.3. Urban heat island (UHI)
- 2.4. Urbanization and global warming
- 2.5. Climate and UHI in Cairo, Egypt
- 2.6. Contemporary climate responsive strategies
- 2.7. Conclusion

## 2.1 Introduction

This chapter explores the influence of urbanization combined with industrialization as a main reason for causing an unfavourable urban climate and urban heat islands (UHI) (Oke, 1995; Kuttler, 1998; Montavez et al., 2000; Tereshchenko and Filonov, 2001). The UHI is linked to changes in energy consumption in the built environment, air quality, greenhouse gases, human health and comfort, and water quality, with an emphasis on the case study city (Cairo, Egypt) in a hot arid climate. The chapter is divided into three main sections:

- The first section covers how urbanization and climate change lead to the phenomenon of UHI
- The second section reviews the effect of the UHI and climate change on Cairo as the case study area, including its impact on climate change, energy consumption and thermal comfort
- The third section deals with a number of climatic responsive strategies which have been developed within the traditional and contemporary architecture for Cairo's climatic zone.

## 2.2 Urbanization and climate

According to the Dictionary of Landscape Architecture and Construction (Christensen, 2005), urbanization may be defined as, “the process of covering a significant portion of a land area with buildings or impervious pavements”. Based on the same dictionary, urban climate may be defined as, “the climate in and near urban areas. It is often warmer, more or less humid, shadier, and has more reflected light than the climate of the surrounding land areas”. Again, the same source defines the urban canyon as, a “City Street lined with buildings” and “Urban physical features that have an effect on airflow, sunlight, humidity, water percolation, heating, cooling of air, soils, etc.” (Christensen, 2005). From these definitions, it is obvious that urbanization can influence climate change within most built up areas (Nakamura and Oke 1988; Yoshida et al., 1990, 1991; Arnfield and Mills, 1994; Asimakopoulos et al., 2001; Hawkes and Foster 2002).

Urbanization growth initiates one of the most dramatic human-induced changes to natural ecosystems through the creation of a largely impervious landscape consisting of stiff and sharp edged rough building blocks (Roth, 2002). These changes, combined

with industrialization, have led to urban heat islands (UHI), creating unfavourable micro urban climates. UHIs occur when the urban areas warm up more quickly and cool down more slowly than their rural surroundings due to their sealed surfaces. This problem will become increasingly heightened in future climate change scenarios and projections of urbanization (Oke, 1995; Kuttler, 1998; Montavez et al., 2000; Tereshchenko and Filonov, 2001; Smith and Levermore, 2008;). Successful adaptation to minimize the occurrence of heat stress is, however, dependent upon a detailed understanding of the processes that lead to elevated urban temperatures within the city context (Landsberg 1981; Oke 1991, Roth 2002; Elsayed 2012).

### 2.2.1 Nature of the urban atmosphere

Urban areas have distinctive topography and biophysical properties, which can differentiate their energy receipts and losses from those of rural areas (Smith and Levermore, 2008). The introduction of new surface materials (concrete, asphalt, tiles, etc.), coupled with the construction of buildings, and the emission of heat, moisture and pollutants which considerably alter the surface and surrounding atmosphere, influences radiation, thermal retention, moisture, roughness and emissions (Oke 1991; Roth 2002), as follows:

- **Radiative changes:** These happen when new surface materials are introduced which have a larger range of albedo and emissivity values than vegetation, and there is a lack of a shading element in urban areas which may lead to the radiative changes becoming higher and uncontrollable. The coupling between buildings and canyon arrangements leads to more complex radiation exchanges than a flat surface. In turn, all these may cause higher ground surface and wall temperatures, which then affect the surrounding microclimate.

The surface albedo is defined as the total reflectance of the surface integrated over all angles of the upward hemisphere (Figure 2.1). It is the ratio of the reflected part of the incoming radiation on a medium of finite thickness to the total incoming radiation (Alexandri, 2005).

$$\text{Albedo } (\alpha) = \frac{\text{reflected part of incoming radiation}}{\text{total incoming radiation}} \text{ (Eq. 2.1)}$$

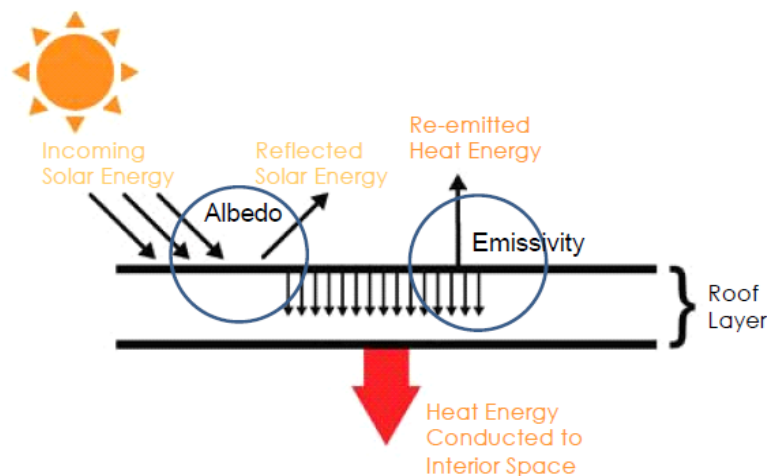
The albedo value is calculated based on several factors such as the incoming radiation wavelength, the sun elevation and the surface characteristics. Surfaces with higher albedo values have lower energy absorbance. Therefore, in urban areas surface

materials such as asphalt for roads and concrete for the walls have lower albedo values, so the surface temperature becomes higher, which increases the air temperature of the surrounding environment.

Although Albedo is the main determinant of a material's surface temperature, thermal emittance, or emissivity, also plays a role. Emissivity ( $\epsilon$ ) is defined as the surface ability to lose heat or emit radiation (Figure 2.1). It is calculated as the ratio of the energy emitted by the surface to energy emitted by the black body of an element. A black body has an ( $\epsilon$ ) equal to 1, while any real object would have ( $\epsilon$ ) < 1.

$$\text{Emissivity } (\epsilon) = \frac{\text{energy emitted from a surface}}{\text{energy emitted from black surface at the same temperature}} \text{ (Eq. 2.2)}$$

The range of urban materials may have high (e.g. red brick 0.9, concrete 0.71-0.94 and asphalt 0.95) or low emissivity (bright-galvanized iron 0.13 and bright aluminium foil 0.04). The choice of these materials during the design and construction phases can reduce the overall urban emissivity, which tends to increase net radiation levels in urban areas. However, the role of emissivity in influencing the urban environment temperature is affected by the urban geometry and sky view factors. Oke et al. (1991) state that in the case of very tight canyons, the emissivity role is minor for higher view factors, which represents a very small difference in urban air temperature. However, combining the albedo with higher emissivity for the materials will allow for greater changes in the air temperature of urban areas.



**Figure 2-1** the emissivity of a material determines how much absorbed solar energy is released or retained.

Shading is another crucial factor affecting the radiative exchange process of ground and wall surfaces. Providing shelter from direct solar gain may cause a reduction in the urban surface temperature, and thus the total radiation absorbed at a site can be manipulated through shading or changing the solar reflectivity of the object (albedo). This will in turn decrease the intercepted solar radiation, and yet will increase the incoming long-wave radiation trapped under trees and shading systems (since trees and other shading object are better emitters than the sky) (Lin et al., 2010; Shahidan, 2011). However, the net result is still a decrease in total radiant energy input (Brown and Gillespie, 1995), and any lack of shading components will lead to a rise in the surface and air temperature values within the urban areas (Fahmy, 2010; Shahidan, 2011).

- **Thermal mass:** Inbuilt up areas, surfaces and structures are often at least partially obstructed by objects, such as neighbouring buildings, and they become large thermal masses that provide a reservoir of heat storage in the daytime which is released at night time.

The high thermal capacity of buildings for heat storage tends to delay the heat transfer to the interior of the building by soaking up excessive heat for several hours. As a result, cities are typically more effective at storing the sun's energy as heat within their infrastructure. Metropolitan areas can absorb and store twice the amount of heat compared to their rural surroundings during the daytime (Christen, and Vogt, 2004). Afterwards, at night the stored heat is slowly released back into the environment due to the difference in the air temperature between the day and night, causing an increase in the night time temperature due to this heat transfer process (Shahidan, 2011).

- **Moisture reduction:** Evapotranspiration is the combination of evaporation and transpiration from soil. Vegetation systems are another moderator and can contribute significantly to reducing urban temperature (Santamouris, 2001). The process describes the transfer of latent heat, what people feel as humidity, from the Earth's surface to the air via evaporating water. Urban areas tend to have less evapotranspiration relative to natural landscapes because cities retain little moisture. This reduced moisture in built up areas leads to dry, impervious urban infrastructure reaching very high surface temperatures, which contribute to higher air temperatures in temperate climates. In arid regions, as the surroundings are usually deserts with a low level of humidity, these causes an increase in the humidity level within the built up areas, combined with a negative impact on the heat stress intensity and duration (Ben Shalom, 2009).

- **Roughness:** There has been a rapid development of obstacles such as buildings and bridges that act as bluff bodies due to their permeability, inflexibility and sharp edges. They create windward positive pressure and leeward negative pressure over their surfaces, leading to flow separation and vortex shedding when exposed to the airflow. In this context, the transport of energy, mass and momentum to and away from the city surface are affected and the turbulences within the built up areas is greater than the homogenous atmosphere over rural areas (Roth, 2002).

Put simply, urban surface roughness reduces sensible heat loss due to the obstruction of airflow by buildings and other large structures (Walsh et al., 2011).

- **Emissions:** Emissions from aerosols, and greenhouse gases from rapid industrialization, affect radiative transfer and act as condensation nuclei; waste heat and water vapour from combustion is added to the urban atmosphere. Furthermore, the anthropogenic heat released through cooling and heating buildings, manufacturing, transportation, and lighting, in addition to human and animal metabolisms are also considered sources of artificial heat that contribute to the warming of the urban atmosphere and increased air temperature (Roth, 2002). Table 2.1 summarizes all the possible urban factors and their effect on the urban environment.

These changes are reflected in an altered energy balance which is a basic and powerful framework used in the analysis of climate processes; this is further explained in Chapter Three. Accordingly, it is not surprising that, as urbanization continues, the associated weather and climate are often modified substantially and a new set of environmental conditions is created, leading to a higher air temperature in densely built up urban areas than the temperatures of the surrounding rural country. This causes what is known as an urban heat island (UHI) phenomenon (Oke, 1978; Landsberg, 1981; Santamouris, 2001; Emmanuel, 2005; Tran et al., 2006; Yu and Wong, 2006; Sailor and Dietch, 2007). The UHI effect can be observed in every town and city and is considered the most obvious climatic indicator of urbanization (Landsberg, 1981; Wong et al., 2007).

**Table 2-1** Possible urban factors and effects on the urban environment (Oke, 1991; Shahidan, 2011)

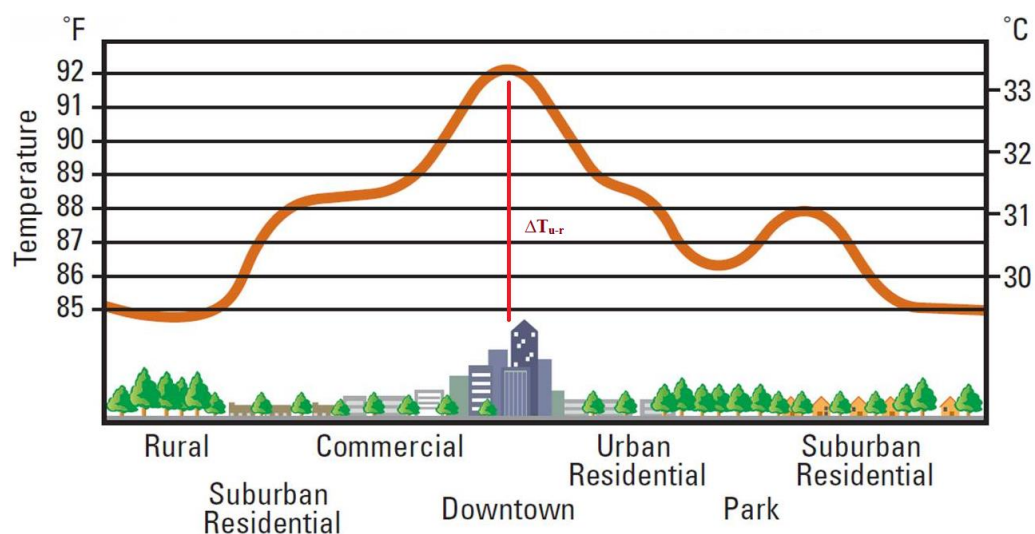
	FACTORS	EFFECTS
1	Canyon radiative geometry (urban geometry and radiation)	Contributes to the decrease in long-wave radiation loss from within the street canyon due to the complex exchange between buildings and the screening of the skyline Infrared radiation is emitted from various buildings and street surfaces within the canyon Buildings replace a fraction of the cold sky hemisphere with much warmer surfaces, which receive a high portion of the infrared radiation emitted from the ground and radiate back an even greater amount
2	Thermal properties (albedo) of material	Increased storage of sensible heat in the fabric of the city during the daytime and release of the stored heat into the urban atmosphere after sunset Replacement of natural soil or vegetation by materials, such as concrete and asphalt used in cities, reduces the potential to decrease ambient temperature through evaporation and plant transpiration
3	Anthropogenic heat	Released by the combustion of fuels from either mobile or stationary sources, as well as from animal metabolism
4	The urban greenhouse effect	Increases in the incoming long-wave radiation from the polluted urban atmosphere. This extra radiative input to the city reduces the radiative drain
5	Canyon surfaces and radiation	Decrease in the effective albedo of the system because of the multiple reflection of short-wave radiation by canyon surfaces
6	The reduction of evaporating surfaces	The city puts more energy into sensible heat and less into latent heat
7	Reduction in turbulent transfer	Reduced transfer of heat form with streets

### 2.3 Urban Heat Island (UHI)

The UHI was first documented in 1833 by Luke Howard in the UK (Jones and Lister, 2009). Howard compared the temperature records of London's weather station with the rural stations. He stated that the cities appeared to be warmer than the surrounding rural areas (Mills, 2003). In 1958, Gordon Manely used the term UHI for the first time to explain this phenomenon. The term 'heat island' is used because warmer city air lies in a 'sea' of cooler rural air and it is caused as a result of the solar energy storage in the urban fabric during the day and its release during the night time back to the atmosphere. The process of urbanisation and development alters the balance between the energy from the sun used for raising the air temperature (heating process) and that used for evaporation (cooling process), because the cooling effect of vegetated surfaces is replaced by impervious surfaces that absorb a high percentage of solar radiation

(Rosenzweig et al., 2006). This effect of the UHI is the most obvious climatic indicator of urbanization (Wong et al., 2007) on increasing air temperature, and has now been well documented by numerous studies (Oke, 1995; Kuttler, 1998; Montavez et al., 2000; Tereshchenko and Filonov, 2001). For instance, in the United Kingdom, the Meteorological Office's Hadley Centre has recorded that the last ten years have been the warmest since the 1880s, and there is an expectation of increase in the temperature by 0.1-0.5°C per decade across the UK and Europe during the 21<sup>st</sup> century (Hulme et al., 2002; IPCC, 2007a). However, Africa has the worst prospects according to the 4th IPCC Assessment Report, which showed evidence that Africa is warming faster than the global average, and this is likely to continue. This warming is greatest over the interior of the semi-arid margins of the Sahara and central southern Africa (IPCC, 2007).

The maximum difference in temperature between the urban and rural areas is referred to as UHI intensity ( $\Delta T_{u-r}$ ) (Oke, 1978; Santamouris, 2001; Roth, 2002; Velazquez-Lozada et al., 2006), which may occur during the day or night, and yet is most pronounced at night time under clear skies and light winds (Santamouris, 2001; Emmanuel, 2005). The UHI is diminished as the wind speeds increase over urban areas, as more thermal energy is transformed by the wind (Alexander and Mills, 2014). Over large metropolitan areas, there may be several plateaus, characterized by weak gradient of increasing temperature, and valleys and peaks based on the type of land use inside the city (Figure 2.2). Generally speaking, the intensity of the UHI effect increases as the size of a city increases, due to the larger size of the built area (Rinner and Hussain, 2011).



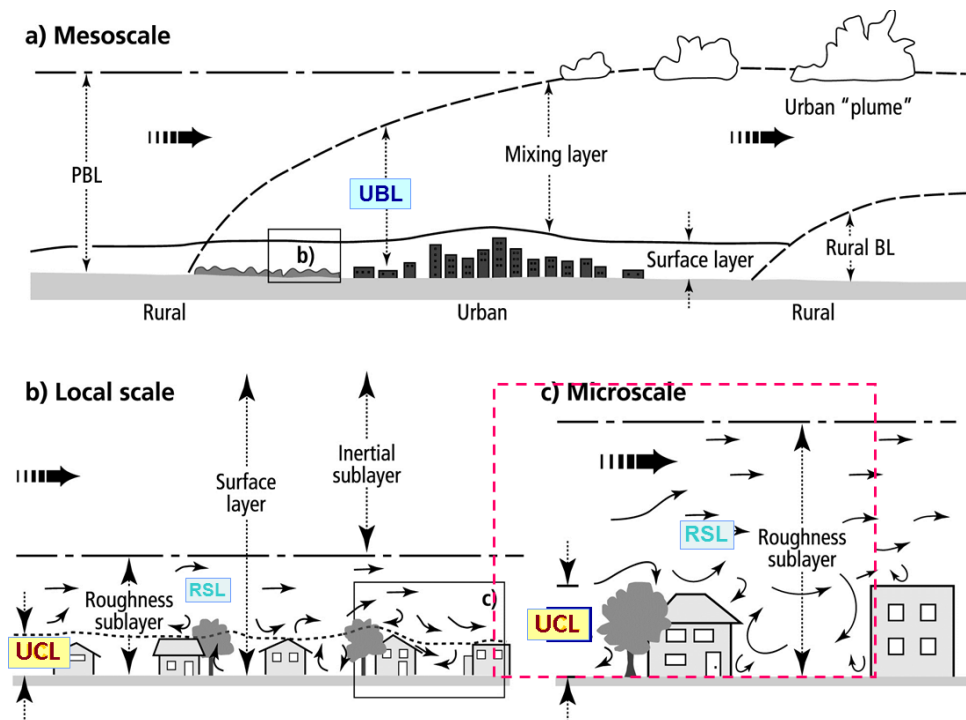
**Figure 2-2** Generalized cross section of a typical urban heat island (Roth, 2001)



There are two common types of UHI, classified by Oke (1995) and simplified by Roth (2002), based on their location and height within the urban atmosphere. These two common types are the air temperature UHI and the surface temperature UHI (Table 2.2). The two types of UHI can be distinguished based on the methods of temperature measurement: (1) the canopy layer heat island and (2) the boundary layer heat island (Oke, 1979). The former consists of air between the roughness elements, e.g., buildings and tree canopies, with an upper boundary just below roof level. The latter is situated above the former, with a lower boundary subject to the influence of the urban surface temperature. According to Emmanuel (2005), most of the climatic effects are predominantly felt in the Urban Canopy Layer (UCL). Therefore; most of the studies seeking to understand air temperature within the UHI phenomenon were conducted at the UCL level (Figure 2.3).

**Table 2-2** Simple classification scheme of UHI types (after Oke, 1995 and Roth, 2002) (Shahidan, 2011)

UHI type	Location
<b>1. Air Temperature UHI</b>	
- Urban canopy layer heat island	Found in the air layer beneath rooflevel
- Urban boundary layer	Found in the air layer above rooflevel; can be affected downwind with the urban plume
<b>2. Surface temperature UHI</b>	Found at the urban horizontal surfaces; such as ground surface, rooftops, vegetation and bare ground. Normally, this depends on the definition of a surface [bird'seye view=2D vs. true 3D surface vs. ground=road)



**Figure 2-3** Schematic of climatic scales and vertical layers found in urban areas. PBL planetary boundary layer, UBL – urban boundary layer, UCL – urban canopy layer. Modified from Oke (1997)

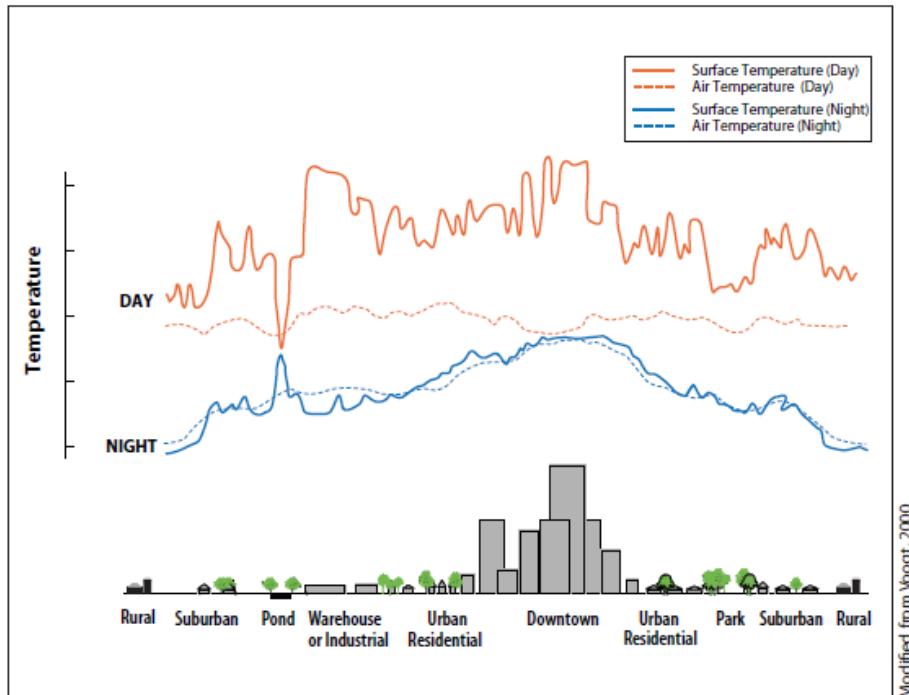
### 2.3.1 Air Temperature UHI

The UHI has a warmer air temperature than surrounding rural areas. The air temperature intensity varies throughout the day and night, where the smallest difference usually occurs in the morning and the difference grows during the day due to the heating up of the surface area, which consequently warms the air (Wong and Yu, 2005). The UHI intensity usually reaches its peak at night when the urban surfaces continue to release heat after sunset and slow the rate of night time cooling (Gratland, 2008) (Figure 2.4).

### 2.3.2 Surface Temperature UHI

Unlike the air temperature UHI, the surface temperature UHI usually reaches its highest value during the daytime, and this is likely to occur in areas filled with a large building mass or paved areas, and minimum value at night (Roth, 2002). Many urban surfaces (e.g. roofs, parking and pavements) may reach a temperature ranging between 27-50°C higher than the air during the daytime as a result of being heated by the sun (Gartland, 2008). The main parameters that may control the level of surface temperature are surface albedo, moisture content, land use, and land cover (Xian, 2007), in addition

to shading devices and vegetation (Fahmy and Sharples 2010; Kato et al., 2010; Reardon, 2013). (Figure 2.4)



**Figure 2-4** Surface and atmospheric temperatures vary over different land use areas. Surface temperatures vary more than air temperatures during the day, but they are both fairly similar at night. The dip and spike in surface temperatures over the pond show how water maintains a fairly constant temperature day and night, due to its high heat capacity. Source: EPA United States Environmental Protection Agency (2008)

## 2.4 Urbanization and global warming

While some heat island impacts seem positive, such as lengthening the plant-growing season, most impacts are negative particularly for hot climate cities, as they can affect a community's environment and quality of life, as seen in Table 2.3 (Oke, 1997b).

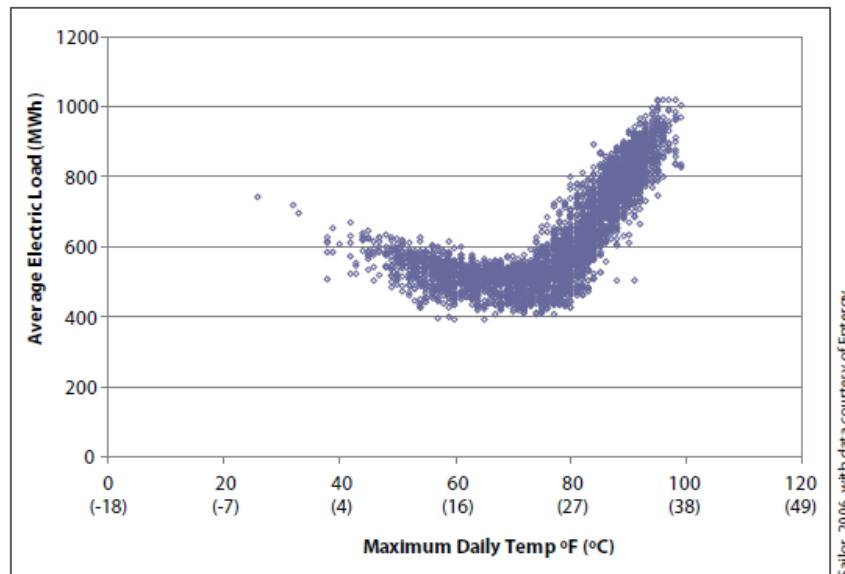
**Table 2-3** Impacts of urban heat islands, and/or a warmer base climate, on temperature-sensitive aspects of cities in cold and hot climate regions after Roth, 2002 (from Oke, 1997b). + - beneficial; - - undesirable ('losers'); (W) – winter; (S) – summer

	Climate impact	
	Cold	Hot
Biological activity (plant growth, disease)	+	Not known yet
Human bio climate (comfort, wind-chill, heat stress)	+ (W) / - (S)	-
Energy use (space heating, air conditioning)	+ (W) / - (S)	-
Water use (garden irrigation – pos. correlation with T)	-	-
Ice and snow (transport disruption)	+	N/A
Air pollution chemistry (weathering photochemistry)	-	-

### 2.4.1 Energy Consumption

If the global climate becomes warmer, cities in cold climates can expect to save fuel for space heating. Cities in hot climates, however, will most likely face an increase in energy demand for cooling and add pressure to the electricity grid during peak periods of demand (e.g. Santamouris, 2007; Ihara et al., 2008; Ewing and Rong, 2008). This demand is further increased by the construction of urban environments with high albedo surfaces that increase the absorption of solar radiation by buildings (Forkes, 2010). As a result, two crucial effects are shown up and these are explained as follows:

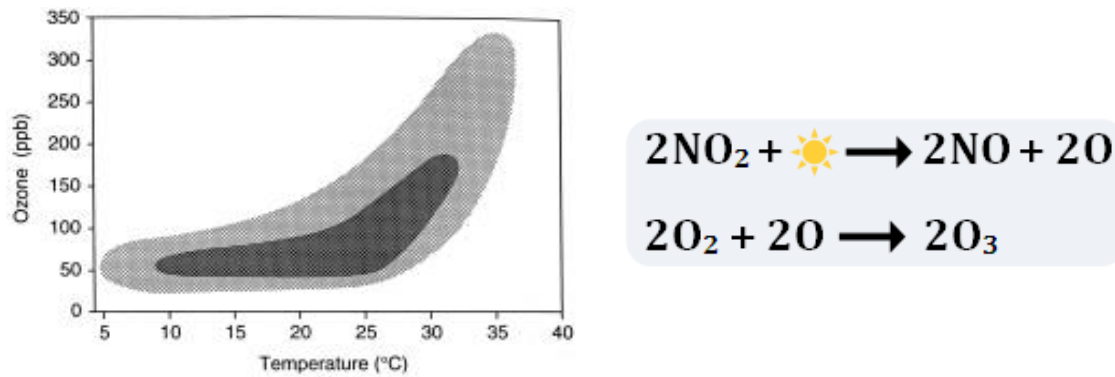
1. Cooling the interiors of buildings results in the release of hot air which contributes to an extra heat load outdoors, which may lead to an additional demand for air conditioning. It has been estimated that 5-10% of community electricity demand results from the need to compensate for the Urban Heat Island effect (Akbari, 2005, Environmental Protection Agency, 2008) (Figure 2.5)
2. The urban heat island effect may be amplified due to a greater cooling demand through the subsequent increase in the release of anthropogenic heat (Shimoda, 2003). Due to the potential to increase peak energy demand as well as greenhouse gas (GHG) emissions, the World Health Organization (WHO) has identified the use of airconditioning as an unsustainable adaptation strategy for extreme heat (World Health Organization, 2004; Health Canada, 2008; De Carolis, 2012).



**Figure 2-5** Increasing Power Loads with Temperature Increases (source: Sailor, 2002). As shown in this example from New Orleans, electrical load can increase steadily once temperatures begin to exceed about 68- 77°F (20-25°C), energy consumption falls as the daily temperature rises (less heating), reaching a minimum of approximately 21°C, and then rises steeply

#### 2.4.2 Air Quality and Greenhouse Gases

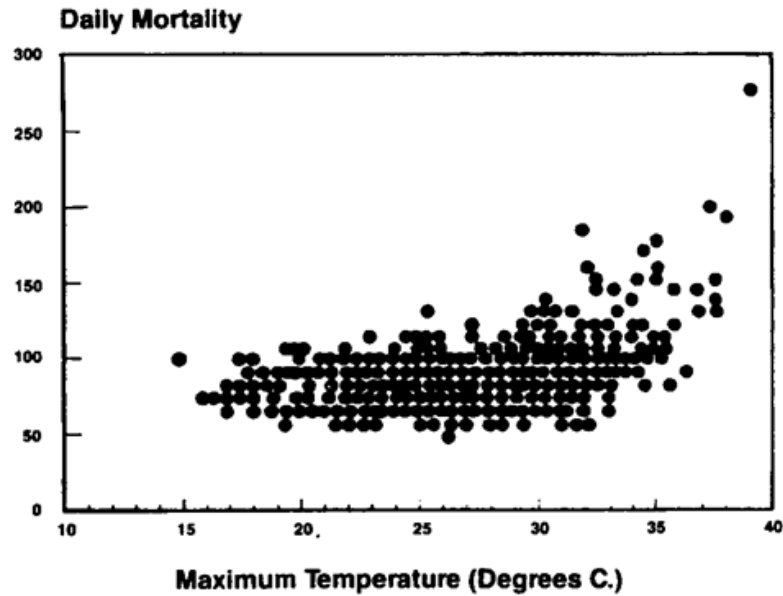
The impact of the UHI on air quality rises with increased temperatures. Temperatures are correlated with the elevated production of ground level ozone ( $O_3$ ), also referred to as photochemical smog, which is the main source for some pollutant compounds such as  $NO_2$  and volatile organic compounds (VOCs) that react in the presence of sunlight, causing an increase in the rate of ozone layer formation as the  $NO_2$  separates and combines with the  $O_2$  in the air to produce  $O_3$  (Figure 2.6). Under normal conditions, the reaction would reverse; however, the presence of VOCs blocks the dissociation of  $O_3$  (Bernstein and Whitman, 2005). All these changes can lead to complex air quality problems such as acid rain, and harm human health. Some studies have linked ozone to impaired lung function and the development of children (Chan et al., 2007).



**Figure 2-6** Relation between daily maximum air temperature and daily maximum ozone concentration in Connecticut (Oke, 1997b) on the left, and the chemical reaction that produces ozone on the right (Source: Roth, 2002)

### 2.4.3 Human Health and Comfort

During extreme weather events such as heat waves, the urban heat island has the potential to prevent the city from cooling down, maintaining nighttime temperatures at a level that affects human health and comfort. The mean core temperature for the human body to function well is 37°C. Above this temperature, there is a risk of heat related illnesses that may lead to mortality (De Carolis, 2012). This relation is well presented in Kalkstein and Smoyer (1993), who provide mortality statistics, which show dramatic increases of heat-related deaths for many cities (Figure 2.7). Similarly, during the 2003 heat wave in Europe there were approximately 35,000 heat-related fatalities, over 2,000 of which were in the UK (Larsen, 2003). In Tokyo, the number of victims of heat stroke has almost tripled since 1985, correlating with an increase in air temperature and the number of “tropical” nights (The Japan Times, 2001). Moreover, in the United States excessive heat exposure contributed to more than 8,000 premature deaths between 1979 and 1999, which exceeds all other natural disasters such as hurricanes, lightning, tornadoes, floods, and earthquakes combined (Center for Disease Control, 2004). The risk of experiencing these health outcomes is greatest when high temperature occurs in companion with high humidity, minimal cloud cover, and low winds (De Carolis, 2012).



**Figure 2-7** Relation between maximum air temperature and mortality in Shanghai from 1980 to 1989.(Oke, 1997b, adapted from Kalkstein and Smoyer, 1993).

#### 2.4.4 Water Thermal Quality

Surface urban heat islands degrade water quality, mainly by thermal pollution. Dark coloured pavements and roof surfaces absorb the sun's energy, reaching surface temperatures of about 27-50°C higher than air temperatures which transfer this excess heat to storm water. A field measurement study reported that urban area runoff was about 11-17°C hotter than a nearby rural area on a typical summer midday with pavement surface temperature 11-19°C higher than air temperature (Roa-Espinosa et al., 2003). This higher temperature storm water drains into storm sewers and raises water temperatures as it is released into streams, rivers, ponds, and lakes. A study in Arlington, Virginia, recorded temperature increases in surface waters as high as 8°F (4°C) just 40 minutes after heavy summer rains (EPA, 2003), which causes thermal shock to aquatic organisms as a result of the increase of water temperatures above normal conditions (EPA, 2008). This thermal shock can lead to many negative effects such as a decline in fish egg production, decreased reproductive rates, altered metabolic rates, impaired juvenile fish development, and fish lethality due to anoxia (Rossi and Hari, 2007). As a result, water bodies that are subjected to thermal shock may experience a decline in species abundance and biodiversity. The precise effects that runoff will have on an aquatic ecosystem depends on the time of exposure, the critical maximum and minimum temperatures specific species can survive within, and the developmental stage of the species, as well as the magnitude of temperature change (Rossi and Hari, 2007).

## 2.5 UHI and climate change in Cairo, Egypt

The IPCC fourth assessment report (IPCC, 2007a) on regional climate projections predicts that warming throughout the African continent and in all seasons is very likely to be larger than global annual warming. The drier subtropical countries such as Egypt are warming more than the moister tropics due to decreased annual rainfall along the Mediterranean Africa and the northern Sahara. According to an earlier version of the same source, the IPCC third assessment report (IPCC, 2001), surface warming in the African continent was reported at approximately 0.7°C during the 20th century. Observation records showed that this warming occurred at the rate of 0.05°C per decade with slightly larger warming in the June-November seasons than in December-May (Hulme et al., 2001). The IPCC fourth assessment report (IPCC, 2007a) predicts the regional climate for North Africa including Egypt in 2080 to 2099 based on climate change results of 1980 to 1999 for an AIB emission scenario<sup>4</sup>, where the projection shows a rise in mean temperature of 2.8°C, a decrease of precipitation by 6%, and the likelihood of fewer wet seasons and more dry seasons (Table 2.4). The results were in agreement with a previous study for the Organization for Economic Co-operation and Development (OECD) (2004) which reported a change in average area temperature and precipitation over Egypt, based upon a dozen recent GCMs (General Circulation Models) using a new version of MAGICC/SCENGEN.<sup>5</sup> The results are shown in Table 2.5. All the climate models estimated a steady increase in temperatures for Egypt, with little intermodal variance. The models estimated more warming for summer than winter.

---

<sup>4</sup> Scenario AIB hypothesizes that economic and demographic trends will continue along current lines, and that energy consumption will remain balanced among multiple sources, rather than shifting decisively away from fossil fuels.

<sup>5</sup>This analysis uses a combination of the 8 best SCENGEN models (CSI2TR96, CSM\_TR98, ECH3TR95, ECH4TR98, GISSTR95, HAD2TR95, HAD3TR00, PCM\_TR00) based on their predictive error for annual precipitation levels. Errors were calculated for each model, and for an average of the 17 models. Each model was ranked by its error score, which was computed using the formula  $100 * [(MODEL - MEAN \text{ BASELINE} / OBSERVED) - 1.0]$ . Error scores closest to zero are optimal. The first eight models had significantly lower error scores than the remaining nine. Therefore, the latter were dropped from the analysis. The error score for an average of the 17 models was 26.7%, the error score for an average of the 8 models was 22%.



Although all the climate models reviewed above predict a steady increase in temperature all over Egypt, the availability of similar studies targeting the city of Cairo was very limited. Ghoneim (2009) conducted satellite remote sensing data studies on the surface temperature characteristics of Cairourban areas, using the thermal infrared band from Landsat Enhanced Thematic Mapper Plus (ETM+) data. The result revealed a significant rise in surface temperature of Cairo betweeb 1980 and 2002 with a general trend of warmer urban areas versus cooler surrounding cultivated land (Figure 2.8) (Ghoneim, AFED 2009).

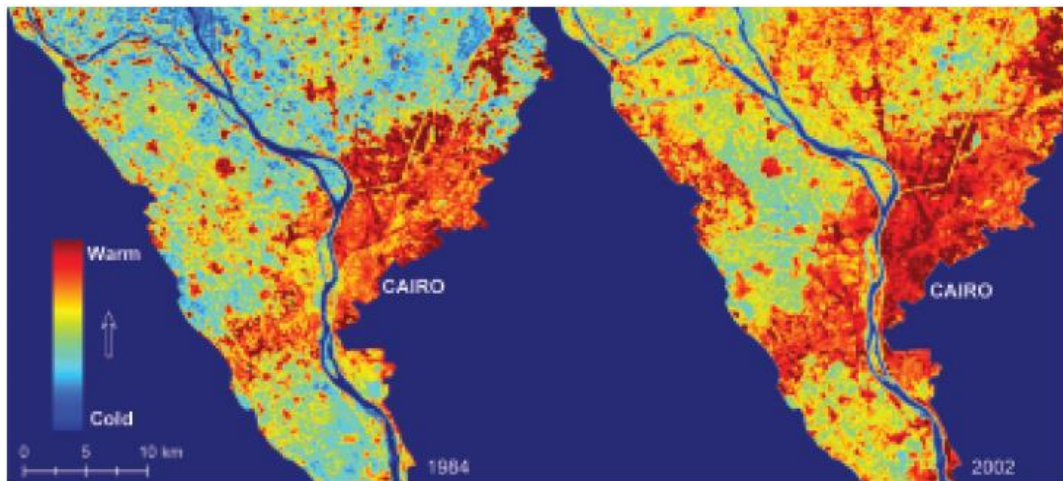
**Table 2-4** Climatic projection in North Africa in 2080 to 2099 (source IPCC, 2007a)

Region	Season	Temperature response (°C)			precipitation response (%)			Extreme Season (%)		
		Min	avg	Max	Min	avg	Max	Warm	Wet	Dry
18N, 20E to 30N, 65E	DJF	2.4	3.2	5	-47	-18	31	97	-	12
	MAM	2.3	3.6	5.2	-42	-18	13	100	2	21
	JJA	2.6	4.1	5.8	-53	-4	74	100	-	-
	SOA	2.8	3.7	5.4	-52	6	64	100	-	-
	Annual	2.8	3.6	5.4	-44	-6	57	100	-	-

DJF= December, January, February; MAM= March, April, May; JJA= June, July, August; SOA= September, October, November

**Table 2-5** GCM estimates of temperature and precipitation change for Egypt. Source OECD (2004)

		Temperature change (°C)		Precipitationchane (%)		
		Mean (Standard deviation)		Mean (Standard deviation)		
Year	Annual	December/ January/ February	June/ July/ August	Annual	December/ January/ February	June/ July/ August
2030	1.0 (0.15)	0.8(0.21)	1.1(0.18)	-5.2	-8.9	10.7(26.35)
2050	1.4(0.22)	1.2(0.30)	1.7(0.26)	-7.6	-12.8	15.49(38.07)
2100	2.4(0.38)	2.1(0.52)	2.1(0.52)	-13.2	-22.3	26.9(66.28)



**Figure 2-8** Rapid urban growth in Cairo between 1984-2002 caused a significant rise in surface temperature (shown in red), referred to as an urban heat island (UHI) effect. Source: CRS-BU, GHONEIM, AFED (2009) report)

### 2.5.1 Climate change and energy consumption in Egypt

Urban heat island has a close relation with the energy consumption in cities particularly the ones with hot arid climate (Chang, 2000; Roth, 2002; Voogt, 2002; Baker et al., 2002; Mills, 2006; Harlan et al., 2006; Rhadi and Sharples, 2013). The more rise of urban temperature will lead to an increase in the use of air conditioning. It follows that there will be a further increase in city temperatures from the dumping of heat from buildings heating ventilation and air conditioning (HVAC) systems and so more air cooling will be required (Takakura, Kitade et al. 2000). This forms a vicious circle or negative reinforcing loop (Uchiyama, 2011). There will also be an impact from increased emissions from cooling if this cooling is provided by fossil fuel based electricity. This will lead to an increased rate of global warming (Happold, 2014). Therefore, the extreme sensitivity of Egypt as a hot city to changes in temperature (Gleick, 1991) added more cooling load on the electricity consumption. This was shown in the *Ministry of Electricity and Energy (MEE, 2010)* fact sheet, where the number of air conditioners used in Egypt has quadrupled in four years (700,000 in 2006 to 3 million in 2010). Figure 2.9 shows sales of air conditioning (AC) units in Egypt exceeded 54,000 units per year between 1996-2009 (Attia et al., 2012). Air conditioners consume around 12% of the maximum productive capacity of power stations and their total consumption is estimated to be 22% of the overall energy production in the Egyptian building sector. If the current consumption trend expands further, which is expected (Georgy and Soliman, 2008), building electricity consumption and peak loads will continue to increase rapidly. As a reaction to this trend, and in order to

accommodate the prognosis for accelerating population growth and rising energy prices, the Egyptian government declared the commencement of its programme for nuclear power plants for electricity production in 2007 (Georgy and Soliman, 2008; Attia, 2012). Driven by the desire to provide cheap electricity to its population, the government considered nuclear energy as the easiest central solution to concentrate its effort to solve the energy problem centrally (UNHDR, 2010). This was done without any thought for reforming the building energy sector or improving the energy conservation policy and environmental protection, in order to avoid falling in the vicious cycle explained earlier in this section between the artificial exhausted heat and the urban heat island, resulting from adding more power plants to serve the increasing load of air conditioning demand which will lead to higher air temperature and urban heat island.

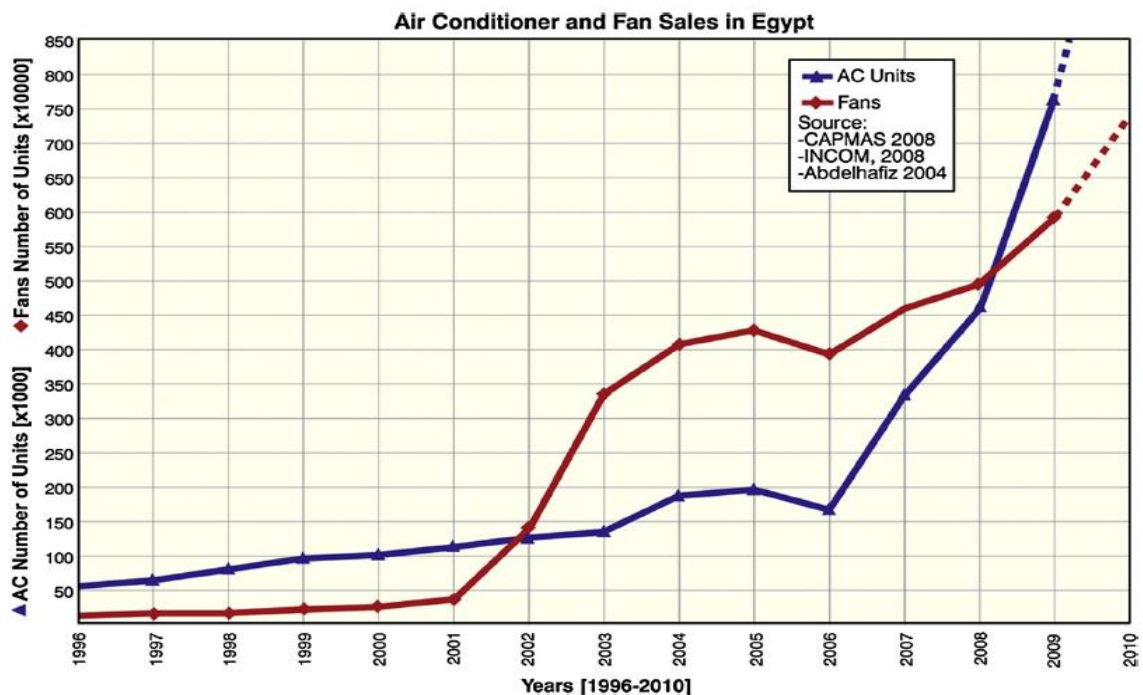


Figure 2-9 Increasing AC and fan sales in Egypt between 1996 and 2009 (CAPMAS, 2008; INCOM, 2008; Abdelhafiz, 2004)

## 2.5.2 Urbanization process and thermal comfort

Thermally comfortable outdoor environments have a positive influence on the indoor climate, leading to lower energy use for space conditioning (Johansson and Emmanuel, 2006). In Bangladesh, Ahmed (2003) reported lifestyle changes among medium and high-income urban dwellers as a direct cause of outdoor discomfort, as these dwellers nowadays tend to spend more time indoors. These changes are likely to contribute to increased use of air conditioning and thus higher energy use, and it may

further increase outdoor temperatures, as the excess heat is emitted to the urban air (de Schillier and Evans, 1998; Baker et al., 2002).

With reference to Cairo, Robaa (2011) researched the effect of urbanization and industrialization processes on outdoor thermal human comfort in Egypt, including central Cairo as a case study. The study revealed that urbanization and industrialization processes have resulted in the modification of the local city climate of Cairo. This modification involves the alteration of the local air temperature, humidity and wind speed, which in turn cause human climate change and increase serious discomfort for humans due to heat. This in turn hinders urban human activities compared to rural conditions. Accordingly, the two hot months of June and July transformed from hot months for all people in central Cairo during the old non-urbanized period, to uncomfortably hot months during the recent urbanized period (Robaa 2011). This has been mainly attributed to two major reasons:

- The distinct increase of air temperature and decrease of both wind speed and relative humidity induced by the urbanization process, which recently occurred in and around the urban area of central Cairo (Robaa, 1999, 2003)
- Passive design strategies, such as shading, orientation, thermal mass, natural lighting and ventilation, are no longer used. According to Attia (2012), traditional techniques and knowledge of appropriate environmental design learned by trial and error over time have been neglected during the last 60 years.

These factors have accelerated the urgent need to improve the current situation and calls for the creation of improved urban climate conditions within on-going urbanization activities.

## **2.6 Traditional and contemporary climate responsive strategies**

According to Ibn-Khaldun,<sup>6</sup> one of the primary tasks of architecture is to create favourable microclimates where humans can live and work (Rotledge and Kegan Paul, 1987). Successive processes of trial and error over long periods of time have given satisfactory answers of architecture concepts and techniques concerning human comfort

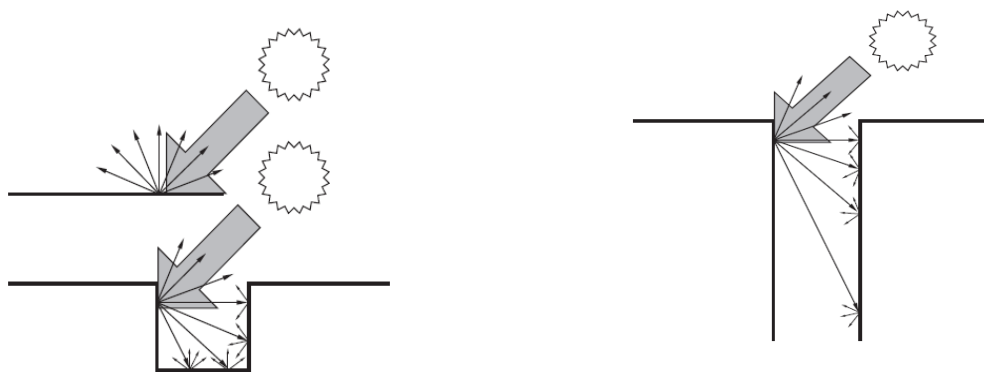
---

<sup>6</sup>Abu Zayd ‘Abd al-Rahman ibn Muhammad ibn Khaldun al-Hadhrami, 14th-century Arab historiographer and historian, was a brilliant scholar and thinker now viewed as a founder of modern historiography, sociology and economics (Stone, 2006).

and the surrounding environment. In Islamic Cairo, a number of strategies attributed to the Arab vernacular architecture and urban design were developed over a long period of time, such as fabric compactness, the high inertia of the construction, shading, night ventilation and evaporative cooling. This can be seen through two main consecutive design scales: (1) the streets' orientation, and (2) the urban fabric.

### 2.6.1 Street Orientation

The objective in a hot, dry climate is to maximise shading for pedestrians and minimise the solar exposure of building facades along streets whilst maintaining optimum urban and building ventilation. This is demonstrated by the street design for Fatimid city in Cairo, which follows a grid in its plan, with its main streets oriented north/south, such as Al-Muizz and Al-Gamalia as the main streets, while the secondary streets are oriented east/west. Most streets are narrow with deep canyons that promote greater shading, thus reducing radiant heat gains on ground surfaces and building facades (Givoni, 1992) (Figure 2.10). This urban design came forth as a good response to the living conditions of both the natural and the social environment, based on age-old regional experience using local building materials and appropriate techniques of climate control (Bianca, 2000). The street canyon geometry's parameters (height-to-width ratio (H/W)) and the street orientation are the most relevant urban parameters responsible for the microclimatic changes in a street canyon (Arnfield and Mills, 1994). These parameters directly affect the potential of airflow at street level, solar access, and therefore urban microclimate (Oke and Nakamura, 1998).



**Figure 2-10** Narrow, deep streets reduce radiant heat gains (Adapted from Givoni, 1998)

### 2.6.2 The Urban Fabric

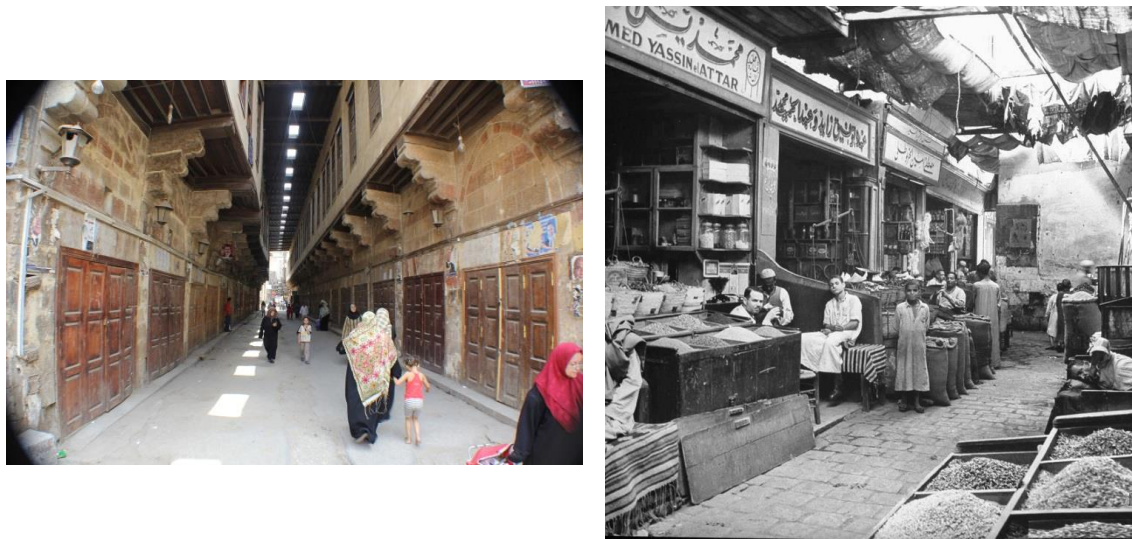
The early concept of compactness can be attributed to the vernacular urban architecture with its famous elements of narrow streets and courtyards, which reveal the distinctive



influence of climatic conditions that are just as important as the cultural dimension. The medium height houses are inward-facing buildings allowing for the compactness of the urban fabric. Only the rooftops and a few facades are exposed to the intense solar radiation. The streets are very narrow and shaded by the neighbouring walls, as shown in Figure 2.11. In some places, these are also covered or further protected from the sun with a trellis, cloth or awning (Figure 2.12). The thermal inertia of the whole system is high, as a consequence of a minimal envelope to volume ratio, also known as surface/volume ratio, where a compact building gains less heat during the daytime and loses less heat at night (Stasinopoulos, 2011). This effect is also owing to the use of heavy materials, mainly stone, which has a high thermal capacity. In addition, using light painted colours in the houses' external facades helps increase the urban reflectance as it might reach twice as much in modern cities (Taha, 1997). However, in the hot arid climate of the desert regions and due to the lack of vegetation with the light colour of the terrain, the problem of glare increases. To reduce the solar radiation and glare, building projections with a selective choice of colours and additional landscape vegetation is employed. The projection elements could be overhangs, wall extensions, and open balconies. These are usually of darker colours than the building surface behind to reduce the glare, as they are the most exposed elements.



**Figure 2-11** Urban compactness and narrow streets shaded by neighbouring walls



**Figure 2-12** Shading techniques across the street

## 2.7 Conclusion

The process of urbanization alters the natural surface and atmospheric conditions so as to create generally warmer temperatures (Landsberg, 1981, Wong & Jusuf, 2008). Oke (1997) suggested that urban atmospheres provide the strongest evidence for the potential of human activities to change climate. In the 20th century, rapid urbanization occurred worldwide, and today the majority of the world's population lives in cities. Increased temperature in cities, termed the UHI effect, is present all around the world and contributes to global climate change and, in turn, is exacerbated by global climate change (Mills, 2007; Sanchez- Rodriguez et al., 2005). With its increasing effect on human health (Harlan et al., 2006), air quality (Cardelino and Ghameides, 1990; Stone, 2004), and energy shortage (Rosenfeld et al., 1998; Grutzen, 2004; Golden et al., 2006; Rhadi and Sharples 2013), the importance of urban temperatures will increase, especially in warm climate cities. Here, it can seriously affect the overall energy consumption of the urban area (Rhadi and Sharples 2013), as well as the comfort and health of its inhabitants (Moonen et al., 2012). Thus, the current priority has been on the less developed regions, mostly located in the subtropics (Roth 2007), as by 2030 Asia and Africa are expected to have more urban dwellers than any other major area (UN, 2006).

In terms of the case study, Africa has been proven to be warming up at a faster rate than the global average, with a steady increase for the air temperature in Egypt (IPCC, 2007), along with an estimated UHI intensity of 4°C in Cairo (Santamouris, 2001). Accordingly, June and July were transformed from comfortable months for all people during the old non-urbanized period to uncomfortable heat months during the

recent urbanized period (Robaa, 2011). Consequently, the city's inhabitants face difficulty finding respite from high summer temperatures, and this threat to human comfort and well-being adds more load to the energy use within the city, which poses a significant challenge for urban planners and designers (Smith and Levermore, 2008). The demand started for tools to adapt the negative effects of air pollution and UHIs (Kratzer, 1956; Geiger, 1965; Landsberg, 1981; Schmalz, 1984; Santamouris, 2001; Grimmond and Oke, 2002) and moved progressively to micro-scales as the urban geometry was found to be decisive in the UHI (e.g. Barry and Chorley, 1978; Landsberg, 1981; Oke, 1987; Escourrou, 1991; Oke et al., 1991; Kuttler, 2004), this could be performed by reducing of daytime radiation load through triggering changes in surface temperature and heat storage in addition to changing street orientation and aspect ratio (Ketterer and Matzarakis, 2014).

Thus, the next chapter discusses the current literature and evidence for the effects of the surface air energy and mass exchanges between the urban canopy and the overlaying boundary layer on the urban microclimate, by highlighting the impact of street design on air temperature, airflow and solar access in an urban canyon. Studies conducted on this term have proved that a street's design is a key factor in mitigating the UHI effect and providing a pleasant microclimate at pedestrian level in an urban canyon (Oke, 1988; Shashua-Bara and Hoffman, 2003; Bourbia and Boucheriba, 2010; Shishegar, 2013; Ketterer and Matzarakis, 2014).



# 3

---

*“The knowledge we have acquired about urban climates should not remain an academic exercise on an interesting aspect of the atmospheric boundary layer. It should be applied to the design of new towns or the reconstruction of old ones. The purpose is, of course, to mitigate or eliminate the undesirable climatic modifications brought about by urbanization” (Landsberg, 1981).*

## **Chapter Three**

---

### **3.Review of Microclimate and Outdoor thermal comfort**

#### Key Concepts

- 3.1. Introduction
- 3.2. Scales of urban climate
- 3.3. Street canyon design
- 3.4. Surface energy balance (SEB)
- 3.5. Outdoor thermal comfort
- 3.6. Indices for assessing heat stress
- 3.7. The mean radiant temperature
- 3.8. Outdoor thermal comfort applications
- 3.9. Recent research of outdoor thermal comfort
- 3.10. Conclusion

### 3.1 Introduction

As seen in the previous chapter, the UHI problem contributes not only to higher temperatures, but also problems of energy use, air quality, human health, and quality of life. Successful adaptation to minimise the occurrence of UHI is, however, dependent upon a detailed understanding of the processes that lead to elevated urban temperatures (Arnfield, 1990; Oke et al., 1991; Swaid, 1993; Souch and Grimmond, 2006). Fortunately, there is a wealth of literature concerned with urban climatology across a range of spatial and temporal scales, which is extensively reviewed in this chapter.

The chapter is, thus, divided into two main sections. The first section considers the urban canyon microclimate including the climatic scale, the main surface energy balance, and urban canyon thermal characteristics. The second section deals with outdoor thermal comfort, such as human energy balance, variables affecting people's thermal sensation, comfort indices, and mean radiant temperature; it concludes with the methodological shortage in outdoor thermal comfort assessment.

### 3.2 Scales of urban climate

The very existence of a city has a significant modification effect on the local climate both within the built up area and in the atmosphere above and beyond its boundaries. The nature of these modifications depends on a wide range of physical variables, which can be observed and evaluated at distinctly different spatial scales (Erell et al., 2011). According to Oke (2006), the spatial dimension of an urban site, regardless of its scale, extends horizontally and vertically. In the vertical direction, the atmosphere can be divided into four distinct layers of different thickness, usually associated with a specific vertical temperature distribution (Jacobson, 1999) in to the troposphere, the stratosphere, the mesosphere and the thermosphere. The troposphere represents the lowest portion of the Earth's atmosphere and contains almost 80% of the atmosphere mass and almost all the water vapour. Within this troposphere layer is located the boundary layer climate, based on Oke's (1987, 2006) extensive studies on different urban climate scales. As seen in Figure 4.1, climate can be divided horizontally as follows:

1. The micro-scale includes buildings, streets, squares, gardens, trees, etc. where every surface and object has its own microclimate in its immediate vicinity. Surface and air temperatures may vary by several degrees in very short distances, and air flow can

be greatly perturbed by even small objects (Oke, 2006). Typical scales of urban microclimates relate to the dimensions of individual buildings, trees, roads, streets, courtyards, gardens, etc. Typical scales extend from less than one metre to hundreds of metres

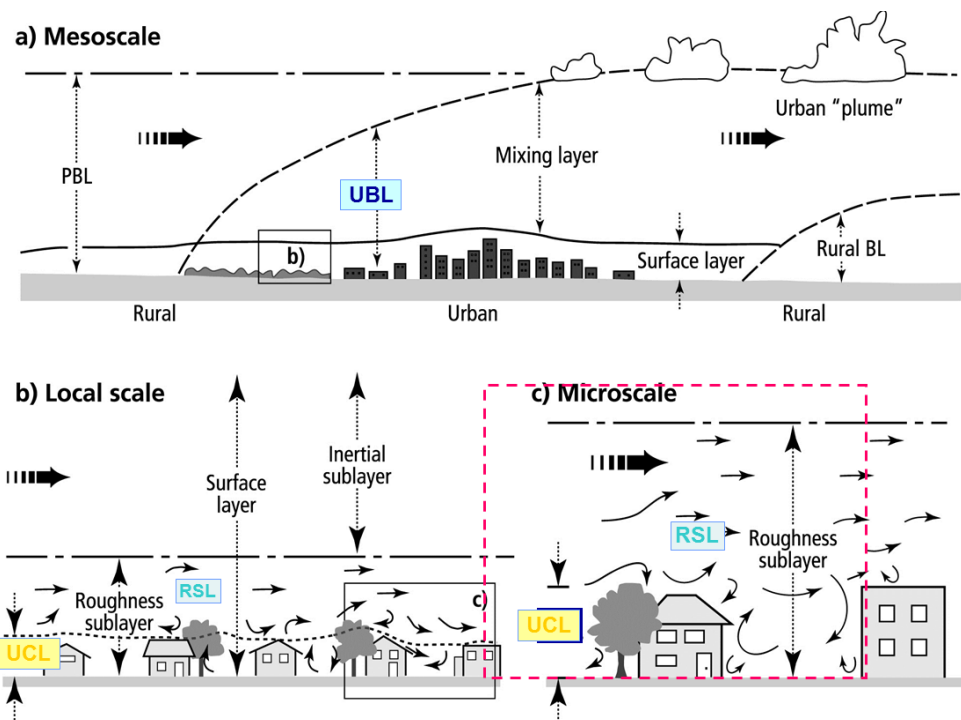
2. The local-scale represents urban neighbourhoods, and this is the scale that standard climate stations are designed to monitor. It includes landscape features such as topography but excludes micro-scale effects. In urban areas, this translates to mean the climate of neighbourhoods with similar types of urban development (surface cover, size and spacing of buildings, activity). Typical scales are one to several kilometres
3. The meso-scale means an entire city. A city influences weather and climate at the scale of the whole city, typically tens of kilometres in extent. A single station is not able to represent this scale
4. The macro-scale is appropriate for describing air masses and pressure systems related to weather (phenomena which are viewed on a scale of hundreds of kilometre, and so is not shown in Figure 3.1). While large urban areas may influence such weather patterns, this level of scale does not resolve the detailed features of cities.

In the urbanized areas, the lowest part of the atmosphere known as the urban boundary layer (UBL) and located within the meso-scale is decisively affected by the nature of the built up areas (Erell et al., 2011), generally considered to be approximately at roof level (Oke, 1976). The UBL can be divided into a number of vertical layers that hold climate interaction as follows (Figure 4.1):

- A. The mixing layer, the flow and potential temperature are rapidly mixed resulting in horizontally homogeneous, vertically uniform profiles. By night, this sub-layer may be further partitioned into a residual of the previous day's mixed layer overlying a surface inversion layer which has been cooled from below. The mixed layer may also be capped by an inversion layer at the top of the boundary layer. Little is known about any differences between urban and rural mixed layers (Roth, 2000)
- B. Inertial sub-layer (ISL), the flow and potential temperature are horizontally homogeneous but can vary in the vertical. The vertical fluxes of momentum, heat and moisture are horizontally homogeneous and uniform in the vertical and are

taken to be equal to the spatially averaged surface value. The lowest atmospheric level of numerical weather prediction models is usually assumed to lie within this layer

- C. The roughness of the sub-layer (RSL) extends from the surface up to a height at which the influence of individual roughness elements on the flow is ‘mixed up’ by turbulence (Raupach et al., 1991). The flow is horizontally heterogeneous, determined by local length scales such as the height of the roughness elements (buildings), their breadth or separation (e.g. Oke, 1988; Roth, 2000), and building shape (Rafailidis, 1997). The depth of RSL is estimated to be 1.8-5 building heights and it has been shown to depend on the stability, separation of the buildings and building shape (Raupach et al., 1980; Oke, 1987; Rafailidis, 1997; Roth, 1999, 2000; Cheng and Castro, 2002)
- D. The lowest part of the urban atmosphere is the urban canopy layer (UCL), which extends from ground level to the height of buildings, trees and other objects. The UCL is characterized by a high level of heterogeneity, since conditions vary widely from one point to another within the canopy volume between buildings (extends from 0-H). Within this layer, the microclimate is site specific and varies greatly within short distances (Arnfield, 2003; Oke, 2004).



**Figure 3-1** Schematic of climatic scales and vertical layers found in urban areas. PBL (planetary boundary) layer, UBL (urban boundary layer), UCL (urban canopy layer) (Based on Oke, 1997).

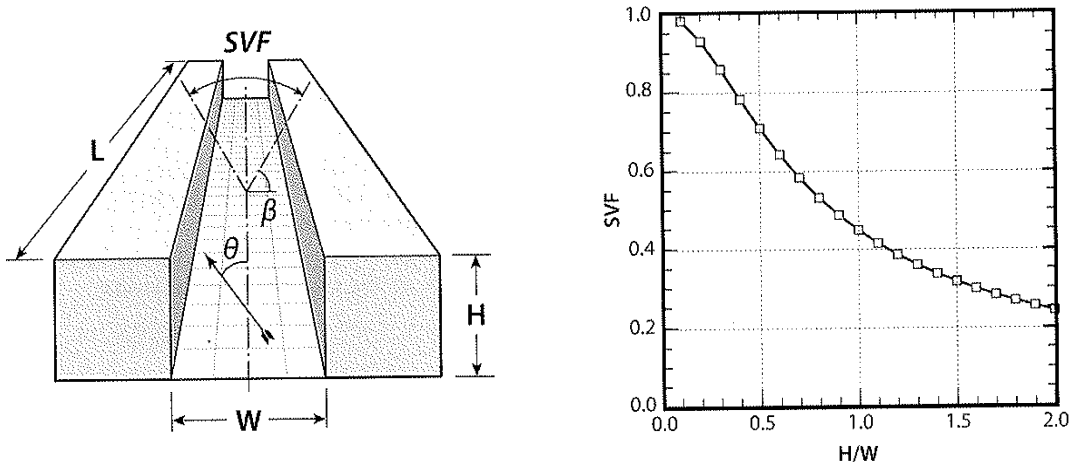
Due to the inherent heterogeneity of the UCL, a unique microclimate is established within any given urban space, with air temperature, wind flow, radiation balance and other climate indicators being determined by the physical nature of the immediate surroundings as well as by the urban and regional environment. Therefore, the attention of urban meteorology has moved progressively to micro-scales as the urban geometry and urban form were found to be decisive in the UHI (Oke, 1991). In this respect, the street design is, hence, a key issue in a global approach for an environmental urban design (Oke, 1988; Ali-Toudert and Bensalem, 2001), and any improvement to urban geometry at street level would reduce the urban heat island in summer and retain the heat during winter (Arnfield and Mills, 1994; Oke, 1998). The proportions of the space, the thermal and optical qualities of the used materials, and the use of landscape vegetation are all design factors that modify climate at the scale of the UCL. This is why urban space microclimate is considered to be an architectural issue as it may have localized impacts such as those on outdoor thermal comfort and building energy load (Erell et al., 2011).

### 3.3 Street canyon design and urban microclimate

A street canyon refers to a linear space, which is formed by two typically parallel rows of buildings or walls separated by a street, and it creates the basic unit of modern cities (Syrios and Hunt, 2008). The geometry of a street canyon is usually expressed by three principle descriptors in terms of quantifiable measures that express its density or other physical properties that may influence the micro-scale climate (Erell et al., 2011):

- The aspect ratio, also known as height to width (H/W) ratio, which describes the sectional proportions of the urban canyon by defining the ratio of the height of the building (H) to the width of the street (W) (Figure 3.2). If the canyon has an aspect ratio of around equal to one with no major openings on the walls it is called a uniform street canyon. A canyon with an aspect ratio below 0.5 is a shallow street canyon, and if there is an aspect ratio of two, this represents a deep street canyon (Shishegar, 2013).
- The canyon axis orientation ( $\theta$ ) represents the direction of the elongated space. Often the canyon axis orientation is described based on the closest cardinal direction such as north to south (N-S), east to west (E-W) or diagonal north west to south east (NW-SE) and north east to south west (NE-SW) (Figure 4.2).

- The sky view factor (SVF) is closely related to its aspect ( $H/R$ ) ratio (Figure 3.2), which represents the fraction of visible sky on a hemisphere which lies centrally over the analyzed location (the quantity of visible sky at a certain location) (Oke, 1981). It is a dimensionless measure between zero and one, representing totally obstructed and free spaces, respectively (Oke, 1988). The higher the aspect ratio, the lower the SVF.



**Figure 3-2** Schematic view of a symmetrical urban canyon and its geometric descriptors (on the left hand side) Sky view factor (SVF) as a function of canyon aspect ratio ( $H/W$ ) (on the right hand side) (Source: Erell, et al., 2011)

### 3.4 The surface energy balance (SEB) of an urban canyon

Urban canyons contain buildings and environments with distinctive topography and biophysical properties. This means that their energy receipts and losses are different from those of rural areas (Smith and Levermore, 2008). Therefore, any attempt to understand the microclimatic behaviour of the urban canyon must start with an analysis of differences in their surface energy balance (SEB).

The concept of an energy balance is derived from the first law of thermodynamics, which states that energy cannot be created nor destroyed, only converted from one form to another. When applied to a simple system, this means that energy input to it must equal the sum of energy output from it, and the difference in energy stored within it (eq. 3.1). However, the energy input and output are most likely to be unequal at any given instant, and they need not be equal at all times; furthermore, the input and output of energy from a system do not necessarily occur in the same form, where typically several modes of energy transfer take places simultaneously. In urban climatology, these temperature differences are attributed to urban geometry (the size, shape, and orientation of buildings and streets) and to the nature of urban surfaces (the

albedo, heat capacity, thermal conductivity, and wetness) (Oke, 1998 and Gordon, 2008). These characteristics alter the radiation balance at the surface, the storage of heat in the urban fabric, and the partitioning of energy into latent and sensible heat (Landsberg, 1981; Oke, 1982, 1987, 1988a, 1995; Toudert and Mayer, 2006) (Figure 3.3). A fuller explanation of this concept is given by Oke (1988) and Arnfield (2003) (Eq. 3.2):

$$\text{Energy input} = \text{energy output} + \text{change in stored energy} \quad (\text{Eq.3.1})$$

$$Q^* + Q_F = Q_H + Q_E + \Delta Q_S + \Delta Q_A \quad (\text{Wm}^{-2}) \quad (\text{Eq.3.2})$$

Where all terms are flux densities; ( $Q^*$ ) is the net all-wave radiation; ( $Q_F$ ) the anthropogenic heat; ( $Q_H$ ) the sensible heat; ( $Q_E$ ) the latent heat; ( $\Delta Q_S$ ) the net heat storage; and ( $\Delta Q_A$ ) the net horizontal heat advection (see Figure 4.3).

Anthropogenic heat ( $Q_F$ ) is often omitted from the measured urban energy balance, both because of its small magnitude in residential settings, and because it is assumed to be embedded in other fluxes (Oke and Cleugh, 1987; Grimmond and Oke, 2002). The latent heat flux ( $Q_E$ ) may be substantial in vegetated areas, but for those dominated by “dry” surfaces, this component can be marginalized as well (Arnfield and Grimmond, 1998; Masson et al., 2002; Oke et al., 1999), especially under arid conditions. Assume that  $Q_F$ ,  $Q_E$ , and  $\Delta Q_A$  are negligible or embedded in the sensible heat ( $Q_H$ ) and the net storage heat flux ( $\Delta Q_S$ ) (Pearlmutter and Berliner, 2005; Masson et al., 2002; Masson, 2006). Then, the urban energy balance can often be simplified to:

$$Q^* = Q_H + \Delta Q_S \quad (\text{W m}^{-2}) \quad (\text{Eq. 3.3})$$

To understand what makes urban microclimate different, each component within equation (3.3) must be considered in detail in terms of those aspects that are affected by the presence of nearby buildings.

( $Q^*$ ) is the net all-wave radiation, defined as the net effect of shortwave solar ( $K$ ) and long wave thermal ( $L$ ) incoming ( $\downarrow$ ) and outgoing ( $\uparrow$ ) radiation, described based on the following balance equation:

$$Q^* = (K_{dir} + K_{dif})(1 - \alpha) + L\downarrow - L\uparrow \quad (\text{Eq. 3.4})$$

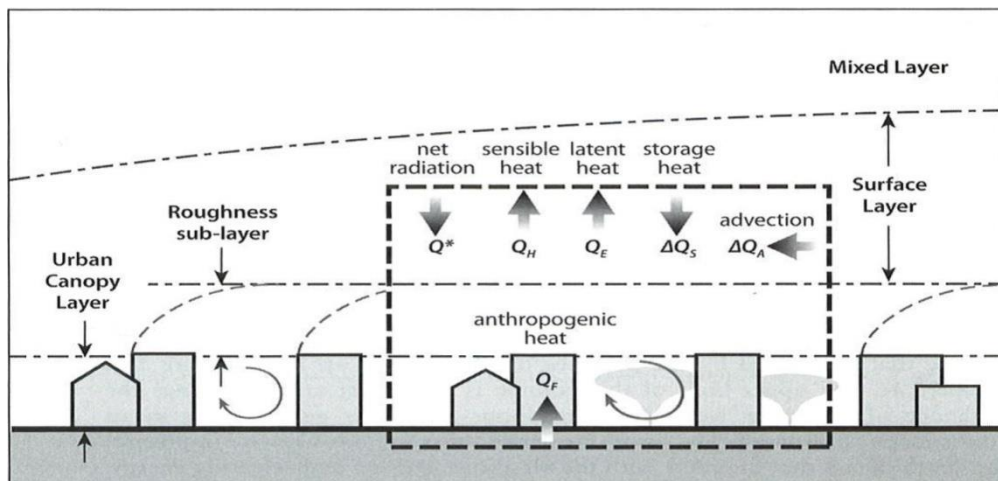
Where  $(Q^*)$  represents the net radiative balance,  $(K_{dir})$  is the direct short-wave radiation (incident solar rays coming directly from sunlight),  $(K_{dif})$  is the diffuse short-wave radiation (solar radiation reflected from clouds or aerosols in the atmosphere, and which makes the entire sky dome appear bright even if the sun itself is hidden),  $(\alpha)$  is the surface of material albedo, and  $(L\downarrow - L\uparrow)$  represents the long-wave radiation emitted by the surface and received by the surface from the sky, respectively.

The sensible heat  $(Q_H)$  is released (or absorbed) depending on the turbulence of the atmosphere and the temperature gradient between the surface and the air. The  $(Q_H)$  released from a surface can be calculated as (Arnfield and Grimmond 1998):

$$QH = h(Ts - Ta) \quad (Eq. 3.5)$$

Where  $(h)$  is the overall heat transfer coefficient from radiation and convection,  $(T_s)$  is the surface temperature and  $(T_a)$  is the air temperature. From equation (3.5), it can be seen that  $(Q_H)$  increases with increased convection and increased air surface temperature difference. Consequently,  $(Q_H)$  is high during the day when both surface temperature and natural convection are high, particularly on sunny days.

The net storage heat flux  $(\Delta Q_S)$  is of particular relevance to the urban environment, because it has been shown to account for over half of the daytime net radiation at highly urbanized sites (Ching, 1985; Oke et al., 1999).  $(\Delta Q_S)$  depends on the materials and structure of the urban surface both in facades and in the ground down to the depth at which each surface is active and its nocturnal release is regarded as a major contributor to the urban heat island (Grimmond and Oke, 1999b).



**Figure 3-3** Schematic section showing urban surface energy balance (SEB) components. (Source: Erell et al., 2011) Arrows pointing inward to the dashed line box represent positive fluxes value (energy gain to the system) while positive values for arrows pointing outward represent energy losses from the system.



Despite the practical difficulties in observing and interpreting the energy balance of an urban area, there are a large number of observational campaigns which studied the major characteristics of urban microclimate, including energy budget, air and surface temperature, air flow, solar access and vegetation (e.g. Nunez and Oke, 1977; Cleugh and Oke, 1986; Grimmond, 1992; Grimmond and Oke, 1995, 1999b, Harman, 2003).

### 3.4.1 Energy budget applications for an urban canyon

The basic knowledge behind the energy balance or budget of an urban canyon was investigated by Nunez and Oke (1977). The findings were then confirmed with further studies (e.g. Arnfield, 1982; Mills, 1993; Sakakibara, 1996; Arnfield and Grimmond, 1998; Masson, 2000; Kusaka et al., 2001; Toudert, 2005; Mazloomi, Hassan, Bagherpour and Ismail, 2010). Nunez and Oke (1977) examined a north-south (N-S) urban canyon located in Vancouver, with an aspect ratio of ( $H1/W=0.86$  and  $H2/W=1.15$ ). The walls were white painted and made of concrete. The energy balance of all wave radiations of both walls and floor were explained by Toudert (2005) as:

$$Q^*_{wall} = Q_H + \Delta Q_S \quad (Eq.3.6)$$

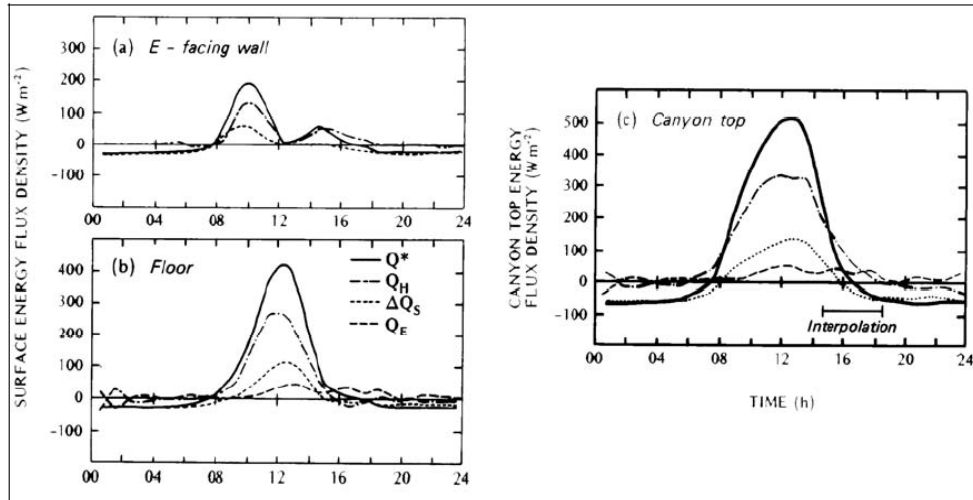
and

$$Q^*_{floor} = Q_H + Q_E + \Delta Q_S \quad (Eq.3.7)$$

$Q^*$	net all-wave radiation
$Q_H$	sensible heat flux
$Q_E$	latent heat flux
$\Delta Q_S$	energy stored in the walls

The main findings were that the urban geometry and the canyon orientation both influence the radiation exchanges, affecting the timing and magnitude of the energy mechanism of the canyon and its energy balance. Figure 3.4 shows the diurnal regime of all fluxes for N-S street orientation, which is similar to the case study of Al-Muizz Street with axis oriented 15 degree north-south. It can be seen that the east facing wall is first to be irradiated in the morning, with a second peak in the afternoon as a result of the reflected diffuse radiation from the west facing wall, which delivers a maximum irradiation in the afternoon. Due to the N-S orientation, the floor is exposed at midday, and the west and east walls about 1.5 hours before and after solar noon. About 60% of the radiant energy surplus was dissipated as a sensible heat flux, 25-30% stored in the materials and 10% transferred to air as latent heat. At night, the net radiant deficit is offset by the release of the energy stored within canyon materials and turbulent

exchange, which is minor. Nunez and Oke (1977) suggested that directing air flow at an angle in relation to the canyon axis may be important to the design pattern.



**Figure 3-4** Daily energy balance of the urban facets of an urban canyon oriented N-S with  $H/W \approx 1$  for a sunny summer day in Vancouver,  $49^\circ\text{N}$  (Nunez and Oke, 1977)

Another numerical model was performed to compare an E-W urban canyon against a parking lot (Sakakibara, 1996), and the results confirmed that urban areas usually absorb more heat during the day time and release more heat during the night time than rural areas or horizontal planes. This was almost the same result as reported by Mills and Arnfield (1993), stating that as the aspect ratio of a street decreases the street becomes more isolated in terms of heat exchange from the overlaying atmosphere.

It is worth mentioning a comprehensive experiment, which studied the E-W and N-S street orientations for all latitudes and seasons with different aspect ratios ranging from 0.25 to 4. Arnfield et al. (1990) investigated the amount of solar access in different urban canyons through numerical modelling. The findings revealed the following:

- The orientation of the street greatly affects the amount of solar energy obtained by walls
- The aspect ratio ( $H/W$ ) influences the availability of solar energy on the ground
- The impact of orientation is more significant in summer than in winter
- There is an easier seasonal solar control for the buildings walls oriented N-S (i.e. E-W streets) as the walls are protected in the summer and exposed in winter.

Another experiment conducted in the hot, arid region of Ghardaia, Algeria (Ali-Toudert and Mayer, 2004) stated that for arid regions it is quite difficult to keep an E-W oriented street canyon in the shade. In E-W orientation, the walls provide very limited

shading, even for very deep street canyons ( $H/W \geq 2$ ). In contrast, N-S oriented street canyons create a more pleasant microclimate as they provide enough shadow and solar energy in summer and winter, respectively. Therefore, the orientation of the street canyon should be chosen based on the area's latitude, as in different latitudes, a different orientation is appropriate. They also investigated the impact of street orientation on solar access and found that the availability of solar energy on the street's facades reduces rapidly with the increase of the aspect ratio of the canyon. These studies indicate that deep and narrow urban canyons ( $H/W \geq 0.5$ ) are more appropriate for hot regions as they generally reduce solar access. Although, Al-Muizz street is consisting from various aspect ratios starting from a very narrow aspect ratio 4.2 to very few wide ones of 0.4, this still might explain the reason that all the main streets within Islamic cities such as Fatimid Cairo, including Al-Muizz Street (figure 3.5), are relatively wide and follow a grid plan with a N-S axis, compared to the secondary streets which are very narrow with an E-W axis, which only keep shadow for a short time. Additionally, most parts within Al-Muizz street including the commercial and some residential sections are having an equal or almost similar heights (H) on both sides as shown in figure 3.6 (Al-Muizz street urban features including aspect ratios are illustrated later in section 5.4)

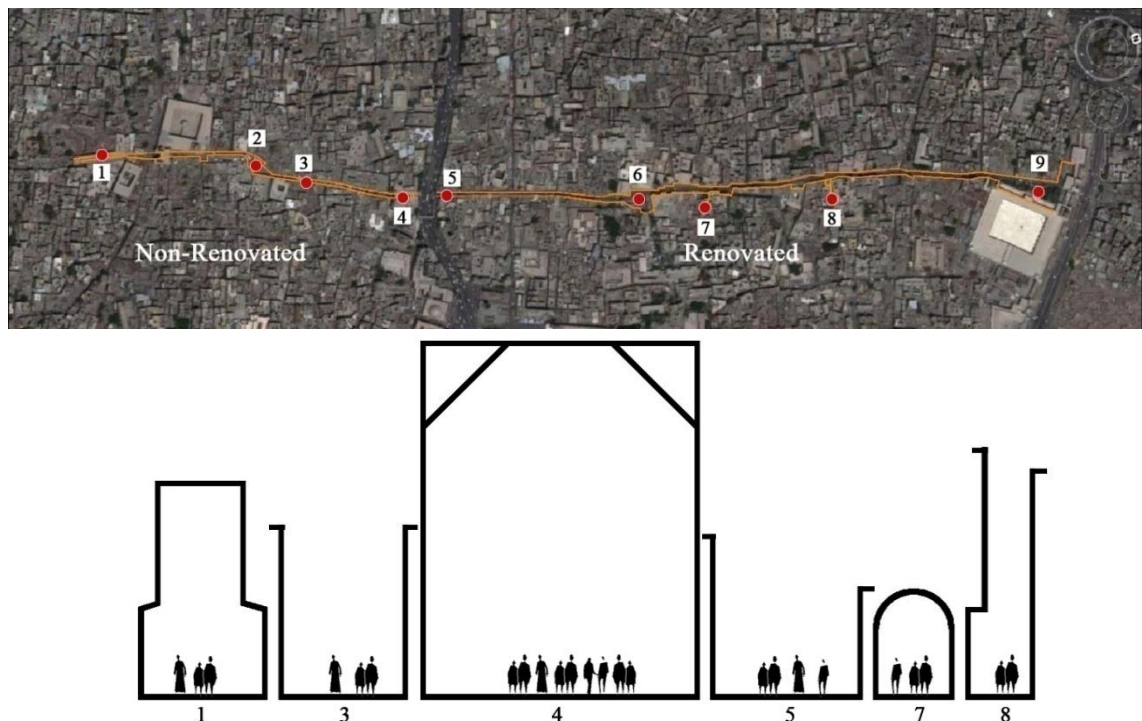
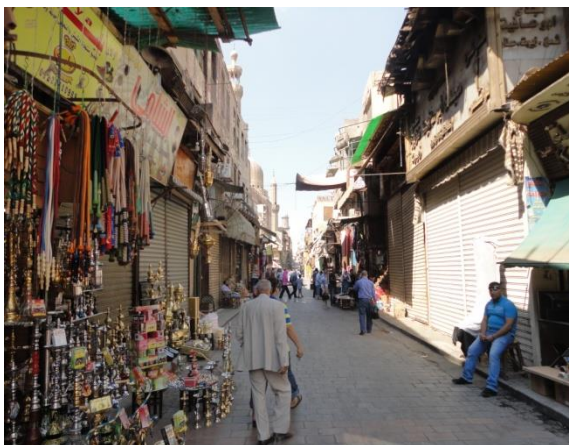
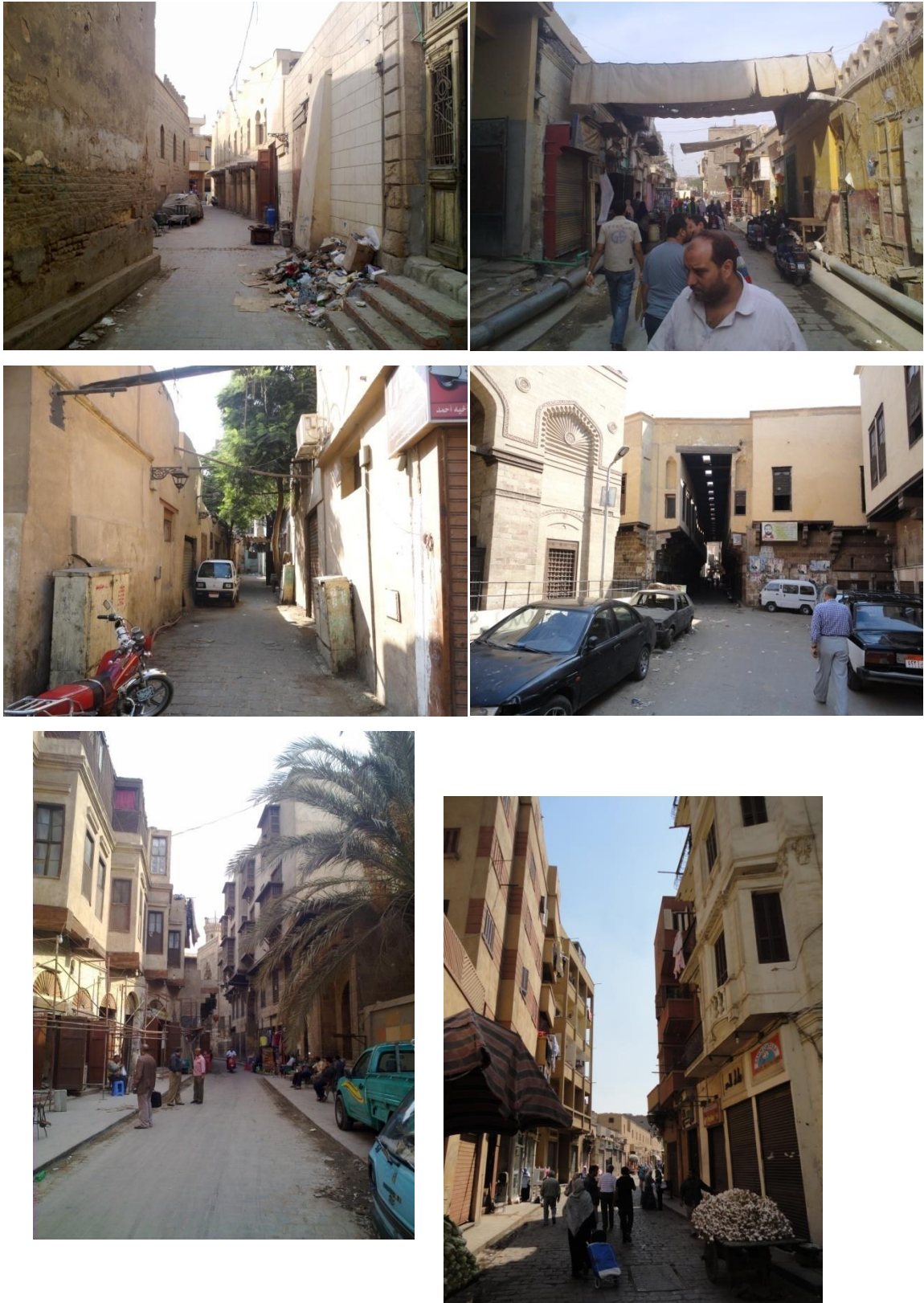


Figure 3-5 Route with the different aspect ratio (H/W) along Al-Muizz Street





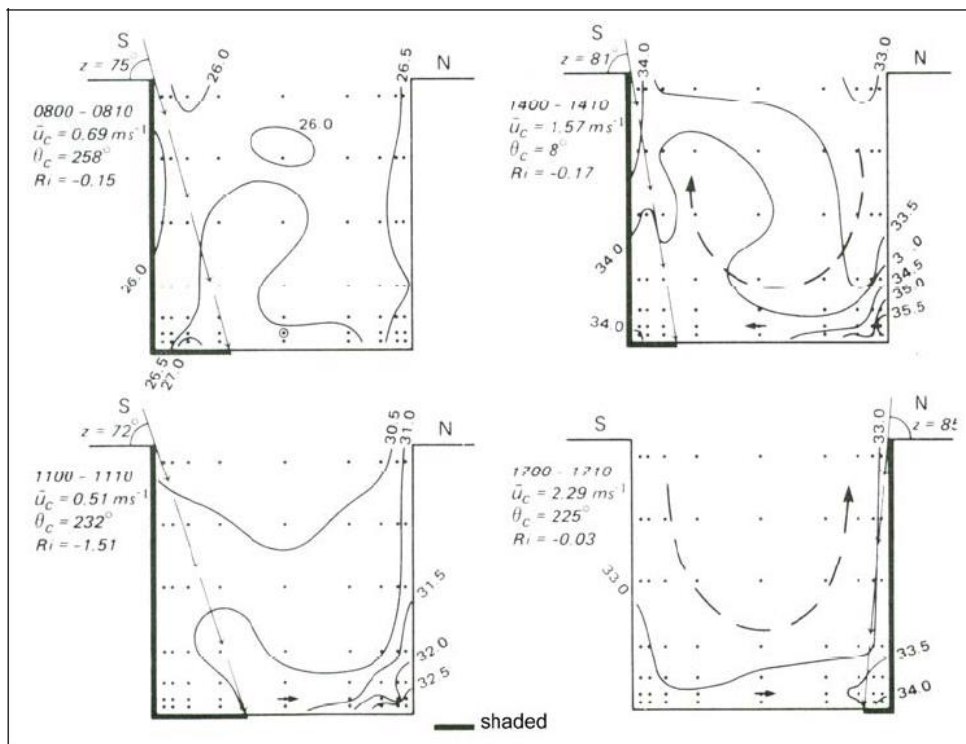




**Figure 3-6** Different photos among different sections within Al-Muizz street showing the similar heights of both sides of the street in several parts

### 3.4.2 Air and surface temperature

Oke (1977) defines a basic urban canyon as being comprised of three main components including the floor, the walls and the air mass in between the walls. In 1988, Oke and Nakamura conducted the first study for the spatial distribution of the air temperature within an urban canyon by fixing a grid network of 63 sensors across a vertical cross section for an E-W urban canyon with an aspect ratio (H/W) of nearly one, during a clear summer day, as a trial to draw a thermal map for the canyon (Figure 3.7). The study outcomes showed a well-mixed turbulent air within and above the canyon, with small differences in the air temperature ( $T_a$ ) of about 0.5-1°C between roof and canyon, and the roof air temperature was cooler during the day and warmer at night. The adjacent air temperature of the irradiated urban facet was slightly higher (2-3K) than the mean value measured at the centre of the canyon.

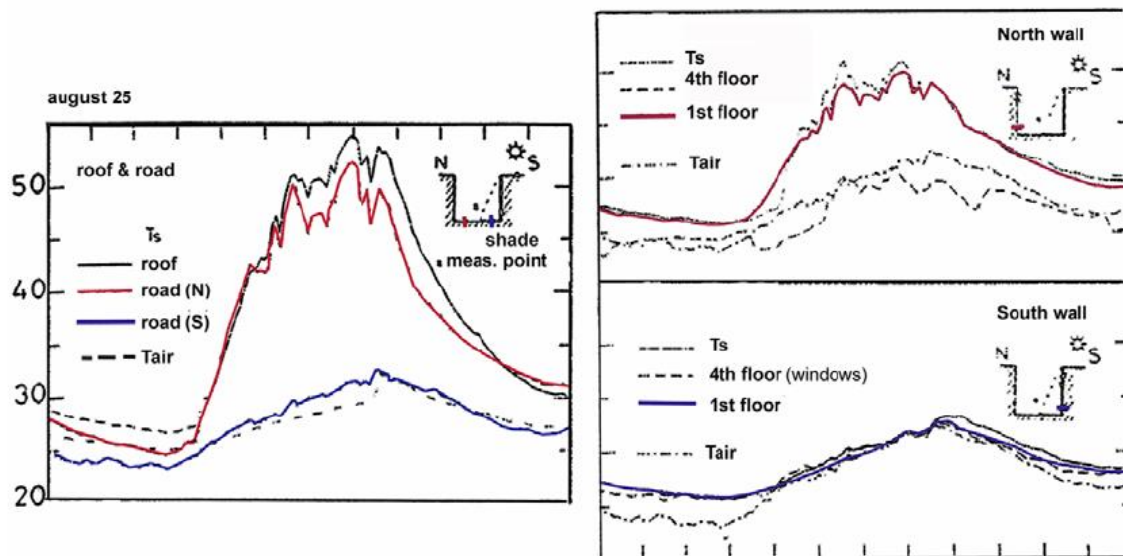


**Figure 3-7** Isotherm distribution across an E-W canyon at selected daytime hours (wind speed, wind direction and stability conditions at 1m height) (Nakamura and Oke, 1988).

Nakamura and Oke (1988) reported a large difference between the surface temperature ( $T_s$ ) and the adjacent air temperature ( $T_a$ ) for the direct irradiated urban facet, where the differences exceeded 10°C, while on the shaded part which only

received diffused radiation, these differences were much smaller. Air temperature ( $T_a$ ) was also sometimes found to be higher than surface temperature ( $T_s$ ) in the shade, likely due to the warming of the whole air volume by turbulent sensible heat flux transfer from sunlit surfaces and its mixing through vortex air circulation. Yoshida et al. (1990/91) reported similar results as Nakamura and Oke (1988) for a generally similar E-W canyon of aspect ratio (0.96) under sunny, summer conditions in Kyoto, Japan (Figure 3.8).

Santamouris et al. (1999) confirmed the previous results with a field study for a NNW-SSE street with aspect ratio ( $H/W$ ) =2.47 under hot weather conditions in Athens, Greece. The vertical ( $T_s$ ) and ( $T_a$ ) distribution was highlighted in deep profiles. Surface temperature ( $\Delta T_s$ ) differences between the various levels of the opposite surfaces were high (14-19°C). By day, the simultaneous difference in ( $T_s$ ) was lower at ground level and increased with height within the canyon. This difference became insignificant in the night-time (<2°C). Furthermore, ( $T_s$ ) stratification was found to be larger for the SW façade (0-10°C) than for NE façade (0-3°C) due to the different daily solar exposure.



**Figure 3-8** Surface and air temperatures of urban canyon facets, for an E-W street of an aspect ratio  $H/W = 0.96$  under sunny, summer conditions for Kyoto, Japan, 35°N (Yoshida et al., 1990/91)

Nazarian et al. (2014) numerically investigated the thermal effects of urban geometry, the surface radiative properties, and the wind direction, to examine surface and canopy air temperature and heat fluxes for a clear, summer day in southern California. Ground surface material (albedo) was found to have the most influence on urban facade temperature and energy balance. Replacing asphalt with concrete as ground

material increased the surface temperature up to 4.5K. For large canyon aspect ratios ( $H/W$ ) =3/2, peak wall temperature decreased by 4K while ground temperatures increased up to 4K larger at night compared to aspect ratio ( $H/W$ ) =2/3. Rotating the wind direction to be 45° off canyon axis altered wall and roof temperature up to 4K and 2.5K, respectively, while ground temperature was not influenced due to the high density of the studied case.

Applying these strategies to Al-Muizz Street, it can be noticed that the ancient town planners seemed to be fully aware of these approaches and the local climate by trying to provide different types of shading patterns as to fully utilize between the different air and surface temperature between the shaded and exposed areas. This was done either by the different urban design forms or shading devices with various openings, to control indirect sunlight into the urban street, while during the night time, these openings should help hot air to be released in order to provide comfortable climate within the urban canopy layer, as there was almost 14°C difference of  $T_{mrt}$  between the shaded and non shaded areas as measured in chapter five.

### 3.4.3 Urban canyon air flow

Urban air flow patterns are determined by the interaction between approaching winds with the built environment. The formation of air flow within a street canyon is essential for pedestrian comfort as well as for building ventilation, air quality and energy use (Memon and Leung, 2010; Yang and Li, 2011). However, the irregularity of the built up urban areas makes the air flow pattern notoriously complex (Erell et al., 2011; Al-Sallal and Al-Rais, 2012). Such as the compact urban configuration of Al-Muizz, by means of its narrow and irregular street network with small spaces in between, with average aspect ratio varying between 0.5-1. Some studies, however, have indicated that the air flow cooling effect could mitigate the UHI effect, and the street canyon is considered to be a key factor in the formation of these urban air flow patterns (Shishegar, 2013). Therefore, the effect of street canyon designs on improving the air flow need to be examined despite of its complexity.

According to Thomas and Fordham (2003), the air over urban areas could be divided into two main layers; the first layer, which is the interested for this research, is the urban canopy layer which is located below the roof tops and between the buildings. The air in this layer is mainly influenced by solar energy falling on building facades and



ground. The other layer is the urban boundary layer, located above the average height of the buildings. The air flow was found to be slower within the urban canopy layer compared to the surrounding rural areas due to the barriers such as buildings and trees located within the urban canopy layer (Okeil, 2010).

The wind flow within an urban canyon is a secondary circulation feature driven by the above-roof dominant flow (Nakamura and Oke, 1988, Santamouris et al., 1999), which is strongly affected by the street orientation and geometry (H: height, L: length, W: width) (Toudert, 2005). In Morocco, Johansson (2005) compared the air flow circulation between deep and shallow street canyons with an aspect ratio of 9.7 and 0.6, respectively, based on 18 months of continuous field measurements. The results confirmed a clear relationship between the urban geometry and microclimate within the street as the wind speeds became slower and more stable in the deep canyon (0.4m/s) in both winter and summer. Another study in Dubai, conducted by Al-Sallal and Al-Rais (2012), stated that narrow street canyons (4m and less) could increase wind speed leading to a better passive cooling performance, and yet create eddies at bending angles. It also recommended that for air flow to reach a deep access inside the narrow streets of the traditional city, the wind speed should not be less than 5m/s so it can have better potential for thermal comfort. Although, Al-Muizz street width varies along the street with the majority of 4m and less, the average air velocity recorded at the pedestrian level (1.4 m) was 0.9 m/s, also the air velocity used to increase when the street becomes shallow reaching 1.6 m/s and decrease when it becomes narrow recording zero speed, validating the relationship between the urban geometry and microclimate (as measured in chapter five). According to Kofoed and Gaardsted (2004), wind flow pattern within the pedestrian level (1.5m above the ground level) in urban areas is still very complex, and can be affected by very little alteration in urban arrangements. Santamouris et al. (2001) investigated ten deep canyons and stated that it is very difficult to get natural ventilation in urban canyons as wind velocity hardly exceeds 1m/s.

In addition to street geometry and orientation, the effect of solar heating on individual surfaces may create substantial thermal flows which affect the air flow patterns (Erell, 2011). If the downwind wall is exposed to direct solar radiation and is substantially warmer than other canyon surfaces, an upwards thermal flow may form near the wall surface. This flow tends to counteract the downwards advective flow, and may lead to the creation of two counter-rotating vortices normally associated with

deeper canyons. The formation of a multi-vortex pattern reduces vertical exchanges, primarily of pollutants but also of heat.

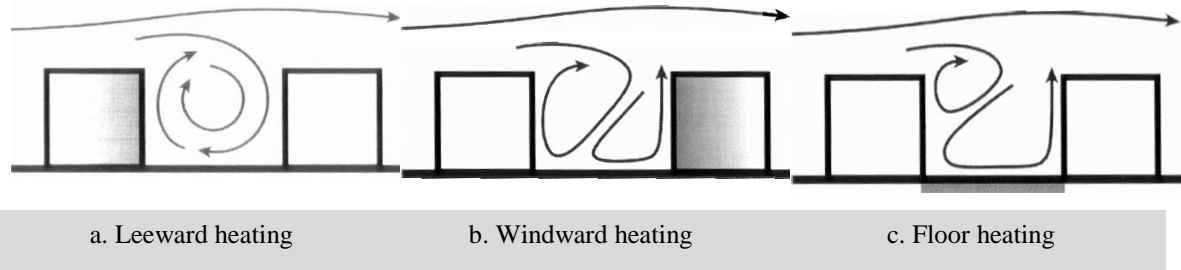
According to Xie et al. (2005), if the wind speed is weak and the radiant loads are strong, buoyancy effects are strong and disrupt the symmetrical lee vortex. This disruption is based upon the location of the heated surface to the approaching wind (Figure 3.9):

- a. Heating of the lee wall: the lee vortex remains symmetrical but is reinforced in magnitude. More ejection of canyon air occurs as a result of buoyant flow near the lee wall
- b. Heating of the wind-facing wall: buoyancy divides the lee vortex into two counter-rotating cells. The advection cell is typically larger than the thermal one, but the relative magnitude of the two depends upon the intensity of the heating upon the velocity of the above-roof flow. Air flows upwards and may be ejected near both canyon walls
- c. Heating of the ground surface: buoyancy divides the lee vortex into two counter-rotating cells, in a pattern that is similar to the one created by the heating of the wind-facing wall. The advection cell may become compressed near the top of the canyon, as buoyancy prevents it from extending down to the canyon floor. Upwind flow may be observed near both canyon walls.

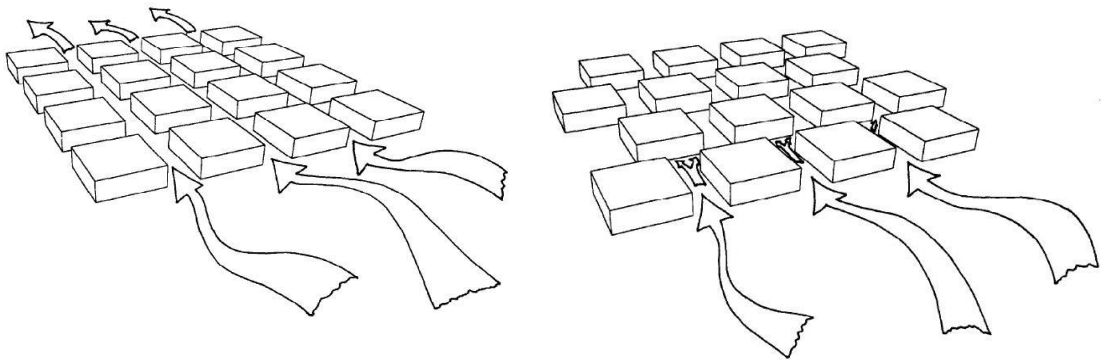
When winds are stronger, advection dominates even in the presence of strong radiant loads, and the overall structure of the canyon flow is affected by thermal buoyancy only to a minor extent.

Additionally, lack of vegetation and appropriate covers in straight streets causes either severe heat (hot, dry climate) or cold (cold, dry climate) wind to blow into the streets due to straight air movement (Santamouris et al., 1999). Narrow and winding streets reduce cold or hot winds and decrease the influence of stormy winds. This pattern is proper for stressful climates (hot-dry and cold-dry) (Santamouris et al., 1999) (Figure 3.10). In the case of very dense urban settlements such as Al-Muizz Street, the wind flow can be hampered, resulting in reduced ventilation cooling, but also preventing the area from the sandstorm such as Al khamasin sandstorm. However, the air circulation can still be improved through wind channelling in shaded narrow streets using the

variations in the aspect ratios along the street. In addition, the solar heating on particular surfaces might cause thermal flow leading to better air flow.



**Figure 3-9** The effect of solar heating on individual surfaces may create substantial thermal flows affecting the air flow patterns (Erell, 2011).



**Figure 3-10** Straight and parallel streets improve air flow into and within a city (on the left hand side) while the narrow and winding streets make air flow slow (Santamouris et al., 1999)

#### 3.4.4 Solar access

The impact of the sun on the climate is prominent. From the urban street canyon point of view, the amount of solar radiation could directly influence the solar access and, hence, thermal comfort at pedestrian level. Therefore, the degree of exposure to solar radiation is one of the main controls on microclimatic conditions, which should be considered in the design of an urban street especially in the hot arid climate such as Cairo (Sheta and Sharples 2010).

Arnfield (1990a) conducted a numerical study in order to examine the street's aspect ratio ( $H/W$ ) and orientation on the amount of solar access for all latitudes and seasons. The study examined various canyons with E-W and N-S orientation and aspect ratio varying from 0.25 to 4. The monthly average irradiation records showed that the aspect ratio ( $H/W$ ) is considered to be the first determinant influencing the amount of solar energy received by the urban canyon, the amount of solar radiation received by the

street surfaces increases as the H/W value becomes wide. On the other hand, the street orientation is more effective in controlling the solar amount gained by the walls; as a result, the solar amount received by the different urban surfaces is not distributed equally, as the ground surfaces are more irradiated than the vertical surfaces or the walls and the H/W appears to have more influence on the streets than the walls.

Table 3.1 indicates the impact of increasing the street width on the total radiation received by the street in the Netherlands ( $52^{\circ} 06' N$  and  $5^{\circ} 11' E$ ) (Van Esch et al., 1995). For all the studied canyons, increasing street width from 15m to 20m increases the radiation yield by 17-20%. In different seasons, the relative increase in radiation yield is more or less equal – about 19% per 5m increase in street width. However, the absolute increase differs quite strongly, as the radiation yield is rather low in winter; an extra 19% means only a few kWh/m, while in summer it is an extra 20-25kWh/m (Robins and Macdonald, 1999). This also shows that in higher latitudes the aspect ratio (H/W) and orientation are of great importance for controlling the receiving solar energy, yet the prime importance is for urban geometry over the orientation in controlling the solar access for the subtropics.

Although the N-S orientation still receives some solar radiation on the shortest day of the year (21st December), even when the street is narrow, it provides thermal comfort in winter, spring and autumn; it can be unpleasant in summer, as there is no shade on the streets during the hottest day of the year. In comparison with N-S oriented streets, streets with E-W orientation provide some shade during the hottest hours of the day. However, E-W oriented streets receive a high percentage of direct solar radiation in the morning and afternoon in summer compared to N-S oriented streets (Robins and Macdonald, 1999).

**Table 3-1** Total radiation yield of the canyon (in kWh/m) for different street directions, typical dates and street widths with flat roofs (Robins and Macdonald, 1999)

Street width (m)	December 21st	March 21 <sup>st</sup>	June 21st
<b>E-W street orientation</b>			
10	13.6	57.8	124
15	16	68	146
20	18.5	78.6	169
25	21	89.2	193
<b>N-S street orientation</b>			
10	13.8	56.6	124
15	16.1	66.8	147

20	18.5	77.2	170
25	20.9	87.6	193

In a similar climatic zone to the case study, in the hot, arid region of Ghardaia in Algeria, the findings pointed out the difficulty of keeping an E-W oriented street in the shade as the walls provide very limited shading even for deep canyons with aspect ratio  $(H/W) \geq 2$ . However, the streets with N-S orientation provide enough shadow in summer and solar energy in winter, leading to more pleasant microclimate (Toudert, 2005). Therefore, one recommendation worth mentioning is that the orientation of the street canyon should be chosen based on the area's latitude, as in different latitudes, different orientations are appropriate; also, by rotating the streets to a NE-SW or NW-SE orientation, comfortable conditions can be created as in summer it will provide better shading areas compared to the E-W oriented street, while in winter more solar access will be available compared to a N-S orientation (Toudert and Mayer, 2004). The study also concluded that deep and narrow urban canyons ( $H/W \geq 0.5$ ) are more appropriate for hot regions as they generally reduce solar access. In contrast, uniform, shallow and generally wide street canyons ( $H/W \leq 0.5$ ) are appropriate for cold areas which require more solar access throughout the whole year.

### 3.4.5 Vegetation

Vegetation is a modifying factor of the local climate. The use of greenery as a strategy to mitigate the UHI and improve the microclimate has been widely emphasized (e.g. Escourrou 1991; McPherson et al., 1994a; Akbari et al., 1995; Avissar, 1996; Taha et al., 1997).

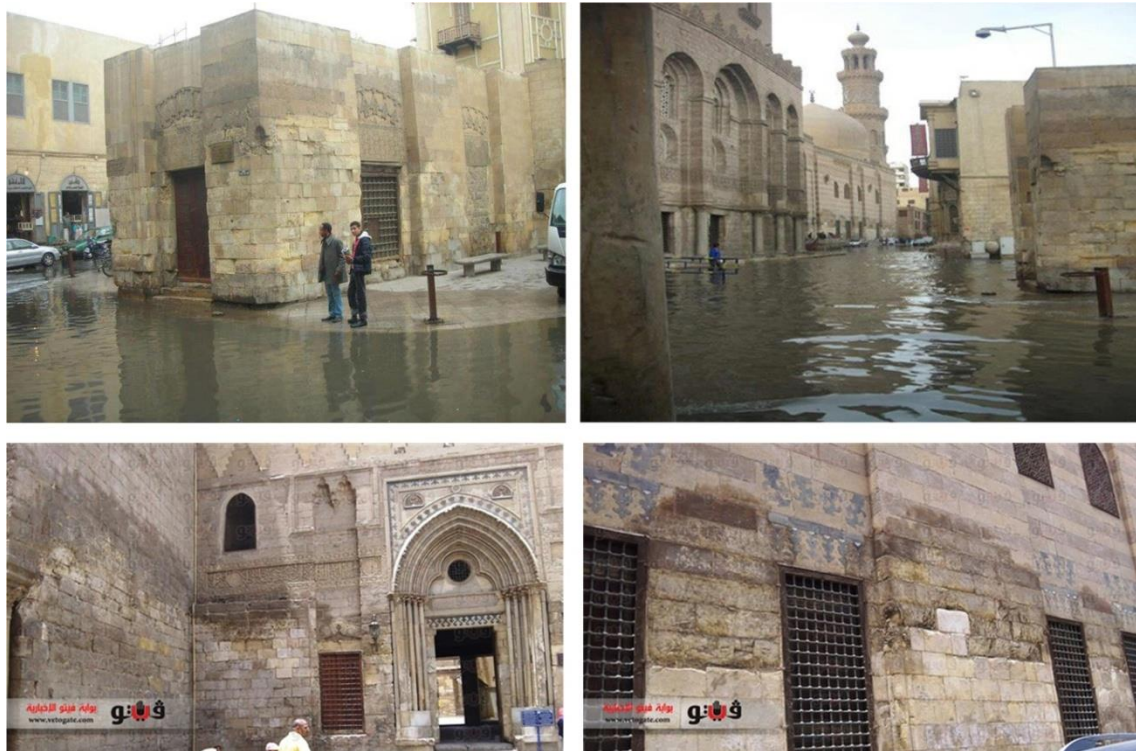
The effects of vegetation on the energy balance are compounded as the radiative, sensible and latent heat fluxes are spatially variable within the vegetative canopy. In tropical climates, the energy balance and cooling energy requirements may be altered by vegetation planted around buildings, avoiding the strong solar radiation and reflected radiation from the surroundings (Robinette, 1968; Brown and Gillespie, 1995; Akbari, 2002; u and wong, 2006; Wong et al., 2007). According to McPherson et al. (1994a), the effect of vegetation on climate can mainly be summarized into shading, evapotranspiration and wind break, in addition to acting as an indirect agent to trap water inside the soil. Thus, any decision to use the vegetation to improve the

microclimate must take into consideration these effects and their impact on the site should be studied well (Moffat and Schiler, 1981).

A comparison experiment conducted in subtropical location showed that some tree-aligned streets and boulevards had 1-2.5°C lower air temperatures than non-vegetated streets during the hottest part of the day (15:00h) (Shashua-Bar and Hoffman, 2004). Using ENVI-met (Bruse, 2006) modelling in Thessaloniki, Greece, Chatzidimitriou et al. (2005) reported a small temperature decrease for tree-aligned streets (less than 1°C), but up to 20°C lower surface temperatures and more than 40°C lower mean radiant temperatures. In Rio de Janeiro, Brazil, Spangenberg (2004) found that an increased amount of urban greenery (tree cover of 30% of the ground and 100% green roofs) could nearly re-create the comfortable conditions of a natural forest. Fahmy et al. (2010) assessed the vegetation impact in the arid climate of Cairo, Egypt. The findings were a 5-15°C reduction in main radiant temperature, and a 1-3°C reduction in air temperature.

It is important to point out that the type and effect of vegetation differs from one climate to another. For hot climates, the best use of the vegetation should benefit from reducing solar radiation and lower air temperature due to shading and evapotranspiration. A sparser vegetation well mixed within the urban structure to produce as much shadow as possible has to be preferred in hot and dry climates (McPherson et al., 1994b). For cold climates, using the vegetation as a screen against high winds is more appropriate, and dense vegetation located at the urban edges is advisable. However, in urban streets, vegetation should be selected carefully to avoid certain common problems. For instance, the trees are often employed as shading devices which provide shade in summer and sunlight in winter, yet this idealized behaviour is not always observed in practice for several reasons (Shashua et al., 2010). Trees, for example, do not always provide shade precisely where desired, the period in which many trees lose their foliage may not coincide with the hot season in a given location, and trees cannot be manipulated to provide shading or be removed in response to changing weather conditions, especially in the transition seasons. Additionally, trees are costly to maintain, and their canopies often interfere with overhead telephone and electric lines. Regarding Al-Muizz's urban configuration, trees cannot be manipulated to provide shading, as the sub-surface water table across Islamic Cairo, including Al-Muizz Street, has risen to catastrophic levels due to the increased disposal of waste water in the

aquifer layers, sometimes as close as 1.5m from the surface (Williams, 2001). This closeness of the water levels to the monuments puts precious building foundations in jeopardy (Figure 3.11).in addition to some other side effects which occur as a result of having greenery in the heritage site, for instance the roots of the vegetation may destroy pavements and underground sewers and harm the foundations of old building in some sites.



**Figure 3-11** The damage caused to monuments and the street by the release of sub-surface water and sewage water in some areas of Al-Muizz

### 3.4.6 Shading consideration in the hot, arid climate

The shade is the dominant factor driving the heat balance equation in the hot, arid regions, as stated by Pearlmutter et al. (2007), who examined heat stress over a summer daily cycle for several aspect ratios and orientations of different urban canyons in the hot, arid climate of south Israel. The main findings were that thermal stress was progressively reduced as the aspect ratio (H/W) increased in the north-south oriented canyon. This effect was less pronounced as the canyon rotated until it disappeared in the east-west orientation. However, during the nighttime the effect of the large aspect ratio (H/W) was largely reversed, which impeded the long wave radiant heat loss to the sky due to the constricted sky view factor (SVF). Such compactness creates a cooler street

environment during the daytime and a warmer one at night. Due to the dense infrastructure in some developed areas that have low SVFs, urban areas cannot easily release long-wave radiation to the cooler, open sky during the nighttime and this trapped heat contributes to the urban heat island (Nakamura and Oke, 1988). A similar study for Lin et al. (2010) based on ten years of meteorological data analysis indicated that a high SVF (barely shaded) causes discomfort in summer and a low SVF (highly shaded) causes discomfort in winter; both conditions reduce the duration of the annual thermal comfort period. The study also revealed that the high shading levels increase thermal comfort during the day in summer, but they can still decrease long-wave radiation loss on the surface, contributing to high temperatures at night. This phenomenon was similar to that which was reported in Chapter Five, where the street locations with low SVF, being covered by shading devices, took a longer time to cool down during the night time compared to other unobstructed locations. However, the results showed the importance of shading for the improvement of day-time comfort. Consequently, it can be concluded that suitable shading is very positive during the summer daytime and well documented, while an investigation is still required for night time comfort. This solution is not an innovative one and has been traditionally used in Al-Muizz Street for centuries (Figure 3.12). Nevertheless, the positive climatic effects of several traditional solutions have recently been questioned, as their effect might be overestimated since they were developed on a qualitative approach of trial and error (Givoni, 199; Toudert, 2005) and quantitative information about the best possible street design, based on scientific methods, in order to regulate the climate comfort is still required (Santamouris, 2001; Hawkes and Foster, 2002; Fahmy and Sharples 2008b; Abdulrahman and Sharples 2014).





**Figure 3-12** Old photos dated to the end of the 18th century for Al-Muizz Street show how people used their own techniques such as the movable tents to avoid direct solar radiation

### 3.4.7 Thermal properties of materials

Further important aspects affecting the microclimate of an urban street are the thermal properties of surface materials and nocturnal cooling (Arnfield, 2003). The reflectivity, or albedo, of surfaces that determines the amount of absorbed shortwave radiation depends mainly on the colour of the surface and varies greatly in urban areas (Table 3.2). Aseada et al. (1996) pointed out the importance of the pavement materials in the resulting heat fluxes and air-ground interface on summer days, where the asphalt pavement was shown to emit an additional  $150\text{Wm}^{-2}$  infrared radiation and  $200\text{Wm}^{-2}$  sensible transport, compared to a bare soil surface. Also, certain configurations of buildings can lead to an increased probability of multiple reflections and absorptions in the canopy layer, resulting in a low urban albedo.

Changes in air temperature near the surface are driven mainly by energy exchange between the surface materials and the surrounding ambient air. This, in turn, is affected by the thermal conductivity and heat capacity of the material. A parameter that combines these properties is the ‘thermal admittance’, which according to Oke (1987) is considered to be the key parameter in determining how much radiation absorbed at the surface will be stored in the sub-surface; the higher the thermal admittance, the more heat is stored in the material, while less energy will be released as sensible heat. At night, the release of energy stored in the canyon materials and the role of the floor and

the façades as a source of sensible heat for the canyon continues at night, causing what is known as nocturnal cooling (e.g. Nunez and Oke, 1977; Nakamura and Oke, 1988; Arnfield and Mills, 1994). The surface temperature of the street remains at 0.5-1 °C lower than the façade temperatures by night, due to a larger sky view of the horizontal surface (Santamouris et al., 1999). During night time, the vertical stratification of the air temperature is low, i.e. less than 0.5 °C for each level, with higher air temperatures measured at the ground level, which decrease with height. At night the simultaneous differences in the surface temperatures are insignificant, with a maximum of 2K (Santamouris et al., 1999). Accordingly, the ancient designers of Middle Eastern cities, including Al-Muizz, have often been credited with a superior understanding of the surrounding environment (Rahamimoff and Bornstein, 1981; Potchter, 1990, 1991; Erell et al., 2011), suggesting that the external colours of Middle Eastern cities were required as a combination of high reflectivity of solar radiation and high emissivity of infrared radiation to the cool sky at night. Light colours and non-shiny surfaces are preferred, and all dark coloured surfaces are avoided. Bright colour contrasts should be in agreement with the general character of the region as shown in Figure 3.13.

**Table 3-2** The albedo and thermal emissivity of typical natural and man-made material Sources: Oke (1987); Garratt (1992)

Surface	Albedo ( $\alpha$ )	Emissivity ( $\epsilon$ )
<b>Man-made</b>		
Asphalt	0.05-0.20	0.95
Concrete	0.10-0.35	0.71-0.90
Brick	0.20-0.40	0.90-0.92
Corrugated iron	0.10-0.16	0.13-0.28
Fresh white paint	0.70-0.90	0.85-0.95
Clear glass (normal incidence)	0.08	0.87-0.94
<b>Natural</b>		
Forest	0.07-0.20	0.98
Grass	0.15-0.30	0.96
Soil	Wet	0.10-0.25
	Dry	0.2-0.4

Notes:

1. The albedo of tropical rainforests lies in the lower part of this range, while that of coniferous or deciduous forests is in the upper part.
2. The albedo of soils depends, in addition to moisture content, on colour: it shows a high correlation with Munsell colour value (Post et al., 2000).



**Figure 3-13** The use of heavy materials, mainly stone, which has a high thermal capacity. In addition, using light painted colours in the buildings' external facades helps increase the urban reflectance

Based on the above, the physical features of the street canyon proved to have an influence on both the outdoor and indoor environments. The relative absorption and reflection of radiation affect the potential for the solar heating of the space outside as well as inside the buildings. Moreover, the accessibility to wind flow affects not only internal building ventilation but also external ventilation and the capability for urban cooling. Subsequently, the street form affects the thermal sensation of people outdoors as well as occupant comfort and energy consumption within buildings.

### 3.5 Outdoor thermal comfort

Thermal comfort as a term has been defined in numerous ways based on how it has been examined. For instance, Fanger's (1970) definition relates thermal comfort to the rate of energy gains and losses by the human body, describing the state of comfort as being when all heat flowing to and from the body are in equilibrium. In his definition, Fanger (1970) mainly used the rational model, which accounts for environmental conditions and physiological regulation of body temperature within a limited range. On the other hand, both the British Standard BS EN ISO 7730 (2013) and ASHRAE (2009) define thermal comfort as "the state of mind that expresses satisfaction with the surrounding environment." This means that comfort is not a state condition, but rather a state of mind, which in turn highlights the social and psychological dimensions. Recent studies have shown that thermal sensations are different among people at the same site due to the combination of a large number of factors, such as length of exposure, social/cultural backgrounds and/ or mood (Fiala et al., 2001; Huizenga et al., 2001; Nikolopoulou, 2001; Humphreys and Nicol, 2002; Nicol and Humphreys, 2002; Nikolopoulou and Steemers, 2003; Emmanuel, 2005a; Humphreys et al., 2007; Lin and

Matzarakis, 2008; Nikolopoulou and Lykoudis, 2009; Lin, 2009; Cohen et al., 2013). Although microclimatic parameters strongly influence thermal sensation, they only accounted for around 50% of the variation between objective and subjective comfort evaluation. The rest could not be measured by physical parameters, whereas psychological adaptation seems to have become increasingly important (Nikolopoulou and Steemers, 2003; Nikolopoulou and Lykoudis, 2009).

### 3.5.1 The heat balance (physiological approach)

Human physiology includes mechanisms for maintaining thermal equilibrium through energy exchanges between the body and its surroundings. The human body continuously produces heat by its metabolic processes, and this heat must be dissipated to the environment in order to maintain a constant internal body temperature (Figure 3.14). From the energy exchange perspective, the state of thermal comfort is reached when metabolic heat production and heat dissipation from the body to the environment are balanced, and when skin temperature and sweat rate are consequently within a defined comfort range (Fanger, 1972). The energy balance equation can be expressed as follows (Hoppe, 1999):

$$M + W + R + C + E_D + E_{Re} + E_{Sw} + S = 0 \quad (\text{Eq. 3.8})$$

where ( $M$ ) is the metabolic heat generated by the human body, ( $W$ ) is the physical work output, ( $R$ ) and ( $C$ ) represent the net radiation and convection heat losses from the body respectively, ( $E_D$ ) is latent heat loss by evaporation of moisture diffused through the skin (imperceptible perspiration), ( $E_{Re}$ ) is the sum of heat flows for heating and humidifying the inspired air, ( $E_{Sw}$ ) is the heat loss due to the evaporation of sweat, and ( $S$ ) is the storage heat for heating and cooling the body mass. The individual terms in this equation have positive signs if they result in an energy gain for the body and negative signs in the case of an energy loss ( $M$  is always positive;  $W$ ,  $E_D$  and  $E_{Sw}$  are always negative). All the heat flows are calculated in watts (W). Many of the most common thermal indices for indoor comfort are based on this heat balance (McIntyre, 1980) as described later in section (3.6). The detailed mathematical statements for each of these terms have been thoroughly documented (e.g. Fanger, 1970; Gagge et al., 1971; Gagge et al., 1986; Höpfe, 1984; VDI, 1998; ASHRAE, 2001a).

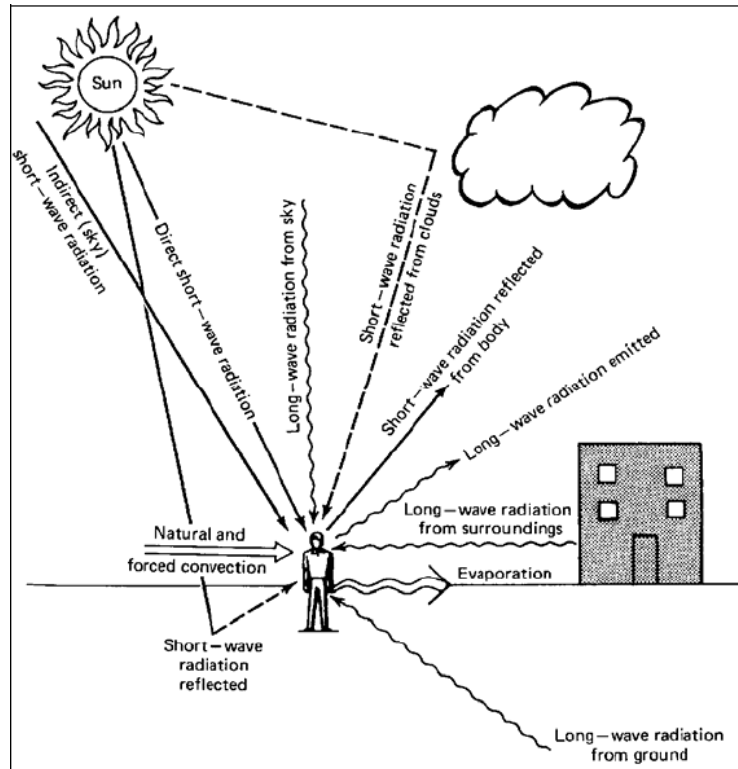


Figure 3-14 The components of the human heat balance (Houghton, 1985)

### 3.5.1.1 Human urban heat exchange

Here, it is important to remember that the outdoor urban setting is different to the indoor as it provides less shelter from sun and wind. There are two important mechanisms related to the outdoor setting, through which the body exchanges energy with the surroundings and achieves thermal comfort (Pearlmutter et al., 1999; Pearlmutter and Shaviv, 2005; Pearlmutter et al., 2007):

*a. The absorption and emission of energy in the form of radiation*

Pedestrians experience wide fluctuations in thermal stimuli due to radiation in two forms: (i) the short wave radiation emitted from the extremely hot surface and mostly referred to as sunlight (ii) long wave radiation which is emitted by the atmosphere and by lower temperature terrestrial surfaces that surround the pedestrians in the built environment. Both forms are combined as a total net exchange of radiation  $R_n$  between the body and the urban environment (Pearlmutter et al., 2006). (Figure 3.15)

$$R_n = (K_{dir} + K_{dif} + K_h + K_v)(1 - \alpha_s) + L_d + L_h + L_v - L_s \quad (Eq. 4.9)$$

- $R_n$  The net radiation of all wave lengths ( $W/m^2$ )
- $K_{dir}$  Direct short wave radiation incident on the body

$K_{dif}$	Diffuse short wave radiation incident on the body
$K_h$	Indirect short wave radiation incident on the body reflected from horizontal surfaces
$K_v$	Indirect short wave radiation incident on the body reflected from vertical surfaces
$\alpha_s$	The albedo of the skin and/or clothing, such that $(1 - \alpha_s)$ is the proportion of all incident short wave radiation that is absorbed by the body
$L_d$	Long wave radiation incident on the body, emitted downwards by the sky
$L_h$	Long wave radiation incident on the body, emitted by horizontal surfaces
$L_v$	Long wave radiation incident on the body, emitted by vertical surfaces
$L_s$	Long wave radiation emitted by the body to the environment

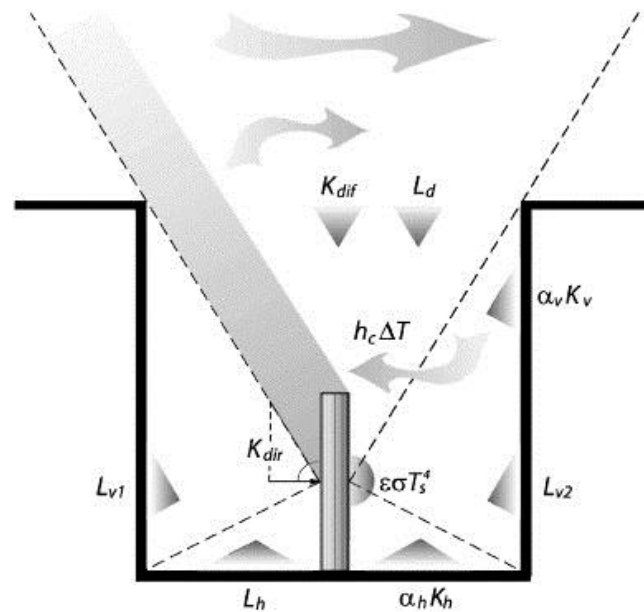
In mid latitude countries like Egypt, pedestrians are likely to suffer most severely from thermal stress due to overheating during the midday hours of the summer season when the short wave radiation is most intense. Therefore, unshaded pedestrians are exposed to direct solar rays (direct radiation) coming directly from the sun and indirect solar radiation known as diffused radiation, which is either scattered by the atmosphere and thus arrives from the entire vault of the sky or from the reflected solar radiation from adjacent buildings and ground surfaces (reflected radiation). In addition to short wave radiation, pedestrians are also exposed to long wave radiation emitted from adjacent buildings and surfaces, as well as from the ground and the sky. The extent of the exposure to these emissions is dependent upon the temperature and emissivity of the respective part of the surrounding environment, and upon its corresponding factor. Moreover, short wave radiation can increase the emission of long wave radiation through increasing the temperature of the adjacent surfaces (Erell et al., 2011).

*b. The absorption (most commonly, dissipation) of heat by convection*

A body exchanges heat with the surrounding air through thermal convection due to local air temperature difference and through forced convection due to wind. Mitchell (1974) calculated the rate of convective heat transfer ( $C$ ) per unit area of the body and measured in  $W/m^{-2}$

$$C = h_c \Delta T \quad (Eq. 3.10)$$

$C$	The convective heat transfer on the sensible flux ( $W.m^{-2}$ )
$h_c$	The transfer coefficient in $W/m^2 \text{ } ^\circ C$ , which is dependent on the number of people in a group, affects forced convection and air speed ( $W.m^{-2}.C^{-1}$ )
$\Delta T$	Difference between body temperature and the surrounding air temperature ( $^\circ C$ )



**Figure 3-15** Schematic depictions of radiation exchanges between a pedestrian and the surrounding urban environment. Net all-wave radiation ( $R_n$ ) at the surface of the vertical cylinder is based on an expression originally given by Monteith and Unsworth (1990) for an open ground plane, which was adapted by Pearlmutter et al. (1999) to account for the additional effects of vertical canyon facets

### 3.5.2 Variables influencing thermal comfort

There are four basic environmental parameters affecting overall thermal comfort: air temperature, radiation, air humidity and wind velocity. Additionally, two personal variables also influence thermal comfort: clothing insulation and the level of activity as metabolic rate (ASHREA, 2009). These factors may be independent of each other, but together they contribute to a body's thermal comfort.

#### 3.5.2.1 Environmental parameters

- **Air Temperature:** defined as the dry-bulb temperature in the shade, it is perhaps the most important for thermal comfort, where it affects the rate of convective and evaporative body heat loss. If the air temperature exceeds the surface temperature of the clothed body, or of the exposed skin, there will be convective heat gain and vice versa. There is actually a fairly wide range of temperatures that can provide comfort when combined with the proper combination of relative humidity, mean radiant temperature (MRT), and air flow. As any one of these conditions varies, the dry-bulb temperature must be adjusted in order to maintain comfort conditions.
- **Radiation:** the absorption of solar radiation and the exchange of long-wave radiation strongly affect the state of thermal comfort of the human body. The concept of

MRT was originally developed for the indoor environment and defined as “the uniform temperature of an imaginary enclosure in which radiant heat transfer from the human body equals the radiant heat transfer in the actual non-uniform enclosure” (ASHRAE, 2009). However, for the outdoor it is much more complicated because of the extensive variation in radiation from different sources. The human body may receive solar radiation as direct and diffuse, as well as reflected radiation from building façades and the ground. Moreover, the body exchanges long-wave radiation with the sky, with urban surfaces and with objects such as trees. The magnitude of the radiation from the different sources varies greatly in space and time.

In warm climates, radiation can make people feel hot and uncomfortable. In contrast, radiation in cold climates can moderate the discomfort caused by low temperature. Radiant temperature has a greater influence than air temperature on losing or gaining heat to the environment. The skin absorbs almost as much radiant energy as a matt black object, although this may be reduced by wearing reflective clothing (HSE, 2013).

- **Humidity:** defined as the amount of water vapour in a given space. An increase in the air’s moisture content, or humidity, can affect the evaporation rate: high humidity restricts the dissipation of heat through sweat evaporation from the skin and respiration, while very low humidity leads to drying out of the mucous membranes as well as the skin, thus causing discomfort. A change in the humidity of the atmosphere affects thermal sensation in that a person feels warmer, sweatier and less comfortable (McIntyre, 1980). Especially under warm conditions, when both convective ( $C$ ) and radiative ( $R$ ) heat losses are small, sweat evaporation ( $E_{sw}$ ) is an important mechanism in maintaining comfort. When the liquid sweat on the skin surface evaporates, latent heat is extracted from the body and a cooling effect is produced. However, Givoni (1998) stated that humidity does not influence thermal sensation below a critical level, and he defined this limit to 80% relative humidity for temperatures up to 25°C. This is because, although the evaporative capacity of the air diminishes with increasing humidity, the body compensates for this by spreading the sweat over a larger area of skin, thus maintaining the required evaporation rate.

- **Wind velocity:** This describes the speed of air moving across the body and may help cool the body if it is cooler than the environment. Air velocity is an important factor in thermal comfort as it significantly affects body heat transfer by convection ( $C$ ) and evaporation ( $E_{sw}$ ). It accelerates convection and increases evaporation of sweat from



the skin, thus producing a physiological cooling effect. The higher the wind speed, the greater the rate of heat flow by both convection and evaporation.

### 3.5.2.2 Personal parameters

- **Metabolic rate:** The metabolic rate is related to the level of physical activity; at higher rates a cooler environment will be preferred to facilitate heat dissipation.
- **Clothing insulation:** Thermal comfort is very much dependent on the insulating effect of clothing on the wearer. Increased clothing insulation leads to a lower temperature difference between the outer surface of the clothed body and the ambient air temperature. Accordingly, the convective  $C$  and radiative ( $R$ ) heat losses decrease with increasing clothing insulation, and it is considered an important adjustment mechanism if the clothes can be freely chosen.

According to Nikolopoulou and Steemers (2003), people adapt physically to an environment by a combination of both strategies of clothing insulation and metabolic rate through adjusting how they dress and move, e.g. slow walking in hot climates, and by avoiding exposure to extreme climate situations.

### 3.5.3 Psychological approach

In urban spaces, people not only seem to accept more extreme thermal stimuli than they do indoors, but studies also indicate that individuals residing in hot and humid regions have better tolerance for high temperatures than those residing in temperate regions (Karyono, 2000; Feriadi and Wong, 2004; Lin and Matzarakis, 2008). These give evidence to the fact that people adapt to the surrounding thermal environment (Barger and de Dear, 1998; Emmanuel, 2005a). The existence of adaptation reflects a “give and take” relationship between the environment and the user, who is no longer a passive recipient for the given thermal environment but rather an active agent interacting with and adjusting to the person-environment system via multiple feedback loops (Brager, 1998). There are three main ways to give such opportunities of human adaptation to comfort including behaviour adaptation, physiological acclimatization, and psychological adaptation (Brager and Dear, 1998; de Dear and Brager, 1998; Givoni, 1998; Fiala et al., 2001; Huizenga et al., 2001; Nikolopoulou, 2001; Humphreys and Nicol, 2002; Nicol and Humphreys, 2002; Nikolopoulou and Steemers, 2003; Humphreys et al., 2007; Lin, 2009).

### **3.5.3.1 Behaviour adaptation and adjustment**

Physical adaptation involves all the physical changes people make to either adjust to the environment, or amend the environment to their needs. Nikolopoulou (1999) identified two different types of physical adaptation: reactive and interactive. In reactive adaptation, the only changes occurring are personal, such as altering one's clothing levels, posture and position, or even metabolic heat with the consumption of hot or cool drinks. In interactive adaptation, people make changes to the environment in order to improve their comfort conditions, such as opening a window, turning a thermostat, opening blinds or using fans. However, it is usually unrealistic to apply the interactive adaptation in the public outdoor space to achieve thermal comfort, since the pedestrian has little capacity to modify the environment. In this context, people's responses to outdoor microclimates may be passive in comparison with indoor climates, but they often result in a different use of open space (Eliasson et al., 2007; Thorsson et al., 2004a, 2004b).

### **3.5.3.2 Physiological acclimatization**

Physiological adaptation implies changes in the physiological responses resulting from repeated exposure to a stimulus, leading to a gradual decreased strain from such exposure (Nikolopoulou and Steemers, 2003). Sachdeva et al. (1995) conducted research on 64 males from a hot, tropical region who were asked to stay for eight weeks in Antarctica. All the subjects worked outdoors for 6-8 hours travelling on foot or on snow vehicles, sleeping in unheated huts (temperature 3-4°C higher than ambient temperature). The results were that when they exposed to severe cold stress, they succeeded in acclimatizing to the climate and prevented cold injuries by increasing finger blood flow and maintaining the temperature of their extremities. In contrast, in hot, arid climate zones, the primary physiological response to heat stress is an increased sweating capacity for a given heat load.

### **3.5.3.3 Psychological adaption**

Different people perceive the environment in a different way, and the human response to a physical stimulus depends on the information that people have for a particular situation. Therefore, the thermal perception of a space is influenced by psychological factors that may influence the perception (Nikolopoulou and Steemers, 2003).

- **Naturalness** was described by Griffiths et al. (1987) as an environment free from artificiality; outdoor environments typically have a wide variation in climatic conditions relative to stable indoor conditions, where people can tolerate climate regarding the transience and mobility of the outdoor conditions, and metabolism and clothing have a significant effect (Fahmy et al., 2010).
- **Expectations** reflect what the environment should be like, rather than what it actually is, where people can predict climate conditions and take necessary precautions. For instance, if thermal conditions are in a different pattern to what people have been experiencing over the previous days, this may cause differences in people's sensation votes or even lead to complaints, as the conditions do not meet their recently-formed expectations (Nikolopoulou and Steemers, 2003). This may explain the variation of expectations between seasons, which in many studies in different climates the minimum comfort temperatures vary between seasons (Liz, 2009; Mahmoud, 2011; Cohen et al., 2013).
- **Experience:** it is important to differentiate between two types of experience. The short term one relates to the memory and seems to be responsible for the changes in people's expectations from one day to the next. The long term experience refers to the schemata people have constructed in their minds. People living in different geographical/climatic zones may have different attitudes towards the sun and staying in outdoor spaces (Knez and Thorsson, 2008), and differences in cultural attributes may be related to geographical/climatic zones to a certain extent. In this context, culture may be defined as "the system of information that codes the manner in which people in an organized group, society or nation interact with their social and physical environment" (Reber, 1985). In the same context, many other researchers have already shown that avoidance or acceptance behaviour is influenced by momentary thermal comfort impressions (Whyte, 1980; Gehl, 1987; Givoni et al., 2003; Eliasson et al., 2007; Katschner et al., 2002, Thorsson et al., 2004; Walton et al., 2007).
- **Time of exposure** bears little relation to discomfort if the stressful condition is for a very short time, such as getting out of a warm car to enter a building in winter. However, this is considered to be a very crucial factor for outdoor spaces which people mainly use for recreational and optional activities, and therefore they are exposed to potentially stressful conditions for long periods (Nikolopoulou and Steemers, 2003).

The time people spent in the different sites varies enormously, but the thermal perception of the environment was an important parameter influencing people's decisions on how long to spend in the area depending on their perception of the surroundings. The perceived stressfulness of the outdoor environment may influence their willingness to travel by foot, for instance, rather than by air-conditioned vehicle. Generally, unless exposure to discomfort is threatening for the living organism, people's tolerance of the thermal environment is great (Nikolopoulou and Steemers, 2003).

- **Perceived control** is widely acknowledged to influence thermal sensation. The higher the degree of control over discomfort that an individual has, the wider the variations are in the thermal environment that he/she can tolerate, and the lower the degree of negative emotional responses. People who have the free will to choose their sitting positions outdoors so that the choice is open to them further reinforces this point. It is not important whether they actually moved position eventually; the critical issue is that the choice was available (Nikolopoulou and Steemers, 2003).

Furthermore, the reason that an individual is present in a certain place can also affect thermal sensation. For instance, people become more tolerant when they expose themselves to the conditions willingly, as in the case of playing outdoors, because they are exercising control and exploiting available choices. In contrast, if he/she feels the need to be in a place so he or she is not exercising control, such as travelling to a workplace, this will lead to less tolerance towards their environment due to the absence of personal will against the external factors.

- **Environmental stimulation** is embodied in a wide range of outdoor thermal conditions. Comfortable conditions have been regarded as those where occupants feel neither warm nor cold, where ambient conditions are 'neutral' (McIntyre, 1980). The comfort zone is often expressed as a temperature range around the neutral temperature. However, it is increasingly believed that a variable, rather than fixed, environment is preferred. It is the effect of aesthetic environment values and personal perception that can be improved by solar shelters, orientation or urban trees (Fahmy et al., 2010). A study by Nikolopoulou and Steemers (2003) reported that the majority of the interviewees voted for +1 (warm) not zero for neutrality, as their actual thermal sensation vote, suggesting that people enjoy feeling warm. The most plausible justification seems to be that they see the external environment with the fresh air, the sun

and the wind as invigorating stimulation for the senses, and wish to spend some time there.

### **3.6 Indices for assessing heat stress**

A comfort index is a single value that integrates the effects of the basic parameters in any human thermal environment such that its value will vary with the thermal strain experienced by the individual (Parsons, 2003; Epstein and Moran, 2006). Since the development of the wet-bulb temperature as the first index or single value to measure the heat stress in 1905 by Haldane, a large number of different indices have been created and are in use throughout the world. Table 3.3 lists the most important indices (Epstein and Moran, 2006); however, there are still more than 100 thermal comfort indices (Blazejczyk et al., 2012).

At the beginning, the index estimation was based on the environmental variables combination effects. Later, the effect of metabolic rate and clothing were also taken into account. However, the most significant progress was made only during the last 30 years for developing universal indices which are capable for evaluating both cold and hot conditions (Cohen et al., 2013). Nowadays, thermal comfort indices can be categorized into rational and empirical indices (McIntyre, 1980; Johansson, 2014); the rational indices are based on heat balance equation for its calculations, while the empirical indices account for the objective and subjective strains.

**Table 3-3** Proposed systems for rating heat stress and strain (heat stress indices). Source: Epstein and Moran (2006)

Year	Index	Authors(s)
1905	Wet-bulb temperature (Tw)	Haldane
1916	Katathermometer	Hill et al.
1923	Effective temperature (ET)	Houghton & Yaglou
1929	Equivalent temperature (Teq)	Dufton
1932	Corrected effective temperature (CET)	Vernon & Warner
1937	Operative temperature (OpT)	Winslow et al.
1945	Thermal acceptance ratio (TAR)	Ionides et al.
1945	Index of physiological effect (Ep)	Robinson et al.
1946	Corrected effective temperature (CET)	Bedford
1947	Predicted 4-h sweat rate (P4SR)	McArdel et al.
1948	Resultant temperature (RT)	Missenard et al.
1950	Craig index (I)	Craig
1955	Heat stress index (HIS)	Belding & Hatch
1957	Wet-bulb globe temperature (WBGT)	Yaglou & Minard
1957	Oxford index (WD)	Lind & Hellon
1957	Discomfort index (DI)	Thom
1958	Thermal strain index (TSI)	Lee & Henschel
1959	Discomfort index (DI)	Tennenbaum et al.
1960	Cumulative discomfort index (CumDI)	Tennenbaum et al.
1960	Index of physiological strain (Is)	Hall & Polte
1962	Index of thermal stress (ITS)	Givoni
1966	Heat strain index (corrected) (HSI)	McKarns & Brief
1966	Prediction of heart rate (HR)	Fuller & Brouha
1967	Effective radiant field (ERF)	Gagge et al.
1970	Predicted mean vote (PMV)	Fanger
1970	Threshold limit value (TLV)	
1970	Prescriptive zone	Lind
1971	New effective temperature (ET*)	Gagge et al.
1971	Wet globe temperature (WGT)	Botsford
1971	Humid operative temperature	Nishi & Gagge
1972	Predicted body core temperature	Givoni & Goldman
1972	Skin wettedness	Kerslake
1973	Standard effective temperature (SET)	Gagge et al.
1973	Predicted heart rate	Givoni & Goldman
1978	Skin wettedness	Gonzales et al.
1979	Fighter index of thermal stress (FITS)	Nunneley & Stribley
1981	Effective heat strain index (EHSI)	Kamon & Ryan
1982	Predicted sweat loss (msw)	Shapiro et al.
1985	Required sweating (SWreq)	ISO 7933
1986	Predicted mean vote (modified) (PMV*)	Gagge et al.
1987	Physiological Equivalent Temperature (PET)	Mayer & Höppe
1996	Cumulative heat strain index (CHSI)	Frank et al.
1998	Physiological strain index (PSI)	Moran et al.
1999	Modified discomfort index (MDI)	Moran et al.
2001	Environmental stress index (ESI)	Moran et al.
2005	Wet-bulb dry temperature (WBTD)	Wallace et al.
2005	Relative humidity dry temperature (RHDT)	Wallace et al.

### 3.6.1 Rational indices (steady state assessment)

Rational indices are based on an analysis of the physics of heat transfer by conducting assumptions that people's exposure to an ambient climatic environment has, over time, enabled them to reach thermal equilibrium, based on the heat balance equation of the human body. Table 3.4 shows details of some of the commonly used indices. The Predicted Mean Vote (PMV) is one of the most widely used indices and was developed by Fanger (1970). It predicts the mean thermal response of a large population of people and consists of a seven point scale ranging from hot (+3) to cold (-3). In practice, PMV is also commonly interpreted by the Predicted Percentage Dissatisfied Index (PPD), which is defined as the quantitative prediction of the percentage of thermally dissatisfied people at each PMV value. It is important to note that PMV was originally developed for indoors, but since it has been widely adopted in outdoor thermal comfort studies in which large groups of people are being surveyed (Nikolopoulou et al., 2001; Thorsson et al., 2004; Cheng et al., 2010).

Another rational index is the Physiological Equivalent Temperature (PET) (Mayer and Höppe, 1987), which is defined as the air temperature at which, in a typical indoor setting, the human energy budget is maintained by the skin temperature, core temperature, and sweat rate equal to those under the conditions to be assessed (Höppe, 1999). PET is a temperature dimension index measured in degrees Celsius ( $^{\circ}\text{C}$ ), making its interpretation comprehensible to people without a great deal of knowledge about meteorology. PET is particularly suitable for outdoor thermal comfort analysis in that it translates the evaluation of a complex outdoor climatic environment to a simple indoor scenario on a physiologically equivalent basis that can be easily understood and interpreted. PET has been widely applied in areas with various climatic conditions (Matzarakis et al., 1999; Toudert and Mayer, 2006; Thorsson et al., 2007; Lin, 2009; Cheng et al., 2010).

Both ISO 7730 (2005) and ASHRAE 55 (2010), which were designed for indoor environments, suggest the use of the Predicted Mean Vote (PMV), whereas the German engineering guidelines VDI 3787 (2008), which were developed for use in outdoor environments, suggest the use of PMV and PET. However, existing standards and guidelines have no recommendations on how to calculate the neutral and preferred index temperatures (Johansson et al., 2014).

**Table 3-4** Selected thermal comfort indices (Fanger, 1970; Givoni, 1963; Givoni, 1976; Hoppe, 1999 and Cohen et al., 2013)

Index	Definition
<b>ET*</b> (°C) New Effective Temp.	The temperature of a standard environment ( $TMRT = T_a$ ; $RH = 50\%$ ; $WS < 0.15$ ms <sup>-1</sup> ) in which a subject would experience the same skin wettedness and mean skin temperature as in the actual environment. Limited to low activity and light clothing
<b>SET*</b> (°C) Stand. Effective Temp.	Similar to ET* but with clothing variable. Extends to include a range of activities and clothing levels
<b>OUT_SET*</b> (°C) Out. Stand. Eff. Temp	Similar to SET* but adapted to outdoors by taking into account the solar radiation fluxes. Reference indoor conditions are: $MRT = T_a$ ; $RH = 50\%$ ; $WS = 0.15$ ms <sup>-1</sup>
<b>PMV</b> Predicted Mean Vote	Based on the human heat balance, expresses thermal comfort on a scale from -3 to +3. Clothing and activity are variables
<b>ITS (W)</b> Index of Thermal Stress	Expresses the rate of heat loss (or gain) required for the body to maintain thermal equilibrium under the given environmental and physiological conditions. Under warm conditions, it is calculated as the required rate of sweat secretion, in terms of equivalent latent heat, that is required to provide sufficient evaporative cooling for maintaining such thermal equilibrium
<b>PET</b> (°C) Physiol. Equiv. Temp.	Temperature at which in a typical indoor setting: $MRT = T_a$ ; $VP = 12$ h Pa; $WS = 0.15$ ms <sup>-1</sup> , the heat balance of the human body (light activity, 0.9clo) is maintained with core and skin temperature equal to those under actual conditions
<b>(UTCI)</b> Universal thermal climate index	Intended for outdoors; No information on the clothing insulation level of the surveyed population is required. Reference condition for activity: metabolic rate of 135 W/m <sup>2</sup> and a walking speed of 1.1 m/s (Cohen et al., 2013)

### 3.6.2 Empirical indices (non-steady state assessment)

The problem with steady-state methods is that they cannot effectively account for the dynamic aspects of the course of human thermal adaptation. According to Hoppe (2002), there are no internationally accepted non-steady-state indices for the solution of this problem and the picture remains unchanged today (Chen and Ng, 2012). In general, people seem to accept more extreme thermal stimuli outdoors than they do indoors, due to markedly different expectations, as mentioned under the psychological adaptation section earlier in this chapter. Therefore, the necessity for observed data from field surveys regarding the perception of the subjective human thermal sensation in the outdoor environments has been recognized, so as to provide a broader perspective to assess thermal comfort in urban spaces (Nikolopoulou and Lykoudis, 2006; Lin, 2009; Kántor and Égerházi, 2012; Kántor, and Unger, 2012; Cohen et al., 2013). These are what is known as empirical thermal indices, which are derived from multivariable regression models, calculating thermal sensation based on measurements of air temperature, solar radiation, humidity and wind speed (Givoni et al., 2003; Nikolopoulou and Steemers, 2003) with the regression coefficients derived from subjective comfort votes given by respondents. These models have been shown to



accurately predict thermal comfort in a given setting, but they are restricted to the type of environment and climate in which the study took place (Johansson, 2006b).

This understanding has enlarged research on this topic in the last decade. Table 3.5 summarizes previous studies that assessed thermal sensation with different thermal indices. Some of the examinations were tested in empirical studies, while others were simulated experiments or involved questionnaire-based field studies. Although the Universal thermal climate index (UTCI) has recently become very common, the most commonly applied index is the PET, which has been tested in field studies in different climate zones (Gulyas et al., 2006; Johansson and Emmanuel, 2006; Matzarakis et al., 2007; Thorsson et al., 2007). Thus, the physiological equivalent temperature index (PET) (Höppe, 1993, 1999) was chosen for the current research, as it shows some benefits for the outdoor environment over other indices. First, PET was developed by considering the effects of short-wave and long-wave radiation fluxes in outdoor environments on the human energy balance, so it is appropriate for outdoor thermal comfort assessment. Second, PET is already included in German VDI 3787 for a human bio-meteorological evaluation of climate in urban and regional planning. Its validity has been proven in hot/ arid and hot/ humid climates (Spagnolo and De Dear, 2003; Ali-Toudert, 2005; Lin, 2009; Yang et al., 2013). Third, PET can be estimated using software packages such as RayMan, which calculates the PET based on air temperature, air humidity, wind speed, mean radiant temperature, human clothing and activity, in addition to the cloud cover, time of year and surrounding obstacles by calculating the sky view factor. Furthermore, parameters such as albedo, the Bowen ratio of the ground surface and the Linke turbidity of air can also be adjusted using RayMan (Matzarakis et al., 2007; Lin et al., 2010). Fourth, PET has been used in urban built-up areas with complex shading patterns and has generated accurate predictions of thermal environments (Matzarakis et al., 1999, 2007; Gulyas et al., 2006; Lin et al., 2006).

**Table 3-5** Summary of studies that assessed thermal sensation with different thermal indices. Modified from Cohen et al. (2013)

Authors	Location	season	Thermal indices	Use of questionnaires (N)
Matzarakis & Mayer, 1996	Freiburg, Germany	Summer	PET	
Nikolopoulou et al., 2001	Cambridge, UK	Spring, Summer & Winter	PMV	1432
Becker et al., 2003	Yotvata, Israel	Summer	PMV	30
Spagnolo & de Dear, 2003	Sydney, Australia	Summer & Winter	TOP, ET*, PET OUT_SET*, PT,	1018
Gomez, Gil, & Jabaloyes, 2004	Valencia, Spain	All year	ID, PE, VINJE, WBGT	1500
Gulyas et al., 2006	Hungary	Summer	PET	No
Johansson & Emmanuel, 2006	Colombo, Sri Lanka	Hot & humid (tropical)	PET	No
Knez & Thorsson, 2006	Göteborg, Sweden, Matsudo, Japan	March & April	PET	106
Nikolopoulou & Lykoudis, 2006	Thessaloniki, Athens, Milan, Freiburg, Kassel, Sheffield, Cambridge	All year	PET, THI, K	9189
Thorsson et al., 2007	Matsudo, Japan	Winter & Spring	PET	1142
Lin & Matzarakis, 2008	Sun Moon Valley, Taiwan	All year	PET	1644
Hussein & Rahaman, 2009	Malaysia	January	PMV, To	375
Lin, 2009	Taichung City, Taiwan	Summer & Winter	PET	505
Shashua-Bar, Pearlmuter, & Erell, 2010	SedeBoker, Israel	Summer	ITS	No
Tseliou et al., 2010	Athens, Thessaloniki, Milan, Fribourg, Cambridge, Sheffield, Kassel	All year	PET, THI, K	9189
Hwang et al., 2011	Taiwan, Huwei	All year	PET	1644
Johansson & Yahia, 2011	Ecuador, Guayaquil	Dry & wet season	PET	537
Novák, 2011		July	UTCI, NET, Humidex, PT(CHMI), HI	Laboratory comparison
Yang, Lau, & Qian, 2011	Shanghai, China	Summer	PET	no
Mahmoud, 2011	Cairo, Egypt	June & December	PET	300
Kántor, Égerházi, et al., 2012 Kántor, Unger, et al., 2012	Szeged, Hungary	Autumn & Spring	PET	967
Schreier et al., 2012	Kiruna, Sweeden, Hamburg, Germany, Messina, Italy	Several years data	UTCI	
Weihls et al., 2012	Germany	Summer & Winter	UTCI	Model work

### 3.7 The mean radiant temperature

The most critical issue in calculating any of the explained outdoor thermal indices is the need for the mean radiant temperature (TMRT), which is defined by ASHRAE (2009) as the uniform temperature of an imaginary black enclosure in which an occupant would exchange the same amount of radiant heat as in the actual non-uniform enclosure. In other words, the TMRT summarizes the effects of all radiant heat fluxes reaching the body. This is why many researchers consider the TMRT as the key variable in evaluating thermal sensation outdoors, especially during warm and sunny weather conditions regardless of the comfort index used (e.g. Mayer and Höppe, 1987; Jendritzky et al., 1990; Mayer, 1993; Spagnolo and De Dear, 2003; Thorsson et al., 2007). However, the calculation of TMRT varies considerably in open spaces compared to indoor situations, and in sunny conditions TMRT can be more than 30°C higher than air temperature as it is subjected to considerable complexities and uncertainties, while in a confined setting of an enclosed room they are approximately equal (Fehrenbach et al., 2001; Thorsson et al., 2007). According to Fanger (1970), the TMRT outdoors can be calculated based on the following equation:

$$T_{mrt} = \left[ 1 / \sigma_B \left( \sum_{i=1}^n E_i F_i + \frac{\alpha_k}{\epsilon_p} \sum_{i=1}^n D_i F_i + \frac{\alpha_k}{\epsilon_p} f_p I \right) \right]^{0.25} \quad (Eq. 3.11)$$

The equation assumes that the entire surroundings of the human body are divided into isothermal surfaces, which have the following properties:

- $E_i$  (Wm<sup>-2</sup>) is the long-wave radiation component ( $E_i = \sigma_B \epsilon_i T_i^4$ )
- $D_i$  (Wm<sup>-2</sup>) is the diffuse and diffusely reflected short-wave radiation component
- $F_i$  is the angle weighting factor
- $I$  (Wm<sup>-2</sup>) is the direct solar radiation impinging normal to the surface
- $f_p$  is the surface projection factor which is a function of the sun height and the body posture,  $\alpha_k$  is the absorption coefficient of the irradiated body surface for short-wave radiation ( $\approx 0.7$ ),  $\epsilon_p$  is the emissivity of the human body ( $\approx 0.97$ ), and  $\sigma_B$  is the Stefan-Boltzmann constant ( $\sigma_B = 5.67 \cdot 10^{-8} \text{ Wm}^{-2}\text{K}^{-4}$ ).

Although the procedure for calculating the angle factor ( $F_i$ ) for simple shapes is given by Fanger (1970), it is still one of the major problems to be calculated if it is divided into several surfaces. For some special cases when the human body is situated on a large flat surface without any horizon obstruction, then the human surrounding will be divided into two spheres, where the ground is the lower one and the sky the upper sphere. The angle factor is set to 0.5 for both spheres (e.g. Jendritzky et al., 1990; Pickup and de Dear, 1999). However, in the case of more complex surface morphology (especially in urban environments), the determination of all relevant radiation fluxes and the individual angle factors are extremely difficult, costly and time consuming.

To overcome all these difficulties, two approaches have been suggested. For urban planners and designers interested in estimating the thermal comfort conditions in different urban spaces, according to ASHRAE (2009), the integral radiation instruments such as the globe thermometer can be used in the case of an existing urban form (Vernon, 1932; Kuehn et al., 1970; de Dear, 1987; Nikolopoulou et al., 1999; Kantor and Under, 2011). The second method, in case of different design scenarios or proposals, is the simulation-based approach using PC software such as RayMan, ENVI-met and SOLWEIG (Bruse, 1999; Toudert, 2005; Thorsson et al., 2007).

The theory of the globe thermometer has been thoroughly explained by Kuehn et al. (1970). Basically, the TMRT is assumed by the globe thermometer to be at equilibrium between the radiation balance and convective heat exchange of the globe (ASHRAE, 2001). It was originally developed for indoor application and was then extended to include outdoor settings (Nikolopoulou et al., 2001). Simply, if the globe temperature, air temperature and air velocity are known, then the TMRT can be calculated according to equation (3.12) given by ASHRAE (2009) with the empirical coefficient as recently refined by Thorsson et al. (2007):

$$T_{mrt} = \left[ (T_g + 273.15)^4 + \frac{1.1 \times 10^8 V_a^{0.6}}{\epsilon_g D^{0.4}} \times (T_g - T_a) \right]^{\frac{1}{4}} - 273.15 \quad (Eq. 3.12)$$

Where ( $T_g$ ) is the globe temperature ( $^{\circ}\text{C}$ ), ( $V_a$ ) is air velocity ( $\text{ms}^{-1}$ ), ( $T_a$ ) is the air temperature ( $^{\circ}\text{C}$ ),  $D$  [mm] is the globe ball diameter, and ( $\epsilon_g$ ) is the emissivity of the sphere (=0.95 for a black globe). The empirical derived parameter  $1.1 \times 10^8$  and the wind exponent ( $V_a^{0.6}$ ) together represent the globe's mean convection coefficient ( $1.1 \times 10^8 V_a^{0.6}$ ).

The second approach of calculating the TMRT by modelling has been recently developed with the aim of simulating the radiation field in outdoor urban context. For instance, the Rayman software (Matzarakis et al., 2000) which models the TMRT, as well as different thermal indices in the urban structure, has shown good results of correlation between the measured and simulated TMRT in certain urban environments (Matzarakis et al., 2000). RayMan divides the 3-dimensional environment into an upper and lower hemisphere with a parting plane between them at 1.1m above the ground, at the height of the weighting centre of a standing human body. By using the software, radiation and thermal comfort conditions can be analysed for complex urban structures and other type of landscapes (Matzarakis et al., 2010). However, the simulations refer

only to one point of the investigated area and do not provide a continuous surface of the obtained values, because it would considerably increase the running time. Such is the case with the 3-dimensional, grid-based ENVI-met model which, on the other hand, models the microclimate including the wind flow, turbulence, temperature, humidity, as well as the TMRT in urban structures, with high spatial (0.5-10m horizontally) and temporal (up to 10s) resolution (Kántor and Under, 2011; Huttner, 2012). The software is based on a three dimensional computational fluid dynamic model and an energy balance model to simulate the surface-plant-air interactions in urban settings for purposes of urban climatology, architecture, urban design and planning (Bruse, 1999, 2006). Both models calculate TMRT at street level (RayMan calculates to one point and ENVI-met to a surface). This is based on Fanger's (1972) concept of dividing the surroundings into many sections (free atmosphere, several building surfaces and the ground surface), for which the direct, diffuse and diffusely reflected short wave and the emitted long wave radiation components are taken into account.

Thorsson et al. (2007) reported a relatively small difference in accuracy between the globe thermometer method and the RayMan simulated TMRT, compared to the more complicated method based on integral radiation measurements and angular factor in estimating outdoor TMRT. However, Katschner and Thorsson (2009) reported a 1°C difference between the TMRT simulated using the ENVI-met software and the TMRT observed from vertical and horizontal measurements and 3°C difference with the globe thermometer.

The main advantage of such models is the possibility of testing the micro-bioclimate effects of different planning scenarios by modifying the dimensions, arrangements, and the radiant properties of the buildings and the vegetation in the model environment (Matzarakis et al., 2007). The TMRT can be easily obtained through the modelling of the available input meteorological parameters, such as air temperature, air humidity, degree of cloud cover, and air clarity (atmospheric turbidity) (Matzarakis et al., 2010). In addition to the atmospheric variables, temporal parameters (day of the year and time of the day) as well as the geographical location must be specified.

### 3.8 Outdoor thermal comfort applications

In order to assess outdoor thermal comfort, there are a number of methodological problems that need to be addressed first, including the following:

- The complicated method of calculating the TMRT based on the integral radiation measurements and angular factors while there is still a lack of validation for other methods, including the globe thermometer and simulation tools for examining different proposal for outdoor spaces
- The lack of validation for available indices to be used outdoors, and the difficult interpretation in respect of people's actual sensations, as some studies have revealed that people living in different geographical or climatic zones may have different attitudes towards the sun and staying outdoor (Thorsson et al., 2007)
- The missing link to urban geometry effects which are important in relation to design. These issues are discussed briefly in the following paragraphs.

Thermal indices applied indoors were extended to outdoors with the assumption that the theory of comfort is also valid outdoors (Spagnolo and de Dear, 2003). However, during the last few years the validity of these outdoor thermal indices has been questioned for two main reasons. The first problem was that the human thermal assessment differs from those predicted and that the indoor setting parameters may not be directly transferable to the outdoor environment (Kenz and Thorsson, 2008); the second problem was related to the interpretation of a comfort index value in a given scale (e.g. a PMV value of + 3 or a PET value of 48°C can at most be interpreted as heat stress, but nothing about the actual degree of discomfort can be drawn with confidence). This difference is mainly related to the distinction between the indoor and the outdoor spaces where the TMRT is almost equal to  $T_a$ , the air movement is weak and the activity mostly sedentary, under indoor conditions, while outdoor the conditions are different due to the large differences in TMRT in space and time, different wind speed, circulations and wide variation in activities. In order to bridge this overlap between outdoor indices and actual thermal sensation, some researchers have focused on redefining the boundaries of the scales of the various indices. These adjustments require calibration that should be carried out using local subjective comfort data (Spagnolo and de Dear, 2003). Different studies (Nikolopoulou and Lykoudis, 2006; Lin and Matzarakis, 2008; Kántor et al., 2012; Cohen et al., 2013) have suggested that

calibration should be carried out using local subjective comfort data conducted from field surveys to provide a broader perspective to assess thermal comfort in urban spaces. Although the general conditions and methods used vary greatly, making any comparison difficult, some common findings still can be drawn.

Spagnolo and de Dear (2003) discussed whether the standards applied indoors are also reliable outdoors, with the main aim of determining the range of a neutral comfort zone outdoors. All relevant meteorological data for comfort were recorded and compared to 1,018 subjective votes of people. The main finding was that the thermal neutrality for outdoor thermal comfort was significantly higher than for indoors (OUT\_SET\* equals 26.2°C versus indoor SET 24°C). This agrees with other studies (de Freitas, 1985; Potter and de Dear, 1999), which have argued that people would prefer slightly warmer conditions, corresponding to a positive value on the ASHRAE seven-point scale, rather than theoretical neutrality. According to Spagnolo and de Dear (2003), people's expectations outdoors are much more variable over space and time since they perceive their lack of control. This suggests a significant widening of the comfort zone for outdoors, and consequently less discomfort than usually interpreted. This led Spagnolo and de Dear (2003) to indicate that indoor standard comfort limits are not directly transferable to the outdoor environment, as the OUT\_SET\* ranging between 23-28°C was found to correspond to the zone of comfort for Sydney, and this is far above the standards adopted indoors. Recently, the lack of control has also been cited to explain the larger tolerance of people in naturally ventilated versus air-conditioned buildings (Brager and de Dear, 1998; Fanger, 2004) and seems to corroborate for outdoors this thesis of increased tolerance in the case of evident lack of control.

The study also conducted a very interesting experiment through calibrating between the most used comfort indices (PMV, PET, OUT\_SET\*, PT, OP, ET\*) and local subjective comfort data. The comparison showed substantial discrepancies between the different indices in the assessment of comfort. PET and OUT\_SET\* seem to provide the closest results (e.g. temperature of neutrality of 24.1°C for OUT\_SET\* vs. 23.4°C with PET), whereas larger differences are found for PT or PMV. However, these results depended on the climate type: the climate of Sydney shows small amplitudes and moderate air temperatures. This does not necessarily reveal how these indices would vary if used for other climate conditions. For instance, a calculation of PET and OUT\_SET\* with the same inputs for extreme hot dry conditions showed that

OUT\_SET\* provides lower values (by 27% less) because of different humidity assumptions (Toudert, 2005).

RUROS project (Rediscovering the Urban Realm and Open Spaces) conducted in a number of European countries agrees with the same results mentioned above (Nikolopoulou and Lykoudis, 2006). The results given on a seven-point scale revealed that thermal sensitivity of the subjects was affected by the adaptation, which usually takes place in different forms such as physical and psychological. Physically, the results proved that there are changes in the clothing insulation and metabolic rate related with the seasonal variation with a tendency for a low metabolic rate activity correlated with the higher air temperature. Psychologically, it was proved that thermal sensation in autumn and spring follows the behaviour of the proceeding season, which is the responsibility of the short-term experience. After the summer, a warmer temperature was desired in autumn, while in spring a cooler temperature was preferred, after the cold winter. Additionally, the same studies revealed that the perceived choice or control had a very high weight in psychological adaptation for avoiding discomfort as the choice of the sitting place and position or being in the area by one's own choice rather than because of compulsory presence. Thus, the physical parameters alone for the microclimate cannot explain the variation between the objective and subjective comfort evaluation as it accounts for only 50%, while the psychological adaptation accounts for the rest (Nikolopoulou and Steemers, 2003).

The third methodological shortage is related to the missing link to urban geometry effects, which are important in relation to design. According to Toudert (2005), studies directly focusing on the consequences of urban design strategies for comfort are severely lacking and the few conducted studies based on the human bio-meteorological approaches within urban structures have highlighted the major dependences of individual factors (air temperature ( $T_a$ ), vapour pressure (VP), wind velocity ( $v$ ), TMRT) on thermal sensation outdoors (e.g. Mayer and Höpfe, 1987; Jendritzky and Sievers, 1989; Mayer, 1993, 1998). The studies reported a positive relationship between the comfort indices including PMV and PET and the TMRT and  $T_a$ . The TMRT showed a linear relationship with strong correlation ( $R^2 > 0.93$ ) with either PET or PMV. In addition, the interdependence of TMRT and the global irradiation  $G$  was as important ( $R^2 > 0.92$ ), with a clear distinction between irradiated and shaded areas being observed. This highlighted the importance of shading in maintaining thermal comfort outdoors, as



the dominant impact of TMRT reduces as a result of decreasing the radiant heat flux because of the shading. This is why TMRT is considered to be of prime importance in typical hot and sunny summer conditions regardless of the comfort index used (e.g. Mayer and Höppe, 1987; Jendritzky et al., 1990; Mayer, 1993; Spagnolo and De Dear, 2003; Thorsson et al., 2007). Furthermore, a statistical regression between  $T_a$  and PET revealed an exponential relationship, albeit with less positive correlation than that observed for TMRT, certainly because PET experiences contrasting values between exposed and shaded locations. Vapour pressure VP fluctuations were found to have an insignificant impact on PET. Increasing the wind speed leads to a decrease of PET, and yet no strong relationship could be found.

### **3.9 Recent research of outdoor thermal comfort**

However, there is no international standard, which covers outdoor thermal comfort studies (Johansson et al., 2014). In the last decade, and due to the advances in techniques in the fields of urban climatology and biometeorology, detailed studies of microclimatic and thermal comfort have been conducted for various outdoor spaces in different climate regions (Chen and Ng, 2012). Some of these studies have focused on modelling and assessment methods from a thermo physiological perspective (e.g. Hoppe, 2002; Gulyas et al., 2006), whereas others have conducted detailed investigations of the climatic parameters that determined the thermal comfort level of humans (e.g. Spagnolo and De Dear, 2003; Nikolopoulou and Steemers, 2003; Cheng and Ng, 2006). This section provides a comprehensive review of the studies conducted during the last decade in regions with hot, arid climates.

Bourbia and Awbi (2004a and 2004b) investigated a group of buildings and shading in an urban street in the hot, arid climate of the city El-Oued in Algeria. The study conducted a field measurement of air and surface temperature, in addition to a shading simulation model. The authors examined the influence of the street's physical attributes, including aspect ratio (H/W) and sky view factor (SVF), on urban microclimate with particular emphasis on the air and surface temperature. The findings highlighted that the examined parameters (aspect ratio and sky view factor) caused a higher variation on surface temperature compared to air temperature. Accordingly, the authors concluded from the simulation results a number of positive relationships between the urban geometry and the microclimate. These started to be very promising in

developing urban design guidelines for the street dimensions and orientation. Nevertheless, the study only examined the air and surface temperature, excluding all other parameters, and these proved to be of great importance for thermal comfort such as solar radiation, wind velocity and humidity. Additionally, the psychological dimension was ignored in the study, as there was no social survey to assess pedestrians' thermal perception.

Another study was conducted by Ali-Toudert and Mayer (2006). The aim of the experiment was to study the effect of urban geometry, including various street aspect ratio ranging from 0.5 to 4 as well as E-W and N-S orientations, on the outdoor thermal comfort in the hot arid climate of Ghardaia in Algeria. The study was based on field measurement and simulation using the ENVI-met software. The outcomes showed distinctive levels of thermal comfort between the streets of different aspect ratios and between different orientations studied. The air temperature was moderately decreased with the higher aspect ratio (H/W) recording a peak difference of 3 K between the canyons with  $H/W = 4$  and 0.5 around 15:00 LST. It also stated that outdoor thermal comfort is very hard to achieve passively in such hot and dry climate, and yet an improvement is still possible. However, the radiation fluxes expressed by the mean radiant temperature are far more decisive. Therefore, the study concluded that the thermal comfort can be improved through successful shading designs as the key strategy for promoting thermal comfort in hot and dry climate. However, the simulations and field measurements analysis were mainly based on the physical approach, including the human balance model, which failed to include many subjective, social and cultural real world situations (Han, 2007).

Johansson (2006a) studied the influence of urban geometry on outdoor thermal comfort in the hot, dry of climate of Fez, Morocco. The study performed field measurements followed by simulations in summer and winter. The author concluded that, during the summer, a deep canyon with a high aspect ratio was fairly comfortable, while a low aspect ratio canyon was extremely uncomfortable, where day-time air temperature was found to peak for H/W ratios of about 1 while a sharp decrease in air temperature was found for H/W ratios of  $\geq 2$  in summer and for H/W ratios of  $\geq 1$  in winter. The study stated that compact cities with deep canyons are better for hot, arid climates, but in winter, the designers should provide some spaces for solar access. However, the study's results were only based on field measurements and simulations

without including any questionnaire surveys in order to refine the boundaries of the calculated Physiological Equivalent Temperature index (PET).

Pearlmutter et al. (2007) examined heat stress over a summer daily cycle for several aspect ratios of 0.33, 0.66, 1.0 and 2.0 and orientations of different urban canyons in the hot, dry Negev Highlands, south of Israel. The main findings were that thermal stress was progressively reduced as the aspect ratio (H/W) increased in the North-South oriented canyon. This effect was less pronounced as the canyon rotated, until it disappeared in the East-West orientation. However, during the night-time the effect of the large aspect ratio (H/W) was largely reversed, which impeded the long wave radiant heat loss to sky due to the constricted SVF. Compactness thus creates a cooler street environment during the daytime and is warmer at night. The results led the authors to conclude that shade is the dominant factor driving the heat balance equation. Still, the study does not represent the real urban situation since it was conducted in an open air model, while a real urban canyon is more complex and includes irregular building heights, different roof shapes and different surfaces material. Also, the thermal comfort index used names as Index of Thermal Stress (ITS) (Givoni, 1976) was developed under laboratory conditions, which does not represent the real responses of pedestrians outdoors.

Djenane et al. (2008) conducted a study regarding the urban morphology impact on microclimate in the hot, dry area of M'zab Valley in Algeria. The study targeted a solution adapted in terms of occupation modes of the ground and urban morphology in the streets as a direct response to the microclimatic constraints. The experiment compared four locations during the summer time, and each location had different street geometry with aspect ratios varying between 1.6 and 9.7, and plot coverage between 10% and 87%. As in all previous studies, the aspect ratio of the street proved to be of high importance for arid regions, where high H/W ratios (until 9.7) adopted in the desert cities allow a good solar protection of the streets during the day; yet they increase its heating during the night. Moreover, the authors demonstrated that the thermal behaviour for adaptation is related to both the solar exposure and the wind speed with the street level. However, the study was solely based on air temperature and wind speed, which cannot be representative for thermal comfort without examining the solar radiation and mean radiant temperature.

Al Jawabra and Nikolopoulou (2009) studied the complex relationship between the microclimate and human behaviour in open public spaces in hot, arid climates. In order to represent a variety of users in a similar climatic context, two cities in two different locations were selected: Marrakech in North Africa, and Phoenix in North America. Field surveys involved structured interviews and human activities observations, along with microclimatic field measurements in two sites in Marrakech and three in Phoenix. These were carried out during the summers and winters of 2008 and 2009. The findings revealed that the number of people and activities outdoors are influenced by the solar radiation especially in summer. Also, people from different social backgrounds located in the same climate have different approaches to using outdoor spaces, which highlights the importance of conducting a social survey to account for the 50% variance between objective and subjective comfort evaluation. However, the study only examined the psychological part of thermal comfort without analysing the urban form impact on microclimate.

Bourbia and Boucheriba (2010) examined the urban morphology impact on microclimate in the hot, arid climate of Constantine, Algeria, in summer. A number of field measurements, including air and surface temperatures, were performed at seven sites with aspect ratios between 1 and 4.8 and a sky view factor between 0.076 and 0.58. The study reported a difference of about 3-6°C in air temperature between the urban and its surrounding rural environment. The authors argued that the larger the sky view factor, the higher the air temperatures reported. On the other hand, the higher the H/W ratio, the lower the air and surface temperatures recorded. Nevertheless, the study did not calculate the mean radiant temperatures or use any thermal index to assess the outdoor thermal environment.

Mahmoud (2011) investigated people's thermal comfort in an urban park in the hot, arid climate of Cairo, Egypt. The study was carried out during the summer and winter seasons using field measurements and questionnaires in nine different zones of the urban park. The Physiological Equivalent Temperature (PET) index was calculated at each location. Results demonstrated differences in the PET index among these zones due to different sky view factors (SVF) and wind speed. It also revealed an alteration in human comfort sensation between different landscape zones. The author argued that the comfort range of PET for the urban parks in Cairo is 22-30°C in summer and 21-29°C in winter. However, the study was only conducted in an urban park, so it is still not

representative for other types of urban spaces in Cairo. Therefore, the thermal comfort range which was found in the study may only be valid for urban parks and it is difficult to generalize the results for other types of urban spaces in Cairo.

Middel et al. (2014) investigated the impact of urban form and landscaping type on the microclimate of hot, arid Phoenix in North America. The study's aim was to find an effective urban form and design strategies to improve temperatures during the summer months. They used the three-dimensional microclimate model ENVI-met after validation with the conducted field measurement. Then, ENVI-met modelling used to simulate five different urban forms that represent a realistic cross-section of typical residential neighbourhoods in Phoenix combined with three landscape designs. The air temperature distribution and variation, ventilation, surface temperatures, and shading were the main parameters analyzed in the study. Findings showed that advection is important for the distribution of temperatures within design and that spatial differences in cooling are strongly related to solar radiation and local shading patterns. In mid-afternoon, dense urban forms can create local cool islands. However, the study was purely following the physical approach of mitigating UHI intensity without counting for other aspects such as thermal comfort.

From the studies discussed above, it can be concluded that microclimate has a significant impact on people's outdoor space usage. Temperature and sunlight are shown to be the most significant factors for achieving thermal comfort in hot, arid climates. However, all these studies have used different ways and methods in studying microclimate and thermal comfort. Some studies used only field measurements without social surveys, while others used a thermal comfort index which was developed based on laboratory conditions and therefore does not represent the complex situation of an urban street. A few studied microclimate and thermal comfort in urban parks only, and recently others used pure simulation analysis. Therefore, this review shows that there is no accepted or general framework in the field of microclimate and thermal comfort in hot, dry regions among scholars. However, Chin and Ng (2012) suggested an interesting assessment framework that should work on at least four levels: physical, physiological, psychological, and social/behavioural (Fig. 3.16). This framework should allow the local *microclimatic* condition to be linked with *human sensations* as well as with the *use of space* in both spatial and temporal terms. In other words, static and objective aspects (i.e. physical and physiological characteristics) should be measured and modelled

effectively to provide ‘climatic knowledge,’ and dynamic and subjective aspects (i.e. psychological and social/behavioural characteristics) require comprehensive field interviews and observations to provide ‘human knowledge’ (Chen and Ng, 2012).

Chapter Three: Review of Microclimate and Outdoor thermal comfort

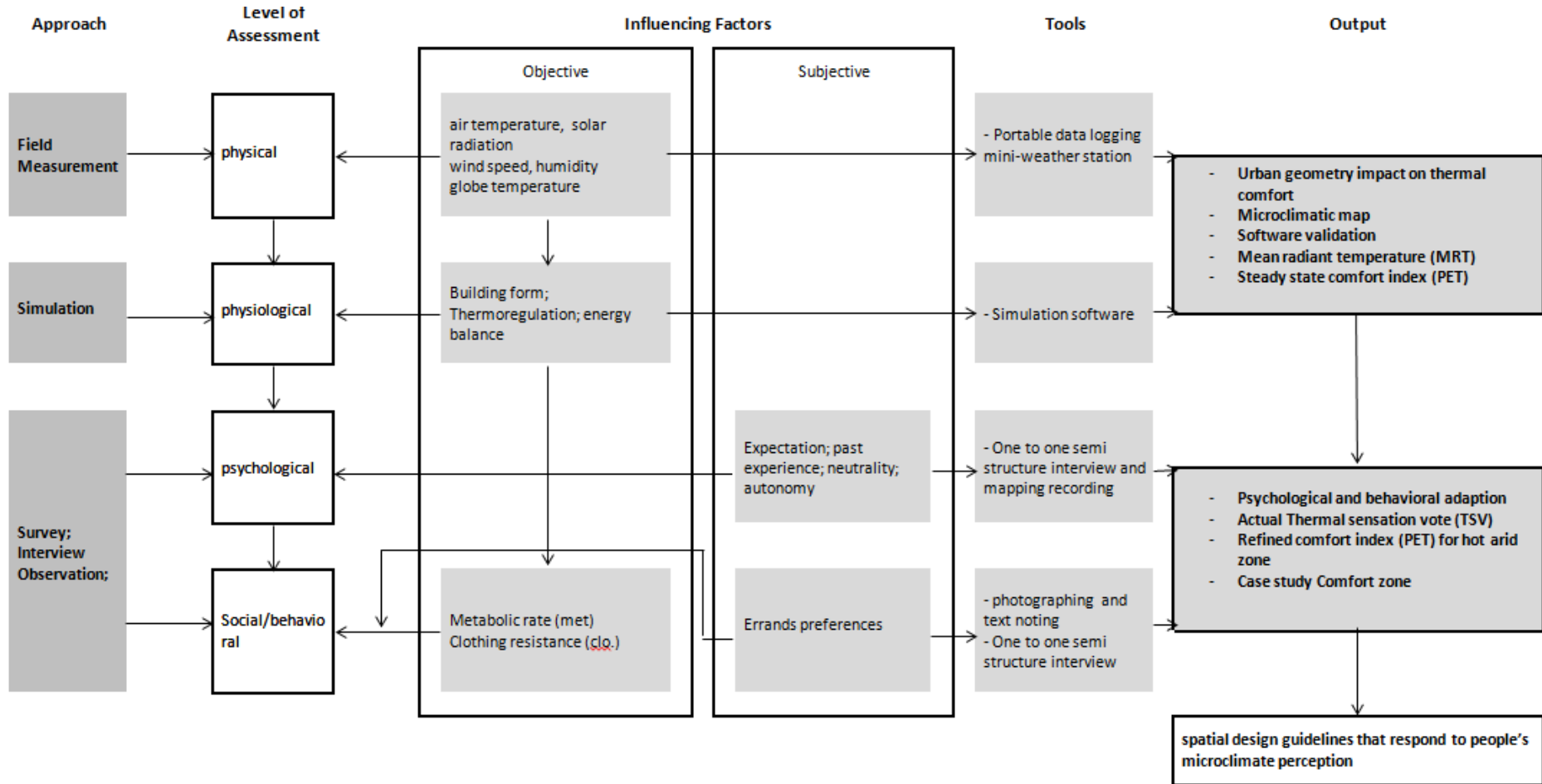


Figure 3-16 Outdoor thermal comfort assessment framework (modified from Chen and Ng, 2012)

### 3.10 Conclusion

Based on Chapter Two, it is clear that cities are warmer than rural areas, especially during night-time, because of the phenomenon known as the UHI effect (Oke, 1987; Voogt, 2004; Velazquez-Lozada et al., 2006, Wong & Jusuf, 2008), which affects human comfort and energy use in buildings (Santamouris, 2007; Ihara et al., 2008; Ewing and Rong, 2008, Radhi et al., 2013). However, the microclimate may vary considerably as a function of the urban design within the urban canopy layer (Givoni 1998; Toudert et al., 2005; Johansson, 2006a; Shishegar, 2013). According to this chapter, the following are concluded:

- Urban microclimate depends both on the type of city in terms of size, geographical location, population size and density, and land use as well as street design features such as height of buildings, street widths and orientation, and subdivision of the building lots. Therefore, the urban design of each neighbourhood in a city creates its own particular local climate (Givoni, 1998; Grimmond et al., 2010; Srivanit and Kazunori, 2011).
- In this respect, the urban street is the element of analysis. Streets are the basic structuring element in the creation of a physical fabric as it appears as the substantial interface between urban and architectural scales. The physical features of the street canyon can climatically affect both outdoor and indoor environments in terms of solar gain in summer and winter, building surfaces' absorption and reflection of solar radiation, wind speed and direction, and their implications for building passive cooling systems and urban ventilation (Toudert, 2005).
- Consequently, the street structure affects the thermal sensation of people as well as the global energy consumption of urban buildings. Therefore, integrating the street design with the climatic consideration is, hence, considered a key issue in a global approach to an environmental urban design (e.g. Oke, 1988; Toudert and Bensalem, 2001; Toudert, 2005; Hathway and Sharples 2012; Shishegar, 2013), especially in the era of climate change.
- Previous studies (section 3.9) stating that, shading is the key strategy for promoting thermal comfort in hot and dry climate particularly in summer (e.g. Ali-Toudert and Mayer, 2006; Pearlmutter et al., 2007; Djenane et al., 2008; Al



Jawabra and Nikolopoulou, 2009; Middel et al., 2014), accordingly this can be reached by (1) a judicious choice of aspect ratios and orientation in case of building up a new districts and (2) arranging complementary solutions, e.g. galleries, planting trees, or shading devices on the facades in case of existing areas development such as Al-Muizz street.

- For this reason, any proposed improvement for an urban development has to be investigated referring to, first, its urban background including street features such as urban morphology, orientation, aspect ratio, and sky view factor, as main aspects affecting outdoor and indoor environments and whether it is climate based or not(examined in chapter 5). Second, the environmental stimulus responsible for shaping people's thermal perception and comfort assessment must also be considered, as studies indicate that people living in hot regions have better tolerance for high temperatures compared to those in temperate regions (Karyono, 2000; Feriadi and Wong, 2004; Lin and Matzarakis, 2008). Therefore, thermal comfort scales developed in the temperate regions are not applicable for the case study, and subsequently this opens the door for using local subjective comfort data conducted from field surveys to provide a broader perspective to assess thermal comfort in urban spaces (assessed in chapter 6) (Nikolopoulou and Lykoudis, 2006; Lin and Matzarakis, 2008; Kántor et al., 2012; Cohen et al., 2013).

# 4

---

*“Although the relationship between a city form and its climate has been intuitively understood, intuition cannot predict how specific future buildings will affect climate conditions (Bosselmann, 1998, p.140). While there is still no single comprehensive model that can predict pedestrian comfort in public open spaces, recent advances in urban microclimatology that combine experimental and computational techniques make evaluation of this aspect of a person interaction with the environment more accessible and realistic” (Erell et al., 2011, p.2).*

## **Chapter Four**

---

### **4. Methodology and Operational Framework**

---

#### Key Concepts

- 4.1. Introduction
- 4.2. Research methodology framework
- 4.3. Primary data collection
- 4.4. Field measurement
- 4.5. Questionnaire surveys
- 4.6. Micro-urban performance simulations
- 4.7. Conclusion

## 4.1 Introduction

The thesis's aim is to investigate the outdoor thermal performance of traditional commercial urban streets, with a special emphasis on summer conditions in a hot arid climate, in order to extend pedestrians' outdoor thermal comfort and use of outdoor spaces.

## 4.2 Research Methodology Framework

The study of outdoor thermal comfort is interdisciplinary, as it incorporates phenomena as diverse as meteorology, urban design, and psychology; however, current investigations lack a general framework for assessment (refer to section 3.9.). Therefore, the research methodology was based on generating a comprehensive framework including the four levels known as physical, physiological, psychological, and social/behavioral, using various research strategies compiled in one full research framework, which summarizes the overall processes and procedures employed to achieve the research objectives and goals of the study (Figure 4.1), including the following phases:

- Primary data collection (phase one)
- Field measurements (phase two)
- Questionnaires survey (phase three)
- Micro-urban performance simulation (phase four)

Each of these phases is achieving one or two of the study objectives. However, all these four phases were compiled together systematically to achieve the overall objective number five, as stated in section 1.3, through proposing the guidelines for improving the microclimate and outdoor thermal comfort based on the case study of Al-Muizz street in Cairo. The processes and procedures of each phase and the objective it is going to achieve are explained in details in the following section.

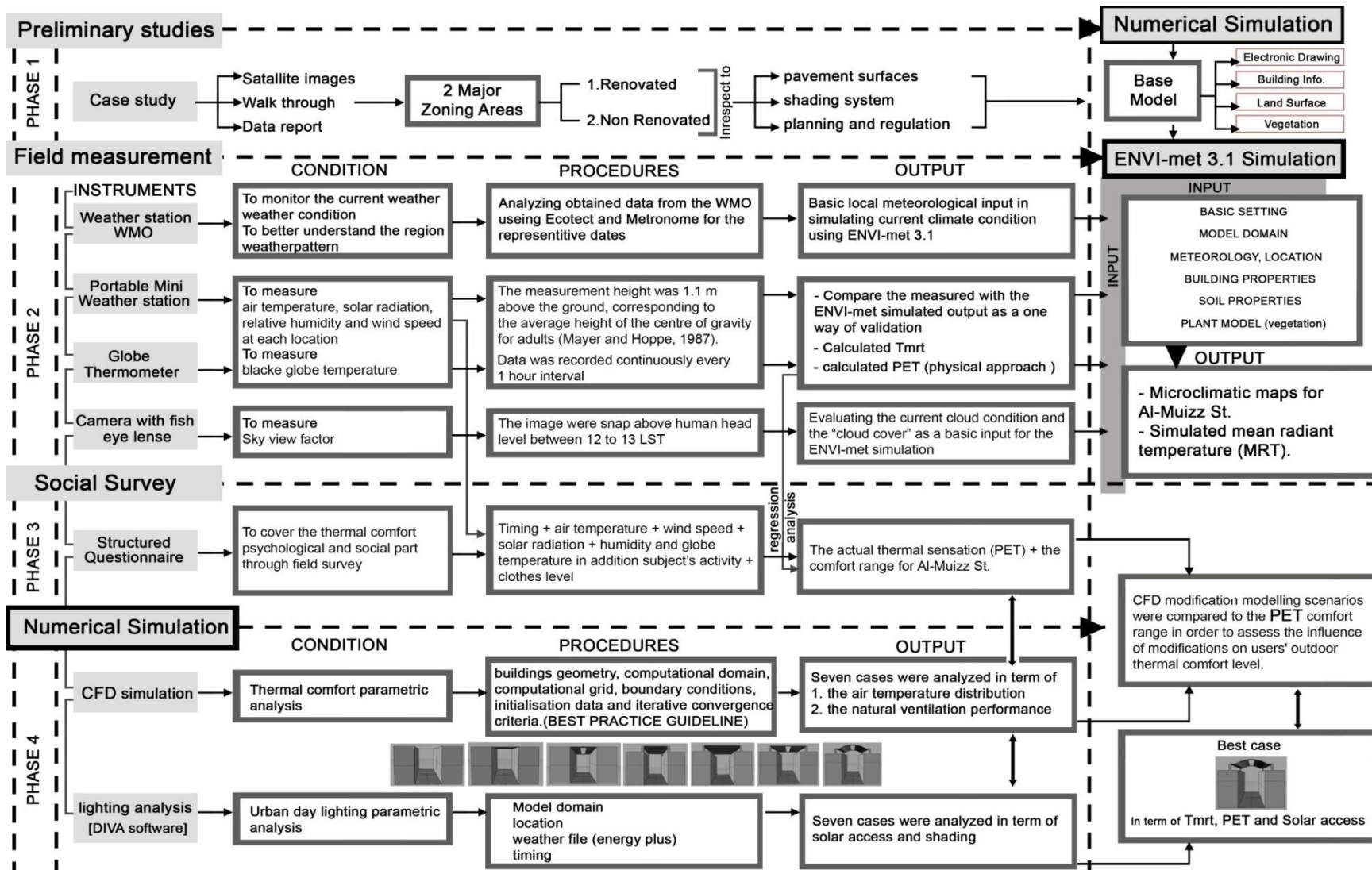


Figure 4-1 Research Methodology Framework

### 4.3 Primary data collection (Phase One)

In phase one, the primary data collection was conducted in order to gather information about the case study, including satellite images, observations, meteorological reports including the weather data, building and electronic documents. Based on this information, a general idea of the current site conditions were generated and Al-Muizz Street was categorized into two major parts, named as renovated and non-renovated (Figure 4.2), the two parts are distinctive in their planning, green and hard surface distribution, and building and urban planning regulations, the characteristics of the two sites are described in Table 4.1. The gathered information was subsequently used in defining the locations and the timing of the study for the following phases through examining the meteorological data and EnergyPlus weather files analyzed by Ecotect analysis 2011.<sup>7</sup>

Based on this phase, summer was chosen as the primary season for the study as it is classified according to the Egyptian energy code as the season when energy consumption peaks in the building sector. Figure 4.3 shows the annual operation profile of electric fans and air conditioners in relation to thermal comfort range in Cairo, which states the high-energy consumption and the long duration of the summer compared to the winter, as the climate is characterized by a hot summer season compared to moderate winter with very little rainfall (Al-Ajmi and Hanby, 2008). Accordingly, the field measurements and the parametric analysis are limited over a week between 26<sup>th</sup> of June and 2<sup>nd</sup> of July, which according to EnergyPlus weather files analysis is the hottest week with the longest daylight duration among the season of 2012. However, only during the questionnaire, the survey was extended to cover extra week in the winter, between 19<sup>th</sup> and 25<sup>th</sup> of December as the shortest daylight duration within the season of

---

<sup>7</sup>Autodesk® Ecotect® Analysis sustainable design software is a comprehensive concept-to-detail sustainable building design tool. Ecotect Analysis offers a wide range of simulation and building energy analysis functionality that can improve the performance of existing buildings and new building designs. Online energy, water, and carbon-emission analysis capabilities integrate with tools that enable you to visualize and simulate a building's performance within the context of its environment.

(<http://usa.autodesk.com/ecotect-analysis/>)

2012, in order to over grab the psychological aspect including peoples’ experience and expectations and to monitor the deviation of their perceptions’ between the two seasons.



Figure 4-2 The two modelling domains and the two measurement points

Table 4-1 The characteristics of Al-Muizz urban canyon studied and their immediate surroundings

Site	General description	Land use	Building	Shaded area	Ground cover (%)	Green (%)
Renovated part	Compact neighbourhood, very close to the old commercial quarter (Khan El-Khalili)	Commercial/residential	Low to 5 floor and over	<5%	Basalt 100%	4.3%
Non-renovated part	Very compact neighbourhood in the heart of the old city. Deep canyon, devoid of vegetation	Commercial with few residential areas	Low to medium rise (2-3 storeys)	55%	Basalt 30% and Road bare ground	1.1%

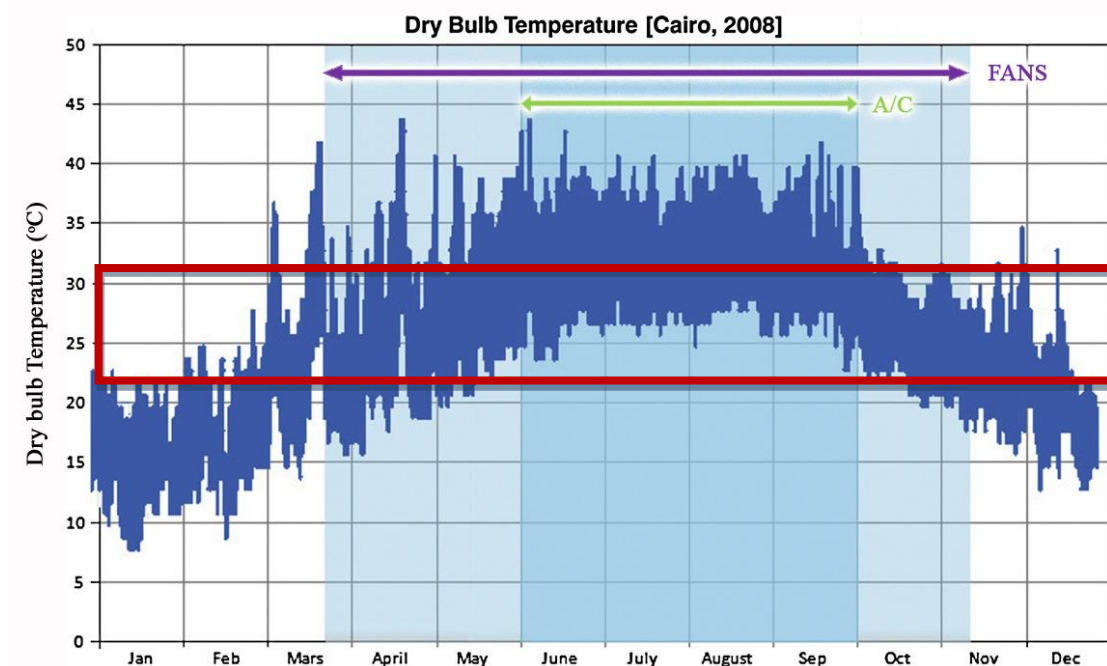


Figure 4-3 Annual fan and air conditioning operation profile in Cairo (Attia et al., 2012) with the PET comfort range.

## 4.4 Field measurements (Phase Two)

In phase two, the main aim was to first explore the link between urbanization and the urban heat island effect phenomenon, second to understand the effect of the urban canyon microclimate and the main surface energy balance (objectives number one and two refer to section 1.3 research aims and objectives). Thus, two field measurement campaigns were carried out in order to map the variations in the microclimate and the outdoor thermal comfort within the street. The first field measurement campaign was undertaken in the two different locations of the street including the renovated and non-renovated part at the same time. The measurements were taken for one week during the summer time with the main aim being to assess the urban heat island (UHI) intensity. Using the meteorological data gathered from the field measurements, a numerical simulation using the ENVI-met 3.1 software was developed. The base model domain was created using the satellite maps, building information, vegetation and ground cover surfaces provided in phase one, while the basic meteorological simulation file was mainly based on the meteorological report from the field measurement. The aim of the numerical simulations was to cover a wider range of urban design, to give the possibility of evaluating the current microclimate situation including the problematic areas. Accordingly, the second field measurements campaign was conducted in the problematic areas including nine different locations along the street for two representative days for a typical hot summer in Cairo; the main aim was to quantify the effect of urban features including aspect ratio, sky view factors and shadings on thermal comfort.

### 4.4.1 First field measurements

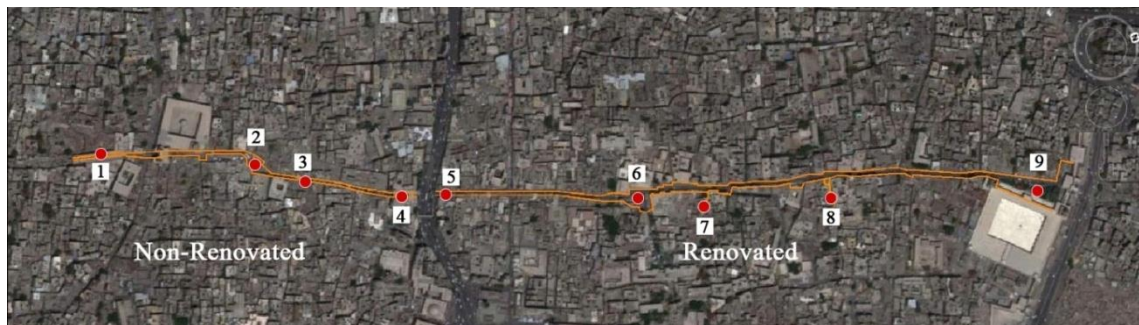
According to the ASHRAE Handbook of Fundamentals (2004, 2009), the four main physical parameters affecting thermal comfort are air temperature ( $T_a$ ), solar radiation ( $W/m^2$ ), relative humidity (RH), and air velocity ( $v_a$ ), in addition to globe temperature ( $T_g$ ) were measured. However, the first field measurements were only performed for the air temperature within Al-Muizz street in the two different locations named previously as the renovated and non-renovated parts over a week in the summer season (figure 4.2), between 26<sup>th</sup> June and 2<sup>nd</sup> July 2012. The outputs were then compared with their temperature obtained from the WMO station No. 623660 located at Cairo International Airport, about 15km North-East of Cairo city centre, at latitude: 30.08, longitude:



31.28 and altitude: 36, to assess the UHI condition in Al-Muizz Street. The other meteorological variables were used as an input to develop a micro-urban performance simulation using the ENVI-met 3.1 software that generated micro-climatic maps for both parts of the street highlighting the problematic locations within the street, which need further analysis for the second field measurements.

#### 4.4.2 Second field measurements

The second field measurements were restricted to only two days 29<sup>th</sup> June and 1<sup>st</sup> July, 2012, which represent the hottest days in the whole week. The field measurements were performed in nine different locations along the street, as shown in figure 4.4, covering the same meteorological parameters measured in the previous field measurements (ASHRAE 2004, 2009). The main output was first to calculate the mean radiant temperature, second to estimate the steady state PET comfort index, third to use the measured values as an input for the simulation programs, and to validate the simulations outputs through comparing with the measured values.



**Figure 4-4** Route with the different measuring points at Al-Muizz Street

#### 4.4.3 The portable weather station adjustments

In order to achieve the field measurement objectives by assessing the main weather parameters at each location point, the Vantage Vue 6250 weather station with a solar radiation sensor, in addition to a Kestrel 4400 heat stress tracker, were used within the spine to collect measurements of the outdoor atmospheric environment.

The sensors are positioned 1.1m above ground level, which corresponds to the average height of the centre of gravity for adults (Mayer and Hoppe, 1987) and at least 1m from the nearest façade, as the temperature and humidity variations within urban canyons have proven to be small except near urban surfaces (Oke, 2004). Figure 4.5 shows the instrument setup for measuring the four basic environmental parameters known to



influence thermal comfort, namely, air temperature, wind speed, humidity and solar radiation. According to the data sheet, presented in table 4.2, the temperature accuracy sensors is ( $\pm 0.5^{\circ}\text{C}$ ), the wind speed accuracy is (1 m/s), the solar radiation range between 0 to 1800 W/m<sup>2</sup> with 5% accuracy of full scale and the humidity accuracy is  $\pm 3\%$  (0 to 90% RH),  $\pm 4\%$  (90 to 100% RH). In addition, globe temperature was calculated using a 25mm black globe thermometer, copper, externally mounted, and calibrated to achieve the same measurements as a standard 150mm globe.



**Figure 4-5** The mobile weather station setup (On the left hand side is the Vantage Vue 6250, while on the right is the Kestrel 4400 heat stress tracker).

**Table 4-2** Davis Vantage Vue 6250 weather station data sheet

<b>Temperature</b>	
<b>Inside Temperature (sensor located in console)</b>	
Resolution and Units	Current Data: 0.1°F or 1°F or 0.1°C or 1°C (user-selectable)
Range	+32° to +140°F (0° to +60°C)
Sensor Accuracy	±1°F (±0.5°C)
Update Interval	1 minute
<b>Outside Temperature (sensor located in ISS)</b>	
Resolution and Units	Current Data: 0.1°F or 1°F or 0.1°C or 1°C (user-selectable) nominal
Range	-40° to +150°F (-40° to +65°C)
Sensor Accuracy	±1°F (±0.5°C) above +20°F (-7°C); ±2°F (±1°C) under +20°F (-7°C)
Radiation Induced Error (Passive Shield)	+4°F (2°C) at solar noon (insolation = 1040 W/m <sup>2</sup> , avg. wind speed ≤ 2 mph (1 m/s)) (reference: RM Young Model 43408 Fan Aspirated Radiation Shield)
Update Interval	10 to 12 seconds
<b>Wind Speed</b>	
Resolution and Units	1 mph, 1 km/h, 0.5 m/s, or 1 knot (user-selectable)
Range	2 to 180 mph, 2 to 156 knots, 1 to 80 m/s, 3 to 290 km/h
Update Interval	Instant Reading: 2.5 to 3 seconds, 10-minute Average: 1 minute
Accuracy	±2 mph (2 kts, 3 km/h, 1 m/s) or ±5%, whichever is greater
<b>Solar Radiation</b>	
Resolution and Units	1 W/m <sup>2</sup>
Range	0 to 1800 W/m <sup>2</sup>
Accuracy	±5% of full scale (Reference: Eppley PSP at 1000 W/m <sup>2</sup> )
Drift	up to ±2% per year
Cosine Response	±3% for angle of incidence from 0° to 75°
Temperature Coefficient	-0.067% per °F (-0.12% per °C); reference temperature = 77°F (25°C)
Update Interval	50 seconds to 1 minute (5 minutes when dark)
<b>Humidity</b>	
<b>Inside Relative Humidity (sensor located in console)</b>	
Resolution and Units	1%
Range	1 to 100% RH
Accuracy	±3% (0 to 90% RH), ±4% (90 to 100% RH)
Update Interval	1 minute
<b>Outside Relative Humidity (sensor located in ISS)</b>	
Resolution and Units	1%
Range	1 to 100% RH
Accuracy	±3% (0 to 90% RH), ±4% (90 to 100% RH)
Temperature Coefficient	0.03% per °F (0.05% per °C), reference 68°F (20°C)
Drift	±0.5% per year
Update Interval	50 seconds to 1 minute

#### 4.5 Questionnaire Surveys (Phase Three)

In phase three, the main aim was to cover the second part of objective number two, which is exploring the effect of urban canyon microclimate on thermal comfort index, through the correlating between the objective PET and the subjective ones so the actual comfort range for the case study is estimated. Then, to fulfil objective number three, the actual comfort range is used to assess between the different proposed modification scenarios generated by the computational fluid dynamics (CFD).

Therefore, and since the actual thermal sensation relies heavily on individual characteristics (Nikolopoulou and Steemers, 2003), an outdoor thermal comfort survey was performed simultaneously while recording the physical measurements and meteorological data in each location. The field surveys were conducted within the two different parts of the street, to evaluate the local people's perception of thermal comfort conditions in the two distinctive outdoor spaces of Al-Muizz. Then, a summary of the users' comfort level perception in the street were analyzed based on the results from the overall field surveys. This helped in calculating the mean radiant temperature and PET as comfort index through the calibrating between the calculated comfort index based on measurements of air temperature, mean radiant temperature, humidity and air velocity with the thermal sensation vote derived from subjective comfort votes given by respondents through using the regression model included in the SPSS software package version 12.0. (For more details, refer to chapter 6).

PET was calculated directly using RayMan software, based on the inputs obtained from the field measurements including air temperature ( $T_a$ ), relative humidity (RH), wind speed ( $v$ ), mean radiant temperature (TMRT), in addition to the subject's clothing value (clo) and metabolic rate acquired from field survey (Matzarakis et al., 2007, 2010). The RayMan model, developed according to Guideline 3787 of the German Engineering Society (VDI, 1998), calculates the radiation flux in simple and complex environments on the basis of various parameters, such as air temperature, humidity, wind velocity, degree of cloud cover, time of day and year, and the albedo of the surrounding surfaces' elevation and location (Cohen et al., 2007). (For more details, refer to section 3.6.2 and 3.7).

#### 4.5.1 Field survey timing and structure

According to ASHRAE (1992), the acceptable temperature range of comfort might be to some extent higher in summer (23-26°C) than in winter (20-23°C). However, studies in different climatic regions have refuted this hypothesis and indicated a wider range of adaptation and tolerance to local conditions where the comfort range may vary from one geographic location to another (Lin and Matzarakis, 2008). Due to this variation between summer and winter, the survey was conducted to cover one week in both seasons as mentioned earlier in phase one. The summer period was the same as the field measurement between 26<sup>th</sup> June and 2<sup>nd</sup> July 2012, while in winter this was between 19<sup>th</sup> and 25<sup>th</sup> December as the shortest daylight period in winter<sup>8</sup>. Then again, in order to cover the climatic variation within the day the survey was conducted three times a day including the morning (8-10), the afternoon (13-15), and the evening at (18-19).

The structured interviews were conducted with respondents who were well acquainted with the area of study; thus, the represented sample was comprised predominantly of local people living or working in the area. In total, 320 structured interviews were conducted (160 in summer and the same in winter, split equally between renovated and non-renovated). The respondents were chosen randomly; both sexes and all age groups were equally represented. Each interview took about 3-5 minutes, and the interviewer recorded the time of the beginning of the interview. Subjects were informed by the author that this survey was voluntary and they had the freedom to accept or reject the survey and that all the data taken for the survey were fully confidential. Subjects were also informed that during the session they were being observed regarding their personal characteristics such as age, clothing and activity. At the beginning of the interview the subject's activity (reclining, sitting, standing, walking), and his/her clothes were recorded and converted into the clo-unit (Spagnolo and de Dear, 2003). The metabolic rate and clothing insulation had to be estimated based on ASHRAE handbook fundamentals (ASHRAE, 2009) (Tables 4.2 and 4.3).

Terminologies used in the questionnaire were translated into Arabic (Appendix C) based on a focus group of four native Arabic speakers researchers in the school of

---

<sup>8</sup>U.S. Department of Energy, 2012  
[http://apps1.eere.energy.gov/buildings/energyplus/cfm/weather\\_data3.cfm/region=1\\_africa\\_wmo\\_region\\_1/country=EGY/cname=Egypt](http://apps1.eere.energy.gov/buildings/energyplus/cfm/weather_data3.cfm/region=1_africa_wmo_region_1/country=EGY/cname=Egypt)

Architecture, Landscape and Planning at Newcastle University. The first part of the questionnaire collected demographic information (e.g. age and sex) and data for activity level, clothing worn and accessories, in addition to the beverage consumption (if the subject was drinking either a hot or soft drink, it was recorded). The second section was concerned with the short-term thermal history, including previous location (indoors/outdoors, sun/shade) prior to arriving at the experimental location, length of time spent outdoors, and then the frequency of presence at the location and reason for being present in order to examine the familiarity with place. The third section asked subjects to rate their current thermal perception and preference. Thermal comfort was rated on the ASHRAE seven point thermal sensation vote (TSV) scale (i.e. -3, cold; -2, cool; -1, slightly cool; 0, neutral; 1, slightly warm; 2, warm; and 3, hot). The McIntyre preference scales (Right now I want to be 'cooler', 'no change' or 'warmer'), directly assessed thermal acceptability (acceptable or unacceptable), and overall thermal comfort (uncomfortable or comfortable). Furthermore, subjects were asked to indicate their level of sensation of and preference for wind and sun on a three point scale with 'I want wind/sun to be weaker', 'no change' and 'I want wind/sun to be stronger'. At the end, the subjects were asked if they had any suggestions or comments, regarding their thermal comfort and microclimate in outdoor spaces.

After the collection of the questionnaires, the investigated thermal sensations according to the ASHRAE seven point scale were respectively compared with calculated PET values from the simultaneous climatic observations as detailed before. Beyond physical conditions, other human factors influencing thermal sensation were examined through responses to the rest of the questions. A multi-variable analysis incorporating these responses, the basic thermal sensation parameter, and the physical metric of PET was then conducted using the SPSS statistical software.

By combining the physical indices based on microclimatic observations and the questionnaire survey, the study examined how the conventional energy balance models can reflect people's thermal sensation in outdoor environments both qualitatively and quantitatively. It is proposed that this methodology and the findings it yields could be helpful to urban planners in developing bioclimatic guidelines for use during the design process.

#### 4.5.2 Metabolic rate (met) and clothing level (clo)

The subject metabolic rate assessment, in addition to the subjects' activity levels, was based on ASHRAE (2009) assumptions (Tables 4.3 and 4.4); however, the subject's metabolic rate was also influenced by food, drink and smoking, and according to Nikolpoulou et al. (2001) the rate changes as follows:

- Cold drink and food –decreased by 10%
- Hot food and drink/ smoking –increased by 5%

Hence, the actual subject's metabolic rate was re-evaluated by the author before further analysis according to their activities and beverage consumption. The clothing level was reviewed by the author according to ASHRAE handbook fundamentals (ASHRAE, 2009).

**Table 4-2** Typical Insulation and Permeation Efficiency Values for Clothing Ensembles (ASHRAE, 2009)

Ensemble Description <sup>a</sup>	$I_{cl}$ , clo	$I_t$ , <sup>b</sup> clo	$f_{cl}$	$i_{cl}$	$i_m$ <sup>b</sup>
Walking shorts, short-sleeved shirt	0.36	1.02	1.10	0.34	0.42
Trousers, short-sleeved shirt	0.57	1.20	1.15	0.36	0.43
Trousers, long-sleeved shirt	0.61	1.21	1.20	0.41	0.45
Same as above, plus suit jacket	0.96	1.54	1.23		
Same as above, plus vest and T-shirt	1.14	1.69	1.32	0.32	0.37
Trousers, long-sleeved shirt, long-sleeved sweater, T-shirt	1.01	1.56	1.28		
Same as above, plus suit jacket and long underwear bottoms	1.30	1.83	1.33		
Sweat pants, sweat shirt	0.74	1.35	1.19	0.41	0.45
Long-sleeved pajama top, long pajama trousers, short 3/4 sleeved robe, slippers (no socks)	0.96	1.50	1.32	0.37	0.41
Knee-length skirt, short-sleeved shirt, panty hose, sandals	0.54	1.10	1.26		
Knee-length skirt, long-sleeved shirt, full slip, panty hose	0.67	1.22	1.29		
Knee-length skirt, long-sleeved shirt, half slip, panty hose, long-sleeved sweater	1.10	1.59	1.46		
Same as above, replace sweater with suit jacket	1.04	1.60	1.30	0.35	0.40
Ankle-length skirt, long-sleeved shirt, suit jacket, panty hose	1.10	1.59	1.46		
Long-sleeved coveralls, T-shirt	0.72	1.30	1.23		
Overalls, long-sleeved shirt, T-shirt	0.89	1.46	1.27	0.35	0.40
Insulated coveralls, long-sleeved thermal underwear, long underwear bottoms	1.37	1.94	1.26	0.35	0.39

**Table 4-3** Typical Metabolic Heat Generation for various activities. Source: ASHRAE (2009)

No.	Activity	Met
1	Sleeping	0.7
2	Reclining	0.8
3	Seated quiet	1.0
4	Standing	1.2
5	Walking	2.0

#### 4.6 Micro-urban performance simulations (Phase Four)

In phase four, the main aim was to fulfill objective number four, which is evaluating the cooling effect of different shading patterns provided by various shading designs, and to predict the optimum cooling potential by comparing Al-Muizz's current conditions and different proposed modification scenarios (refer to section 1.3 research aims and objectives). According to figure 4.6, the main model domain was first simulated using ENVI-met 3.1, in order to generate microclimatic maps for the current situation by highlighting the areas with comfort problems; to analyze the urban morphology impact on microclimate, and to estimate the mean radiant temperature (MRT). Although the results have been validated with the field measurements, it still has some limitations including the underestimation of the long wave radiation by night and the negative consideration for the material heat storage, as explained later in details. Therefore, the computational fluid dynamics (CFD), Fluent code 13.0, was used as it can calculate the heat transfer, air temperature distribution and wind flow simulation through outdoor environment. However, this method is computationally very expensive and almost impossible to perform for a long-period energy simulation, even with the high speed of nowadays supercomputers (Zhang et al., 2013). Therefore, an alternative approach was to couple the CFD program with the building energy simulation (BES). The DesignBuilder<sup>9</sup> software, which is an interface for the whole building energy simulation program named as EnergyPlus, that is capable in calculating solar gains on surfaces, surface temperatures and radiant exchanges (<http://www.designbuilder.co.uk>), was chosen as BES handles the external surface temperature for the main building surrounding the street, while Fluent as CFD simulates the street airflow and air temperature. Such coupling method, which transfers enclosure surface temperatures

<sup>9</sup> DesignBuilder is being explained in details in section 7.4.1



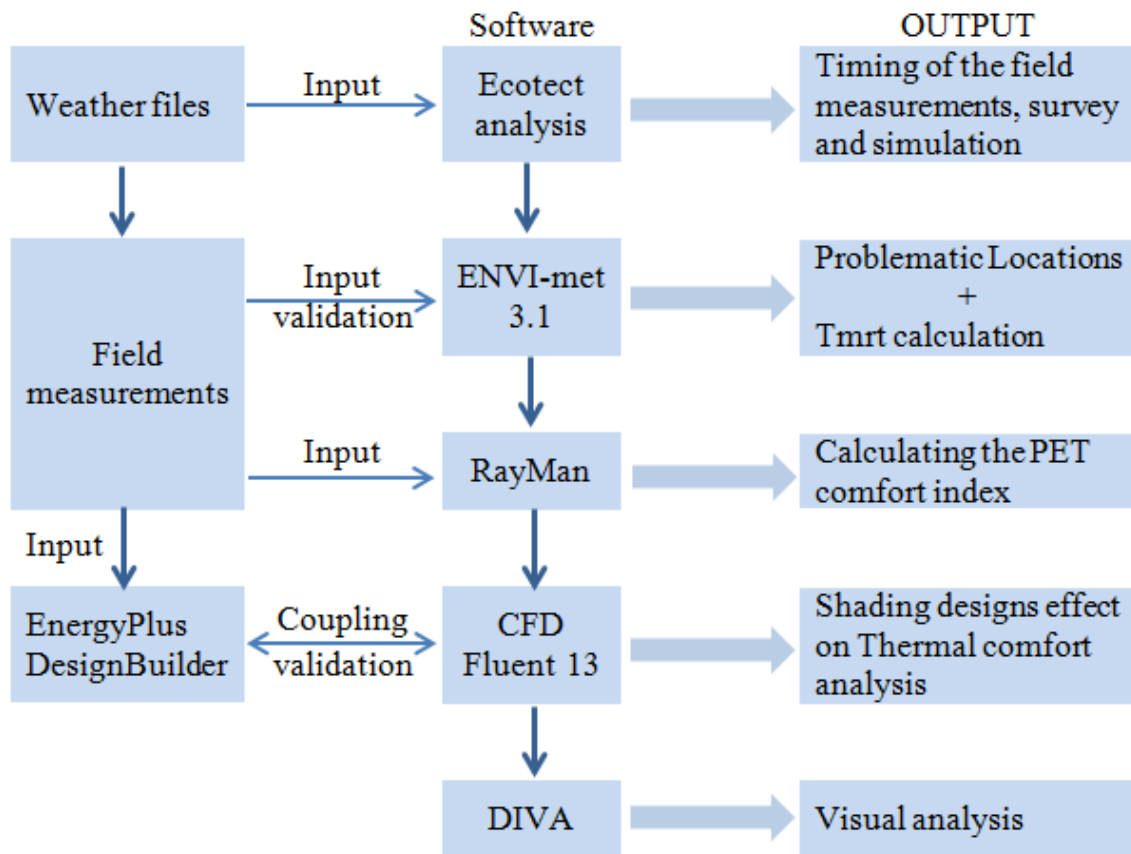
from BES to CFD, is more reliable and efficient than other coupling methods (Zhai and Chen 2003, 2005). The comparative analysis was then performed for the base case in addition to six other different scenarios with different shading patterns. The regular validation was applied through comparing the CFD output with the field measurement values. In confirming the benefit from these modifications, the meteorological outputs from each simulation were used to analyze the impact on the local people's outdoor thermal comfort through the calculation of the mean radiant temperature and the PET comfort index. One of the passive shading systems shortcomings is the reduction of the daylight received underneath, so solar access analysis was performed in order to assure visual comfort and have a complete evaluation for the efficiency of the shading patterns not only thermally but visually as well. Diva for Rhino10 was used to perform a detailed day lighting analysis for each case of the seven scenarios using Radiance/DAYSIM with thermal load simulations and EnergyPlus within. According to Jakubiec and Reinhart (2011), Diva is a powerful tool that can be used on an urban or building scale.

The details regarding the model's relevance to the study, the model general structure, the programme validation and limitation are explained in the following section.

---

<sup>10</sup>Diva for Rhino is a sustainable analysis plugin for the Rhinoceros 3D Nurbs modelling program.





**Figure 4-6** The relation between the different softwares and their outputs

#### 4.6.1 Numerical Models predicting urban microclimate

According to Table (4.5), ENVI-met has the advantage in calculating the mean radiant temperature (TMRT), which, in section 3.7, is considered as a main parameter in assessing people's thermal sensation outdoors under sunny and warm conditions (e.g. Mayer and Höppe, 1987; Jendritzky et al., 1990; Mayer, 1993; Spagnolo and De Dear, 2003; Thorsson et al., 2007). However, the CFD code Fluent 13.0 is better in calculating the heat transfer and wind flow through outdoor environment and both programs are validated in the area of concern whether it is TMRT for ENVI-met or heat transfer and wind flow in the Fluent 13.0. ENVI-met is open access software which is free to download, and can be used on a personal computer or a laptop. On the other hand, an educational version of Fluent Code 13.0 was already provided by the School of Architecture, Planning and Landscape at Newcastle University on a highly configured computer.

**Table 4-4** Comparison between CFD codes that can serve the research scope and the strongly desired features

FEATURES	FLOW 3D (VERSION 3.2)	FLUENT (VERSION 13)	PHOENICS (VERSION 1.6 AND 'FLAIR')	ENVI-MET 3.1
Solution technique	FVM <sup>1</sup> , co-located grid	FVM <sup>1</sup> , co-located grid, multi-grid	FVM <sup>1</sup> , staggered	3D Finite Difference (Incompressible flow)
Dimension	2D, 3D	2D, 3D	2D, 3D	2D graphical user interface, for fabric, vegetation, location and solar path
Coordinate systems	Cartesian, cylindrical polars, BFC	Cartesian, cylindrical polars, BFC	Cartesian, cylindrical polars, BFC	Cartesian coordinates
Mesh type	Structured, multi-block	structured	structured	Structured
geometry and mesh generation	GUI, command language	Menu driven (keyboard)	GUI, PHOENICS input language	Menu driven and input language
Flexibility and boundary condition	Very (command interface or fortran user routines)	Very (command interface or fortran user routines)	Very (command language or fortran user routines)	Very(Open, forced/closed, or cyclic LBC)
transient/ steady	Both	Both	Both	Both
Turbulence model	$k - \epsilon$ , low Re. no. $k - \epsilon$ , ASM <sup>2</sup> , RSM <sup>2</sup> , DSM <sup>4</sup> , Reynolds flux model	$k - \epsilon$ , RSM <sup>2</sup> , RNG <sup>2</sup>	$k - \epsilon$ , $k - l$ , constant eddy viscosity RSM <sup>2</sup> (not available with BFCs)	$k - \epsilon$ model 1.5 order closure, RSM <sup>2</sup> , flux balance model
Natural ventilation	Good	Good	Good	Good
Monitoring and solution (residuals and absolute values)	Yes (graphical using and user-defined monitoring point)	Yes (graphical and numerical)	Yes (graphical using and user-defined monitoring point)	Yes (graphical and numerical)
Computational resources	Only highly configured PC for large models simulations	Super computer for large models simulation	Super computer for large models simulation	Only highly configured PC for large models simulations
Core calculation model	Doesnot include soil, or plant models	Heat transfer and wind flow simulation through outdoor environment. Plants can be coded but without its complete thermal effect	All type of radiant interaction except surface temperature, wind flow and plants but without complete thermal effects, also it doesnot include a soil model	All types of radiant interaction, wind flow, plants, soils and pm10 and gaseous emissions but without considering their thermal effect
Input data	Input formulae and graphical user interface	Input formulae and graphical user interface	Input formulae and graphical user interface	Databases and graphical user interface
output	All meteorological, but not vegetation, soil or TMRT	All meteorological, but not vegetation, soil or TMRT	All meteorological, but not vegetation, soil or TMRT	All meteorological, vegetation and soil parameters and TMRT
validation	Yes	Yes	Yes	Only for radiation, TMRT, RH whereas the package has been used my many research studies
Comfort index	NO	NO	NO	PMV index
Availability	Should be bought <a href="http://www.etasimulation.com/web/html/sales_en.htm">http://www.etasimulation.com/web/html/sales_en.htm</a>	Through the university	Should be bought <a href="http://www.cham.co.uk/default.php">http://www.cham.co.uk/default.php</a>	Freeware: <a href="http://www.ENVImet.com">www.ENVImet.com</a>

(1) FVM = Finite Volume Method (2) ASM – algebraic stress model, RSM – Reynolds stress model, DSM – differential stress model, RNG – renormalisation Group Theory  $k - \epsilon$  Model (3)  $k - \epsilon$  – two equation model of Launder and Spalding (1974)

#### 4.6.2 The numerical model ENVI-met 3.1<sup>11</sup>

Environmental Meteorology or ENVI-met is a computer program that predicts the microclimate in urban areas (Bruse, 2006). According to the developer team, it is defined as “a three dimensional microclimate model designed to simulate the surface-plant-air interactions in urban environment with a typical resolution of 0.5 to 10m in space and 10sec in time. ENVI-met is a prognostic model based on the fundamental laws of fluid dynamics and thermo-dynamics. The model includes the simulation of flow around and between buildings, exchanges processes of heat and vapours at the ground surface and at walls, turbulence, exchange at vegetation and vegetation parameters, bioclimatology, particle dispersion.” (ENVI-met website: [www.envi-met.com](http://www.envi-met.com)).

ENVI-met has almost all the algorithms of a CFD package such as the model Navier Stokes equation for wind flow,  $K - \epsilon$  atmospheric flow turbulence equations, energy and momentum equation and boundary condition parameters (Bruse, 2004; Huttner, 2012). However, as mentioned in the table, it is more developed than a specialist CFD package as it simulates the soil/ plant/ surface/ air relation by applying a numerical model for each (Toudert and Mayer, 2006). It almost has the ability to simulate built environments from the microclimate to local climate scale at any location (Spangenberg, 2008). ENVI-met's combination of bio-meteorological output provides an in-depth understanding of climate urban canopy layer (Fahmy and Sharples, 2010) and better assessment for the outdoor comfort levels based on human biometeorology (Fahmy, 2010). It is one of the very rare software programs where all the factors influencing thermal comfort like wind speed and direction, TMRT, and air temperature are simulated integrally to derive thermal comfort indices, in the case of PMV (Lenzhölzer, 2010). ENVI-met has been frequently used in the literature and has been validated for assessing the built environment (Wong et al, 2007; Ali Toudert and Mayer, 2007a, 2007b; Bourbia and Mansouri, 2008; Fahmy and Sharples, 2009). A comprehensive summary of the model is provided by Ali-Toudert (2005).

---

<sup>11</sup>A comprehensive discussion of ENVI-met 3.1 General structure is available at appendix 'B2'

#### 4.6.2.1 Relevance of ENVI-met to the present study

According to the scope and objectives of the present work, ENVI-met distinguishes itself from other CFD-models through several advantages:

1. it is one of the first models to seek to reproduce the major processes in the atmosphere that affect microclimate on a well-founded physical basis (i.e. the fundamental laws of fluid dynamics and thermodynamics) (Bruse, 1999, 2004)
2. ENVI-met simulates the microclimatic dynamics within a daily cycle. The model is non-stationary and non-hydrostatic and prognoses all exchange processes including wind flow, turbulence, radiation fluxes, temperature and humidity
3. The software is adequately capable for assessing pedestrian thermal comfort, where the key variable for outdoor comfort, i.e. PMV index and mean radiant temperature TMRT, are calculated (Fahmy, 2010)
4. The high spatial resolution (up to 0.5m horizontally) and the high temporal resolution (up to 10s) allow a fine reading of the microclimatic changes, especially sensible to urban geometry and pertinent for comfort issues (Ali Toudert, 2005, 2007)
5. The model requires a limited number of inputs and provides a large number of outputs including calculation and output of mean radiant temperature ( $T_{mrt}$ ), as key variable in outdoor thermal comfort (Ali Toudert and Mayer, 2006)
6. The ENVI-met has a strong advantage over other CFD models through implementing a detailed and sophisticated vegetation model which describes the interaction of local vegetation, not only on the wind field, but also on the thermodynamic processes. This makes the model particularly suitable for a recent research programme initiated by the Air Quality Innovation Project (IPL), founded by the Dutch Ministry for Transport, Public Works and Water Management (Rijkswaterstaat) and the Ministry of Housing, Spatial Planning and the Environment (Ministry of VROM).

#### 4.6.2.2 ENVI-met limitation and validation

The model has a well-founded physical basis and offers many advantages in comparison to many other available urban microclimate models (Toudert, 2005). However, ENVI-met still has a few shortcomings. One of the limitations is that the input parameters for

the initial conditions, which are given at 2,500m height and using a 1D model to create the surrounding environment, are kept constant at 2,500m during the simulation (potential temperature, air humidity, and wind speed). This makes it difficult for some locations where the wind is strongly influenced by the local climate to be simulated. The soil input parameters such as temperature and humidity are kept constant at 1.75m depth. Another limitation is the fact that the indoor temperature of buildings has to be constant during the simulation period. Furthermore, the material heat storage is not taken into account, as the heat stored in the building and transferred through walls and roof is calculated by conducting U-values, while in real cases, each material has its own thermal properties expressed by thermal admittance  $\mu = (KC)^{0.5}$  where ( $K$ ) represents the thermal conductivity and ( $C$ ) represents the heat capacity. Therefore, the lack of heat storage in the ENVI-met leads to the overestimation of the long wave radiation emitted by walls in the daytime, and underestimation by night where no heat can be released after sunset. Based on these limitations, ENVI-met does not perform well in analyzing design interventions, including different surface materials particularly after sunset where the radiated long wave is under estimated. Therefore, the necessity for other software to cover this gap must include CFD or wind tunnel experiments.

#### 4.6.3 The numerical model CFD code Fluent 13.0

Although the wind tunnel can perform the research contribution well through conducting different design interventions. CFD (computational fluid dynamics) has some important advantages compared to wind tunnel testing. Wind tunnel measurements are generally only performed at a few selected points in the urban model, and do not provide a whole image of the flow field. CFD on the other hand provides whole-flow field data, i.e. data on the relevant parameters in all points of the computational domain. Unlike wind tunnel testing using scaled models, CFD does not suffer from potentially incompatible similarity requirements because simulations can be conducted at full scale. This is particularly important for extensive urban areas such as the case study. CFD simulations easily allow parametric studies to evaluate alternative design configurations, especially when the different configurations are all *a priori* embedded within the same computational domain and grid (see e.g. van Hooff and Blocken, 2010a). When it comes to ENVI-met 3.1., the CFD code Fluent 13.0 has the advantage in calculating the heat transfer, air temperature distribution under shades and

wind flow within the micro urban environment. Because of these advantages, CFD is increasingly used to study a wide range of wind environmental problems in urban areas, such as natural ventilation of buildings (e.g. Jiang and Chen, 2002; Evola and Popov, 2006; Chen, 2009; van Hooff and Blocken, 2010a, 2010b; Norton et al., 2010; van Hooff et al., 2011a), convective heat transfer (e.g. Blocken et al., 2009; Defraeye et al., 2010, 2011a, 2011b; Defraeye and Carmeliet, 2010; Karava et al., 2011; Saneinejad et al., 2011), wind energy (e.g. Milashuk and Crane, 2011), and other applications (e.g. Neofytou et al., 2006; Wakes et al., 2010). Thus, the CFD code Fluent 13.0 was chosen in this study due to the variety of the core calculation model compared to other well known codes reviewed in Table 4.4, as it serves the research scope and desired features well.

#### **4.6.3.1 CFD requirements**

CFD requires a large number of decisions to be made by the user, and some of these variables are the approximate equations describing the flow (steady RANS, unsteady RANS (URANS), LES or hybrid URANS/LES), the level of detail in the geometrical representation of the buildings, the size of the computational domain, the type and resolution of the computational grid, the boundary conditions, the discretisation schemes, the initialisation data, and the iterative convergence criteria. Care is required in specifying these variables because the output might completely change if the specified variables are wrongly specified (Sørensen and Nielsen, 2003; Blocken et al., 2010). This reinforces the importance of the best practice guideline (BPG) (Blocken et al., 2012) and their integration in the CFD studies. The establishment of these guidelines has been an important step towards more accurate and reliable CFD simulations. According to numerous publications (Casey and Wintergerste, 2000; Menter et al., 2002; Sørensen and Nielsen, 2003; Chen and Zhai, 2004; Franke et al., 2004, 2007, 2011; Wit, 2004; Franke et al., 2007; Blocken et al., 2012), these guidelines address the five main categories, including: defining the physical model, the geometry of the studied problem, the computational domain dimensions, the computational domain boundary conditions, and the computational mesh. These are explained in Table 4.6, which will be explicitly included in the framework presented by Blocken et al., (2012), as shown in Figure 4.7, with the sub-chart in Figure 4.8.

According to the best practice guideline (BPG) flowchart Figure 4.7, there are three different cases where CFD studies are required:

- Case 1: new developments within an existing urban configuration, for which on-site measurements are available or will be conducted
- Case 2: new developments within an existing urban configuration, for which no on-site measurements are available or will be conducted
- Case 3: development of a new urban configuration, for which – evidently – no on-site measurements are available during the design stage.

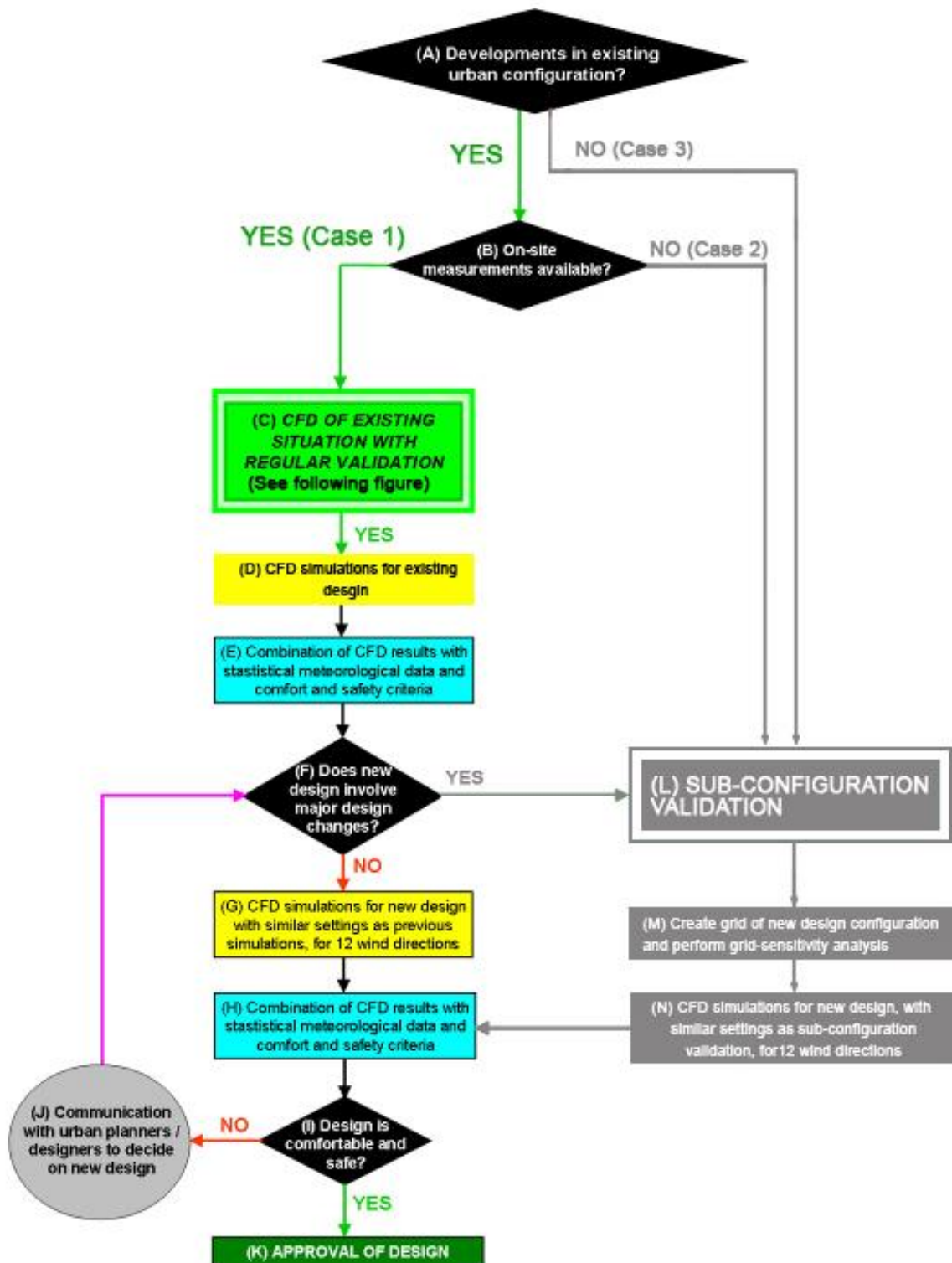
Due to the availability of on-site measurements, as Al-Muizz street is considered a new development within an existing urban configuration (case one), it is therefore recommended for a regular validation using on-site measurement to take place, as indicated by step C in the flowchart, which is further outlined in Figure 4.8. According to Blocken et al., (2012), the on-site measurement validation represents the complex reality without simplifications and is therefore the true validation data for numerical models. During the simulations, one should differentiate between the computational variables and setting that are well described by the BPG and others which are not well defined due to their inherent complexity, as stated in C3 and C4 respectively (Figure 4.8). The domain size, computational grid, boundary conditions, discretisation schemes, algorithms for pressure interpolation and pressure-velocity coupling are all well prescribed by BPG. The extent to which the geometry is reproduced in the model, the choice of the turbulence model and of the type of wall functions are less well prescribed, because it is more difficult to provide general guidelines about these parameters. However, the available best practice guideline's (BPG) information and experience with previous simulations can guide their selection. Based on these variables the first simulation is conducted for the existing urban form for the sake of the validation label (C) in the flowchart (Figure 4.7 and 4.8). This is followed by the grid sensitivity analysis (C4), where simulation on different grids which are coarsened and refined are performed and compared till sufficient grid independence has been established based on the most economical grid. The results on this grid are compared with the on-site measurements (C5). In case inadequate results are obtained, based to some extent on the judgment and expectations of the modeler, increasing the level of geometrical detail of the model and/or selection of another turbulence model and/or

other wall functions is necessary (C7). On the other hand, if the results are considered to be accurate enough (C6), then the simulations can move to the second level by applying it to the different scenarios (step D in Figure 4.7) and subsequently combined with the statistical meteorological data, the terrain-related transformation model, and the comfort and safety criteria (E). This provides the level of wind comfort and safety for the existing urban configuration. When the new developments in this existing urban configuration do not incur major changes, (the term “major” in the urban and building aerodynamics refers to a major changes in the flow field such as the occurrence of a new or additional flow feature that requires additional validation efforts) the same computational parameters and settings can be used for the CFD simulations of this new urban configuration (G-H).

**Table 4-5** Requirements for a consistent CFD simulation (AboHela et al., 2012).

Solution method	Second order schemes or above should be used for solving the algebraic equations
Residuals	in the range of $10^{-4}$ to $10^{-6}$
Mesh	Multi-block structured mesh Carrying out sensitivity analysis with three levels of refinements where the ratio of cells for two consecutive grids should be at least 3.4 Mesh cells to be equidistant while refining the mesh in areas of complex flow phenomena If cells are stretched, a ratio not exceeding 1.3 between two consecutive cells should be maintained
Turbulence model	Realizable k- $\epsilon$ turbulence model
Accuracy of studied buildings	Details of dimension equal to or more than 1m to be included
Domain dimensions	If H is the building height; lateral dimension = 2H+building width Flow direction dimension = 20H+building dimension in flow direction Vertical direction = 6H While maintaining a blockage ratio below 3%
Boundary conditions	Inflow: Horizontally homogenous log law ABL velocity profile Bottom: No-slip wall with standard wall functions Top and side: symmetry Outflow: pressure outlet





**Figure 4-7** Flowchart illustrating the framework for the assessment of pedestrian wind comfort and safety with CFD. Part C is further outlined in Figure 4.8 (after Blocken et al., 2012)

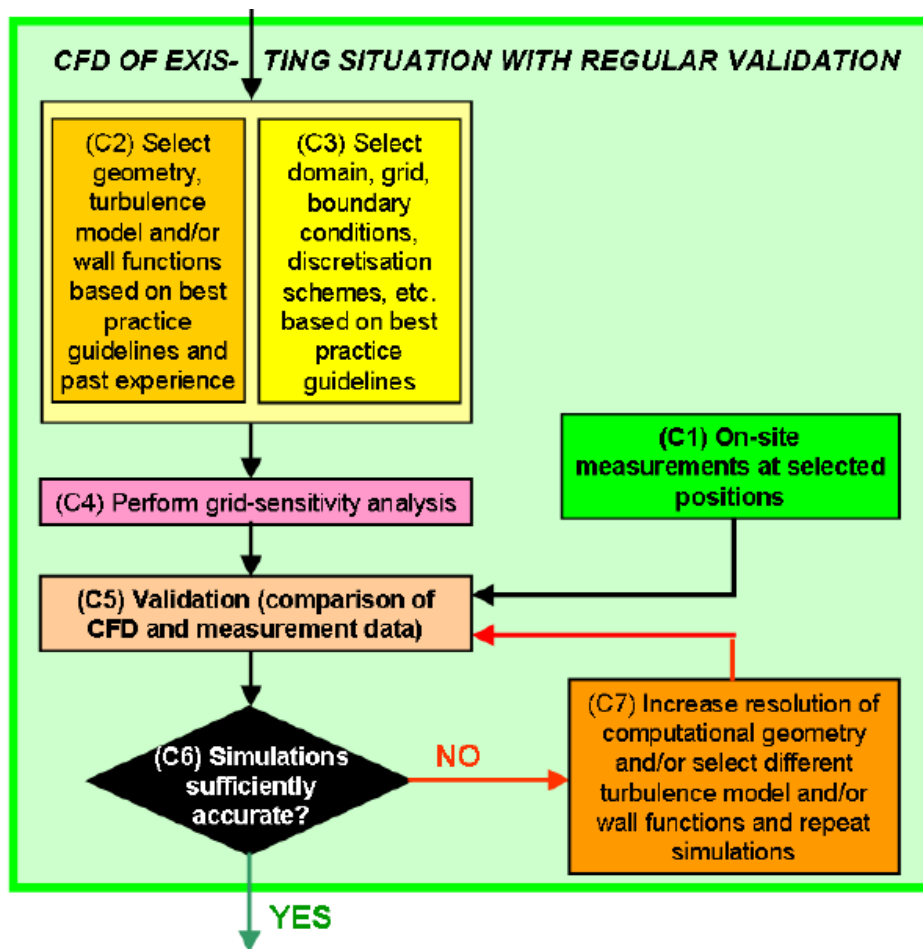


Figure 4-8 Flowchart outlining part C of the large flowchart in Figure 4-7 (Blocken et al., 2012)

#### 4.6.3.2 CFD simulation: Mathematical Model, Geometry and Solution Domain and Boundary Condition

##### The mathematical model adjustments

The turbulent wind flow and temperature distribution around and inside the proposed structures are solved with the 3D steady Reynolds-averaged Navier-Stokes (RANS) equations and the realizable  $k-\varepsilon$  turbulence model as it is a well acknowledged model for wind flow around buildings (Franke et al., 2004; Janssen et al., 2013). The model was developed based on modifying the dissipation rate ( $\varepsilon$ ) equation to satisfy certain mathematical constraints on the normal stresses consistent with the physics of turbulent flows, which is not satisfied by either the standard or the RNG  $k-\varepsilon$  models, makes the realizable model more precise than both models at predicting flows such as separated flows and flows with complex secondary flow features. (Cable 2009; Mollinedo et al., 2013). Blocken et al. (2011) investigated the application of different turbulence models

within the CFD in building performance simulation for the outdoor environment and concluded that the Realizable  $k-\varepsilon$  is the optimum model in terms of yielding consistent results with relatively required low computational power. The model is supplemented with the Boussinesq model for thermal effects. Special attention is given to CFD solution verification by grid-sensitivity analysis and to CFD validation with in-situ measurements. The coupled CFD modelling approach is used to analyze the ventilation rates for the different alternative configurations, which allows the proper calculation of air flow in the proximity of and through the ventilation openings between the outdoor environment and an enclosed or semi-enclosed indoor environment and/or local density differences (buoyancy) (van Hooff and Blocken, 2010). Although the radiation parameter is one of the major factors to be considered in the hot arid region, yet according to van Hooff and Blocken (2010) it does not need to be taken into account if all surface temperatures are imposed inside the model. (Refer to appendix B3, for the detailed mathematical models equations)

### **Computational domain dimension**

The computational domain should be large enough to avoid artificial acceleration of the flow. According to Franke et al. (2007) and Tominaga et al. (2008), the minimum distance from the building to the side, to the inlet and to the top of the domain should be at least five times ( $5H$ ) the tallest building ( $H$ ), and the distance from the building to the outlet should be fifteen times the height ( $H$ ) (figure 4.9). The maximum blockage ratio is equal to 3%, (Franke et al., 2007; Tominaga et al., 2008b), where the blockage is defined as the ratio of the projected area of the building in flow direction to the free cross section of the computational domain.

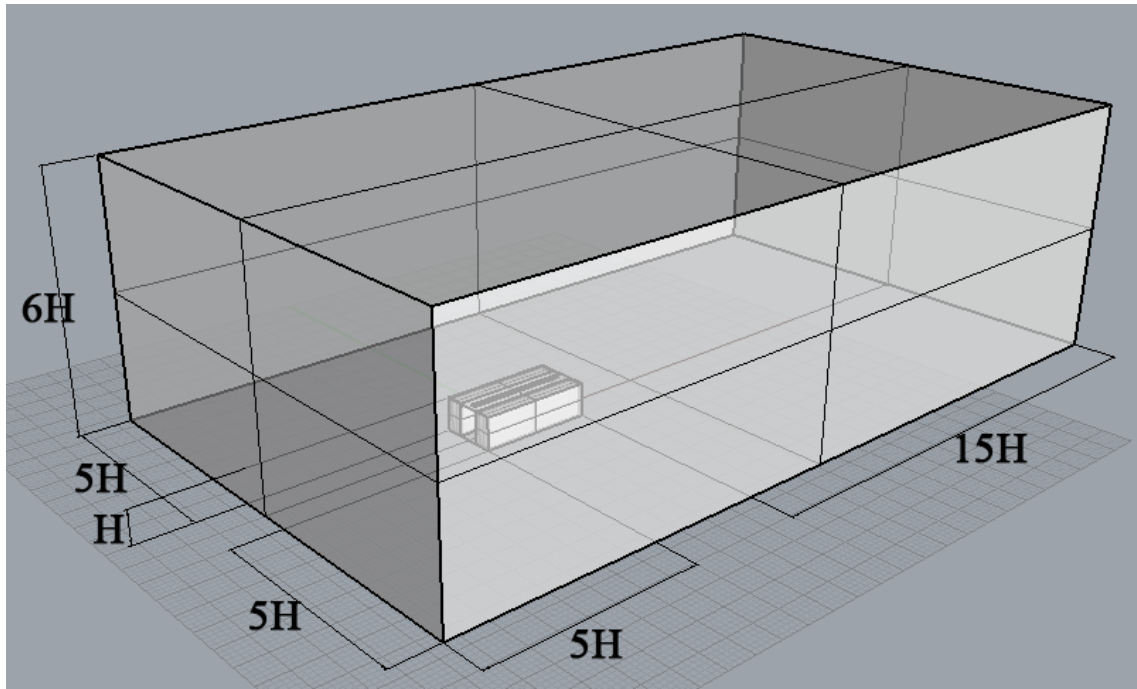


Figure 4-9 Computational domain dimensions for a flow around the model of height H.

### Computational domain boundary condition

The boundary conditions' main function is to simulate the physical quantities in the real flow problem. It consists of five boundaries that need to be assigned to external flow problem as follows:

- The inflow boundary condition: The atmospheric boundary layer (ABL) inflow at the inlet of the domain consists of the profiles of mean wind speed, turbulent kinetic energy and turbulence dissipation rate. According to Blocken et al. (2012), the mean wind speed profile is prescribed by the logarithmic law corresponding to the upwind terrain through the roughness length ( $z_0$ ). According to Jha (2010), the velocity profile can be computed using the logarithmic function described as following:

$$\frac{V(z)}{V(10)} = \frac{\ln\left(\frac{z}{z_0}\right)}{\ln\left(\frac{10}{z_0}\right)} \quad (\text{Eq. 4.1})$$

Where  $V(z)$  is the wind speed at operating height  $z$  (m/sec),  $z_0$  is the roughness length, and  $V(10)$  is the wind speed (m/sec) at a reference height 10m from the ground.

Another important characteristic about the inlet velocity profile is the horizontal homogeneity, which means that the flow variables should not change until the built area is reached (Blocken et al., 2007b; Hargreaves and Wright, 2007). Fulfilling this requirement is explained in the next section.

- At the outflow boundary, the boundary behind the studied area serves as an outlet for all of the fluid to leave the domain, and zero static pressure is specified at the outlet
- At the sides and the top of the domain, symmetry boundary conditions are imposed (i.e. zero normal velocity and gradients), and according to Franke et al. (2007) symmetry boundary conditions enforce a parallel flow at the top and the sides of the domain. This means that the velocity component normal to the boundary, as well as other flow variables, will vanish, and may be different from the inflow boundary profile; thus, the best results can be obtained
- The ground boundary condition of the domain: the standard wall functions by Launder and Spalding (1974) with the sand grain roughness modification by Cebeci and Bradshaw (1977) are used. In order to have an accurate description of the flow near the ground surface, Franke et al. (2007) emphasized that the equivalent sand-grain roughness height  $k_s$  (m) and the roughness constant  $C_s$  need to be in accordance with the aerodynamic roughness length  $z_0$  (m). According to Blocken et al. (2007), for ANSYS Fluent software, this condition is:

$$k_s = \frac{9.793 z_0}{C_s} \quad (Eq. 4.2)$$

The roughness length differs according to the nature of the terrain. The case study of Al-Muizz is considered as roughness length ( $Z_0$ ) of equal 2.0 which is described according to Davenport et al. (2000) for rough country as City centres with mixture of low-rise and high-rise buildings, or large forests of irregular height with many clearings (Table 4.7).

### **Horizontal homogeneity of the atmospheric boundary layer (ABL) profile through the computational domain**

Atmospheric Boundary Layer (ABL), also known as Planetary Boundary Layer (PBL), is the lower part of the Earth's atmosphere and its behaviour is directly influenced by the contact with the Earth's surface. One of the main parameters affecting the reliability of the CFD simulation results is the horizontal homogeneity of the ABL profile, which means the absence of streamwise gradients in the vertical profiles of the mean wind speed and turbulence quantities. This flow type occurs when the vertical mean wind speed and turbulence profiles are in equilibrium with the roughness characteristics of the ground surface.

Fulfilling this requirement, the following wind profile of horizontal velocity( $u$ ), turbulent kinetic energy ( $k$ )and dissipation rate ( $\varepsilon$ )for atmospheric boundary layer flows are widely adopted (Richards, 1989; Harris and Deaves, 1981):

$$U = \frac{u^*}{k} \ln \left( \frac{z+z_0}{z_0} \right) \quad (\text{Eq. 4.3})$$

$$K = \frac{u^{*2}}{\sqrt{C_u}} \quad (\text{Eq. 4.4})$$

$$\varepsilon = \frac{u^{*3}}{k(z+z_0)} \quad (\text{Eq. 4.5})$$

Where ( $u^*$ )is the friction velocity(m/s), ( $k$ ) is the von Kármán constant (= 0.40 or 0.42), ( $C_u$ ) is the turbulence model constant, ( $z$ ) is the height (m) and ( $z_0$ )is the aerodynamic roughness length (m), which is 0.5m or 1.0m depending on the wind direction. It is determined based on the updated Davenport roughness classification (Wieringa, 1992) (Table 4.7).

**Table 4-6** Davenport's classification of effective terrain roughness (Davenport, 2001)

no.	Class		Landscape features
	name	Roughness length: $Z_0$ m	
1	sea	0.0002	Open sea or lake (irrespective of wave size), tidal flat, snow covered flat plain, featureless desert, tarmac and concrete, with a free fetch of several kilometres
2	smooth	0.005	featureless land surface without any noticeable obstacles and with negligible vegetation e.g. beaches, pack ice without large ridges, marsh and snow-covered or fallow open country
3	open	0.03	Level country with low vegetation (e.g. grass) and isolated obstacles with separations of at least 50 obstacle heights e.g. grazing land without windbreaks, heather, moor and tundra, runway area of airport. Ice with ridges across-wind
4	roughly open	0.10	Cultivated or natural area with low crops or plant covers, or moderately opens country with occasional obstacles (e.g. low hedges, isolated low buildings or trees) at relative horizontal distance of at least 20 obstacles heights
5	rough	0.25	Cultivated or natural area with high crops or crops of varying height, and scattered obstacles at relative distances of 12 to 15 obstacles heights for porous objects (e.g. Shelterbelts) or 8 to 12 obstacles heights for low solid objects (e.g. buildings)
6	very rough	0.5	Intensive cultivated landscape with many rather large obstacles groups (large farms, clumps for forest) separated by open spaces of about 8 obstacles heights. Low densely-planted major vegetation like bush land, orchards, young forest. Also, area moderately covered by low buildings with interspaces of 3 to 7 building heights and no high trees
7	closed	1.0	Landscape regularly covered with similar-size large obstacles, with open spaces of the same order magnitude as obstacle heights e.g. mature regular forests, densely built up area without much building height variation
8	chaotic	$\geq 2.0$	City centres with mixture of low-rise and high-rise buildings, or large forests of irregular height with many cleanings

#### 4.6.3.3 Mesh independence test

One of the main factors affecting the quality of a CFD simulation is mesh creation, which is according to Asfour and Gadi (2007) one of the most critical variables to consider for a successful CFD simulation. Therefore, BPG and Blocken (2012) have agreed the importance of carrying out test runs on different mesh sizes and configurations until the solution does not change significantly with the change in mesh sizes and configurations in what is called a mesh independence test (Liaw, 2005; Ariff et al., 2009a; Salim and Cheah, 2009). However, Franke et al. (2007) limited this test to three systematically refined/coarsened meshes. The ratio of cells for two consecutive grids should be at least 3.4, and when this is not applicable due to computational limitations, it is advised to locally refine the mesh in the area of interest or areas where important physical phenomena are likely to occur (Abohela, 2012). Therefore, three meshes with different resolution were used, the first mesh had a resolution of 0.48m around the street model and throughout the rest of the computational domain. The second mesh had a resolution of 0.24m around the street model and 0.48m throughout the rest of the computational domain and the third had had a resolution of 0.12m around the street model and 0.48m throughout the rest of the computational domain. (Refer to section 7.3.1)

#### 4.6.3.4 CFD limitation

One of the factors affecting the choice of the CFD technique is the available computational power. According to the available computational power, one of the Reynolds Average Navier Stokes models (RANS), namely the Realizable  $k-\varepsilon$  turbulence model, has been used to yield reliable results with relatively low computational requirements. However, it should be acknowledged that other techniques such as using Direct Numerical Simulations (DNS), Large Eddy Simulation (LES), Detached Eddy Simulation (DES) or Unsteady RANS, which are known for yielding more consistent results, could have been used if more computational power was available (Abohela, 2012).

Another limitation is the inability of the CFD in the assessment of thermal comfort by developing a comfort index which appropriately reflects the comfort sensation of a person in a given situation (Moonen et al., 2012). However, the physical parameters of the urban microclimate on which the comfort indices are based can be obtained from



measurements (Mayer et al., 2008; Katzscher and Thorsson, 2009), or by means of calculation models based on the simulation outputs (Moonen et al., 2012).

#### 4.6.4 Solar access analysis

In order to have a full evaluation for any street design solution to assure thermal comfort, the design has to assure visual comfort as well. Therefore, DIVA-for-Rhino was used to perform a detailed day lighting analysis for the proposed scenarios. DIVA, which stands for Design Iterate Validate Adapt, is an environmental analysis plugin for the Rhinoceros 3D Nurbs modelling program (McNeal, 2010). DIVA performs a daylight analysis on an existing architectural model via integration with Radiance and DAYSIM (Reinhart et al., 2011). Users of the plug-in can then construct a simple perimeter one-zone volume for energy analysis based on the existing detailed architectural geometry. Schedules generated by the day-lighting analysis are then automatically shared with the energy simulation. This method allows the rapid visualization of daylight and energy consequences from an architectural design model, where users can easily test multiple design variants for daylight and energy performance without manually exporting to multiple soft-wares.

The analyses were based on calculating the amount of incident solar radiation received on the three different surfaces underneath the shading devices including the east and west walls, and the ground surface (energy per area ( $\text{W}/\text{m}^2$ )) annually and during the summer and winter. The output for each scenario was evaluated using the ANSI/ASHRAE/IESNA Standard 90.1-2007<sup>12</sup> for lighting, which states that the lighting power densities for the outdoor sales for open areas including vehicle sales lots should not be less than  $5.4 \text{ W}/\text{m}^2$ .

#### 4.6.5 Pre-simulation procedures

- Overview and understanding of climatic processes of different scales, the subtropical particularities, the natural parameters (such as topography, vegetation etc.) and the urban (man-made) parameters (building density, soil sealing etc.) of the case study areas and their surroundings

---

<sup>12</sup> IESNA is the Illuminating Engineering Society of North America  
ANSI is the approved American National Standard

- Detailed investigation and survey of the case study areas (the simulation models) in particular concerning the soils, detailed information about surface sealing, their materials and albedos, the geometry of the buildings and vegetation. Collection and definition of the environment-referred parameters essential for the ENVI-met input database
- Using the field monitoring (Section 4.4) in order to estimate the reliability of the results and validate the simulations output of the microclimate
- Collection and interpretation of available local climatic data from local meteorological stations, hour-by-hour weather data, which should have been collected during longer periods of time
- Use the climatic data input, based on 30 years of WMO station no. 623660 recorded at Cairo international airport close to the case study mentioned under monitoring dates (Section 4.4)
- Meteonorm 7.0, which is a comprehensive meteorological reference that gives the access to a catalogue of meteorological data for solar applications and system design at any desired location in the world ([www.meteonorm.com](http://www.meteonorm.com)), and Ecotect analysis 2011 were used to calculate the representative dates for field measurement as well as for simulation process out of the weather files gained before in order to generate a typical summer week and a representative winter week day for hot arid regions because thermal cold stress never occurs
- Simulations (go-through) of various “if-what” scenarios, which allow a large number of variations and combinations.

#### 4.6.6 Reliability of data

To test the reliability of the simulation tools and the assumed variables, triangulation of simulation results with the measured values generated from the field measurements (Phase two) were carried out as the empirical validation of the simulation results. Each urban climate conditions is simulated to have meteorological plots at the same certain points of the site measurements. Then, average outdoor meteorology for each case were observed and compared with the modelling output. Subsequently, the results were matched to previous research results using the same software and field measurement techniques presented on research of outdoor thermal comfort. The next chapter on field measurement illustrates and discusses the validity framework of the thesis in detail.

## 4.7 Conclusion

In this chapter, the research methodologies employed have been discussed. Measurement procedures and instrumentation used in field measurement were explained and the monitored dates were justified. Outdoor thermal comfort survey were designed according to the ASHRAE fundamental handbook (2009) in order to correlate the actual human thermal sensation vote gathered through the field survey with the obtained comfort index from the field measurement. In the main modelling process, the general structure of ENVI-met 3.1 and CFD code Fluent 13.0 have been explained in order to define the capability of, and simulation procedures for, the models. As ENVI-met 3.1 was limited in highlighting the areas with discomfort issues and calculating the mean radiant temperature (TMRT) for the current conditions. While, the CFD code Fluent 13.0 is responsible for estimating the heat transfer and wind flow through outdoor environment. Moreover, DIVA-for-Rhino was reviewed in order to examine a full day lighting analysis for the proposed different shading scenarios as stated by ANSI/ASHRAE/IESNA Standard 90.1-2007.

The results of each phase and type of assessment are explained in three subsequent chapters. These chapters are, Chapter Five: The field measurements: Findings and Discussion; Chapter Six: Outdoor Subjective Thermal Comfort: The Questionnaire Survey Findings and Discussion; and Chapter Seven: The numerical assessment: Findings and Discussion.

# 5

---

*“Most (if not all) literature on climate and built environment design assumes climate to be central or even starting point for urban design Olgyay and Olgyay (1963, p.11).*

## **Chapter Five**

---

### **5. The Field Measurements**

The Physical Approach

---

#### Key Concepts

---

- 5.1. Introduction
- 5.2. Cairo climate analysis
- 5.3. Current conditions of air temperature in Al-Muizz Street
- 5.4. Measuring Sites
- 5.5. Result analysis
- 5.6. Thermal comfort analysis (PET)
- 5.7. Validation of ENVI-met model
- 5.8. ENVI-met microclimatic map
- 5.9. Conclusion

## 5.1 Introduction

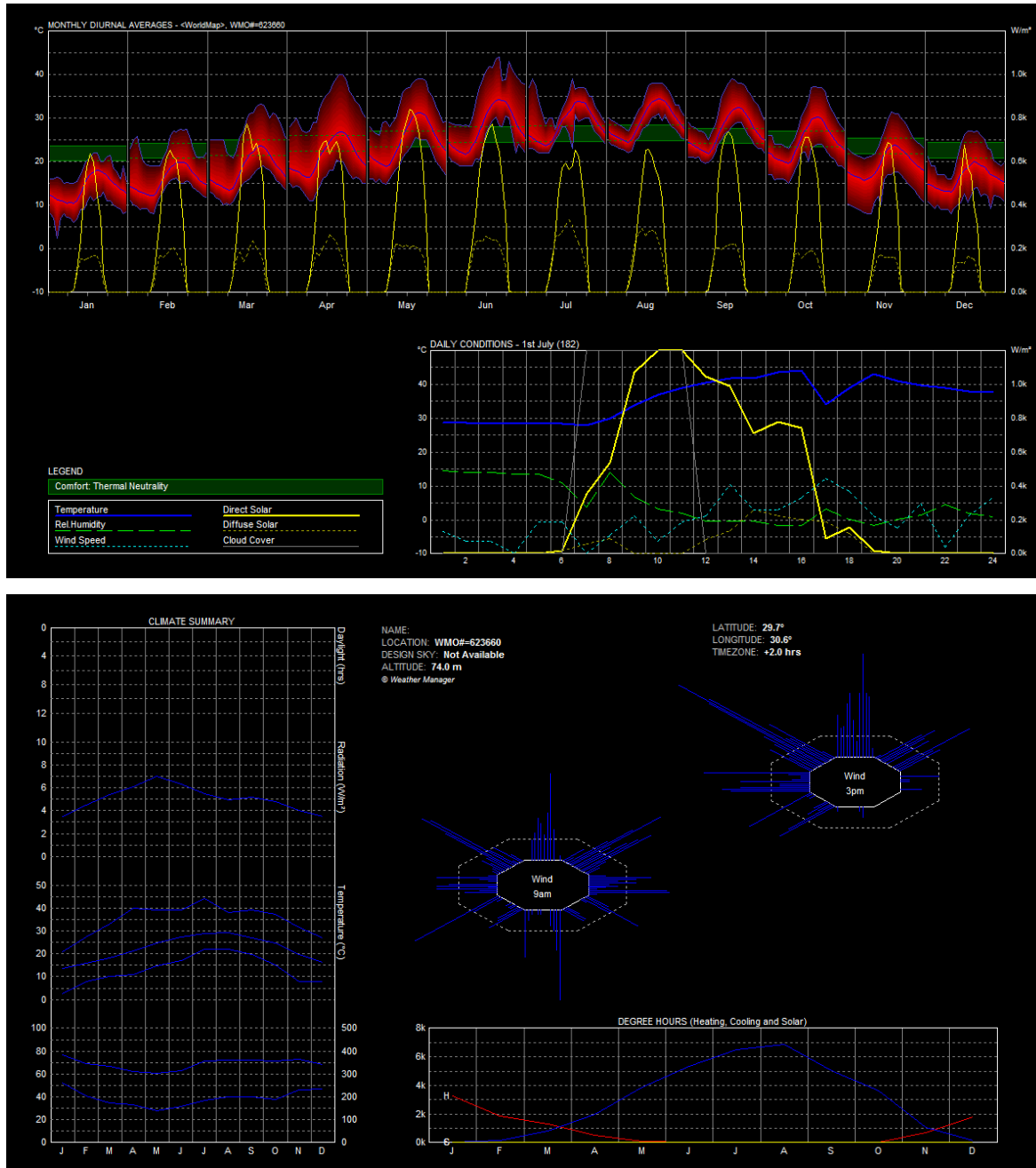
This research interest focuses on the micro-scale climate modifications that take place within the urban canopy layer (UCL), which extends up to the average building height. The microclimate is site specific and varies greatly within short distances (Arnfield, 2003; Oke 2004). This makes the data provided by the standard climate stations (WMO) alone insufficient for examining the street microclimate, as they were designed to monitor the climate within the local scale excluding the micro-scale effect (Erell et al., 2011). Thus, meteorological field measurements were conducted within the UCL of the two parts of Al-Muizz Street, representing the two distinctive urban forms of the renovated and non-renovated parts during the summer period.

This chapter focuses on investigating the effects of urban morphology and design on thermal comfort from a physical approach. Thus, the chapter is divided into three main sections: the first section examines the current condition of air temperature in the street compared to the WMO observed values (micro-scale against local scale) in order to assess the UHI intensity. The second section investigates the microclimate along the street, and the investigation was carried out with a comprehensive field measurement on nine different spots along the path, each with different physical features, and the comfort index (PET) for each location was calculated in order to be correlated with the subjective votes conducted from the survey in the following chapter in order to estimate the actual PET. The third section discusses the computer simulation results, including the microclimatic maps and the validation of ENVI-met model.

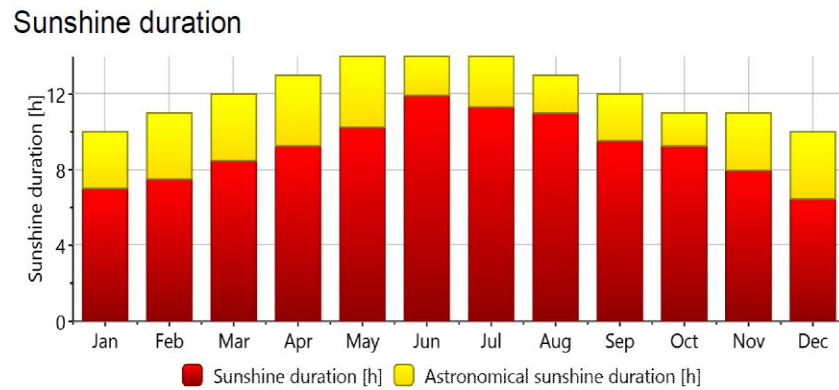
## 5.2 Cairo climate analysis

Based on 30 years of data from the WMO Station no.623660 (Latitude: 30.13, Longitude: 31.4 and Altitude: 64) records at Cairo international airport (U.S. Department of Energy, 2012) were analysed by Meteonorm 7 and Ecotect analysis software (Figure 5.1). The extreme hot week period in 2012 was expected to lie between 26<sup>th</sup> June and 2<sup>nd</sup> July. The maximum average air temperature (Ta) was 44.0°C, and the maximum average summer relative humidity (RH) was 42% and 49% at midday in June and July, respectively. The maximum average wind speed was 3.5m/s in June and July and the maximum average monthly global radiation was 7385, 73196, 6893 Wh/m<sup>2</sup> for May, June and July, respectively. The maximum daily direct solar radiation

was 773 Wh/m<sup>2</sup> on 14th June, and 26th June was the longest diurnal time, at 14 hours and 4 minutes (Figure 5.2).



**Figure 5-1** Cairo monthly average meteorology based on 30 years records of WMO station no. 623660 calculated by Ecotect weather tool. The monthly diurnal average is on the top and shows the four main parameters of air temperature, relative humidity, wind speed and solar radiation. The same parameter for 1<sup>st</sup> July is analysed as well as the climate summary for the whole year on the bottom left side.



**Figure 5-2** The sunshine duration analysis conducted by Meteonorm 7

### 5.3 Current conditions of air temperature in Al-Muizz Street

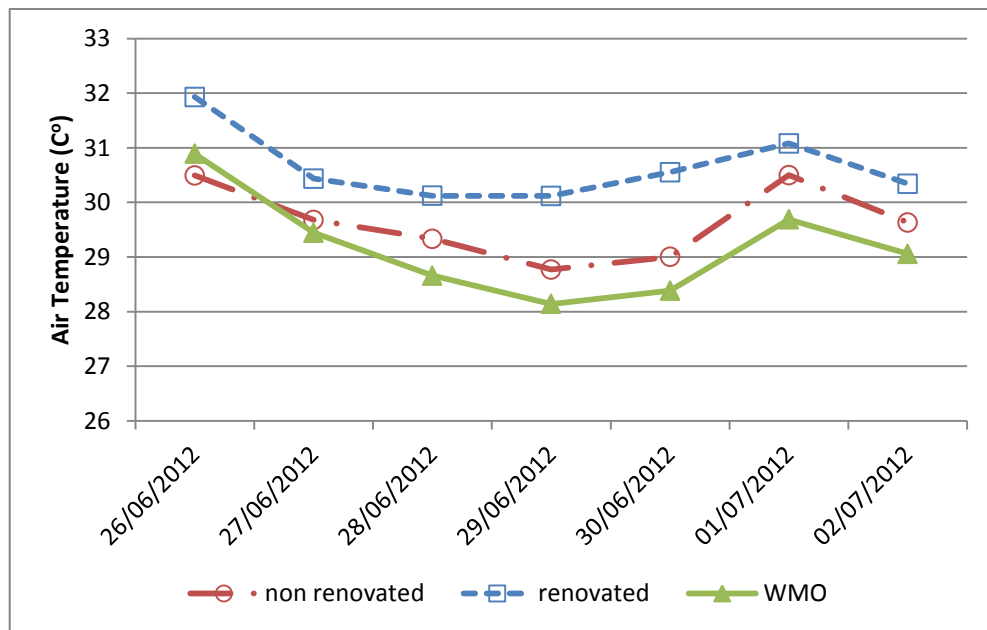
The first field measurements were conducted in two different locations within Al-Muizz street, covering the renovated and the non-renovated part as shown in Figure 5.3. The data were acquired at 60 minute intervals over a period of one week during the summer between 26<sup>th</sup> June to 1<sup>st</sup> July 2012 (refer to section 4.4.1). The main aim was, first, to assess the urban rural air temperature difference (UHI intensity) and, second, to use these as reference points for simulation analysis and validation.



**Figure 5-3** The two locations of the portable weather stations within Al Muizz street, Cairo, Egypt

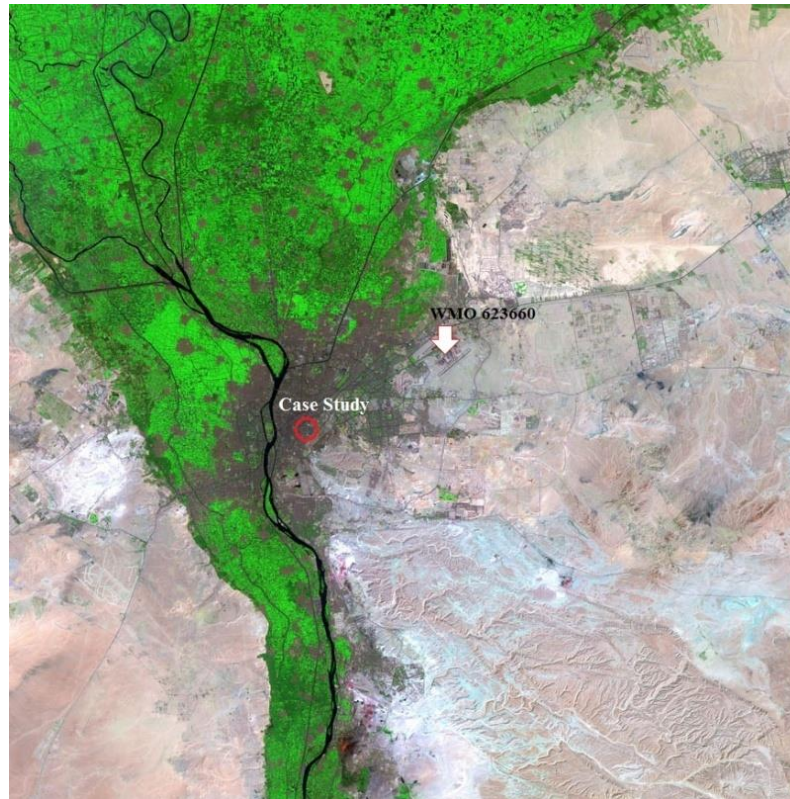
As shown in Figure 5.4, the air temperature observed by the mini weather stations at 1.1m above the ground level were plotted against the reading obtained by the Cairo Airport WMO Station no.623660. The graph reveals a consistent pattern of higher urban temperatures within the urban street compared to the WMO station, as the mean daily temperature for the renovated part of the street has the highest value compared to other readings, as it recorded 30.7°C for the average air temperature compared to 29.6°C for the non-renovated and 29.1°C for the WMO, which is mostly at the bottom of the graph. This indicates the presence of an urban heat island (UHI) in the two parts of the street during the measurement period. Basically, air temperature ( $T_a$ ) within the canyon varies between 23.2°C and 38°C, which is a much wider range in comparison to the average

monthly value for Cairo (22.8°C to 35.5°C) recorded by the WMO at the airport. This may be attributed to the dissimilarity of environmental conditions in both sites. The WMO location is almost outside the city core where the area within 40 km of the station is covered by croplands (55%), grasslands (25%), built-up areas (9%), forests (8%), and lakes and rivers (2%) (Figure 5.5). Al-Muizz's street pattern represents the highest number of hard surface materials, such as buildings and pavements, where the heat release from these surfaces reaches their maximum during the peak hours of daytime. With less vegetation, the sensible heat from hard surface materials which are exposed to the air works to increase the air temperature. Also, the different urban climate scale for both weather stations may also influence the results, as the WMO was designed to monitor at the local city scale (typical scales are one to several kilometres) while the field measurements were conducted within the UCL (typical scales extend from less than one metre to hundreds of metres).



**Figure 5-4** Average air temperature of the two mini weather stations within the UCL and the airport weather station during the week of field measurements

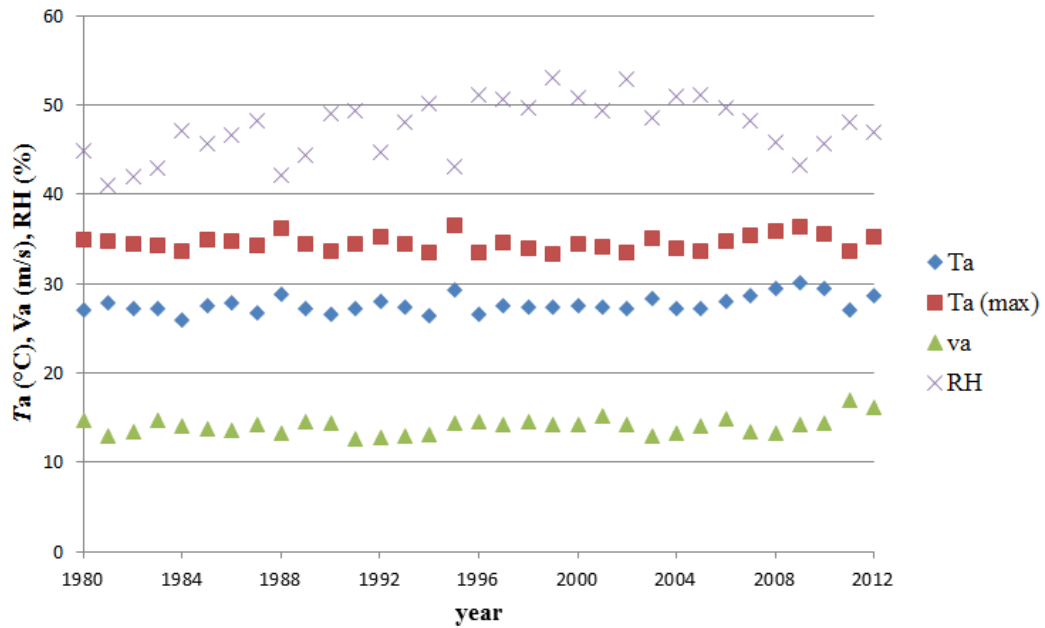




**Figure 5-5** The WMO station location to the case study (the area within 40km of this station is covered by croplands (55%), grasslands (25%), built-up areas (9%), forests (8%), and lakes and rivers (2%))

### 5.3.1 The microclimate in the canyon

The data collected from the WMO Station no.623660 records at Cairo international airport for the last 30 years highlighted the homogeneity of the climatic conditions in the Cairo summer, as shown in Figure 5.6, i.e. hot, sunny and cloudless. Therefore, comprehensive meteorological measurements were carried out on two days (30<sup>th</sup> June and 1<sup>st</sup> July 2012). Although the period of data collection was short, the prevailing conditions on these two days were considered representative of a typical hot summer in Cairo. The physical parameters of air temperature ( $T_a$ ), relative humidity (RH), and air velocity ( $v_a$ ), in addition to globe temperature ( $T_g$ ), was measured using the Kestrel 4400 heat stress tracker at height of 1.1m above the ground, corresponding to the average height of the centre of gravity for adults (Mayer and Hoppe, 1987).



**Figure 5-6** The homogeneity of the climatic conditions in Cairo over a long term period (1980-2012) including the mean values of air temperature (Ta), relative humidity (RH), and wind speed (va) in June at Cairo WMO Station no.623660 at Cairo International Airport

## 5.4 Measuring Sites

Consistent with the objectives of this study, measuring points were selected in nine different locations along the path (four points located in the non-renovated part and the other five located at the renovated one), as shown in Figure 5.7, with various orientations and aspect ratios along the Al-Muizz spine, Cairo, Egypt (Table 5.1). The street is approximately one mile long and follows a grid in its plan with axis oriented 15 degree north-south. The street is flanked by different buildings average heights ranging from five to two storeys. Most parts of the street are narrow, with presence of a number of deep gaps or canyon intersections on both sides. The street surface is made of a mix of basalt and bare ground. More details about the selected measuring sites and its properties are illustrated in Figure 5.8 and Table 5.1.

The meteorological measurements were performed consecutively starting at Point 1 from 6:00 to 24:00 LST (local standard time) and lasting 15minutes on average at each point. The measurements were recorded every three hours for each location.

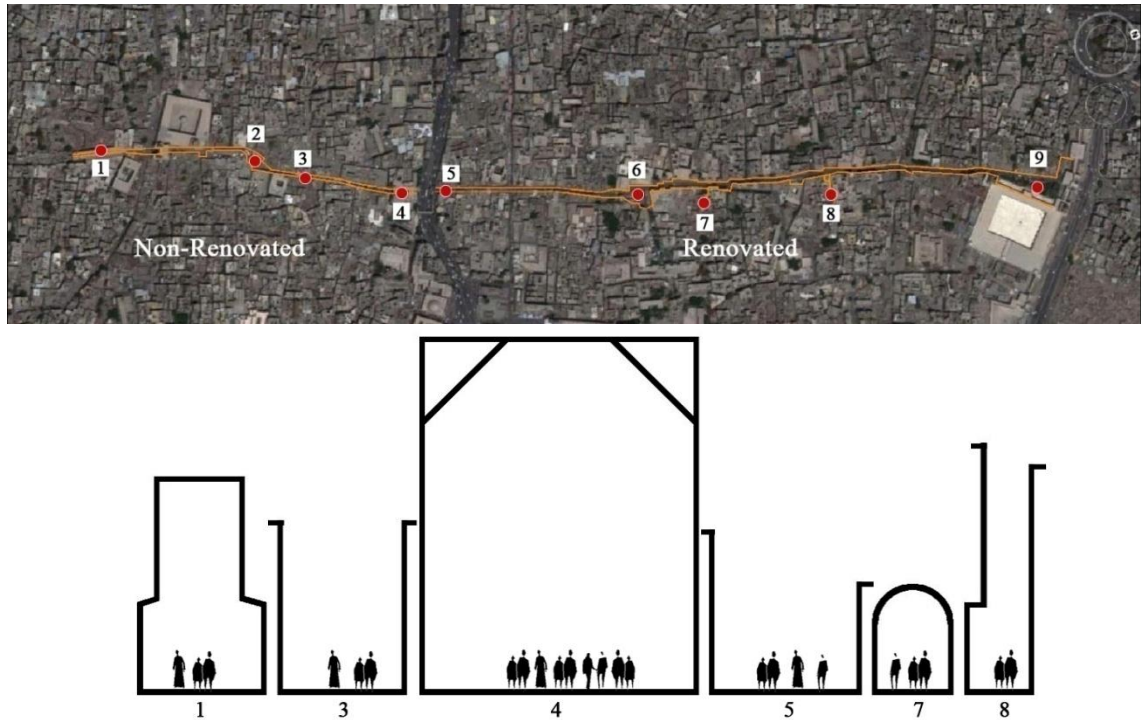


Figure 5-7 Route with the measuring points at different street geometries and at Al-Muizz Street

Table 5-1 Canyon properties at all measuring points in Fatimid Cairo, Egypt

	Points	Street width (m)	Aspect ratio H/W	SVF*	Ground albedo	Ground cover
un-renovated	1	5.00	H/W= 1.8; covered	0.05	0.17	bare ground
	2	unobstructed	H1/W=0.6; H2/W=0.5	0.69	0.17	bare ground
	3	4.80	H/W=1.5; semi covered	0.19	0.17	bare ground
	4	12	H/W=1.5; covered	0.29	0.15	Mix basalt/bare ground
renovated	5	6	H1/W=0.75; H2/W=1.1	0.54	0.11	basalt
	6	unobstructed	H1/W= 2 ;H2/W=2.4	0.81	0.11	basalt
	7	3	H/W=1.3; vault covered	0	0.11	basalt
	8	2.4	H1/W= 3.8 ;H2/W=4.2	0.24	0.11	basalt
	9	unobstructed	H/W=0.2	0.90	0.11	basalt

\*Sky-view factor (SVF) calculated by RayMan (Matzarakis et al., 2000) at the centre of the street



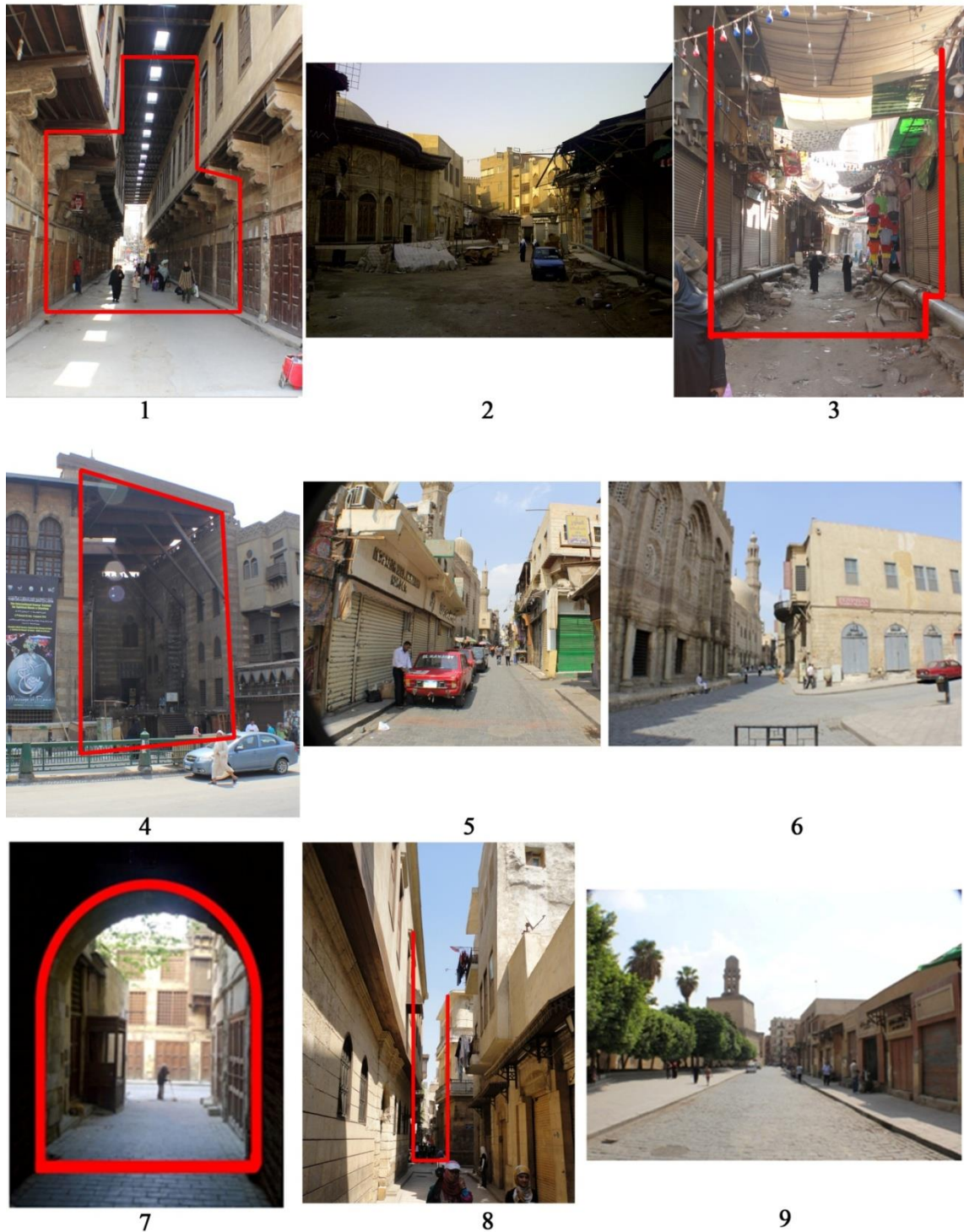


Figure 5-8 Photographs of the nine selected measuring sites

## 5.5 Result Analysis

According to the meteorological data, the two measurement dates of 29<sup>th</sup> June and 1<sup>st</sup> July, 2012 were clear, hot and calm summer days, with a daily mean air temperature of 28.3°C and 29.7°C respectively (maximum 36.6°C and 36.8°C) and a mean wind speed

of 4.47m/s and 5.91m/s. The sun rose at 4:57a.m. and set at 7:00p.m. The solar elevation reached its maximum of  $83.1^\circ$  at 1:00p.m.

### 5.5.1 Air Temperature

Figure 5.9 shows the air temperature ( $T_a$ ) for all the measuring sites which were obtained on 29<sup>th</sup> June and 1<sup>st</sup> July 2012. The highest value of  $T_a$  was recorded around 15:00 LST (local standard time) at the sunlit Point 9, which has the lowest aspect ratio ( $H/W=0.2$ ), reaching  $37.7^\circ\text{C}$  in the first day and  $38.4^\circ\text{C}$  in the second day. According to Emmanuel (2007), as the height to width ratio increases, the maximum daily temperature within the urban canyon decreases.  $T_a$  showed a small difference between the various urban streets in the morning until 9:00 LST. After 10 LST, the disparity in  $T_a$  became larger between the different locations due to the change of the sun path and its elevation angle on the street, which caused an increase in the turbulent transfer of heat induced by the irradiated surfaces (Nakamura and Oke, 1998); accordingly, the difference in  $T_a$  became larger between non-shaded and shaded areas. A peak difference  $\Delta T_a = 3^\circ\text{C}$  was reached between 15:00 and 18:00 LST on both days of measurement. Measuring Points 1, 7 and 8 showed a tendency to be slightly cooler during the day than the others and this can mostly be attributed to their lower exposure to direct solar irradiation (Makaremi et al., 2012). As illustrated in Figures 5.7 and 5.8 and Table 5.1, point 1 is a tent market that is covered by a wooden canopy with some holes in the centre to allow sunlight. Point 7 is a vaulted covered pathway and point 8 is an extremely deep canyon oriented close to E-W with an aspect ratio ( $H1/W=3.8; H2/W=4.2$ ), which allows a longer time of protection from direct solar radiation (Toudert and Mayer, 2005). After 21:00 LST and before reaching 24:00 LST, when  $T_a$  averages  $31.2^\circ\text{C}$  for the measurement days, almost no difference ( $\Delta T_a$ ) was found ( $\leq 1^\circ\text{C}$ ) between all investigated urban locations. Although the unobstructed points 2, 6 and 9 recorded the highest  $T_a$  through the day, they cooled faster, as they lost more than  $9.5^\circ\text{C}$  at midnight in comparison to the other enclosed measuring points. This may be assigned to the high sky view factor (SVF) of these three points which allows a rapid dissipation of heat. According to Oke (1981) and Barring et al. (1985), the low sky view factor delays the cooling surface during clear calm nights. The urban streets have low SVF values and therefore the heat released from the canyon materials is trapped in the canyon air volume (Svensson, 2004). In Japan, Kakon and Nobuo (2009) reported that increasing

SVF by 10% would decrease UHI by 0.3% at night time, and this may explain why points such as 1, 8 and 3 with low SVF were warmer by 1°C and 2°C than point 9 after 21 LST till 3 LST for both days of measurement (Toudert and Mayer, 2005).

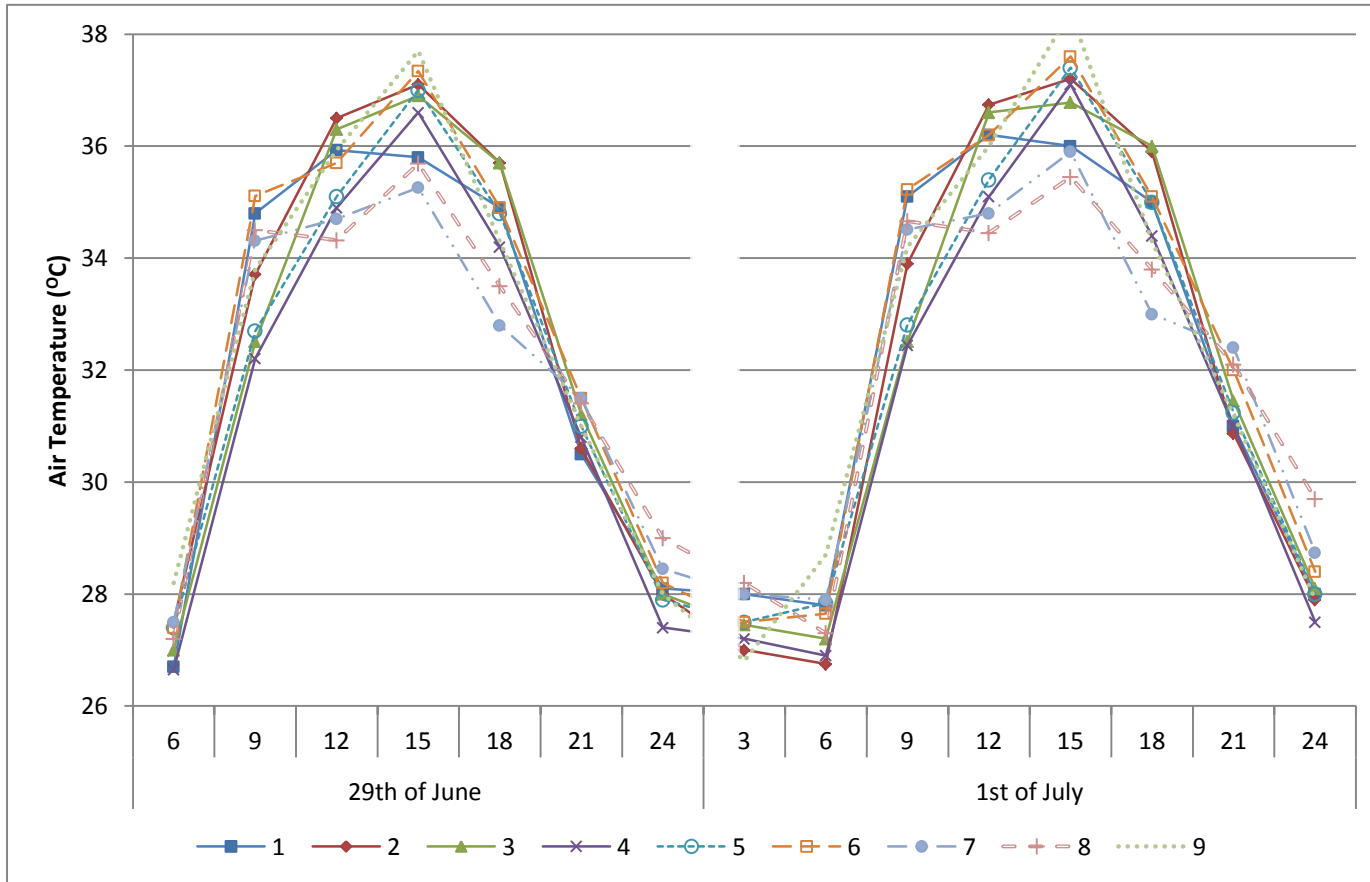
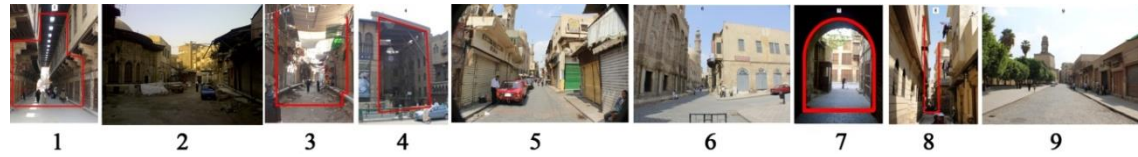


Figure 5-9 The in-situ air temperature ( $T_a$ ) measured during the two summer days measurements

### 5.5.2 Wind speed

Although the two-day measurement campaign included the wind velocity to be used in calculating the mean radiant temperature (TMRT) and PET comfort index, it was not enough to give a comprehensive assessment of the wind flow pattern within the street. However, some observations are worth mentioning.

Table 5.2 lists the wind speed recorded. The wind flow within the urban canopy is negatively affected by a higher aspect ratio (H/W) (Emmanuel, 2007). Therefore, the points with low aspect ratios and unobstructed locations recorded higher values than the ones with high aspect ratios. The unobstructed measuring point 6 recorded the highest air speed average of 1.2m/s, with maximum air speed records of 1.9m/s at 15:00 LST. This may be attributed to its location, which is an intersection point between Al-Muizz Street (north-south) and Beet Al-Qadi Street (east-west) giving it the privilege of the different orientation. This is followed by point 4 and 5, which recorded the average of 1.1m/s due to its proximity to Al-Azhar Street (32m width) where the street width and the vehicle movements may influence the results. Moreover, it is worth mentioning point 9, which is an unobstructed area recording an average air speed of 0.9m/s. Point 8, even though it is an extremely deep canyon with the highest aspect ratio, it recorded a high wind speed compared to other urban canyons as it reached 1.5m/s at 15:00 LST and an average of 0.9m/s. This may be attributed to the design of the street, with a wide opening toward the wind direction coming from Al-Muizz that acts as a wind catcher (Figure 5.11). However, point 7 has the same orientation as point 8, and yet it is covered and enclosed (Figures 5.7 and 5.8) and this prevents it from having the same performance as it was the only location which recorded zero m/s wind speed at 6 and 9 LST. This agrees with the point mentioned in the literature review (section 3.4.3), as a very dense urban settlement can hamper the wind flow, resulting in reduced ventilation cooling (Sharmin et al., 2012).



**Table 5-2** Average wind velocity (m/s) measured on 29<sup>th</sup> June and 1<sup>st</sup> July 2012

	29 June 12							1 July 12							
	6	9	12	15	18	21	24	3	6	9	12	15	18	21	24
1	0.6	0.3	0.6	1	0.6	0.3	0.2	0.9	0.7	0.4	0.7	0.9	0.5	0.2	0.4
2	0.9	0.7	0.8	1.2	0.9	0.6	0.5	1	0.8	0.6	0.9	1.1	0.8	0.4	0.5
3	1	0.5	0.9	1.3	1	0.7	0.6	1.1	1	0.5	0.8	1.3	1.1	0.6	0.7
4	0.9	1	1.1	1.6	1.3	1	0.9	1.4	0.8	0.9	1	1.5	1.3	1	0.9
5	0.7	1.5	1.2	1.6	1.2	0.9	0.8	1.2	0.6	1.4	1.3	1.4	1.3	1	0.9
6	0.9	0.7	1.4	1.8	1.5	1.2	1.1	1.2	0.9	0.8	1.3	1.9	1.4	1.1	1.2
7	0	0	1.1	1.4	0.8	0.5	0.4	0.6	0.5	0	1	1.5	0.9	0.6	0.4
8	0.6	0.4	1.1	1.5	1.3	0.9	0.8	0.7	0.6	0.5	1	1.6	1.2	0.9	0.7
9	0.5	0.5	1	1.4	1.1	0.8	0.7	1	0.5	0.6	1.3	1.6	1.2	1	0.9

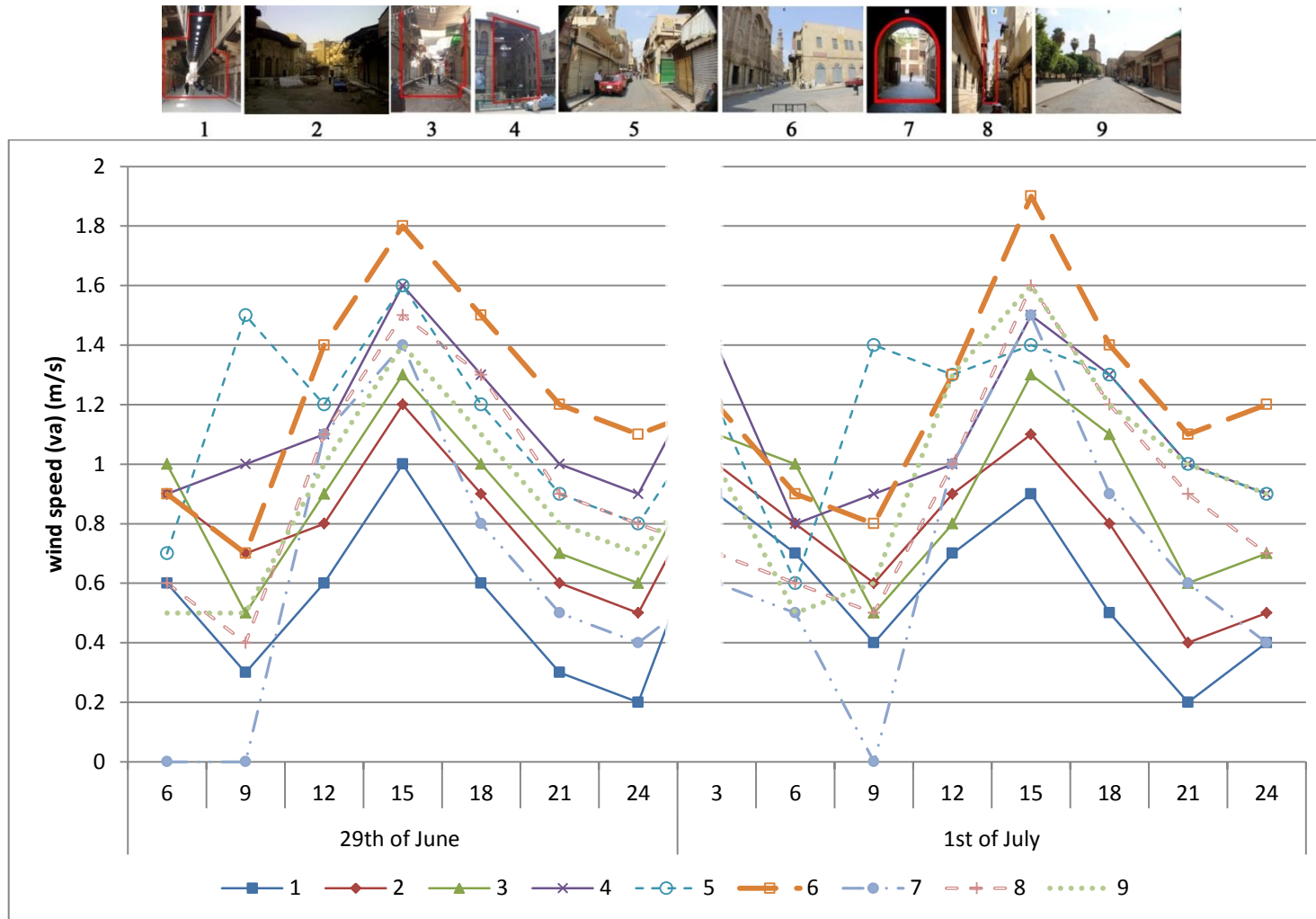


Figure 5-10 The in-situ wind speed (va) (m/s) measured on 29th June and 1st July 2012

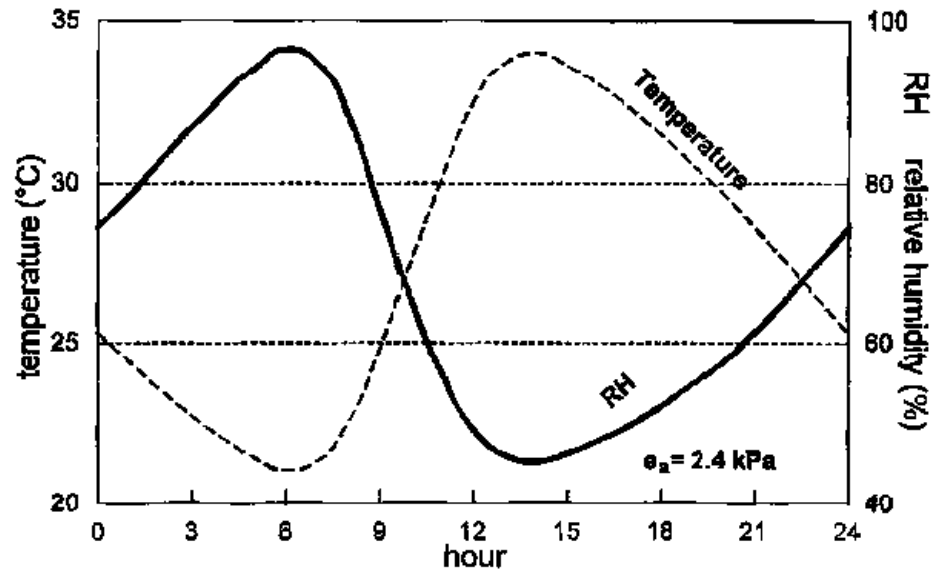


**Figure 5-11** The deep canyon for location 8 and how it was designed to become narrower

### 5.5.3 Relative Humidity

According to Akinnubi et al. (2007), the solar radiation absorbed by the atmosphere and the heat emitted by the earth increase the air temperature and as the air temperature increases after sunrise, the relative humidity decreases, reaching its lowest point when the maximum temperature is realized. This was exactly the case for the measured relative humidity which showed a negative relationship with the air temperature (Figure 5.12). As can be seen in Figure 5.13, at 6:00 LST when the air temperature of all locations recorded values close to below 28°C (Figure 5.9), all the measured points of relative humidity reached almost equal values in the morning between 46% and 50%. At 9:00 LST when the air temperature started to vary between the different locations, the relative humidity in the different locations started to follow the same path by registering wider records of between 40% to 55% on day one and 45% to 54% on day two. At 15:00 LST, as the air temperature of the observed values reached its maximum, the relative humidity values hit troughs of between 33% and 38%, until midnight when they reached their maximum values (67% and 72%) when there is no solar radiation and the air temperature are very low. Thus, locations with a higher air temperature such as point 9, which recorded the highest air temperature, also recorded one of the lowest values of relative humidity. However, locations with a lower air temperature, such as the shaded point 1, recorded a higher relative humidity as the shading canopy may block the humid air from escaping easily (Sharmin, 2012).

It should be mentioned that there is a great deal of output from air conditioning units located on the street side of location no 5, and thus local sources of heat and humidity might have influenced these results (Figure 5.16).



**Figure 5-12** As the temperature changes during the day, the relative humidity also changes substantially.

Source: Richard et al. (1998)

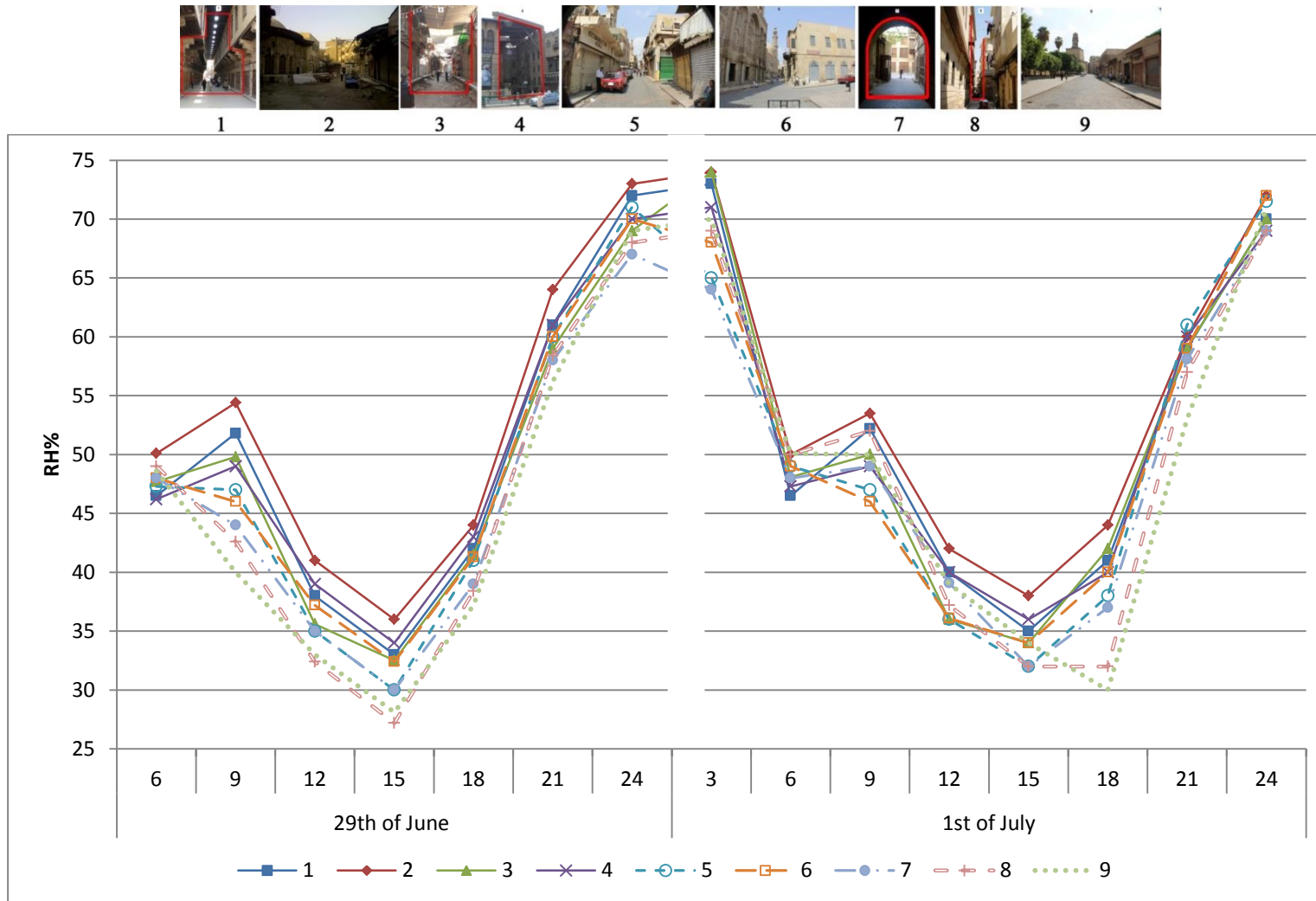


Figure 5-13 Relative Humidity (RH%) at 1.2 m a.g.l. during the two summer days' measurements

### 5.5.4 Mean Radiant Temperature

The mean radiant temperature (TMRT), which is a function of absorbed short-wave and long-wave fluxes, was calculated through the globe thermometer, as shown in Table 5.3 (Nikolopoulou et al. 2001); this is in accordance with equation (5.1) given by ASHRAE (2009), with the empirical coefficient recently refined by Thorsson et al. (2007) as:

$$TMRT = [(T_g + 273)^4 + \frac{1.1 \times 10^8 V_a^{0.6}}{\epsilon_g D^{0.4}} \times (T_g - T_a)]^{1/4} - 273 \quad (Eq. 5.1)$$

Where ( $T_g$ ) is the globe temperature ( $^{\circ}\text{C}$ ), ( $V_a$ ) is air velocity (m/s), ( $T_a$ ) is the air temperature ( $^{\circ}\text{C}$ ),  $D$  is the globe diameter (mm) (= 25mm in this study), and ( $\epsilon_g$ ) is the globe emissivity (= 0.95 for black-colour globe). The empirically derived parameter  $1.1 \times 10^8$  and the wind exponent ( $V_a^{0.6}$ ) together represent the globe's mean convection coefficient ( $1.1 \times 10^8 V_a^{0.6}$ ).

**Table 5-3** Measured globe temperature ( $^{\circ}\text{C}$ ) on 29<sup>th</sup> June and 1<sup>st</sup> July 2012

	29 June 2012							1 July 2012							
	Time in hours							Time in hours							
	6	9	12	15	18	21	24	3	6	9	12	15	18	21	24
1	24.9	36.2	39.4	44.9	38.8	29.7	26.1	25.5	25.4	37.1	39.9	45.2	39.1	30.1	26.9
2	25.4	38.1	42.6	49	39	29.4	27.2	26.1	26.5	38.6	43.1	49.4	39.7	29.5	27.1
3	25.1	35.8	40.1	47.1	38.9	30.7	27.1	26.2	25.9	36	40.5	46.9	39.3	31.1	27
4	25.4	36.1	45.1	49.3	38	31.7	28.1	25.9	26.1	37.1	45.3	50	39.1	31.9	28.7
5	27	37.2	47.6	49.8	40	32.2	28.9	27	27.1	37.6	48.2	51.1	41.5	33.1	29.7
6	26.4	40	47.9	50.9	39.3	32.7	27.8	26.6	26.8	41.2	48.6	52.2	41.1	34.2	27.5
7	26.1	31	37.4	39.9	34.2	29.8	25.9	25.6	26.1	32.1	38.5	41.1	34.9	29.9	26
8	23.9	35.5	40.8	45.4	36.2	30.4	27.1	25.6	25.3	36.3	41.2	45	36.3	30.6	27.3
9	26.6	39.3	45.3	56.7	38.7	32	26	26	27.2	40.2	45	57.1	39.5	32.6	26.2

As shown in Figure 5.14, the mean radiant temperature (TMRT) was noticeably lower within the sheltered urban streets than in the unobstructed locations with low aspect ratios (e.g. point 9 vs. points 8 and 7). The difference between sheltered and exposed measuring points reached about  $26^{\circ}\text{C}$  at the hottest time of the day (e.g. between points 7 and 9 around 15:00 LST). The difference between air temperature and the TMRT was more than  $30^{\circ}\text{C}$  in some cases, while in the sheltered locations such as point no 7, the maximum air temperature on 29th July was  $39.6^{\circ}\text{C}$  and at the same time the TMRT was  $39.8^{\circ}\text{C}$ . The same findings have been reported in several studies, for instance Kántor and Unger(2011) found that in sunny conditions TMRT can be more than  $30^{\circ}\text{C}$  higher

than air temperature in exposed locations and even up to 5°C in shaded parts due to the diffuse and reflect solar radiation components (Toudert and Mayer, 2005). Another study conducted by Toudert (2005) in the hot dry climate of Beni-Isguen in Algeria reported a difference of 36°C between sheltered and exposed locations at the hottest time of the day.

The exposed locations, represented by points 6 and 9, experienced the highest TMRT values at 15:00 LST recording 62.6°C and 70°C respectively on 29<sup>th</sup> June and 65.1°C and 71.2°C on 1<sup>st</sup> July. Similar TMRT values were reported by Shahidan (2011) in Malaysia during the summer season reaching 76°C, while Toudert (2005) in Freiburg in Germany reported 66°C as a maximum TMRT registered. Beni-Isguen in Algeria reported values ranging between 60-75°C as the highest TMRT experienced.

TMRT differences between the different urban streets are clearly higher than ( $T_a$ ) (Nakamura and Oke, 1988). The lowest TMRT values were calculated for points 1 and 7, as they are covered paths and not directly affected by solar radiation. Point 1 showed values varying between 22.9-51.1°C while point 7's values were the lowest (SVF = 0) between 24.1-45.7°C. Point 8 is a protected location, except at midday when the sun is at its highest position; at that time, the TMRT reached 53.3°C due to its E-W orientation, which is quite difficult to keep in shade at noon time despite its high aspect ratio. However, being a very deep twisted canyon with aspect ratio ( $H1/W= 3.8$ ;  $H2/W=4.2$ ) and SVF of 2.4 can also prevent the access of solar radiation for a long time during the day. Point 3 reached its highest value between 12:00 and 15:00 LST as 43.2°C and 54.9°C, and this may be attributed to local interventions as the street is semi-covered by tents in some places. This also prevents direct solar radiation from being focused on one place for long hours (Figure 5.15). After 19:00 LST, and because of less solar radiation and a lower sun position, there was a negligible difference ( $\leq 4^\circ\text{C}$ ) registered between all urban streets and TMRT averaged 31.5°C. Despite the day time when the TMRT was for the most part higher than  $T_a$ , at night time the TMRT was approximately equal to  $T_a$  and was even less than  $T_a$  between 21:00 LST till 24:00 LST. Furthermore, point 5 recorded one of the highest TMRTs during the day and the highest TMRT after sunset at 18:00 LST. Despite its North-South orientation and the aspect ratio of  $H1/W= 0.75$ ;  $H2/W=1.1$ , it should be mentioned that this area is mainly for jewellery traders and most of them use mechanical cooling which may, in fact,

further increase outdoor temperatures, as the excess heat is emitted to the urban air and more cooling will be needed as a result of the vicious circle created in this situation (Figure 6.16) (de Schillier and Evans, 1998; Baker et al., 2002).

After sunset at 18:00 LST, TMRT decreases drastically because the short-wave irradiation becomes negligible and hence results in a reduction of the surface temperatures. As a consequence, less heat is radiated. Therefore, the unobstructed areas which recorded the highest TMRT at midday had a higher cooling rate than other locations at night time. Point 9 lost almost 46°C in TMRT between 15:00 till 24:00 LST, and location 6 was almost 35°C cooler TMRT at 24:00 LST than what it recorded at 15:00 LST. By contrast, the protected locations such as 1, 3 and 8 recorded 25.5 °C, 26.5 °C and 25.7 °C respectively higher than the unobstructed point 9, which recorded 24.6°C at 24:00 LST on 29<sup>th</sup> June and 24°C on 1<sup>st</sup> July compared to the protected points mentioned before which recorded 26.4°C, 26.3°C and 25.7°C, respectively. This may be attributed to the greenhouse type effect, as the tents or the canopies may trap or reduce the absorbed heat. The high shading levels can decrease long-wave radiation loss on the surface, contributing to high temperatures at night (Lin et al. 2010). At night, TMRT values remained between 25°C and 34°C, which is attributable to the surplus heat released by the surfaces.



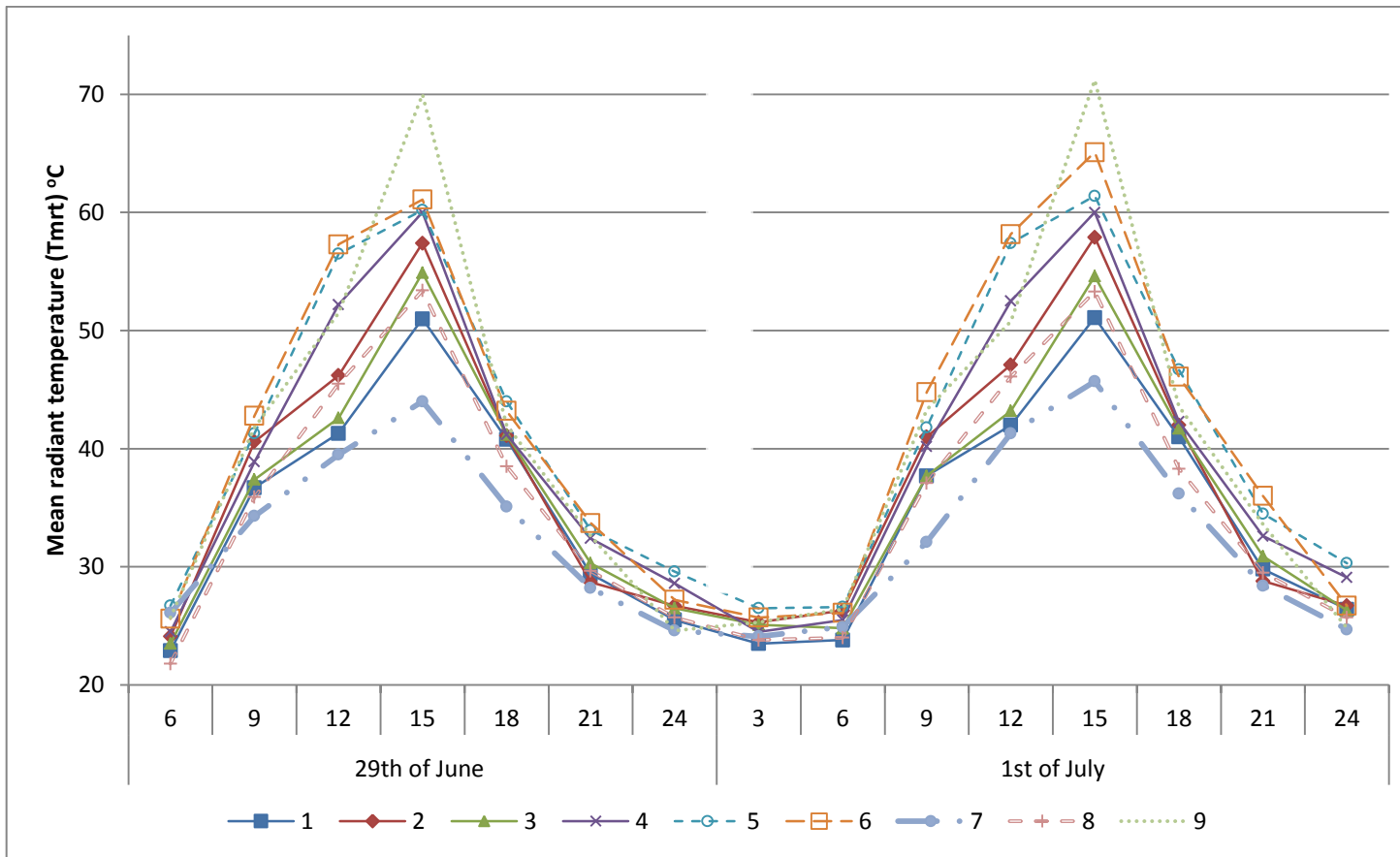
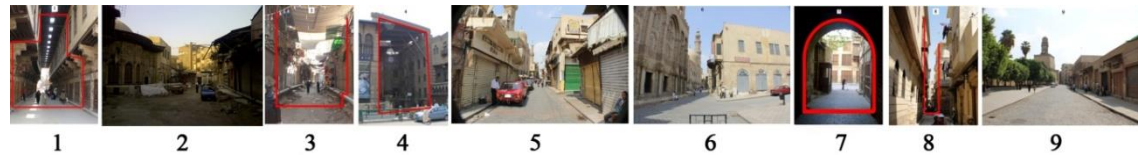


Figure 5-14 Mean radiant temperature (TMRT) at 1.1 m a.g.l. during the two summer days of measurement



**Figure 5-15** A local intervention, as the street is semi-covered by tents in some places which prevent direct solar radiation from focusing in one place for too long



**Figure 5-16** The excess heat is emitted from the mechanical ventilation to the urban air, which may increase the air temperature in the street

## 5.6 Thermal comfort analysis (PET)

Once  $T_a$ ,  $v_a$ , RH and TMRT are known, a thermal index, as a single value that integrates the effects of the basic parameters in a human thermal environment, can be calculated. Several thermal indices developed for outdoor settings can be used, e.g. the physiologically equivalent temperature, PET (Höppe, 1993, 1999), the standard equivalent temperature adapted for outdoors, OUT-SET\* (Pickup and de Dear, 1999) or the predicted mean vote also adjusted for outdoors PMV\* (Jendritzky et al., 1990). Although all of these indices are based on the same physical basis of Fagner's comfort equation (Fagner, 1970) and incorporate the additional solar and terrestrial radiation fluxes, they still have some differences (for more details refer to Sections 3.6). In this study, PET, based on the human energy balance model MEMI (Munich Energy Model for Individuals), was used. PET is defined as the physiological equivalent temperature at any given place (outdoors or indoors). It is equivalent to the air temperature at which, in a typical indoor setting, the heat balance of the human body (work metabolism 80W of light activity, added to basic metabolism; heat resistance of clothing 0.9 clo) is maintained with core and skin temperatures equal to those under the conditions being assessed (Esmaili et al., 2011). It is a function of the air temperature, air humidity, wind speed and mean radiant temperature. PET has been widely applied in areas with various climatic conditions (Toudert and Mayer, 2006; Cheng et al., 2010; Lin, 2009; Matzarakis et al. 1999; Thorsson et al. 2007).

The PET was calculated using the RayMan model (Matzarakis et al., 2007, 2010). The RayMan model was developed in the Meteorological Institute (University of Freiburg, Germany), according to Guideline 3787 of the German Engineering Society (VDI, 1998). This model computes the radiation flux inside urban structures based on meteorological parameters including time of day and year, air temperature, air humidity, degree of cloud cover, and the albedo of the adjacent surfaces as shown in Figure 5.17 (Gulyas et al., 2006). To calculate the thermal sensation, the following requirements were adjusted as constants: body surface area has been standardized to  $1.9\text{m}^2$ , which represents a human with a height of 1.75m and a bodyweight of 75kg (Mayer and Höppe, 1984, 1987; Becker, 2000 and Potchter et al., 2006); the rate of metabolic energy transformation (work metabolism) based on 80W for a standing person and the insulation factor of clothing ( $I_{clo}$ ) has been standardized to 0.9 for an indoor business

suit (Figure 5.17) (Jendritzky et al., 1990; VDI, 1998). Lin and Matzarakis (2010) reported that RayMan model was more successful in simulating nature-like rather than urban settings. Previous studies of hot and humid regions reported the validity of the RayMan model (Lin et al. 2010). Therefore, this study argues that the model can be applied to hot and arid regions.

The screenshot shows the RayMan 1.2 software interface with the following input parameters:

Section	Parameter	Value
Date and time	Date (day.month.year)	1.7.2013
	Day of year	182
	Local time (h:mm)	23:36
Geographic data	Location	Ägypten (Kairo)
	Geogr. longitude (..°..E)	31°15'
	Geogr. latitude (..°..N)	30°3'
	Altitude (m)	0
	time zone (UTC + h)	2.0
Current data	Air temperature Ta (°C)	38.4
	Vapour pressure VP (hPa)	22.9
	Rel. Humidity RH (%)	34.0
	Wind velocity v (m/s)	1.0
	Cloud cover C (octas)	0
	Global radiation G (W/m²)	
	Mean radiant temp. Tmrt (°C)	71.2
Personal data	Height (m)	1.75
	Weight (kg)	75.0
	Age (a)	35
	Sex	m
	Activity (W)	80.0
Clothing and activity	Clothing (clo)	0.9
	Activity (W)	80.0
Thermal indices	<input checked="" type="checkbox"/> PMV	
	<input checked="" type="checkbox"/> PET	
	<input checked="" type="checkbox"/> SET*	

**Figure 5-17**The RayMan 1.2 interface showing the input parameters for calculating the PET

The thermal comfort index (PET) was calculated for each location and plotted on Figure 5.18, which shows the similarity between the PET and TMRT patterns, where the regressions analyses between PET and TMRT lead to coefficients of determination of  $R^2 = 0.972$  for a linear relationship (Figure 5.19 and 5.20), which confirms the strong influence of the mean radiant temperature on evaluating thermal sensation outdoors under summer sunny conditions regardless of the comfort index used (Mayer and Höpfe, 1987; Mayer, 1993; Gomez et al., 2001). The most uncomfortable locations are those exposed to the direct sun rays. PET peak values occurred at 15:00 LST and ranged from 52.8°C for point 9 and 47.7°C for point 6 on 29<sup>th</sup> June and 53.7°C for point 9 and 49.4 for point 6 on 1<sup>st</sup> July. By contrast, the lowest PET value for the same time was determined for location 7, which recorded 38.9°C on the first day and 40.1°C on the second day (SVF=0). In the early morning and late afternoon, PET did not reveal clear differences between the sites within street canyons, i.e. PET≈30°C before 9:00 LST

and  $\approx 34^{\circ}\text{C}$  after 21:00 LST. PET differences between the various streets were pronounced at 12 LST at points 5, 6 and 9, indicating a higher level of heat stress reaching  $44.5^{\circ}\text{C}$ ,  $45.1^{\circ}\text{C}$  and  $43.1^{\circ}\text{C}$  on the first day and  $45.1^{\circ}\text{C}$ ,  $49.1^{\circ}\text{C}$  and  $42.6^{\circ}\text{C}$  on day two, respectively. Points 1 and 3 showed a slightly lower level of heat stress recording  $38.8^{\circ}\text{C}$ ,  $39.6^{\circ}\text{C}$  on day one and  $39.3^{\circ}\text{C}$ ,  $40.1^{\circ}\text{C}$  on day two, respectively, as they are semi-shaded from the direct solar radiation. PET values decreased very slowly at night and roughly equalled the air temperature at midnight.

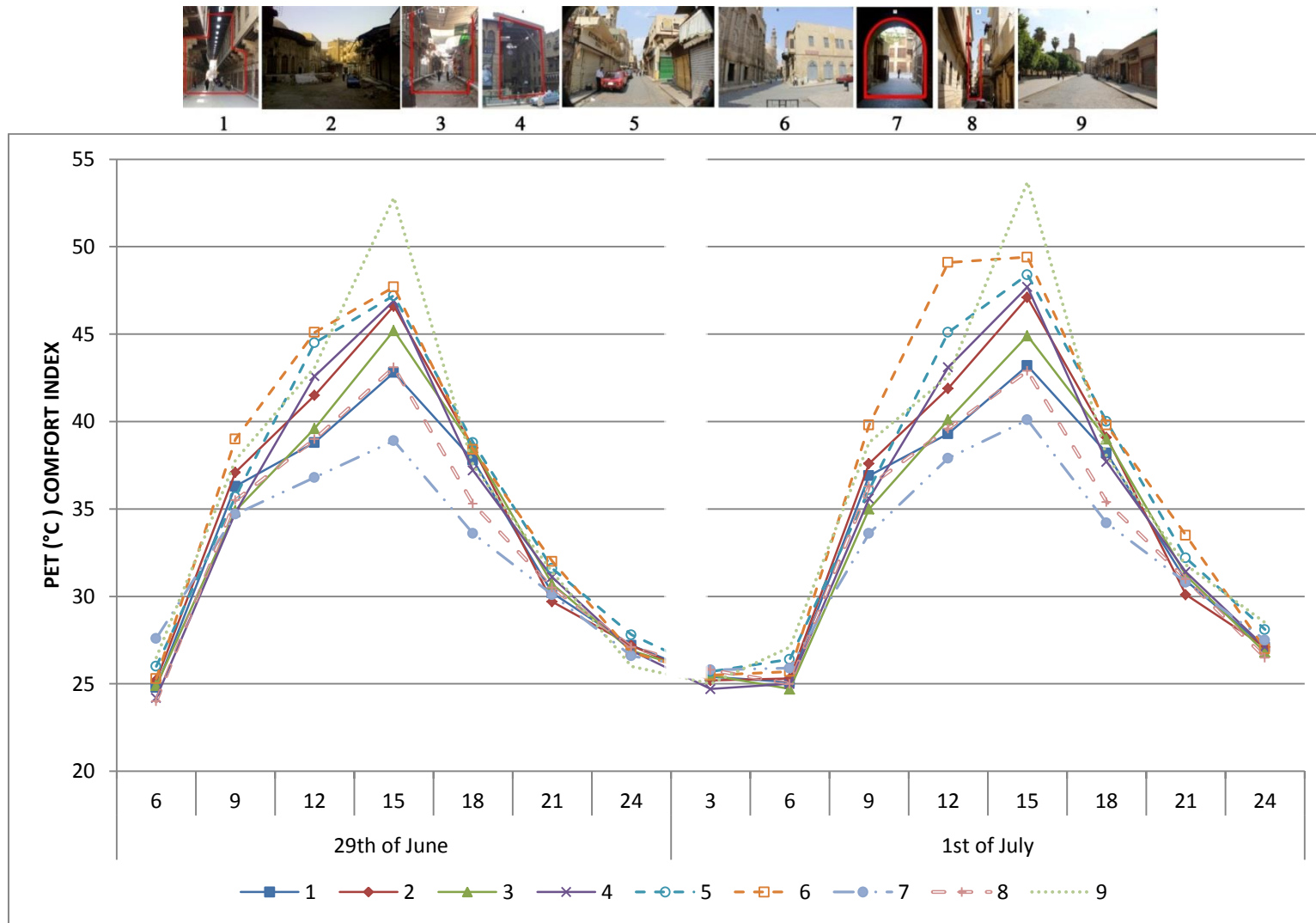


Figure 5-18 Physiologically equivalent temperature (PET) at 1.2 m a.g.l. during the two measurement days



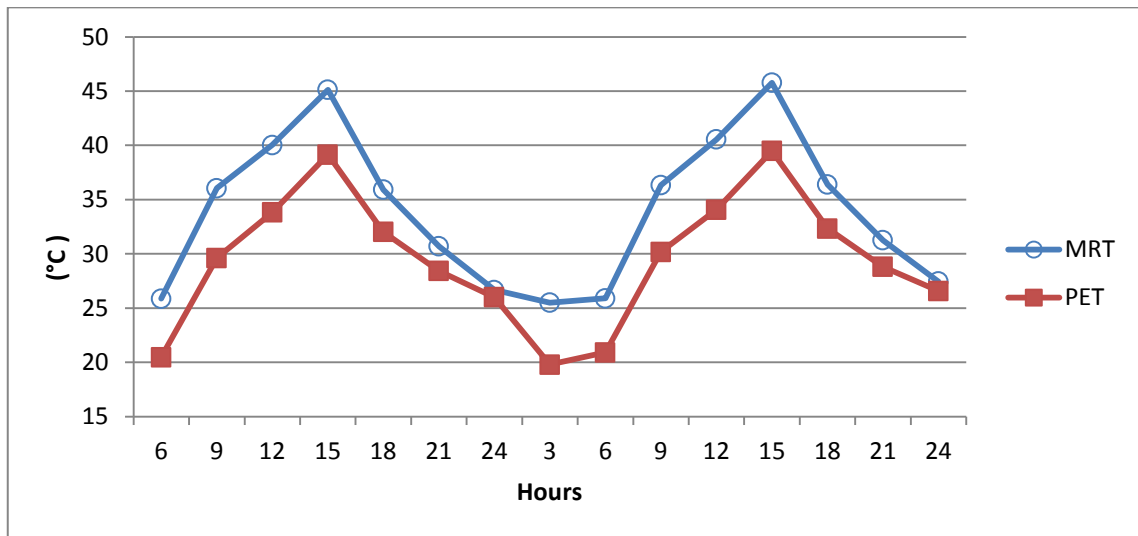


Figure 5-19 The average patterns of the TMRT and PET for the two measurement days

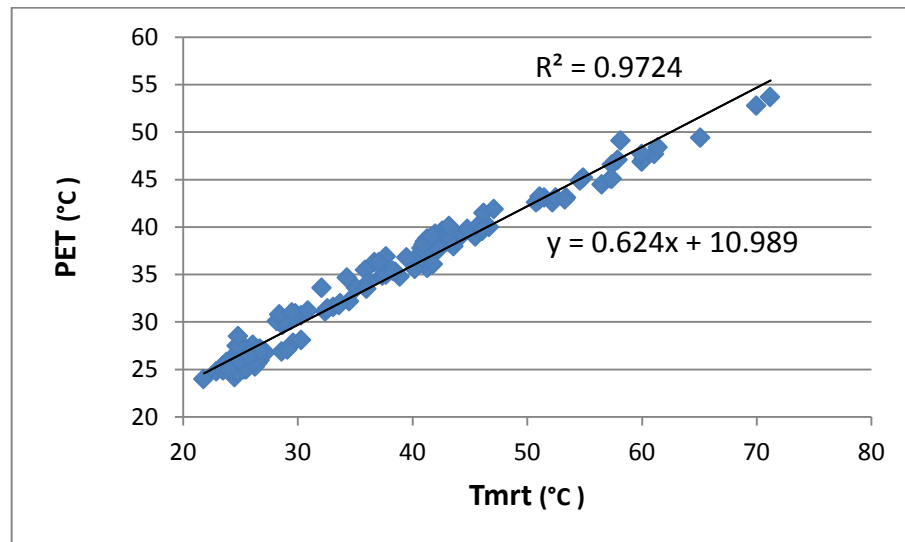


Figure 5-20 Correlation between PET and thermal sensation in summer 2012

## 5.7 Validation of ENVI-met model: computed and measurement comparison

The air temperature and TMRT become the main concern in the overall condition when it comes to thermal comfort in the hot, arid climate (Nikolopoulou, 1998; Shahidan, 2011). It was very important to simulate the existing situation for both parameters of air temperature and TMRT in order to cover wider areas along the path as a double check to validate the results concluded from the field measurements campaign. Therefore, simulations were carried out for the two parts of Al-Muizz Street under the same boundary conditions that occurred during the monitoring period, and then the simulation

results were compared against the measured data in order to increase the confidence in the ENVI-met as a tool.

The model simulation was performed on 1<sup>st</sup> July 2012 as the hottest day on the measurements period. The area around Al-Muizz Street has been transformed into two model grids, where the area of interest must be reduced to fit the available ENVI-met grid cells (180 x 180 x 30 and 100 x 100 x 30 grid cells) as a compromise has to be found between the accuracy and resolution of the model and the number of treatable grid cells. Therefore, based on the different parts dimensions the street was divided into renovated part with the dimension 40 x 160 x 30 with a resolution of 2m x 2m x 3m for the renovated part and the dimension 20 x 80 x 30 grids with a resolution of 2m x 2m x 3m for the non-renovated one. Note that the model area is rotated 15° out of grid north. Table 5.4 shows the simulation input data for 1<sup>st</sup> July 2012 which is an extreme summer day for Cairo. Two snapshot receptors were located at the same spots of the measurement campaign to record Ta, RH, V, solar radiation and globe temperature at 1.2m above ground level (Figure 5.21). Outputs were then compared with the local climate scale averaged records for the same parameters observed from the site measurement.

**Table 5-4** Main input data used for ENVI-met

<i>PARAMETER</i>	<i>VALUE</i>
Ta, air dry bulb temperature	34.85°C
RH, relative humidity	59%
Va, wind speed	3.5m/s at 10m height
soil temperature	302 at (0-0.5m) and 299 at (0,5-2m)
U value walls	1.7
U value roofs	2.2
Albedo walls	0.4
Albedo roofs	0.15



**Figure 5-21** The two modelling domains and the two measurement points which are the same receptors in ENVI-met

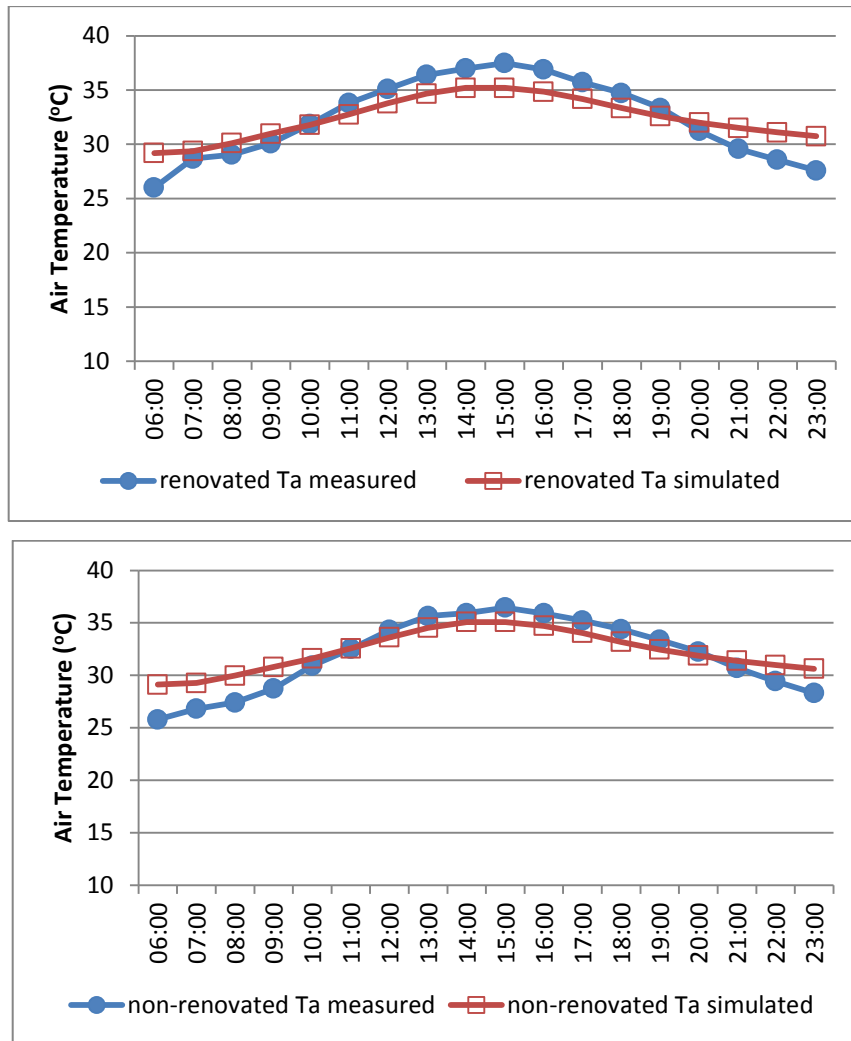


### 5.7.1 Results analysis

According to the in-situ measurements, 1<sup>st</sup> July 2012 was a clear, hot and steady summer day, with a daily mean air temperature of 31°C (maximum 38.4°C) and a mean wind speed of 0.56m/s. The sun rose at 4:56 a.m. and set at 7:00 p.m. The solar elevation reached its maximum of 83.28 degrees at 1:00.

#### 5.7.1.1 Simulated and Measurement Air Temperature (Ta)

Figure 5.22 shows a comparison between the measured air temperature at the two measurement points in 1.1 m a.g.l and the corresponding model results at 1.2 m a.g.l (due to the vertical model resolution). Two model simulation outputs are plotted against the data observed for the two parts of Al Muizz Street. ENVI-met estimation for the dry air temperature (Ta) was in a good approximation with the monitored temperatures in both parts. The regressions analyses between the measured and computed air temperature were calculated with correlation coefficients  $R^2=0.942$  for the renovated area and  $R^2= 0.970$  for the non-renovated for a linear relationship. Thus, the measured and computed ENVI-met for air temperature is well correlated and considered reliable in presenting the current air temperature condition of Al-Muizz Street.



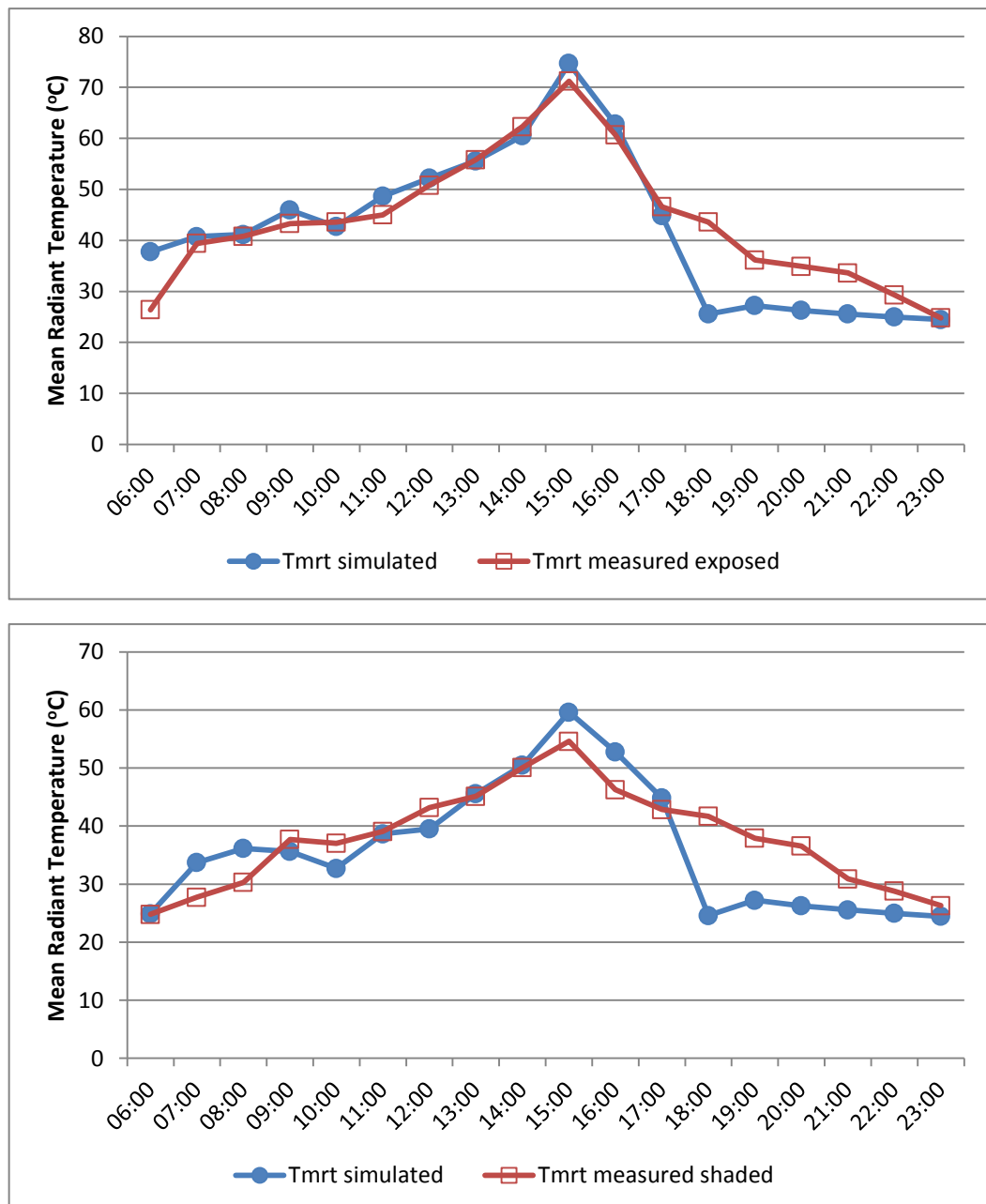
**Figure 5-22** Comparison between the air temperature measured and the ENVI-met output (the renovated above and the non-renovated below).

### 5.7.1.2 Computed and Measured mean radiant temperature (TMRT)

Figure 5.23 illustrates the measured TMRT using the 25mm black globe thermometer compared to the TMRT estimated by ENVI-met. The globe temperature measured by the black globe sensor had to be recalculated using the observed in-situ values, as shown in Table 5.5, using equation (5.1) explained in Section 5.5.4.

Despite the complexity of the three dimensional environment, ENVI-met is found to represent well the trends of the TMRT with a calculated correlation coefficient ( $R^2$ ) during the daytime between the measured and computed equal to 0.916 for unshaded area and equal to 0.850 for the shaded part. However, simulated values of TMRT were under-estimated for both parts after sunset in comparison to the field data. This may be attributed to the decrease in short wave radiation after sunset, as it can decrease by 20°C

of the main radiant temperature (Katzschner and Thorsson, 2009). Additionally, the material heat storage is not taken into account during the simulation, where the heat stored in the building and transferred through walls and roof is calculated by conducting U-values. In real cases, however, each material has its own thermal properties expressed by thermal admittance, i.e. lack of nocturnal heat release process as no heat stored in the building fabrics (Toudert, 2005; Fahmy et al., 2010).



**Figure 5-23** TMRT simulated by ENVI-met plotted against measured TMRT (the above graph for the unshaded TMRT and below the shaded TMRT)

**Table 5-5** The observed in-situ values used in equation (5.1) for calculating the TMRT estimated from the globe temperature ( $T_g$ ), air temperature ( $T_a$ ) and air velocity ( $V_a$ ).

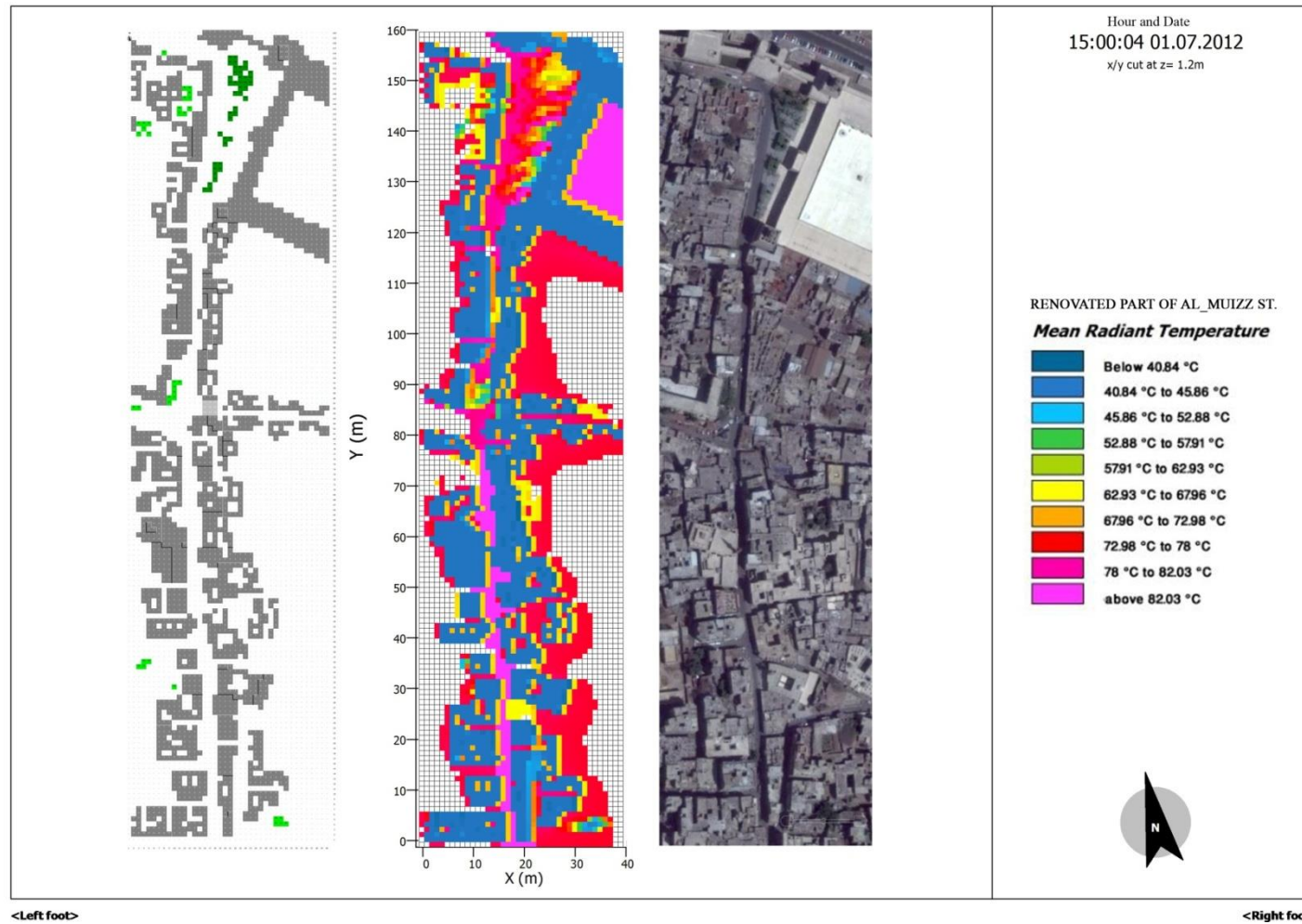
Renovated Part (Exposed)				Time	Non-Renovated (Shaded)			
$T_g$	$T_a$	$V_a$	TMRT		$T_g$	$T_a$	$V_a$	TMRT
27.2	28.7	0.5	<b>25.4</b>	06:00	26.6	27.2	1	<b>26.8</b>
40.2	34.2	0.6	<b>43.3</b>	09:00	36	32.5	0.5	<b>37.7</b>
45	36	1.3	<b>50.8</b>	12:00	40.5	36.6	0.8	<b>43.2</b>
57.1	38.4	1.6	<b>71.2</b>	15:00	46.9	36.8	1.3	<b>54.6</b>
39.5	34.3	1.2	<b>43.6</b>	18:00	39.3	36	1.1	<b>41.7</b>
31.6	31.2	1	<b>31.6</b>	21:00	32.1	31.5	0.6	<b>32.9</b>
26.2	27.9	0.9	<b>24.8</b>	00:00	27	28.1	0.7	<b>26.3</b>

## 5.8 ENVI-met microclimatic map

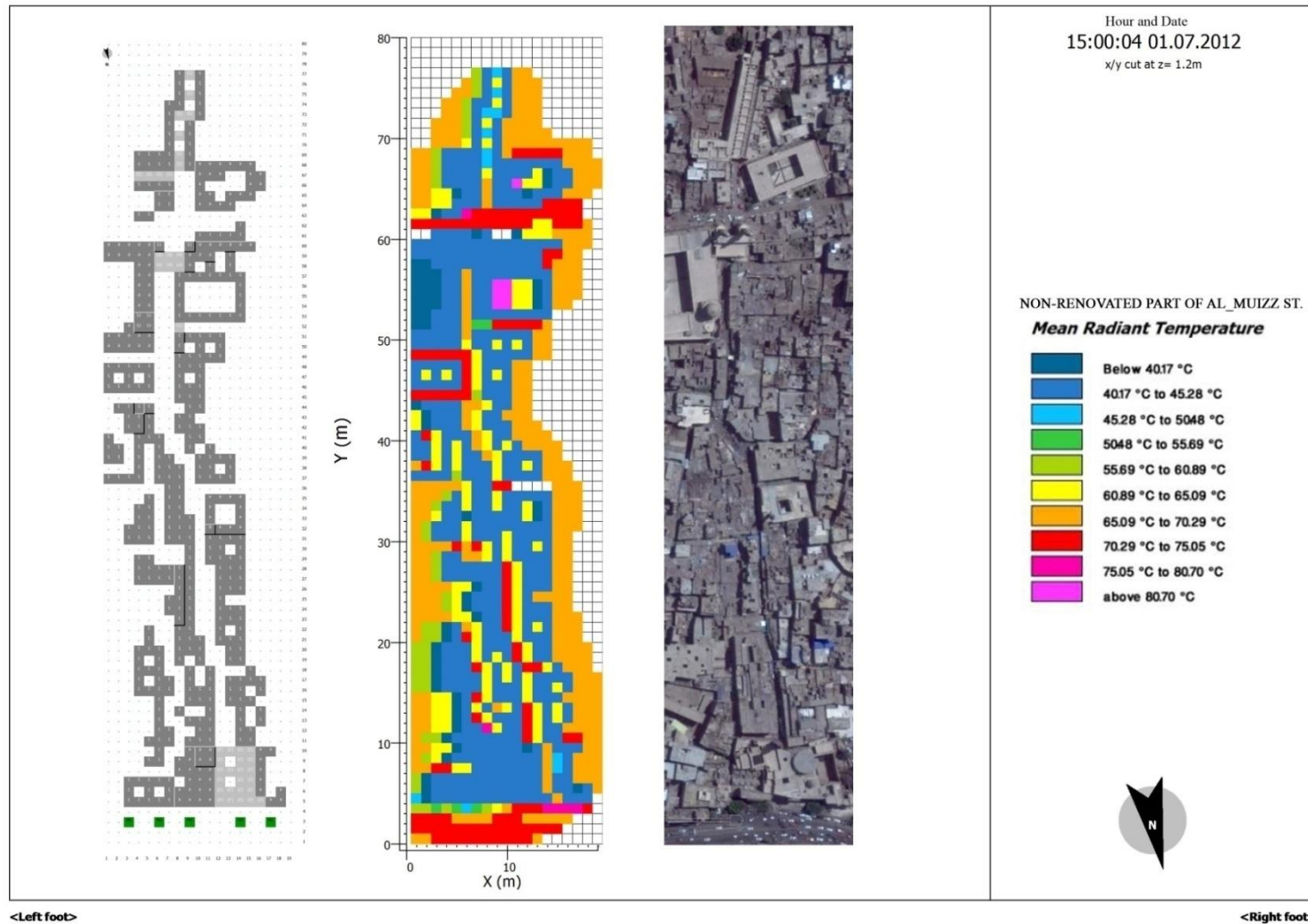
According to the field measurement findings, the peak temperature time in Al-Muizz Street was at 15:00 LST. In regions with a hot, arid climate, the maximum temperature is important; it determines the UHI intensity of the urban area and it influences people's thermal comfort and determines the loading of the air conditioning systems (Wong et al, 2007; Wong and Yu, 2009). Therefore, a comparison was conducted between the different conditions of the renovated and non-renovated parts of the street during this hour at 1.2m height, in order to understand the impact of different urban modifications between the two parts towards the TMRT, as shown in Figures 5.24 and 5.25, which in turn affects the pedestrians' thermal comfort and the use of the outdoor spaces.

The image shows the gradient colour marked from a blue to magenta colour, representing the lowest to highest TMRT. Based on the renovated part current condition profiles (Figure 5.24), during the daytime the spot of magenta colour is focused at the centre of the street and clearly represents the highest TMRT with yellow spots close to the west buildings which is attributed to the buildings shadings effect on decreasing the short wave radiation (Katzschner and Thorsson, 2009). The most affected areas are located in the centre of the street which has a high sky view factor (SVF). Also, it is

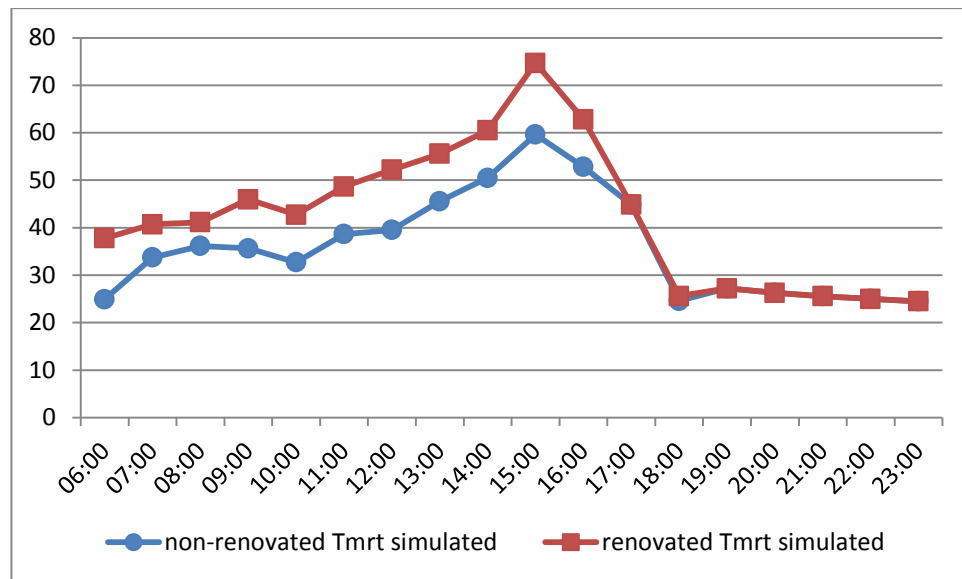
believed that the highest TMRT may be the result of a lack of vegetation, high building density within the area and the severe lack of shading, particularly at the centre of the street where most activities are occur during the daytime. This is in contrast to the non-renovated part current conditions (Figure 5.25) where the magenta spots become very few and replaced by the mix of red and yellow. This indicates that TMRT is lower compared to the renovated part as more shaded areas are found in the non-renovated part. These shading adjustments show an improvement in TMRT reduction (Figure 5.26). The same results were reported in the field measurement results where the non-shaded locations showed a high thermal discomfort with high values of TMRT. This verifies the hypothesis that the urban TMRT conditions may be enhanced if the shading pattern improved. Accordingly, this affects the outdoor thermal comfort and extending the continuity of the acceptable thermal conditions during the day, as the average patterns of the TMRT and PET proved to be very strongly correlated, as illustrated in Figure 5.19 and 5.20.



**Figure 5-24** The renovated part spatial pattern of the Mean Radiant Temperature (TMRT) for 1st July 2012 by ENVI-met. The highest mean radiant temperature was located in the centre of the street, particularly in the areas with high sky view factors (SVF) while in the areas close to the west buildings the TMRT became lower due to its shading effects



**Figure 5-25** The non-renovated part spatial pattern of the Mean Radiant Temperature (TMRT) for 1st of July 2012 by ENVI-met. The non-renovated part shows a lower mean radiant temperature compared to the renovated one in figure (6.24) due to the smaller sky view factor resulting from the different shading adjustments



**Figure 5-26** The difference mean radiant temperature (TMRT) between the shaded and non-shaded for 1st July 2012 by ENVI-met

## 5.9 Conclusions

Two in-situ meteorological measurements were carried out in Al Muizz Street, located in the historical quarter of Cairo, of the air temperature for one week during the summer in order to investigate the urban rural air temperature variance (UHI intensity) and to use this as a reference point for simulation analysis and validation. The other in-situ meteorological measurements, including the four main meteorological parameters according to ASHRAE (2009), in addition to TMRT during an extreme hot summer covering two days, were taken to examine the effectiveness of the climatic responsive methodology that was found in the vernacular urban areas of Al-Muizz Street. The experimental results were quantitatively analysed and provided the following information:

- By comparing the one week field measurement with the data obtained from the WMO station, the existence of an urban heat island within the urban street of Al-Muizz was pointed out. The average daily air temperature ( $T_a$ ) within the canyon varies between  $23.2^{\circ}\text{C}$  and  $38^{\circ}\text{C}$ , which is a much wider range in comparison to the average value for the same period ( $22.8^{\circ}\text{C}$  to  $35.5^{\circ}\text{C}$ ) recorded by the WMO at the airport
- In the non-shaded location, there was high thermal discomfort as the TMRT and PET recorded very high values of  $71.2^{\circ}\text{C}$  and  $53.7^{\circ}\text{C}$ , respectively compared to the PET



comfort values range between (23°C and 32°C). The results showed the importance of shading for the improvement of day time comfort. For instance, the TMRT dropped by almost 14°C between the unobstructed location 9 and the shaded location 7 at 15:00 LST. A similar difference in TMRT between solar exposure and shade was found by Ali-Toudert et al. (2005) in a city in southern Algeria, and by Johansson (2006) in the hot, humid city of Colombo, Sri Lanka. These indicate the importance of how compact urban form (high aspect ratios (H/W)) can provide more comfort than dispersed urban form

- The sheltered streets had the lowest PET values as these design elements reduce the amount of direct sun during the daytime, thus improving thermal comfort and reducing sun exposure, which can improve the ambient air temperature by up to 15% based on a study conducted by Arizona State University in Phoenix, which is classified as a hot, arid climate (Love, 2009). This in turn opens the door for the good design of shadings as an efficient solution for pedestrian pathways in hot arid regions
- Streets with a low sky view factor and high thermal capacity showed a time delay in heat releasing during the night time compared to the unobstructed location. According to Lin et al. (2010), the low sky view factor can decrease long-wave radiation loss on the surface, contributing to high temperatures at night
- According to the field study, points 7 (fully covered) and 8 (high aspect ratio varies between 3.8 and 4.2) performed the best during the day time and this was mainly assigned to their urban design form. However, when comparing between the renovated and non-renovated part, the points located in the non-renovated area performed better than the ones in the renovated part as they recorded lower TMRT and PET. This may be owing to the changing behaviour and ways of adaptation to the microclimate between the inhabitants of both sides, where the property owners on the old part regard the pavement area as a legitimate extension to their facades and feel free to create an appropriate setting for selling and living, while in the renovated part the new regulations prevent the local people from acting according to their microclimate needs. Therefore, the life moves back into the houses, and these changes are likely to contribute to the increased use of air conditioning and thus higher energy use with further increases in outdoor temperatures, as the excess heat

is emitted to the urban air. This happened with point 5 located in the jewellery segment within the renovated part

- ENVI-met proved to be a reliable tool to generate microclimatic maps and simulate the different urban scenarios to some extent, based on the program limitations mentioned under Section 4.6.2.2. ENVI-met has been validated through comparing outputs of different parameters results to receptors output. The average outdoor meteorology for each case was observed and compared with the modelling output. ENVI-met reproduces the observed data with a sufficient accuracy.

Based on the above findings, the TMRT proves to have the major effect on thermal perception during the hot season where the solar radiation and the level of shading at various locations play more important roles than air temperature and wind speed when calculating thermal indices. As stated by numerous researchers, (such as Ali-Toudert and Mayer, 2006; Pearlmutter et al., 2007; Djenane et al., 2008; Al Jawabra and Nikolopoulou, 2009; Middel et al., 2014), the shading is the dominant factor driving the heat balance equation in the hot, arid regions. However, during the night time the effect of the high shading patterns was largely reversed, which impeded the long wave radiant heat loss to sky due to the constricted SVF. The compactness creates a cooler street environment during the daytime and warmer at night (Nakamura and Oke, 1988; Lin et al. 2010). Hence, as a strategy to improve the local microclimate, high shading level is required in outdoor environments to increase thermal comfort and extend the continuity of the acceptable thermal conditions during the day (Ali-Toudert and Mayer, 2006; Makaremi et al., 2012; Middel et al., 2014). However, the environmental behaviour of these shading patterns needs to be investigated during the night-time to encourage ventilation and run off of the heat release which is stored in the thermal mass during the day to the night sky. One of the issues of shading strategies is the shortage in daylight availability (Tzempelikos and Athienitis, 2007), and therefore a daylight analysis is also needed in order to have a full evaluation for the shading strategies presented.

The present experiment is based on an energy-model approach, which assesses comfort by means of comfort indices. Although these assessment methods can serve well as analytical tools to assess human thermal comfort, they failed to include many subjective, social and cultural real world situations (Han, 2007). Such work is particularly lacking in such severe climates, where people's subjective perception of the

climate may play an important role in their sensation of comfort (Ali-Toudert, 2005). Therefore, in Chapter Six an intensive social survey based on the psychological approach was conducted to develop more knowledge of the reliability of these indices and refine their scaling.

# 6

---

*“Discussion of and research into human thermal comfort has a long history. The results are illuminating but far from unambiguous. In all cases, at least of the more thorough work, the authors have had to limit and qualify their conclusions. Sometimes they hold only for a limited range of environments, or a special group of people, and usually they involve acceptance of a theoretical standpoint with regard to the definition, and hence the measurement or even the measurability of 'comfort' itself (Markus and Morris, 1980).*

## **Chapter Six**

---

### **6. Outdoor Thermal Comfort Analysis**

#### The Subjective Approach

---

#### Key Concepts

---

- 6.1. Introduction
- 6.2. Anthropometric profile of subjects and observations
- 6.3. Thermal sensation
- 6.4. Thermal adaptation mechanism
- 6.5. The difference thermal sensation votes (TSV) within Al-Muizz
- 6.6. Correlation between predicted and subjective thermal sensation
- 6.7. Non-environmental variables
- 6.8. Conclusion

## 6.1 Introduction

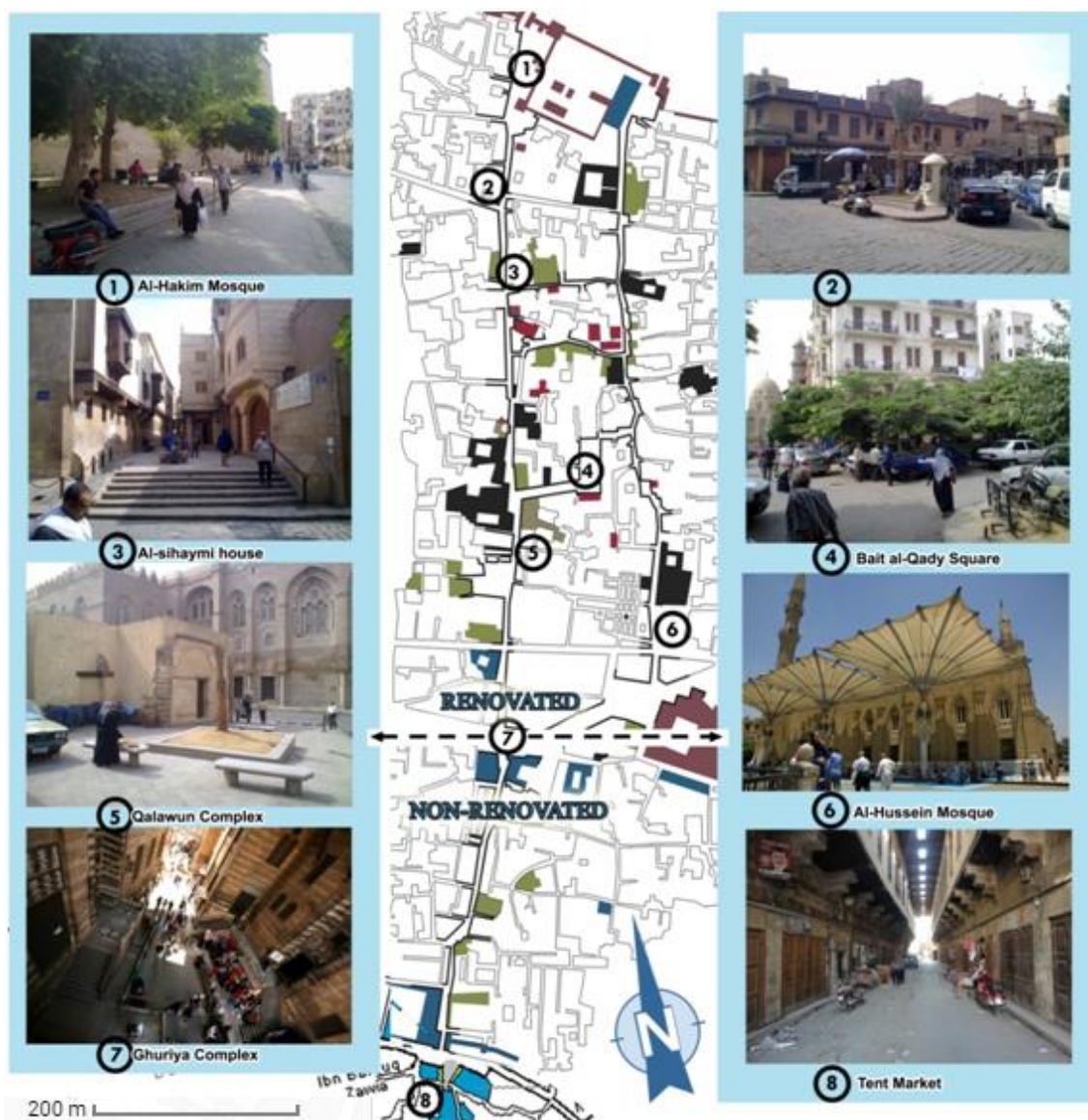
Although the PET and TMRT assessment methods, examined in the previous chapter, can serve well as analytical tools to assess human thermal responses to the local thermal environment, the international comfort standard such as ASHRAE standards and the ISO are almost exclusively based on theoretical analyses of human exchange in mid-latitude climates in North America and Europe (Han, 2007). Additionally, according to the same author, the climatic chamber method used to underpin these indices failed to include many subjective, social and cultural real world situations. Numerous studies conducted in different climatic regions indicated a wider range of adaptation and tolerance to local conditions, such as the study by Cohen et al. (2013) on outdoor thermal perceptions in the Mediterranean climate of Tel Aviv, where it was reported that the thermal acceptance range for the PET value was higher by 3°C PET than the European scale and lower by 5°C PET than the lower boundary of the subtropical climate in Taiwan (Cohen et al., 2013). Therefore, in order to obtain better agreement between indices and actual thermal sensation, different scholars (e.g. Nikolopoulou and Lykoudis, 2006; Lin and Matzarakis, 2008; Kántor, Égerházi, and Unger, 2012; Cohen et al., 2013) have suggested the necessity for observed data from field surveys regarding the perception of the subjective human thermal sensation in the outdoor environments, to maximize the correlation between the indices and the actual recorded votes. This chapter provides empirical data from field survey coupled with in-situ measurements conducted in the previous chapter, with the main objectives to be covered including the followings:

1. Evaluating the pedestrians' thermal comfort perception and preference in outdoor urban spaces of Cairo
2. Calibrating the boundaries of the human thermal sensation scale under the hot, arid climate in comparison to other climatic zones
3. Investigating the impact of thermal adaptation and behaviours on human thermal sensation in outdoor spaces.

## 6.2 Anthropometric profile of subjects and observations

A total sample size of 320 subjects (68.4% males and 31.6% females) split equally between the renovated and non-renovated parts of Al-Muizz Street was undertaken

twice, 160 during the hottest week of the summer between 26<sup>th</sup> June and 2<sup>nd</sup> July 2012, and the same between 19<sup>th</sup> and 25<sup>th</sup> December 2012. This represents winter conditions with the shortest diurnal time, undertaken three times a day between 8-10 in the morning, 13-15 in the afternoon and 18-19 in the evening. In each part of the street, the surveyor installed the equipment for measuring outdoor climatic parameters in proximity to the subjects. To ensure stable outdoor climatic conditions were achieved and recorded, each session continued for approximately ten minutes. As the measurement of the physical environment proceeded, the voluntary subject was interviewed by the surveyor and a questionnaire completed (for more details see Section 4.5).



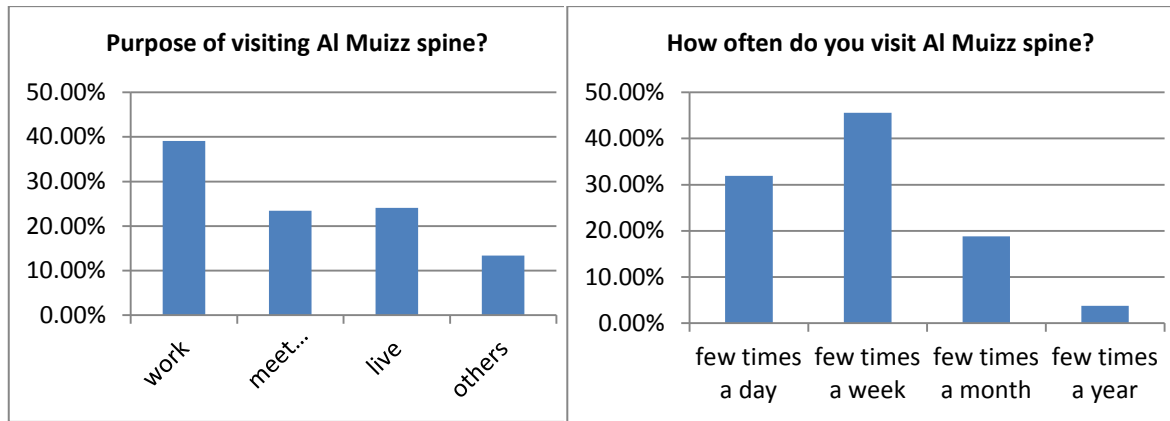
**Figure 6-1** Al-Muizz Street: renovated and non-renovated parts where the questionnaire was carried out

Table 6.1 shows the gender and the age distribution. Most of the sample was comprised of people who had direct and regular contact with Al-Muizz Street, consisting of 39.1% working in the area, 23.4% meeting people, 24.1% living in the street, and 13.4% other activities such as shopping (Figure 6.2a). 96.3% visited the place on a regular basis varying between few times a day (31.9%), a few times a week (45.6%), a few times a month (18.8%) and a few times a year (3.8%), with an outdoor staying time of more than 20 minutes (Figure 6.2b). During the survey, the observations were made and seven clothing units (Clo) in addition to four metabolic rates were estimated in accordance with ASHRAE standards 55-2009 (2009) (explained under Section 4.5.2) to be used as inputs in RayMan to calculate each subject's Physiological Equivalent Temperature (PET) (Matzarakis et al., 2010).

**Table 6-1** The gender and age distribution for the 320 questionnaires

Gender		Age group						Total
		15-24	25-34	35-44	45-54	55-64	+65	
MALE	Count	83	34	50	30	18	2	217
	% within gender	38.2%	15.7%	23.0%	13.8%	8.3%	0.9%	100.0%
	% within age group	62.9%	61.8%	78.1%	69.8%	81.8%	50.0%	67.8%
	% of Total	25.9%	10.6%	15.6%	9.4%	5.6%	0.6%	67.8%
FEMALE	Count	49	21	14	13	4	2	103
	% within gender	47.6%	20.4%	13.6%	12.6%	3.9%	1.9%	100.0%
	% within age group	37.1%	38.2%	21.9%	30.2%	18.2%	50.0%	32.2%
	% of Total	15.3%	6.6%	4.4%	4.1%	1.3%	0.6%	32.2%
%Total	Count	41.3%	17.2%	20.0%	13.4%	6.9%	1.3%	100.0%





**Figure 6-2** Distribution percentage of people purpose of visiting (on the left handside) and distribution percentage of how often they visit the area of study (on the right handside)

### 6.3 Thermal Sensation

The 7-point scale is used traditionally as a thermal sensation scale (Nicol, 2008), and is proposed by ISO 10551. According to Miller (1956), it is likely to be the ideal number of discrete categories to describe sensation. The common in use 7-point scales are the ASHRAE and Bedford scales. The scale of ASHRAE is a measure of the cold and heat and contains the concept of thermal sensation while the scale of Bedford embodies the concept of comfort (Pantavouet al., 2013). As a result, the questionnaire utilized in this study to recognize the thermal requirements of the outdoor users for Al-Muizz Street was designed from the seven point thermal sensation vote (TSV) scale originated by the ASHRAE (i.e. -3, cold; -2, cool; -1, slightly cool; 0, neutral; 1, slightly warm; 2, warm; and 3, hot). In the questionnaire, the thermal sensation vote (TSV) was determined by asking:

*How do you feel right now in this spot? Please choose a grade from the following thermal sensation scale that best reflects your current sensation*

-3	-2	-1	0	1	2	3
Cold	Cool	Slightly cool	Neutral	Slightly warm	Warm	Hot

Figure 6.3, illustrates the percentage distribution on number of thermal sensation votes (TSV's) of all subjects in both summer and winter. In the summer, the percentage of people who felt warm (TSV= 2) was the highest with value of (30%), whereas the percentage of those who were slightly cool (TSV= -1) was the highest with value (37.5%) in the winter. In the summer, (53.8%) of TSVs were within the three central



categories (“slightly cool”, “neutral”, “slightly warm”, TSV= -1, 0, 1), and as many as 43.1% reported that they felt warm or hot (TSV = 2, 3). In winter, 53.8% of TSV's were within the three central categories; while 26.9% voted for cool and 19.4% for cold.

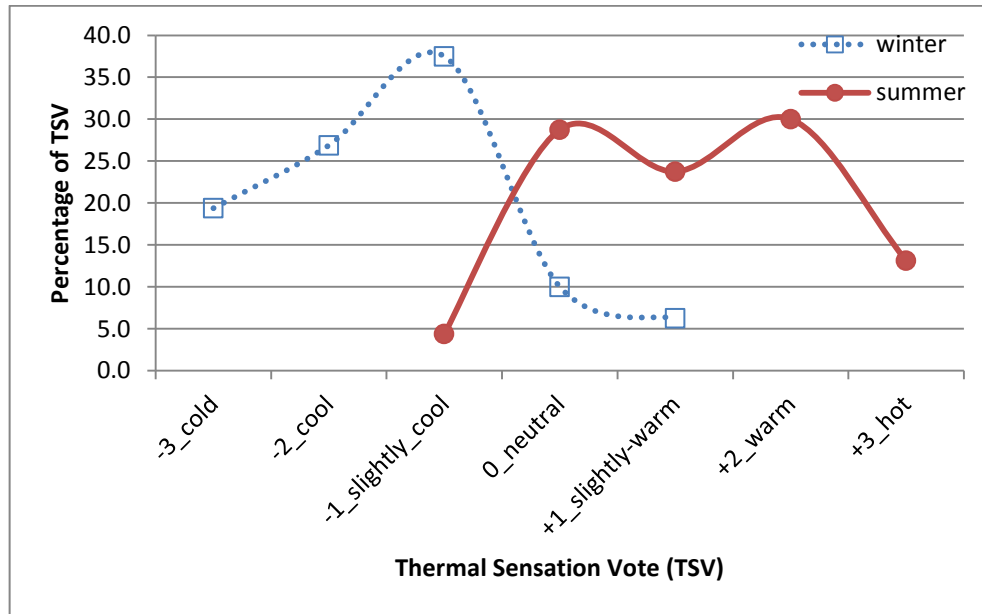


Figure 6-3 Percentage distributions of thermal sensation votes (TSVs) in cool and hot seasons

### 6.3.1 Thermal acceptable range

The ASHRAE Standard 55(2009) specifies that, satisfactory thermal conditions should be tolerated by a minimum 90% of occupants in a space when a high standard is applied; i.e.,  $\leq 10\%$  of occupants feel unacceptable”, while de Dear and Fountain (1994) defined it as the votes outside the three central categories of the TSV scale are “unacceptable” (i.e. -1, 0, +1). Therefore, the relationship between the subjective thermal responses such as acceptable, un-acceptable, and commonly accepted measure of thermal sensation can be obtained. Applying the de Dear and Brager (1998), method, the percentage of unacceptability in each  $1^{\circ}\text{C}$  PET interval group was calculated in order to estimate the PET range based on votes as shown in figure 6.4. The second-degree polynomial fitted curves were then applied over the plot, where its intersection with the unacceptability line are the 90% acceptability limits, which is 23 -  $32.5^{\circ}\text{C}$  PET. If compared with the thermal acceptable range of different climatic zones such as Western/middle European scale which is according to Matzarakis and Mayer (1996) is  $18 - 23^{\circ}\text{C}$  PET, and hot humid climate of Taiwan which is much higher with  $21.3 - 28.5^{\circ}\text{C}$  (Lin, 2009). This indicates that people in different regions have different thermal perceptions (Kenz and Thorsson, 2008). Although the  $R^2$  value (65.7) is in-

definitive, a similar range of 21-30°C was reported by Mahmoud (2011) who investigated an urban park close to the case study.

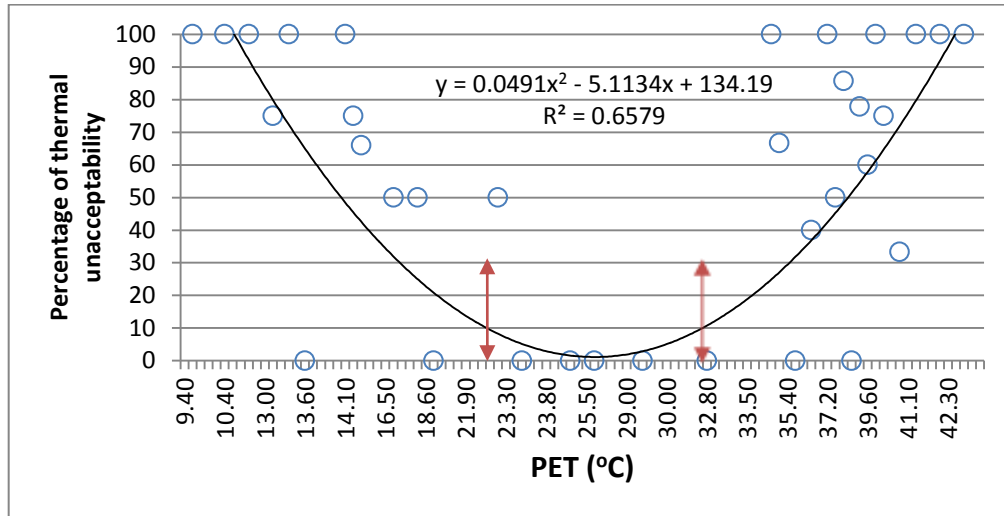


Figure 6-4 Thermal acceptable range for respondents in the street

#### 6.4 Thermal adaptation mechanism

From the adaptive principle point of view, if a change occurs to produce discomfort, people react in ways, which tend to restore their comfort (Nicol and Humphreys, 2002). Therefore, self-regulatory actions will take place. There are three main means of adaptive mechanisms: physiological, psychological, and behavioural adaptations, respectively (de Dear and Brager, 1998). However, there is general agreement that physiological acclimatization does not play a role in adaptive procedures (Fanger and Toftum, 2002) as such a mechanism becomes crucial in extreme environments, as the physiological responses start changing from repeated exposure to a stimulus, leading to a gradual decreased strain from such exposure (Nikolopoulou and Steemers, 2003) which is not the case in the current research. Thus, this study focuses on the psychological adaptation, and includes *experience*, *expectations* and *perceived control* as the most influential factors (Lin, 2009), and behavioural adjustment, which is also an important factor.

### 6.4.1 Psychological adaptation experience factor

The long term experience refers to the schemata people have constructed in their minds, where the level of adaptation to particular environmental dimensions, established as a function of past exposure, and act as strong determiners of the individual's evaluation of the surrounding environment (Wohlwill, 1974).

In order to verify this hypothesis, it was important to calculate the temperature at which the people feel comfortable in both seasons. The most common method used to model the relationship of thermal sensation and various factors is multiple regressions. The study conducted an analytical examination of thermal sensitivity applying the “One Way ANOVA” test, using TURKEY’S-B (equal variance assume) test, comparing values of subjective Thermal Sensation Votes (TSV) to objective PET values. This enabled examination of the homogenous groups of votes in order to grade the PET scale for the case study climate of Cairo.

The mean thermal sensation votes (MTSVs) were estimated as function of the PET consistent with weather collected data of both seasons as shown in the figures 6.5 and 6.6, where the correlation between the (MTSVs) and PET are described as follows:

$$\begin{aligned} \text{In summer} \quad \text{MTSV} &= 0.0998 (\text{PET}) - 2.947 && (\text{Eq. 6.1.}) \\ & && (R^2 = 0.83) \end{aligned}$$

$$\begin{aligned} \text{In winter} \quad \text{MTSV} &= 0.0881 (\text{PET}) - 2.1411 && (\text{Eq. 6.2.}) \\ & && (R^2 = 0.81) \end{aligned}$$

In the summer, the slope (0.099) of the fitted regression line indicates the thermal sensitivity of respondents to PET variations, which can be interpreted as each sensation level corresponding to 10°C of PET. About 83.47% of the variance in subjective thermal sensations can be explained by PET with the linear regression line. In the winter, the  $R^2$  value indicated that 81% of the variance in subjective thermal sensation is accounted for by the variation in PET with slope value equal (0.088) corresponding to 11.5°C PET per sensation unit. Comparative results indicate that respondents’ thermal sensation in summer is more sensitive than in winter. In order to verify the effects of experience on respondents’ thermal perception in Al-Muizz Street, neutral temperatures were considered. The neutral temperature is the temperature at which people feel thermally neutral (neither cool nor warm), and can be assessed using fitted equations

number 6.1 and 6.2 with  $MTSV = 0$ . The neutral temperatures for the summer and winter seasons were found to be  $29.5^{\circ}\text{C}$  and  $24.3^{\circ}\text{C}$  PET, respectively. This appears to suggest that people accept a higher temperature in summer more readily than they do in winter as shown in Table 6.2.

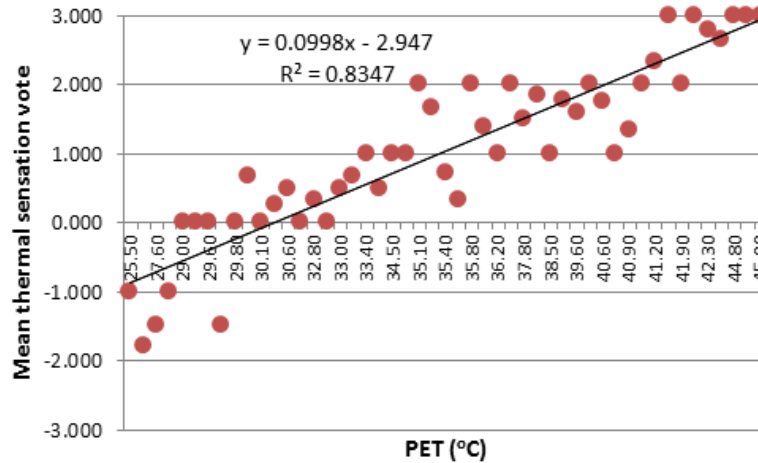


Figure 6-5 Correlation between PET and thermal sensation in summer 2012

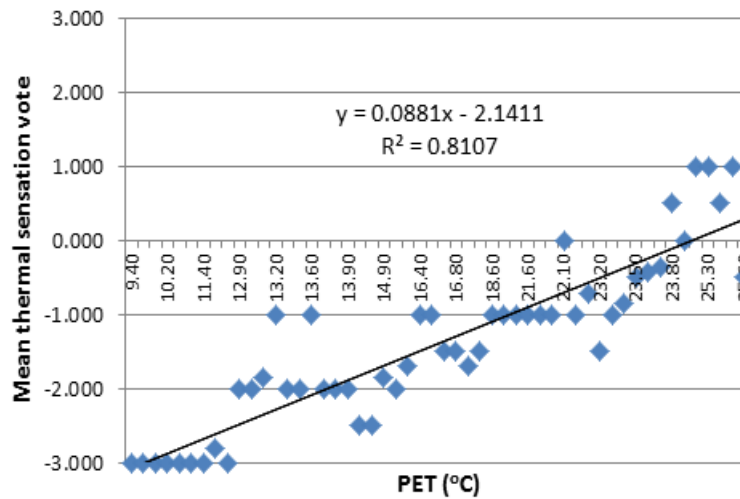


Figure 6-6 Correlation between PET and thermal sensation in winter 2012

Accordingly, these results indicate that people adjust their thermal perception during these two seasons according to the schemata they have constructed in their minds refers to as experience factor which reminds people that air temperature in the summer of Cairo is higher than those in the winter, therefore, their tolerance for high temperatures in hot season is better, and their neutral temperature is higher than that in the cool season (Nikolopoulou and Steemers, 2003). Conversely, since the summer season in Cairo is almost three times longer than the winter season, people are typically adapted to the hot conditions.

**Table 6-2** Physiology equivalent temperature (PET) at different levels of thermal sensation

MTSV	Thermal sensation	PET	
		Summer (°C)	Winter (°C)
-1	Slightly cool	19	12.9
0	Neutral	29	24
1	Slightly warm	39	35
2	Warm	49	> 35
3	Hot	> 49	-

### 6.4.2 Psychological adaptation and the expectation factor

In order to verify the expectation impact on thermal perception, the study examined the relationship between people's expectations and the thermal environmental variables including, air temperature, wind speed and solar radiation in the questionnaires. Then, a qualitative analysis based on preferred temperatures was performed.

#### 6.4.2.1 Expectations for thermal environmental factors

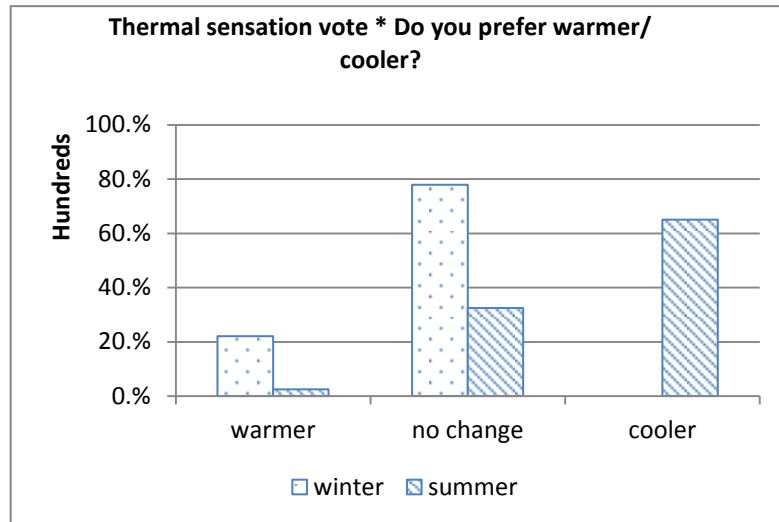
The respondents who felt comfortable with thermal environmental factors were selected in order to assess their preferences toward air temperature, wind speed and solar exposure. For instance, the subjects who voted for the three central categories on the TSV scale accounted for 177 subjects of the total sample (55.3%) as shown in table 6.3. Then the percentages of these subjects who want cooler, warmer, or unchanged air temperature were calculated for both seasons. The same method were applied in computing the percentages of the respondents who prefer stronger or weaker (sun and wind) for both seasons (Fig. 6.7).

Nikolopoulou and Steemers (2003) pointed towards deviations in expectations as a result of what people previously used to experience, which may cause a difference in people's sensation vote, as their expectations had changed. In winter, 77.9% of people felt that the thermal conditions were 'just right' while in summer 32.5% voted for no change and the rest (68.5%) mostly voted for a cooler temperature (Figure 6.7a). Similarly, most respondents prefer higher wind velocities in the summer 95.1% and lower wind velocities in the winter 72.2% (Figure 6.7b). For sunshine (Figure 6.7c), 97.8% preferred lower levels of direct solar radiation in the summer, while 88.3%

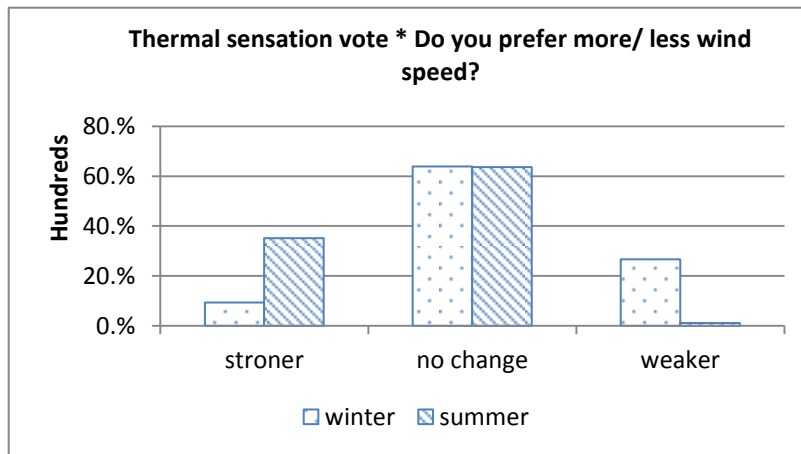
preferred higher solar radiation in the winter. Accordingly, this may explain the variation of expectations between seasons as individuals have different expectations or preferences for the examined thermal environmental factors and these expectations affect the respondents' thermal perception (Nikolopoulou and Steemers, 2003; Lin 2009). These findings are consistent with findings from other large scale studies such as the one performed by Nikolopoulou and Lykoudis (2006), in three different countries in Europe, Italy, Greece and Switzerland, highlighted that in Italy and Greece people have learned to cope with the expected hot summers, while in Switzerland, where the summers are cooler, a higher percentage of thermal discomfort from the heat was reported even though microclimate conditions were more favorable than in Italy and Greece for the same season.

**Table 6-3** Thermal sensation vote \* summer\_winter Crosstabulation

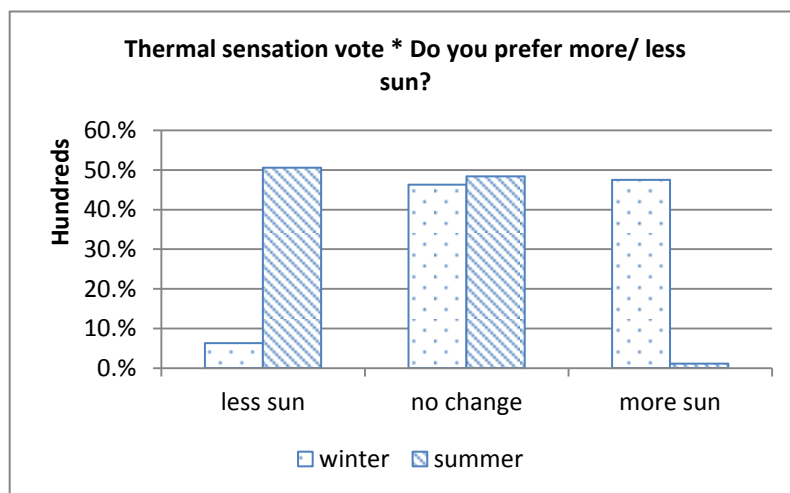
			summer	winter	Total
Thermal Sensation Vote	-3_cold	Count	0	31	31
		% within thermal sensation vote	0.0%	100.0%	100.0%
		% within summer_winter	0.0%	19.4%	9.7%
		% of Total	0.0%	9.7%	9.7%
	-2_cool	Count	0	43	43
		% within thermal sensation vote	0.0%	100.0%	100.0%
		% within summer_winter	0.0%	26.9%	13.4%
		% of Total	0.0%	13.4%	13.4%
	-1_slightly_cool	<b>Count</b>	<b>7</b>	<b>60</b>	<b>67</b>
		% within thermal sensation vote	10.4%	89.6%	100.0%
		% within summer_winter	4.4%	37.5%	20.9%
		% of Total	2.2%	18.8%	20.9%
	0_neutral	<b>Count</b>	<b>46</b>	<b>16</b>	<b>62</b>
		% within thermal sensation vote	74.2%	25.8%	100.0%
		% within summer_winter	28.8%	10.0%	19.4%
		% of Total	14.4%	5.0%	19.4%
	+1_slightly-warm	<b>Count</b>	<b>38</b>	<b>10</b>	<b>48</b>
		% within thermal sensation vote	79.2%	20.8%	100.0%
		% within summer_winter	23.8%	6.3%	15.0%
		% of Total	11.9%	3.1%	15.0%
+2_warm	Count	48	0	48	
	% within thermal sensation vote	100.0%	0.0%	100.0%	
	% within summer_winter	30.0%	0.0%	15.0%	
	% of Total	15.0%	0.0%	15.0%	
+3_hot	Count	21	0	21	
	% within thermal sensation vote	100.0%	0.0%	100.0%	
	% within summer_winter	13.1%	0.0%	6.6%	
	% of Total	6.6%	0.0%	6.6%	
total	Count	160	160	320	
	% within thermal sensation vote	50.0%	50.0%	100.0%	



A. Percentage of preference vote for air temperature



B. Percentage of preference vote for wind



C. Percentage of preference vote for sun

Figure 6-7 Percentage of preferences votes including air temperature, wind speed and sun exposes



### 6.4.2.2 Preferred temperature

The neutral temperature is defined as the temperature at which people feel comfortable. However, the preferred temperature is the condition in which individuals prefer neither warmer nor cooler temperatures (Fanger 1973), in other words is the temperature, which people want. Probit analysis is useful for determining thermal neutralities, that is, temperatures most frequently coinciding with "neutral" thermal sensations (Ballantyne et al., 1977), using the preference votes in questionnaires, accordingly the impact of expectations on thermal comfort is verified.

Figure (6.8) depicts results of the probit analysis from logistic regression examining the preferred temperature base on the questionnaires' preference votes of "prefer cooler" and "prefer warmer" against each 1°C PET intervals. The preference percentage of each group is calculated and fitted separately within the probit model. The intersection of the two fitted probit lines was the preferred temperature at which individuals did not prefer either a cooler or a warmer temperature (de Dear and Fountain, 1994). The preferred temperature in the cold and hot seasons was 24°C PET, which is lower than the neutral temperature in summer by 5°C and 0.5°C in winter yet the preferred temperature still falls within the thermal acceptance range (23°C - 32°C). It is also interesting to mention that the values are very similar to what reported by ASHRAE (1992) as stated in table 6.4, although it is for the indoor environment.

In summer, the survey indicated neutral temperatures of 29°C under section (6.4.1.) yet the probit analysis indicates much lower preferred PET decreasing to 24°C. This comparative result demonstrates the impact of expectations on respondents' thermal comfort, indicating that there is a wider temperature preference gap between the maximum tolerated temperatures and those preferred in summer than there is in winter. The finding also proves that people are looking after cool conditions in a hot climate, the results were found consistent with the assumption by McIntyre (Steemers, 2003) and Lin (2009) studies.

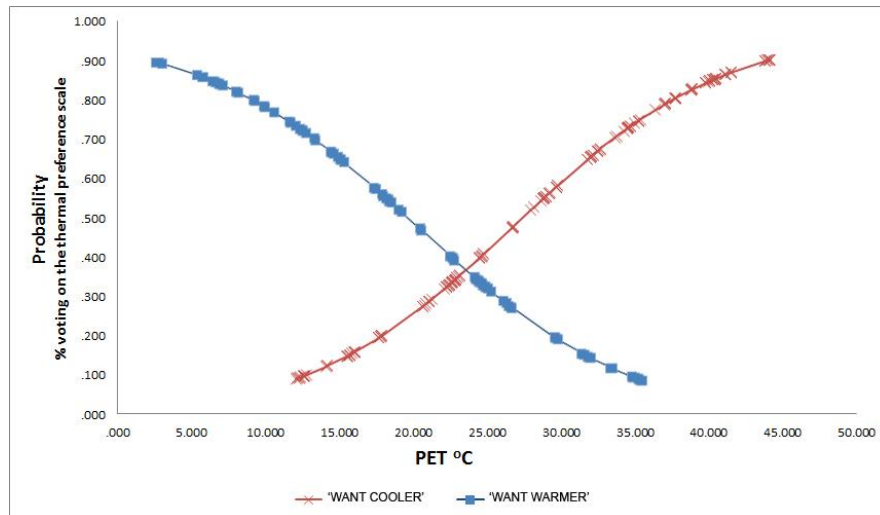


Figure 6-8 Preferred temperature by Probit model

Table 6-4 Thermal Comfort Conditions –ASHRAE Standard 55 (1992) Source: Charles (2003)

Season	Optimum Temperature <sup>a</sup>	Acceptable Temperature Range <sup>a</sup>	Assumptions for other PMV inputs <sup>b</sup>
winter	22°C	20-23°C	relative humidity: 50% mean relative velocity: < 0.15 m/s mean radiant temperature: equal to air temperature metabolic rate: 1.2 met clothing insulation: 0.9 clo
summer	24.5°C	23-26°C	relative humidity: 50% mean relative velocity: < 0.15 m/s mean radiant temperature: equal to air temperature metabolic rate: 1.2 met clothing insulation: 0.5 clo

a: refers to operative temperature, defined as “the uniform temperature of an imaginary black enclosure in which an occupant would exchange the same amount of heat by radiation plus convection as in the actual nonuniform environment. Operative temperature [ $t_o$ ] is numerically the average of the air temperature ( $t_a$ ) and mean radiant temperature ( $\bar{t}_r$ ), weighted by their respective heat transfer coefficients ( $h_c$  and  $h_r$ ): (ASHRAE Standard 55, 1992, p.4)

$$t_o = (h_c t_a + h_r \bar{t}_r) / (h_c + h_r) "$$

b: if the value of these assumptions differs, refer to comfort zone diagrams and tables given in ASHRAE Standard 55, for appropriate temperature ranges.

### 6.4.3 Perceived control factors for psychological adaptation

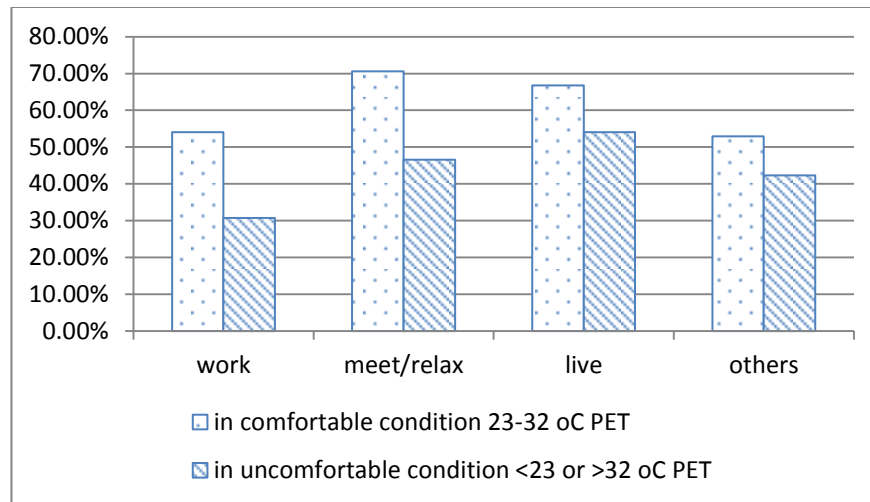
It is now widely acknowledged that people, who have a high degree of control over their environment and a source of discomfort, tolerate wide variations, and the negative emotional responses are greatly reduced (Nikolopoulou and Steemers, 2003). For instance people who have control over the windows and the fans in a naturally ventilated indoor space adjust their neutral temperatures to the thermal condition they experience (Barger et al., 2004), indicating an acceptance of adaptive behavioural measures leading to a tolerance of a wider range of thermal comfort temperatures than

those occupying completely sealed and mechanically ventilated buildings. The same approach applied in outdoor environment such as the choice availability for sitting in the sun or shade (Nikolopoulou and Lykoudis, 2006; Nikolopoulou and Steemers, 2003). Thus, in this section, the thermal perceptions of four groups visiting the street for different reasons are compared and the effects of perceived control on thermal comfort are discussed.

The subjects were asked about the main purpose for passing by or visiting the street to investigate whether respondents chose to come to the square autonomously; four answers were provided for this question. The first answer is working in the area, so there is no much choice to leave or stay. The second option is to meet people and relax for social activities participate in social or cultural activities, indicating that people simply want to relax. The third option is living on the street; where in this case they have the option to stay indoors if they feel thermally uncomfortable. The final category was passer-by's for a shortcut to another destination. The respondents were then divided based on these four options and the percentage of respondents who felt comfortable in a "comfortable condition" and in an "uncomfortable condition" were calculated on the bar chart of figure 6.9.

The "comfortable condition" was defined according to the thermal comfort range of  $23^{\circ}\text{C} - 32^{\circ}\text{C}$  PET, based on the earlier analysis of thermal acceptable range (figure 6.4). The "uncomfortable condition" was defined as the thermal condition outside this range, i.e.,  $\text{PET} < 23^{\circ}\text{C}$  or  $\text{PET} > 32^{\circ}\text{C}$ . "Feeling comfortable" is defined as when respondents chose "yes" in response to the question of "do you perceive the overall thermal environment as comfortable or not?". Figure 6.9, highlights the impact of 'the ability to control one's environment on thermal perception. The largest percentage who felt comfortable was people who were visiting the street to socialise and relax (70.6%). This was followed by people who lived in the area (54%), while people who worked on the street reported the lowest percentage of satisfaction with the thermal conditions. According to Nikolopoulou and Steemers (2003), the reason that an individual is present in a certain place can also affect thermal sensation. For instance, people indicated more tolerance when they exposed themselves to the conditions willingly, as in the case of playing outdoors, because they are exercising control and exploiting available choices. In contrast, the perception of being obliged to be in a place for work

led to decreasing the perception of exercising control leading to less tolerance of the thermal conditions. These comparative results highlighted the importance role of the Perceived control and the ability to control the length of exposure to the perceived uncomfortable conditions on influencing the thermal sensation.



**Figure 6-9** Percentage of users visiting the street for different reasons who felt overall thermally comfortable and uncomfortable under comfortable conditions  $PET > 23^{\circ}\text{C}$  or  $PET < 32^{\circ}\text{C}$

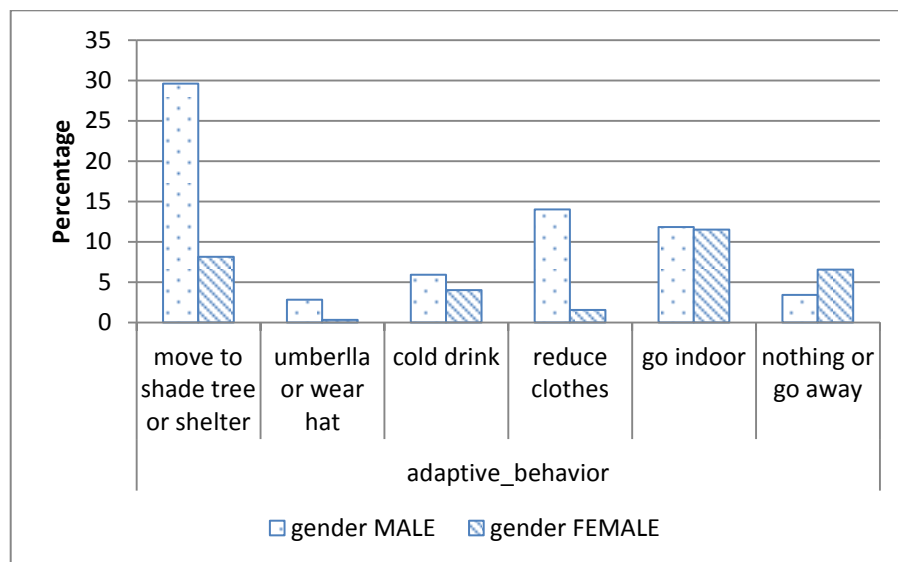
#### 6.4.4 Behavioural adaptation

Human adaptation and the sensation of the thermal environment is the comprehensive effect of the three behaviour adjustments (Yao et al., 2009). If the person is dissatisfied with the uncomfortable condition, they undertake some behavioural adjustments, which can be classified into personal, environmental and cultural adjustments (de Dear and Brager, 1998).

During the survey, the respondents were asked to rank in order what action or behaviour, from five given behaviour adjustments, they would prefer to take if they felt it was too hot in the outdoor spaces. Figure 6.10 shows the cross-tabulation analysis of the survey and respondents' gender. The analytical results reveal that moving to shade appears to be the preferred behaviour where almost half of the sample (48%) voted for it. However, only 8% of the females chose to do the same, which may be explained by the conservative culture of separation between men and women in this old district. Men usually occupy the street's shaded areas to engage in commercial activities, while the females have to walk in the unshaded centre of the street to avoid physical proximity to men.

Secondly, almost 15% of males chose to reduce clothing layers against a very low percentage of females (<2.0%). For females, although reducing clothing layers is a thermally adaptive and autonomous behaviour, the percentage of respondents utilizing this alternative was low due to the cultural constraints in the area, where it is still unacceptable for females to remove the veil or wear light revealing clothes even for the necessity of adapting to thermal conditions.

Thirdly, for people living and working in the area almost the same percentage of (12%) females and males opted for going indoors as a mechanism to manage their thermal environment, referring to as the perceived control mechanism where the respondents have a high degree of control over a source of discomfort.



**Figure 6-10** Percentage of males and females who adopted adaptive behaviours

Figure 6.11 examines the clothes worn by male in correlation with PET, represented as (clo.) mean value, in compliance with ASHRAE standards 55-2009 (2009), the results reveals a direct relation between the PET and the amount of clothes worn by the respondents as these amount increases gradually when PET increases, the clothes worn by respondents, remain at approximately 0.6 (clo.). Thus, the amount clothing which can be reduced is limited, whereas other actions are required to adapt to high temperatures. While for females the level of clothing to be adaptable is limited due to the tradition and culture constrains where most the women have to cover their arms and hair.

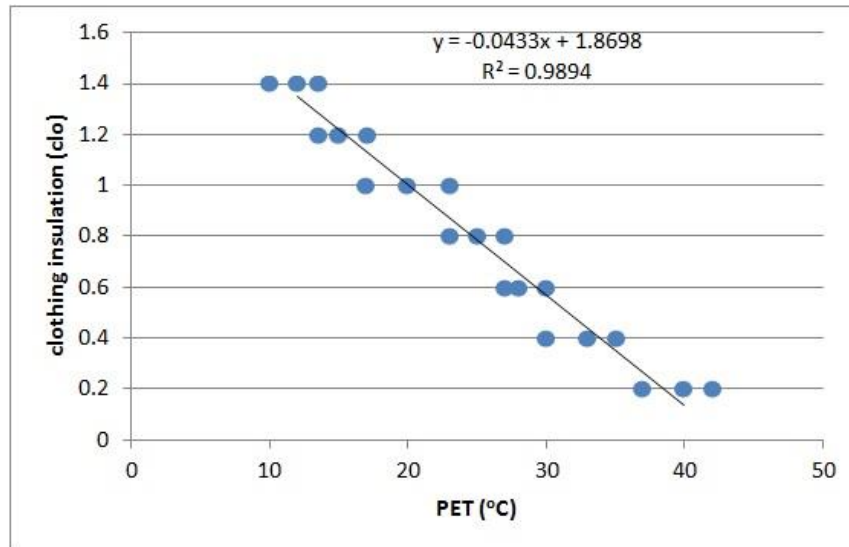
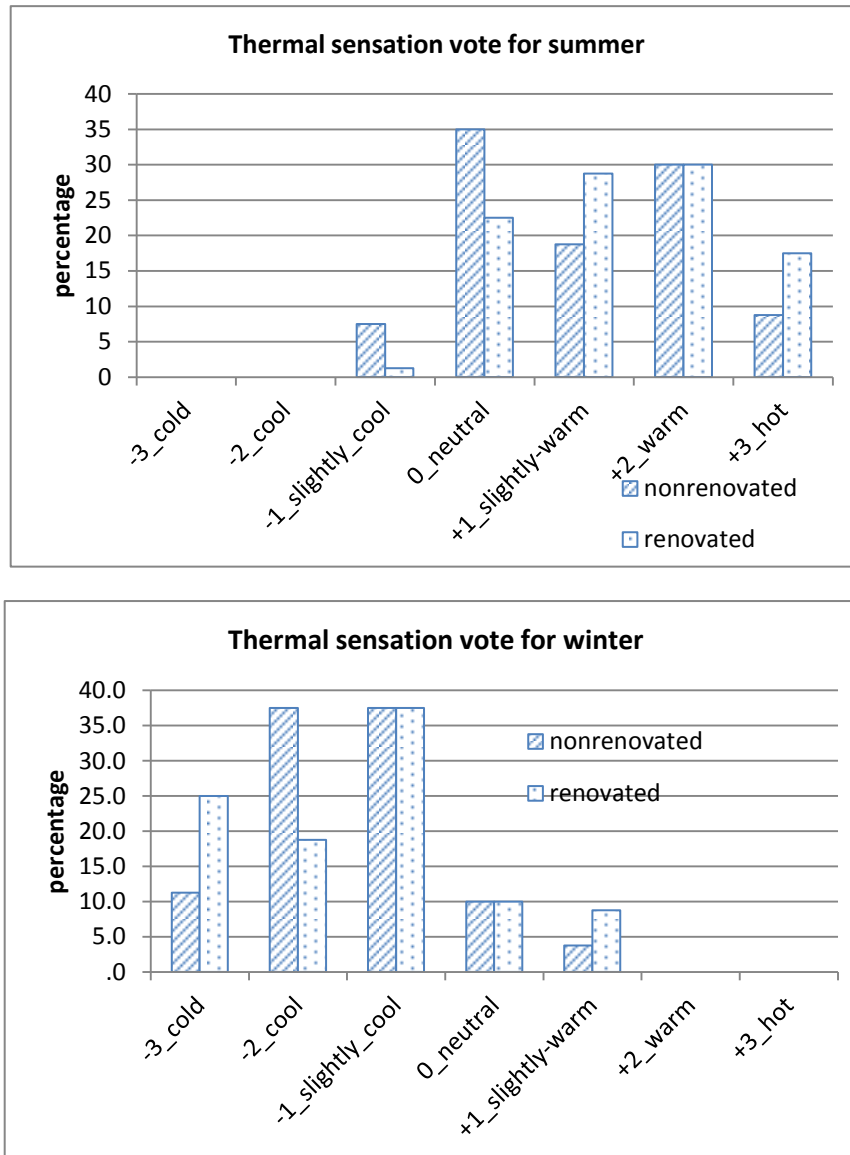


Figure 6-11 Clothes worn by males under different PET segments

### 6.5 The thermal sensation votes (TSV) difference within Al-Muizz's two locations

Al-Muizz Street includes a diversity of zones, as each part of the street, the renovated and non-renovated, has its own urban distinctive features and different levels of adaptation regarding local people settings for comfort. In order to investigate the difference in the occupants' thermal perception, the subjective votes about the thermal environment for each part of the street were compared and presented (Figure 6.12). Only the votes of -1, 0, and +1 describe satisfactory thermal environments, following Fanger's theory (Fanger, 1972).



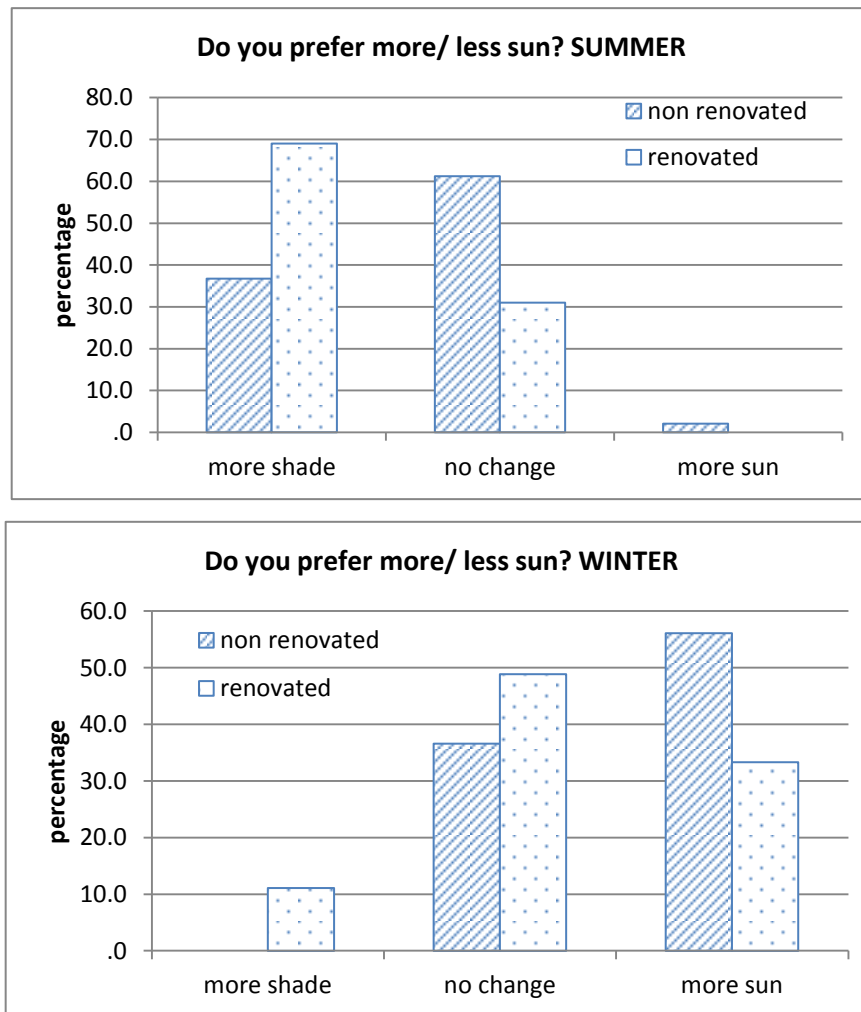
**Figure 6-12** The subjective thermal sensation votes (TSV) in the two different parts of Al-Muizz

In summer, it can be noticed that a higher percentage of people within the non-renovated part (61.3%) accepted the thermal environment, compared with (52.6%) in the renovated side. During the winter, the difference in percentage of satisfied people between both parts was less than the summer, where people's acceptance of the thermal environment in the renovated part was higher, recording 56.5% against 51.5% for the non-renovated. This may be attributed to the difference between the direct solar radiations received on both parts, where there is almost a complete absence of the direct solar radiation in the non-renovated part, which is the most severe climatic element throughout the daytime in summer for pedestrians in hot, arid cities. This affects the mean radiant temperature unlike the wind speed and relative humidity, where changes

have less effect on the thermal sensation votes. This correlates with the Nikolopoulou's (1998) study, stating that the mean radiant temperature and air temperature proved to have a higher impact on the outdoor thermal comfort level. Thus, the study selected the respondents who voted for the three central categories on the TSV scale, and then calculated the percentage of these respondents who prefer more shade or more sun (Figure 6.13). The results illustrated that in summer the respondents who voted for no change was 61.2% in the non-renovated part, against 31% in the renovated one, while almost 70% asked for more shade in the renovated part compared to 36.7% in the non-renovated one who asked for the same option.

During the winter, the results revealed that almost 50% of the renovated parts agreed with no change compared to 36.6% in the non-renovated, with 56.1% reported for more sun against 33.3% for the renovated segment. According to these analytical results, the non-renovated section seemed to have better thermal comfort conditions than the renovated one during the summer time. However, the renovated part acts a little bit better in the winter season by allowing more sun to reach the occupants.





**Figure 6-13** The percentage of preference votes for more shade, no-change, or more sun in the two parts of Al-Muizz

## 6.6 Correlation between predicted thermal comfort and subjective thermal sensation

The calculated PET based on microclimatic measurements (from the previous chapter) was correlated with perceived thermal sensation (on a 7-point scale), and the slope of the resulting linear regression (Figures 6.5 and 6.6, solid line) indicates that pedestrians tended to highly tolerate the varying thermal conditions in the outdoor environment as the thresholds for 'warm' and 'hot' conditions occurred at successive increments of about 10°C against 11.5°C in winter. At the same time, compared to the PET indoor from previous studies, the regression line has a shallower slope corresponding to a higher increment value, which suggests that pedestrians had a larger tolerance to outdoor conditions than indoor (Nikolopoulou et al., 2001; Thorsson et al., 2004b). About 83.4% of the variability in subjective thermal sensations can be explained by the

PET regression line in the hot seasons, while it was 81% for the cool seasons. This discrepancy between predicted thermal comfort and perceived thermal sensation is expected to reflect other non-environmental factors which might influence a subject's thermal feeling. In the following section, a series of detailed statistical analyses in relation to thermal sensation are explained.

## 6.7 Non-environmental variables

In addition to the question of thermal sensation and thermal adaptation, the questionnaire also covers other non-environmental variables such as personal thermal sensitivity and preference, short-term thermal history, and frequency of and reason for presence in the place. The general results from these questions are reported here.

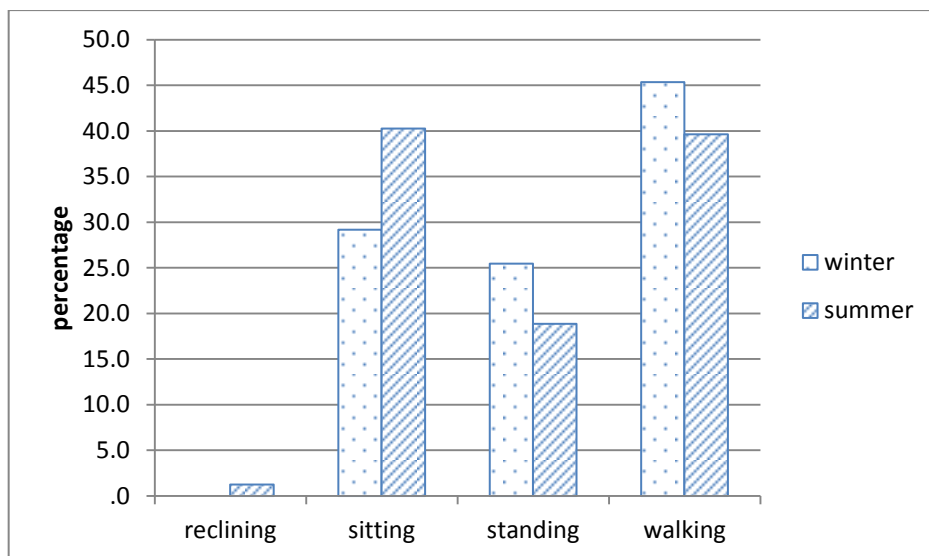
The question "How long have you been outdoors?" provided pedestrians with three options (less than 2 minutes, between 2 and 10 minutes and more than 10 minutes), and was accompanied by the question "Just before you arrived at this location, were you indoors (conditioned or not) or outdoors (in sun or shade)?" These two questions aimed to investigate to what extent the short-term thermal history of interviewees would influence their expressions of thermal sensation (Spagnolo and de Dear, 2003; Nikolopoulou and Steemers, 2003) (for more details, see Section 3.5.3.3).

As shown in Table 6.5, in summer close to half the number of interviewees (46.9%) had been outdoors for 2-10 minutes prior to arriving at the experimental locations. The majority of pedestrians (85%) who had been exposed to the outdoor conditions for this period of time or longer were sheltered from direct solar radiation by staying in the shade (70.6% indoor, 14.4% outdoor shade). In winter, it was different as the majority of pedestrians (61.9%) who had been exposed to the outdoor conditions for the same period of time or longer were spending their time outdoors with 35% staying under direct sun and 26.9% in shade, with 60% of the interviewees being outdoors for more than ten minutes before the interview. Neither the location of prior activity (indoors with conditioned or not, or outdoors with shaded or not), nor the time spent outdoors, were found to be statistically significant. There seems to be no sign of short-term acclimatization to a particular location.

**Table 6-5** Contingency table of short-term thermal history

summer_winter		before arriving at this place				Total	%
		indoor_conditi oned	indoor_ventilat ed	outdoor_sun	outdoor_shade		
summer	2-10min	22	31	12	10	75	46.9
	+10min	20	40	12	13	85	53.1
	Total	42	71	24	23	160	
	%	26.3	44.4	15.0	14.4		100
winter	2-10min	6	17	20	21	64	40
	+10min	6	32	36	22	96	60
	Total	12	49	56	43	160	
	%	7.5	30.6	35.0	26.9		100

An additional question regarding previous physical activity just prior to the interview based on the interviewer's observations revealed that among the visiting pedestrians, the majority of interviewees in summer had either been sitting (40%) or walking (39%), while in winter walking was the predominant activity (45.6%) followed by sitting (28.8%), as shown in Figure 6.14.

**Figure 6-14** Percentage distributions of the respondents' activities

The analysis showed that physical activity led to a significantly warmer thermal sensation under the same PET. The analysis of Variance (One-Way ANOVA) was applied, and the overall correlation between the thermal sensation votes and the metabolic rate as shown in Figure 6.15 was ( $R^2 = 0.84$ ). This indicated that 84% of the

variance in subjective thermal sensation was accounted for by variation in physical activity.

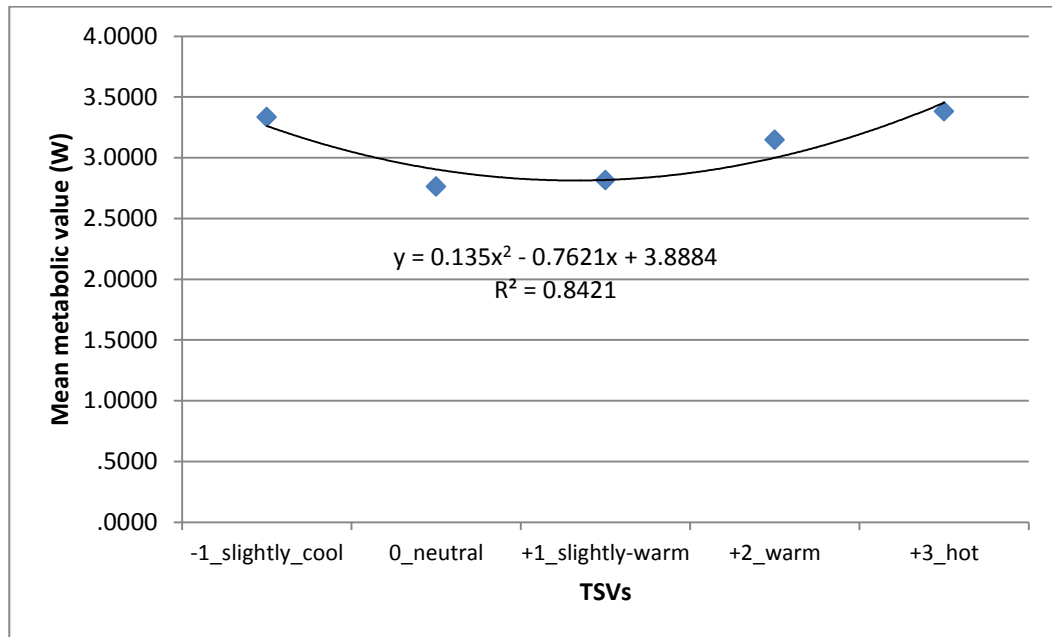


Figure 6-15 Adjusted correlation between TVS and physical activities under outdoor conditions

### 6.7.1 Frequency of visitation

The statistical analysis indicated that the frequency at which respondents were present in the location played a less significant role in the respondents' thermal sensation. This in fact was not a surprising result, since most of the interviewees were residents or people who had regular contact with the street and would be expected to pass by this location often and to be uniformly familiar with the space and the local microclimate.

### 6.7.2 Personal variables

Neither gender nor clothing made a significant contribution to explaining variations in thermal sensation by PET. Observations show that almost all the pedestrians in the summer survey were wearing summer clothes with low thermal resistance, except for the majority of the females whose clothing habits were influenced by the culture rather than the surrounding climate. Any differences in clothing which may have been present did not have a noticeable influence on subjective thermal sensation. The situation in winter might be quite different, as both genders seemed to wear clothes corresponding with the climate with high thermal resistance, which greatly restricts heat loss from the

body and can allow pedestrians to feel relatively warm under considerably cold conditions.

## 6.8 Conclusion

The study presents the methodology and the findings of an outdoor comfort survey in Cairo in an attempt to enrich the knowledge of the relationship between subjective thermal sensation and outdoor thermal environment, also to figure out the acceptable comfort index range which can fit into the study context in order to be used as the baseline in assessing the different scenarios proposed in chapter seven. However, since thermal comfort ranges vary in different climates, the outcomes of this study could be considered indicative of expectations in a hot, arid climate of a conservative cultural nature. The main findings of the chapter were as follows:

- People were asked to indicate their thermal sensation while objective and subjective measurements were taking place. The calculated PET based on microclimatic measurements (for one week in both summer and winter, 2012) was correlated with perceived thermal sensation (on a 7-point scale). The thermal comfort range was 22-32°C PET, which is 1-2°C higher than previous studies conducted in Cairo urban Green Park where the range was 21-30°C. The thermal comfort analysis for the psychological and behavioural factors shows some evidence for the willingness to undertake adaptive behaviours.
- The length of exposure and the ability to exercise control affected the perceptions of the thermal environment where the summer neutral temperature (29.5°C PET) was 5°C PET higher than in winter (24.5°C PET). This suggests that people accept a higher temperature in summer than in winter as a result of their experience, which reminds them that the temperature in summer is higher than winter so their tolerance for a higher temperature is enhanced. The same conclusion was reported in several studies, for instance a study in the UK indicated that the difference in summer (28°C) and winter (8°C) for neutral temperatures is approximately 20°C and in the hot, humid climate of Taiwan the difference between summer (25.6°C PET) and winter (23.7°C PET) is 1.9°C PET (Lin, 2009). Further research in the Mediterranean climate of Tel-Aviv (Cohen et al., 2013) reported that the difference

between the neutral temperature during the cold season (22.7°C PET) and the neutral temperature in the hot season (23.9°C PET) is 1.2°C.

- The expectation mechanism was also examined, indicating that the respondents' preferences for a low air temperature and lower levels of exposure to direct solar radiation in the hot summer season are stronger than that in the winter season (Lin, 2009). This assumption was reported by McIntyre (Stemmers, 2000).
- The preferred temperature was 24°C PET for both seasons, which is lower than the neutral temperature in summer by 5°C and 0.5°C in winter.
- Additionally, the Perceived control analysis showed that people who can exercise control and take advantage of available choices are more tolerant toward the surrounding thermal environment, such as in the case of socializing. People with a low level of autonomy such as people going to work have lower tolerances than people who are willingly exposed to the conditions.
- From the behavioural adjustment analysis, seeking shade was the predominant adaptive behaviour. However, culture appears to influence the respondents' choices, particularly the females, as the amount of clothing worn by the females differs than males.

Finally, in relation to the first and second research hypotheses mentioned in Chapter One regarding the extent to which subjective human parameters affect people's assessment of the outdoor environment, the analysis suggested that all the examined meteorological, psychological and behavioural variables were significantly correlated with the thermal sensation vote. Accordingly, Nikolopoulou and Stemmers (2003) demonstrated through regression analyses that only approximately 50% of the variance between objective and subjective comfort evaluations could be explained by physical and physiological conditions. They speculated that the difference was attributable to psychological factors such as naturalness, past experience, perceived control, time of exposure, environmental stimulation, and expectations. In terms of implications for planning, the physical environment, psychological adaptation and a deep understanding of the cultural context is argued to be complementary rather than contradictory, and consideration of this duality could increase the use of the city's open spaces.

# 7

---

*“Where science is a collected body of theoretical knowledge based upon observation, measurement, hypothesis and test...design is the collected body of practical knowledge based upon sensibility, invention, validation and implementation” (Archer, 1979, p. 18).*

## **Chapter Seven**

---

### **7. The Comparative Numerical Assessment**

---

#### Key Concepts

- 7.1. Introduction
- 7.2. Tent performance and CFD
- 7.3. CFD simulation settings
- 7.4. CFD simulation validation
- 7.5. Comparative study
- 7.6. Conclusion

## 7.1 Introduction

It was concluded in the previous chapters that in the hot arid climate more than 70% of the solar radiation reaches the Earth's surface, while this proportion reaches only about half in Central Europe. Also, it was seen that the mean radiant temperature ( $T_{mrt}$ ) has a major effect on thermal perception during the hot season, where the intensity of solar radiation and the clarity of the sky are the main reasons for the extreme levels of heat encountered in Cairo (Sheta and Sharples 2010). In Chapter Five, the non-shaded locations contribute to a high thermal discomfort sensation with a difference in  $T_{mrt}$  equal to 14°C between the shaded and non-shaded areas which is a very important indicator to be considered in achieving better outdoor thermal environment. In Chapter Six, the respondents' thermal sensation was more sensitive to the summer than winter climatic variations, and the correlation with the high air temperature and  $T_{mrt}$  were found to be more significant, and seeking shade was the predominant adaptive behaviour with thermal comfort range between 22 - 32°C. Human thermal comfort in the outdoor spaces of the hot, arid region may depend as much on the radiant load to which a pedestrian is exposed than the temperature of the air. While the designers' ability to control air temperature in outdoor spaces is very limited, it is fairly simple to control exposure to the direct solar radiation. Additionally, shade is still the main variable to be taken into consideration when aiming for the rehabilitation of traditional retail streets, and its implementation in locations characterized by outdoor hot discomfort conditions for pedestrians (Marques de Almeida, 2006) (figure 7.1). However, in order to specify the optimum shading design and typology, an investigation of the environmental behaviour is required, particularly after sunset as it was reported in chapter three (literature review) and five (field measurements) that the street locations with low SVF, being covered by shading devices, took a longer time to cool down during the night time compared to other unobstructed locations. The assessment including the wind flow, the air temperature distribution and solar access underneath the different shading patterns. Thus, this chapter focuses on investigating the effect of different shading configurations, particularly to enhance occupants' comfort level underneath, using a computational fluid dynamics (CFD) simulation,

The chapter is divided into two main sections; the first section reports the choice of the CFD and the validation results based on field measurement comparison; and the



second section reports the investigated variables for the different case studies and is further divided into three subsections. The first subsection reports the results of different wind flow for all the investigated cases; the second subsection reports the results of different air temperature distribution patterns underneath each case, and the last subsection reports the results of the solar access analyses for the best and base cases.



Calle Marqués de Larios, Málaga (Spain)



Calle Sierpes, Seville (Spain)



The hot streets of Agueda (Portugal)



San Antonio, Texas

**Figure 7-1** Shading canopies across the full width of pedestrian streets in different hot countries

## 7.2 Shading performance and CFD

The topology and form of the tensile structure can be used to alter the quantity and direction of solar radiation entering the enclosure. These can also be used to modify the airflow underneath the structure and in its vicinity. Fabric membranes can only be used to create an intermediate climate or meso-climate that acts as a buffer between the external climate and the environmentally semi-enclosed spaces to moderate and regulate them.

The membrane form and orientation and the associated thermal mass (walls, floors, patios, etc.) can be designed to suit different seasons and climates. For example, in summer, the fabric structure should be shaped and oriented to provide shade by screening solar radiation and the fabric material chosen should be such that it absorbs and transmits a minimum amount of solar heat into the space, and work in conjunction with thermal mass distributed within the enclosure to stabilise temperatures. It should be designed with a number of different openings so that the internal heat finds a place to escape at night through the openings, or it could also be folded at night, so as to encourage ventilation and escape of the heat through radiation that is stored in the thermal mass during the day to the night sky. In winter, the opposite should occur, as the structure should be designed to maximise the absorption of daytime solar energy through solar absorption by thermal mass (such as buildings, terraces, paving, patios, walls) and reradiate it into the enclosure and at the same time screen the chill wind. Accordingly, as mentioned in Section 4.6.3, it was decided to obtain these design contributions using the numerical model CFD code Fluent 13.0, following the best practice guidelines (BPG) (Blocken, 2012). This enables a large number of choices to be made by the user and ensures the reliability of the results and their validity (Franke et al., 2004, 2007, 2011; Wit, 2004; Franke et al., 2007; Blocken et al., 2012) (for more detail, refer to Section 4.6.3.1).

### **7.3 CFD simulation settings**

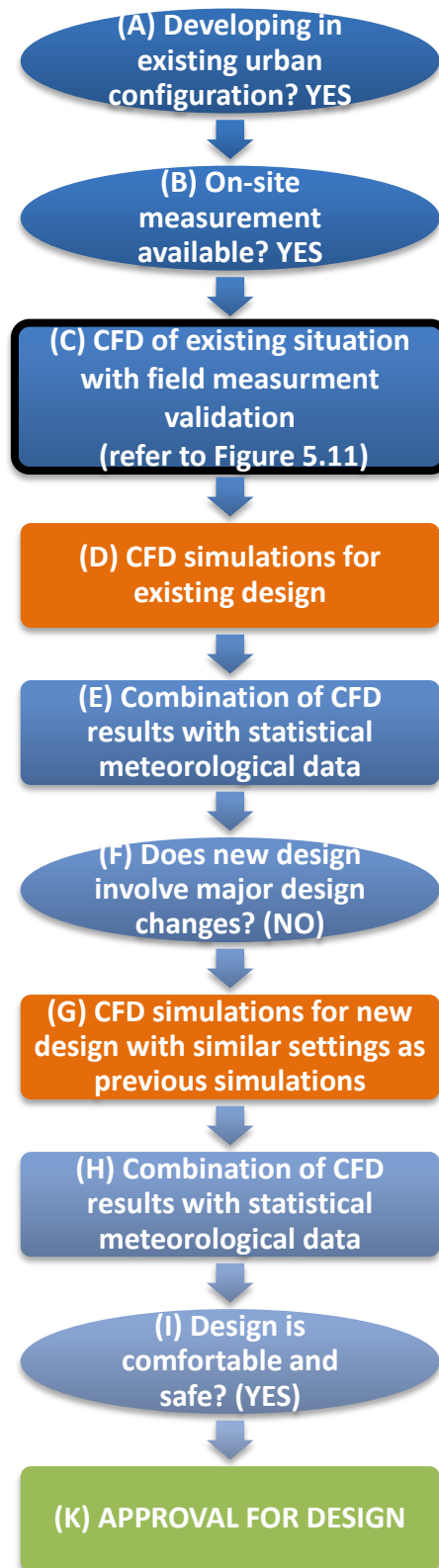
All the following simulations were all adjusted according to the best practice guidelines (BPG) scenario for developing existing urban configurations, as illustrated in Figure 7.2 and explained in Section 4.6.3.1, and the CFD requirements in Section 4.6.3.2. The adjustments concerned the essential configurations and requirements for the mathematical model, the geometry and solution domains, and the boundary conditions as stated in table 7.1.

**Table 7-1** Requirements for a consistent CFD simulation (AboHela et al., 2012).

Solution method	Second order schemes or above should be used for solving the algebraic equations
Residuals	in the range of $10^{-4}$ to $10^{-6}$
Mesh	Multi-block structured mesh Carrying out sensitivity analysis with three levels of refinements where the ratio of cells for two consecutive grids should be at least 3.4 Mesh cells to be equidistant while refining the mesh in areas of complex flow phenomena If cells are stretched, a ratio not exceeding 1.3 between two consecutive cells should be maintained
Turbulence model	Realizable k- $\epsilon$ turbulence model
Accuracy of studied buildings	Details of dimension equal to or more than 1m to be included
Domain dimensions	If H is the building height; lateral dimension = $2H$ +building width Flow direction dimension = $20H$ +building dimension in flow direction Vertical direction = $6H$ While maintaining a blockage ratio below 3%
Boundary conditions	Inflow: Horizontally homogenous log law ABL velocity profile _velocity inlet Bottom: No-slip wall with standard wall functions Top and side: symmetry Outflow: pressure outlet

### 7.3.1 Computational domain dimension

The model was placed in a computational domain with dimensions 147m x 85m x 45m as X, Y and Z (length, width and height), respectively. In order to avoid the artificial acceleration of the flow, the minimum distance from the building to the side, to the inlet and to the top of the domain were adjusted to be at least five times (5H) the tallest building (H) and the distance from the building to the outlet was adjusted to fifteen times the height (H) (Franke et al., 2007; Tominaga et al., 2008). The maximum blockage ratio is 1.5%, which is below the recommended maximum of 3% (Franke et al., 2007; Tominaga et al., 2008b).



**Figure 7-2** Flowchart illustrating the scenario framework for the assessment of pedestrian comfort using CFD for the case study (the milestone questions which lead to this scenario are given in ellipses). Part C is further outlined in Figure 4.8 (after Blocken, 2012, refer to Figure 4.7).

### 7.3.2 Horizontal homogeneity of the atmospheric boundary layer (ABL) profile through the computational domain

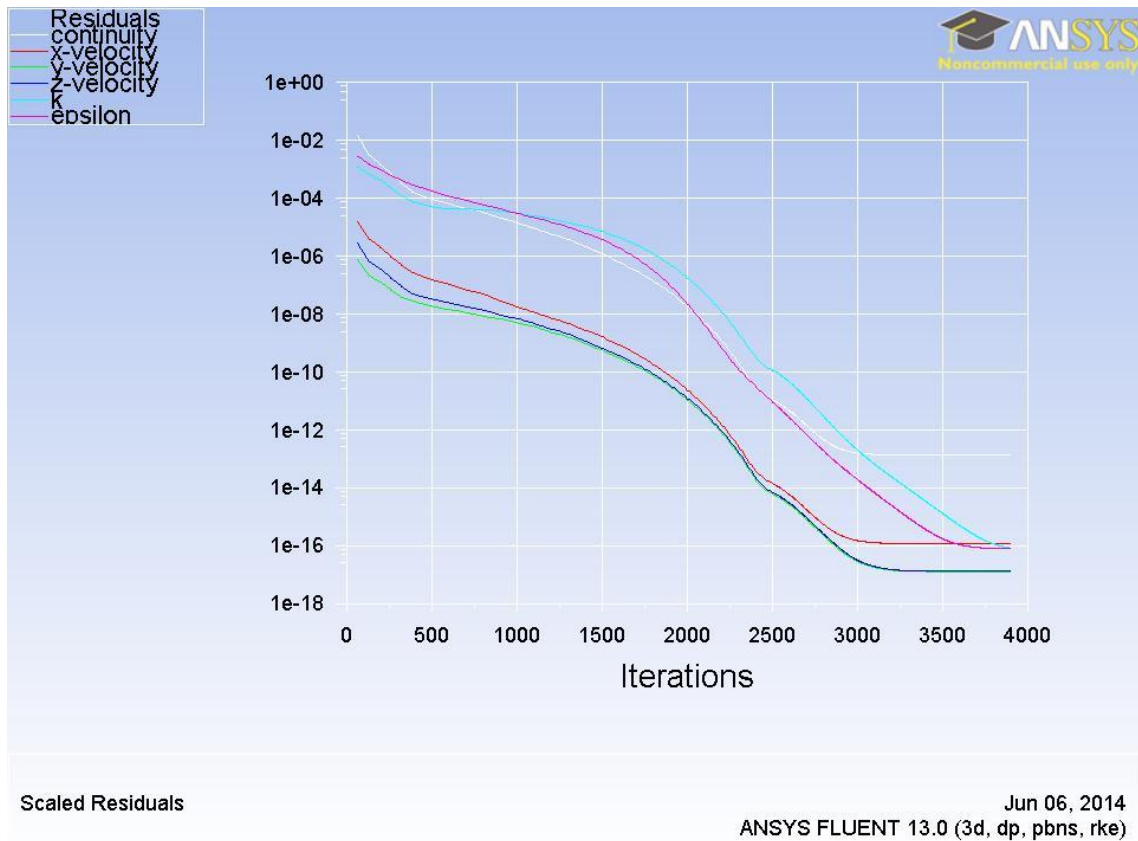
The simulation was first carried out in a 3D empty computational domain with the same dimensions mentioned above ( $X \times Y \times Z = 147\text{m} \times 85\text{m} \times 45\text{m}$ ). The reason for using an empty domain is that the horizontal homogeneity of the ABL profile is dependent on the roughness of the bottom wall boundary and on the boundary condition at the top boundary of the computational domain. The user defined function (UDF) was used to specify the inlet boundary conditions satisfying equations (4.5), (4.4) and (4.5) for the velocity ( $u$ ), turbulent kinetic energy ( $k$ ) and turbulent dissipation rate ( $\varepsilon$ ) respectively as mentioned by Richards and Hoxey (1993). The bottom boundary condition was assigned as a rough wall and standard wall functions were used; the roughness height ( $k_s$ ) and roughness constant ( $C_s$ ) were determined according to the relationship between  $k_s$ ,  $C_s$  as derived by Blocken et al. (2007b) satisfying equation (4.2). All the sides and top boundary conditions were assigned as symmetry conditions, while the pressure outlet was imposed for the outlet boundary. The CFD simulations were then performed using the commercial CFD code Fluent 13.0 and the 3D steady RANS equations. Closure is provided by the realizable  $k$ - $\varepsilon$  turbulence model (Shih et al., 1995). The choice for this turbulence model is based on the recommendations by Franke et al. (2004) and on earlier successful validation studies for pedestrian-level wind conditions (Blocken et al., 2004, 2007a, 2008b; Blocken and Carmeliet, 2008; Blocken and Persoon, 2009). Pressure velocity-coupling is taken care of by the SIMPLE algorithm.<sup>13</sup> Pressure interpolation is second-order, and second-order discretisation schemes were used for both the convection terms and viscous terms of the governing equations (Blocken et al., 2012). The iterations were terminated when the scaled residuals (Fluent Inc., 2006) did not show any further reduction with an increasing number of iterations, and the chosen convergence criterion was specified so that the residuals decrease to  $10^{-6}$  for all the equations (Figure 7.3). The velocity, turbulent dissipation rate (TDR) and

---

<sup>13</sup>The SIMPLE algorithm was developed by Prof. Brian Spalding and his student Suhas Patankar at Imperial College, London in the early 1970s. Since then it has been extensively used to solve Navier-Stokes equations for different kinds of fluid flow and heat transfer problems. SIMPLE is an acronym for Semi-Implicit Method for Pressure Linked Equations (for more detail, please refer to Patankar, 1980; Versteeg and Malalasekera 1995).

turbulent kinetic energy (TKE) were plotted along three equidistant vertical lines in the stream wise direction of the domain ( $X=0, 65,$  and  $145\text{m}$ ) (Figure 7.4).

Horizontal homogeneity of the ABL means that the plots of velocity, turbulent dissipation rate (TDR) and turbulent kinetic energy (TKE) should coincide along the three lines (Figure 7.4). Horizontal homogeneity for velocity (Figure 7.5) and TDR (Figure 7.6) and TKE profiles (Figure 7.7) profiles were achieved throughout the computational domain. The profile was written from the outlet to be used as the inlet profile for all the simulations in the research.



**Figure 7-3** The iterations were terminated when the scaled residuals (Fluent Inc. 2006) did not show any further reduction with an increasing number of iterations, and the chosen convergence criterion was specified so that the residuals decrease to  $10^{-6}$  (Liaw, 2005 and AboHela et al., 2012)



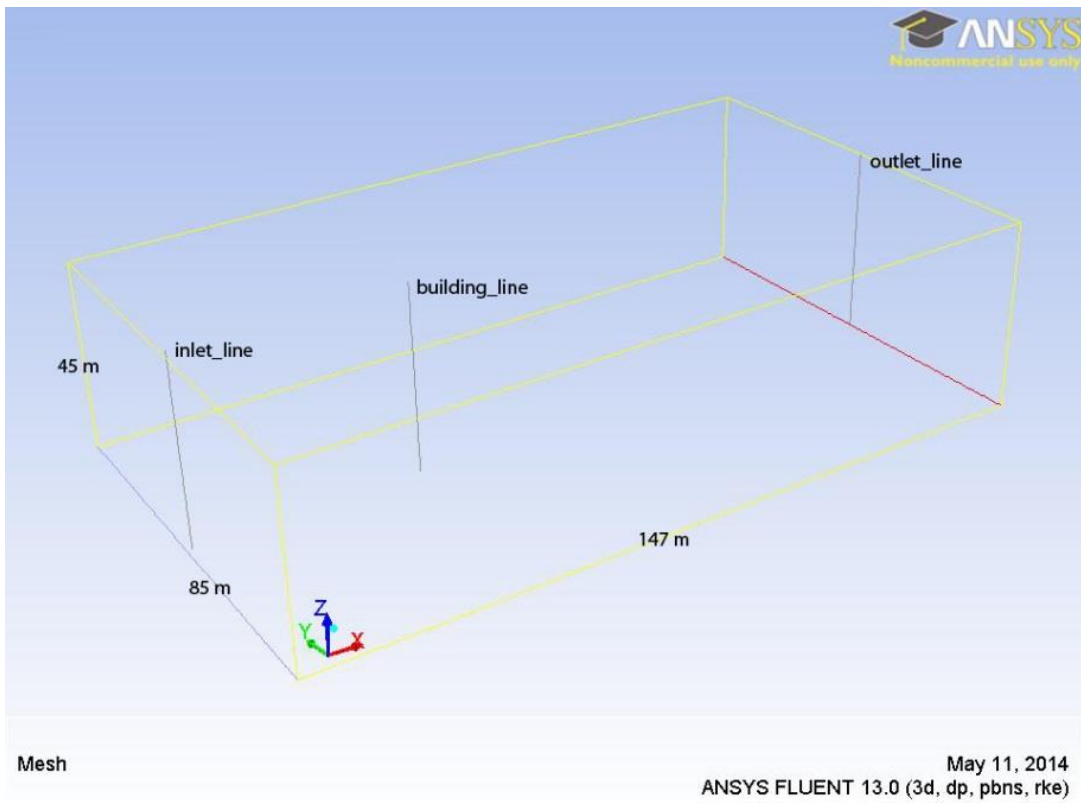


Figure 7-4 Computational domain dimensions and positions of the lines

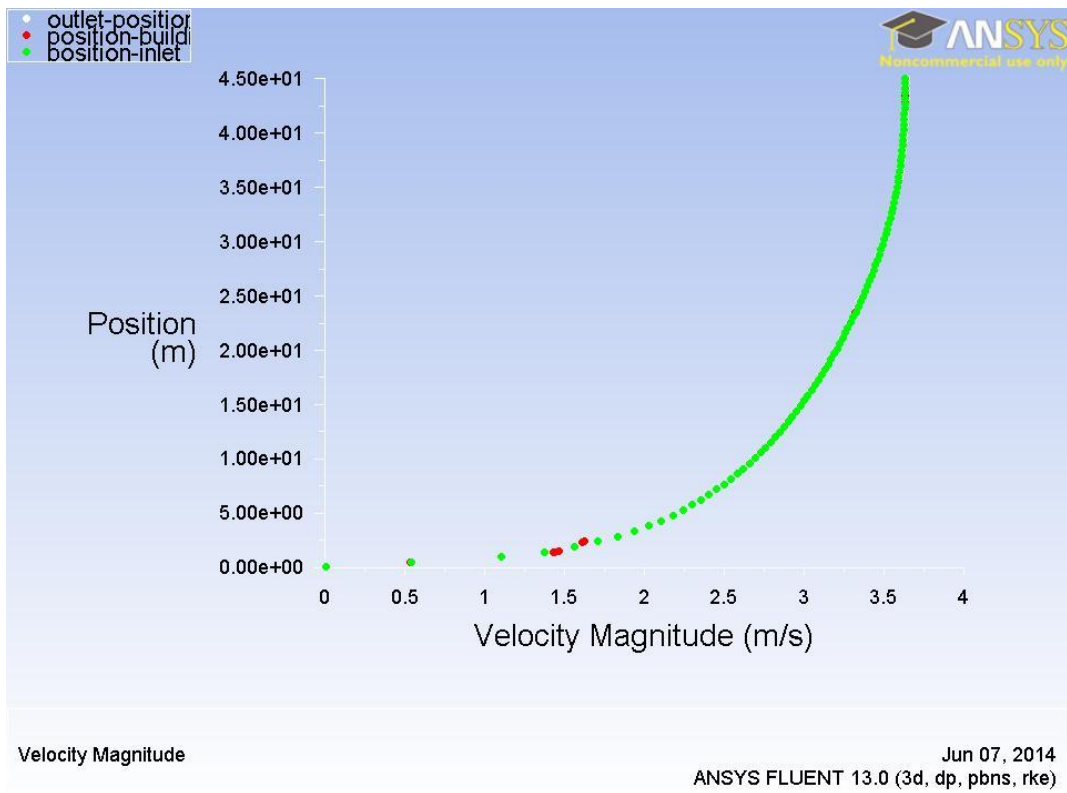


Figure 7-5 Velocity magnitude graph showing the horizontal homogeneity of the velocity profile

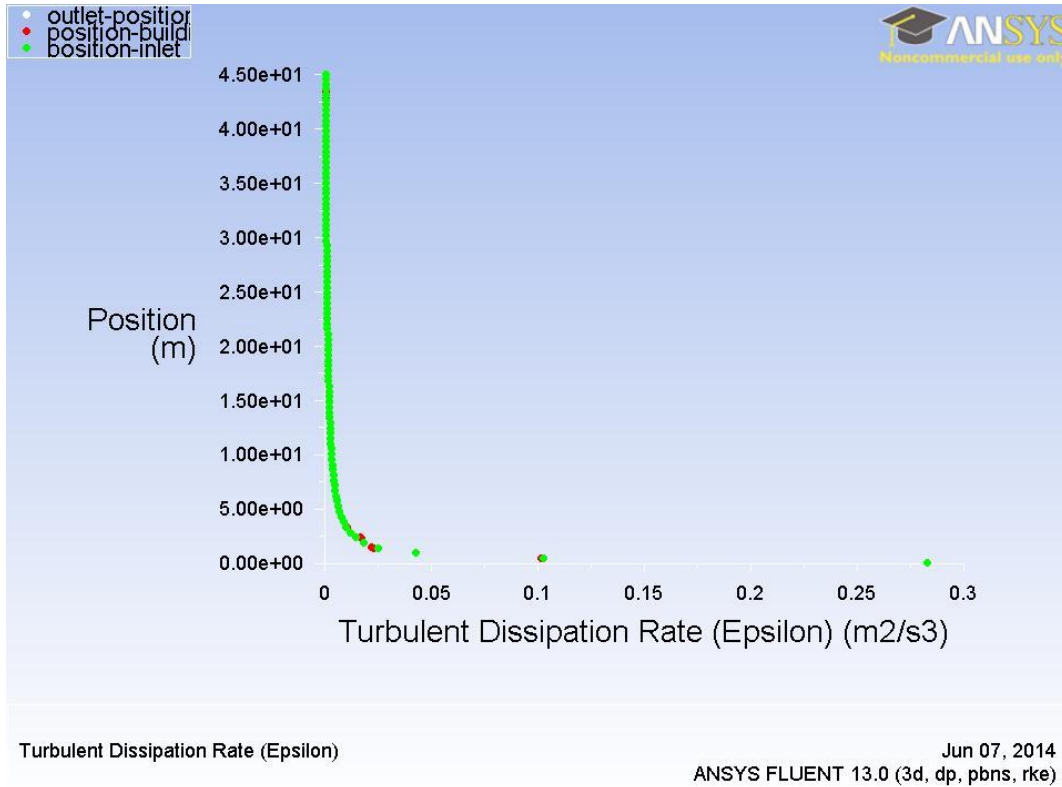


Figure 7-6 TDR graph showing the horizontal homogeneity of the TDR profile

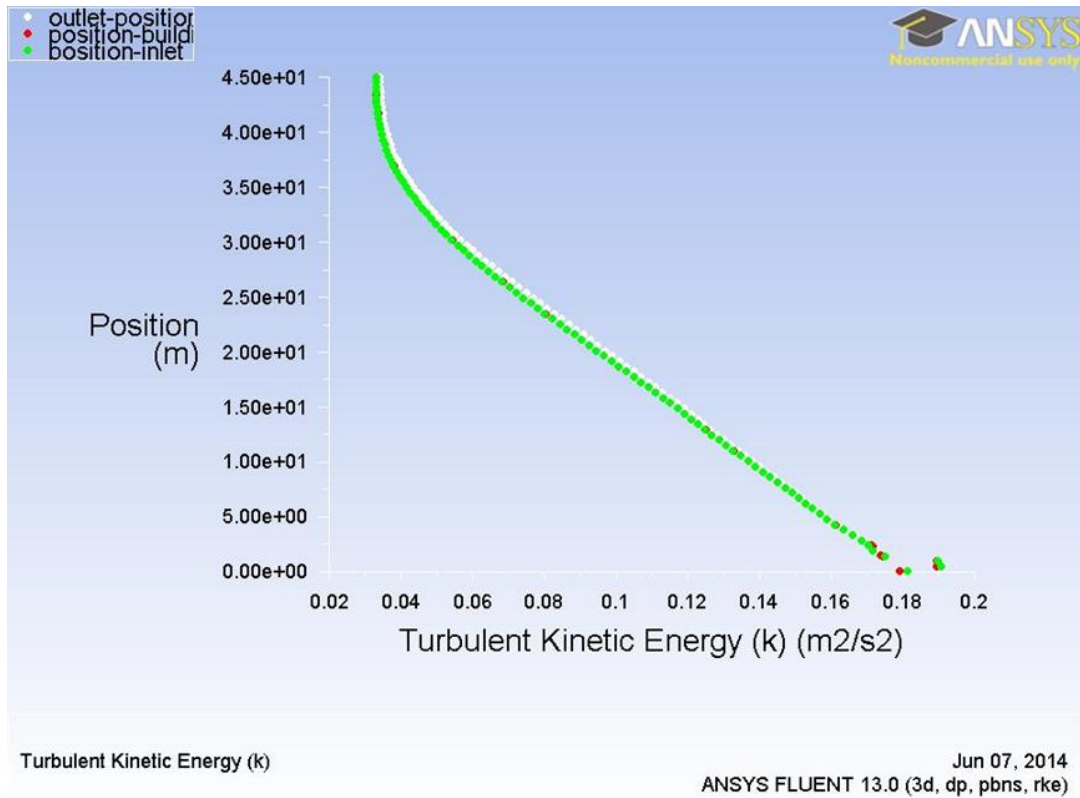


Figure 7-7 TKE graph showing the horizontal homogeneity of the TKE profile



### 7.3.3 Computational mesh

The same simulation settings used for achieving a horizontally homogeneous ABL profile (explained in Sections 4.6.3.1 and 4.6.3.2) in addition to table (7.1) were used for the following simulations. Due to the availability of the on-site measurements, the existing case scenario as illustrated in the flowchart (Figure 7.2) was selected for the validation and the mesh independence test. Firstly, a representative street segment with dimension 20m x 12m x 7m was created for the simulations, as shown in Figure 7.8. Secondly, the area around the street model where the important physical phenomena are likely to occur was refined, the structured mesh was chosen as it is more suitable for simple shapes such as square or rectangular sections (AboHela 2012), The mesh resolution was gradually refined until a constant solution is achieved (Franke et al. 2007), and the compromise between the accuracy and resolution of the model and the number of treatable grid cells is found, therefore, the mesh was coarsened in areas away from the street model with 0.48 m as a spacing mesh which was the minimum spacing to achieve the recommended skewness below 0.98 (ANSYS FLUENT tutorial 2006) and refined in areas close to the street model reaching 0.24 m for the mesh spacing (as explained in the following section). Therefore, a new multi-block mesh was constructed where the area around the street model extending 22m in the leeward direction and 10m in the windward direction, sides and above the cube were assigned a resolution of 0.24m in the X, Y and Z directions. As for the rest of the computational domain, the mesh resolution was set to 0.48m in the X, Y and Z directions (Figure 7.9).

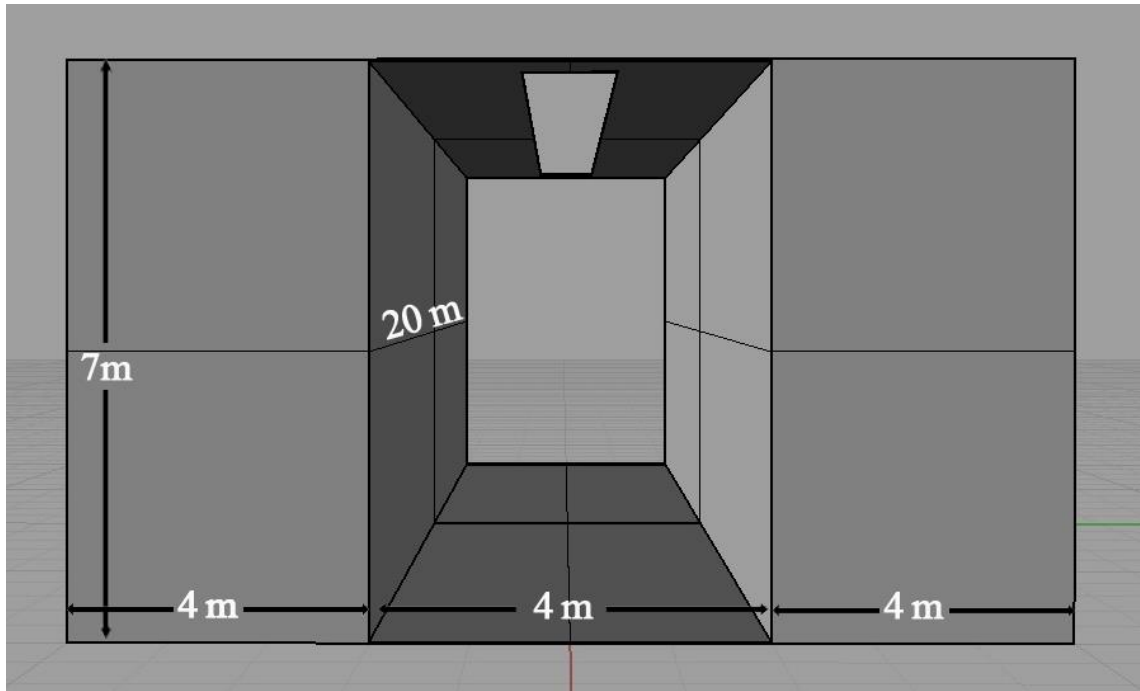
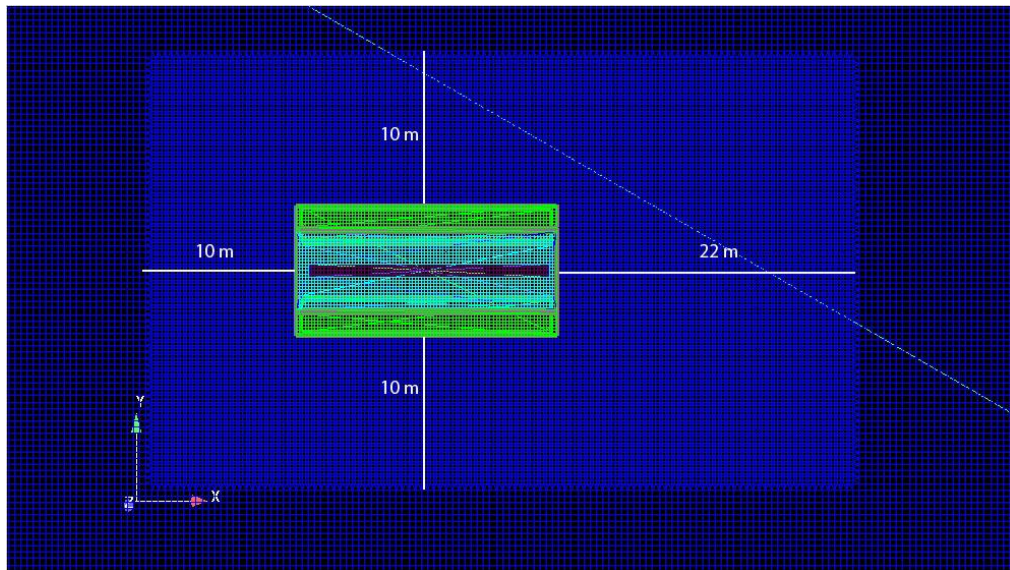
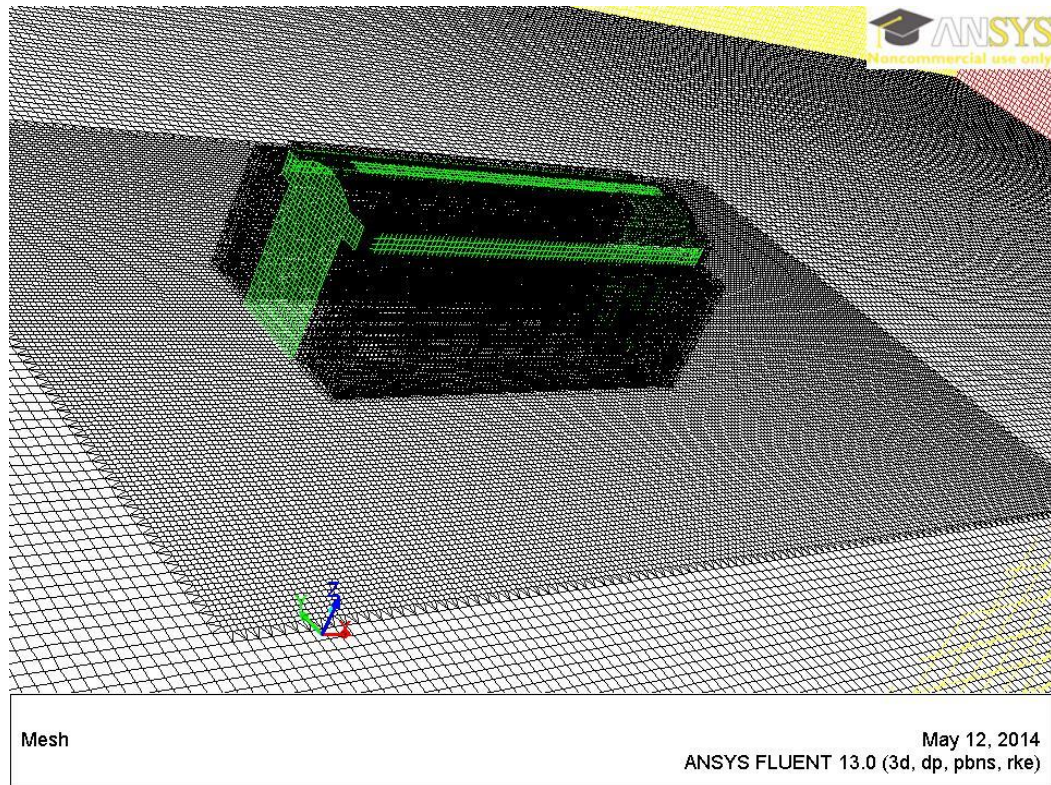


Figure 7-8 The simulated street segment dimensions in CFD





**Figure 7-9** Mesh refinement area around the model and extended to 10m height above the model

### 7.3.4 Mesh independence test

A mesh independence study was carried out to determine the dependence of the flow field on the refinement of the mesh, as stated in the BPG presented as step C4 in Figure 4.8. According to several authors (Liaw, 2005; Ariff et al., 2009a; Salim and Cheah, 2009), it is essential to run a test on different mesh sizes and configurations until there is no significant change in the output solutions with the change in mesh configurations and size. Franke et al. (2007) limited this test to three systematically refined/coarsened meshes. Therefore, two other meshes were used; the first mesh had a resolution of 0.48m around the street model and throughout the rest of the computational domain. The second mesh had a resolution of 0.12m around the street model and 0.48m throughout the rest of the computational domain. These mesh sizes were based on the balance between the three main variables responsible for the effectiveness of a mesh type including orthogonal quality, aspect ratio and skewness<sup>14</sup> (Franke et al. 2004 and de Oliveira et al. 2013).

<sup>14</sup>Orthogonal quality of a cell is the minimum value that results from calculating the normalized dot product of the area vector of a face and a vector from the centroid of the cell to the centroid of that face and the normalized dot product of the area vector of a face and a vector from the centroid of the cell to the

Figure 7.10 shows a comparison between the mean wind velocity vertical profiles captured at the centre line of the model for the three meshes; the mean wind velocity path lines plots for the 0.48m mesh are the same as in the 0.24m and the 0.12m mesh. All three meshes were able to capture similar wind velocity for the same point located on the centre line of the model across the prevailing wind direction. Thus, to decrease computational demand and time, it can be concluded that the 0.24m mesh is sufficient for running a mesh independent simulation.

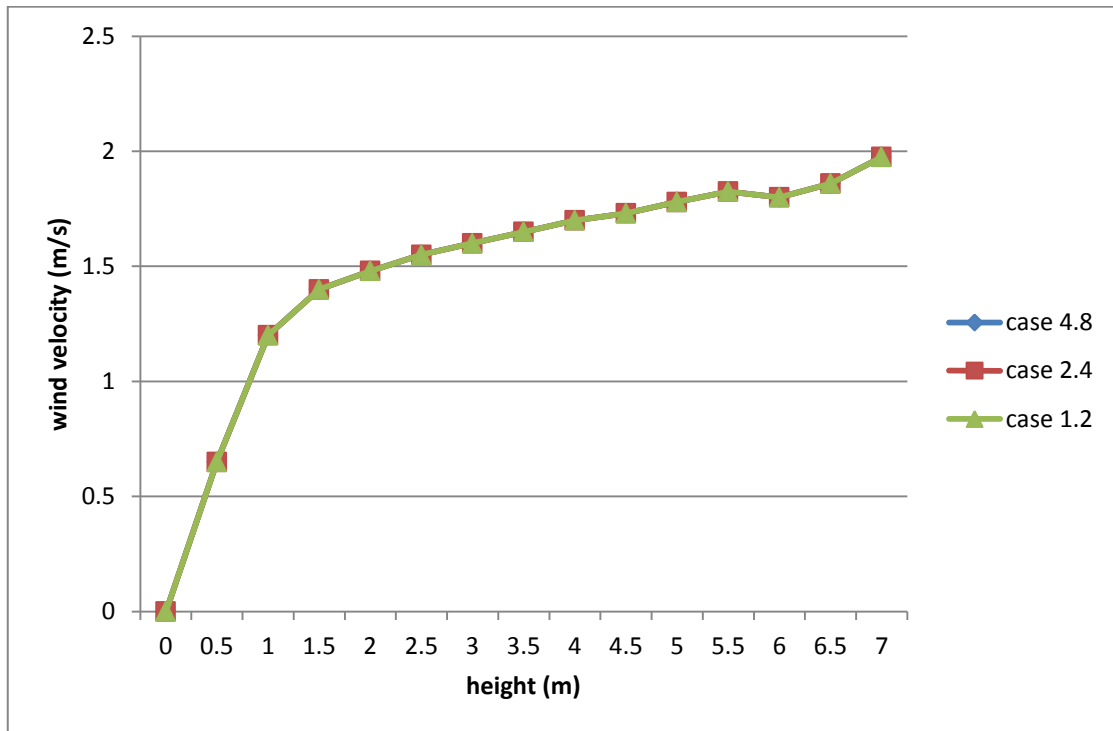


Figure 7-10 wind velocity profile captured at the centre line of the model for the three meshes

## 7.4 CFD simulation validation

### 7.4.1 CFD simulation: model validation

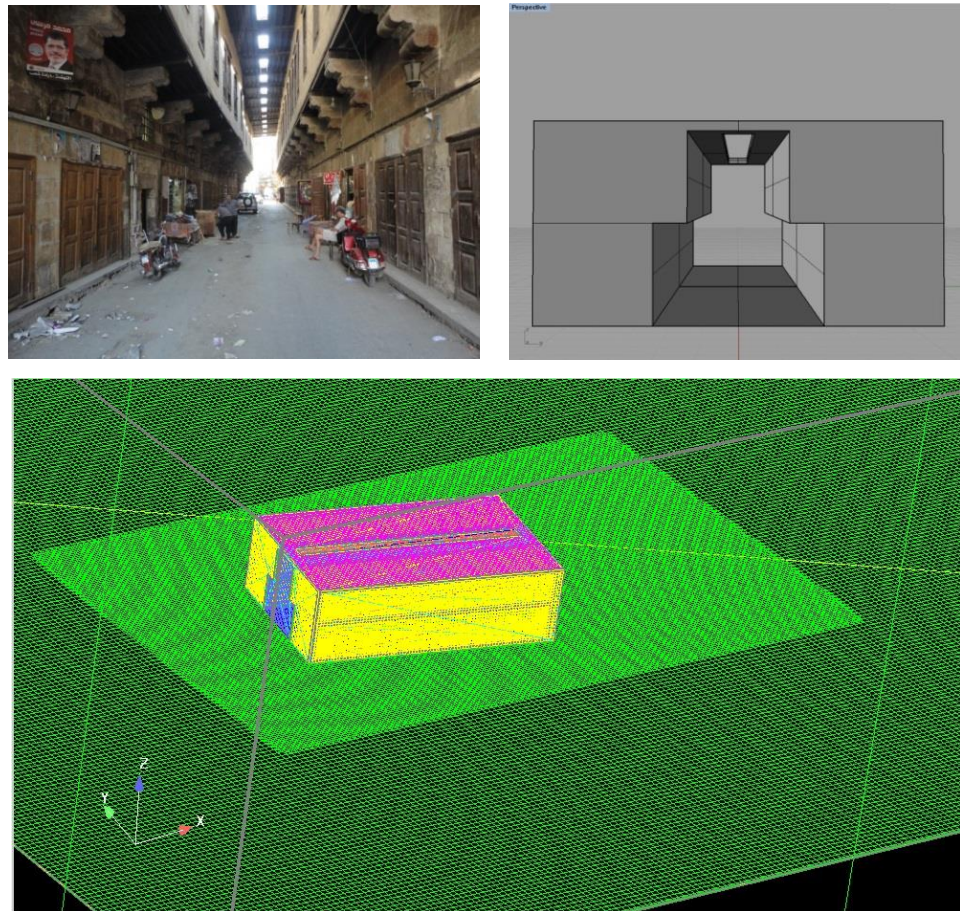
According to the best practice guideline (BPG), as illustrated in Figure 7.2, the study was developed in an existing urban configuration with the availability of on-site field measurement. Therefore, the validation was based upon regular validation through comparing the CFD output with the field measurement values reported in Chapter

---

centroid of the adjacent cell that shares that face. Therefore, the worst cells will have an orthogonal quality closer to 0 and the best cells will have an orthogonal quality closer to 1. Aspect ratio is a measure of the stretching of the cell. Skewness is defined as the difference between the shape of the cell and the shape of an equilateral cell of equivalent volume. Highly skewed cells can decrease accuracy and destabilize the solution (Fluent tutorial release 13.0)



Five for the existing case (Figure 7.11). The measurement point was located in the middle of the tent market (for more information, please refer to location one, Section 5.4, Figures 5.7 and 5.8).



**Figure 7-11**The existing case study the CFD model and meshing domain

According to Zhang et al. (2013), theoretically, CFD programs that accurately describe the heat transfer in solid materials and calculate the air velocity and temperature distribution can predict the energy demand if all of the heat factors are set as dynamic boundary conditions and heat generators. However, this method is computationally very expensive and almost impossible to perform for a long-period energy simulation (i.e. a season or a year), even though the calculation speed of supercomputers has increased greatly over the years (Zhang et al., 2013). Therefore, an alternative approach was to couple the CFD program with the building energy simulation (BES). The idea of coupling BES and CFD was first developed by Negrão (1995), who focused on the necessity for the two models to exchange appropriate boundary conditions. Indeed, CFD requires a surface temperature to accurately describe the flow condition (Barbason and Reiter, 2014). Therefore, Designbuilder as BES handles the external surface

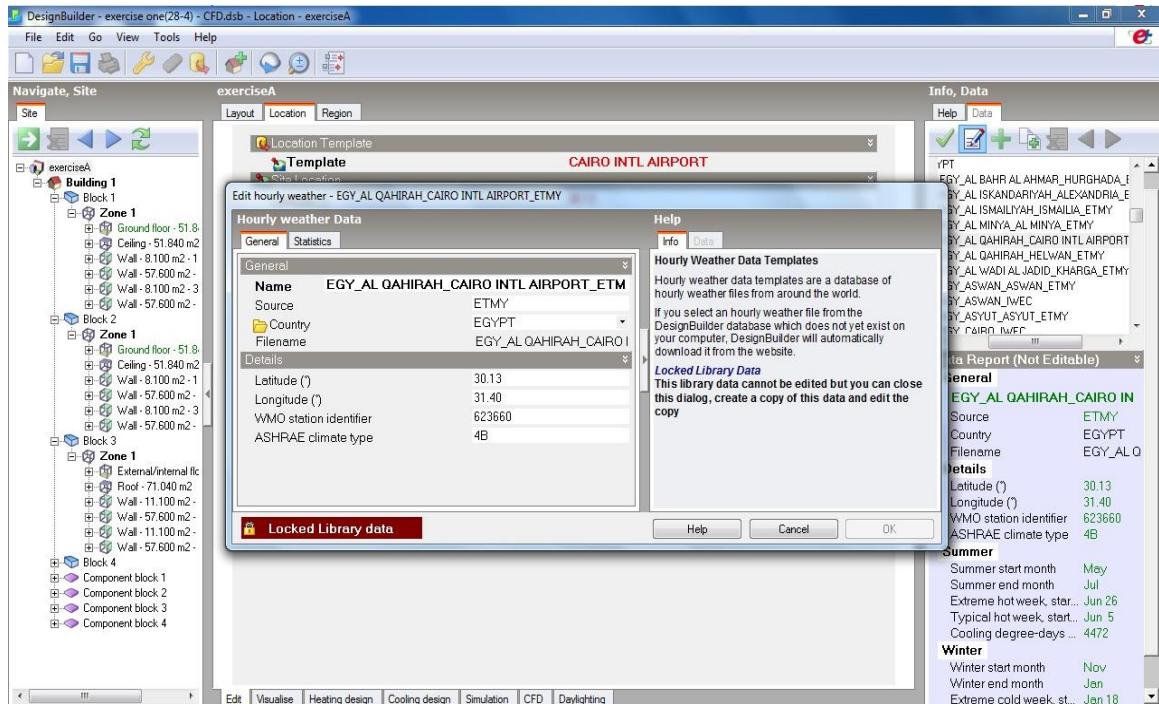
temperature for the main building surrounding the street or the semi- enclosed areas, while Fluent as CFD simulates the street air flow and air temperature. Such a coupling procedure largely reduces computing time because it does not solve the flow field during the transition from one time step to another (Zhai et al., 2002; Zhai and Chen, 2003; 2006; Zhang et al., 2013). As concluded by Zhai and Chen (2003, 2005), the coupling method which transfers enclosure surface temperatures from BES to CFD is more reliable and efficient than other coupling methods. The method can unconditionally satisfy the convergence condition. Moreover, if all surfaces temperatures are presumed inside the model then the radiation model can be neglected (van Hooff and Blocken, 2010), which will also save more time and load on the computational power.

#### **7.4.1.1 The DesignBuildersimulation**

The DesignBuilder is an interface for the EnergyPlus simulation engine. EnergyPlus is a ‘Qualified Computer Software’ for calculating energy savings for purposes of the energy-efficient commercial building in the USA (Pedersen, 2007) and it has a proven track record from previous research studies of Middle East housing (Abdulrahman and Sharples 2014). Expert users can get access to the source code allowing for third-party validation, which adds to the software’s credibility and long-term reliability. EnergyPlus has been validated under the comparative Standard Method of Test for the Evaluation of Building Energy Analysis Computer Programs BESTEST/ASHRAE STD 140. EnergyPlus requires climatic data to run valid simulations based on a given location. The climatic data or the weather file used in the simulation has been extracted from the EnergyPlus website for the WMO Station no.623660 records at Cairo International Airport in hourly timesteps over a period of ten years.<sup>15</sup> These climatic data are added as a separate weather file before running the simulations, as shown in Figure 7.12.

---

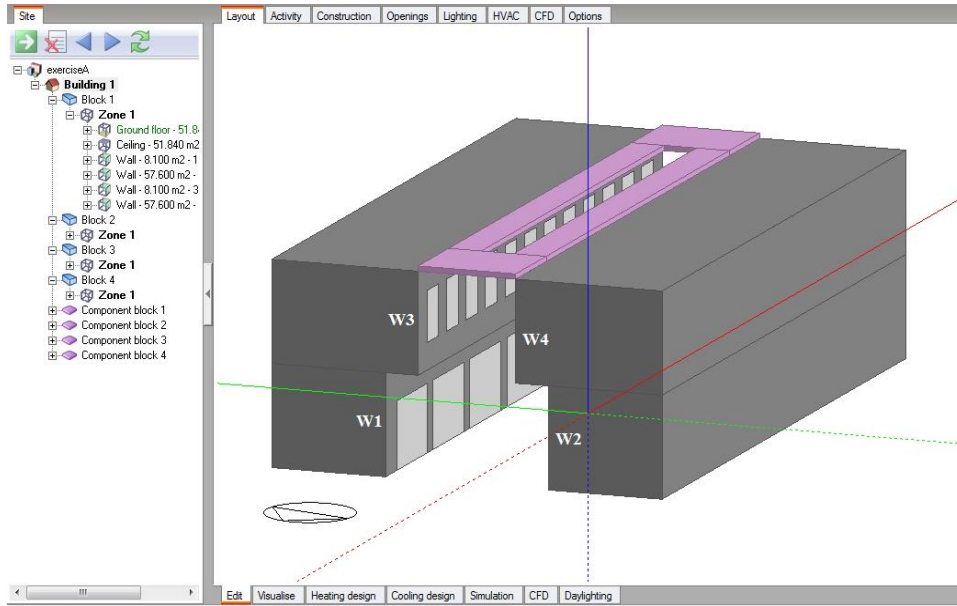
<sup>15</sup>[http://apps1.eere.energy.gov/buildings/energyplus/cfm/weather\\_data3.cfm/region=1\\_africa\\_wmo\\_region\\_1/country=EGY/cname=Egypt](http://apps1.eere.energy.gov/buildings/energyplus/cfm/weather_data3.cfm/region=1_africa_wmo_region_1/country=EGY/cname=Egypt)



**Figure 7-12** The weather profile preliminary data from the WMO Station no.623660 records at Cairo International Airport

#### 7.4.1.2 The DesignBuilder Results

Table 7.2 shows the complete data set simulated by DesignBuilder for the surface temperature of all walls and roofs, which were used later as an input for the CFD simulations. As shown in Figure 7.14, the given surface temperature started at 1:00am, and the wall values were almost similar until sunrise between 5:00 and 6:00am, when these values started to vary, as the solar position changed. The distribution of shadow inside the semi-enclosed space varies accordingly and, so, according to Figure 7.13, the surface temperature of walls (2) and (4) started to increase each with different values according to the degree of exposure to the sun and the gallery design, which keep wall (2) always partly shaded. On the other side, walls (1) and (3) remained on trend as they were still in shade until noon-time, when all the values were close again. Then the sun started to move to the other side facing walls (1) and (3) so their surface temperature started to increase (each with a different value based on the different degree of exposure and the self-shaded wall (1), while walls (2) and (4) started to cool down in the shade. This occurred until sunset, between 18:00 and 19:00, when all the walls started to cool down again and reached close values.

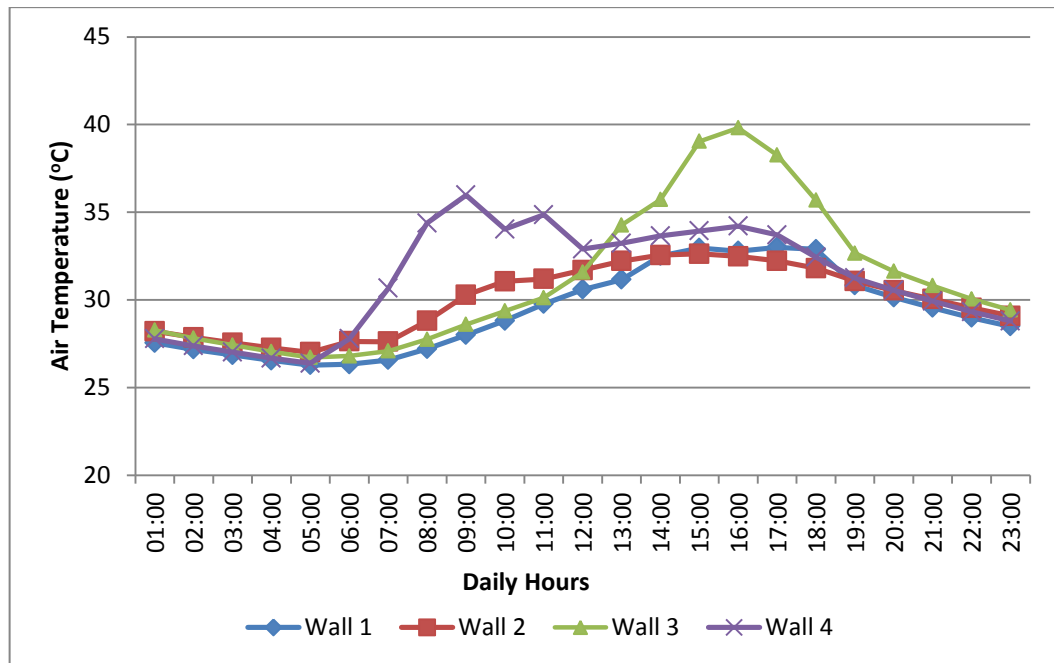


**Figure 7-13** The model as drawn in DesignBuilder with the name of the four simulated walls as W1, W2, W3 and W4

Table 7-2 Output data simulated by DesignBuilder

	Wall 1	Wall 2	Wall 3	Wall 4	Roof
<b>hour</b>	<b>Surface temperature (°C)</b>				
<b>01:00</b>	27.54	28.20	28.27	27.78	32.18
<b>02:00</b>	27.17	27.85	27.81	27.37	31.62
<b>03:00</b>	26.85	27.55	27.42	27.01	31.14
<b>04:00</b>	26.54	27.26	27.04	26.67	30.70
<b>05:00</b>	26.27	27.01	26.72	26.37	30.32
<b>06:00</b>	26.32	27.63	26.80	27.77	30.19
<b>07:00</b>	26.57	27.61	27.08	30.66	30.43
<b>08:00</b>	27.20	28.80	27.75	34.38	32.20
<b>09:00</b>	27.99	30.27	28.60	35.98	33.21
<b>10:00</b>	28.80	31.05	29.36	34.03	34.66
<b>11:00</b>	29.76	31.19	30.12	34.85	36.45
<b>12:00</b>	30.59	31.69	31.57	32.89	37.70
<b>13:00</b>	31.15	32.21	34.27	33.22	38.56
<b>14:00</b>	32.50	32.55	35.71	33.65	38.99
<b>15:00</b>	32.95	32.62	39.03	33.92	39.23
<b>16:00</b>	32.77	32.48	39.81	34.20	39.29
<b>17:00</b>	32.99	32.22	38.25	33.70	39.07
<b>18:00</b>	32.87	31.80	35.68	32.43	36.68
<b>19:00</b>	30.82	31.07	32.66	31.24	35.86
<b>20:00</b>	30.13	30.53	31.63	30.54	34.93
<b>21:00</b>	29.55	30.04	30.80	29.92	34.08
<b>22:00</b>	28.98	29.53	30.05	29.31	33.27
<b>23:00</b>	28.48	29.08	29.41	28.78	32.53





**Figure 7-14** Surface temperature for all walls mentioned in Figure 8.16

Table 7.3 and Figure 7.15 display the summer time design air temperature assumed by the DesignBuilder from the weather files for the study site, compared to the air temperature reported from the field measurement in Chapter Five for the same period for 1<sup>st</sup> July 2012. The data used by DesignBuilder show a good agreement with the observed ones and that the temperature average differences was 2.1°C, with both lines sharing the same trend over the day (Figure 7.15), which might give a confident result when using the surface temperature generated from DesignBuilder into the CFD simulations.<sup>16</sup>

<sup>16</sup>For more information about EnergyPlus validation:

[http://simulationresearch.lbl.gov/dirpubs/valid\\_ep.html](http://simulationresearch.lbl.gov/dirpubs/valid_ep.html);

[http://apps1.eere.energy.gov/buildings/energyplus/energyplus\\_testing.cfm](http://apps1.eere.energy.gov/buildings/energyplus/energyplus_testing.cfm))

Table 7-3 The air temperature assumed by DesignBuilder for the site compared to the field measurement

Hour	Ta measured	Ta assumed
06:00	25.8	28.1
07:00	26.8	29.4
08:00	27.4	30.7
09:00	28.7	32.3
10:00	30.9	33.8
11:00	32.5	35.2
12:00	34.3	36.4
13:00	35.6	37.3
14:00	35.9	37.9
15:00	36.4	38.1
16:00	35.9	37.9
17:00	35.2	37.3
18:00	34.4	36.4
19:00	33.3	35.2
20:00	32.2	33.8
21:00	30.7	32.3
22:00	29.4	30.7
23:00	28.3	29.4

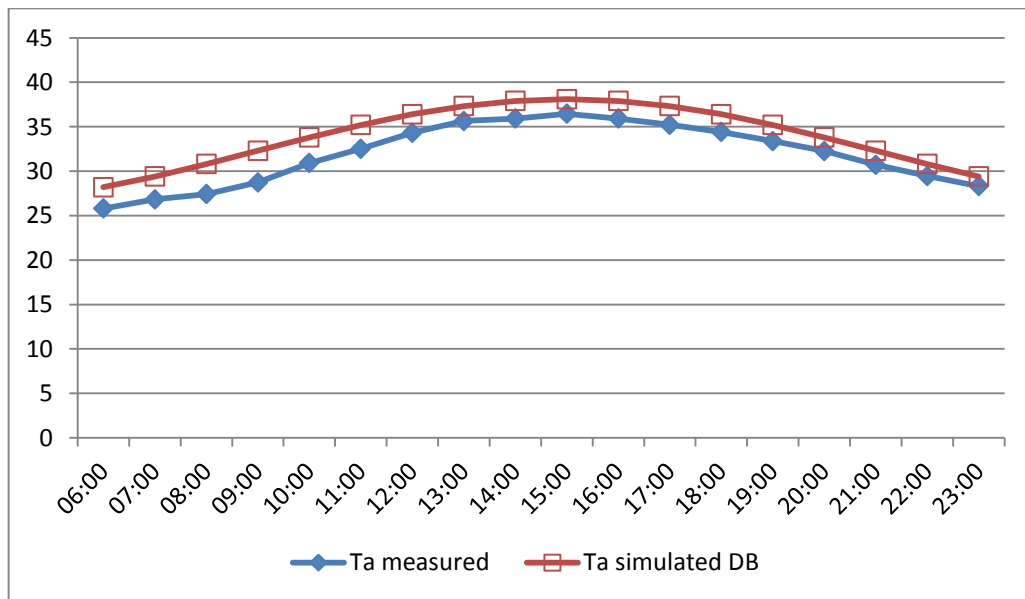


Figure 7-15 DesignBuilder assumed air temperature for the study location and the field measurements

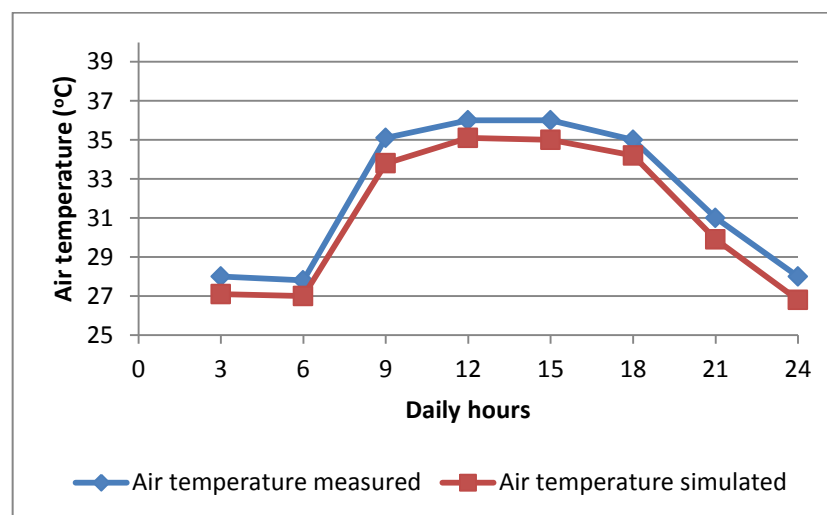
#### 7.4.2 The CFD model validation

In Table 7.4, the complete data set including the measured and simulated air temperatures and the DesignBuilder imported surface temperature used as an input in

the CFD simulation are provided. The simulated CFD output was validated against the experimental measurement for the existing case. According to step E in the BPG flowchart (Figure 7.2), the results of the validation are presented within the graph as shown in Figure 7.16, and the simulated air temperature is compared with the in-situ air temperature measurements taken at three-hour intervals starting from 3:00 until 24:00 on 1<sup>st</sup> July 2012. It can be observed that the simulation results show a consistent trend with the observed ones and that the temperature differences are within 0.8°C to 1.2°C. It could be concluded that the designed model is capable of estimating the air temperature patterns for the existing case under steady state conditions which add more confidence in testing iterations for the suggested shading configurations.

**Table 7-4** Data table for the validation air temperature and the input surface temperature data

Hours	Measured	Simulated	Wall-1	Wall-2	Wall-3	Wall-4	Roof
	Air temperature (°C)		Surface temperature (°C)				
3.00	28.0	27.1	26.8	27.5	27.4	27.0	31.1
6.00	27.8	27.0	26.3	27.6	26.8	27.7	30.2
9.00	35.1	33.8	28.0	30.3	28.6	35.9	33.2
12.00	36.0	35.1	30.6	31.7	31.6	32.9	37.7
15.00	36.0	35.0	33.0	32.6	39.0	33.9	39.2
18.00	35.0	34.2	32.8	31.8	35.7	32.4	36.7
21.00	31.0	29.9	29.5	30.0	30.8	29.9	34.1
24.00	28.0	26.8	28.5	29.1	29.4	28.8	32.5



**Figure 7-16** Comparison between the air temperature measured and the CFD output for the existing case on 1st July at pedestrian height of 1.4m

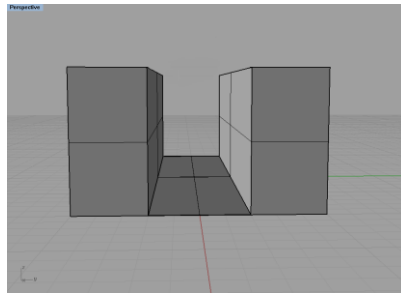
## 7.5 Comparative study

The current research used the parametric approach to obtain the air temperature distribution and natural ventilation performance underneath seven shading structure configurations. In the parametric study, cross-comparing the effects of different design issues is easier by observing changes in the heat flow rate and the natural ventilation performance in different testing scenarios, and then relating this to predicted thermal conditions outdoors. The comparative analysis is labelled under letter (G) in the BPG (Figure 7.2), after the validation step, where the CFD simulations should be conducted for the new design different scenarios with the same settings as previous simulations used for validation. Accordingly, seven different scenarios were set up in the same prevailing wind direction with the same CFD code Fluent 13.0 settings to further evaluate the air flow rate and the air temperature distribution patterns beneath.

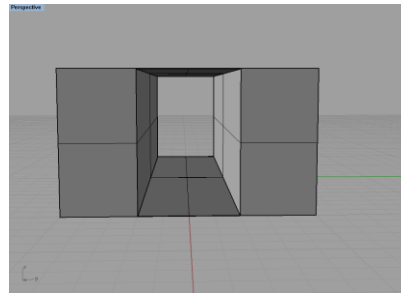
Each tested scenario consists of one specific geometrical change in the roof structure shapes and opening locations, as shown in Figure 7.17. The appropriate boundary conditions were set according to the same date used in the validation on 1<sup>st</sup> July 2012 as a representative for an extreme hot day. However, the choice of day is not critical as the results are not specifically related to real conditions. All results were recorded at 1.4m above the ground level representing the thermally affected height by the pedestrians (Ali-Toudert and Mayer, 2007a, 2007b; Fahmy et al., 2010). The exact choice of the night time for the simulation was based on the reported findings (Nakamura and Oke, 1988; Pearlmutter et al., 2007; Lin et al., 2010) that the high shading levels increase thermal comfort during the day in summer, yet at night they can decrease long-wave radiation loss on the surface, contributing to high temperatures; this was also concluded from the field measurement in Chapter Five.

As shown in Figure 7.17, the aspect ratio (H/W) was the same for all the cases in being equal to 1.5, while the roof structure varied between the different cases. For instance, there was no roof for case number one, while case number two was fully covered, case number three was fully covered with one opening in the middle, and case number four had a roof 1m higher than the previous cases, with one opening on both sides. In case number five, the side openings were the same as case four but with one metre shifted locations on each side, and case six was the same as case five, but with an extra opening

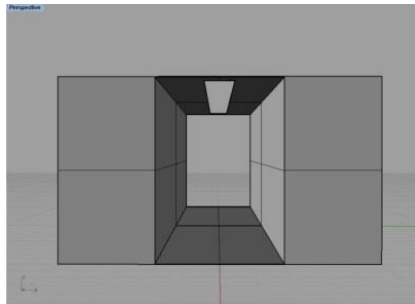
in the middle. Case number seven had the same number and locations of opening as case six but in a vaulted shape.



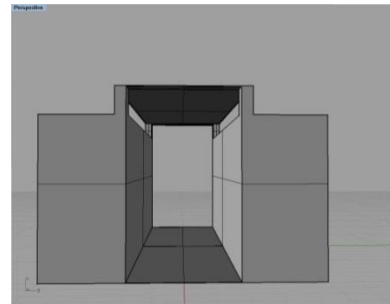
Case no. 1



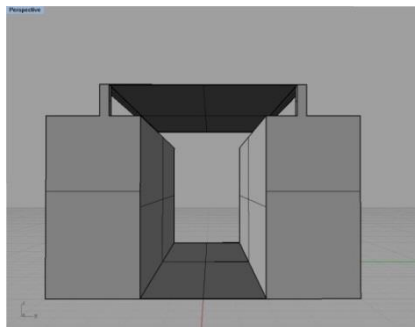
Case no. 2



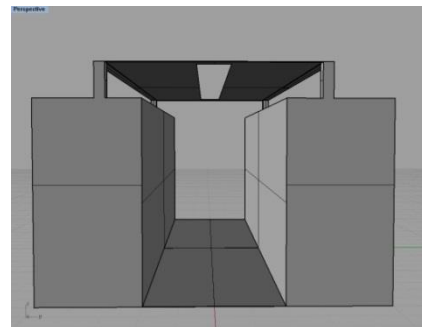
Case no. 3 (Base Case)



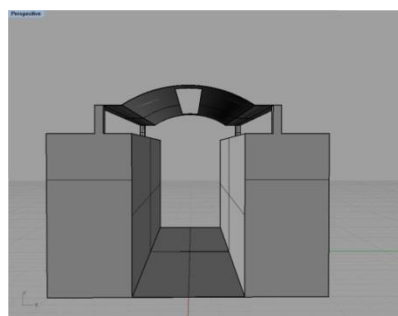
Case no. 4



Case no. 5



Case no. 6



Case no. 7

**Figure 7-17** The alternative configurations for each case study with specific changes in the roof shape and opening locations

## 7.5.1 CFD simulations: comparative results

### 7.5.1.1 Comparison of the vertical profiles of the mean wind velocity

For the performance-based analysis of the simulation results, a wind speed classification based on outdoor thermal comfort is derived (Murakami and Deguchi, 1981; Cheng and Ng, 2006), the current study classification is based on the outdoor thermal comfort in relation to the wind force on pedestrians or buildings. Ng et al. (2008) conducted a study to obtain the pedestrian-level wind speed threshold values, in order to achieve outdoor thermal comfort for the subtropical climate, using physiological equivalent temperature (PET). On a typical summer day when air temperature is 27.9°C and relative humidity is about 80%, a wind speed of 0.6-1.3m/s is required to achieve neutral thermal sensation (neutral PET: 28.1°C). In another study for outdoor thermal comfort for the subtropical climate, the researchers reported that, in summer, a decrease in wind speed from 1.0m/s to 0.3m/s was equal to a 1.9°C temperature increase, and for outdoor thermal comfort under typical summer conditions 1.6m/s wind speed was required (Cheng et al., 2011).

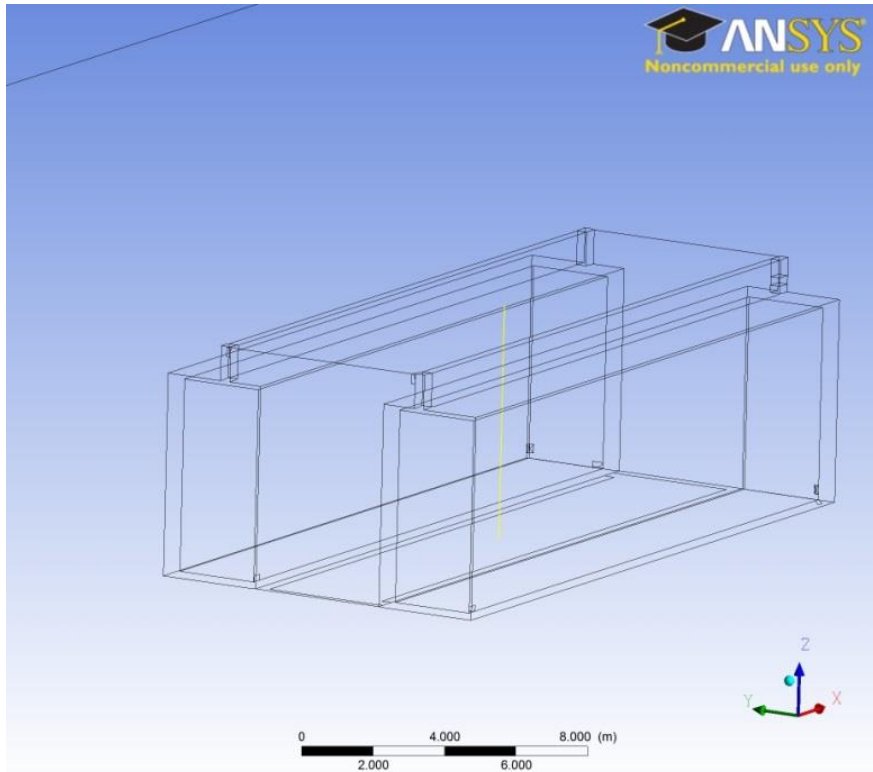
Accordingly, the classification of the pedestrian-level wind speed ( $u$ ) is assigned as shown in Table 7.5, including five different classes named as “stagnant,” “poor,” “low,” “satisfactory,” and “good” pedestrian-level natural ventilations in street canyons (Yuan and Ng, 2012).

**Table 7-5** The classification of the pedestrian-level natural ventilations in street canyons (Yuan and Ng, 2012)

Class 1	$u < 0.3 \text{ m/s}$	stagnant
Class 2	$0.6 \text{ m/s} > u \geq 0.3 \text{ m/s}$	poor
Class 3	$1.0 \text{ m/s} > u \geq 0.6 \text{ m/s}$	low
Class 4	$1.3 \text{ m/s} > u \geq 1.0 \text{ m/s}$	satisfactory
Class 5:	$U \geq 1.3 \text{ m/s}$	good

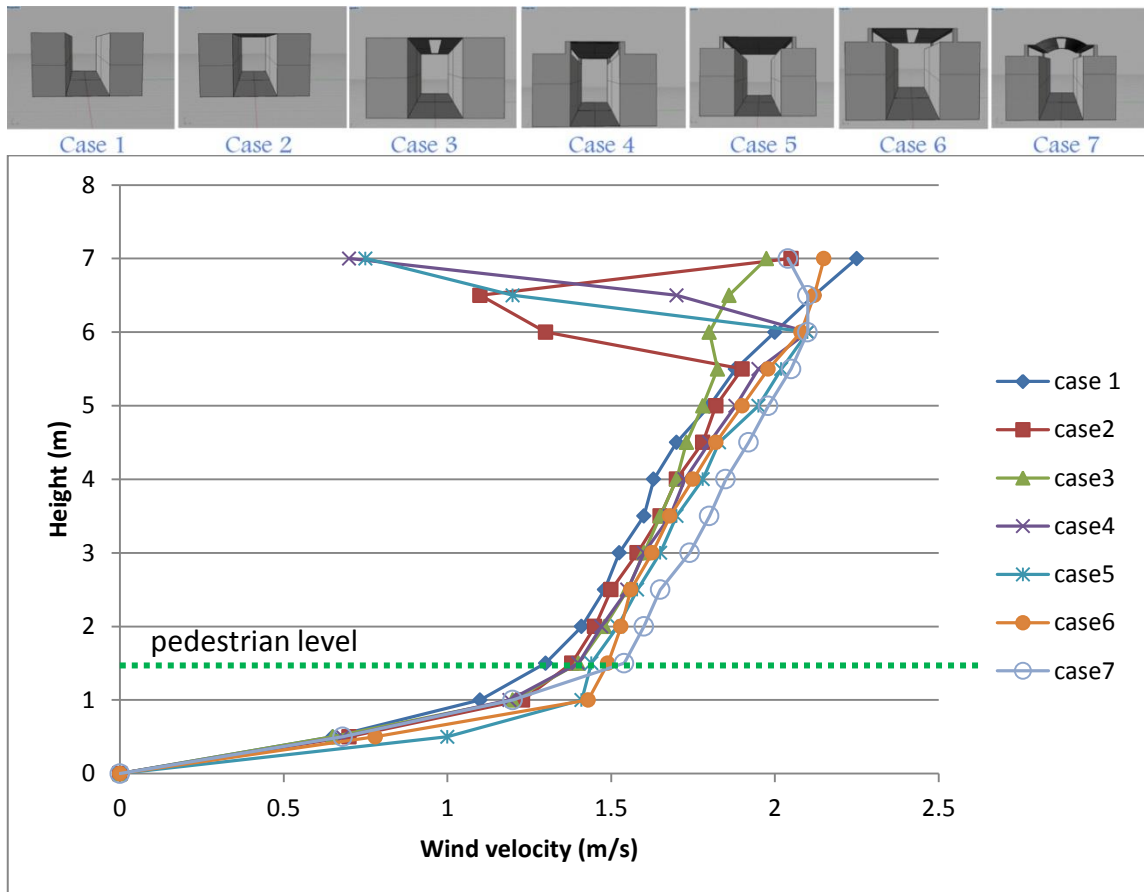
In order to examine the effect of wind speed at the pedestrian level, the vertical profiles of the mean wind velocity were measured at a point on the centre line of the street across the prevailing wind direction with a reference wind speed equal to 3m/s at U10 (at 10m height) (Figure 7.18). Figure 7.19 shows the vertical profiles of all the cases from 0m at the ground level to 7m at the roof level. As can be seen, all cases may have

had a similar profile until they started getting closer to the roof and the openings when the vertical profiles started to vary. This is except for case number one, which was without a roof so its vertical profile kept on its increasing trend. In cases 2 and 3, they had almost the same velocity vertical profile with very close values until they reach the top roof level (+6 m above the ground level) when case 2 saw a decrease in wind velocity from 1.9m/s to 1.1m/sec as the roof tent was fully closed. In case 3, the centre roof opening assisted the wind to rise smoothly without much slowing down of its speed (almost 0.05m/sec velocity reduction). On contrary to case 4, where there was no opening in the roof centre, the wind velocity had to slow down and was released through the two side openings instead. Cases 4 and 5 shared the same two side openings but with different positions on the roof, and had almost the same vertical profiles up to the top of building at 6m above the ground level, when the wind velocity reached its maximum for both cases, at 2.1m/sec, before it declined by reaching roof level and had almost equal values between (0.70m/sec and 0.75m/sec). However, cases 6 and 7, which shared the same three openings (one on each side and one on the roof), had the same vertical profile of the mean wind velocity and there was no sudden decrease in the wind velocity under the roof, as with cases 4 and 5. This was because the roof opening helped the air to rise while keeping its speed. This indicates that roof structure and different openings significantly affect the wind profiles beneath. The result is consistent with a previous study by Ng et al. (2011), which stated that the wind environment at the pedestrian level is not affected by building height but is significantly influenced by urban geometry in the pedestrian level. Also, it is important to mention that all the cases fall within class number five (wind speed  $\geq 1.3\text{m/s}$ ). As seen in Table 7.5, they all achieved the comfort zone for the pedestrian classification for natural ventilation mentioned, except case 1, which recorded 1.3m/s and is thus classified as class four. Although some cases recorded very similar values, case number 7 had the exact value for the optimum condition mentioned by Cheng et al. (2011) of 1.6m/sec under typical summer time conditions, while all other shading scenarios led to lowering the wind velocity to a less satisfactory level according to a study by Cheng et al. (2011).



**Figure 7-18** The vertical profiles of the mean wind velocity were measured at a point on the centre line of the street across the prevailing wind direction





**Figure 7-19** The vertical profiles of the mean wind velocities from the CFD simulation located at the centre line of the street (from 0m on the ground level to 7m on the roof level)

**Table 7-6** The vertical profiles of the mean wind velocities from the CFD simulation located at the centre line of the street

Height	Case 1	Case2	Case3	Case4	Case5	Case6	Case7
Metres	Velocity (m/sec <sup>-1</sup> )						
0	0	0	0	0	0	0	0
0.5	0.65	0.7	0.65	0.68	1	0.78	0.68
1	1.1	1.23	1.2	1.19	1.41	1.43	1.2
1.5	1.3	1.38	1.4	1.4	1.44	1.49	1.54
2	1.41	1.45	1.48	1.47	1.52	1.53	1.6
2.5	1.48	1.5	1.55	1.55	1.58	1.56	1.65
3	1.525	1.58	1.6	1.6	1.65	1.625	1.74
3.5	1.6	1.65	1.65	1.68	1.7	1.68	1.8
4	1.63	1.7	1.7	1.725	1.78	1.75	1.85
4.5	1.7	1.78	1.73	1.8	1.83	1.82	1.92
5	1.8	1.82	1.78	1.88	1.95	1.9	1.98
5.5	1.88	1.9	1.825	1.95	2.02	1.98	2.05
6	2	1.3	1.8	2.1	2.1	2.08	2.1
6.5	2.12	1.1	1.86	1.7	1.2	2.12	2.1
7	2.25	2.05	1.975	0.7	0.75	2.15	2.04

### 7.5.1.2 Comparison of ventilation flow rate and air exchange rate

The mean flows and air exchange rate are significant factors for UCL ventilation (Hang et al., 2009) and pollutant removal (Hang et al., 2012) within the urban canopy layer (UCL) ventilation, which has been known as one of the possible mitigations to improve urban air environments (Oke, 1988; Bady, 2008; Deng, 2012; Hu and Yoshie, 2013 and Hang et al., 2013). To describe the air flow in street canyons further, both ventilation flow rate and air change rate per hour (ACH) have been examined (Kim, 2010; Hang and YG, 2010; ZW and YG, 2011; Graça et al., 2012) to quantify and assess the effectiveness of different ventilation configuration across the different cases.

#### 7.5.1.2.1 The ventilation flow rate

According to Hang et al. (2013), different semi-open street roofs may produce various flow patterns and ventilation capacities, and to quantify this effect Table 7.7 shows the normalized flow rates ( $Q^*$ ) in the seven test cases. Positive values denote air entering UCLs and negative ones represent air-leaving UCLs. Case 7 represented the highest flow rate ( $Q^*$ ) compared to other cases. The following points are worthy of attention:

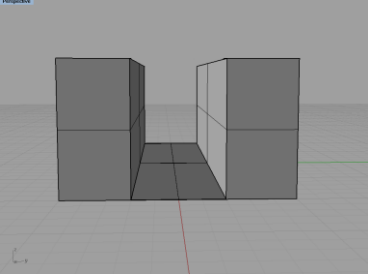
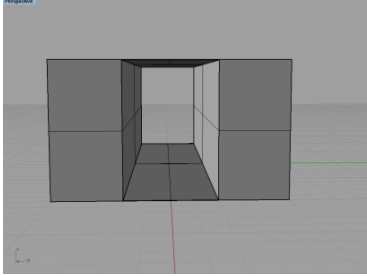
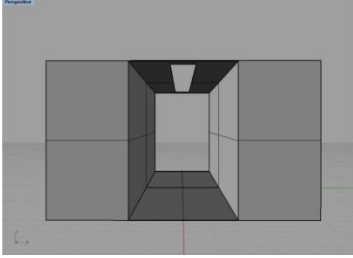
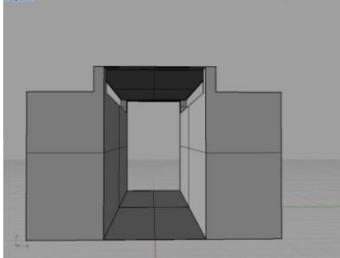
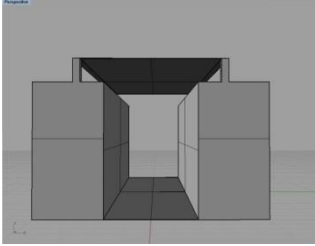
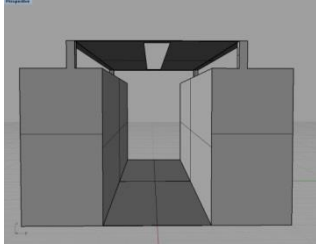
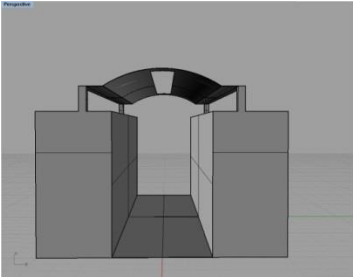
When comparing the first three cases, as they share the same volume ( $464\text{m}^3$ ), it was found that case number 1 recorded the highest volume flow rate which was expected due to the full open roof; however, case number 1 should be excluded from the analyses as it is not a semi-open street roof, as stated by Hang et al. (2013). By comparing case number 2 (fully covered) with case number 3 (roof opening), it was found that the volume flow rate increased by more than 10% in case number 3 due to the roof opening, compared to the lack of openings in case number 2; the roof opening was responsible for 23.5% of the total volume flow rate for case number 3.

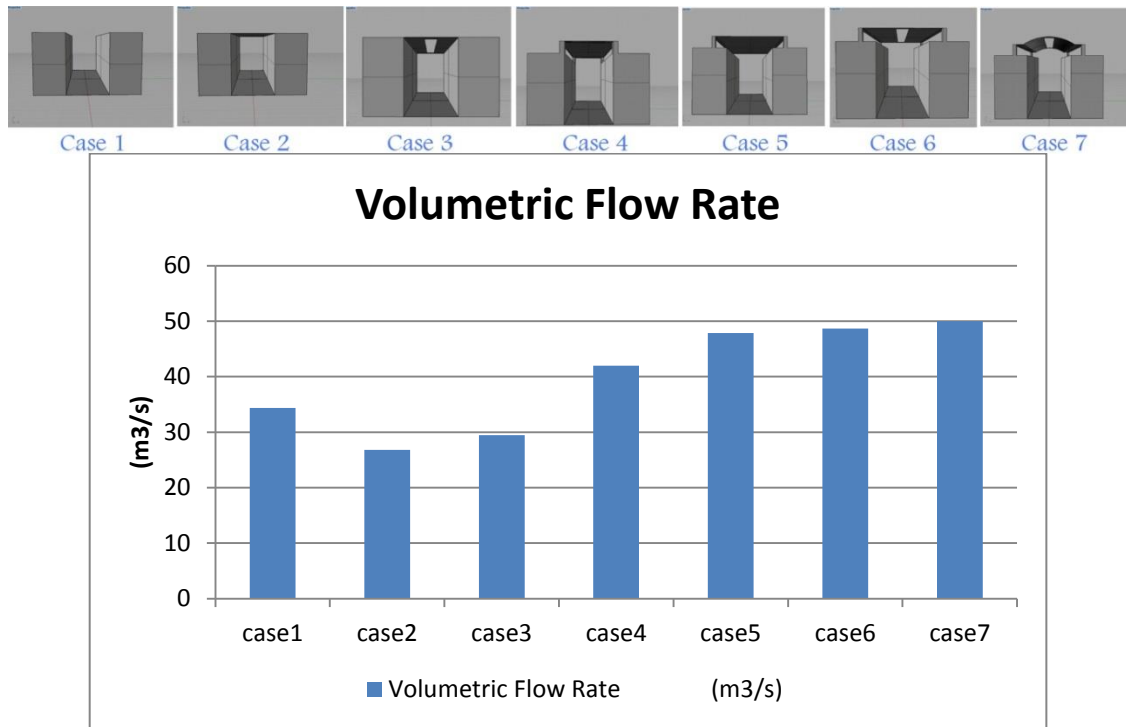
Second, although case number 5 had a larger volume space ( $584\text{m}^3$ ) compared to case number 4 ( $544\text{m}^3$ ), both having the same number and size of openings. It was noted that case number 5 had a higher volume flow rate than case number 4 due to the difference in the volume size, for both cases the two top side openings were responsible for almost the equal value of 30% of the total volume flow rate.

Third, by comparing the two cases number 5 and 6 which had the same volume size of  $584\text{m}^3$  with an extra opening in the mid roof for case number 6, the analysis revealed that case 6 had a higher volume flow rate of 2% compared to case 5, and the three openings of case 6 were responsible for 27% of the total volume flow rate against 30% for the two openings in case 5.

Fourth, cases 6 and 7 shared the same number, size and location of openings with the only difference being the shape of the roof, as case 6 was a flat roof while 7 was vaulted; case 7 recorded a 2.8% improvement in the volume flow rate than case 6. Furthermore, the total openings shared the same percentage of almost 27% of the total volume rate within both cases; however, the roof opening in case 7 recorded almost 10% for the total volume flow rate against 7.4% for the roof opening in case 6, which might be attributed to the vault shape of the roof as it may facilitate the air movement underneath. Based on these analyses, and as stated in Figure 7.20, it can be concluded that case 7 had the best performance compared to all other cases.

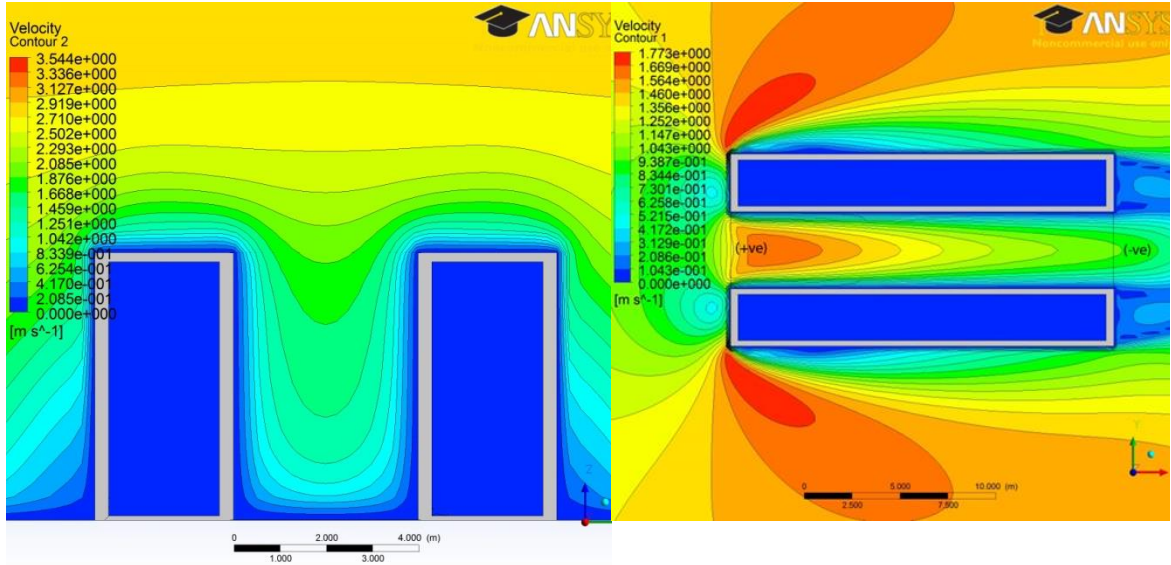
**Table 7-7** The (Q) or the Volumetric Flow Rate (m<sup>3</sup>/s) through the street opening or street roof note that positive values of (Q) denote air entering (inlet) and negative values represent air leaving (outlet)

<b>Case 1</b>	 <p>Front opening+<b>34.346294</b> Back opening-19.985943 Roof opening -14.360367</p>	<b>Case 2</b>	 <p>Front opening+<b>26.778683</b> Back opening -26.778683</p>
<b>Case 3</b>	 <p>Front opening+<b>29.482895</b> Back opening -22.538654 Roof opening -6.9445729</p>	<b>Case 4</b>	 <p>Front opening+<b>41.991043</b> Back opening-29.845551 Upper left opening -6.0431418 Lower right opening -6.102366</p>
<b>Case 5</b>	 <p>Front opening+<b>47.880123</b> Back opening-36.509018 Upper left opening-5.6316333 Upper right opening-5.7394876</p>	<b>Case 6</b>	 <p>Front opening+<b>48.663147</b> Back opening-35.384422 Upper right opening -4.8697925 Upper left opening -4.7942924 Roof opening -3.6146126</p>
<b>Case 7</b>	 <p>Front opening+<b>49.999229</b> Back opening-36.696915 Upper left opening -4.280737 Upper right opening -4.0979248 Roof opening-4.9237744</p>		

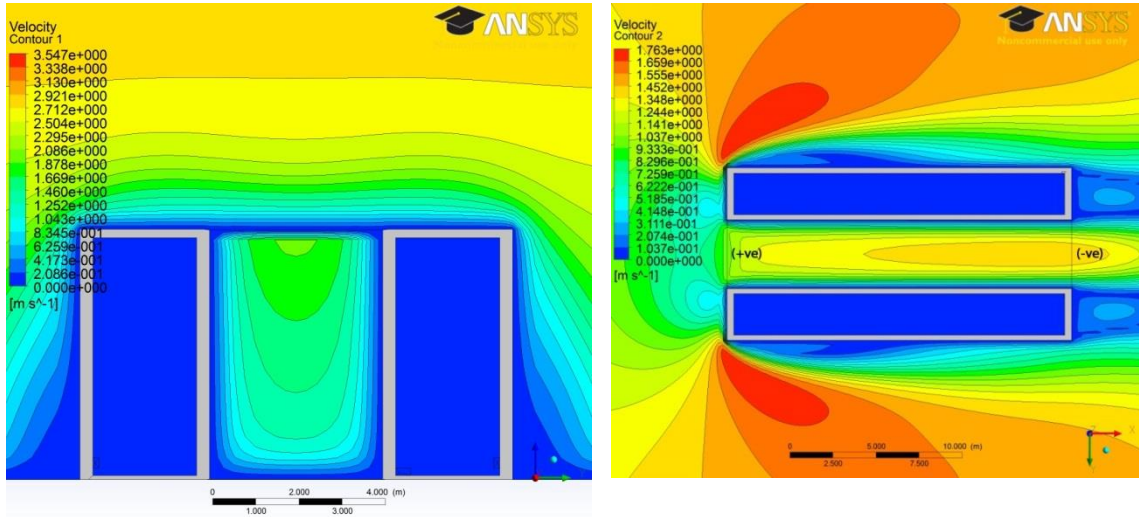


**Figure 7-20** The total volume flow rate (m<sup>3</sup>/s) for each case

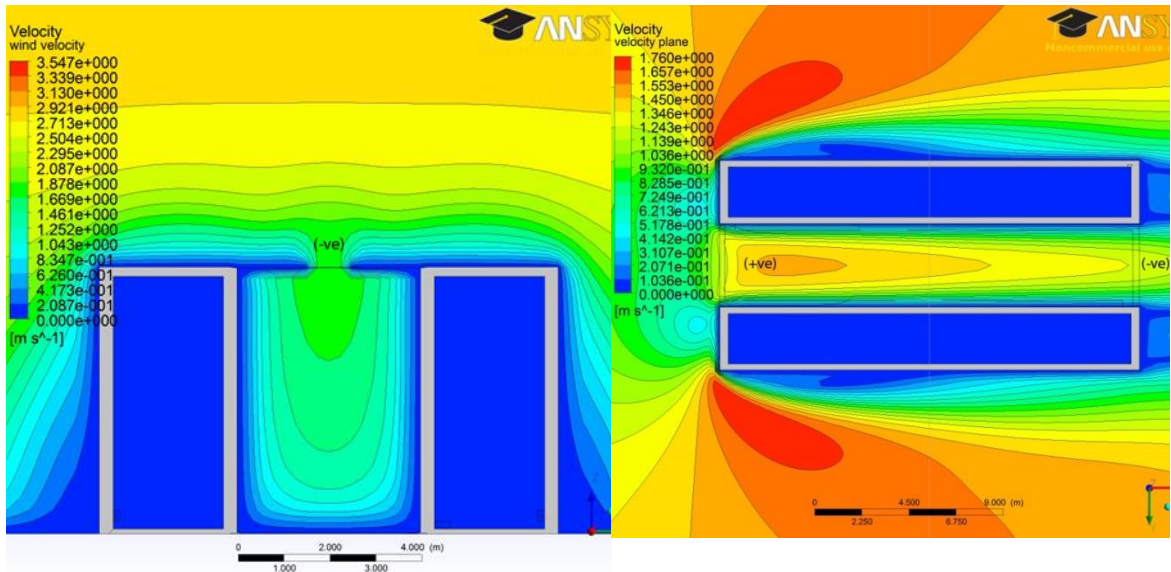
Case 1



Case 2

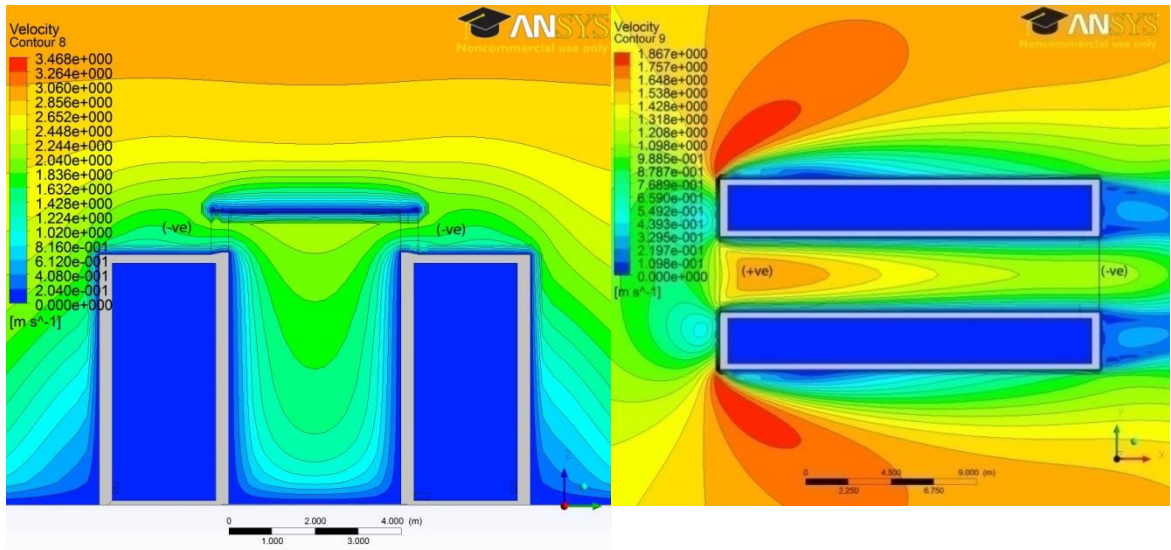


Case 3

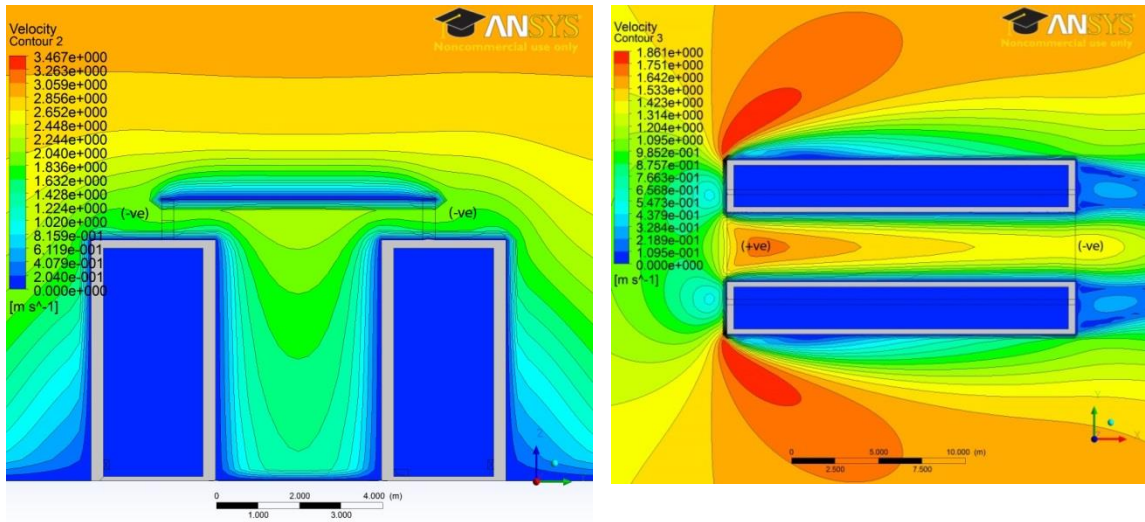




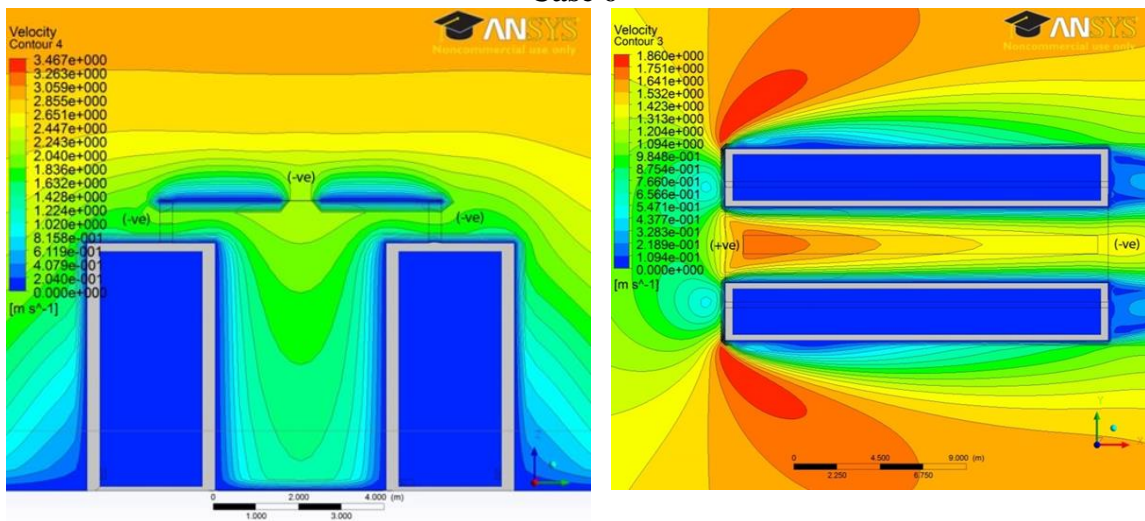
Case4

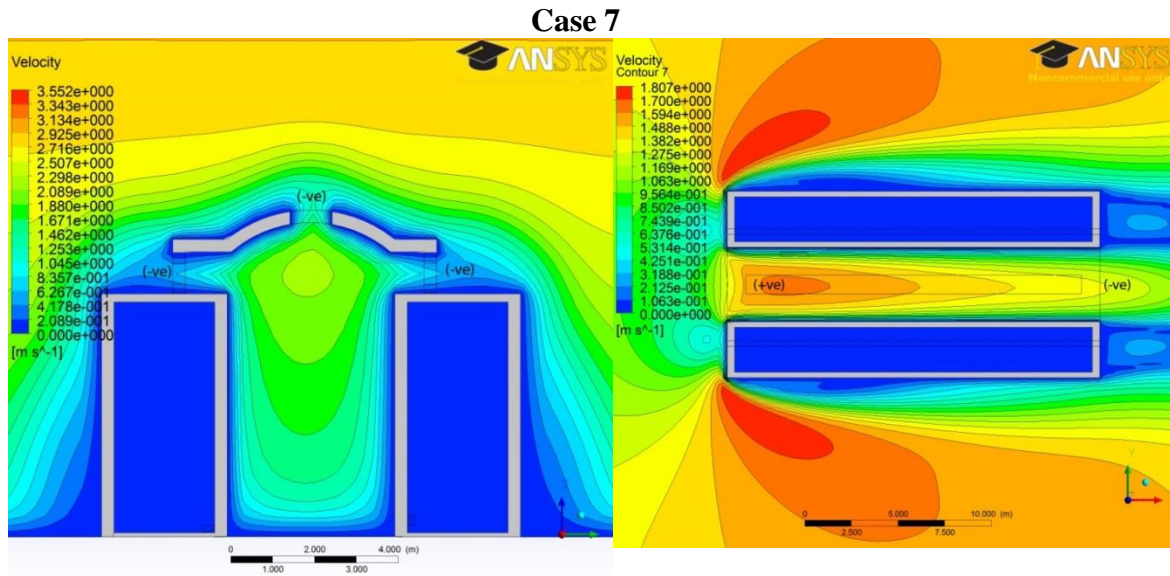


Case 5



Case 6





**Figure 7-21** The vertical wind speed contours at the centre line of the model on the left hand side and the horizontal wind speed contours at 1.4m above the ground level on the right hand side. Note that positive values of Volumetric Flow Rate (Q) denote air entering and negative values represent air leaving

#### 7.5.1.2.2 The air exchange rate per hour

One of the essential aspects of air exchange rate is to examine the different shading configurations' effect on the ventilation and the air exchange rate within the urban street, and to reduce any negative effect it might cause. The effectiveness of the different ventilation configurations is assessed using the air exchange rate, (Kim, 2010; Hang and YG, 2010; ZW and YG, 2011; Graça et al., 2012) which is the number of times each hour that the semi- enclosed total volume of air is exchanged with fresh air, as defined by ASHRAE (2005):

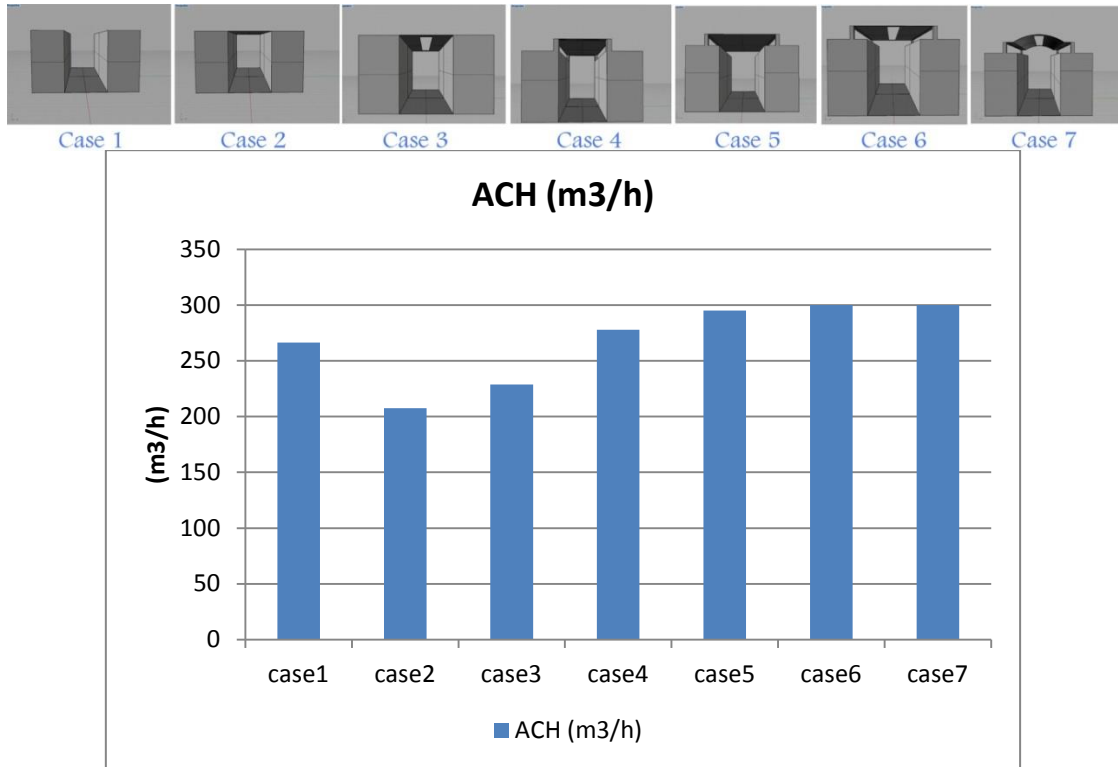
$$ACH = \frac{Q (3600)}{V} \quad (Eq. 7.1)$$

Where Q is the volumetric air flow rate into the enclosure ( $m^3/s$ ), V the volume of the enclosure ( $m^3$ ) and 3,600 the conversion per hour (60 minutes multiplied by 60 seconds). For each ventilation configuration, the simulated volume flow rates through each opening are used to determine the ACH using equation (7.1). The results of the total calculated ACH are shown in Figure 7.22 and the flow rates percentage across the roof and side openings are then presented in Figure 7.23. Based on these figures, the following can be pointed out;

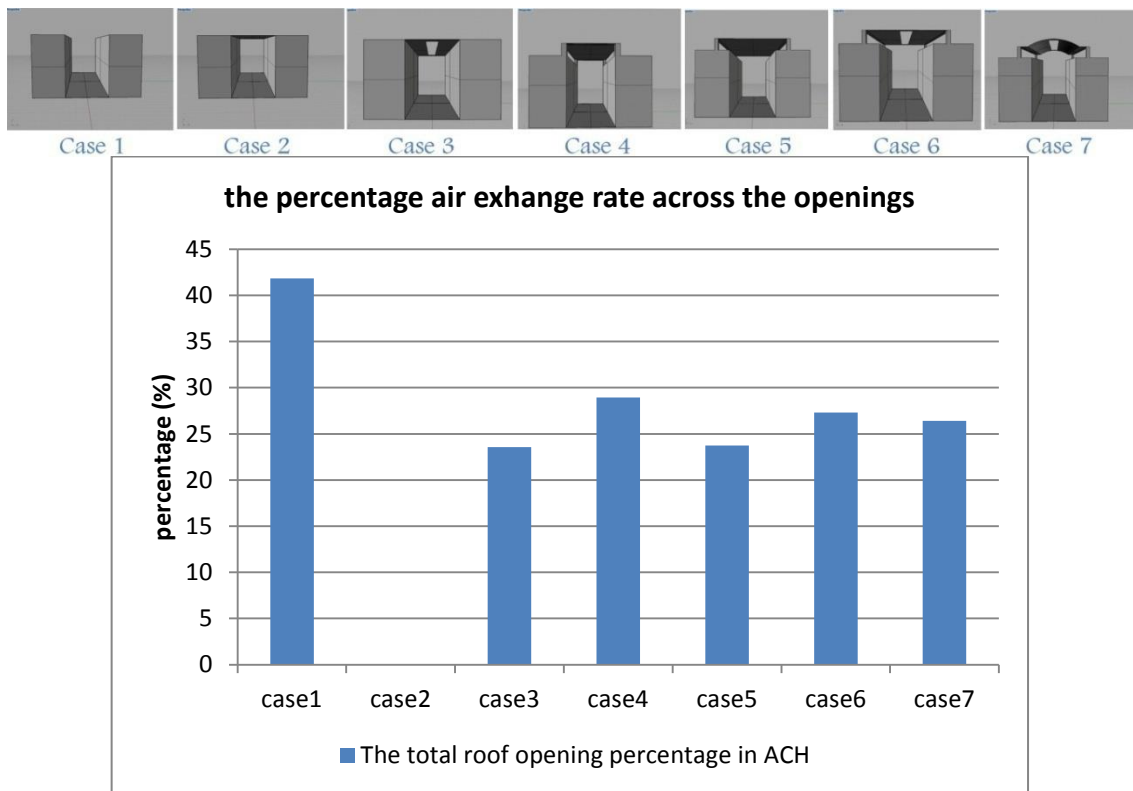


Case 1 recorded a higher air exchange rate of 28.3% than case 2 and 16.5% than case 3, which was expected due to the high sky view factor for case 1 (without a roof). However, when compared to the other cases, case 1 recorded the lowest air exchange ratio, and yet this is not a representative for better performance of the other cases compared to case 1 because according to equation (7.1) it is being calculated based on the volumetric air flow rate into the enclosure ( $m^3/s$ ) and, as stated, the other cases had a larger volume. This explains how the opening performance contributes to better ACH, as in Figure 7.22. Case 1's roof opening recorded the highest in ACH (41.8%) followed by the opening of case 4 (28.9%), and then cases 6 and 7, and then 5.

It also can be concluded that although cases 6 and 7 had the highest ACH, the number of openings was not the only reason as it may be attributed to the volume size which encourages more air circulation. This was confirmed through calculating the openings flow rate percentage of the total flow rate (Figure 7.23) as the results showed that not having a roof in case 1 caused more than 42% of the total air change rate in the canyon. Also, the roof openings in case 4, which had less volume than the following cases and only two sided openings, achieved 29% of the total air change rate against 27% and 26.4% for the three openings in cases 6 and 7, respectively.



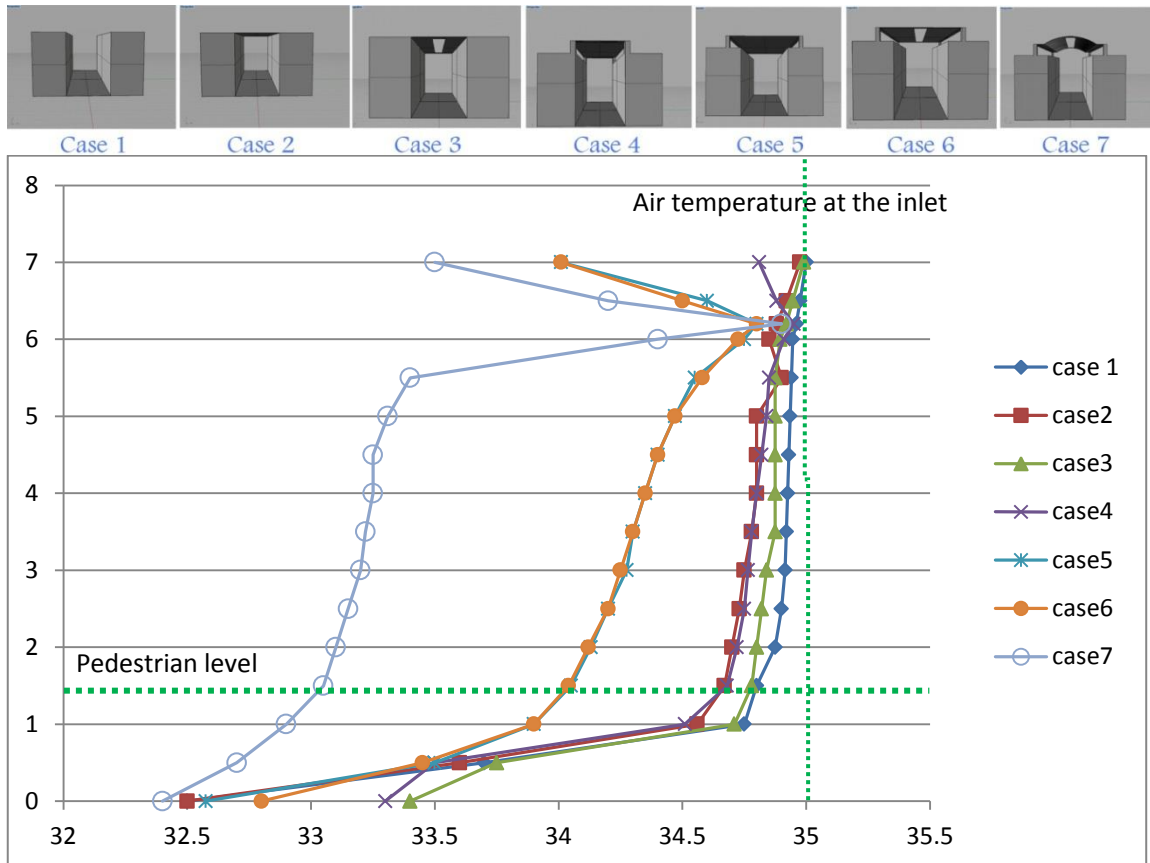
**Figure 7-22** Calculated air change rate per hour (ACH) for the different ventilation configurations for reference wind speed  $U_{10} = 5\text{m/s}$



**Figure 7-23** Flow rate percentages across the roof and side openings (case no. 2 is excluded due to its fully covered roof without any openings to be estimated)

### 7.5.1.3 Comparison of air temperature distribution

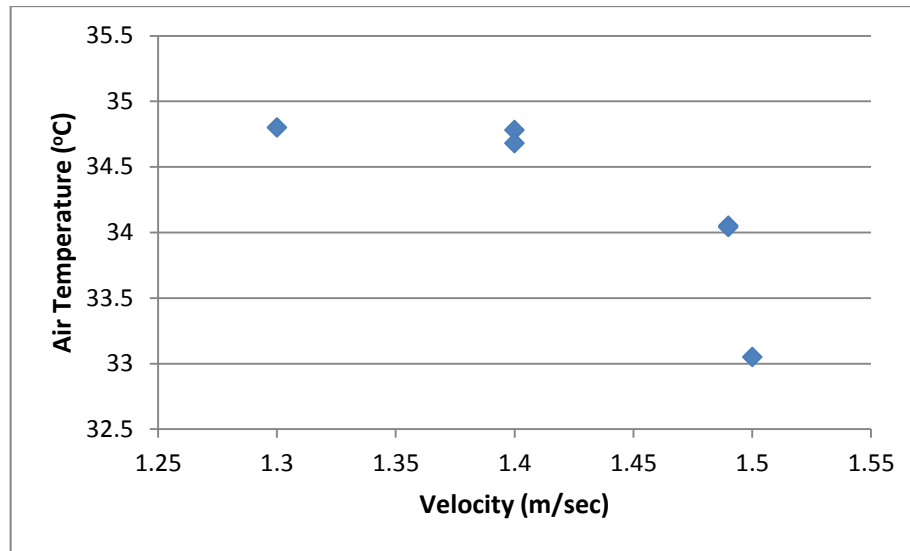
The vertical profiles of the mean air temperature were measured at a point on the centre line of the street across the prevailing wind direction with a reference air temperature at the inlet equal to 35°C, as conducted from the field measurement. As illustrated in Figure 7.24, the air temperature vertical profiles were plotted for all the cases from 0m to 7m above the ground level.



**Figure 7-24** The simulated vertical profiles of the air temperature located at the centre line of the street (from 0m on the ground level to 7m on the top roof level)

All cases started between 32.4°C to 33.4°C at level zero as the surface temperature, which is lower than the inlet temperature due to the shading effect. Once the vertical profiles reached the pedestrian level (1.4m) above the ground level, case 1 recorded the highest air temperature followed by cases 2, 3 and 4, all with minimal difference less than (0.2°C). The same four cases had the same trend of the vertical profile till reaching the roof level when case 2 faced a slight increase in air temperature directly under the roof while 4 had the same increase of air temperature at the building roof before decreasing again at the side opening level. Cases 5, 6 and 7 had different vertical trends.

Although case 6 had one more opening in the roof compared to case 5, which had only two side openings above the top buildings, they both had the same trend and recorded almost the same air temperature, which was lower than the previous cases. Therefore, it seems the extra opening or the location of the opening in the middle had less effect on air temperature than on the air velocity, as mentioned in the previous section. Even though case 7 had the same location and number of openings as case 6, it recorded the lowest air temperature through all 7m of vertical line except when it reached the side openings, when it suddenly increased by  $1.5^{\circ}\text{C}$  to reach the same temperature as the outlet ( $35^{\circ}\text{C}$ ), due to natural heat transfer from the undershade and the outside air temperature (Al-Kayiem et al. 2010). Then, once it passed the side opening, it declined again and lost the  $1.5^{\circ}\text{C}$ , again recording  $33.5^{\circ}\text{C}$  under the roof. This difference between cases 7 and 6 may be attributed to the vaulted shape of the roof in the former, as the mid opening had no effect on air temperature when cases 5 and 6 are compared. Therefore, it can be concluded that case 7 represented the best performance for having the lowest air temperature at the pedestrian levels between (1m to 2m above the ground level), as it kept  $1^{\circ}\text{C}$  difference with cases 6 and 5, and  $1.63^{\circ}\text{C}$  difference with the base case 3. For all cases, the highest air temperature stratified at the top (Al-Kayiem et al. 2010). The air temperature distribution was directly proportional to level height: the higher the level, the higher the air temperature till the vertical profile meets the side openings when the air temperature suddenly increased due to the direct contact with the external air temperature at  $35^{\circ}\text{C}$ . This migration of warm air to the top of the enclosure offers potentially more comfortable conditions resulting from cooler air collecting at ground level in the inhabited zone. Further, the high level hot air reservoir could have been discharged through upper level vents and thus generated a cooling airflow in the inhabited zone driven by the stack effect. Moreover, the results indicated a negative correlation between the air temperature distribution underneath the different roof shapes and the ambient wind speed, as the wind speed increased about 1.4m and there was a rapid drop in temperature, as shown in Figure 7.25. This effect of wind velocity has been reported by numerous studies (Ng et al., 2008; Yuan and Ng, 2012), including Cheng et al. (2011), who reported that a 1.0m/s to 0.3m/s decrease in the wind speed is equal to a  $1.9^{\circ}\text{C}$  temperature increase, and Memon et al. (2010), who stated that air temperatures rose as high as 1.3K when ambient wind speed decreased from 4 m/s to 0.5 m/s.



**Figure 7-25** The inverse correlation between the air temperature distribution underneath the different roof shapes and the ambient wind speed at the pedestrian level

**Table 7-8** The vertical profiles of the air temperature conducted from the CFD simulation located at the centre line of the street

Height	Case 1	Case2	Case3	Case4	Case5	Case6	Case7
Metre	Air temperature (°C)						
0	32.5	32.5	33.4	33.3	32.5	32.8	32.4
0.5	33.7	33.6	33.7	33.5	33.5	33.4	32.7
1	34.7	34.5	34.7	34.5	33.9	33.9	32.9
1.5	34.8	34.6	34.8	34.6	34.1	34.0	33.1
2	34.9	34.7	34.8	34.7	34.1	34.1	33.1
2.5	34.9	34.7	34.8	34.7	34.2	34.2	33.1
3	34.9	34.7	34.8	34.7	34.2	34.2	33.2
3.5	34.9	34.8	34.9	34.8	34.3	34.3	33.2
4	34.9	34.8	34.9	34.8	34.3	34.3	33.3
4.5	34.9	34.8	34.9	34.8	34.4	34.4	33.3
5	34.9	34.8	34.9	34.8	34.5	34.5	33.3
5.5	34.9	34.9	34.9	34.9	34.5	34.5	33.4
6	34.9	34.9	34.9	34.9	34.7	34.7	34.4
6.2	35.0	34.9	34.9	34.9	34.8	34.8	34.9
6.5	35.0	34.9	34.9	34.9	34.6	34.5	34.2
7	35.0	35.0	35.0	34.8	34.0	34.0	33.5

#### 7.5.1.4 The mean radiant temperature and PET

Although the ambient air temperature and air velocity were analysed, the assessment of air temperature or air velocity was insufficient to evaluate the overall thermal comfort in semi-outdoor and outdoor spaces (Danial et al., 2013). Thus, the PET were calculated using a proprietary application, Rayman (Matzarakis et al., 2007), based on the dominant microclimatic parameters including air temperature ( $T_a$ ), relative humidity (RH), wind velocity ( $v$ ) and mean radiant temperature ( $T_{mrt}$ ) of the surroundings. Except for  $T_{mrt}$ , these parameters were given either by the CFD simulation output including air temperature and wind velocity or from the field measurements, such as the relative humidity as a constant value.

The  $T_{mrt}$  was calculated for each case based on equation (5.1) given by ASHRAE (2009), as follows (for more details, refer to Sections 3.7 and 5.5.4):

$$T_{mrt} = \left[ (T_g + 273.15)^4 + \frac{1.1 \times 10^8 V_a^{0.6}}{\epsilon_g D^{0.4}} \times (T_g - T_a) \right]^{\frac{1}{4}} - 273.15 \quad (Eq. 5.1)$$

Where ( $T_g$ ) is the globe temperature ( $^{\circ}\text{C}$ ), ( $V_a$ ) is air velocity (m/s), ( $T_a$ ) is the air temperature ( $^{\circ}\text{C}$ ),  $D$  [mm] is the globe diameter (=25 mm), and ( $\epsilon_g$ ) is the emissivity of the sphere (=0.95 for a black globe). The empirically derived parameter  $1.1 \times 10^8$  and the wind exponent ( $V_a^{0.6}$ ) together represent the globe's mean convection coefficient ( $1.1 \times 10^8 V_a^{0.6}$ ). However, the globe temperature ( $T_g$ ) has to be calculated first based on each scenario air temperature and air velocity using the following equation (Dimiceli et al., 2011, 2013):

$$T_g = \frac{B + CTa + 7680000}{C + 256000} \quad (Eq. 7.2)$$

Where ( $T_a$ ) is air temperature while  $B$  and  $C$  are defined as follow

$$B = S \left( \frac{f_{ab}}{4 \sigma \cos(z)} + \left( \frac{1.2}{\sigma} \right) f_{dif} \right) + (\epsilon_a) T_a^4 \quad (Eq. 7.3)$$

$$C = \frac{h v^{0.58}}{(5.3865 \times 10^{-8})} \quad (Eq. 7.4)$$

Where ( $T_a$ ) is the air temperature ( $^{\circ}\text{C}$ ), ( $\sigma$ ) Stephan-Boltzman constant =  $5.67 \times 10^{-8}$ , ( $S$ ) is solar irradiance, ( $f_{ab}$ ) is the direct beam radiation from the sun, ( $f_{dif}$ ) is the diffuse radiation from the sun, ( $z$ ) is the solar angle to zenith, ( $s$ ) is the solar irradiance ( $\text{W}/\text{m}^2$ ), ( $h$ ) is the convective heat transfer coefficient, ( $v$ ) the wind velocity (mph) and ( $\epsilon_a$ ) is the

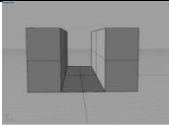
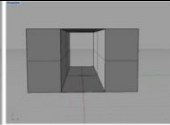
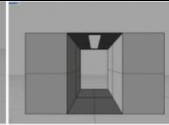
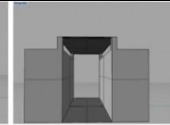
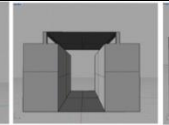
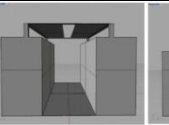
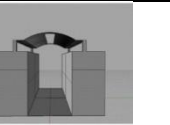
thermal emissivity and according to Hunter and Minyard (1999) it can be calculated using the following:

$$\epsilon_a = 0.575ea^{\frac{1}{7}} \quad (Eq. 7.5)$$

Where ( $ea$ ) is the atmospheric vapour pressure.

The equation was proved by Dimiceli et al. (2011, 2013) to estimate the globe temperature very accurately, as the experiments showed that the estimations were within about 0.27°C. All input variables are readily available in Table 7.9 and some of these variables are constant among all the cases as they shared the same location and conditions such as the atmospheric vapour pressure, solar angle to zenith, and solar irradiance, while the air temperature and wind speed was different in each case. Once the globe temperature ( $T_g$ ) was calculated, and then air temperature ( $T_a$ ), air velocity( $v_a$ ), relative humidity (RH) and mean radiant temperature ( $T_{mrt}$ ) are known, the physiologically equivalent temperature, PET (Höppe, 1993, 1999), as a thermal index is ready to be calculated using the RayMan model (Matzarakis et al., 2007, 2010).

Table 7-9 Calculated globe temperature, mean radiant temperature and PET for the different case studies in addition to the inputs used in the equations(  $f_{db}$ ) is the direct beam radiation from the sun,  $z$  is the solar angle to zenith,  $s$  is the solar irradiance ( $W/m^2$ ) were calculated based on solar radiation calculator attached in appendix E)

								
	Case 1	Case 2	Case 3	Case 4	Case 5	Case 6	Case 7	
<b>v (m/h)</b>	4680	4968	5040	5040	5220	5364	5544	
<b>v (m/sec)</b>	1.3	1.38	1.4	1.4	1.45	1.49	1.54	
<b>Ta</b>	34.8	34.67	34.78	34.68	34.05	34.04	33.05	
<b>B</b>	2708960.49	2668708.03	2702738.3	2671788.3	2482871	2479955.6	2203796.82	
<b>C</b>	756743640	783414319	789979636	789979636	806222801	819048598	834879223	
<b>Tg</b>	<b>34.80</b>	<b>34.67</b>	<b>34.78</b>	<b>34.68</b>	<b>34.05</b>	<b>34.04</b>	<b>33.05</b>	
<b>Tmrt</b>	<b>34.92</b>	<b>34.75</b>	<b>34.84</b>	<b>34.79</b>	<b>34.16</b>	<b>34.15</b>	<b>33.06</b>	
<b>PET</b>	<b>35.3</b>	<b>35.2</b>	<b>35.2</b>	<b>35.1</b>	<b>34.2</b>	<b>34.2</b>	<b>32.9</b>	
<b>The constant values used in equations (7.2), (7.3), (7.4) and (7.5)</b>								
<b>z</b>	90.22			<b>s</b>	0 (at the night time)		<b>f<sub>db</sub></b>	0

The thermal comfort index (PET) was calculated for each case and plotted in addition to the  $T_{mrt}$  on Figure 7.26. As can be noticed from the graph, the similarity between the PET and  $T_{mrt}$  patterns (Chapter Five reported that the regressions analyses between PET and  $T_{mrt}$  of  $R^2 = 0.972$  for a linear relationship) again confirms the strong influence of the mean radiant temperature on evaluating thermal sensation outdoors under summer sunny conditions (Mayer and Höppe, 1987; Mayer, 1993; Gomez, Tamarit, and Jabaloyes, 2001). The thermal acceptable range was estimated in Chapter Seven between 24°C to 32°C PET. Although none of the seven cases successfully achieved the acceptable range, they were still located within the slightly warm category. Also, it is very important to mention that the study was conducted on the hottest day of the year, which means that some cases can still achieve the thermal acceptable range during typical summer days, such as case 7, which positively achieved a 2.3°C reduction, compared to the base case 3, followed by cases 5 and 6 with a 1°C difference than the base case.

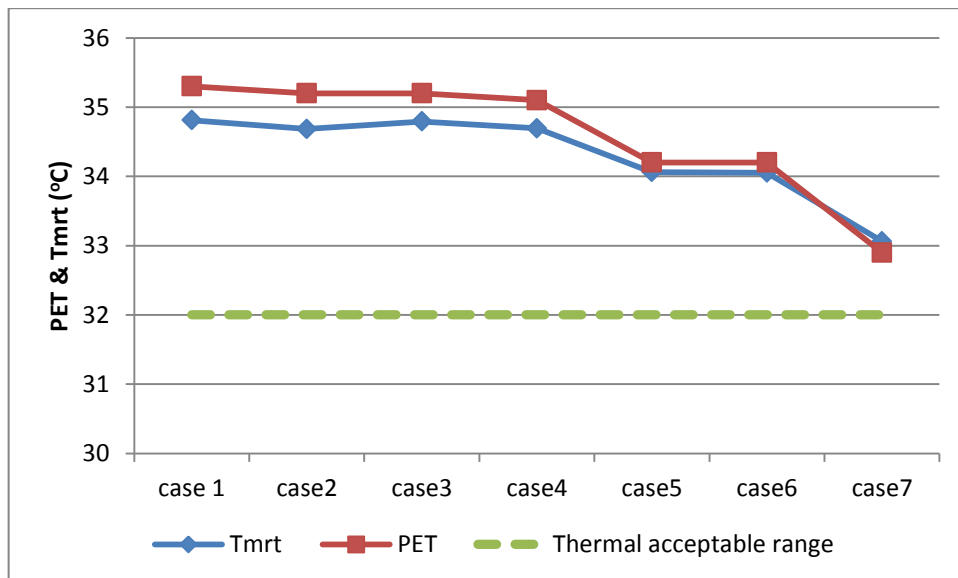


Figure 7-26 The estimated PET and  $T_{mrt}$  for the seven cases

### 7.5.1.5 Overall results

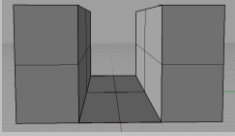
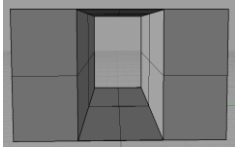
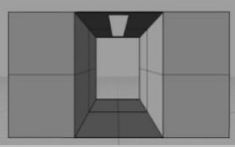
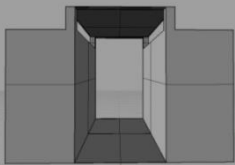
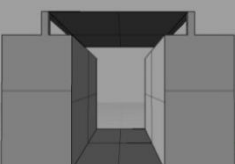
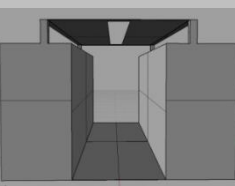
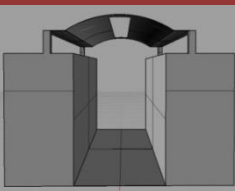
As the main concern of the study was to evaluate the optimum cooling effect made by different typologies of roofs as shading structures for urban streets during the night time, a summary of the results is presented in Table 7.10, showing the different



modification results for air temperature, air velocity and PET. This conditions leads to an improvement of the cooling effect at the street level. It is evident from the findings that the modification was due to the change in the shape and opening location within the covering structures.

The findings show that the structures' typology and the opening locations are one of the paramount factors in providing a temperature reduction on the urban scale. This modification in these properties leads to a large reduction of air temperature with 2.3°C for the best case compared to the base case. The reduction in air temperature was due to the vaulted shape of the tent with three openings as it causes a higher air velocity and higher air exchange rate underneath, which has a positive effect in decreasing the air temperature. Also, the vault shaped roof had a curved surface area and was considerably larger than the base, and so receives less solar heat per unit area, thus lowering surface temperatures and facilitating re-radiation after sunset(SKAT, 1988). Continuously, this process improved the thermal comfort of the area, as the PET for the best case 7 was about 32.9°C against 35°C for the base case, which was only 0.9°C, close to the thermal acceptable range on the hottest day of the year.

Table 7-10 Comparison between the different cases including the base case 3 and best case 7

Cases	Volume flow rate (m3/s)	Air velocity (m/sec)	Air exchange rate (m3/h)	% ACH through the openings (%)	Air temperature (°C)	PET (°C)
Case 1 	34.34	1.3	266.43	41.81	34.8	35.3
Case 2 	26.77	1.38	207.7	n/a no roof openings	34.67	35.2
Case 3 	29.48	1.4	228.7	23.55	34.78	35.2
Case 4 	41.99	1.4	277.8	28.93	34.68	35.1
Case 5 	47.88	1.45	295	23.72	34.05	34.2
Case 6 	48.66	1.49	299	27.29	34.04	34.2
Case 7 	49.99	1.54	300	26.4	33.05	32.9

### 7.5.2 Solar access simulation

Shading systems leads to a reduction of the heat gain at pedestrian level, which may lead to cooling systems not being operated frequently. Nonetheless, they have the drawback of reducing daylight availability (Tzempelikos and Athienitis, 2007). According to the Illuminating Engineering Society of North America (IESNA, 2000), it is essential that daylight effects be considered in any space where daylight is admitted, even if it is not exploited as a light source, in order to reduce the need for artificial lighting. Therefore, an analysis of solar access and shading is necessary for a complete evaluation of the climate efficiency of any street design solution to assure thermal and visual comfort underneath the shading tents.

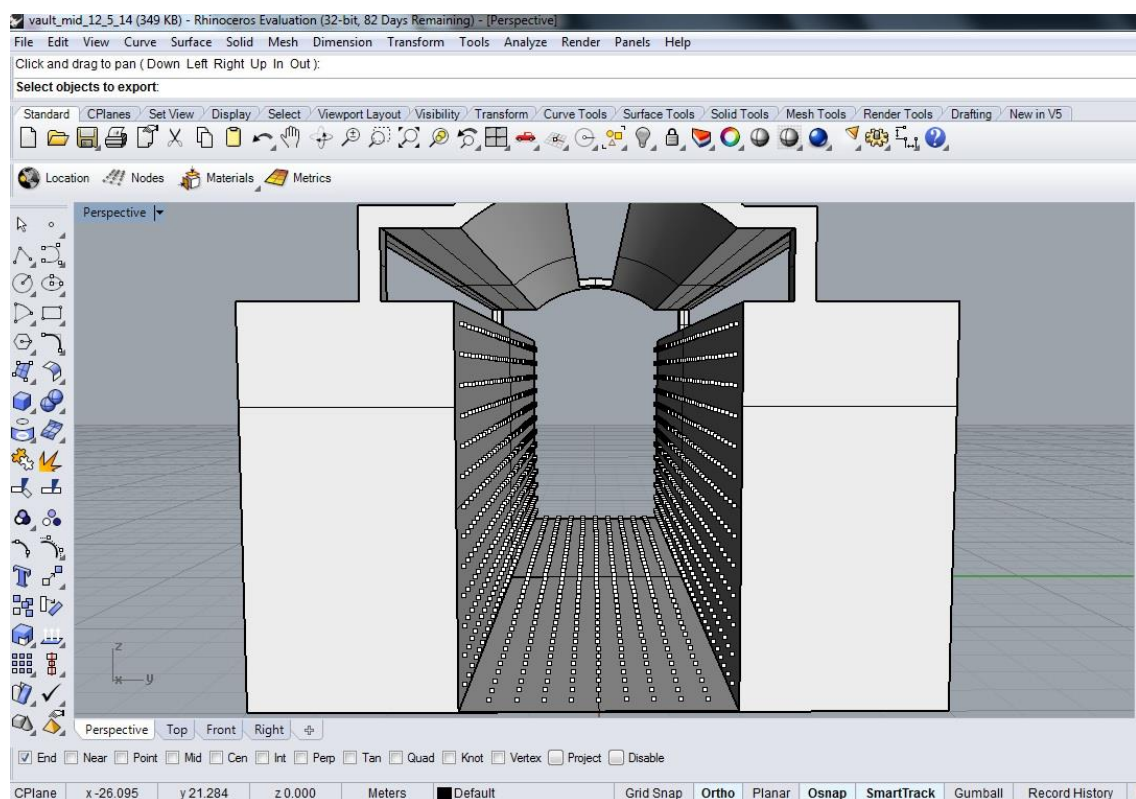
#### Simulation Setup

DIVA, which stands for Design Iterate Validate Adapt, is an environmental analysis plugin for the Rhinoceros 3D Nurbs modelling program (McNeal, 2010) and is used to examine the impact of each of the seven scenarios on solar access underneath. DIVA performs daylight analysis on an existing architectural model via integration with Radiance and DAYSIM with thermal load simulation using EnergyPlus within, which is a powerful tool that can be used on an urban or building scale (Reinhart et al., 2011). Radiance and DAYSIM employ a reverse ray tracing algorithm based on the physical behaviour of light in a volumetric, three-dimensional model which should most accurately represent reality (Ward, 1994). Radiance, on the other hand, utilizes the split flux method based upon a representation of complex geometries as planes when predicting interior daylight levels (US Department of Energy, 2010).

According to IESNA, daylight availability represents the annual amount of daylight coming from the sun and the sky at a specific location, time, date and sky condition. Based on the study objective for radiation maps, a grid based simulation was chosen which generates climate-specific annual surface irradiation images and calculates annual irradiation at node locations. This tool is powerful and was mainly developed to be used on an urban scale to identify locations in need of shading due to excessive solar exposure or areas with solar energy conversion potential.

The DIVA for Rhino simulation tool was used to model the case studies based on the grid based radiation map approach for three different timings: annual calculations, and both summer and winter seasons, which could help in optimizing the shading devices to minimize the summer exposure while maximizing the winter gain.

Data of direct and diffuse solar radiation are included in the weather file titled as “Cairo Intl Airport 623660 (ETMY)” which was uploaded within the software extracted from the EnergyPlus weather file data. The grids of sensor nodes were adjusted on the ground surface and the two walls with spacing every 0.5m in both directions (X) and (Y), as seen in Figure 7.27.



**Figure 7-27** The grid sensor nodes scattered within the model

## Metric

As seen in Figure 7.28, the cumulative sky method was selected which according to Robinson and Stone (2004) is described as harnessing a Radiance module called GenCumulativeSky to create a continuous cumulative sky radiance distribution. This cumulative sky is then used in a Radiance backwards ray-trace simulation. Compared to other approaches which use hourly calculations, this approach is significantly faster with a minimal sacrifice in accuracy. Simulation radiance parameters are presented in

Table 7.11 and explained in Box 7.1, as illustrated in the DAYSIM tutorial (Reinhart, 2006); they should thus yield reliable results.

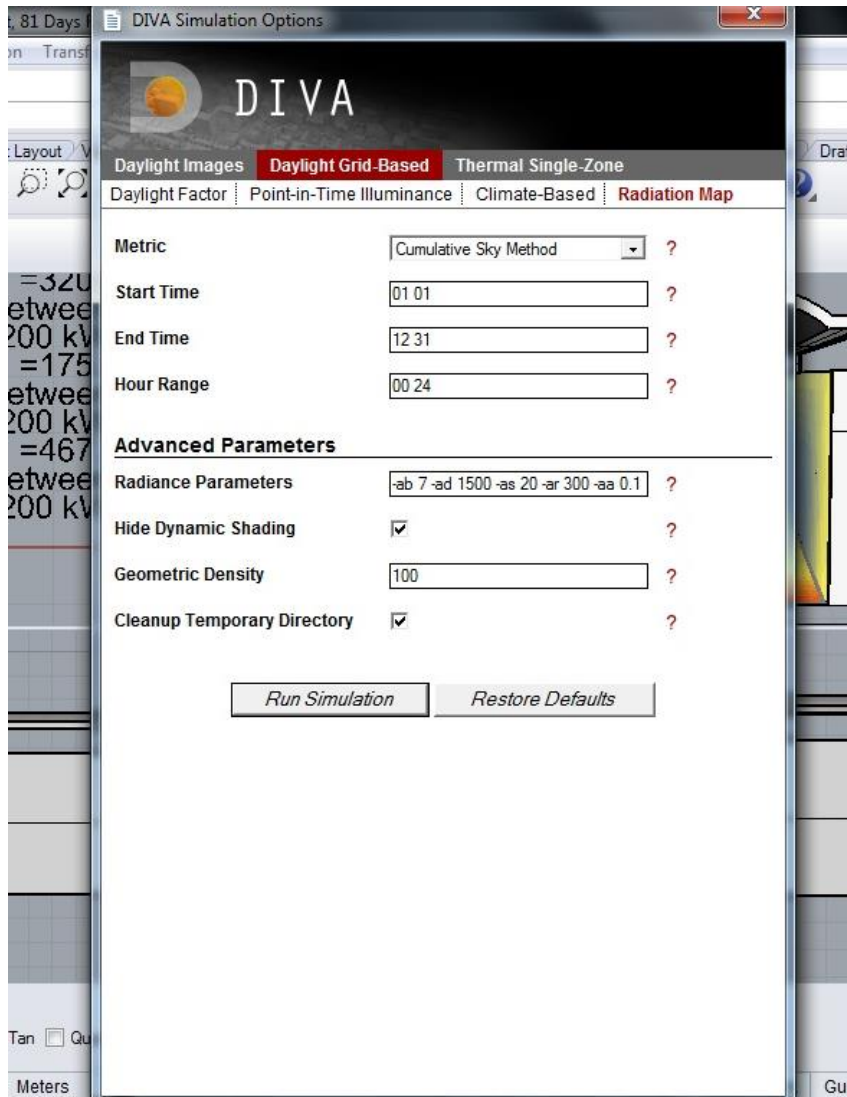


Figure 7-28 The grid sensor nodes scattered within the model

Table 7-11 The grid sensor nodes scattered within the model

Ambient bounces	Ambient divisions	Ambient super-samples	Ambient resolution	Ambient accuracy	Direct threshold	Direct sampling
ab	ad	as	ar	aa		
7	1500	20	300	0.1	0	0

**Further justifications for the choice of parameters...**

**ambient bounces (ab=5):** This parameter describes the number of diffuse inter-reflections which will be calculated before a ray path is discarded. An ab-value of 5 is already sufficient for a standard room without any complicated facade elements. This parameter significantly increases the required calculation time and should be set with care. It has to be even higher if interior rooms of facades including venetian blinds are considered, as rays may be reflected several times they find their way out of the building.

**ambient division (ad=1000) and ambient sampling (as=20):** The ad-parameter determines the number of sample rays that are sent out from a surface point during an ambient calculation. This parameter needs to be high if the luminance distribution in a scene with a high brightness variation. An ambient sampling parameter greater than zero determines the number of extra rays that are sent in sample areas with a high brightness gradient.

**ambient accuracy (aa=0.1) and ambient resolution (ar=300):** The combination of these two parameters with the maximum scene dimension provides a measure of how fine the luminance distribution in a scene is calculated. According to page 385 in *Rendering with Radiance*, the combination of aa=0.1, ar=300 and a maximum scene dimension of 100m yields a minimum spatial resolution for cached irradiances of:

$$\frac{\text{maximum scene dimension} \times \text{ambient accuracy}}{\text{ambient resolution}}$$

The simulation resolution will be  $(100\text{m} \cdot 0.1) / 300 \sim 3\text{cm}$ . This is sufficient if the facade/roof openings through which the daylight enters the building feature no details below 3 cm. The formula reveals that it is advantageous to keep your scene dimensions as small as possible.

**direct threshold (dt=0):** This option switches off the selective source testing, i.e. each light source is equally considered during each shadow testing. This option is automatically set to zero when direct daylight coefficients are calculated using DAYSIM.

**direct sub sampling (ds=0):** This option switches off the direct sub sampling threshold, i.e. only one ray is always sent into the center of each light source. As during the calculation of the direct daylight coefficients only solar discs with an angular size of  $0.5^\circ$  are present, disabling direct sub sampling speeds up the calculation without impeding its accuracy.

---

**Box 8.1.** The simulation parameters as explained in the “tutorial on the Use of Daysim/Radiance Simulations for Building Design – version: Aug-06” (Reinhart, 2006)

---

### 7.5.2.1 Daylight simulation results

The analyses were based on calculating the incident solar radiation on the three different surfaces underneath the shading devices including the east and west walls, and the

ground surface. The incident solar radiation is the amount of solar radiation energy received on a given surface during a given time (energy per area ( $\text{W}/\text{m}^2$ )). All seven cases were examined seasonally and annually and the overall results are illustrated in Table 7.12 and analysed in Figure 7.29 and 7.30, as compared to ANSI/ASHRAE/IESNA Standard 90.1-2007<sup>17</sup> for lighting.

According to ANSI/ASHRAE/IESNA Standard 90.1-2007, the lighting power densities for the outdoor sales for open areas including vehicle sales lots should not be less than  $5.4 \text{ W}/\text{m}^2$ . Case 1 was excluded from the comparative analysis as it is a fully exposed street without any shading device adjustments; this explains the highest radiation values recorded compared to other scenarios, as shown in Figures 7.29 and 7.30.

Case 2 recorded the lowest values of solar radiation received among the three surfaces, including the walls and the ground in both seasons. This is mainly attributed to its fully covered tent system with no openings for sunlight to pass through (Figures 7.29 and 7.30), as the west wall and the ground could not achieve the minimum lighting power densities requirement during the winter time, as stated by ANSI/ASHRAE/IESNA Standard 90.1-2007.

Although case 3 only had one opening in the middle of the roof and it can be considered as the base case used by the ancient town planners in Al-Muizz Street to provide shading without preventing the daylight from entering the place (Figure 7.30 and 7.31). The case recorded very close values compared to the best cases of 6 and 7, and it performed better than cases 4 and 5, which had two side openings without any openings in their roof. It can be concluded that the roof opening acted better than the side opening in providing sunlight underneath, particularly in the summer time when the sun altitude is higher than in winter. This also explains the close values between cases 3 and 4 in winter when the sun altitude is very low; then, the side opening in case 4 performed well based on the sun angle, which can reach up to 36.4 degrees compared to 83.2 degrees in summer (Figures 7.29 and 7.30).

Cases 4 and 5 both shared similar side openings; however, the only difference was in case 4, in which the openings were in alignment with the west and east walls

---




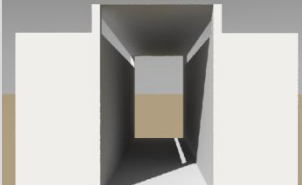
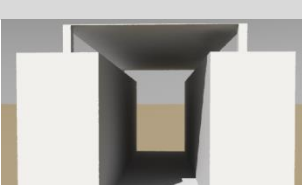
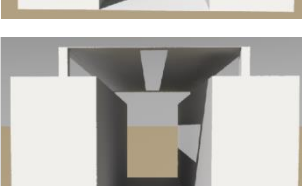
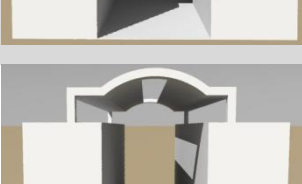
<sup>17</sup> IESNA is the Illuminating Engineering Society of North America  
ANSI is the approved American National Standard

underneath, while in case 5 the openings were 1m shifted beyond the walls, as seen in Figure 7.29 and 7.30. Based on this modification, case 4 recorded higher values than case 5, which could not achieve half the minimum ANSI/ASHRAE/IESNA Standard 90.1-2007 for the west wall and barely passed the required lighting power densities for the ground during the winter time, as the sun rays in some angles may hit the inside roof without reaching the walls or the ground. In case 4, the passing rays from both windows most probably reached either the ground or one of the walls.

Case 6 in general is considered to be the best case in daylighting and solar radiation analysis. However, due to the vaulted shape in case 7, this caused both east and west walls to receive more solar incidence in summer, while due to the same vaulted shape, the roof was half a metre higher than the flat roof in case 6, and as a result the ground in case 6 received more solar incidence than the ground surface in case 7, due to the high sun altitude during the summer. As illustrated in Table 7.12 and Figures 7.29 and 7.30, although case 6 recorded the best results in providing daylighting underneath, the values were very close to case 7; such a minimal difference does not give much advantage for case 6, as both cases had already achieved the lighting power density requirements, except for the west wall during the winter time as cases 6 and 7 recorded 4.58 and 4.35  $W/m^2$  respectively. These were below but very close to the minimum requirement (5.4  $W/m^2$ ) which means that both cases may use an artificial light to achieve these differences. Therefore, both cases may be considered similar in terms of daylight performance.



**Table 7-12** solar radiation and incident analysis between the different cases

Cases	Time	East (W/m <sup>2</sup> )	West (W/m <sup>2</sup> )	Ground (W/m <sup>2</sup> )
Case 1 	Summer	61.93	33.31	104.95
	Winter	30.80	9.75	12.40
	Yearly	92.35	42.89	116.61
Case 2 	Summer	9.70	7.41	26.23
	Winter	5.70	2.12	5.10
	Yearly	15.36	9.51	31.29
Case 3 	Summer	21.26	13.42	46.51
	Winter	11.85	4.03	6.87
	Yearly	32.83	17.38	53.37
Case 4 	Summer	16.26	11.87	31.93
	Winter	11.71	4.01	6.36
	Yearly	27.92	15.82	38.19
Case 5 	Summer	13.37	10.08	30.01
	Winter	7.935	2.99	5.63
	Yearly	21.27	13.04	35.56
Case 6 	Summer	25.17	15.54	47.08
	Winter	13.55	4.58	7.04
	Yearly	<b>38.48</b>	<b>20.17</b>	<b>54.42</b>
Case 7 	Summer	25.30	15.69	46.48
	Winter	11.61	4.35	6.89
	Yearly	36.69	20.02	53.57

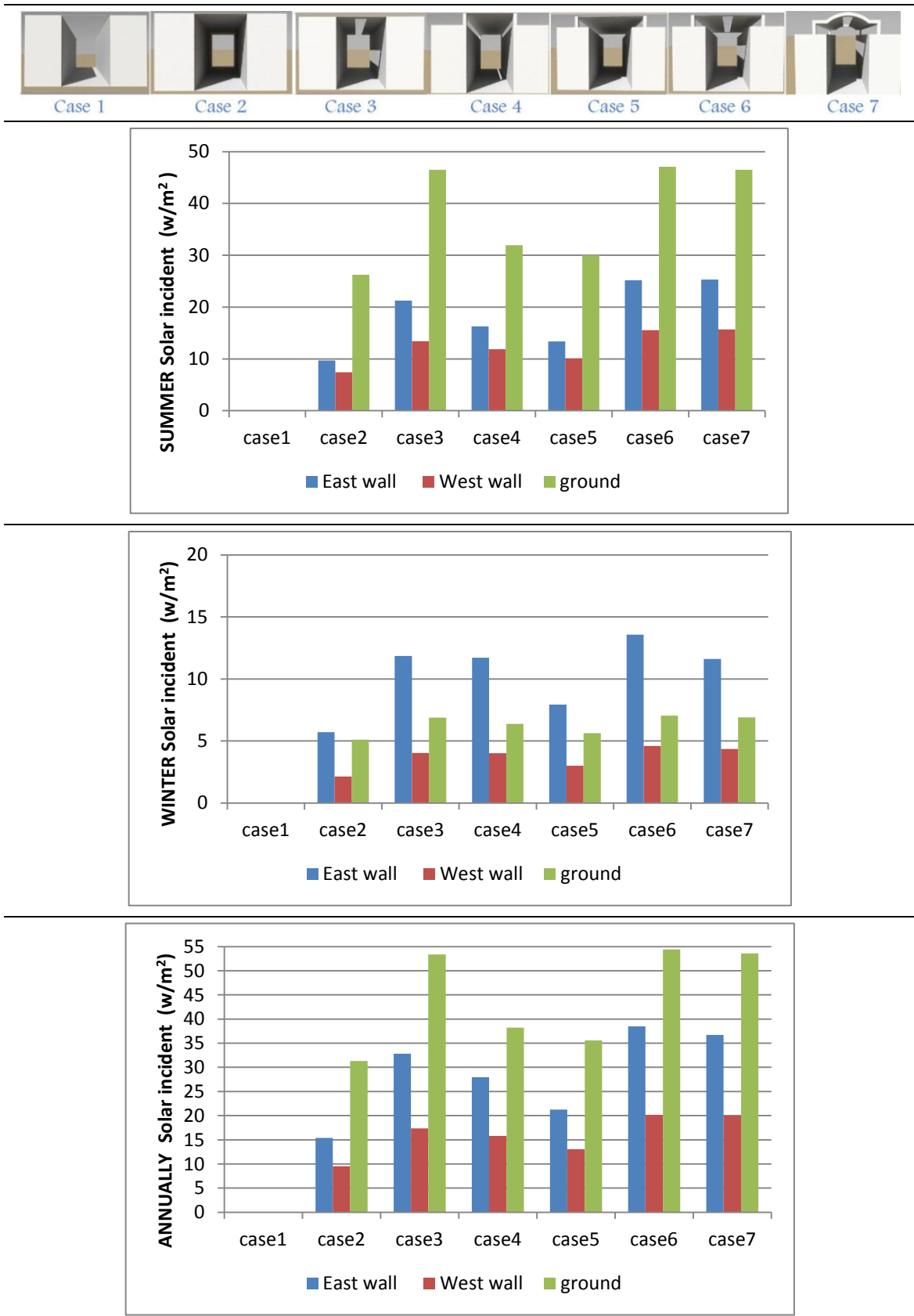
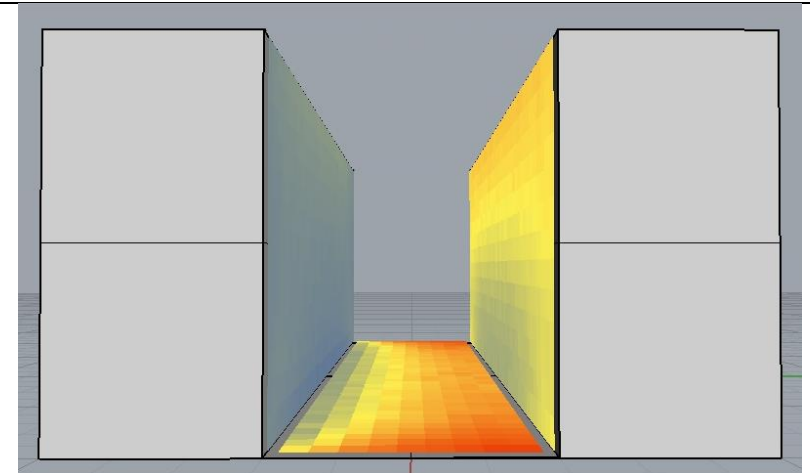
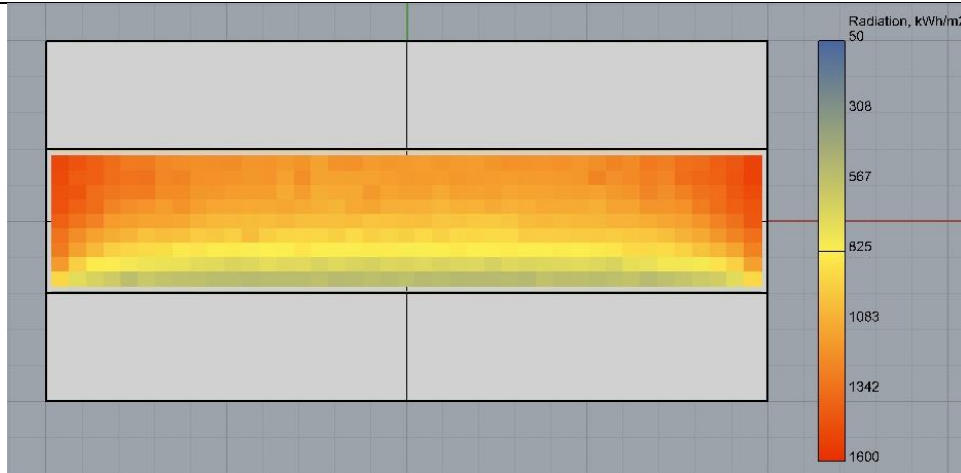


Figure 7-29 The solar incident analysis for all cases for the summer and winter, and annually, excluding

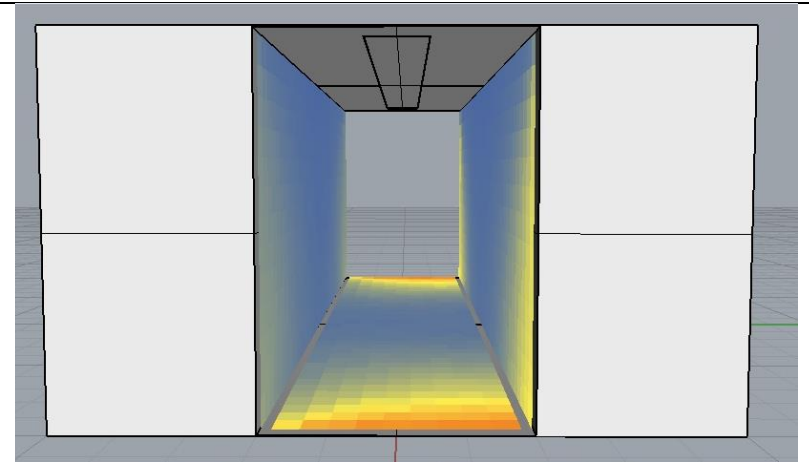
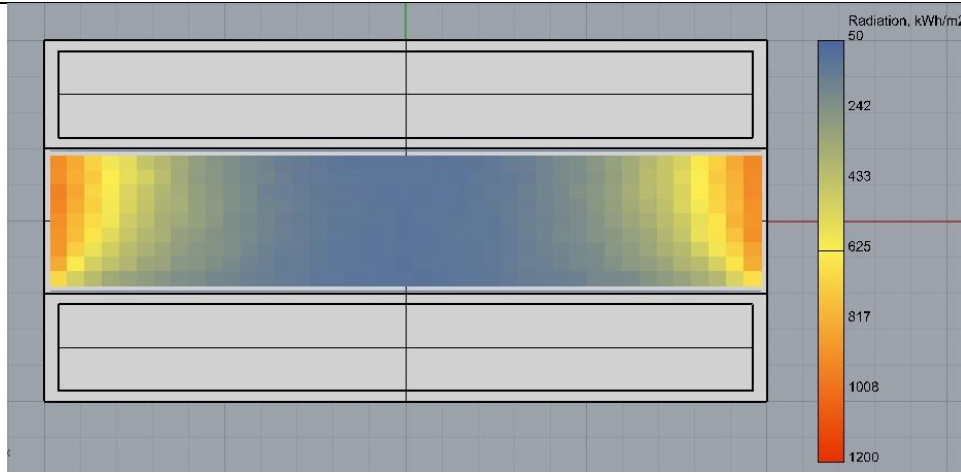
---

case 1 as it is a fully exposed without any shading roofs

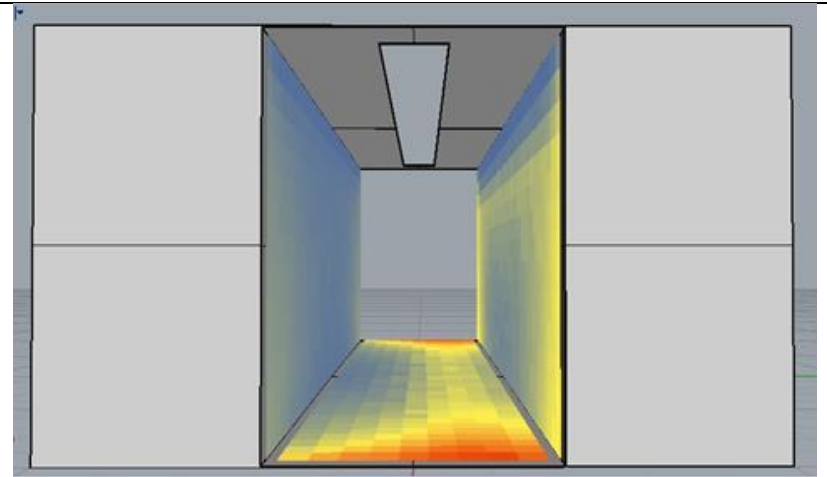
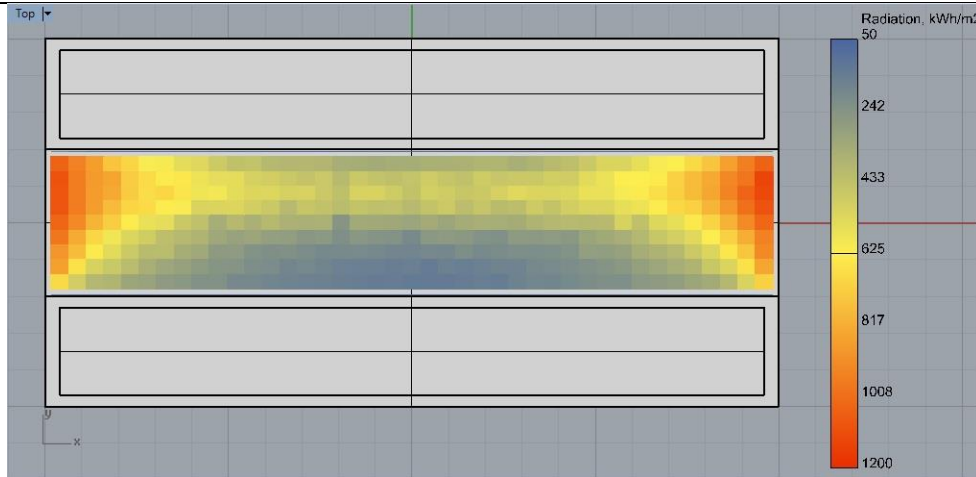
Case 1



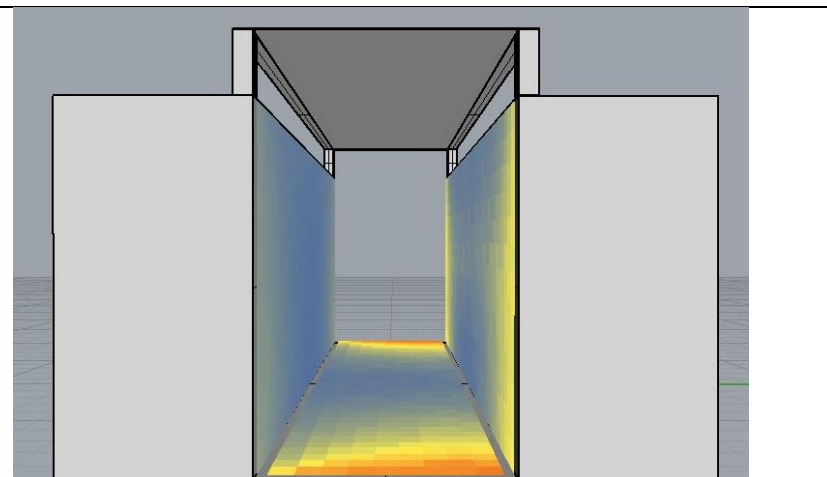
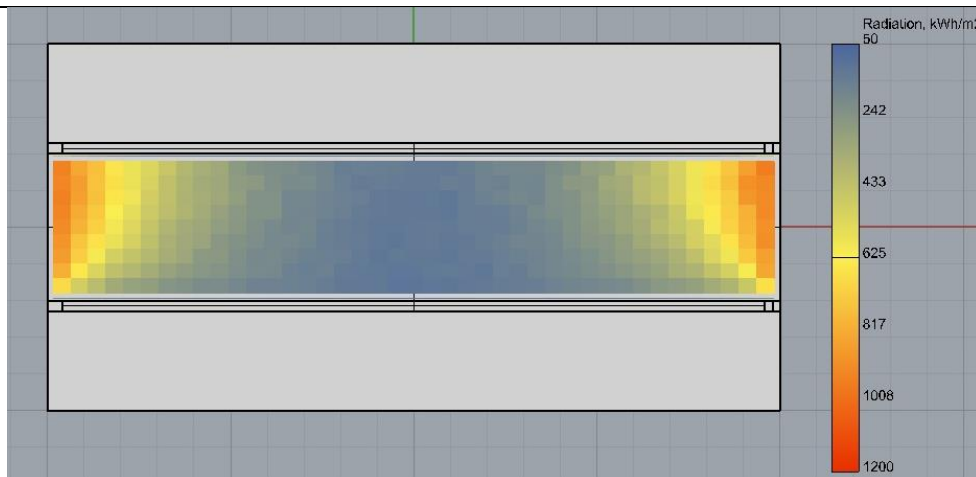
Case 2



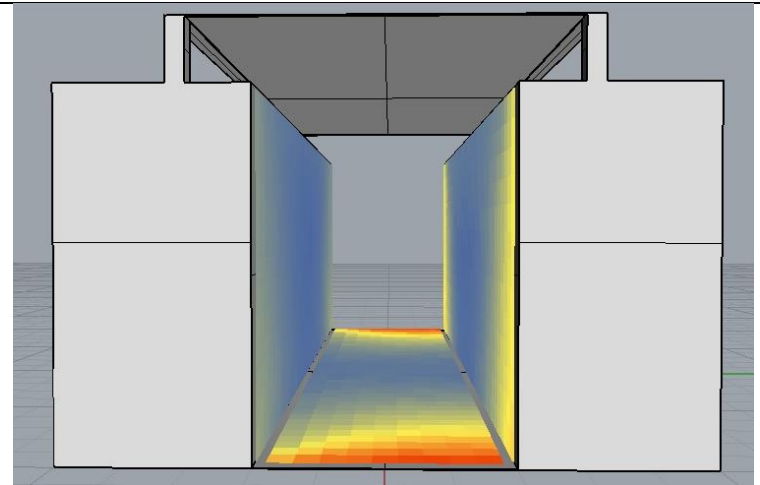
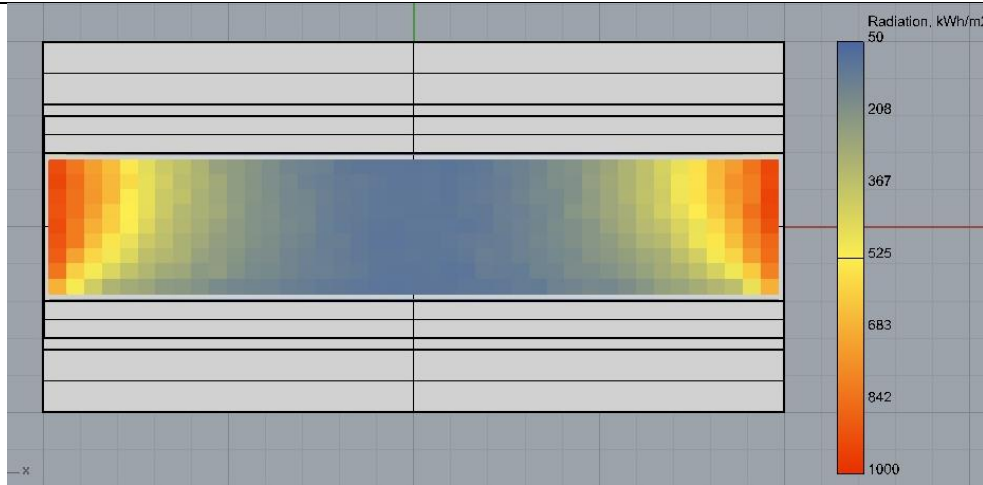
Case 3



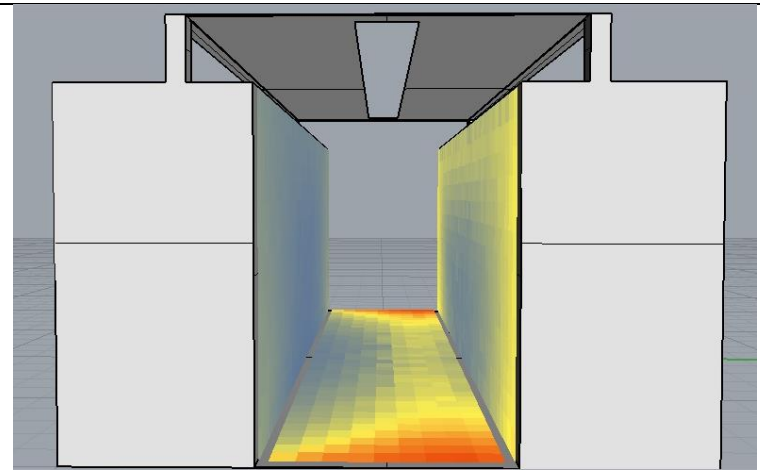
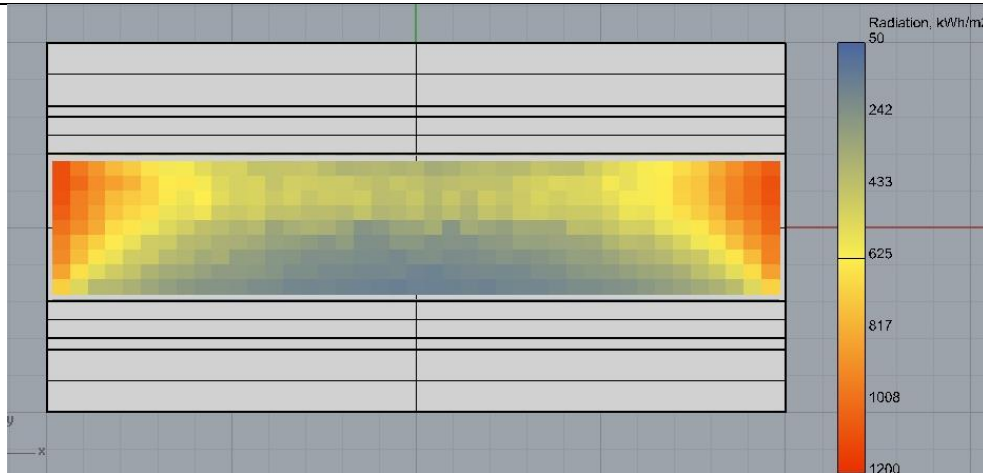
Case 4



Case 5



Case 6



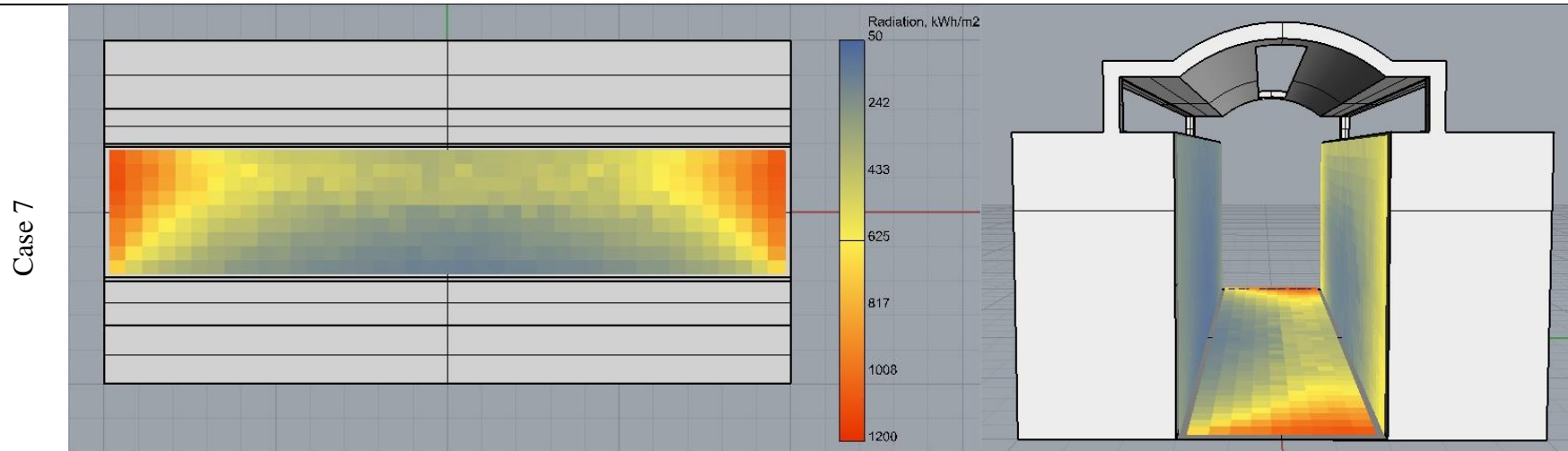


Figure 7-30 DIVA Radiation Map –annual grid based simulation output for the seven case studies



Figure 7-31 The base case, as used by ancient town planners in Al-Muizz Street to provide both shading and daylight

## 7.6 Conclusion

The solar radiation and the level of shading were proved to be the dominant components driving the heat balance equation for the hot, arid climate (Pearlmutter et al., 2007), where the  $T_{mrt}$  was found to have a stronger effect on pedestrian thermal perception than the air temperature under hot, sunny conditions (Spagnolo and de Dear, 2003; Toudert et al., 2005; Johansson, 2006). Although shading is not a new solution as it had been used historically under different climate conditions, its positive climatic effects as a traditional solution have recently been questioned, as they might have been overestimated (Givoni, 1997; Toudert, 2005). The high shading levels may increase thermal comfort during the day in summer, and contribute to high temperatures at night as they decrease the long wave radiation loss on surfaces (Lin et al., 2010). In order to regulate climate comfort, a quantitative based study was still required for different shading patterns. Because vegetation as a shading device is not applicable for Al-Muizz Street as the sub-surface water has risen to catastrophic levels, the appropriate solution was the use of shading devices such as tents and canopies.

The chapter was divided into two parts. In the first part of the chapter, the choice of the computational fluid dynamics (CFD) Fluent code 13.0 as a tool in order to explore the environmental behaviour of these shading structures was discussed, in addition to the appropriate settings based on the literature review and best practice guide lines (BPG) (Blocken, 2012) for the CFD simulation. This included the mathematical model, geometry and solution domains, and the boundary condition. The CFD results were validated based on the in site measurement comparison with the existing case modelling. In the second part, the possible use of the different shading designs including topologies and opening locations, particularly to enhance occupants comfort level within the semi-enclosed spaces, was the main discussion using the comparative analysis reported by the CFD for seven different cases based on three main environmental aspects, including the air velocity, air temperature distribution and solar access.

First, the air velocity was examined in terms of the wind velocity vertical profile so as to examine the effect at the pedestrian level, and then the volume flow rate and air exchange rate were examined to quantify the mechanisms of air exchange and the effectiveness of the design (Hang et al., 2013). The results indicated that all of the



examined wind vertical profiles followed almost the same pattern, with the highest velocity recorded for the pedestrian level being 1.55 (m/sec) for case 7, until they all reached the building top near the roof, when the velocity profiles started to vary according to the different roof shapes and opening locations. This meant that the roof typology and opening significantly affected the wind profiles beneath. All of the seven cases fell within the comfort range of wind velocity ( $U \geq 1.3$  m/s) except case 1, and yet case 7 was the closest to the optimum wind speed of 1.6m/sec under typical summer time conditions, according to a study by Cheng et al. (2011). Then, the ventilation capacity and volume flow pattern was examined as it may vary due to the different semi-open street roofs (Hang et al., 2013). It was concluded that in all cases the side and roof openings performed about 23%-30% better with an increase in the volume flow rate underneath the shading roofs. In addition, the influence of the roof shape as the vaulted roof recorded 10% for the total volume flow rate against 7.4% for the flat roof. The effectiveness of the different ventilation configurations was assessed using the air exchange rate (Kim, 2010; Hang and YG, 2010; ZW and YG, 2011; Graça et al., 2012). Although cases 6 and 7 recorded the best ACH, the number of openings was not the only reason as the volume sizes played a role in encouraging more air to pass through. Therefore, by estimating the openings percentage in contributing for the total flow rate it was found that two openings in cases 4 had a higher performance for ACH rate than the three openings in cases 6 and 7. However, case 7 followed by case 6 recorded the highest values for the total ventilation flow rate and ACH.

Secondly, the air temperature distribution was investigated underneath the different roof configurations using the vertical line air temperature measurements located at the centre of the street with a reference air temperature at the inlet equal to 35°C as conducted from the field measurements. The air temperature distribution was positively correlated with the level height, and the higher the level was, the higher the air temperature till the vertical line reached the side opening when the air temperature suddenly increased because of the suction effect between the indoor air temperature and the outdoor ones. This migration of warm air to the top of the semi-enclosure offers potentially more comfortable conditions resulting from cooler air collecting at ground level in the inhabited zone. On the other side, there was a negative correlation between the air temperature distribution and the wind velocity underneath, as the wind increased the air temperature but used to decrease and this has been reported through different studies

(Ng et al., 2008; Memon et al., 2010; Cheng et al., 2011; Yuan and Ng, 2012). Even though the air temperature and air velocity were analysed, they are still not enough indicators for outdoor thermal comfort, and thus the mean radiant temperature and the comfort index PET were calculated for each case. Again, case 7 represented the best performance for having the lowest  $T_{mrt}$  and PET at the pedestrian levels with a 1°C difference with cases 6 and 5, and a 2.3°C difference with the base case 2.

Although the shading provided a favourable reduction of the heat gained by the pedestrians and the buildings underneath (up to 14°C as reported in chapter 5), one of its drawbacks is still the reduction in daylight availability underneath (Tzempelikos and Athienitis, 2007). Therefore, in the third subsection of part three, the solar access and lighting analyses were conducted in order to complete the evaluation of the street design solution. Radiation maps were generated using DIVA for Rhino for all the seven cases in summer, winter and annually, and the three surfaces of the two walls and ground were analysed based on the amount of solar incident received on their surfaces. All cases performed well according to the ANSI/ASHRAE/IESNA Standard 90.1-2007, except in winter where the west wall for all cases did not achieve the minimum requirements (excluding the without roof case 1). Cases 6 and 7 proved to be the best cases with very minimal differences between both cases values, and also the base case 3 came third in allowing daylight to penetrate underneath, which gives the privilege for the roof centre openings among the side openings for better daylighting.

# 8

---

*“We often think of people living their life inside buildings and we may not see that in fact for one reason or another we spend much of our time outside” (Gehl, 1986).*

## **Chapter Eight**

---

### **8. Conclusions and Recommendations**

---

#### Key Concepts

- 8.1. Introduction
- 8.2. Overview based on the thesis aims and objectives
- 8.3. The operational framework
- 8.4. Guidelines for improving the microclimate in the hot, arid climate
- 8.5. Outline for possible future research
- 8.6. Limitation of the study
- 8.7. Contribution of the study

## 8.1 Introduction

This chapter discusses the results of the previous chapters and their implications for climate-conscious urban design in hot, arid climates, illustrated by Al-Muizz Street in the Islamic quarter of Cairo. It includes the following sections. The first section is an overview of the thesis aims and objectives. In the second section, guidelines are discussed for improving outdoor thermal comfort strategies for hot, arid climates. The third section contains an outline for possible future research and the contributions of the study.

## 8.2 The theoretical part based on the research aims and objectives

The assessment of outdoor thermal performance in the urban streets of the selected hot, arid context was the main driver of this research. Accordingly, the urban development of the street had to be investigated first in Chapter One, and Al-Muizz Street had to be analysed in terms of size, geographical location, and land use, as well as street design features such as the height of buildings, street widths and orientation, and subdivision of the building lots (appendix A). The main findings were that the spatial geometry of the traditional urban fabric of Al-Muizz Street seems to have developed from a lack of planning. The principle of privacy might have contributed to the development of the narrow and winding streets apart from the climatic adaptation by ‘shading’. Other urban strategies look like they were developed mainly as a result of the harsh desert climate such as the street orientation and the street aspect ratio, which are the two most relevant urban parameters responsible for the microclimatic changes in a street canyon (Todhunter, 1990; Bianca, 2000; Erell et al. 2011; Shishegar 2013). This is well expressed by the street design for the Fatimid city in Cairo, which follows a grid in its plan, with Al-Muizz as the main street oriented N-S. This creates a more pleasant microclimate, as the N-S orientation provides enough shadow and solar energy in both summer and winter (Toudert and Mayer, 2005). In contrast, E-W oriented streets are quite difficult to keep in shade (Pearlmutter et al. 2007), and therefore they were always narrower and higher in aspect ratio than the N-S streets. Furthermore, the high thermal inertia for the whole system as a result of a minimal envelope to volume ratio makes the compact buildings gain less heat during the daytime and lose less heat at night. The use of heavy stones with a big cut creates a high thermal capacity, and using light colours on external facades helps to reduce the urban reflectance of the whole

site. Consequently, the effect of urbanization and industrialization on modifying the local city climate through elevating the air temperature (Oke, 1995; Kuttler, 1998; Montavez et al., 2000; Tereshchenko and Filonov, 2001) was discussed in Chapter Two. It was noted that poor design planning and an unbalanced urban energy process as a direct effect of urbanization can lead to an uncomfortable rise in urban temperature in hot and cold regions, which is known as the urban heat island effect (UHI). By analysing the UHI mechanism, it was found that strategies for mitigating the UHI need to be based on specific climatic parameters and the location of the city. Based on this literature, it was found that during the hot season, UHI intensity can reach 8.0°C. This condition can become more extreme, especially in hot, arid climates or the tropical climate, due to high exposure to solar radiation. This was shown in the 4<sup>th</sup> IPCC Assessment Report, which stated that Africa is warming faster than the global average and this warming is greatest over the interior of semi-arid margins of the Sahara and central southern Africa (IPCC, 2007). In the hot, arid regions, air temperature, surface temperature, relative humidity and the radiation regime are the variables most affected regarding changing the entire microclimate in an urban area. The changes in an urban hot arid climate can directly impact on bioclimatic influences that are more focused on human thermal comfort and building energy performance for cooling (Emmanuel, 2005). This is important when considered in the context of the MOEE (2010) fact sheet where the number of air conditioners used in Egypt has quadrupled in four years (700,000 in 2006 to 3 million in 2010). In the context of Cairo, as described in Section 2.5, the few available examples of works providing evidence of UHI occurrence concluded a steady increase in temperatures for Egypt, with more warming estimated for summer than for winter (ACED, 2004). Cairo showed a significant rise in surface temperature with a general trend of warmer urban areas versus cooler surrounding cultivated land (Ghoneim, AFED, 2009), with heat intensity close to 4K occurring during the night and early morning in the summer period over the city of Cairo (Fouli, 1994). In 2011, another study stated that the two hot months of June and July transformed from comfortable months for all people in central Cairo during the old non-urbanized period to uncomfortable heat months during the recent urbanized period (Robaa, 2011). The urban temperature threatens to continue increasing, and based on future scenarios there will be a rise of mean temperature by 2.8°C (ACED, 2004). It has been considered necessary in this study to assess the UHI intensity for old city centre of

Cairo, represented by Al-Muizz Street based on a comparison between the in site field measurements and the data obtained from the WMO located at Cairo international airport. According to the literature review, most studies have suggested that one of the major strategies for mitigating the UHI is through increasing the amount of shade, so the urban temperature would decrease (Sections 2.5 and 2.6). However, this study has taken a further step towards improving these strategies by providing theoretical evidence and assessing the potential of modifying the physical properties of shading devices to give the optimum cooling effect at street level.

This UHI phenomenon is conducted at the Urban Canopy Layer (UCL) (Oke, 1994; Roth, 2004) as well as most of the climatic effects that humans feel (Emmanuel, 2005). Therefore, in Chapter Three, the climate scale, including the UCL, and the surface-air energy exchanges and mass exchanges between the urban canopy and the overlaying boundary layer (Mills, 1997) were explained. It was concluded that urban climate is influenced by several factors such as urban morphology and density, the properties of urban surfaces and vegetation cover. The appropriate use of these factors such as improvements to urban geometry at street level could reduce the UHI in summer and retain the heat during winter (Oke, 1998). In the second part of the chapter, outdoor thermal comfort was reviewed, including the physical and social approaches. A number of drawbacks were revealed: first, although the crucial role of the mean radiant temperature in analysing the UHI and outdoor thermal comfort was noted, there is still no easy and reliable method of estimation despite its importance for hot, arid regions. Second, international comfort standards such as ASHRAE standards and the ISO are almost exclusively based on theoretical analyses of human exchange in mid-latitude climatic in North America and Europe (Han, 2007). Moreover, the climatic chamber method used to underpin these indices failed to include many subjective, social and cultural real world situations (Han, 2007). In addition to the lack of validation for the available comfort indices, the reliance on the energy balance of the human body still faces the issue of a lack of interpretation. For instance, there is a lack of clarity about the meaning of a PMV value of -2 or +2, or a PET value of 34°C, in terms of heat stress, and the actual degree of comfort or discomfort cannot be drawn with confidence in the given scale, unless a comparison with social surveys is established (Touder, 2005; Cohen et al., 2013). Third, the physical microclimatic parameters only account for 50% of the variation between the objective and subjective comfort evaluation. The rest

cannot only be measured by the energy balance, as the psychological adaptation seems to be increasingly important (Nikolopoulou and Steemers 2003). There is a deep need to understand the psychological adaptation and the cultural context as it is argued to be complementary rather than contradictory, and consideration of this duality could increase the use of the city's open spaces. Therefore, the study suggests that all these drawbacks need to be inserted in a reliable and comprehensive framework, including UCL field measurements for the main climatic parameters, not only relying on the city's metrological data, but also examining the predominant climatic factors, and studying their effects on the pedestrian level from both the physical and the social dimensions. Then, there is the need to develop the actual thermal sensation vote for the case study through examining the relationship between the subjective thermal sensation and the outdoor thermal environment.

### **8.3 The operational framework based on the research questions**

Based on the theoretical background of the thesis, there were four main knowledge gaps which needed to be identified, as follows:

- Although about one third of the Earth's land is covered by desert, arid regions have not often been the focus of urban climate research (Pearlmutter et al., 2007; Aljawabra and Nikolopoulou, 2010) and the existing ones are mainly based either on the pure heat balance approach without any contribution for the social dimension and vice versa
- Although traditional and contemporary architects have attempted to design urban streets according to climate, quantitative information about the best possible street design to regulate climate comfort, based on scientific methods, is yet required (Hawkes and Foster, 2002; Thomas, 2003; Toudert, 2005) as there is still a lack of climate knowledge regarding the optimum design (Oke, 2006)
- The influence of thermal comfort on outdoor activities is a complex issue comprising both climatic and behavioural aspects; however, current investigations lack a general framework for assessment, as most of the research has been focused on physical issues explained by the energy balance of the human body, ignoring the significant effect of the psychological and behavioural factors, which is also known as thermal adaptation (Brager and de Dear, 1998;

Nikolopoulou et al., 2001; Nikolopoulou and Steemers, 2003; Spagnolo and de Dear, 2003; Hwang and Lin, 2007; Chen and Ng, 2012)

- Although people's subjective perceptions and responses to the urban environment are various and not yet well understood, simulation and scenario-testing tools are always of particular importance in an assessment framework because they provide a platform for the integration of knowledge from various perspectives and comparisons of various design scenarios (Givoni et al., 2003; Chen and Ng, 2012).

Thus, an interrelated methodological framework in compliance with the research questions (section 1.2) was designed in order to cover these gaps of knowledge, as follows:

**Q1. Which are the main design parameters influencing the urban microclimate and outdoor thermal comfort in the hot arid climate?**

- The case study selection
- Physical measurements to quantify the urban form impact on microclimate and thermal comfort by calculating the mean radiant temperature and PET comfort index based on the heat balance approach

**Q2. What are the thermal comfort perception and preference of people in outdoor urban spaces? What are the impacts of thermal adaptation on human thermal sensation in outdoor spaces?**

- A field survey which contributes to the understanding of the relationships between microclimate and human behaviour in open public spaces in a hot, arid climate and to refine the comfort zone for the study context based on the actual thermal perception

**Q3. How can shading designs be modified to promote a significant optimum cooling effect?**

- Numerical modelling as a predicating tool allows various design alternatives to be compared and tested in terms of attractiveness and effectiveness.

**Q4. How can an urban street bounded by the existing urban boundaries be designed to improve the microclimate and thermal comfort at street level?**

- Based on the interrelated relation between the given findings and conclusion of the above questions (section 8.4).



Chapters	Method	Research Questions
5	<ul style="list-style-type: none"> <li>• The case study selection</li> <li>• Field measurement</li> </ul>	Q1. Which are the main design parameters influencing the urban microclimate and outdoor thermal comfort in the hot arid climate?
6	<ul style="list-style-type: none"> <li>• A field survey</li> </ul>	Q2. What are the thermal comfort perception and preference of people in outdoor urban spaces? What are the impact of thermal adaptation on human thermal sensation in outdoor spaces?
7	<ul style="list-style-type: none"> <li>• Numerical modelling</li> </ul>	Q3. How can shading designs be modified to promote a significant optimum cooling effect?



8 Q4. How can an urban street bounded by the existing urban boundaries be designed to improve the microclimate and thermal comfort at street level?

### 8.3.1 The case study

More than a quarter of the urban areas are usually covered by streets, and designing streets is a key issue in a global approach for an environmental urban design. Therefore, in order to provide a pleasant microclimate in urban areas, designing urban streets in a way which brings about appropriate airflow and utilizes solar access is essential. This could affect global climate and energy consumption of buildings. In this respect, Al-Muizz Li Din Allah Street, located in the hot arid climate of the Islamic quarter of Cairo as a basic element of an urban structure, was chosen as the case study in order to serve question number one and overgab the lack of microclimate studies in hot arid regions in

addition to other many reasons, as mentioned in Chapter One: first, the essential street pattern of Al-Muizz Street has been preserved and reflects a climatic-conscious design developed over centuries of building experience. Its convoluted street system and compact urban structure limits the possibility of adopting modern large scale developments. Thus, a quantitative examination for the traditional and contemporary architecture solution based on scientific methods, in order to regulate the climate comfort, can be achieved. Second, the street piloted the first large-scale pedestrianisation scheme in 2010 in Egypt. This is relevant in supporting one of the thesis objectives that pedestrianized areas encourage longer durations of use and therefore allows for the examination of pedestrian thermal comfort in urban streets. Finally, Al-Muizz Street and its surroundings were exposed to an extensive restoration project by the Egyptian government, which transformed the street into an open-air museum. The first part of the street was fully restored and opened to the public in early 2010. The second part of the street has yet to undergo restoration, leaving behind two different urban structures located in the same street. This allows for a comparative case study between the two contexts and their impact on use and thermal comfort in the varying urban environments.

### **8.3.2 Field measurement**

Two in-situ meteorological measurements were carried out in Al Muizz Street. The first was hourly field measurement for one week in two different locations during the summer (26 June - 2 July 12), with the aim of assessing the UHI intensity in the urban street by comparing the two observed values with the one conducted from the readings obtained by the Cairo Airport WMO Station no.623660. The second in-situ measurement was every three hours carried out for two days in summer covering nine different locations along Al-Muizz Street. This was performed first to provide answers for question number 1 by exploring the main design parameters influencing the urban microclimate and outdoor thermal comfort in the hot arid climate, second to explore the link between urbanization and the urban heat island effect as one of the research objectives. The experimental results were quantitatively analysed to provide the following information.

The presence of an UHI in these two urban locations during the period of measurement was noted, as the urban canopy layer recorded higher urban temperature compared with

the WMO station. However, the renovated part of Al-Muizz had the highest UHI intensity when compared with the non-renovated, with an average of 1.5°C.

There was high thermal discomfort at the non-shaded locations, where the  $T_{mrt}$  and PET recorded very high values of 71.2°C and 53.7°C, respectively. On the other hand the sheltered streets had the lowest PET values as these design elements reduced the amount of direct sun during the daytime, thus improving thermal comfort and reducing sun exposure. However, during the night time due to very low SVF, this might lead to a decrease in long-wave radiation loss, as radiation may be trapped in the canyon air volume, causing a high level of discomfort. Increasing SVF by 10% would decrease UHI by 0.3% at night time (Kakon and Nobuo, 2009); this may explain why some locations such as 1, 8 and 3 with low SVF were warmer by 1°C and 2°C than point 9 after 21 LST until 3 LST for both days of measurement. Thermal comfort is very difficult to reach passively in hot, arid climates at either tropical or subtropical latitude and summer conditions (Toudert, 2005) (e.g. in Cairo:  $T_a$  Max.34-35°C, RH = 32-84%). In effect, Arnfield (1990a) and Bourbia and Awbi (2004) suggested the substantial irradiation of the street surface for the subtropics (20°N to 40°N), even for deep geometries. PET maxima reached 53.7°C and PET minima during the day were in all cases a few degrees higher than air temperature. Nevertheless, an improvement is possible by means of appropriate design since both solar orientation and shading were found to affect strongly the outdoor thermal comfort at street level.

Wide streets, e.g.  $H/W \leq 0.5$ , are highly uncomfortable during the largest part of daytime. They are largely irradiated and have high air temperatures (almost equal to that above an unobstructed surface). However, N-S streets have a small advantage over E-W streets as the thermal conditions at their edges along the walls are less stressful. Hence, for shallow canyons, implementing shading strategies at street level (galleries, trees, etc.) is the only way to improve the comfort situations substantially (Toudert, 2005).

### **8.3.2.1 The ENVI-met spatial microclimatic map and validation**

The ENVI-met simulation model has been used to describe the spatial pattern of mean radiant temperature. In view of global climate change and the mitigation of the urban heat island, the obtained microclimatic map provided some problematic areas (UHI) concerning pedestrian thermal comfort, even after the restoration project, and these need to be studied and avoided in the future. However, the non-renovated part of the alley

revealed reductions in the whole neighbourhood pedestrian comfort records. This was due to several reasons, as the higher aspect ratio (H/W) and different shading system caused less direct solar radiation to enter the alley and generally led to lower  $T_{mrt}$  values throughout the most of the day. In addition, it increases the albedo of the ground surface within the non-renovated part, as it is a mix of basalt road and bare ground, against the basalt and granite of the renovated one with a lower albedo value. This leads to strong solar irradiation in the renovated part compared to the non-renovated, which strongly influenced the  $T_{mrt}$ . ENVI-met estimation of the  $T_{mrt}$  and air temperature was a good approximation with the observed ones from the field measurements (Toudert and Mayer, 2006). However, the incapability of ENVI-met in modelling the  $T_{mrt}$  under shading conditions and its lack of heat storage should be taken into account.

### 8.3.3 Field survey

In order to serve the research second question including, the thermal comfort perception and preference of people in outdoor urban spaces and the impact of thermal adaptation on human thermal sensation in outdoor spaces. A field survey included structured interviews with a standard questionnaire and observations of the human activities, along with the previous microclimatic monitoring, carried out during winter and summer 2012. The survey assessed the microclimate of the outdoor urban environment and investigated the relationship between different thermal comfort indices and people's actual thermal sensation for Al-Muizz Street. Thermal conditions of different outdoor environments vary considerably, mainly as a function of solar access. In summer, it was noticed that the non-renovated part performed better than the renovated, while in winter this was vice versa. It was concluded that the urban design in Cairo needs to include well shaded spaces for pedestrians to protect pedestrians in summer as well as open spaces to provide solar access in winter. Furthermore, this study found that the summer and winter comfort zones and acceptability limits for PET were 23-32°C for the hot, arid climate of Cairo, while the preferred temperatures were 29°C PET in summer and 24.5°C PET in winter. This is important information for urban designers aiming for a climate conscious urban design, as people in hot arid region could be more tolerant with the heat stress than people in temperate or hot humid climate. The study also shows the influence of culture and traditions on clothing. While most people choose the clothing according to the climate, some people in Al-Muizz are influenced by their cultural

traditions when they choose how to dress. Finally, the analysis suggested although microclimatic parameters strongly influence thermal sensation, they cannot fully account for the wide variation between objective and subjective comfort evaluation, whereas, psychological adaptation and behavioural variables seem to be becoming increasingly important. Accordingly, in terms of implications for planning, the physical environment, psychological adaptation and a deep understanding of the cultural context, the study suggests that, similar studies should be conducted in other climatic zones in order to enlarge the spectrum of knowledge and understanding of human thermal perception, as it is argued to be complementary rather than contradictory, and consideration of this duality could increase the use of the city's open spaces.

### 8.3.4 Numerical modelling

Based on the field measurements and the survey analysis, thermal conditions of different outdoor environments vary considerably, mainly as a function of solar access. From a climatic point of view, shading is the key strategy for promoting comfort in the hot, arid climate because it leads to:

- A reduction of the direct solar radiation absorbed by a standing person
- A reduction of the heat released by the surroundings, in particular the ground
- A decrease of the air temperature as a secondary effect.

Many design possibilities are, hence, possible for controlling the microclimate. However, the main problem for shading devices such as tents or canopies mainly occurred during the night-time as they usually act as obstacles at this time as the heat release can be trapped underneath, contributing to the UHI (Nakamura and Oke, 1988). This is because they decrease the long-wave radiation loss on the surface, thus contributing to high temperatures at night (Lin et al. 2010). Nevertheless, if the topology, form and opening of the roof structure are well considered and examined in the design, the internal heat can find a place to escape at night through the openings, as ventilation and escape of heat through radiation that is stored in the thermal mass during the day to the night sky will improve.

Therefore, in order to fulfill question number three as how shading designs can be modified to promote a significant optimum cooling effect, in addition to the third and fourth objectives stated in section (1.1), the computational fluid dynamic (CFD) Fluent code 13.0 was chosen to further evaluate the air flow rate and the heat transfer patterns

underneath seven different scenarios in addition to the existing case study for purpose of validation. Each testing scenario consists of one specific geometrical change in the roof shape and opening locations.

#### **8.3.4.1 Validation study**

The extracted best practice guidelines for CFD simulations, which Chapter Seven concluded with, were used as the start point for the validation study. This study investigated the air temperature underneath the existing case study and compared the obtained CFD results with in-situ measurements. It can be argued that the obtained CFD simulation results in this work compared favourably with the reviewed results. The obtained results contributed to the examination of the main hypothesis for the seven different cases. Thus, CFD simulation was considered a reliable assessment tool for yielding consistent results. In addition, the simulation variables used can be relied on for investigating the effect of the different shading designs including the shapes and opening locations in providing a better microclimate at the pedestrian level.

#### **8.3.4.2 Comparative study**

Chapter Seven addressed the answers for the third question of the study where the form and opening of the roof structure as shading devices are the main factors affecting their performance. It was concluded that in order to assess the effect of roof shape, and opening design configurations on pedestrian thermal comfort within the street level, three dependant variables should be investigated. These were the air temperature distribution, wind velocity, and solar access, as these were the main variables affecting the performance of the shading roofs. In order to examine the first two variables, the air temperature distribution patterns and the wind flow displays underneath the investigated cases were plotted and the recorded wind velocities and air temperatures were compared against each other at the same location under the same conditions. It can be concluded that:

- The shading roof typology and the opening locations were one of the paramount factors in providing a temperature reduction in urban scale. This modification in the shading roof properties led to a large reduction of air temperature with (2.3°C) for the best case compared to the base case

- The PET as a thermal comfort index was also reduced for the best case, which was 7, at about 32.9°C against 35°C for the base case, which is only 0.9°C away from the thermally acceptable range on the hottest day of the year
- The shading roofs typology and opening significantly affected the wind profiles beneath as the results showed that all wind vertical profiles were followed almost the same pattern until they reached the building top near the roof, when the velocity profiles started to vary based on the shading roofs shape and opening locations
- There was a negative correlation between the air temperature distribution underneath and the ambient wind speed, since as wind velocity increased, the air temperature decreased for the same point on the vertical line. This effect of wind velocity has been reported by numerous studies (Ng et al., 2008; Memon et al., 2010; Cheng et al., 2011; Yuan and Ng, 2012)
- The air temperature distribution was positively correlated with the height level; the higher the level was, the higher the air temperature. This migration of warm air to the top of the semi-enclosure offered potentially more comfortable conditions resulting from cooler air collecting at ground level in the inhabited zone
- In terms of ventilation flow rate, the cases which were accompanied by side and roof openings performed better by about a 23%-30% increase in the volume flow rate underneath the shading roofs, compared to cases with either side or roof opening. In addition, the influence of the roof shape as a vaulted roof recorded 10% for the total volume flow rate against 7.4% for the flat roof
- Over all, case 7 showed the best performance compared to all other cases (Table 8.1), as the curved surface area of the vaulted roof in case 7, which was considerably larger than the base, received less solar heat per unit area, thus lowering surface temperatures and facilitating re-radiation after sunset (SKAT, 1988).

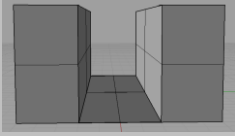
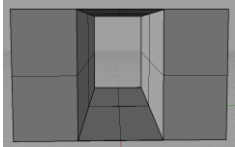
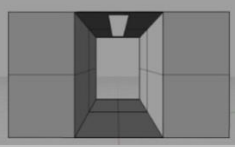
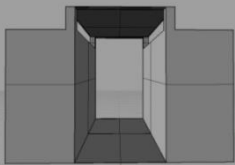
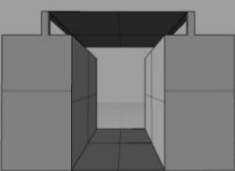
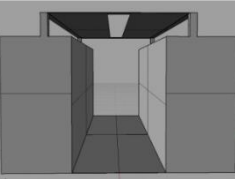
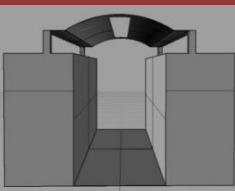
In order to ensure the solar radiation levels underneath the shading roofs, the solar access as a third variable needed to be examined. DIVA for Rhino, daylight analysis software, was used with the seven cases and a grid based radiation map was produced for each case for annual, summer and winter solar access conditions for the three

surfaces (the two walls and the ground). The results were then evaluated against ANSI/ASHRAE/IESNA Standard 90.1-2007 for lighting and the following was concluded:

- All cases performed well during the summer time; however, during the winter, the cases failed to achieve the minimum lighting power densities for the outdoor spaces for open areas which should not be less than  $5.4 \text{ W/m}^2$  (ANSI/ASHRAE/IESNA Standard 90.1-2007) for the west wall, and for the ground surface for case 2, excluding case 1, which was without a roof
- Case 6 had the best performance in terms of daylight analysis. However, the values were very close to case 7. Both cases achieved the lighting power density requirements, aside from the west wall during the winter time, where both cases recorded very close values, at  $4.58$  and  $4.35 \text{ W/m}^2$ , respectively. According to these results, both cases can be dealt with as similar in terms of daylight performance
- The middle roof opening proved to be much better in terms of visual comfort, while the side openings proved to have the upper hand for thermal comfort.



Table 8-1 Comparison between the different cases including the base case 3 and best case 7

Cases	Volume flow rate (m3/s)	Air velocity m/sec	Air exchange rate m3/h	% ACH through the openings %	Air temperature (°C)	PET (°C)
Case 1 	34.34	1.3	266.43	41.81	34.8	35.3
Case 2 	26.77	1.38	207.7	n/a no roof openings	34.67	35.2
Case 3 	29.48	1.4	228.7	23.55	34.78	35.2
Case 4 	41.99	1.4	277.8	28.93	34.68	35.1
Case 5 	47.88	1.45	295	23.72	34.05	34.2
Case 6 	48.66	1.49	299	27.29	34.04	34.2
Case 7 	49.99	1.54	300	26.4	33.05	32.9

#### **8.4 Guidelines for improving the microclimate within the UCL in the hot, arid climate**

Based on the research findings and conclusion in accordance with study question number four "How can an urban street bounded by the existing urban boundaries be designed to improve the microclimate and thermal comfort at street level?", the potential guidelines for improving the outdoor thermal comfort and microclimate strategies are as follows:

1. Overall, the results of the series of simulations emphasize the importance of shading in the hot, arid context in lowering PET. The investigations carried out demonstrate that the acceleration of shading urban areas brings thermal benefits to the urban climate in hot arid cities. These can even reverse (or at least moderate) the negative climatic effects affiliated to urbanism. Besides thermal comforts, shade provides a large number of social and human benefits, and is moreover sustainable.
2. The choice of the right shading device should ideally be based on its physical characteristics such as the topology, the geometry and the openings. Making the right choice of type of tent or canopy would result in more effective and better radiation interception and lower urban temperature. The vaulted or domed roof is usually recommended for the hot, arid region as its shape offers better quality of shade and cooling (Gadi, 2000).
3. The study defines the summer and winter comfort zones and acceptability limits for PET in the hot, arid climate of Cairo. This is important information for urban designers aiming for a climate-conscious urban design. The study also shows the influence of culture and traditions on clothing. While most people choose the clothing according to the climate, some people in Cairo are influenced by their cultural traditions when they choose how to dress.
4. An establishment for the practical and educational background of the importance of numerical simulations to the field of urban planning is needed due to the complexity and the wide range of research fields and urban environment elements involved at local climate scale. This is in order to relate passive design and climate knowledge to real practice and improve its sustainability.

5. The design of outdoor public spaces without specific awareness of the microclimate is usually caused by insufficient knowledge about microclimate processes in many landscape architects and urban designers (Eliasson, 2000; Katzchner, 2006). In order to overcome this problem, more effort still has to be made. Easily applicable design guidelines should be generated in order to encourage a better inclusion of microclimate issues in urban space design.
6. The research recommends using simulation tools such as ENVI-met as a preliminary tool for examining any large scale development in its early stages. Even though it still faces some shortages, ENVI-met has proven to be a reliable tool to simulate different urban scenarios, and thus it is advisable for use in any planning process, or architectural intervention spatial distribution maps for the microclimate conditions, similar to the one presented in the thesis.
7. The study highlighted the importance of a climate-conscious urban design and design flexibility. It is important to consider microclimate and thermal comfort in the urban design process and requirements, for a climate conscious urban design should preferably be included in the planning regulations for cities such as Cairo. In addition, existing urban environments in Cairo could be modified in order to provide a better outdoor thermal environment. Such studies could enhance the thermal comfort and suggest improvements to the existing urban planning regulations.

Although the study was mostly completed for a hot arid location with a hot, arid climate for summer conditions, it is believed that the design recommendations discussed here can be more efficient for transitional seasons and also applicable to more extreme climates with typical hot summers such as Gulf countries in the Middle East. The Mediterranean basin, for instance, experiences to a large extent similar irradiation potentials in the hot season (see Arnfield, 1990a). Obviously, some adjustments related to sun course geometry (zenith and azimuth angles) accounting for latitude differences have to be considered (Arnfield, 1990a; Mills, 1997).

### **8.5 Outline for possible future research**

The findings and recommendations stated are limited to the scope of this study. Many related issues and detailed findings need further investigation, in order to improve on

outdoor thermal comfort and to minimize the UHI effect. Several suggestions for future research are recommended to refine the detailed procedures carried out for this thesis:

1. As this study has provided substantial possibilities based on the weaknesses and strengths of CFD, DesignBuilder and ENVI-met modelling of Cairo's urban climate perspectives, the author suggests further research may apply these models in the design and assessment of outdoor public spaces within the old and new parts of the city of Cairo, and then through all of Egypt. This tool will be further upgraded from time to time as new assessments will be obtained from the advanced versions of these models
2. Future comparisons of different urban parts within the same cities should be explored. This will allow more understanding of the actual ability for the various types of shade in providing cooling effects. It will include further research on tents' physical aspects such as the materials, height and form of the tents. Also, different locations, wind directions, and solar zenith angles for the different types of tents should be examined
3. The study has exposed the actual outdoor thermal comfort conditions in the old city of Cairo by identifying comfort zones that are suitable for local users in this city area. However, due to the time and instrumentation limitations of fieldwork, the site measurement for outdoor thermal comfort was carried out with limited instrumentation, time and numbers of environmental locations. This opens up new research possibilities to conduct further research on site assessment using better instruments and focusing on a larger area throughout the whole city of Cairo in order to develop the comfort zone and acceptability limits for each climatic zone within the whole country. Such limits are essential in the development of urban spaces in the city in harmony with the microclimate. Additionally, it is important to develop urban planning regulations in every city according to the climatic requirements. Thus, further studies to analyse the existing regulations from a climatic point of view are needed
4. In this study, CFD Fluent code 13.0 and DesignBuilder were linked via the feeding outputs of one program to the other. It is recommended that this process is automated via a suitable software approach. Alternatively, an integrated

simulation tool could be developed, capable of considering the continuous interaction of indoor and outdoor environments through walls and windows

5. Gaps in research also exist concerning the assessment of the effect of outdoor shading roof designs in improving thermal comfort indoors. To extend the thesis case study, further studies are required on in-situ measurements as well as a comparative analysis of the mean radiant temperature and the air flow within the different shops underneath
6. This study showed the importance of overhead shading in warm climates. Future studies should include both the effects of shading and vegetation together to develop more detailed knowledge on the field of improving the microclimate and outdoor thermal comfort
7. The evaluation of the economical impact of the improvement of outdoor thermal comfort remains a highly interesting aspect. This is a very specific task, which demands profound knowledge of the consumption and efficiency of the cooling devices, the energy market, and costs in Egypt
8. Finally, this thesis was aimed at providing help and guidance to those involved in the process of decision-making at the earliest stages of the design procedure. This in itself could be made into a tool that enables its users to proceed faster in those early stages of the design instead of manually going through all the stages given in this thesis. Such a tool will be improved even further if the proposed improvements to an outdoor thermal index and a reliable integrated simulation tool have been delivered. The development of such a comprehensive tool will be of great benefit to all stakeholders in the design process of a building or an urban development and in the long term will be beneficial to the users and occupiers of the buildings by offering more flexibility for them in using both indoor and outdoor spaces, and also in reducing their dependence on fossil fuels for the heating and cooling of their homes. The work presented in this thesis provides the basis for such future developments.

## 8.6 Limitations of the study

It is important for the study to highlight the limitations of the study for further research suggestions and to ensure validation in future work. There are some issues and approaches in this study that need to be highlighted and improved for further study:

1. The instruments used in measuring the globe temperature need to be reconsidered, as the use of a black globe thermometer needs to be replaced with a grey globe thermometer which is more suitable for outdoor thermal comfort studies. The use of a black globe thermometer without the correction of people's solar thermal reflectivity assumes that all in the sun are wearing black clothing, thus overestimating  $T_{mrt}$  in these conditions (Nikolopoulou and Lykoudis 2006). Importantly, the study suggested that further research needs to consider a grey globe thermometer that can evaluate globe temperature with consideration for people's solar thermal reflectivity
2. Methodologically, ENVI-met 3.1 was revealed to be a good tool for the prognosis of microclimatic modifications due to urban environments and for assessing the thermal comfort of pedestrians. Indeed, the model has a well-founded physical basis and offers many advantages in comparison to many other available urban microclimate models. However, the incapability of ENVI-met in modelling the  $T_{mrt}$  under shaded conditions and its lack of heat storage and thermal mass of the buildings should be taken into account in further studies. This information helps the understanding of the limits of the present investigation, and gives an overview of the eventual refinements of the model
3. The findings of this study are for the conditions of an average wind speed from one direction and one solar zenith angle. Wind direction variations and different solar zenith angles could thus have an effect on the results of this study. Local patterns of seasonal winds and solar angles have always been an important factor in determining the final design of an urban area.

## 8.7 Contribution of the study

The outcome of this study not only offers a solution to some issues and problems concerning pedestrians or local people who are using the public open spaces, but at the same time enriches the knowledge in this field. The study has identified efforts in

improving the outdoor thermal comfort strategies in hot, arid climates by assessing the potential optimum cooling effect of different shading designs. The proposed guidelines would be useful in improving the development of the streets:

1. The study provided a new insight into the perception of Cairo urban designers, especially architects, planners, landscape architects and the government, regarding the importance of shade and its physical properties when designing urban area. This knowledge is important for opening up a new perspective and capabilities regarding the technical aspects of providing a better climate effect underneath. By knowing the facts and figures, the designer can better allocate effort in designing urban space to maximize the cooling potential from shade
2. The study has provided a basic database on the level of outdoor thermal comfort for Cairo users during peak hours, which can be used as a reference for Cairo, in order to evaluate the impact of outdoor space design throughout the city area
3. Finally, the combined method framework in this study, starting with field measurements and the ENVI-met prognosis model, has enhanced the current microclimate assessment at the street level. It then used the field survey to correlate between the measured index and actual thermal sensation or perception for the local people before examining different scenarios using the CFD for the optimum solution for the case study. To the author's knowledge, this is the first time such a process and research framework have been combined for both physical and social dimensions to offer a better understanding and advanced solutions for enhancing the outdoor spaces thermal comfort quality in Cairo.

As a final point, the author strongly believes that the work carried out in this study has contributed to improving the quality of urban life in present and future developments. It is hoped that these contributions will broaden the scope of researchers in both the current and related fields.

## References

'A'

- Abdulrahman, A and Sharples, S (2014) 'Analysing and optimizing the performance of hybrid housing design in the Middle East'. In: 2nd IBPSA-England Conference, UCL.
- Abohela, I., (2012) 'Effect of Roof Shape, Wind Direction, Building Height and Urban Configuration on the Energy Yield and Positioning of Roof Mounted Wind Turbines' [PhD thesis]. Newcastle, UK: Newcastle University; 2012.
- Adam, S., (2000), 'Poverty and Charity in Medieval Islam: Mamluk Egypt, 1250-1517', Cambridge: Cambridge University Press Article: Mamluk, pp. 750-751 in Encyclopaedia Britannica, 15th ed., Vol 7)
- Akbari, H. (2005) 'Energy Saving Potentials and Air Quality Benefits of Urban Heat Island Mitigation', Retrieved 2 Jul. 2008 from <<http://www.osti.gov/bridge/servlets/purl/860475-UIH-WIq/860475.PDF>>.
- Akinnubi, R.T., Akinwale, B.F., Ojo, M.O., Ijila, P.O., and Alabi, O.O., (2007) 'Characteristic Variation of Relative Humidity and Solar Radiation over a Tropical Station Ibadan, Nigeria', Research Journal of Applied Sciences, 2: 1266-1269.
- Alatas, Syed Farid (2006), 'From Ja`mi`ah to University: Multiculturalism and Christian-Muslim Dialogue', Journal of Current Sociology pp 112–32.
- Alexander, P.J., and Gerald Mills, G., (2014) 'Local Climate Classification and Dublin's Urban Heat Island' Journal of *Atmosphere* 2014, 5, 755-774.
- Ali-Toudert F. and Mayer, H. (2007) 'Effects of asymmetry, galleries, overhanging facades and vegetation on thermal comfort in urban street canyons'. Solar Energy; 81:742–54.
- Ali-Toudert F. and Mayer, H. (2006) 'Numerical study on the effects of aspect ratio and solar orientation on outdoor thermal comfort in hot and dry climate', Journal of Building and Environment 41: 94-108.
- Ali-Toudert F. (2005) 'Dependence of outdoor thermal comfort on street design'. PhD Thesis, University of Freiburg, Freiburg
- Ali-Toudert F. and Mayer H. (2005) 'Numerical study on the effects of aspect ratio H/W and orientation of an urban street canyon on outdoor thermal comfort'. Journal of Building and Environment; DOI: 10.1016
- Al Jawabra, F and Nikolopoulou, M., (2009) 'Outdoor Thermal Comfort in the Hot Arid Climate, the effect of socio-economic background and cultural differences', 26th Conference on Passive and Low Energy Architecture PLEA, Quebec City.
- Al-Kayiem, H., M. Firdaus Bin M. Sidik, M.F., and Munusammy, R.A.L., (2010) 'Study on the Thermal Accumulation and Distribution Inside a Parked Car Cabin', American Journal of Applied Sciences 7 (6): 784-789, 2010 ISSN 1546-9239
- Allen, R.G., Pereira, L.S., Raes, D., and Smith, M., (1998) 'Crop evapotranspiration - Guidelines for computing crop water requirements', FAO - Food and Agriculture Organization of the United Nations Rome, 1998 ISBN 92-5-104219-5
- Al-Muqaddassi, M.A. ( 1906 ), 'Ahsan Al- Taqasim fi Ma'rifat Al-Aqalim' ( The Best Division in the Knowledge of Countries ), Edited by De Goeje, M.J. (1994) Brill Publication, Leiden.
- Al-Sallal, A. and Al-Rais, A. (2012) 'Outdoor airflow analysis and potential for passive cooling in the modern urban context of Dubai', Journal of Renewable Energy, vol.38, pp. 40-49.
- Al-Sayyad, N., (1981), 'Streets of Islamic Cairo - a configuration of urban themes and patterns', Aga Khan Program for Islamic Architecture, Harvard University and the Massachusetts Institute of Technology
- Al-Tabari, A. J., (1963), 'Tarikh al-Rusul Wa al-Muluk', Dar al-Ma'aref, Cairo.
- American Society of Heating, Refrigerating, and Air-Conditioning Engineers. (2009) 'ASHRAE Handbook Fundamentals'. (Inch-pound Edition) ISBN: 978-1-933742-54-0.



- American Society of Heating, Refrigerating and Air-Conditioning Engineers (2007) 'ANSI/ASHRAE Standard 90.1 -2007' Energy Standard for Buildings Except Low-Rise Residential Buildings (SI Edition) ISSN 1041-2336
- American Society of Heating, Refrigerating, and Air-Conditioning Engineers. (2004) 'ASHRAE Standard 55-2004. Thermal environmental conditions for human occupancy', Atlanta.
- American Society of Heating, Refrigerating and Air-Conditioning Engineers. (1992) 'Thermal environmental conditions for human occupancy'. Atlanta, GA: ASHRAE.
- Antoniou G., Bianca S., Al-Hakim S., Lewcock R. and Welbanc M., (1985) 'The Conservation of the Old city of Cairo'. UNESCO, Technical report RP/PP/1979-1980/4/7, 6/05.
- Antoniou, J. (2009) 'Historic Cairo, A Walk Through the Islamic City' The American University Press, Fifth Printing.
- Arnfield J., Herbert JM., and Johnson GT. (1998) 'A numerical simulation investigation of urban canyon energy budget variations'. American Meteorological Society, Second Symposium on Urban Environment, Albuquerque, NM.
- Arnfield J., and Mills, G. (1994) 'An analysis of the circulation characteristics and energy budget of a dry, asymmetric, east-west urban canyon', International Journal of Climatology, vol. 14, pp.239-261
- Arnfield, J., (1990b) 'Canyon geometry, the urban fabric and nocturnal cooling: a simulation approach', Physical Geography, Vol. 11, pp. 209-239.
- Australian Government website "<http://www.yourhome.gov.au/passive-design/shading>", Passive shading design (2013) Principal author: Caitlin McGee Updated by Chris Reardon, 2013 (last access 21 November 2013)
- Assimakopoulos, D. N., Assimakopoulos, V. D., Chrisomallidou, N., Klitsikas, N., Mangold, D., Michel, P., Santamouris, M., and Tsangrassoulis, A. (2001) 'Energy and climate in the urban built environment', 1st edition, James & James. London, UK.
- Attaher, S., Medany, M.A., Abdel Aziz, A.A. and El-Gindy, A. (2006) 'Irrigation water demands under current and future climate conditions in Egypt', Journal of Agricultural Engineering, 23, 1077-1089.
- Auliciems, A., (1981) 'Towards a psycho-physiological model of thermal perception', International Journal of Biometeorology, 25:109-122.
- Ayman, H.A. (2011) 'An analysis of bioclimatic zones and implications for design of outdoor built environments in Egypt', Journal of Build and Environment 46, 605-620.
- Ayman, H.A. (2011) 'An analysis of the microclimatic and human comfort conditions in an urban park in hot and arid regions'. Journal of Build and Environment 46, 2641-2656.

**'B'**

- Bady, M., Kato, S., and Huang, H. (2008) 'Towards the application of indoor ventilation efficiency indices to evaluate the air quality of urban areas', Journal of Build Environment; 43(12):1991-2004.
- Baker, L.A., Brazel, A.J., Selover, N., Martin, C., McIntyre, N., Steiner, F.R., Nelson, A., and Musacchio, L. (2002) 'Urbanization and warming of Phoenix (Arizona, USA): Impacts, feedbacks and mitigation'. Journal of Urban Ecosystem. 6:183-203.
- Ballantyne, E.R., Hill, R.K., and Spencer, J.W. (1977) 'Probit analysis of thermal sensation assessments', International Journal of Biometeorology 1977; 21:29-43.
- Barbason, M., and Reiter, S., (2014) 'Coupling building energy simulation and computational fluid dynamics: Application to a two-storey house in a temperate climate', Journal of Building and Environment, Vol 75, pg 30-39. 1
- Becker, S. (2000) 'Bioclimatological rating of cities and resorts in south Africa according to the climate index', International Journal of Climatology, 20: 1403-1414 (2000)
- Behrens-Abouseif, D., (1992) 'Islamic Architecture in Cairo: an Introduction', E.J Brill Publishing Leiden, ISBN9004096264.
- Bianca, S., (2000) 'Urban Form in the Arab World Past and Present', Institute fur Orts, Regional- und Landesplanung, ETH Zurich
- Bianca, S. (2000). Urban form in the Arab world: Past and present. Thames and Hudson Ltd, London, UK

- Blocken, B., Janssen, W.D., and van Hooff T. (2012) 'CFD simulation for pedestrian wind comfort and wind safety in urban areas: General decision framework and case study for the Eindhoven University campus', *Journal of Environmental Modeling & Software* 30: 15-34.
- Blocken, B., Stathopoulos, T., Carmeliet, J. and Hensen, J.L.M. (2011) 'Application of computational fluid dynamics in building performance simulation for the outdoor environment: an overview', *Journal of Building Performance Simulation*, 4(2), pp. 157-184.
- Blocken, B., Stathopoulos, T., Carmeliet, J. and Hensen, J. (2010) Application of CFD in building performance simulation for the outdoor environment: an overview. Available at: [http://sts.bwk.tue.nl/WindEngineering/pdf/2010\\_JBPS\\_Preprint\\_BB\\_TS\\_JC\\_JH.pdf](http://sts.bwk.tue.nl/WindEngineering/pdf/2010_JBPS_Preprint_BB_TS_JC_JH.pdf) (Accessed: 18 October 2010).
- Blocken, B. and Persoon, J. (2009) 'Pedestrian wind comfort around a large football stadium in an urban environment: CFD simulation, validation and application of the new Dutch wind nuisance standard', *Journal of Wind Engineering and Industrial Aerodynamics*, 97(5-6), pp. 255-270.
- Blocken, B., Stathopoulos, T. and Carmeliet, J. (2007b) 'CFD simulation of the atmospheric boundary layer: wall function problems', *Journal of Atmospheric Environment*, 41(2), pp. 238-252.
- Blocken, B., Carmeliet, J., and Stathopoulos, T. (2007) 'CFD evaluation of wind speed conditions in passages between parallel buildings e effect of wall-function roughness modifications for the atmospheric boundary layer flow', *Journal of Wind Engineering and Industrial Aerodynamics* ;95:941-62.
- Blocken, B. and Carmeliet, J. (2004) 'Pedestrian Wind Environment around Buildings: Literature Review and Practical Examples', *Journal of Thermal Envelope and Building Science*, 28(2), pp. 107-159.
- Bodart, A.M., and De Herde, (2002) 'Global energy savings in offices buildings by the use of daylighting', *Journal of Energy and Buildings* 34; 421-429.
- Bonan, G.B. (2008) 'Ecological Climatology', Cambridge University Press Paperback , October 2008, ISBN: 978-0-521-69319-6
- Bottema, M. (1996) 'Roughness parameters over regular rough surfaces: experimental requirements and model validation', *Journal of Wind Engineer*; 64:249-65.
- Bouchahm Y., Fatiha B., and Bouketta S. (2012) 'Numerical simulation of effect of urban geometry layouts on wind and natural ventilation under Mediterranean climate', The sixth International Conference of the Arab Society for Computer Aided Architectural Design ASCAAD
- Bouchlaghem N. (2000) 'Optimizing the design of building envelopes for thermal performance', *Journal of Automation in Construction*, 10:101-12.
- Brager, G.S., and de Dear, R.J. (1998) 'Thermal adaptation in the built environment: a literature review', *Journal of Energy Buildings*, 27:83-96.
- Brager, G.S., Paliaga G, and de Dear, R.J. (2004) 'Operable windows, personal control, and occupant comfort', *ASHRAE Transactions*; 110:17-35.
- Bruse, M. (2006) 'ENVI-met 3 – a three dimensional microclimate model', Ruhr University at Bochum, Geographischer Institut, Geomatik. <http://www.envi-met.com>.
- Bruse M., Anwendung von mikroskaligen Simulations modellen in der Stadtplanung. In: Bernhard L., Küger T. (Eds.), (2000) *Simulation raumbezogener Prozesse: Methoden und Anwendung* [Application of microscale simulation models in urban planning]. Münster, 2000 (in German)
- Bruse M., Stadtgrün und Stadtklima (2003) *WiesichGrünflächen auf das Mikroklima in Städtenauswirken* [Urban green and urban climate. impacts of the green spaces on the urban microclimate]. *LÖBFMitteilungen*, 2003, 1, 66-70 (in German)
- Bruse M. (2000) 'Assessing thermal comfort in urban environments using an integrated dynamic microscale biometeorological model system. Third Symposium on the Urban Environment, AMS Conference, Davis
- Bruse, M. (1999) 'The influences of local environmental design on microclimate', Ph.D Thesis University of Bochum, Bochum (in German)
- Buccolieri, R., Sandberg, M., and Di Sabatino, S., (2010) 'City breathability and its link to pollutant concentration distribution within urban-like geometries', *Journal of Atmospheric Environment*, 44(15):1894-903.

- Cable, M., (2009) 'An Evaluation of Turbulence Models for the Numerical Study of Forced and Natural Convective Flow in Atria' Master Thesis, Queen's University Kingston, Ontario, Canada
- Cai, X.M., (2012) 'Effects of differential wall heating in street canyons on dispersion and ventilation characteristics of a passive scalar', *Journal of Atmospheric Environment*, 51:268-77
- Capuleto I., Yezioro A., Shaviv G.E., (2003) 'Climatic aspects in urban design - a case study', *Journal of Building and Environment*, 38, 827-835.
- Capuleto I., Shaviv G.E., (1997) 'Modelling the urban grids and fabric with solar rights considerations', *Solar World Congress*, ISES International Energy Society, Korea.
- Carfan, A.C., Galvani, E., and Nery, J.T., (2012) 'Study of thermal comfort in the City of São Paulo using ENVI-met model', *Investigaciones Geograficas* 01/2012; 78.
- CDC. 2004. Extreme Heat: A Prevention Guide to Promote Your Personal Health and Safety. Retrieved 27 July 2007 from <[http://www.bt.cdc.gov/disasters/extremeheat/heat\\_guide.asp](http://www.bt.cdc.gov/disasters/extremeheat/heat_guide.asp)>.
- Centre for Environmental Economics and Policy in Africa (CEEPA) (2006) 'Assessing the impacts of climate change on agriculture in Egypt: a ricardian approach', Discussion Paper No. 16, Special Series on Climate Change and Agriculture in Africa, University of Pretoria, Pretoria, 1-33.
- Chang, S.C. (2000) 'Energy Use'. Environmental Energies Technology Division. Retrieved 18-06-2009.
- Chao, Y., and Ng, E., (2012) 'Building porosity for better urban ventilation in high-density cities A computational parametric study', *Journal of Building and Environment* 50;176-189
- Charles, K.E., (2003) 'Fanger's Thermal Comfort and Draught Models', IRC Research Report RR-162 Institute for Research in Construction National Research Council of Canada, Ottawa, K1A 0R6, Canada
- Cheng, V., and Ng, E., (2006) 'Thermal comfort in urban open spaces for Hong Kong', *Journal of Architectural Science Review* 2006;49(2):179-82.
- Cheng, V., Ng E., Chan, C., Givoni, B., (2011) 'Outdoor thermal comfort study in a subtropical climate: a longitudinal study based in Hong Kong', *International Journal of Biometeorology*; 2012 Jan;56(1):43-56. doi: 10.1007/s00484-010-0396-z.
- Chen, Q., (2009) 'Ventilation performance prediction for buildings: a method overview and recent applications', *Journal of Build Environment*, 44:848-58.
- Chin, L and Ng, E (2012) ' Outdoor thermal comfort and outdoor activities: A review of research in the past decade' *Cities, The International Journal of Urban Policy and Planning*, 29 (2), pp. 118–125
- Chrag, D., Ramachandraiah, A. (2010) 'The Significance of Physiological Equivalent Temperature (PET) in outdoor thermal comfort studies' *International Journal of Engineering Science and Technology* Vol. 2(7), 2010, 2825-2828
- Christen, A., and Vogt, R. (2004) 'Energy and Radiation Balance of a Central European City', *International Journal of Climatology*. 24(11):1395-1421.
- Christopher, S., (2006) 'Comparative analysis of urban reflectance and surface temperature', *Remote Sensing of Environment*, Volume 104, Issue 2, p.168-189.
- Cohen, P., Potchter, O., and Matzarakis, A. (2013) 'Daily and seasonal climatic conditions of green urban open spaces in the Mediterranean climate and their impact on human comfort' *Journal of Building and Environment*, 51,285;295.
- Cohen, P., Potchter, O., and Matzarakis, A. (2013) ' Human thermal perception of Coastal Mediterranean outdoor urban environments', *Journal of Applied Geography* 37 (2013) 1-10
- Community Design Collaborative (CDC), (1997) 'AI-Darb al-Ahmar: an agenda for revitalization - conservation and development proposals for a historic district in Cairo', final report published by Community Design Collaborative in collaboration with the Near East Foundation, Cairo.
- Compagnon, R., Haefeli, P. and Weber, W., (2006) 'The 23rd Conference on Passive and Low Energy Architecture (PLEA)'. Université de Genève, Haute Ecole Spécialisé de Suisse occidentale: Geneva. 2006

- Coronel, J.F., and Alvarez, S. (2001) 'Experimental work and analysis of confined urban spaces', *Journal of Solar Energy* 70:263–273
- Crawley, D.B., and Drury, B. (2008) 'Estimating the impacts of climate change and urbanization on building performance', *Journal of Building Performance Simulation* 1 (2) 91–115.

**'D'**

- da Graça, G.C., Martins, N.R. and Horta, C.S. (2012) 'Thermal and airflow simulation of a naturally ventilated shopping mall', *Journal of Energy and Buildings* 2012;50:177-88.
- De Carolis, L., (2012) 'the urban heat island effect in Windsor, ON: assessment of Vulnerability and Mitigation strategies', City of Windsor report, Canada.
- de Dear, R., Nicol, F., Roaf, S. (2013) 'The wicked problem of designing for comfort in a rapidly changing world', *Journal of Architectural Science Review*, 56(1).
- de Dear, R., Brager, G. (2010) 'ASHRAE Adaptive Comfort Standard (American Society of Heating, Refrigerating and Air Conditioning Engineers - American standard for buildings)', *ASHRAE Adaptive Comfort Standard (American Society of Heating, Refrigerating and Air Conditioning En*, 2010, (pp. 1 - 44). Atlanta, United States of America: American Society of Heating, Refrigerating and Air-Conditioning Engineers, Inc..
- de Dear, R.J., and Fountain, M.E. (1994) 'Field experiments on occupant comfort and office thermal environments in a hot-humid climate'. *ASHRAE Transactions*, Vol.100 (2), pp.457-475
- de Dear R.J. and Brager G.S. (1998) 'Developing an Adaptive Model of Thermal Comfort and Preference', *ASHRAE Transactions*., V.104(1a), p.145-167
- Djenane, M., Farhi, A., Benzerzour, M and M. Musy (2008) 'Microclimatic behaviour of urban forms in hot dry regions, towards a definition of adapted indicators', 25th International Conference on Passive and Low Energy Architecture PLEA, Dublin.
- del Rio, V., Levi, D. and Duarte, C. (2010) 'Perceived livability and sense of community: Lessons for designers from a favela in Rio de Janeiro, Brazil'. In F. Wagner & R. Caves (eds.) *Livable Communities* (in press).
- Deng, Q., He, G., Lu, C. and Liu, W. (2012) 'Urban ventilation e a new concept and lumped model. *International Journal of Ventilation*;11:131-40.
- de Schiller S., and Evans J.M., (1998) 'Sustainable urban development: design guidelines for warm humid cities', *Urban Design International Journal* 3(4):165–184
- De Wilde, P. and W. Tian, W. (2010) 'Predicting the performance of an office under climate change: a study of metrics, sensitivity and zonal resolution', *Journal of Energy and Buildings* 42 (10) 1674–1684.
- Djongyang, N., Tchinda, R., and Njomo, D., (2010) 'Thermal comfort: A review paper', *Renewable and Sustainable Energy Reviews* 14, 2626–2640
- Duffie, J.A., and Beckman, W.A., (2013) 'Solar Engineering of Thermal Processes' (4 ed.). Wiley. pp. 13, 15, 20. ISBN 978-0-470-87366-3.
- Dimiceli, V.E., Piltz S.F., and Amburn S.A (2011) ' Estimation of Black Globe Temperature for Calculation of the Wet Bulb Globe Temperature Index', the World Congress on Engineering and Computer Science (WCECS) 2011 Vol II, San Francisco, USA
- Dimiceli, V.E., Piltz S.F., and Amburn S.A (2011) 'Estimation of Black Globe Temperature for Calculation of the Wet Bulb Globe Temperature Index', the World Congress on Engineering and Computer Science (WCECS) 2011 Vol II, San Francisco, USA
- Dimiceli, V.E., Piltz S.F., and Amburn S.A (2011) ' Black Globe Temperature Estimate for the WBGT Index', *IAENG Transactions on Engineering Technologies*, chapter 26.

**'E'**

- EEHC. (2008) 'Annual Report' Egyptian Electricity Holding Company. Cairo.
- Eliasson, I., (2000) 'The use of climate knowledge in urban planning', *International Journal of Landscape and Urban Planning*, 48(1-2), 31-44

- Eliasson, I., Knez, I., Westerberg, U., Thorsson, S. and Lindberg, F. (2007) 'Climate and behaviour in a Nordic city', *International Journal of Landscape and Urban Planning*, 82, 72-84
- Elnabawi M, Hamza N, Dudek S. (2013) Use and Evaluation of The Envi-met Model for Two Different Urban Forms in Cairo, Egypt: Measurements and Model Simulations. In: 13th International Conference of the International Building Performance Simulation Association (IBPSA 2013), Chambéry, France.
- Elnabawi M, Hamza N, Dudek S. (2015) Numerical Modelling Evaluation for the Microclimate of an Outdoor Urban Form in Cairo, Egypt. *Journal of Housing and Building National Research Center (HBRC)*, Volume 11, Issue 2, Pages 246–251.
- Emmanuel, R. (2005) 'An urban approach to climate-sensitive design strategies for the tropics'. Spon Press, London.
- Emmanuel, R., Rosenlund, H. and Johansson, E. (2007) 'Urban shading—a design option for the tropic. A study in Colombo, Sri Lanka', *International Journal of Climatology*, 27, 1995-2004, 2007.
- ENVI-met Official website: [www.envi-met.com](http://www.envi-met.com) (last access on 25 June 2013)
- EPA. (2003) 'Beating the Heat: Mitigating Thermal Impacts', *Nonpoint Source News-Notes*. 72:23-26.
- Epstein, Y., and Moran, D. S. (2006). 'Thermal comfort and the heat stress indices', *Journal of Industrial Health*, 44, 388-398.
- Erell E., Pearlmutter D., and Williamson T., (2011) 'Urban Microclimate: Designing the Spaces Between Buildings', Earthscan/James & James Science Publishers, London.
- Esmaili R., Gandomkar A. and Nokhandan H.M. (2011) 'Assessment of Comfortable Climate in Several Main Iranian Tourism Cities Using Physiologic Equivalence Temperature Index' *Physical Geography Research Quarterly*, No. 75, Spring 2011
- Ewing, R. and Rong, F., (2008) 'The impact of urban form on U.S. residential energy use', *Housing Policy Debate Journal* 19 (1) 1–30.

**'F'**

- Fahmy, M., Sharples, S., Yahiya, M. (2010) 'LAI based trees selection for mid latitude urban developments: A microclimatic study in Cairo, Egypt', *Journal of Building and Environment*, 45 (2), pp. 345-357 <http://dx.doi.org/10.1016/j.buildenv>.
- Fahmy, M., (2010) 'Interactive urban form design of local climate scale in hot semi-arid zone, in School of Architecture', University of Sheffield: Sheffield.
- Fahmy, M. and Sharples, S., (2008a) 'Extensive Review for Urban Climatology: Definitions, Aspects and Scales', 7th International Conference on Civil and Architecture Engineering, ICCAE-7. Military Technical Collage, Cairo May 27-29.
- Fahmy, M. and Sharples, S., (2008b) 'The Need for an Urban Climatology Applied Design Model' [Online]. Available At: [Http://www.Urban-Climate.Org/lauc028.Pdf](http://www.Urban-Climate.Org/lauc028.Pdf)." The online newsletter of the International Association for Urban Climatology 2008(28): 15-16.
- Fahmy, M. and Sharples, S., (2008c) 'Passive Design for Urban Thermal Comfort: A Comparison between Different Urban Forms in Cairo, Egypt', PLEA 2008 - 25th Conference on Passive and Low Energy Architecture. University Collage of Dublin, Dublin, 22nd to 24th October 2008.
- Fahmy, M. and Sharples, S. (2009a), 'On the Development of an Urban Passive Thermal Comfort System in Cairo, Egypt', *Journal of Building and Environment* 44(9): 1907-1916.
- Fahmy, M. and Sharples, S. (2009b) 'Once Upon a Climate: Arid Urban Utopia of Passive Cooling and the Diversity of Sustainable Forms', SUE-MoT2009 Second International Conference on Whole Life Urban Sustainability and its Assessment . Loughborough University April 22-24.
- Fahmy, M. and Sharples, S., (2010) 'Urban Form Adaptation Towards Minimizing Climate Change Effects in Cairo, Egypt. 1st Housing Conference for the Arabic Region. HBRC, Housing and Building Research Centre: Cairo, December. 23-26.
- Fahmi, W. and Sutton, K. (2003) 'Reviving Historical Cairo through Pedestrianisation: The Al-Azhar Street Axis', *International Development Planning Review*, 25, 407–431

- Fanger, P.O. and Toftum, J. (2002) 'Extension of the PMV model to non-air-conditioned buildings in warm climates', *Journal of Energy and Buildings*, 34, 533-536
- Fanger P.O., (1973) 'Conditions for thermal comfort-a review', *Proceedings of Symposium on Thermal Comfort and Moderate Heat Stress (CIB W45)*, Garston, UK, pp. 3–15.
- Fanger P.O., (1972) 'Thermal Comfort', McGraw Hill place City Book, State New York, country-region USA.
- Fathy, H. (1986) 'Natural Energy & Vernacular Architecture' principles and examples with reference to Hot Arid climates p. 63, UN Press
- Fehrenbach, U., Scherer, D., and Parlow, E. (2001) 'Automated classification of planning objectives for the consideration of climate and air quality in urban and regional planning for the example of the region of Basel/Switzerland', *International Journal of Atmospheric Environment*, 35:5605–5615.
- Feriadi, H., and Wong, N.H. (2004) 'Thermal comfort for naturally ventilated houses in Indonesia', *Journal of Energy and Buildings*, 36:614–26.
- Fernando, H. J. S., Zajic, D., Di Sabatino, S., Dimitrova, R., Hedquist, B., and Dallman. A. (2012) 'Flow, turbulence, and pollutant dispersion in urban atmospheres' *AIP physics of fluid*, Volume 22, Issue 12.
- Fiala, D., Havenith, G., Bröde, P., Kampmann, B. and Jendritzky, G. (2012) 'UTCI-Fiala multi-node model of human heat transfer and temperature regulation', *International Journal of Biometeorology*, 56, 429-441.
- Finney, D.J. (1971) 'Probit analysis', Cambridge University Press, Cambridge.
- Florides G.A., Tassou S.A., and Kalogirou S.A, Wrobel, L.C. (2002) 'Measures used to lower building energy consumption and their cost effectiveness', *Journal of Applied Energy*,73:299–328.
- Fouli R.S. (1994) 'Effect of Urbanization on some meteorological elements in greater Cairoregion', In the Report of the Technical Conference on Tropical Urban Climates. WMO, Dhaka.

**'G'**

- Gadi M. B., (2000) 'Design and simulation of a new energy conscious system, (Basic Concept)', *Journal of Applied Energy*, Vol. 65: pp. 349-53.
- Gagge A.P., Fobelets A.P., and Berglund L.G., (1986) 'A standard predictive index of human response to the thermal environment', *American Society of Heating, Refrigerating, and Air-Conditioning Engineers Transactions*, 1986, 92, 709-731
- Gaitani, N., Mihalakakou, G., Santamouris, M., (2007) 'On the use of bioclimatic architecture principles in order to improve thermal comfort conditions in outdoor spaces', *Journal of Building and Environment*, 42:317-24.
- Gehl, J., (2008) 'Life between Buildings: Using Public Space', Indiana University.
- Gehl, J. and Gemzoe, L. (2001) *New City Spaces*. Copenhagen: The Danish Architectural Press.
- Georgy R., and Soliman A., (2007) 'Energy efficiency and renewable energy' Egypt-national study. Cairo: NREA.
- Gharib, R.Y. (2011) 'REVITALIZING HISTORIC CAIRO: THREE DECADES OF POLICY FAILURE' , *International Journal of Architectural Research*, Volume 5 - Issue 3 - November 2011 - (40-57)
- Ghoneim, E. (2008). 'Optimum groundwater locations in the northern Unites Arab Emirates'. *International Journal of Remote Sensing*, 29 (20): 5879-5906.
- Ghoneim, E., and El-Baz, F. (2007). 'Relics of ancient drainage in the eastern Sahara revealed by radar topography data', *International Journal of Remote Sensing*, 28 (8): 1759-1772
- Ghoneim, E. and El-Baz, F. (2007). 'The application of radar topographic data to mapping of a mega-paleodrainage in the Eastern Sahara', *Journal of Arid Environments*, 69: 658-675
- Givoni B. (1997) 'Climate Considerations in Building and Urban Design', New York.ITP; 1997.
- Givoni, B. (1994) *Urban design for hot humid regions*. *Journal of Renewable Energy*, 5(II), 1047-1053.
- Givoni, B., Khedari, J., Wong, N.H., Feriadi, H. and Noguchi, M. (2006) Thermal sensation responses in hot, humid climates: effects of humidity. *Journal of Building Research and Information*, 34, 496-506.

- Givoni, B., Noguchi, M., Saaroni, H., Pochter, O., Yaacov, Y., Feller, N. and Becker, S. (2003) Outdoor comfort research issues. *Journal of Energy and Buildings*, 35, 77-86.
- Gómez, F., Tamarit, N., and Jabaloyes, J. (2001) 'Green zones, bioclimatic studies and human comfort in the future development of urban planning', *Journal of Landscape and Urban Planning*, 55(3):151-161
- Goosse H., P.Y. Barriat, W. Lefebvre, M.F. Loutre and V. Zunz (2010) 'Chapter 2. The Energy balance, hydrological and carbon cycles', *Introduction to climate dynamics and climate modelling* - <http://www.climate.be/textbook> 2010
- Goshayeshi, D., Jaafar, M.Z., Shahidan, M.F., and Khafi. F., (2013) 'Thermal comfort differences between polycarbonate and opaque roofing material installed in bus stations of Malaysia', *European Online Journal of Natural and Social Sciences*, vol.2, No.3, pp.379-393; ISSN 1805-3602
- Grimmond, C. S. B., Roth, M., Oke, T. R., Au, Y. C., Best, M., Betts, R., Carmichael, G., Cleugh, H., Dabberdt, W., Emmanuel, R., Freitas, E., Fortuniak, K., Hanna, S., Klein, P., Kalkstein, L. S., Liu, C. H., Nickson, A., Pearlmutter, D., Sailor, D., and Voogt, J., (2010) 'Climate and More Sustainable Cities: Climate Information for Improved Planning and Management of Cities (Producers/Capabilities Perspective)', *Procedia Environmental Sciences*, vol. 1, pp.247-274.
- Groat, L., and Wang, D., (2002) 'Architectural Research Methods', New York: John Wiley & Sons.
- Grundström, K., Johansson, E., Mraissi, M., and Ouahrani, D., (2003) 'Climat & Urbanisme – La Relation entre le Confort Thermique et la Forme du Cadre Bâti, Report 8, HDM', Lund University.
- Gulyas A., Unger J., and Matzarakis A., (2006) 'Assessment of the microclimatic and human comfort conditions in a complex urban environment: modelling and measurements', *Journal of Building and Environment*, 41:1713-22.

**'H'**

- Haag, M. (2006) 'Cairo Illustrated' the American University Press, Cairo, Egypt.
- Han, J. (2007) 'Field study on occupant's thermal comfort and residential thermal environment in a hot climate of China', *Journal of Building and Environment*, 42, 4043-4050
- Hang, J., Luo, Z., Sandberg, M., and Gong, J., (2013) 'Natural ventilation assessment in typical open and semi-open urban environments under various wind directions', *Journal of Building and Environment*, 70,318-333
- Hang J, Li Y, Buccolieri R, Sandberg M, Di Sabatino S. (2012) 'On the contribution of mean flow and turbulence to city breathability: the case of long streets with tall buildings', *Science of the Total Environment*, 416:363-73.
- Hang J, Li Y, Sandberg M, Buccolieri R, and Di Sabatino S. (2012) 'The influence of building height variability on pollutant dispersion and pedestrian ventilation in idealized high-rise urban areas', *Journal of Building and Environment*, 56:346-60.
- Han, J. (2007) 'Field study on occupant's thermal comfort and residential thermal environment in a hot climate of China'. *Journal of Building and Environment*, 42, 4043-4050
- Hakim, B. S., (1986) 'Arabic-Islamic Cities-Building and Planning Principles' KPI.
- Hakim, B. (1988) 'Recycling the experience of traditional Islamic urbanism', *Preservation of Islamic architecture heritage*, Arab Urban Development Institute, Riyadh.
- Hardy, J. E., Mitlin, D. and Satterthwaite, D. (2001) 'Environmental Problems in an Urbanizing World', Earthscan, London.
- Harlan, S.H., Brazel, A.J., Prashad, L., Stefanov, W.L. and Larsen, L. (2006) 'Neighborhood microclimates and vulnerability to heat stress', *Journal of Social Science and Medicine*, 63:2847-2863.
- Hathway, A and Sharples, S (2012) The interaction of rivers and urban form in mitigating the urban heat island effect: a UK case study. *Journal of Building and Environment*, 58. pp. 14-22.
- Hawkes, D., and Foster, W. (2002) 'Energy efficient buildings, Architecture, Engineering, and Environment', 1st edition, W.W. Norton and company, New York: USA.
- HBRC. Code: ECP 306-2005. The Egyptian Code for enhancing energy use in buildings, vol. 1. Cairo, Egypt: Housing and Building Research Center (HBRC); 2006.

Health and Safety executive 'Thermal Comfort; Basic Six Factors'

<http://www.hse.gov.uk/temperature/thermal/factors.htm> (Last access 25 June 2011)

- Hisham, M. (2003) 'Traditional Islamic principles of built environment', Routledge. p. viii. ISBN 0-7007-1700-5.
- Holmes, M.J. and Hacker, J.N. (2007) 'Climate change, thermal comfort and energy: meeting the design challenges of the 21st century', *Journal of Energy and Buildings* 39, 802–814.
- Höppe, P., (2002) 'Different aspects of assessing indoor and outdoor thermal comfort', *Journal of Energy and Buildings*, 34:661-5.
- Hoppe, P. (1999) 'The physiological equivalent temperature - a universal index for the biometeorological assessment', *International Journal of Biometeorology*, 43, 71-75.
- Höppe, P., (1993) 'Heat balance modelling', *Experientia* 49: 741–746.
- Hu, T., and Yoshie, R., (2013) 'Indices to evaluate ventilation efficiency in newly-built urban area at pedestrian level' *Journal of Wind Engineering and Industrial Aerodynamics*, 112 (2013) 39–51
- Huang, L.M., Li, H. T., and Zhu, D. H. (2008) 'A fieldwork study on the diurnal changes of urban microclimate in four types of ground cover and urban heat island of Nanjing, China', *Journal of Buildings and environment*, vol. 43, pp. 7-17.
- Huttner, S. (2012) 'Further development and application of the 3D microclimate simulation ENVI-met', Mainz University, Germany
- Hu, T., and Yoshie R., (2012) 'Indices to evaluate ventilation efficiency in newly-built urban area at pedestrian level', *Journal of Wind Engineering and Industrial Aerodynamics* 2013;112:39-51

## T

- Ibn-Khaldun, (1377) 'The Muqaddimah' ,translated from the Arabic by Franz Rosenthal, (London: Rotledge and Kegan Paul, 1987), vol. 2 p. 357.
- ICOMOS Review Sheet on the Nomination of the Historical Center of Cairo on the World Heritage List, April 10, 1979.
- Ihara, T., Kikegawa, Y., Asahi, K., Y. Genchi, Y., and Kondo, H. (2008) 'Changes in year-round air temperature and annual energy consumption in office building areas by urban heat-island countermeasures and energy-saving measures', *Journal of Applied Energy* 85 (1) 12–25.
- Intergovernmental Panel on Climate Change (IPCC). (1990) 'Potential impacts of climate change'. Report of Working Group 2, Intergovernmental Panel on Climate Change, 1-1 to 2. Geneva: World Meteorological Organization (WMO)/United Nations Environment Programme (UNEP).
- Intergovernmental Panel on Climate Change (IPCC) Plenary XXVII (2007) Climate Change: Synthesis Report (Valencia, Spain, 12-17 November 2007)
- ISO (1998) International Standard 7726. Ergonomics of the thermal environment–Instruments for measuring physical quantities. International Standards Organization, Geneva.
- ISO (2005) International Standard 7730. Ergonomics of the thermal environment–analytical determination and interpretation of thermal comfort using calculation of the PMV and PPD indices and local thermal comfort criteria. International Standard Organization, Geneva.

## J

- Jabareen, Yosef. 2006. Sustainable urban forms: Their typologies, models, and concepts. *Journal of Planning Education and Research* 26(1), 38-52.
- Happold, B., (2014) 'Urban Heat Island' designing buildings.  
[http://www.designingbuildings.co.uk/wiki/Urban\\_heat\\_island](http://www.designingbuildings.co.uk/wiki/Urban_heat_island) (Last access 25 August 2011)
- Jakubiec, J and Reinhart, C. (2011) DIVA 2.0: integrating daylight and thermal simulations using rhinoceros 3d, daysim and energyplus 12th Conference of International Building Performance Simulation Association, Sydney, 2011.



- Janssen, W., Blocken, B., and van Hoff, T., (2013) 'Use of CFD simulations to improve the pedestrian wind comfort around a high-rise building in a complex urban area' 13<sup>th</sup> Conference of International Building Performance simulation association, Chambéry, France, August 26-28.
- Jendritzky G., Sönning W., Swantes H.J., Einobjektives Bewertungsverfahren zur Beschreibung (1979) 'des thermischen Milieus in der Stadt- und Landschaftsplanung (Klima-Michel-Modell)' [An objective assessment procedure to specify the thermal environment in urban and landscape planning]. *Beiträge der Akademie für Raumforschung und Landesplanung*, 28, 85p (in German)
- Jendritzky G., and Nübler W., (1981) 'A model analysing the urban thermal environment in physiologically significant terms', *Archiv für Meteorologie, Geophysik und Bioklimatologie, Serie B*, 29, 313-326
- Jenkins, D., Liu, Y. and Peacock, A.D. (2008) 'Climatic and internal factors affecting future UK office heating and cooling energy consumptions', *Journal of Energy and Buildings* 40 (5) 874–881.
- Johansson, E., (2014) 'Instruments and methods in outdoor thermal comfort studies – The need for standardization', *Journal of Urban Climate*, <http://dx.doi.org/10.1016>.
- Johansson E., and Emmanuel R., (2006) 'The Influence Of Urban Design On Outdoor Thermal Comfort In The Hot, Humid City Of Colombo, Sri Lanka', *International Journal of Biometeorology* (2006) 51:119-133
- Johansson, E., (2001) 'Street canyon microclimate in traditional and modern neighborhoods in a hot dry climate- A case study in Fez, Morocco', In *The 18th International Conference on Passive and Low Energy Architecture*. Florianopolis, Brazil, 7-9 November (2001), pp.661-665.
- Jones P.D. and Lister D.H. (2009) 'The urban heat island in Central London and urban-related warming trends in Central London since 1900', *Weather – December 2009, Vol. 64, No. 12*
- Jared, N. and Rabiun A B et al. (2006) *Inter-Relationships Between Solar Radiation Intensity (Rd) And Relative Humidity (Rh) In Kenya 2nd Un/Nasa Workshop On IHY and Basic Space Science*. Indian Institute of Astrophysics, Bangalore November 27- December 1, 2006

**'K'**

- Kakon, A.N., Mishima, N. and Kojima, S. (2009) Simulation of the urban thermal comfort in a high density tropical city: Analysis of the proposed urban construction rules for Dhaka, Bangladesh. *Journal of Building Simulation*, 2, 291-305.
- Kántor, N., Égerházi, L., and Unger, J. (2012). Subjective estimation of thermal environment in recreational urban spaces part 1: investigations in Szeged, Hungary. *International Journal of Biometeorology*, 56. <http://dx.doi.org/10.1007/s00484-012-0523-0>.
- Kántor, N., Unger, J., & Gulyas, A. (2012). 'Subjective estimations of thermal environment in recreational urban spaces: part 2 international comparison', *International Journal of Biometeorology*, 56. <http://dx.doi.org/10.1007/s00484-012-0564-4>.
- Kántor, N., Unger, J., (2011) 'The most problematic variable in the course of human-biometeorological comfort assessment – the mean radiant temperature' Department of Climatology and Landscape Ecology, University of Szeged, Hungary
- Kántor, N., and Unger, J. (2010) 'Benefits and opportunities of adopting GIS in thermal comfort studies in resting places: An urban park as an example', *Journal of Landscape and Urban Planning*, 98(1), 36–46.
- Karyono, TH., (2000) 'Report on thermal comfort and building energy studies in Jakarta-Indonesia', *Journal of Building and Environment*, 35:77–90.
- Kato, S., Matsunaga, T., and Yamaguchi, Y., (2010) 'Influence of shade on surface temperature in an urban area Estimated by aster data', *International Archives of the Photogrammetry, Journal of Remote Sensing and Spatial Information Science*, Volume XXXVIII, Part 8, Kyoto, Japan.
- Kato, S., Murakami, S., Takahashi, T., and Gyobu, T., (1997) 'Chained analysis of wind tunnel test and CFD on cross ventilation of large-scale market building', *Journal of Wind Engineering and Industrial Aerodynamics*, 67e68:573-87.

- Katzschner, L. (2006). 'Behaviour of people in open spaces in dependence of thermal comfort conditions', In Paper presented at the PLEA2006 – The 23rd conference on passive and low energy architecture, Geneva, Switzerland.
- Kenny, N. A., Warland, J. S., Brown, R. D., and Gillespie, T. G., (2009) 'Part A: Assessing the performance of the COMFA outdoor thermal comfort model on subjects performing physical activity', *International Journal of Biometeorology*, 53, 415–428.
- Ketterer, C., and Matzarakis, C., (2014) 'Human-biometeorological assessment of the urban heat island in a city with complex topography – The case of Stuttgart, Germany', *Journal of Urban Climate* 573–584
- Khatri, K. B., Van der Steen, P., and Vairavamorthy, K., (2007) 'climate change: Alexandria, Egypt' UNESCO-IHE, Delft, the Netherlands.
- Kipper, R., (2009) 'Cairo: A Broader View', ed. Regina Kipper & Marion Fischer (Cairo: GTZ Egypt, 2009), p. 13.
- Kim, T., Kim, K., and Kim, B.S. (2010) 'A wind tunnel experiment and CFD analysis on airflow performance of enclosed-arcade markets in Korea', *Journal of Building and Environment*, 45: 1329–38.
- Knez I, Thorsson S, Eliasson I, and Lindberg F., (2009) 'Psychological mechanisms in outdoor place and weather assessment: towards a conceptual model', *International Journal of Biometeorology*, 53:101–11.
- Knez, I., and Thorsson, S., (2008) 'Thermal, emotional and perceptual evaluations of a park: cross-cultural and environmental attitude comparisons', *Journal of Building and Environment*, 43:1483–1490
- Knez, I., and Thorsson, S., (2006) 'Influences of culture and environmental attitude on thermal, emotional and perceptual evaluations of a public square', *International Journal of Biometeorology*, 50, 258–268. doi:10.1007/s00484-006-0024-0.
- Knowles R.L., (2003) 'The solar envelope: its meaning for urban growth and form', *Energy and Buildings*, 35, 15-25.
- Kofoed, N and Gaarsted, M., "Considerations of the wind in Urban spaces", In Nikolopoulou, M. (Eds.) *Designing open spaces in the urban environment: a Bioclimatic approach*. Greece, Centre of renewable energy sources, department of building 2004
- Krüger, E., Drach, P., Emmanuel, R. and Corbella, A. (2013) 'Assessment of daytime outdoor comfort levels in and outside the urban area of Glasgow, UK'. *International Journal of Biometeorology*, 57, 521-533.
- Kuehn, L. A., (1970) 'Theory of the Globe Thermometer', *Journal of Applied Physiology*, Vol. 25, No. 5, 750-757.

**'L'**

- Lam, T.N.T., Wan, K.W., Wong, S.L. and Lam, J.C. (2010) 'Impact of climate change on commercial sector air conditioning energy consumption in subtropical Hong Kong', *Journal of Applied Energy* 87, 2321–2327.
- Lawson, T. (2001) 'Building aerodynamics', London: Imperial College Press; 2001.
- Lee, D. O., (1984) 'Urban climates,' *Progress in Physical Geography*, vol. 8, no. 1, pp. 1–31. View at Scopus
- Liaw, K.F. (2005) 'Simulation of Flow around Bluff Bodies and Bridge Deck Sections using CFD'. PhD thesis. University of Nottingham [Online]. Available at: [www.theses.nottingham.ac.uk/125/1/KFL\\_thesis.pdf](http://www.theses.nottingham.ac.uk/125/1/KFL_thesis.pdf).
- Lin, T.P., Tsai, K.T., Hwang, R.L. and Matzarakis, A. (2012) Quantification of the effect of thermal indices and sky view factor on park attendance. *Journal of Landscape and Urban Planning*, 107, 137–146.
- Lin, T.P., de Dear, R.J. and Hwang, R.L. (2011) Effect of thermal adaptation on seasonal outdoor thermal comfort. *International Journal of Climatology*, 31, 302-312.

- Lin, T.P., and Matzarakis, A., (2011) 'Tourism climate information based on human thermal perception in Taiwan and Eastern China', *Journal of Tourism Management*, 32:492-500.
- Lin, T., Matzarakis, A., and Hwang, R., (2010) 'Shading effect on long-term outdoor thermal comfort', *Journal of Building and Environment*, 45:213-221.
- Lin TP., (2009) 'Thermal perception, adaptation and attendance in a public square in hot and humid regions', *Journal of Building and Environment*, 44:2017-26.
- Lin, Z., and Deng, S., (2008) 'A study on the thermal comfort in sleeping environments in the subtropics - developing a thermal comfort model for sleeping environments', *Journal of Building and Environment*, 43:70-80.
- Lin, T.P., and Matzarakis, A., (2008) 'Tourism climate and thermal comfort in Sun Moon Lake, Taiwan', *International Journal of Biometeorology*, 52:281-90
- Littlefair, P. (2001) 'Daylight, sunlight and solar gain in the urban environment', *Journal of Solar Energy*, 70(3):177-85.
- Love, J., (2009) 'Improved Pedestrian Thermal Comfort through Urban Design' Master dissertation. Arizona State University.
- Lu, N., Taylor, T., Jiang, W., Jin, C., Correia, J., Leung, L.R. and P.C. Wong, P.C. (2010) 'Climate change impacts on residential and commercial loads in the Western U.S. grid', *IEEE Transactions on Power Systems* 25-1.

**'M'**

- Mahmoud, A.H.A. (2011) Analysis of the microclimatic and human comfort conditions in an urban park in hot and arid regions. *Journal of Building and Environment*, 46, 2641-2656.
- Mahmoud A.H.A. (2011) 'An analysis of bioclimatic zones and implications for design of outdoor built environments in Egypt', *Journal of Building and Environment*, 46: 605-20.
- Mansura, E.T., Mendelsohn, R., and Morrison, W., (2008) 'Climate change adaptation: a study of fuel choice and consumption in the US energy sector', *Journal of Environmental Economics and Management* 55, 175-193.
- Matzarakis, A., Rutz, F., and Mayer, H., (2010) 'Modelling radiation fluxes in simple and complex environments: basics of the RayMan model', *International Journal of Biometeorology*, 54, 131-139
- Matzarakis, A., Rutz, F., and Mayer, H., (2007) 'Modelling radiation fluxes in simple and complex environments – application of the RayMan model', *International Journal of Biometeorology*, 51: 323-334.
- Matzarakis A, Rutz F, Mayer H. (2000) 'Estimation and calculation of the mean radiant temperature within urban structures'. In: de Dear RJ, Kalma JD, Oke TR, Auliciems A, editors. *Biometeorology and urban climatology at the turn of the millenium. Selected papers from the ICB-ICUC'99 conference, Sydney, WCASP-50, WMO/TD No. 1026*. Geneva: World Meteorological Organization; 2000.
- Matzarakis, A., and Mayer, H., (1996) 'Another kind of environmental stress: thermal stresses, WHO collaborating centre for air quality management and air pollution control. Newsletters, 18:7-10.
- Mavrogianni, A., Davies, M., Batty, M., Belcher, S.E., Bohnenstengel, S.I., Curruthers, D., Chalabi, Z., Croxford, B., Demanuele, C., Evans, S., Giridharan, R., Hacker, J.N., Hamilton, I., Hogg, C., Hunt, J., Kolokotroni, M., Martin, C., Milner, J., Rajapaksha, I., Steadman, J.P., Stocker, J., Wilkinson, P., and Ye, Z.Z., (2011) 'The comfort, energy and health implications of London's urban heat island', *Building Services Research and Technology* 32 (1) 35-52.
- Mayer, H., (1993) 'Human Biometeorology - Urban Bioclimatology', *Journal of Experientia*, 49(11), 957-963.
- Mayer, H., and Höppe, P., (1987) 'Thermal Comfort of Man in Different Urban Environments' *Theoretical and Applied Climatology*, 38(1), 43-49.
- Mayor of London & GLA, (2010) 'The Draft Climate Change Adaptation Strategy for London' Public Consultation Draft, Greater London Authority, London, 2010.
- McIntyre, D.A. (1980). *Indoor climate*. Applied Science Publishers, Essex, England.

- Memon R.A., and Leung, D.Y.C. (2010) 'Impacts of environmental factors on urban heating', *Journal of Environmental Sciences-China*, vol. 22, no. 12, pp.1903-1909.
- Meyer, G., (1990) 'Economic and Social Change in the Old City of Cairo', Middle East Studies Association of North America, Texas.
- Middela, A., Häbb, K., Brazelc, A.J., Martind, C.A., and Guhathakurtae, S., (2014) 'Impact of urban form and design on mid-afternoon microclimate in Phoenix Local Climate Zones', *Journal of Landscape and Urban Planning* 122 (2014) 16– 28
- Mills, G., (2007) 'Cities as agents of global change', *International Journal of Climatology*. 27:1849–1857.
- Mills, G., (2006) 'Progress toward sustainable settlements: A role for urban climatology', *Theoretical and Applied Climatology*. 84:69–76.
- Miller G.A., (1956) 'The magical number seven, plus or minus two: some limits on our capacity for processing information', *Psychological Review*, 63:81-97.
- Mills G. (1997) 'An Urban Canopy-Layer Climate Model', *Theoretical and Applied Climatology*. 57,229-244.
- Mollinedo H., Ramirez J., Huerta O., Mendoza V.X., Martinez S.A., 2013, Effect of the type of impellers on mixing in an electrochemical reactor, *Chemical Engineering Transactions*, 35, 721-726 DOI:10.3303/CET1335120
- Montavez, J. P., Rodrigues, A. and Jimenez, J. I., (2000) 'A study of the Urban Heat Island of Granada', *International Journal of climatology*. 2000; 20, 899-911
- Moonen, P., Defraeye, T., Dorer, V., Blocken, B., and Carmeliet, J., (2012) 'Urban Physics: Effect of the micro-climate on comfort, health and energy demand', *Frontiers of Architectural Research*, 1, 197–228
- Moriwaki, R., and Kanda, M. (2004) 'Seasonal and diurnal fluxes of radiation, heat water vapor, and carbon dioxide over a suburban area', *Journal of Applied Meteorology*, 2004; 43(11), 1700-1710.
- Moughtin C. 2003: *Urban design, street and square*. Architectural Press. Amsterdam.
- Murakami S., and Deguchi K. (1981) 'New criteria for wind effects on pedestrians', *Journal of Wind Engineering and Industrial Aerodynamics*, 7:289-309.

## 'N'

- Nakamura, Y., and Oke, T. R. (1998) 'Wind, Temperature and Stability conditions in an East-West Oriented Urban Canyon', *Journal of Atmospheric Environment* 22(12):2691-2700.
- NASA (2005) 'The Balance of Power in the Earth-Sun System'. FS-2005-9-074-GSFC ([http://www.nasa.gov/pdf/135642main\\_balance\\_trifold21.pdf](http://www.nasa.gov/pdf/135642main_balance_trifold21.pdf))
- Nasser, N. (2000) 'URBAN DESIGN PRINCIPLES OF A HISTORIC PART OF CAIRO: A dialogue for sustainable urban regeneration', School of Architecture. University of central England, Birmingham (PhD dissertation)
- Negrão, C. (1995) 'Conflation of computational fluid dynamics and building thermal simulation' [PhD thesis]. Glasgow, UK: University of Strathclyde.
- Ng, E., Cheng V., and Chan C. (2008) 'Urban climatic map and standards for wind environment - feasibility study. Technical input report no. 1: methodologies and finds of user`s wind comfort level survey. Hong Kong Planning Department. Available at: [http://www.pland.gov.hk/pland/en/p\\_study/prog\\_s/ucmapweb/ucmap\\_project/content/reports/Comfort\\_Level\\_Survey.pdf](http://www.pland.gov.hk/pland/en/p_study/prog_s/ucmapweb/ucmap_project/content/reports/Comfort_Level_Survey.pdf); 2008.
- Ng, E., Yuan, C., Chen, L., Ren, C., and Fung, J.C.H. (2011) 'Improving the wind environment in high-density cities by understanding urban morphology and surface roughness: a study in Hong Kong', *Journal of Landscape Urban Planning*, 101(1):59-74.
- Nicol, J.F. (2008) 'A handbook of adaptive thermal comfort towards a dynamic model', University of Bath, editor. Bath.
- Nicol, J.F. and Humphreys, M.A. (2002) 'Adaptive thermal comfort and sustainable thermal standards for buildings', *Journal of Energy and Buildings* 34(6) pp 563-572 (ISSN 0375 7788)

- Nikolopoulou M., and Lykoudis S. (2006) 'Thermal comfort in outdoor urban spaces: analysis across different European countries', *Journal of Building and Environment* ,41,1455–70.
- Nikolopoulou M., and Steemers K. (2003) 'Thermal comfort and psychological adaptation as a guide for designing urban spaces', *Journal of Energy Buildings*;35:95-101.
- Nikolopoulou M., Baker N., and Steemers K. (2001) 'Thermal comfort in outdoor urban spaces: understanding the human parameter', *Journal of Solar Energy*;70:227-35.
- Nikolopoulou, M. (1998) 'Thermal comfort in outdoor urban spaces', PhD. Dissertation, Department of Architecture, University of Cambridge, Cambridge, United Kingdom.

## 'O'

- Obbonna, A.C., Harris, D.J. (2008) 'Thermal Comfort in sub-Saharan Africa: field study report in Jos-Nigeria', *Journal of Applied Energy*, 85:1-11
- Oke, T.R. (2006) 'Initial guidance to obtain representative meteorological observations at urban sites' report no.: instruments and observing methods report no. 81 World Meteorological Organization. Available at:  
<http://www.wmo.int/pages/prog/www/IMOP/publications/IOM-81/IOM-81-UrbanMetObs.pdf>;
- Oke, T. R. (1977) 'The Energy Balance of an Urban Canyon', *Journal of Applied Meteorology* 16(1):11-19.
- Oke T., Johnson, G.T., Steyn., D.G., and Watson, I.D. (1991) 'Simulation of surface urban heat islands under “ideal” conditions at night', Part 2: Diagnosis of causation. *Boundary Layer Meteorology Journal*, 56: 339-358.
- Oke, T.R. (1988) 'Street design and canopy layer climate', *Journal of Energy and Buildings*. vol.11, pp.103-113
- Oke, T.R. (1978) 'Boundary Layer Climates', 339-390, Methuen & Co., New York, New York.
- Okeil, A., (2010) 'A holistic approach to energy efficient building forms', *Journal of Energy and Buildings*, vol. 42(9), pp. 1437-1444.
- Oliveira, S., and Andrade, H. (2007) 'an initial assessment of the bioclimatic comfort in an outdoor public space in Lisbon', *International Journal of Biometeorology*, Oct 3;52(1):69-84
- Omonijo, A.G., Adeofun, C.O., Oguntoke, O. and Matzarakis, A. (2013) 'Relevance of thermal environment to human health: a case study of Ondo State, Nigeria', *Theoretical and Applied Climatology*,113, 205-212.
- Organization for economic Co-operation and development (OECD) (2004). Development and climate change in Egypt: focus on costal Resources and the Nile: working party on global and structural policies working party on development Co-operation and Environment, pp.68.  
<http://www.oecd.org/environment/cc/33330510.pdf>

## 'P'

- Pearlmutter D, Bitan A, Berliner P (1999) 'Microclimatic analysis of ‘compact’ urban canyons in an arid zone', *Journal of Atmospheric Environment* 33:4143–4150
- Pearlmutter D., Berliner P., and Shaviv, E., (2006) 'Physical modeling of pedestrian energy exchange within the urban canopy', *Journal of Building and Environment*, vol 41, no 6, pp783-795
- Pearlmutter D., Berliner P., and Shaviv, E., (2007a) 'Integrated modeling of pedestrian energy exchange and thermal comfort in urban street canyons', *Journal of Building and Environment*, vol 42, no 6, pp2396-2409
- Pearlmutter D., Berliner P., and Shaviv, E., (2007b) 'Urban climatology in arid regions: Current research in the Negev desert', *International Journal of Climatology*, vol 27, no 14, pp1875-1885
- Peel, M. C., Finlayson, B. L., and McMahon, T. A. (2007) 'Updated world map of the Köppen-Geiger climate classification', *Hydrology and Earth System Sciences*; 11, 1633-1644, doi: 10.5194/hess-11-1633.

- Pereira F.O.R., Nome Silva C. A., Turkienikz B., (2001) 'A methodology for sunlight urban planning: a computer-based solar and sky vault obstruction analysis', *Journal of Solar Energy*, 70:3, 217-226.
- Peterson, J. T. (1973) 'The climate of cities: a survey of recent literature', *Climate in Review*, G. McBoyle, Ed., pp. 264–285.
- Priyadarsini R., and Wong, N. (2005) 'Parametric studies on urban geometry, airflow and temperature' *International journal on architectural science*, vol. 6, no. 3, pp. 114-132.
- Potchter, O., (1990-1991) 'climatic aspects in the building of ancient urban settlements in isreal', *Journal of Energy and Buildings*, vols 15-16, pp93-104
- Potchter, O., Cohen, P., and Bitan, A., (2006) 'Climatic behavior of various urban parks during hot and humid summer in the Mediterranean city of Tel Aviv, Israel international journal of climatology,. 26: 1695–1711, published online 16 may 2006 in Wiley interscience (www.interscience.wiley.com) doi: 10.1002/joc.1330

## 'Q'

## 'R'

- Radhi, H and Assem, A and Sharples, S (2014) 'On the colours and properties of building surface materials to mitigate urban heat islands in highly productive solar regions', *Journal of Building and Environment*, 72. pp. 162-172.
- Radhi, H and Fikiry, F and Sharples, S (2013) Impacts of urbanisation on the thermal behaviour of new built up environments - a scoping study of urban heat island in Bahrain. *Journal of Landscape and Urban Planning*, 113. pp. 47-61.
- Radhi, H and Sharples, S (2013) Quantifying the domestic electricity consumption for air-conditioning due to urban heat islands in hot arid regions. *Journal of Applied Energy*, 112 . pp. 371-380.
- Rajagopalan, P., Wong, N.H. and Cheong, K.W.D. (2008) 'Microclimatic modeling of the urban thermal environment of Singapore to mitigate urban heat island', *Journal of Solar Energy*, 82, 727-745.
- Rahamimoff, A. and Bornstein, N. (1981) 'edge conditions- climatic considerations in the design buildings and settlements', *Journal of Energy and Buildings*, vol 4, pp43 - 49
- Ratti C. and Richens P., (2004) 'Raster analysis of urban form', *Environment and Planning B: Planning and Design*, 31:2, 297-309.
- Ratti C. and Baker N., Steemers K., (2005) 'Energy consumption and urban texture', *Journal of Energy and Buildings*, 37:7, 762-776.
- Ratti C. and Morello E., (2005) 'SunScapes: extending the 'solar envelopes' concept through 'iso-solar surfaces', *Proceedings of the 22nd International Conference on Passive and Low Energy Architecture*, Beirut, Lebanon.
- Raymond, A., (1993) 'Le Caire, Fayard'. *International Journal of Middle East Studies*, volume 26; issue 03, pp 501-502
- Rees, W. (2001b) 'Global Change, Ecological Footprints , and Urban Sustainability' In : 'How Green is the City', D. Devuyst, L. Hens and W. de Lannoy (Eds), Columbia University Press
- Reinhart, C.F. and Jan Wienold, J., (2011) 'The daylighting dashboard e A simulation-based design analysis for daylit spaces', *Journal of Building and Environment* 46 (2011) 386-396
- Reinhart, C.F. (2006) 'Tutorial on the Use of Daysim Simulations for Sustainable Design', Institute for Research in Construction. National Research Council Canada, Ottawa, Ont., K1A 0R6, Canada, August 29, 2006
- Rizwan, A. M., Dennis Y.C. Leung, Chun-Ho Liu (2010) 'Effects of building aspect ratio and wind speed on air temperatures in urban-like street canyons', *Journal of Building and Environment* 45, 176–188
- Robaa, S. M.(2011) 'Effect of Urbanization and Industrialization Processes on Outdoor Thermal Human Comfort in Egypt', *Atmospheric and Climate Sciences*, vol. 1, pp. 100-112, 2011.
- Robaa, S. M. (2003) 'Urban-Suburban/Rural Differences over Greater Cairo, Egypt,' *International Journal of Atmosfera*, Vol. 16, No. 3, pp. 157-171.

- Robaa, S. M. (1999) 'Impact of Urbanization on Meteorology and Human Comfort in Greater Cairo, Egypt', Ph.D. Thesis, Cairo University, Cairo, Egypt.
- Robins, A. and Macdonald, R. (1999) 'Review of Flow and Dispersion in the Vicinity of Buildings', Atmospheric Dispersion Modeling Liaison Committee Annual Report.
- Robinson, D. and Stone, A., (2004) 'Irradiation modeling made simple: the cumulative sky approach and its applications', Plea2004 - The 21st Conference on Passive and Low Energy Architecture. Eindhoven, The Netherlands, 19 – 22 September 2004
- Rogot E, Sorlie PD, Backlund E (1992). Air-conditioning and mortality in hot weather. *American Journal of Epidemiology*, 136:106–116
- Russell, D., (1962) 'Medieval Cairo and the Monasteries of Wadi Natrun – a historical guide', Weidenfeld and Nicholson, London.

## 'S'

- Sailor, D. J. (2002) 'Urban Heat Islands, Opportunities and Challenges for Mitigation and Adaptation', Sample Electric Load Data for New Orleans, LA (NOPSI, 1995). North American Urban Heat Island Summit. Toronto, Canada. 1-4 May 2002. Data courtesy Entergy Corporation. Shalom H. Potchter, O., and Tsoar, H., (2009) 'the effect of the urban heat island and global warming on thermal discomfort in a desert city, the case of Beer Sheva, Israel' The seventh International Conference on Urban Climate, 29 June - 3 July 2009, Yokohama, Japan
- Santamouris, M., (2007) 'Heat island research in Europe—the state of the art', *Advances in Building Energy Research (ABER)* 1 (1) 123–150, Earthscan.
- Santamouris, M., (2002) 'Sustainable Cities Realistic Targets for a Utopian Subject', Paper presented at Green City Conference, Westerloo, Belgium.
- Santamouris, M., Papanikolaou, N.; Koronakis, I., Georgakis, C., Argiriou, A., and Assimakopoulos, D.N., (2001) 'on the impact of urban climate on the energy consumption of buildings', *Journal of Solar Energy* vol. 70, no. 3, 2001, pp. 201-216
- Santamouris, M., Papanikolaou, N., Koronakis, I., Livada, I., Assimakopoulos, D. (1999) 'Thermal and air flow characteristics in a deep pedestrian canyon under hot weather conditions' *Journal of Atmospheric Environment* 33:4503–4521
- Seinfeld, J.H., and Pandis, S.N., (2006). 'Atmospheric Chemistry and Physics, from Air Pollution to Climate Change' Wiley. p. 130. (2 ed.). ISBN 978-0-471-72018-8.
- Shashua-Bar, L., and Hoffman, M.E., (2003) 'Geometry and orientation aspects in passive cooling of canyon streets with trees', *Journal of Energy and Buildings* 35, 61–68.
- Sheta, W. and Sharples, S. (2010) 'A building simulation sustainability analysis to assess dwellings in a new Cairo development'. In: Fourth National Conference of IBPSA-USA, New York University
- Smith, C., and Levermore, G., (2008) 'Designing urban spaces and buildings to improve sustainability and quality of life in a warmer world', *Energy Policy*, doi:10.1016/j.enpol.2008.09.011
- Spagnolo, S., and de Dear, R. (2003) 'A field study of thermal comfort in outdoor and semi-outdoor environments in subtropical Sydney Australia', *Journal of Building and Environment*, 38, 721-738.
- Srivanit, M., and Kazunori, H. (2011) 'The Influence of Urban Morphology Indicators on Summer Diurnal Range of Urban Climate in Bangkok Metropolitan Area, Thailand', *International Journal of Civil & Environmental Engineering*, vol. 11, no. 5, pp: 34-46.
- Stasinopoulos, T., (2011) 'Assessing Building Forms through Envelope to Volume Ratio', *Architecture and sustainable Development PLEA 2011*, Louvain la Neuve, Belgium
- Stemmers, K. (2003) 'Cities, energy and comfort: a PLEA 2000 review', *Journal of Energy and Buildings*, 35:1e2.
- Stewart, D. (2003) 'Heritage planning in Cairo. Multiple heritages in a mega-city', *International Development Planning Review* 25 (2), 129-152
- Stewart, D., (1999) 'Changing Cairo: The Political Economy of Urban Form', *International Journal of Urban and Regional Research*, vol 23.

- Stone, C. (2006) 'Ibn Khaldun and the Rise and Fall of Empire\_ Saudi Aramco World (Arab and Islamic Cultures and Connections)' Saudi Aramco World print edition. Volume 57, Number 5,
- Sukhatme, S. P. (2008) 'Solar Energy: Principles of Thermal Collection and Storage' Tata McGraw-Hill Education. p. 84. (3 ed.). ISBN 0070260648.
- Sutton, K., and Fahmi, W., (1997) 'The rehabilitation of Old Cairo', Habitat International 2002a, 26 (1), 73–93. United Nations Development Program. Rehabilitation of Historic Cairo. Final Report. UNDP Technical Co-operation Office: Cairo, Egypt, 1997.
- Svensson, M.K., (2004) 'Sky view factor analysis implications for urban air temperature differences' Journal of Applied Meteorology 11, 201–211 (DOI:10.1017/S1350482704001288)
- Syrios, K., and Hunt, G. R. (2008) 'Passive air exchanges between building and urban canyon via openings in a single façade', International Journal of Heat and Fluid Flow, vol.29, pp. 364–373.
- Szokolay S.V., (2004) 'Introduction to architectural science: the basis of sustainable design', Elsevier, Architectural Press, Amsterdam, Boston.

**'T'**

- Taha, MR., Douglas, S., and Haney, J., (1997) 'Mesoscale meteorological and air of quality impacts of increased urbane albedo and vegetation', Journal of Energy and Buildings 25:169–177
- Takakura, T., S. Kitade, et al. (2000). "Cooling effect of greenery cover over a building." Journal of Energy and Buildings 31(1): 1-6.
- Tan, C.L., Wong, N.H. and Jusuf, S.K. (2013) Outdoor mean radiant temperature estimation in the tropical urban environment. Journal of Building and Environment, 64, 118–129.
- Taye, M.T., Willems, P., Terwisscha, C., Scheltinga, V., and Kroeze, C., (2012) 'The Lived Experience of Climate Change: Water case study on the Nile and Rhine river basins', Climate change: from science to lived experience. T869 LECH-e Water Case Study 2012
- Thomas, R., and Fordham, M. (2003) 'Sustainable Urban Design: An environmental approach', London and New York: E & FN Spon.,
- Thorsson S., Lindberg F., Eliasson I., and Holmer B. (2007) 'Different methods for estimating the mean radiant temperature in an outdoor urban setting', International journal of climatology. 27: DOI: 10.1002
- Thorsson, S., Honjo, T., Lindberg, F., Eliasson, I., and Lim, E. M. (2007) 'Thermal comfort and outdoor activity in Japanese urban public places', Journal of Environment and Behavior, 39(5), 660-684.
- Thorsson, S., Lindqvist, M., and Lindqvist, S., (2004) 'Thermal bioclimatic conditions and patterns of behaviour in an urban park in Göteborg, Sweden', International Journal of Biometeorology, 48:149-56.
- Todhunter, P. E. (1990) 'Microclimatic Variations Attributable to Urban Canyon Asymmetry and Orientation', Journal of Physics and Geography, vol. 11, pp.131-141.
- Tseliou, A., Tsiros, I. X., Lykoudis, S., and Nikolopoulou, M. (2010) 'An evaluation of three biometeorological indices for human thermal comfort in urban outdoor areas under real climatic conditions', Journal of Building and Environment, 45, 1346-1352
- Tzempelikos A, and Athienitis AK. (2007) 'The impact of shading design and control on building cooling and lighting demand', Journal of Solar Energy, 81:369–82.

**'U'**

- Uchiyama, K., (2011) 'Cities and Heat-island', BBJ Research Center on Global Warming Discussion Paper Series No. 43 (7/2011)
- UNESCO Technical report 1985
- United Nations Environmental Program : Global Environmental Outlook, 2002.
- UN-Habitat (2003) Global Report on Human Settlements 2003, The Challenge of Slums, Earthscan, London; Part IV: 'Summary of City Case Studies', pp195-228.



UNHDR. United Nations Human Development Report. Egypt Human Development Report; 2010 <<http://www.undp.org/Default.aspx?tabid=227>> [retrieved 17.11.10].

U.S. Department of Energy, 2012.

[http://apps1.eere.energy.gov/buildings/energyplus/cfm/weather\\_data3.cfm/region=1\\_africa\\_wmo\\_region\\_1/country=EGY/cname=Egypt](http://apps1.eere.energy.gov/buildings/energyplus/cfm/weather_data3.cfm/region=1_africa_wmo_region_1/country=EGY/cname=Egypt)

## 'V'

Van Hooff, T., Blocken, B. and van Harten, M. (2011) '3D CFD simulations of wind flow and wind-driven rain shelter in sports stadia: Influence of stadium geometry', *Journal of Building and Environment*, 46(1), pp. 22-37.

Vanos, J.K., Warland, J.S., Gillespie, T.J. and Kenny, N.A. (2010) 'Review of the physiology of human thermal comfort while exercising in urban landscapes and implications for bioclimatic design', *International Journal of Biometeorology*, 54, 319-334.

VDI (1998) VDI 3787. Part I: Environmental meteorology, methods for the human biometeorological evaluation of climate and air quality for the urban and regional planning at regional level. Part I: Climate. VDI guideline 3787. Part 2. Berlin: Beuth; 1998.

Voogt, J.A. (2002) 'Urban heat island', p. 660–666. In I. Douglas (ed.) *Causes and consequences of global environmental change*. Vol. 3. John Wiley and Sons, Chichester, UK.

Voogt, J.A., and Oke. T.R., (1997) 'Complete urban surface temperatures', *Journal of Applied Meteorology and Climatology*. 36:1117–1132.

## 'W'

Walsh C.L., (2011) 'Assessment of climate change mitigation and adaptation in cities' *Journal of Urban Design and Planning* Volume 164 Issue DP2

Wang, X., D. Chen, D., and Ren, Z., (2010) 'Assessment of climate change impact on residential building heating and cooling energy requirement in Australia', *Journal of Building and Environment* 45, 1663–1682.

Waziry, Y., (2002) 'Application on Environmental architecture; solar Design Studies of courtyard in Cairo and Toshky', in Arabic. Cairo, Madbuli Publishing.

Waszeri U. (2002) 'Practice on environmental architecture- the sunny design for interior court- studies on Cairo and Toshki'. Cairo: Madboli Publishing

Wieringa, J., Davenport A.G., Grimmond C.S.B., and Oke T.R., (2001) 'New revision of Davenport roughness classification', 3EACWE (3rd European and African conference on Wind Engineering), Eindhoven, Netherlands.

Wiet, G., (1964), Cairo: City of Art and Commerce, translated from French into English by Seymour Feiler, University of Oklahoma Press, Norman.

Williams, C., (2001) 'Islamic Cairo: A Past Imperiled', *The Massachusetts Review* Vol. 42, No.4, Egypt (Winter 2001/2002), pp 591-608.

Williams, C., (1983) 'The Cult of 'Alid Saints in the Fatimid Monuments of Cairo, Part I: The Mosque of al-Aqmar. Muqarna'. Yale University Press.

Willard, B. (2011). "3 Sustainability Models" citing *The Power of Sustainable Thinking* by Bob Doppelt, and *The Necessary Revolution* by Peter Senge et al. Retrieved on: 2011-05-03.

Wohlwill JF. Human adaptation to levels of environmental stimulation. *Journal of Human Ecology* 1974;2:127–47.

Wong, N. H., & Jusuf, S. K. (2008) 'GIS-based greenery evaluation on campus master plan', *Journal of Landscape and Urban Planning*, 84, 166–182.

Wong, N.H. and Yu, C. (2009) 'Tropical urban heat islands: climate', *Buildings and greenery*. Taylor and Francis, New York, USA.

Wong, N.H., Kardinal J.S., Aung La Win, A., Kyaw Thu, H., Syatia Negara, T. and Xuchao, W. (2007). Environmental study of the impact of greenery in an institutional campus in the tropics. *Journal of Building and Environment*, 42(8), 2949-2970.

- World Health Organization (WHO) (2013) 'Annual Report' center of health development. [http://www.who.int/kobe\\_centre/publications/en\\_annualreport\\_2013.pdf?ua=1](http://www.who.int/kobe_centre/publications/en_annualreport_2013.pdf?ua=1)
- World Health Organization (WHO) (2004) 'Heat-waves: risks and responses, Health and Global Environmental Change', SERIES, No. 2\_ <http://www.euro.who.int/globalchange>
- World Urbanization Prospects (2011) 'The 2011 Revision' Department of Economic and Social Affairs Population Division United Nations New York, 2012 ESA/P/WP/224 March 2012 English only United Nations New York, 2012

## 'X'

## 'Y'

- Yang, L., and Li, Y., (2011) 'Thermal conditions and ventilation in an ideal city model of Hong Kong', *Journal of Energy and Buildings*, vol. 43, no. 5, pp.1139-1148.
- Yang, W., Nyuk Hien Wong, N.H., and Kardinal J.S (2013) 'Thermal comfort in outdoor urban spaces in Singapore', *Journal of Building and Environment*, 59, 426-435.
- Yang, X., Lihua Zhao, Michael Bruse, M., and Qinglin Meng, Q., (2012) ' An integrated simulation method for building energy performance assessment in urban environments' *Journal of Energy and Buildings* Volume 54, Pages 243–251
- Yang, X., Li, Y., and Yang, L., (2012) 'Predicting and understanding temporal3D exterior surface temperature distribution in an ideal courtyard. *Journal of Building and Environment*, Volume 57, Pages 38–48
- Yang Z, Li HX, Hu YF., (2006) 'Study on solar radiation and energy efficiency of building glass system', *Journal of Applied Thermal Engineering*, 26:956–61.
- Yao, R., Li, B. and Liu, J. (2009) 'A theoretical adaptive model of thermal comfort – Adaptive Predicted Mean Vote (aPMV)', *Journal of Building and Environment*, 44 (10). pp. 2089-2096. ISSN 0360-1323
- Yoshida A, Tominaga K, Watani S., (1990/1991) 'Field measurements on energy balance of an urban canyon in the summer season', *Journal of Energy and Buildings* 15/16:417–423
- Yousry M., and Aboul Atta, T., (1997) 'The Challenge of Urban Growth in Cairo', *The Urban Challenge in Africa: Growth and Management of its Large Cities*, New York, United Nations University Press.

## 'Z'

- Zacharias, J., Stathopoulos T., Wu, H. (2004) Spatial behavior in San Francisco's plazas: the effects of microclimate, other people and environmental design. *Journal of Environment and Behavior*, 36, 5, 638-658.
- Zacharias, J., Stathopoulos, T., and Wu, H. (2001). Microclimate and downtown open space activity. *Journal of Environment and Behavior*, 33, 2, 296-315.
- Zhai, Z., Chen, O., (2003) 'Solution characters of iterative coupling between energy simulation and CFD program', *Journal of Energy and Buildings* 35, 493-505
- Zhai, Z., Chen, O., Haves, P., and Klems J.H., (2002) 'On approaches to couple energy simulation and computational fluid dynamics programs', *Journal of Building and Environment* 37, 857 – 864
- Zhang, A., Gao, C. and Zhang, L. (2005) 'Numerical simulation of the wind field around different building arrangements', *Journal of Wind Engineering and Industrial Aerodynamics*, 93(12), pp. 891-904.
- Zhang, R., Zhang, Y., Lam, K.P. and Archer, D.H. (2010) 'A prototype mesh generation tool for CFD simulations in architecture domain', *Journal of Building and Environment*, 45(10), pp. 2253-2262.
- Zhang, W., Hiyama, K., Kato, S., and Ishida, Y., (2013) 'Building energy simulation considering spatial temperature distribution for non-uniform indoor environment' *Journal of Building and Environment* 63, 89-96
- Zhang, Y.W., Gu, Z.L., Lee, S.C., Fu, T.M. and Ho, K.F. (2011) 'Numerical Simulation and In Situ Investigation of Fine Particle Dispersion in an Actual Deep Street Canyon in Hong Kong', *Journal of Indoor and Built Environment*, 20(2), p. 206.

## **Appendix 'A'**

### **Al-Muizz Street Urban Development**

---

*“He who has not seen (Islamic) Cairo does not know the grandeur of Islam... the thronging place of nations and the anthill of the human race” written by Ibn Khaldun, famous Arab scholar at the end of the thirteen century (Ibn Khaldun, 1951 :256-7).*

## • Cairo urban development

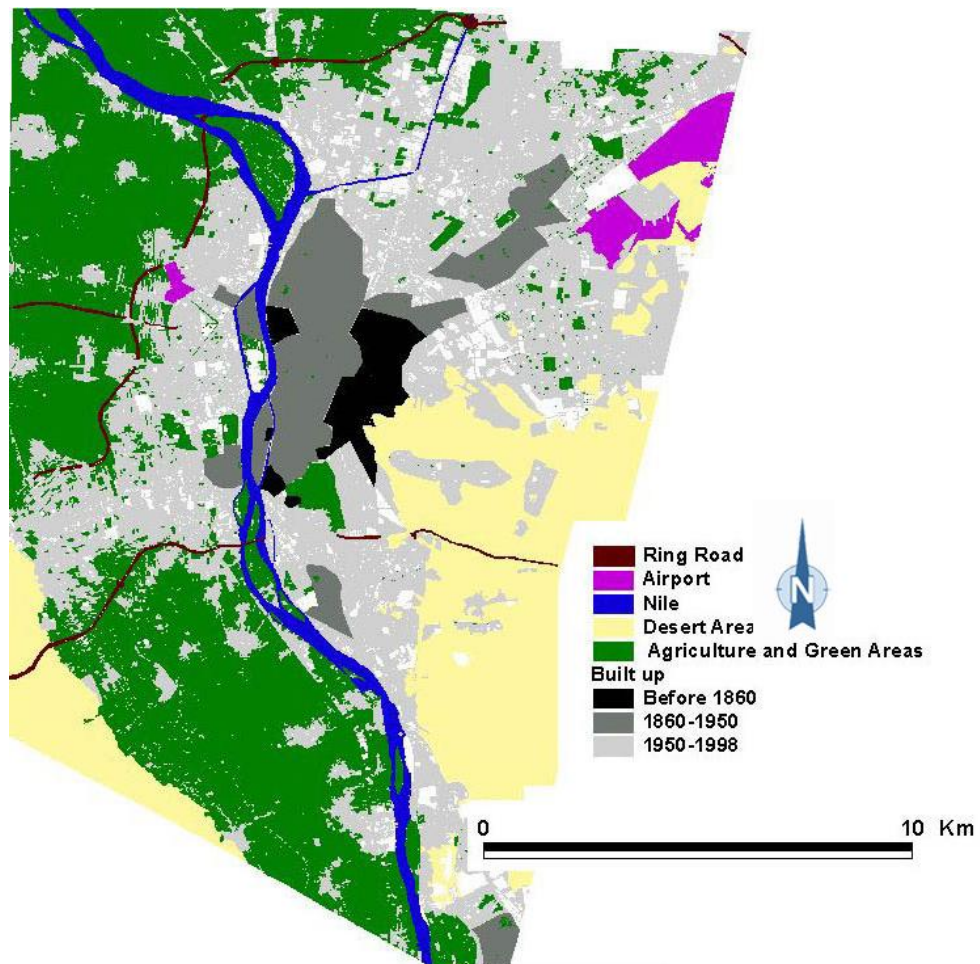
Al-Qahira (the conquerer or the victorious), a name which passed into English as Cairo, was founded in AD969 on land adjacent to Fustat, another Islamic city established at the dawn of Islam in AD641. These cities were themselves preceded by Roman and Pharaonic settlements (Babylon and Memphis) in the same approximate location at the strategic southern apex of the Nile Delta (UN-Habitat, 2003). Islamic rule continued in the country for more than nine centuries till the French invasion in 1879. During this period, a climate conscious design was developed in order to deal with the extreme hot desert climate of Cairo. Different passive techniques were established such as the streets and buildings orientations, (near to the orientation of north to south), the courtyard concepts, and a compact urban structure. After the mid-18th century, it became common practice to superimpose western town planning principles on the city's local conditions, with the introduction of new technologies where the narrow and irregular street systems in the old city could not be maintained. This includes the modern urban expansion under Ismail Pasha and his successors, and was concentrated to the west of the historical city up to the Nile, north to Abbassia, Shubra, and Heliopolis, and south to Maadi and Helwan. Only in the post-war period did Cairo's expansion extend across the Nile into Giza and north into Shubra el Kheima Governorate (Figure 0.1A).

Cairo's expansion has predominantly been on rich agricultural land. Only the eastern districts, most notably NasrCity, Nozha (and earlier Abassia and Heliopolis), have been created on what was desert land. This led the built environment to witness many changes that affect local climate. In fact, all Cairo's development trends were mainly motivated by political and economic shifts. This was demonstrated based on field surveys and GIS technical work for different maps of Cairo (Stewart, 1999; Stewart et al., 2004; Yin et al., 2005), which divided Cairo into four time periods of urban planning development, including the following:

1. Islamic (Settling; 969AD to the French occupation; 1798AD), urban key features are Al-Fustat, The Fatimid Cairo, the citadel
2. Imperialist (French occupation; 1798AD to the July revolution; 1952AD), urban key features are the Central Cairo, Al-Zamalek, and Garden City

3. Arabic socialist (July Revolution; 1952AD –Transitory; 1987AD), urban key feature is NasrCity
4. Capitalism (Transitory; 1987AD to now); urban key features are the satellite developments of the new town rings.

Al-Muizz Street belongs to the Islamic urban planning period dated back to 969AD. However, it has been affected by all the subsequent urban development periods where the historic Islamic quarters were affected by a consequent rise in population and a higher demand for services. For instance, the water supply design in the historic quarters is insufficient for such an increase in demand. Additionally, the informal electricity ‘hook-up’ raised by the informal settlers causes significant electricity supply problems (Yousry et al., 1997). Thus, it was essential to study the impact of each transitional period on the urban pattern of Al-Muizz.



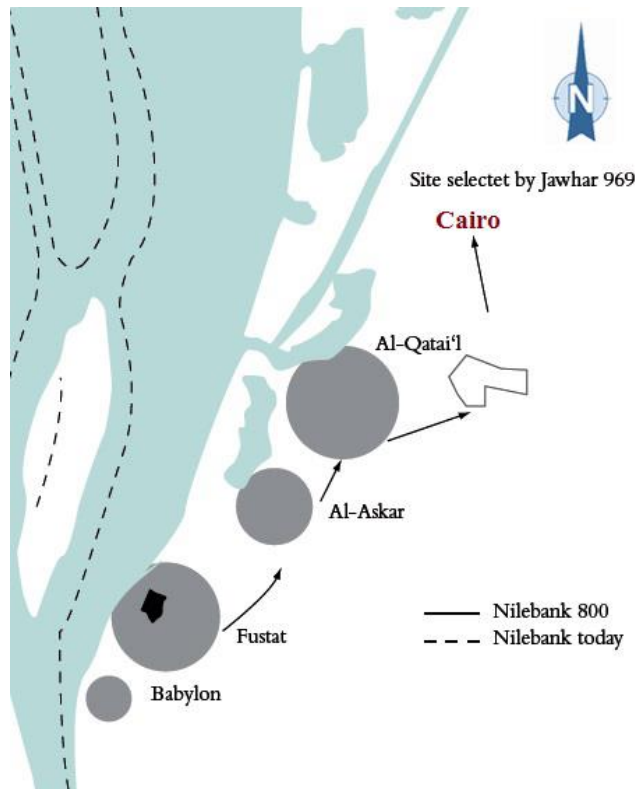
**Figure 0-1A** The expansion of the main built up areas of greater Cairo according to three periods, pre-1860, 1860-1950, and 1950 to the present (source: [www.ucl.ac.uk/dpu-projects/Global Report/home.htm](http://www.ucl.ac.uk/dpu-projects/Global%20Report/home.htm))

- **The development of Al-Muizz Street**

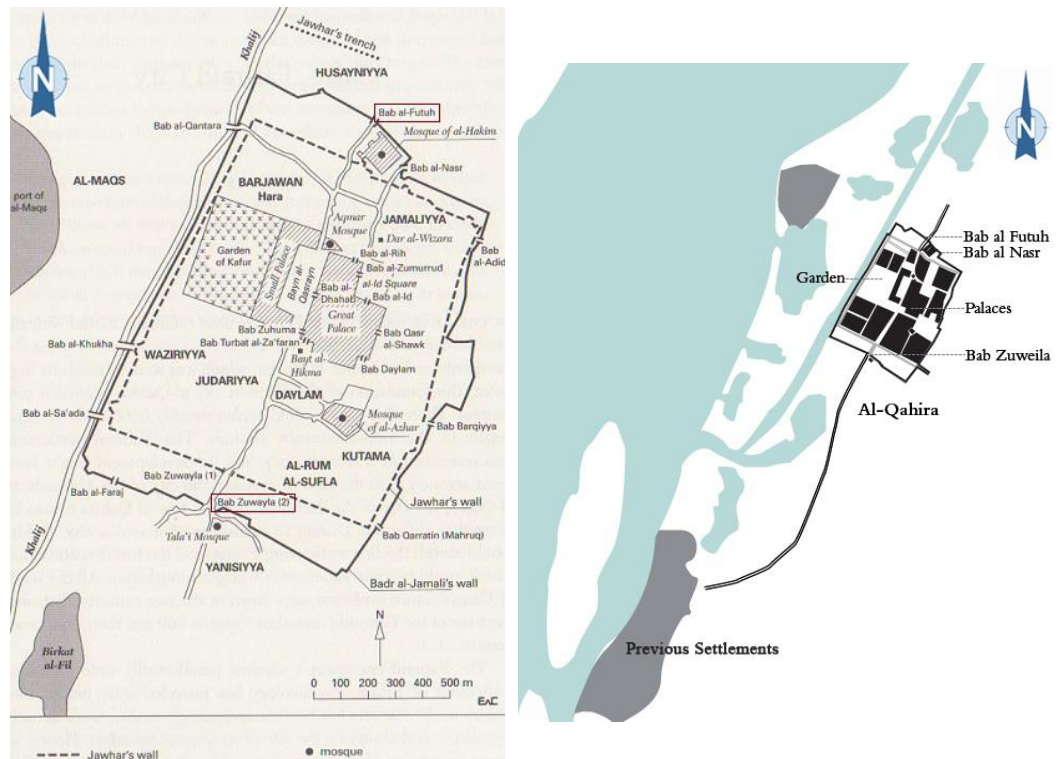
The Islamic settlement in the area of Cairo dates back to 641AD and the foundation of Al-Fustat, which became Egypt's first capital under Islamic rule (Richard, 2006). The city's urban design started by building the first mosque in Africa at the city centre to act as a focal point to unite the inhabitants of Egypt's new capital in prayers. Separate living quarters were assigned for the various clans in the army, and each quarter was divided from the next by a vast expanse of land to prevent internal tribal war (Rezk, 2011). This method of urban planning allowed the city of Fustat to grow rapidly, becoming an important urban centre in Egypt and later in the Islamic Empire (Antoniou, 2009). The birth of Fustat marked the beginning of Egypt's transformation, and a new Islamic society was formed that would change the country's architecture, laws and beliefs (Rezk, 2011). Al-Fustat remained relatively small for the first 100 years of its existence; this was primarily due to the fact that the Islamic empire was ruled by the Umayyad dynasty from Damascus, while Al-Fustat was too far and too small to attract attention. This situation changed with the rule of the Abbasid dynasty in 749AD and the removal of the seat of the Caliphate from Syria to Iraq (Antoniou, 2009). In Egypt, this meant the displacement of the governmental functions of the region to a newly built suburb just north of Fustat, named Al-Askar, to serve as a new urban centre (Ashmawy, 2004). Al-Askar expanded but failed to attract enough residents to compete with Fustat due to its costly real estate and limited access (Antoniou, 2009; Rezk, 2011). However, during the century or more that followed, the two communities merged so that the combined settlements of Al-Fustat and Al-Askar stretched along the axis of the Nile (Figure 0.2A).

The growing decadence of the Abbasids in the late ninth century led to the increasing independence of parts of the Abbasid Empire, and Ahmed Ibn Tulun quickly seized the opportunity and proclaimed himself as the independent ruler of Egypt, founding a new dynasty called the Tulunid dynasty (Parker et al., 2008). In 870AD, Ibn Tutun started a new town, north west of Al-Askar, called Al-Qatai, which was modelled after Samarra in Iraq. It had magnificent open spaces built for sport and tournaments, and large mosques were constructed amongst them, such as the famous Ibn Tulun mosque, which still stands (Haag, 2006). Al-Qatai had attractive markets for luxury consumer goods, and the bulk of economic activity remained in Al-Fustat. However, in 905AD, the Abbasid troops succeeded in regaining the country for the empire and destroyed

most of the monuments, which had been constructed within the city of Al-Qatai, leaving Al-Fustat once again the premier city in Egypt (Antoniou, 2009; Rezk, 2011). The Abbasid rule of Egypt would not last, however, and in 969AD General Gawhar Al-Siqilli conquered Egypt for the Fatimid Caliphate, and thereby established their imperial city, Al-Qahira or Cairo (Rezk, 2011). At the time of the Fatimid invasion, the inhabited areas of the populous cities of Al-Fustat, Al-Askar, and Al-Qataie were joined together into a triple city called collectively 'Misr.' Its length, according to Maqaddassi (AD985), was about three kilometres. The site chosen for Al-Qahira or Cairo lay immediately to the north of Al-Fustat, as shown in Figure 0.2A. The city is rectangular in shape, half a square mile and surrounded with fortified walls in all four directions (Figure 0.3A.). The main spine is named after the Caliphate, Al-Muizz Street, which is probably the oldest and most stable street of Fatimid Cairo (Al-Sayyad, 1981; Rezk, 2011), and ran from north to south, connecting the gate of Bab Al-Futuh with the gate of Bab Zuwaila. These main gates were built to guard the entrance of the city, as it was built in the first place to be the residence of the Caliph and his court, his slaves and officials, and his troops; common people were not allowed in Cairo without a special permit issued by the royal house. As time went on, the population of the triple city 'Misr' had grown and gradually moved to the immediate vicinity of the imperial stronghold. By the extinction of the Fatimid dynasty, the population overflowed into the enclosure of Cairo, causing all the cities to merge into one big city within an area no larger than 5km<sup>2</sup>, known today as Islamic Cairo (Rezk, 2011). Al-Muizz Street is still the predominant route for pedestrians, dividing the Islamic quarter into two parts. Al-Muizz is bounded in the east by Salah Salim Road and by Port Said Road in the west. The northern boundaries of Islamic Cairo start with the 11<sup>th</sup> Century walls of Badr Al-Jamali and the southern part ends with Saliba Road (Figure 0.4A).

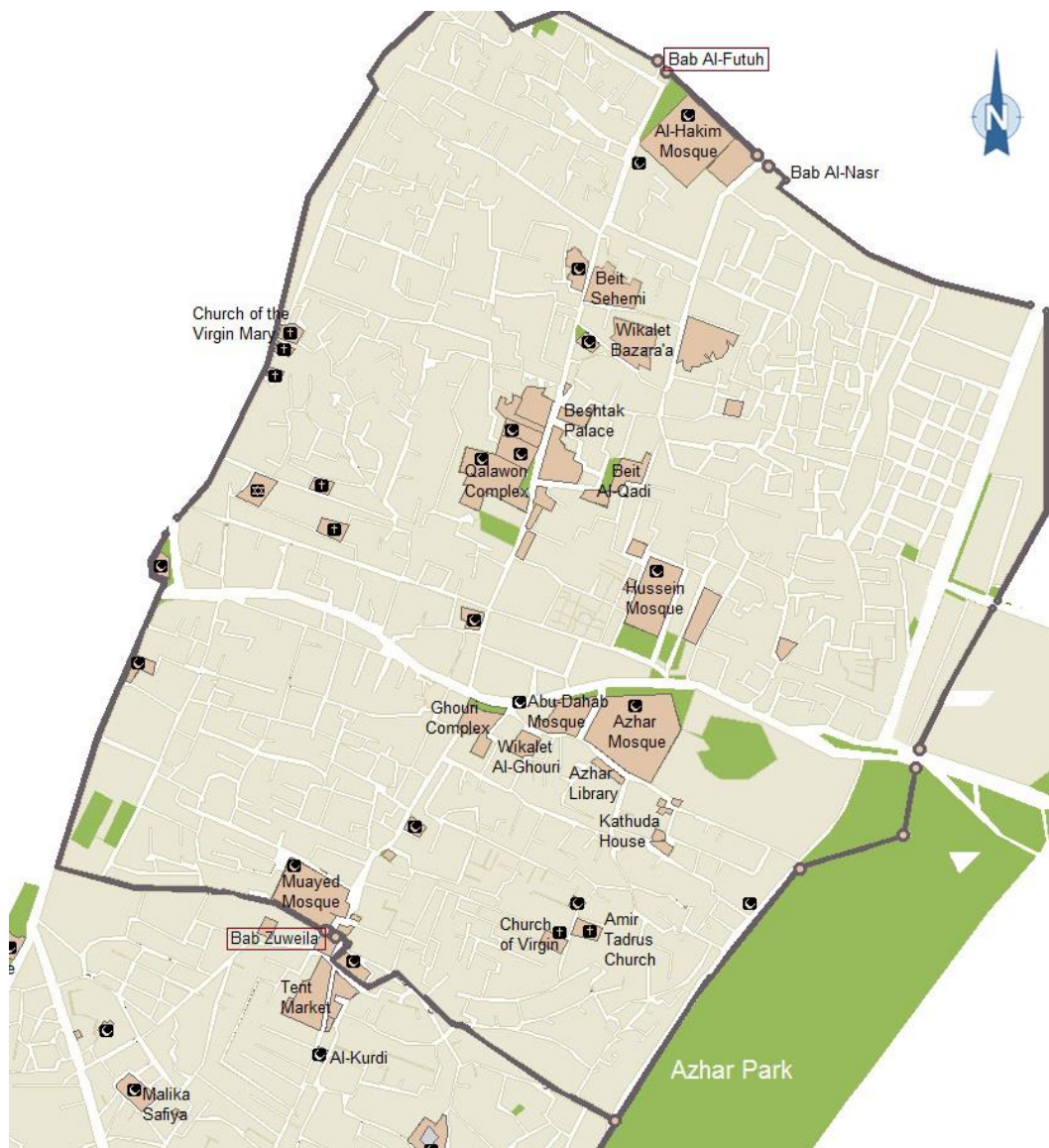


**Figure 0-2A** Cairo development, starting from Al-Fustat to the north of the Roman fort Babylon in 641AD (on the right) (source: <http://www.studiobasel.com/publications/books/nile-valley.html>)



**Figure 0-3A** The plan of Fatimid Cairo and its location to previous settlements (source: <http://www.studio-basel.com/publications/books/nile-valley.html>)



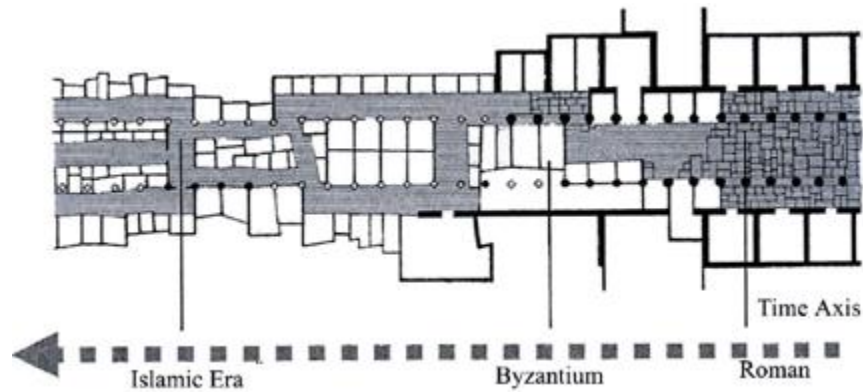


**Figure 0-4A** The Al-Muizz spine and Gate Al-Futuh in the north, and Zuweila in the south (Mortada, 2003)

### **Al-Muizz Street urban pattern type**

As stated by Vorgelegt and Jaber (2013), it has been acknowledged that the most complex and far-reaching changes in urban design between the Greek and Roman periods and the emerging Muslim cities in late antiquity and the early Islamic period were the altered street layout, as shown in Figure 0.5A. This change was from large central avenues that crossed at right angles in Hellenistic times in cities of Syria, to an

irregular, narrow, winding pattern, such as that seen in Al-Muizz Street in Cairo. The understanding of different pattern effects is essential, especially since the beneficial climatic effects of numerous traditional solutions have been questioned. These solutions may reflect culture specifications rather than climatic Daptation (Giovani, 1997). To comply with the study objective, Al-Muizz Street's urban pattern formation and its physical development requires analysis.



**Figure 0-5A** The transformation of a colonnaded street in the early Islamic era, as merchants started erecting their booths along the main pedestrian flows, first as temporary, then as permanent structures (source: Bianca 2000, p.127, original drawing by Sauvagat)

#### **Al-Muizz urban pattern under the Fatimids (969-1171AD)**

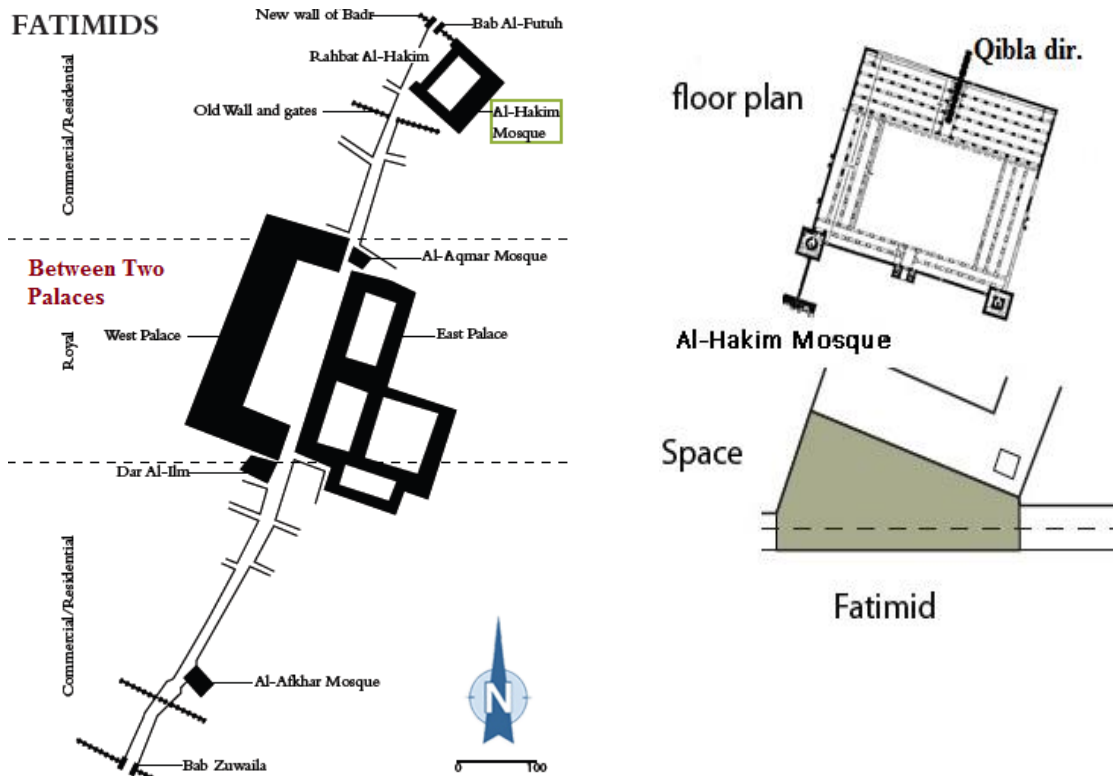
Al-Muizz Street was founded in 969AD by the Fatimids. At that time, it is possible to assume that Al-Muizz Street was at its widest, at approximately 18-23m, and was served by secondary streets approximately 7-9m wide (Al-Tabari, 1963; Al-Sayyad, 1991). The street tended to be broad to fulfil public functions, and recent archaeological evidence suggests that even the narrow streets of Fustat were widened by the Fatimids (Scanlon, 1981). In his book *The Streets of Islamic Cairo*, Al-Sayyad (1981) examined the development of Al-Muizz Street. The street was composed of three segments by that time, with a major segment in the middle, as a royal space, between the two palaces; its main function was for ceremonies and public occasions. The other two segments acted as an introduction to the major ceremonial route in the core. All three segments were composed of palaces, mosques and shops and performed different functions ranging from residential to commercial. According to Al-Maqrizi, the size of the area between two palaces was such that ten thousand troops, both cavalry and soldiers, could be marshalled on it (Lane-Poole, 1902). Despite the space between the two palaces, there were no major nodes for urban activities along the

street except those near the gates. The space in front of Bab Zuwayla has been reported to be a node of commercial activity, while the space inside Bab Al-Futuh was used as a meeting place (Figure 0.6A).

In earlier Muslim settlements such as Al-Fustat and Al-Qata'i, they started with a mosque in the centre, around which the city then started to grow (Amr Ibn El ass Mosque and Ibn Tulun Mosque). However, this was not the case in Fatimid Cairo, where the palaces were designed to occupy the core, while the main mosque Al-Azhar was in a peripheral location. This in turn affected the internal city structure and, accordingly, Al-Muizz Street acted as a network to connect the palaces with the city gates and the main mosques.

Building density was low in those quarters for the administrators, and a great deal of land within the ownership plots was allocated to private stables and orchards. There is no adequate archaeological evidence to determine the percentage of built up land to open space or how the residential buildings were arranged. Both residential and secular buildings were arranged perpendicular to the street pattern. However, the most prominent building arrangement was the religious buildings, as the main influencer for the orientation of these buildings is the Qibla direction, as shown on Figure 0.6A. Also, it should be noted that these structures were built before the street pattern had been fully planned, so there were no restrictions on their form, and as a result the abundance of space in and outside the Fatimid city enclosure did not interfere with the awkward angles of these structures. The only mosque that did not follow this rule was the mosque of Al-Aqmar, which is considered by some scholars to be an important development in Islamic urban architecture in Cairo, as it is the earliest building whose facade was adjusted to the line of the street (Al-Sayyed, 1981). None of these mosques appear to have influenced neighbouring plots and buildings during this time.

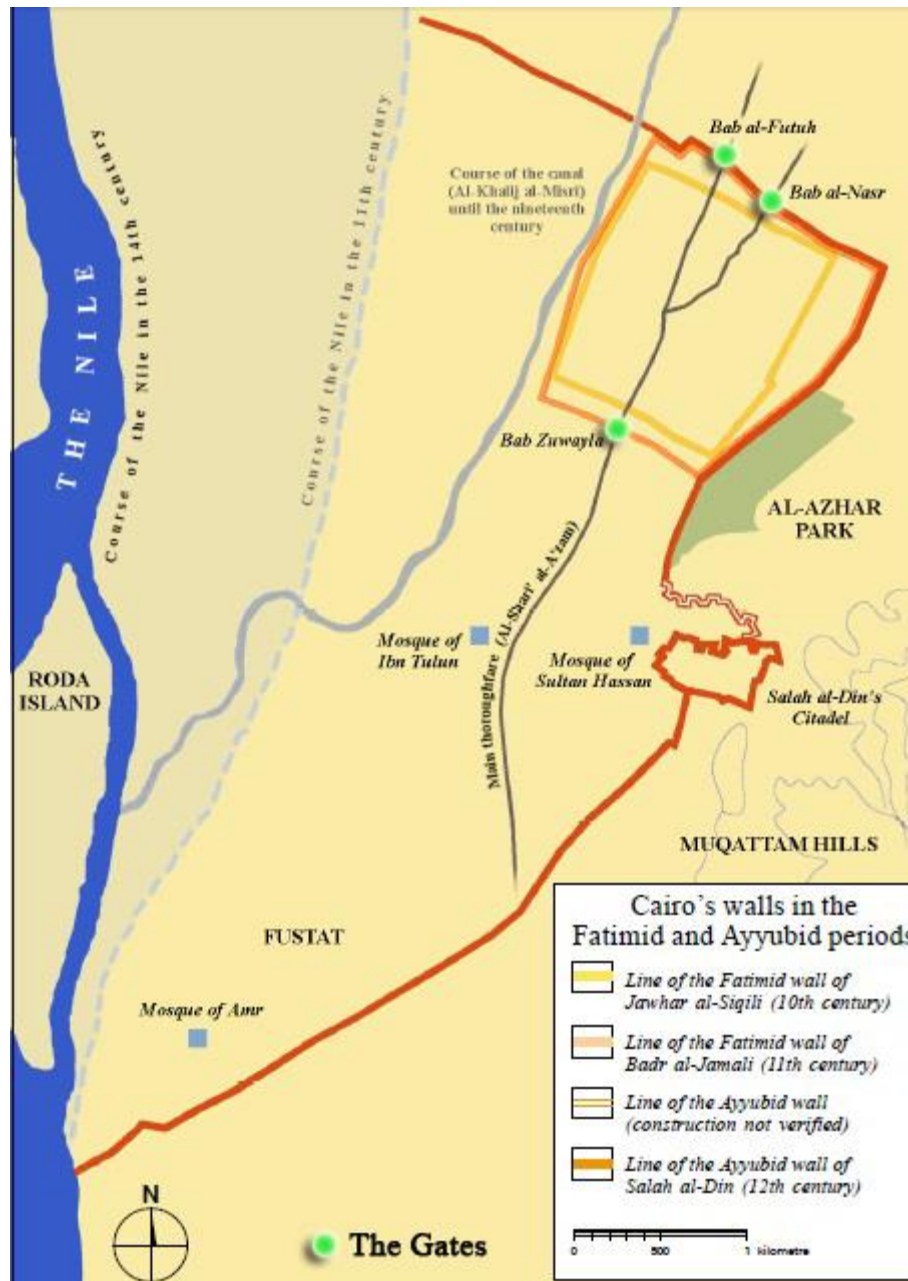
There was a variety of urban proportions within Fatimid Cairo; the mosques walls were not too high and did not have what is called monumental dimensions. The dimensions of the walls indicate a tendency towards a human scale, yet the overall scale judgement is hard to achieve due to the lack of information about the spaces in front of them.



**Figure 0-6A** The Al-Muizz spine and the area between the western and eastern palaces (on the left). The Qibla direction was a main influencer for the street orientation (on the right) (source: <http://www.studio-basel.com/publications/books/nile-valley.html>)

### **Al-Muizz urban pattern under the Ayyubids (1171-1252AD)**

Under the Ayyubids, the walls enclosing Cairo proper were once again extended. The extensions were limited to the eastern and western walls, in which six new gates were constructed. The Al-Qantara Gate was extended, along with Al-Sa'ada Gate, and a new gate, Al-Khokha, was constructed. Al-Muizz Street lay between the two walls and became known by its literal translation of Bein Al-Surein (between the two walls) (Figure 0.7A). On the eastern wall, a new gate called Al-Mahruq Gate was added, and Al-Barqiya Gate was extended, with the wall then stretching northwards; a new gate was believed to have been constructed called Al-Gedid Gate, but this remains a tentative point.



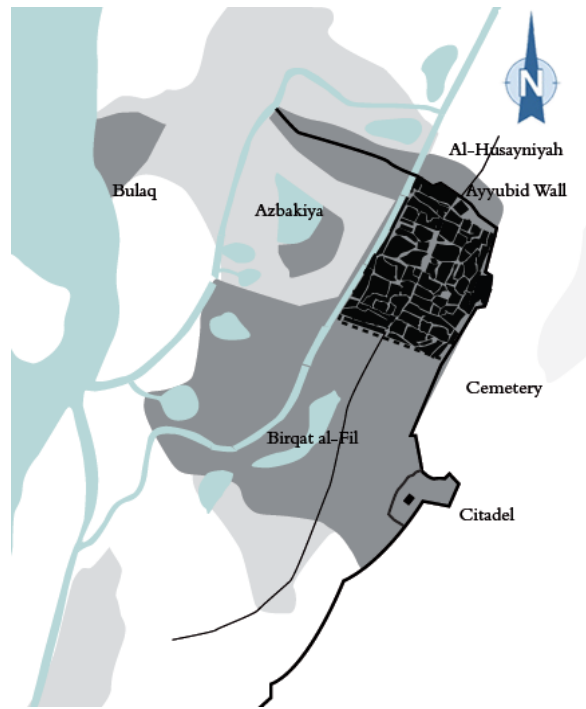
**Figure 0-7A** The expansion of Cairo's town plan under the Ayyubids (source: HCSP technical report)

Al-Muizz Street underwent its most severe change during the time of the Ayyubids due to the arrival of a large number of residents. This urgent need to provide shelters meant that buildings were constructed without sufficient regulation by the state. As a result, the street pattern changed dramatically from the original wide streets of the Fatimid city, as shown in Figure 0.3A, into a very dense urban pattern, as shown in Figure 0.8A. It is easy to expect that because Al-Muizz Street was one of the widest streets during the Fatimid's era, it had its share of that development. People started to build in the spaces between the former detached palaces and their gardens. Most of the

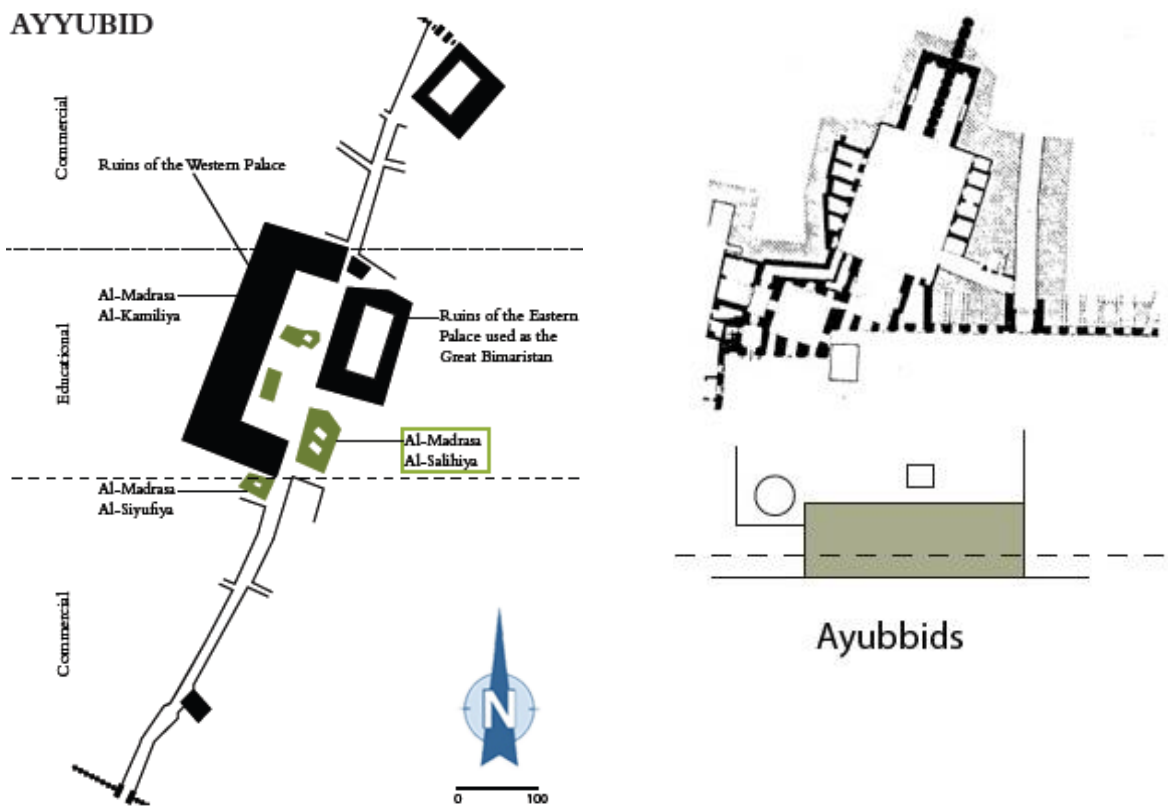
villas were converted into commercial structures. Some parts of the Fatimid Palaces have been used as hospitals, while the spaces between them were occupied with some schools. The three Fatimid segments were retained but with different mixed functions (commercial, educational and cultural), while the continuity of the street from Zuwayla Gate to Al-Futuh Gate was achieved. A number of major nodes for urban activities such as market places and meeting places along Al-Muizz started to appear, and yet the area between the two palaces is still the main node in Cairo. Al-Muizz remained the major thoroughfare in the city attracting all the major markets (Figure 0.9A).

Unlike in the Fatimid era, the religious structures built by the Ayyubids had their exterior facades parallel to the centre line of the street, even though the interior was bent to orient the prayer hall towards the Qibla. They were recessed to create spaces in front of them, signifying an important structure whilst also shaping the streetscape (Al-Sayyad, 1981). The exterior walls were usually short and of human proportion (Figure 0.9A). On the other hand, commercial and residential buildings lay perpendicular to the main streets concentrated along the thoroughfares, between the public buildings. Public and commercial buildings tended to occupy the entire plot of land with shops aligning the street frontage and the inner courtyard. Residential buildings up to five and six storeys were very common, creating a feeling of narrowness along the street to increase their inward looking nature onto a main courtyard for ventilation and light.





**Figure 0-8A** The narrow street pattern under the Ayyubid dynasty (source: <http://www.studio-basel.com/publications/books/nile-valley.html>)



**Figure 0-9A** Mixed land use pattern of Al-Muizz spine under the Ayyubids (on the left), and the schools and religious buildings had exterior walls parallel to the street centre line (on the right) (source: <http://www.studio-basel.com/publications/books/nile-valley.html>)

### **Al-Muizz urban pattern under the Mamluk (1252-1517AD)**

The Mamluk generals, who were originally slaves serving as soldiers in the Ayyubid army, used their power to establish a dynasty that ruled Egypt and Syria from 1250 to 1517AD. Historians have traditionally broken the era of Mamluk rule into two parts, starting with the Bahri period covering 1252-1382AD, and then the Burji from 1382-1517AD; this calls attention to the change in the ethnic origin of the majority of Mamluks.

#### **Al-Muizz urban pattern during the Bahri Mamluk**

The Mamluk period saw a continuation of the original plot pattern during the Ayyubids by constructing a new building in the area between two palaces, which was repeated during the time of the Bahri Mamluk. Three schools were constructed between the earlier Ayyubid ones in addition to the famous Qalawun complex, which was built by the Bahri Mamluk. The sequential structure of the spine was almost maintained except for new functions, which were added to the node between the two palaces, creating a separate internal district with a number of new landmarks. The Bahri Mamluks thus created the character that Al-Muizz Street was to maintain for the following centuries (Al-Sayyed, 1981). The street was irregular, 6-7m wide, and seemed to have three major spaces, one in the middle segment and one at each end. Major buildings were located in the middle segment and surrounded these major spaces (Figure 0.10A).

The way the Bahri Mamluk dealt with the shaping and treatment of the exterior elements had a great impact on the evolution of irregular spaces of different widths along the street. Twelve out of 14 major schools and mosques built at that time had staggered exterior facades with at least one side parallel to the street centre line (Figure 0.10A). These facades had coloured brick courses and large openings, and a few steps were used for the first time in front of the mosque entrances, which were mostly either recessed or lined up with the facades.

#### **Al-Muizz urban pattern during the Burji Mamluk**

By the time of the Burji Mamluk, Al-Muizz Street as a main spine of the city was already filled with numerous buildings from the Fatimid, Ayyubid and Bahri Mamluk eras. Therefore, the Burji Mamluk had to find another way to build around



these plentiful monuments, which had a major influence on Al-Muizz Street's pattern. The Burji Mamluks attempted to shift the current major node of the street from the area between two palaces, by their construction of the Al-Ghuri complex. Their addition of other monuments along the path has enriched its structure. Most of the spaces created along the path were either in front of Burji Mamluk structures or in front of older structures renewed by the Mamluks. It is therefore suggested that the hierarchy of spaces along the street was probably generated during the rule of the Burji Mamluks. They conducted a policy of decentralization in which buildings were constructed in huge complexes in well-chosen vacant spaces along Al-Muizz in an attempt to change the existing physical node of the area between the two palaces (Figure 0.11A). The same design of spaces created by the Bahri Mamluk continued during the Burji yet it was smaller in size and embraced by buildings. The narrow streets were sectioned off with gates for privacy and security against strangers and thieves (Wiet, 1964).

The lack of available space meant that religious and school buildings had to be smaller than the earlier ones, the central open courtyard was eliminated (Wiet, 1964), and the exterior facades were neither parallel to the street centre line nor perpendicular to the Qibla direction, as shown on the right hand side of Figure 0.11A. Commercial buildings such as *khans*<sup>18</sup> and *wikalas*<sup>19</sup> were arranged perpendicular to the street, around a central courtyard, and occupying the entire plot. The common appearance of the *rab*<sup>20</sup> in the Mamluk period was used as a revenue generating building, occupied by shops on the ground floor, with two to three bedroom apartments on the top storeys.

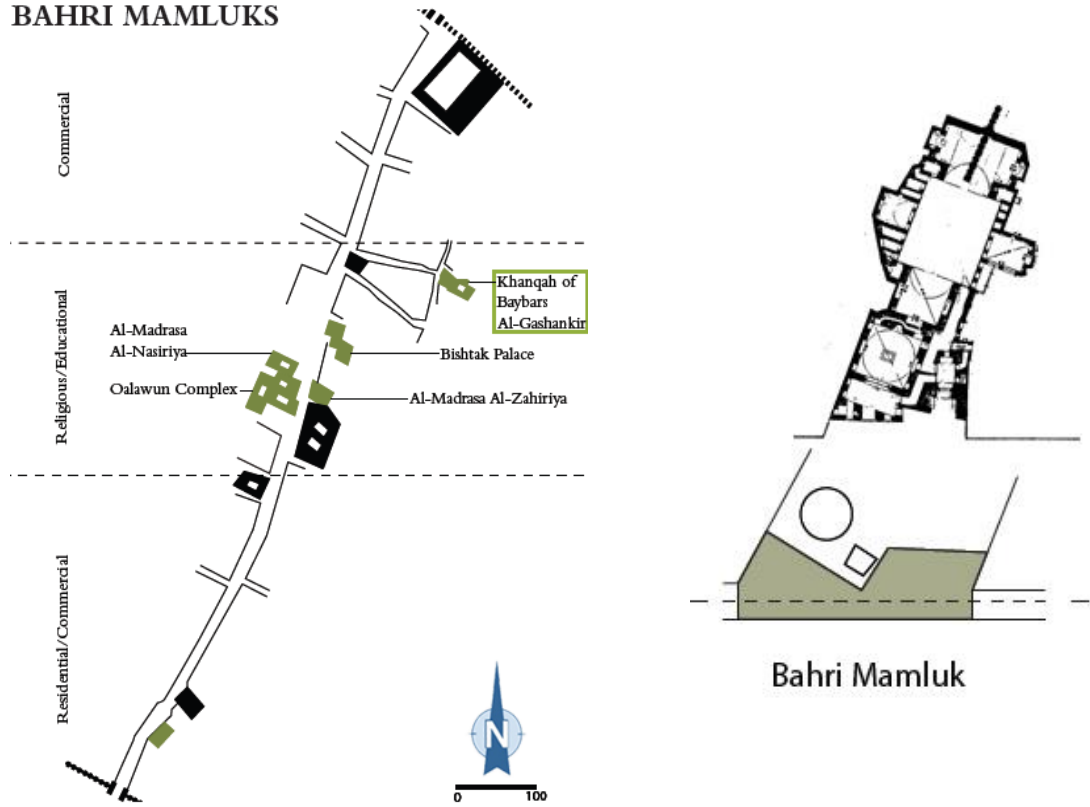
---

<sup>18</sup>Hostel/ commercial buildings with special places assigned for the main groups of craftsmen or traders.

<sup>19</sup> A building specialised in storage of local and international commodities, accommodating itinerant traders in the upper storeys.

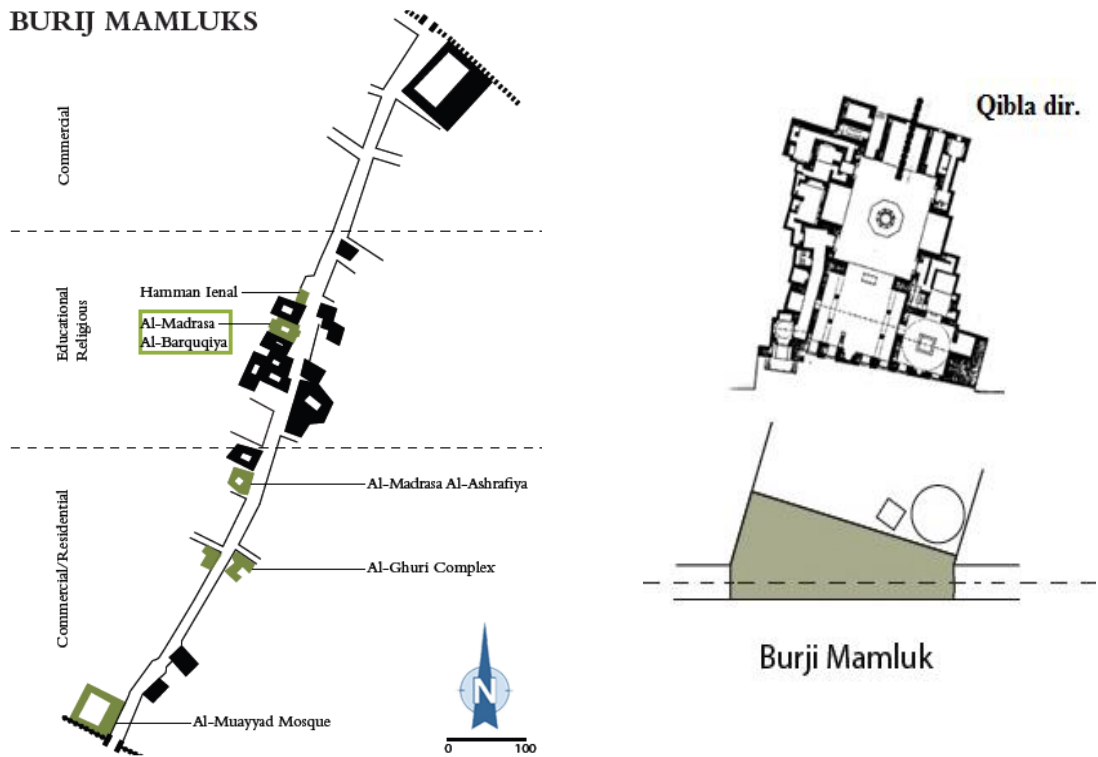
<sup>20</sup> A common building type in the middle ages with the upper storeys consisting of permanent lodgings and a separate entrance and little courts, while the ground floor was let out as shops.

**BAHRI MAMLUKS**



**Figure 0-10A** Mixed land use pattern of Al-Muizz spine under the Bahri Mamluk (on the left), and the exterior walls treatment to the street centre line (on the right) (source: <http://www.studio-basel.com/publications/books/nile-valley.html>)

**BURIJ MAMLUKS**



**Figure 0-11A** Mixed land use pattern of Al-Muizz spine under the Burji Mamaluk (on the left), and the exterior walls' treatment to the street centre line (on the right) (source: <http://www.studio-basel.com/publications/books/nile-valley.html>)

In conclusion, Cairo had become a 'prototypical' Islamic city as shown in Figure 0.12A, with an established market network, an irregular street pattern, and a citadel. Raymond (1993) attests to the size of Cairo's markets during the Mamluks, as he maintains that between the northern gate of Bab al-Futuh and the southern gate of Bab al-Zuweila was a surface area of 38 hectares within which was a total of 48 markets and 44 commercial houses. The streetscape was characterised by small shops that constituted the markets. Wiet (1964: 71) describes the shops in the northern part of Al-Muizz Street. Here, it is lined by mysterious portals, there by shops, some of which are of such tiny dimensions that they look like large cases with one side removed so as to expose the interior. In front of the shop is a stone bench or little platform as long as the shop entrance and wide enough for a man to sit on.



**Figure 0-12A** Transformation of Fatimid Cairo under the Mamluk dynasty (source: <http://www.studio-basel.com/publications/books/nile-valley.html>)

**Al-Muizz urban pattern under the Ottoman Cairo (1517-1805), including the French expedition (1798AD)**

By the time of the French Expedition in 1798 AD, Cairo consisted of three separate but functionally related communities: the walled city with its extensions (where Al-Muizz Street is located), plus the two port suburbs of Bulaq and Misr Al-Qadima (the name given to the former Fustat, as shown in Figure 0.12A). During the Ottoman period between 1517 and 1805, the city had expanded extensively, with the development of two new neighbourhoods along the western border of the walled city, known as Al-Azbakiya and Birkat Al-Fil, as shown in Figure 0.13A. With these new developments came the movement of the elite class out of Al-Muizz and the walled city leaving a social vacuum, as described by Raymond (1993), who stated that between 1496-1517 only 15% of the elite residences were left in central Cairo. The older aristocratic zone within the walled city left mansions vacant and buildings quickly deteriorated to be replaced with commercial houses and the residence of the new bourgeoisie of powerful merchants.



**Figure 0-13A** Under the Ottomans, Cairo became a provincial capital. The old part of the city became less important as the centre moved toward Azbakiya and Birkat Al-Fil (source: <http://www.studio-basel.com/publications/books/nile-valley.html>)

By the end of the Ottoman period, the Al-Muizz street pattern appears to have stabilised with minor buildings being added to, either along the empty segments of the path or in areas of previous buildings (Al-Sayyad, 1981). In addition, there was the creation of a new internal district located between Al-Silehdar Mosque and Al-Aqmar Mosque named Al-Nahassein in Al-Muizz which specialized in the production of metal crafts, especially copper. Concerning the space structure along Al-Muizz according to the first reliable map generated by the French (Figure 0.14A), it can be noticed that, firstly, the number of public spaces increased but were smaller in size as a result of the informal construction which took place inside these spaces. Secondly, the system of streets was regular, open in the centre, more tortuous, and often closed in residential regions (Nasser, 2000). Thirdly, ‘atfa’<sup>21</sup> or a blind alley became much more common in Al-Muizz street due to security issues. In general, the Al-Muizz Street

<sup>21</sup>A passage that formed part of a circulation unit that provided access to a group of dwellings.

pattern can still reveal its Fatimid origins spatially as part of the organisation of the city. However, streets were much narrower and many streets were shorter, with a greater number of streets being sealed off by encroaching buildings.

Most of the large spaces created in the preceding dynasties have either disappeared or been replaced by informal structures; as a result, it was impossible to find any vacant land within the walled city, so it was normal for Ottomans to rebuild over the ruined monuments. This may explain why most of the Turkish mosques built inside the walled city had very small spaces in front of them, with seven out of ten having exterior facades that had no relation to the centre line of the street or to the direction of Qibla; however, the facades were very elegant and with large openings (Al-Sayyed, 1981), as shown in Figure 0.15A. This illustrates the relation between the mosque's main exterior wall and the centre line of Al-Muizz Street.

Residential buildings became much smaller due to the high value of land and the displacement of residential functions by commercial ones. The high density of the smaller residences meant that there was no garden or stable, but instead a large central courtyard. Houses occupied the entire plot, and were built wall to wall, facing inwards for privacy, with the need for open space being fulfilled by the central courtyard. On the other hand, commercial buildings, public paths, shop compounds, and apartment blocks remained in the same form, with new shop compounds (*wikala*) constructed aligning the major streets, and traditional designs of central courtyards.

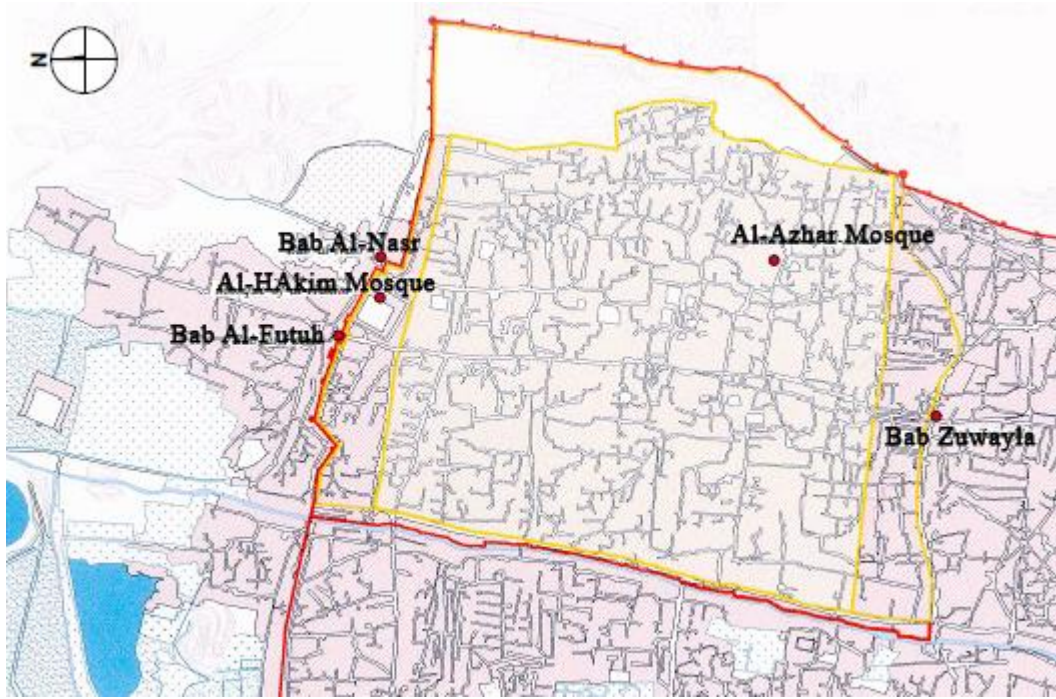


Figure 0-14 The Fatimid Cairo urban fabric in 1800 (based on the Description de l'Egypte map, 1980)

OTTOMAN

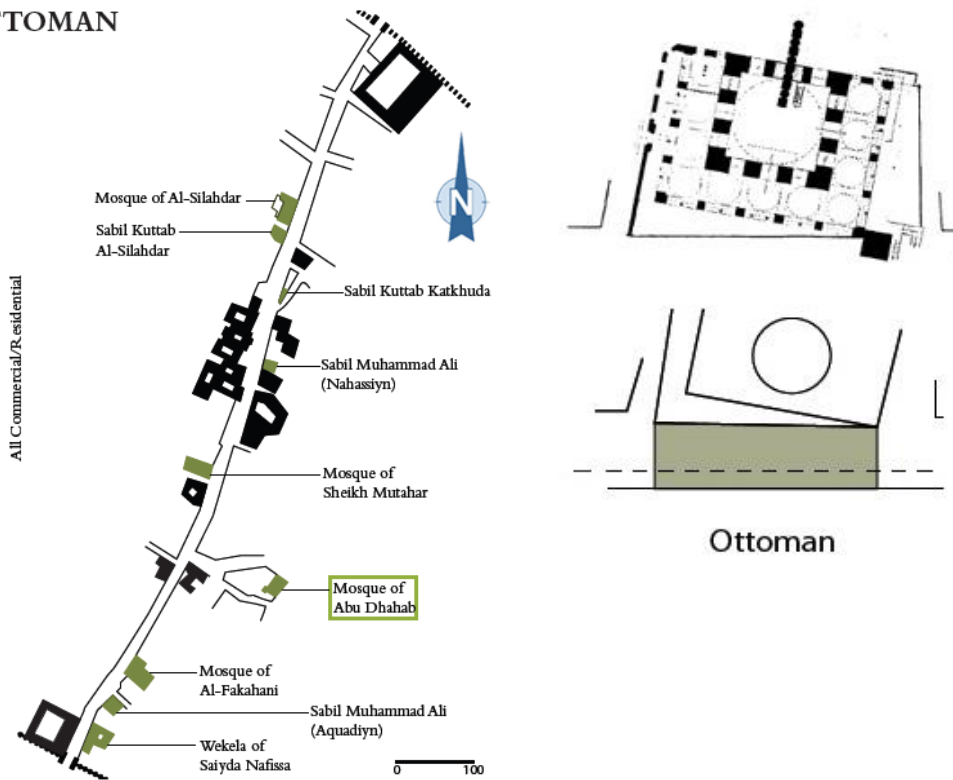
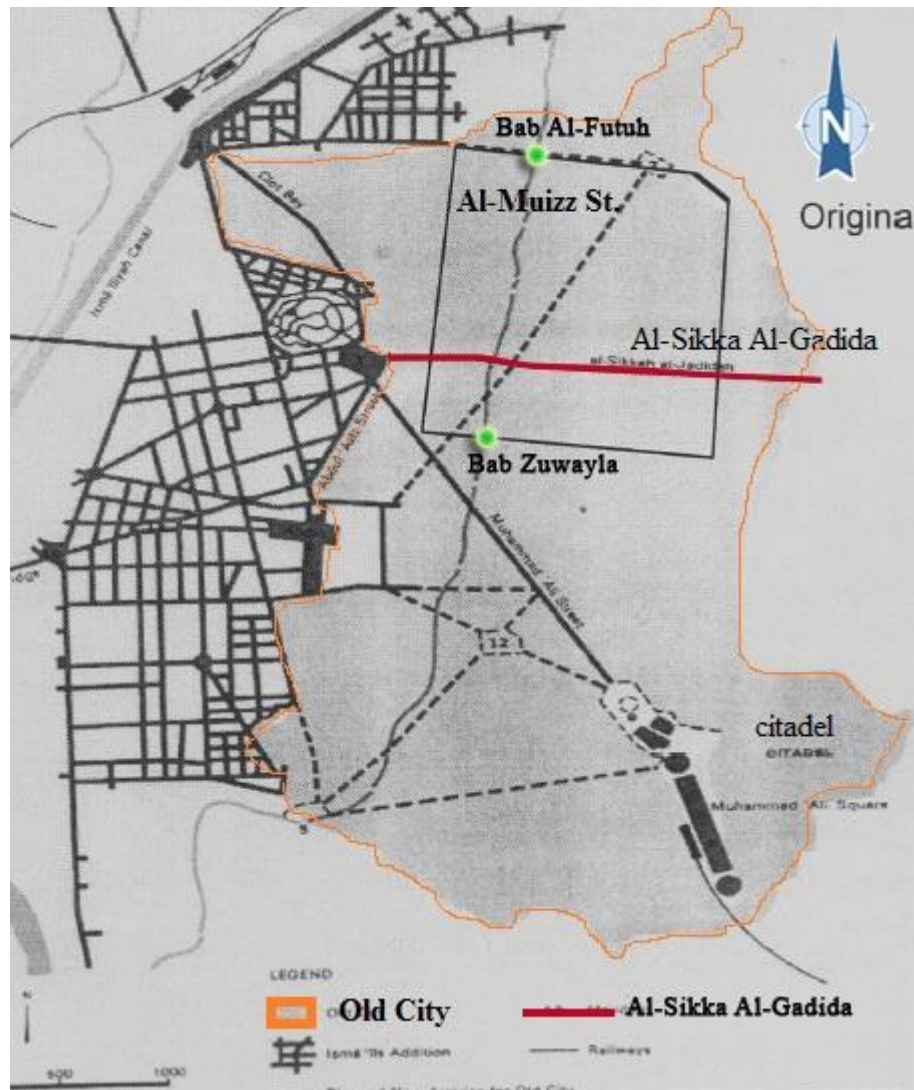


Figure 0-15A Mixed land use pattern of the Al-Muizz spine under the Ottomans (on the left), and the relation between the religious building exterior walls to the street centre line (on the right) (source: <http://www.studio-basel.com/publications/books/nile-valley.html>)

### **The Effects of Modernisation on the Historic City of Cairo**

The modern era is identified by Mohammed Ali's rise to power in 1805, with a vision to modernise Egypt and create modern institutions parallel to the traditional ones. The walled city, with its convoluted street system, could not possibly support the needs of such large scale developments (Nasser, 2000). This led to a gradual shift from the walled city into Bulaq as a new residential area to the north and discontinuity between Cairo's past and future architectural value (Abu Lughod, 1971). Once again, the old city with its irregular roads and poor infrastructure could not fulfil Khedive Ismail's (1863-1879) dream, and his era is described by historians as the first modernisation attempt since Mohammed Ali. Therefore, the old city experienced further neglect and isolation. By that time, Egypt's population was experiencing its first increase in the modern era after centuries of decline. Therefore, new residential districts were constructed; Ismailiya and Azbakiya in the west were developed; Garden City was developed along the Nile; Heliopolis to the east; Ma'adi to the south, and the Nile river island of Gezira was also developed. European-style villas were the dominant residential style, reflecting the shift to European values. Cairo became divided into two realms depicted as east/west or traditional/modern, each defined in stark contrast to the other (Stewart, 1999). In late 1870s, and due to the construction of new residential districts to face the first rapid population growth, there was a pressing traffic problem which was solved by extending Al-Muski Street. It was first named Al-Sikka Al-Gadida and was started by Mohammed Ali. He split Al-Muizz Street and the walled city into two parts, so that it became the first modern street in the walled city (Figure 0.16A).





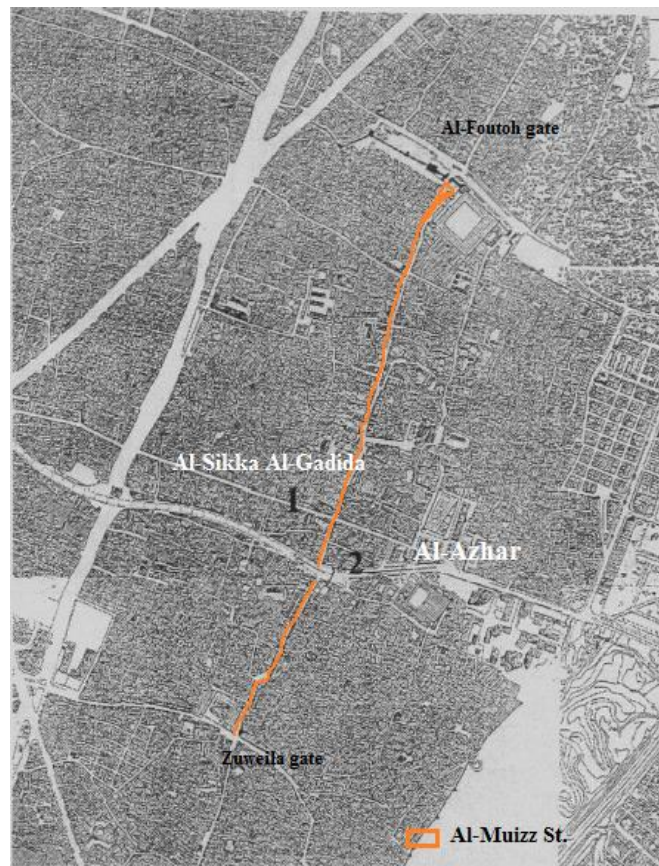
**Figure 0-16A** The city developments added by Ismail (1870)

### **British Occupation (1882-1956)**

Under British rule (1882-1956), Greater Cairo expanded along the lines laid down by Ismail.

The social and functional division of the city became more severe between the old and new parts (Stewart 1999). The explosion of vehicular traffic in the 1930s and 1940s encouraged the widening and cutting of new streets to ease circulation in the city (Nasser, 2000). Among these was Al-Azhar Street; it constructed in the late 1920s and was at first built at the expense of and for the use of the Tramway Company. Nowadays, it is one of the most congested streets and moves traffic from the central Cairo business district to Heliopolis (a northern suburb of Cairo). Passing through the old city, it has divided it into the north section that consists of Khan al-Khalili and Al-Foutoh Gate,

and the southern section from Al-Azhar Mosque to Zuweila Gate, which is part of the Darb Al-Ahmar district (Figure 0.17A). Almost entirely disconnected, each district has become self-contained with limited movement between. However, the old city remained neglected with a fixed area and ruined infrastructure. Nevertheless, the good part of being isolated or neglected was that the historic city was almost preserved intact, with the exception of the two main roads, Al-Sikka Al-Gadida and Al-Azhar, which cut through the dense urban fabric. Not just physical preservation, but social and economic preservation existed until very recently (Nasser, 2000) (Figure 0.13A).



**Figure 0-17A** Al-Sikka Al-Gadida (1) and Al-Azhar (2) streets cut across the dense urban fabric Al-Azhar, dividing Khan Al-Khalili and Al-Foutoh Gate to the north, and the southern section from Al-Azhar Mosque to the Zuweila Gate in the south

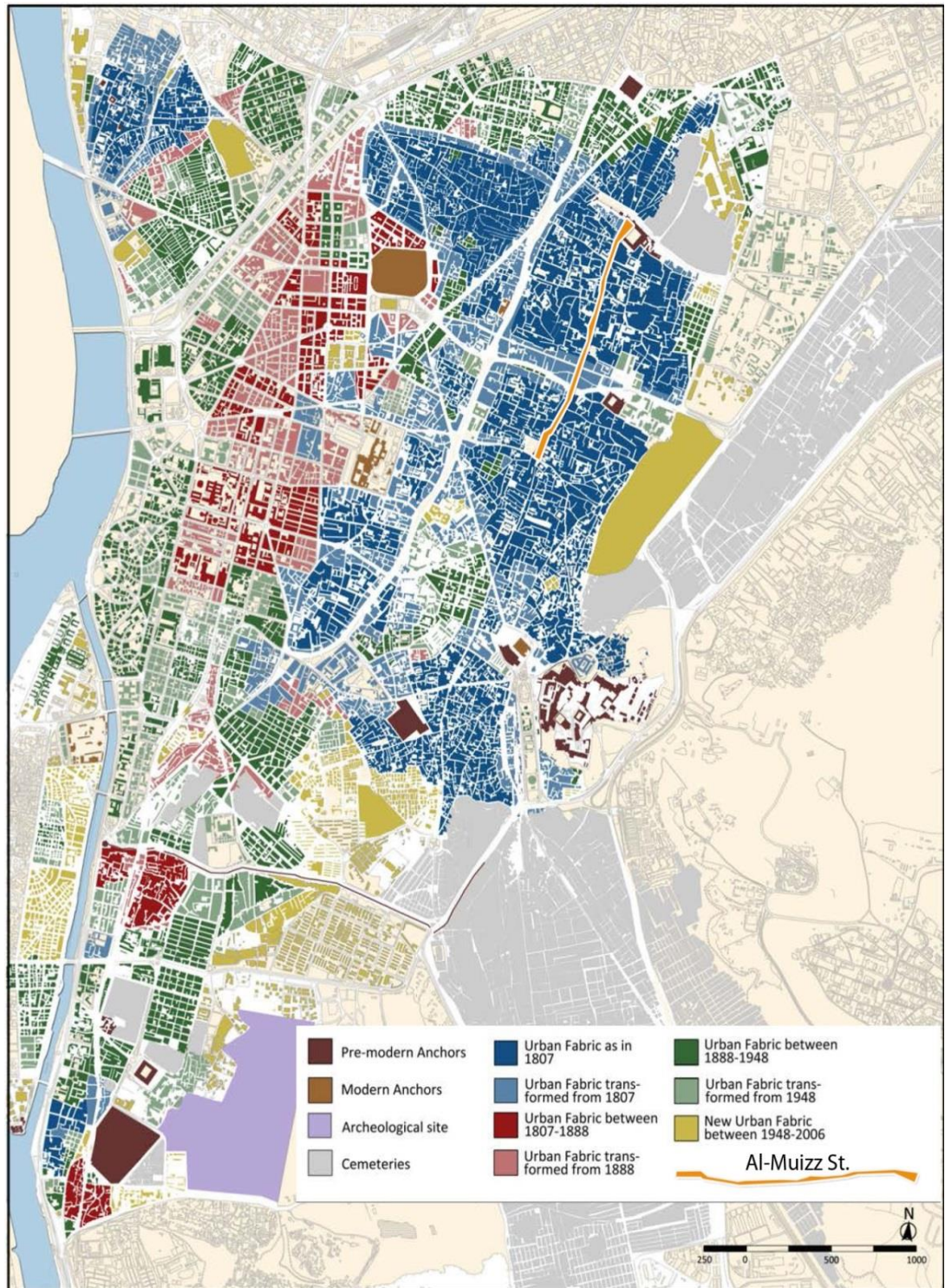
### **The Free Soldiers Revolution 1952 – until being officially listed as a world heritage site**

After the 1952 revolution and during the Nasser Era, the district continued its deterioration as a result of policies that forced land reforms and intensive and unsympathetic construction. Historic buildings were subjected to rent freezes, leaving little capital for maintenance and repair. This led to the rapid deterioration of several

buildings (Amedi et al., 2009) until 1974, when Al-Sadat came to power as Egypt's second president. The government implemented what was known as an 'open-door' policy in which foreigners were once again permitted to visit Egypt, since the doors were closed in the Socialist revolution of 1952. Therefore, the country faced a dramatic rise in tourists who were fascinated by visiting historic Cairo; this new policy awakened interest in the conservation of the heritage sites from an economic point of view. These changes have had an impact on the economic and social structure of the old city, particularly in commercial enterprises such as Khan Al-Khalili market within Al-Muizz Street and on small-scale manufacturing in the peripheral parts of the old city (Meyer, 1990). By the end of President Sadat's era, UNESCO recognised the advantage of tourism within the Egyptian context. In 1979, UNESCO declared Old Cairo a world heritage site and produced a generic development plan for the whole area. The medieval economic function changed from transit trade to the tourism industry, leading to the challenge of improving the built environment of the Islamic city once again by safeguarding its historical and cultural qualities as assets and sources of income.

Figure 0.18A shows a comparison between the most recent maps of Cairo (CAPMAS, 2006) and the map of the French Expedition (Cairo in 1807). This reveals that the pre-modern fabric kept its main attributes (focal points, street patterns, built-up areas and voids) throughout the development in the 19th century.





**Figure 0-18A** Urban fabric modification between 1807-1888, 1888-1948 and 1948-2006 (Source: URHC and UNESCO)

- **Al-Muizz as a World Heritage Site (WHS)**

Historic Cairo was inscribed on the World Heritage List in 1979 under the title of “Islamic Cairo,” recognizing its absolutely unquestionable historical, archaeological and urban importance. On the recommendation of the International Council for Monuments and Sites (ICOMOS), its inscription was based on criteria I, V and VI of the World Heritage Operational Guidelines, including the following justifications:

- (I) Several of the great monuments of Cairo are incontestable masterpieces
- (V) The centre of Cairo groups numerous streets and old dwellings, and thus maintains, in the heart of the traditional urban fabric, forms of human settlement which go back to the Middle Ages
- (VI) The historic centre of Cairo constitutes an impressive material witness to the international importance, on the political, strategic, intellectual and commercial levels of the city during the medieval period.

The site was described as an historic fabric covering an area of around 32 square kilometres on the eastern bank of the River Nile and surrounded by the modern quarters of Greater Cairo, where vast areas are still intact and many focal points have emerged, starting with Al-Fustat in the south. These also include the mosque of Amr Ibn Al-As (founded in 641), Babylon, with its Coptic churches, the mosque of Ahmad Ibn Tulun (founded in 876), the Citadel area, the mosque of Sultan Hasan (1356-1359), and Darb al-Ahmar with Mamluk and Ottoman monuments. There is also the Fatimid nucleus of Cairo from Bab Zuwaila to the North Wall with the city gates of Bab Al-Futuh and Bab an-Nasr.

#### **The Islamic quarter heritage conservation overview**

The extent of heritage preservation in Egypt is usually related to the ruling system. The first preservation effort took place during the period of French colonialism by Napoleon in 1798, and the production of the well-known book ‘Description de l’Egypte’ in 1809, which included the first reliable map of the urban fabric of Fatimid Cairo. By 1881, Khedive Tawfiq established the Comité de Conservation des Monuments de l’Art Arabe, as the first attempt to identify buildings of historical and architectural significance in historic Cairo (Lamie, 2005; Aslan 2007). The main task was to survey and record the valuable architectural buildings and, in addition, conduct a physical investigation to demonstrate the

architectural value with full, as-built drawings. However, the greater part of indexing was under the initiative of King Fouad in 1930; hundreds of architectural structures and remnants were indexed based upon the intrinsic criteria of architectural beauty or age. The Comite's approach was in accordance with the SPAB manifesto (the Society for the Protection of Ancient Buildings). Founded in 1877, listed buildings were to be restored to the authentic style of their historic period with their authentic materials preserved *in situ*. The major achievement of the Comite was to restore the building elements (columns, windows, doors, and pillars). Their efforts focused on rich historic complexes such as the Qalawun complex in Al Muizz Street. In addition, the Comite had a different vision for the ruined monuments by cutting them down to be presented as valued pieces in the Museum of Islamic and Coptic art (Stewart, 2003).

Since the revolution in 1952, the process of selecting buildings has transferred from the Comite to the establishment of the Egyptian Antiquities Organisation. However, the last of the monuments was undertaken in 1951 due to the political and military challenges the nation was facing in the region (Aslan, 2007). Thus, in 1997 and after the historic core of Cairo was listed as a WHS in 1979, the Technical Co-operation Office (TCO) administrated another survey where they found that since the last index in 1951, 65% of the buildings on the index had been destroyed or were seriously deteriorated, while others still needed to be added to the list. According to the TCO report, there were some 1,200 historic buildings in Cairo and by 1951, the list had been reduced to 622. Today, there are a total of 527 monuments (including 100 'new' listings added since 1951). This remarkable changed occurred during the President Sadat era, when the open door policy was adapted and foreign missions were encouraged to interfere in the conservation process with the issuing of Decree 2828. This stated that the Supreme Council of Antiquities was responsible for working with foreign organizations under the supervision of the Ministry of Culture. As a result, a number of foreign missions and other organisations have been associated with the restoration of various monuments. However, these missions are reluctant to become involved in extensive restoration programmes and subsequently attention tends to focus on small projects related to buildings with architectural and/or aesthetic significance, and occasionally political significance, such as the Al-Hakim Mosque that has historically been associated with the Ismaili Shi'ite sect. However, according to the Community Design Collaborative (CDC) (1997), the general quality of the

urban fabric, comprised of significant groups of facades, streetscape elements, open spaces and green areas, is without recognition. This is because there are numerous buildings which still enhance the historic area as a whole even though they do not possess exceptional architectural features; they are thus unprotected from demolition and uncontrolled transformation. Moreover, not all the indexed monuments benefit equally from restoration efforts; these are focused only on those monuments which are the most popular with tourists and which are located in easily accessible sites, or are religious buildings which have never been in danger of demolition as they still have a daily function in the life of an orthodox Islamic society (Nasser, 2000). All these reasons gave Al-Muizz Street the priority to be labelled as the 'Heritage Corridor' in proposals by both UNESCO (1980) and the Technical Cooperation Office (1997), as it contains the greatest concentration of medieval architectural treasure in the Islamic world (UNESCO Technical Report, 1985). Since then, generic development plans for the whole area have been produced.

#### **UNESCO Study, 1980: "The Conservation of the Old City of Cairo"**

According to the final report undertaken by the Urban Regeneration of Historic Cairo (URHC) project in 2012, an early study of Islamic Cairo was carried out by UNESCO consultants between February and August 1980. The plan generally focused on producing conservation recommendations for the whole urban setting, including traffic management, the main urban spines' traffic load, infrastructure upgrading, local awareness development, and the definition of five minor zones to produce interventions. Clearly, this was the first time a local or international body had proposed such development on an urban scale, rather than for individual historic buildings. The report indicated that each zone had to deal with its own monuments, initiate architecture design frameworks for new buildings, and introduce new uses for the old buildings and housing programmes (UNESCO, 1980). In 1983, the essential Decree No. 17 was announced for the safeguarding of the historic buildings. The policy focused on protection from deterioration and theft, in addition to setting out some criteria and regulations for dealing with foreign development organizations. Basically, the issued policies initially targeted built heritage protection without any proper urban planning development by working on singular buildings rather than the whole or even part of the historic quarter. Ghaleb and Abdallah (2003) noted that

Egyptian legislation never grasped the meaning of the historic quarter's preservation, according to policy four in 1912, until Decree No. 117 was enacted in 1983. Thus, polices were not enough to interpret UNESCO's recommendations after the declaration of Historic Cairo as a WHS. In 1992, Cairo experienced a major earthquake in which the structural integrity of many buildings within the Historic Cairo sustained major damage. As a result, national and international organizations turned their attention to the conservation issues of Egypt's built environment with reinvigorated interest. Among a conspicuous list of interventions and studies, the following should be taken into account due to their importance and impact on Al-Muizz Street.

### **Al-Darb Al-Asfar Alley Rehabilitation Project, 1994-2001**

Al-Darb Al-Asfar is an alley in the district of Gamaliya located off Al-Muizz Street, near Bab Al Futuh Gate (Figure 0.19A). In 1994, the Ministry of Culture and Supreme Culture Antiquities funded by the Kuwait-based Arab Fund for Social and Economic Development (AFSED) began the documentation and establishment of a conservation strategy for the area, which had become a neglected backwater of decaying buildings and services. The project carried out the restoration of three medieval houses in the alley, which were rehabilitated and restored and these were Al Suhaymi House (1648), Mostafa Gaafar House (1713), and Al Khorazati house, a living example of residential architecture of the 19th century. As restoration proceeded in the three houses, the surroundings were also improved. Electricity, water, and sewage systems were renovated. The alley was made a pedestrian only zone and paved with limestone. Facades of other building were painted, doors renovated, and lighting posts replaced, as seen in Figure 0.19A. They were then all allocated adaptive functions to fit within the wider development of the area (Bianca and Siravo, 2005).

The project of Al-Darb Al-Asfar exemplifies a real experiment for limited restoration, but wider conservation (Shehayeb and Abdel-Hafiz, 2006). Therefore, this phase of restoration was extended and introduced as the first rehabilitation project in historic Cairo, exceeding the single restoration of monuments by applying a renovation strategy of the landmark's background (Ministry of Culture Press, 2002).



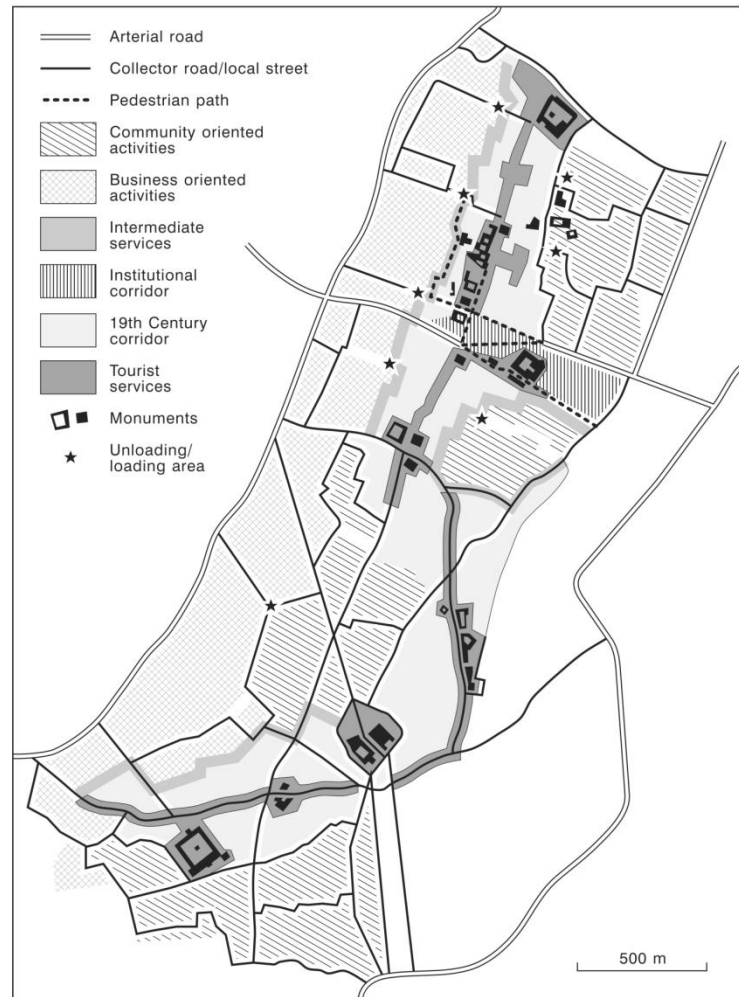


**Figure 0-19A** Al-Darb Al-Asfar Alley after restoration

### **UNDP Report, 1997: “Rehabilitation of Historic Cairo”**

The 1997 UNDP plan, which has yet to be comprehensively put into action, covered an area of about four square kilometres in Historic Cairo from Al-Futuh located in Al-Muizz in the north to Ibn Tulun mosque in the south (TCO, 1997). The UNDP, Technical Co-operation Office (TCO) framework plan was based on a rehabilitation strategy articulated in five urban areas: the heritage corridor (Al-Muizz Street), the institutional corridor, the 19th century corridor, the transformation zone, and the community zone (Figure 0.20A). Urban policies would guarantee a feasible implementation of rehabilitation strategies, while community participation was identified as another tool for protecting Historic Cairo’s outstanding value. The report provided an important reference for large-scale urban rehabilitation actions in Cairo, such as the pedestrianization of the central spine along Al-Muizz Street, labelled the Heritage Corridor (UNDP 1980), and some other streets, between 9.00am and 9.00pm, with one-way streets being suggested to ease traffic congestion. A key contribution would be ‘adaptive reuse’ of restored buildings, suggesting that a significant *sabil-kuttub* (former fountains and Quranic schools combined) be used as a tourist information centre. The plan aimed to revive the old ‘*al-fina*’ (outside courtyard) concept, whereby shops and workshops can extend their activities out on to the street in front of their premises. Therefore, streets in Historic Cairo would again consist of

central public space for pedestrians and traffic and semi-private space for use by local residents for trading and other uses. However, due to the lack of official action, Historic Cairo's safeguarding efforts remained limited to the piecemeal restoration of a limited number of monuments and a few demonstration projects (Sutton and Fahmi, 2002).

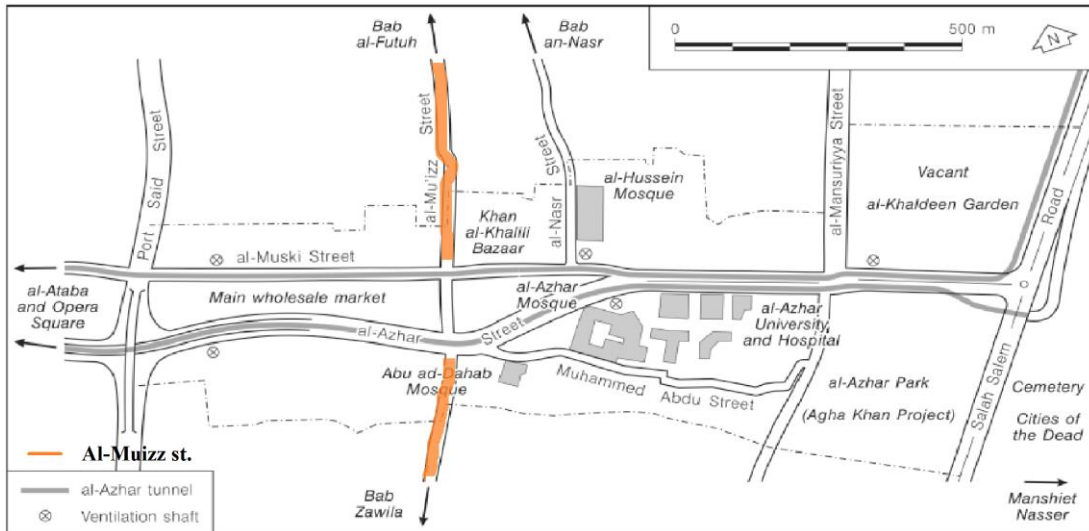


**Figure 0-20A** UNDP rehabilitation plan, 1997 (source: UNDP Technical Co-operation Office: Cairo, Egypt, 1997)

### **Historic Cairo, Al-Azhar Tunnel Project, 2001**

Despite the availability of the UNDP 1997 Rehabilitation Plan, in 2001 the Egyptian government pursued its own conservation policies by giving priority to Al-Azhar Square. This started two years devoted to restoration projects for the Al-Azhar and Al-Hussein mosques, to avoid Al-Azhar Bridge's heavy traffic and its serious environmental consequences for the safety of historic monuments within Al-Muizz Street's main spine and the Khan Al-Khalili bazaar area (Figure 0.21A). The Al-Azhar

underground tunnel was constructed under Al-Azhar Street in late 2001. As a result, the area between the two mosques was planned to be pedestrianized and transformed into a new plaza which would have direct access to the central spine of Al-Muizz Street and the Khan Al-Khalili bazaar area.



**Figure 0-21A.** Al-Azhar axis – main streets, buildings and localities (source: Fahmi, and Sutton, 2003)

### The Revival of Al-Muizz, 2009

In recent decades, the idea of area conservation instead of the restoration of single monuments has been established. In 2000, the Egyptian government proposed the huge Historic Cairo Rehabilitation Project (HCRP), aiming to protect and conserve historic Cairo with a view to developing extensive areas into an open-air museum, with the main priority given to Al-Muizz Street. In 2009, the government and UNESCO began a national campaign for the maintenance and restoration of Al-Muizz Street to regain its beauty after the completion of the development of the infrastructure facilities. The restoration started from Al Fotouh gate up to the intersection of Al-Azhar Street, at a total value of 23 million EGP. The houses and overlooking shop facades were totally renovated on both sides of the street, while buildings higher than the level of the monuments were brought down to size and painted an appropriate colour. Road surfaces were treated and fitted with benches and low-profile pavements in the spirit of the original thoroughfare (Table 0-A), 11 new sets of electronic bollards were built around the main entrances of the street to ensure pedestrianization (Figure 0.22A), and a new sewage system and piping network were built to prevent water leakage along the street. As an integral part of this project, the illuminations of this

monumental area had the purpose of skilfully enhancing, through expert use of colour and light, the beauty of these architectural masterpieces.

Unfortunately, as a result of the political unrest in Egypt after the 2011 revolution, the other part of the street starting from Zuwaila Gate up to the intersection of Al-Azhar Street, has been delayed and the project duration expanded to 42 months without a fixed date. This has left behind two distinctive urban forms within the same alley. Figure 0.23A clearly reveals the contrasts of the ambient conditions for each part of the same alley, with its own urban distinctive features, regulation, materials, shadings, vegetation, and surfaces.

**Table 0-A** The street new material installed (source: Arab contractors)

Item	Material restored	Quantity
Street	Black Aswan granite	7500m <sup>2</sup>
Pavement	Gondola granite slabs	4900m <sup>2</sup>
Pavement blocks	Gondola granite	2900ml



**Figure 0-22A.** Electronic bollards control the traffic at the entrance to Al-Muizz





**Figure 0-23A.** The difference between the two parts of Al-Muizz: the renovated on the left and the non-renovated on the right

## • Conclusion

Religious, environmental, socio-economic and cultural factors have been cited as having influences on the elements of the traditional urban fabric. However, the environmental and climatic conditions have a major impact on the formation of many cities in North Africa. This was expressed by Hakim (1986), whose studies are based on the Qur'an and Sunna<sup>22</sup> with the support of two Arabic manuscripts on the subject of building solutions. Both manuscripts are based upon the interpretation of building solutions as seen through the Maliki<sup>23</sup> School of Islamic Law based in Andalusia (Muslim Spain), and Tunisia. Hakim (1986:23) stated that both manuscripts illuminate three things: the remarkable similarity of 'solutions' that are 350 years apart, the dependency on similar references within the Maliki School of Islamic law, and the similarity of solutions across the vast geographic area of North Africa and Al-Andalus, resulting in a consistent urban design approach modified by variations in response to local setting, climate variation, and the availability of building materials.

In this chapter, there has been an attempt to analyse Al-Muizz Street's built environment and the factors that shaped its urban form, according to different maps at the end of each ruling dynasty. These are clarified as follows:

- In the first instance, the origin of the city could have been based on environmental, socio-economic or religious considerations. The availability of water or good agricultural land may have served as a considerable environmental factor for locating traditional cities (as all the cities were built beside the

---

<sup>22</sup>*Sunna or Sunnah* –this is an established custom or conduct and a cumulative tradition, typically based on Muhammad. For example, the actions and sayings of Muhammad are believed to complement the divinely revealed message of the Qur'an. J.P. Esposito, *The Oxford Dictionary of Islam*, 2003

<sup>23</sup>Islamic Jurisprudence comprises of the laws that govern a Muslim's daily life. The Prophet Muhammad explained and practically demonstrated these laws. The jurists studied the Qur'an and the Prophet's life and they adopted a refined methodology which they used to extract legal rulings and verdicts. This methodology is known as the Principles of Jurisprudence. Eventually, the Muslim world was left with four schools of jurisprudence that are present to this day. There are differences between these schools on some issues but these differences never caused conflict. These schools, referred to respectively as the Hanbali, Hanafi, Maliki, and Shafei, are followed by different Muslim states either entirely or in part.

NileRiver). After this, the city was developed in an incremental manner without a 'formalized' plan, but with a general concept of harmony, coherence and liveability

- The spatial geometry of the traditional urban fabric seems to have developed from a lack of planning. Aside from that, the structures are planned but the planning principles are flexible enough to allow for acceptable diversity; the principles were applied by the individuals in the society as there was limited civic planning. The main sources of these principles could have been religious tenets derived from the Islamic law (Qur'an and Sunna), yet this needs more investigation which is outside the scope of this study
- The principle of privacy might have contributed to the development of the narrow and winding streets, apart from the climatic adaptation by 'shading'. However, other urban strategies appear to have been developed mainly as a result of the harsh desert climate without any link to Islamic law, such as the street orientation, which represents, with the street aspect ratio, the most relevant urban parameters responsible for the microclimatic changes in a street canyon (Todhunter, 1990; Bianca 2000). This is well expressed by the street designs for the Fatimid city in Cairo, which follows a grid in its plan, with Al-Muizz as the main street oriented north/south(N-S), creating more pleasant microclimate as the N-S orientation provides enough shadow and solar energy in summer and winter, respectively (Toudert and Mayer 2005). In contrast, East-West (E-W) oriented streets are quite difficult to keep in shade, as the walls provide very limited shading, even for very deep street canyons ( $H/W \geq 2$ ), and this may explain why the secondary streets of the Fatimid city are always narrower and higher in aspect ratio than the N-S streets. Furthermore, the whole system has high thermal inertia as a result of the minimal envelope to volume ratio, which makes the compact buildings gain less heat during the daytime and lose less heat at night. It also used heavy stones with a big cut to make use of their high thermal capacity, and light colours were used for the external facades to help to reduce the urban reflectance of the whole sites.

Finally, all these successive techniques developed over a long period of time have given satisfactory answers of architecture concepts and techniques concerning

human comfort and the surrounding environment. As mentioned in the introduction of this chapter, for any proposed development for an urban area, it is crucial for the urban area background, including land use, master plane and urban form, to be investigated, whether it is climate based or not. However, some scholars have recently raised concerns about these techniques, by questioning whether they have been over estimated (Givoni, 1997; Meier et al., 2004). Moreover, when the Fatimid city was first established, it was meant to be a royal city with a low density of buildings and a great deal of land and wide streets, but over time it was transformed into a very highly urbanized area with a high population density and irregular narrow streets (Figure 0.27). Therefore, in the literature review of Chapter three, the effect of urbanization and climate change with reference to Cairo is presented, while the urban form impact on microclimate and thermal comfort is reviewed in Chapter four.



## Appendix 'B'

## Appendix 'B1'

### General structure of ENVI-met 3.1

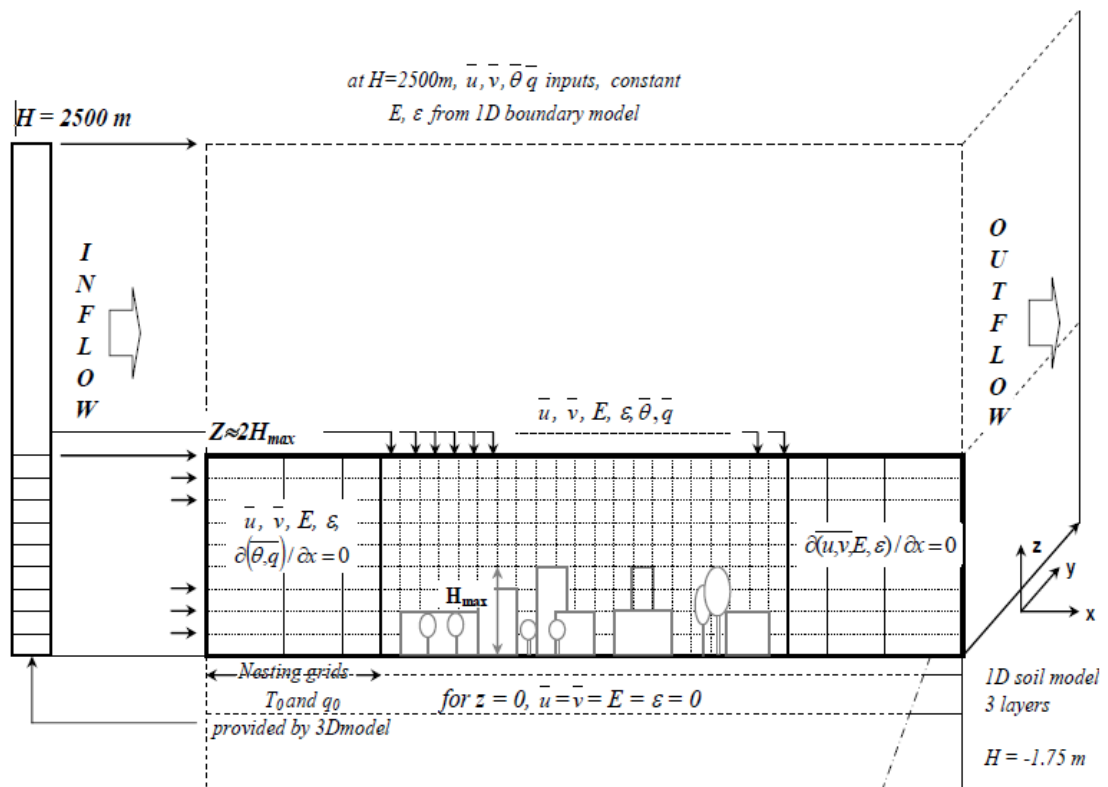
By understanding the basic knowledge of the model, it is important to describe the general structure of ENVI-met in order to obtain an overview of how the model works. The main model is designed in 3D core model and 1D border model with two horizontal dimensions (x and y) and one vertical dimension (z) (Figure 1.1B). Inside this main model, the typical elements that represent the area of interest are placed: buildings, vegetation, and different types of surfaces, where the main function of the 3D model is to simulate all processes inside the actual model area. The upper horizontal boundary and the vertical windward boundary act as the interface of the 1D border model and the 3D core model. To allow an accurate simulation of the boundary layer, the 1D model extends the simulated area to the height  $H = 2500\text{m}$  (i.e. an average depth of a boundary layer) and transfers all start values to the upper limits of the 3D volume needed for the actual simulation, as it is not possible (and not necessary either) to extend the complete 3D model up to this height.

The core area to be simulated is a volume of the dimensions (x, y, z) plotted into the grid modules. Selecting the correct size of the model domain is a central aspect in successful numerical modelling. The horizontal dimension is more or less given by the dimension of the subject of interest. Therefore, (z) is determined by the maximum height  $H_{\text{max}}$  of the urban elements within the model ( $z \geq 2H_{\text{max}}$ ), which means the total height of the model will be twice or more the tallest object in the simulation area (especially if it is a building) and at least 30m in total (Bruse, 2004; Todert 2005; Malekzadeh 2009). Envi-met allows two different types of vertical grids according to the type and the objective of the study, for instance, at street level, the first grid is vertically subdivided into five equal parts in order to record thoroughly the microclimate near the surface. This is called the equidistant grid (A), and is a telescoping grid (B1, B2 and C) where the grid size expands with the height (Figure 1.2B).

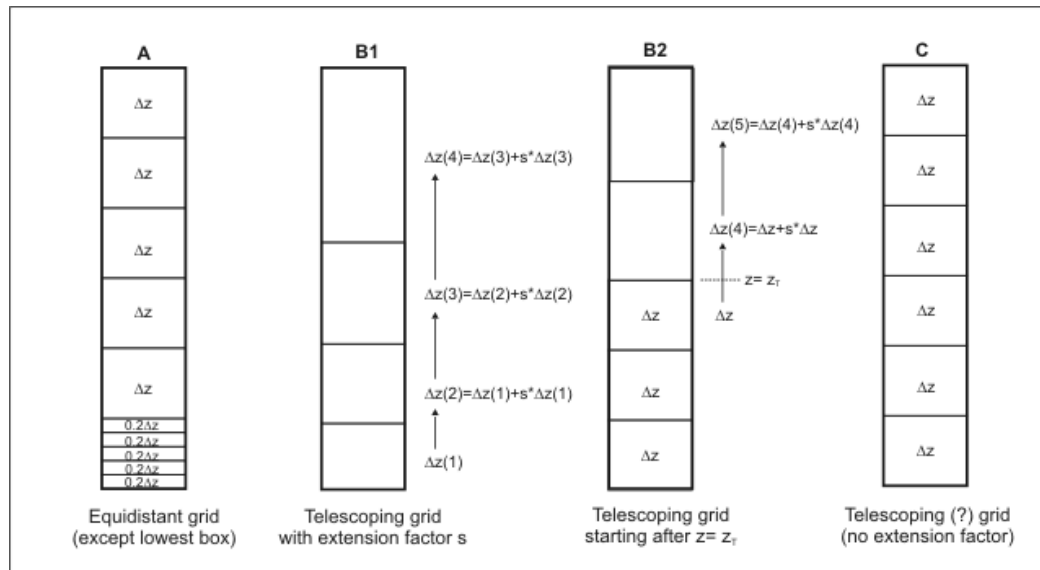
Another concept of covering more horizontal space without too much refining of the grid cells is the usage of the Nesting Area, which is a band of grid cells surrounding the core of the 3D model. This acts as a buffer zone in order to avoid numerical disturbance. The nesting grids also ensure a representative 3D profile of the wind at the windward

boundary by adjusting the initial 1D wind profile. These grids get progressively larger as their distance from the core model increases, and this allows the movement of the model's borders away from the core without wasting too many calculation cells, and yet it is still possible to assign two different soil profiles to the nesting area. The nesting area is at least double the size of the highest obstacle in the model area ( $2H_{\max}$ ) beyond the actual modelled area.

Finally, a soil model is needed to calculate the heat transfer from the surfaces into the ground and vice versa. The model takes into account the hydrological and thermodynamical processes and consists of ten nodes in a vertical profile with a depth of -1.75m where the temperature and the humidity settings are divided into three layers (0-20cm, 20-45cm, and 45-175cm) and each layer corresponds to a soil type. The deep soil temperature (-2.00m) is kept constant during simulation.



**Figure 1-1B** General EVI-met model's structure including the boundaries. Source: Bruse (2009) and Ali Toudert (2005)



**Figure 1-2B** Different types of vertical grids in ENVI-met. Source: www.envimet.com

The ENVI-met are ruled by too many equations to be presented thoroughly here and the model is well documented and regularly updated (Bruse and Fleer, 1998; Bruse, 1999, 2004, 2008). Only the mean radiant temperature ( $T_{mrt}$ ) determination is reported below, which is considered one of the most important meteorological parameters influencing the outdoor thermal comfort and sensation under sunny conditions (Mayer and Hoppe, 1987; Mayer, 1993; Spagnolo and de Dear, 2003). However, a comprehensive summary of the model is provided by Ali-Toudert (2005) and is available in the Appendix.

### Determination of $T_{mrt}$ by ENVI-met modelling

The ENVI-met software models the microclimate, including the mean radiant temperature ( $T_{mrt}$ ) in urban structures, and is based on a three dimensional computational fluid dynamic model and an energy balance model (Bruse, 1999, 2012). According to Huttner (2012), the mean radiant temperature ( $T_{mrt}$ ) is calculated for a cylindrical shaped body as in equation (1.1B) (Huttner, 2012):

$$T_{mrt} = \left( \frac{1}{\sigma} (Q_{lw,in} + \frac{ak}{\epsilon} \times (Q_{sw-diff,in} + Q_{sw-dir,in})) \right)^{0.25} \quad (\text{Equation 1.1B})$$

Where the emission coefficient of the human body ( $\epsilon$ ) is set to 0.97 and ( $ak$ ), the absorption coefficient of the human body for short wave radiation, is set to 0.7. ( $\sigma$ ) is the Stefan Boltzmann constant,  $Q_{sw-diff,in}$  and  $Q_{sw-dir,in}$  is the diffuse and direct incoming short wave radiation respectively. As the influence of the radiation of the ground decreases with increasing height; ENVI-met assumes that the incoming long wave

radiation  $Q_{lw,in}$  originates as 50% from the upper hemisphere (sky, buildings, and vegetation) and 50% from the ground, based on equation (1.2B):

$$Q_{lw,in} = 0.5 \times (vf_{veg}\overline{\varepsilon_{veg}}\sigma\overline{T_{veg}}^4 + vf_{bldg}\overline{\varepsilon_{bldg}}\sigma\overline{T_{bldg}}^4 + vf_{bldg}Q_{lw,sky} + vf_{bldg}(1 - \overline{\sigma_{bldg}})Q_{lw,sky}) + 0.5 \times (\sigma\varepsilon_{ground}T_{ground}^4) \quad (Equation 1.2B)$$

The view factors (vf) give the percentage of vegetation/ buildings/ sky that can be seen from the specific grid point. The physically correct approach would be to calculate the long wave radiation fluxes based on the average emissivity ( $\overline{\varepsilon}$ ) and temperature ( $\overline{T}$ ) of all plants/ building surfaces within view (Huttner, 2012). The incoming long wave radiation from the sky ( $Q_{lw,sky}$ ) is calculated based on the air temperature, air humidity and some empirical parameters (Oke, 1978). For long wave radiations coming from the ground, only the emissivity and surface temperature of the grid's corresponding grid cell are taken into account.

The diffuse incoming short wave radiation ( $Q_{sw-diff,in}$ ) is derived from equation (1.3B) accordingly:

$$Q_{sw-diff,in} = 0.5 \times (vf_{bldg}\overline{rf_{bldg}}Q_{sw-dir,sky} + vf_{sky}Q_{sw-diff,sky}) + 0.5 \times (rf_{ground}Q_{sw,ground}) \quad (Equation 1.3B)$$

(rf) is the reflectivity and ( $Q_{sw,ground}$ ) is the overall shortwave radiation at the ground surface of the corresponding grid cell. The incoming direct short wave radiation ( $Q_{sw-dir,in}$ ) is calculated as the direct short wave radiation within the grid cell multiplying with an projection factor pf equation (1.4B):

$$Q_{sw-dir,in} = pf \times Q_{sw-dir} \quad (Equation 1.4B)$$

This projection factor depends on the azimuth angle of the sun<sup>24</sup>( $\Phi$ ) equation (1.5B):

$$pf = 0.42 \times \cos \Phi + \sin \Phi \quad (Equation 1.5B)$$

---

<sup>24</sup>The solar azimuth angle is the [azimuth](#) angle of the [sun](#). It defines in which *direction* the sun is, whereas the [solar zenith angle](#) or its [complementary](#) angle [solar elevation](#) defines how high the sun is (Sukhatme, 2008; Seinfeld and Spyros, 2006; Duffie and Beckman, 2013).

“In spite of the different methods used for calculating  $T_{mrt}$ , ENVI-met simulated results provided a satisfactory agreement with measured data given the complexity of the urban environment when the projection factor (pf) is appropriately set” (Toudert, 2005).

### **Simulation course and boundary condition**

In the simulation process, the set up description and boundary conditions are very critical, and thus it is highly advisable to understand the process behind it. According to Figure 1.3B, which illustrates the ENVI-met work flow, it can be divided into two main simulation procedures, namely, setting up the model and running the model. In setting up the model phase, it consists of four sub-models, where all input information regarding the area definition (basic meteorology, building properties, soil properties, land properties and biometeorology) was collated and loaded within the input database named as the configuration file. Then, the area input file is mainly related to the position and height of buildings, the position of plants, the distribution of surface materials and soil types, and the position of sources, the position of receptors, the database links and the geographic position of the location on earth (Bruse, 2009). All inputs were required for simulating the complete model. After the first step was completed, the next step regarding the running model was implemented.

The boundary condition must be carefully understood to compare the results of a numerical simulation with measured data or to simulate a specific meteorological development. The equations used in the boundary model are a 1D simplified form of those used in the 3D model with some parameterisations when necessary.

Firstly, the vertical inflow boundary up to 2500m was calculated with the 1D model by applying a logarithmic law, based on the input values of the horizontal wind ( $u$ ,  $v$ ) at 10m height and on the roughness length  $z_0$ . Then, the potential temperature ( $\theta_{start}$ ) was given as an input parameter at a height of 70m, set to the whole vertical profile assuming start conditions of neutrality. A vertical gradient forms if the initial surface temperature differs from the initial air temperature. The surface temperature is then given to the 1D model by the soil sub-model, and is calculated on the basis of three input values of soil temperatures and soil humidity included in the soil properties setting. The surface temperature is then calculated on the basis of three input values of soil temperatures and soil humidity in the soil sub-model and provided to the 1D model. The linear air humidity profile was calculated by means of input values at 2,500m i.e.  $q_{2500m}$

and functioned as local friction velocity  $u^*$ . Subsequently, the surface temperature and humidity are provided by the 3D model as mean values of the nesting area related values. The initialization of the 1D model is run during a period of eight hours with a time step of  $\Delta t=1s$  until the interactions between all start values reach a stationary state (Bruce, 2009). Then, the atmospheric equations were solved by integration of the variables based on the following sequence:  $u$ ,  $v$ ,  $\theta$ ,  $q$ , local turbulence ( $E$ ) and its dissipation rate ( $\varepsilon$ ) and the exchange coefficients of mean air flow ( $Km$ ) and diffusion coefficients of heat ( $Kh$ ) and vapour ( $Kq$ ).

In the 3D Model, the start values at the inflow boundary are provided by the 1D boundary model calculation results as a vertical profile. However, this transition from 1D to 3D schemes needs an adjustment in a non-homogenous boundary urban environment. Therefore, the 3D nesting area is used to solve it. In contrast, on the horizontal boundary, homogeneity is assumed. Wall and roof temperatures are calculated at all physical boundaries in the model area. Then, the wind speed components at building grids are set following a no-slip condition where  $u=v=w=0$ . The wind field is adjusted gradually during the initializing phase (diastrophic phase) according to the existence of the obstacles.

On the other hand, at the ground surface ( $z=0$ ) and on the walls,  $E$  and  $\varepsilon$  are calculated as a function of  $u^*$  from the flow components tangential to the surface the model assuming that no gradient exists between the two last grids close to the outflow border (Toudert, 2005). According to these processes, the actual 3D simulation was comprised based on the following order: the calculations of soil parameters ( $T, \eta$ ), surface quantities ( $T_0, q_0, as$ ), radiation update, the update of wind components ( $u, v, w$ ), pressure perturbation  $p'$ , turbulence quantities  $E, \varepsilon, Km, Kh, Kq$ , and air temperature and humidity  $\theta, q$ . The cycle of the process is repeated once the 1D model is updated again.

In relation to the numerical aspects, all differential equations are approximated using the finite difference method and solved forward-in-time (Bruse, 2009). Thus, there is a variation of time steps adopted based on the quantity to be calculated. The wind flow calculation requires ten minutes as a main time step, whereas smaller time steps are used for E- $\varepsilon$  system to obtain a numerically stable solution (3 minutes). However, 30 seconds time steps are used for surface temperature and humidity (Bruse, 1999). As for solar radiation, this is usually updated in larger time-steps and can be set by the user. In

micro-scale simulations, obstacles creating steep pressure gradients require very small time steps to solve the set of wind field equations. Therefore, although in ENVI-met the wind field is not treated as a 'normal' prognostic variable, it is updated in accordance with the interval time. A larger simulation time is required if the wind field is treated as a normal variable. As a result, the simulation needs a quick and implicit solution to solve the advection-diffusion equation, and this is why the dynamic pressure is removed from the equations of motion (equations 3.1 to 3.3 Appendix) and auxiliary flow components are calculated. These are then corrected by incorporating the dynamic pressure which has been separately defined by means of the Poisson equation (Bruse, 2004).

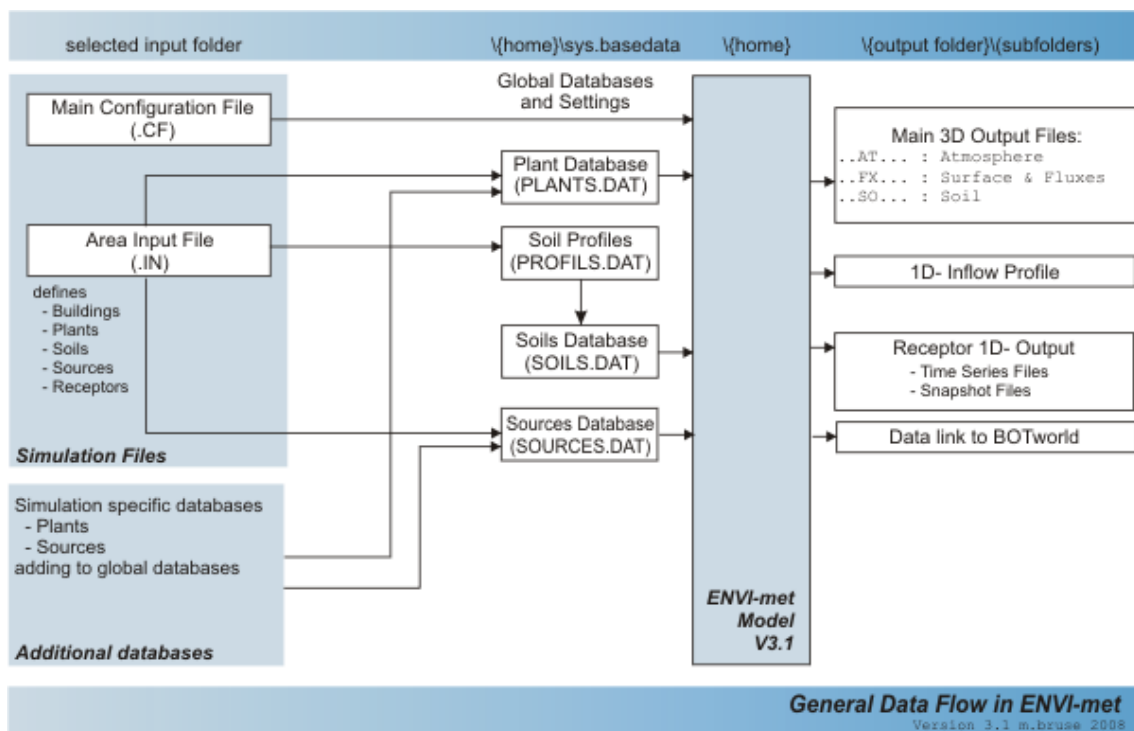


Figure 1-3B Flow diagram of ENVI-met (Bruse, 2008)



## Appendix 'B2'

### CFD model equations

#### Transport equations

The present flow and transport phenomena for air flow and the heat transfer are described by the Navier-Stokes equations. The time-averaged Navier-Stokes equations for the momentum, mass and energy transport are given as follows:

$$\text{Continuity equation} \quad \frac{\partial U_i}{\partial x_i} = 0 \quad (\text{eq. 1.6B})$$

$$\text{Momentum conservation} \quad \rho U_j \frac{\partial U_i}{\partial x_i} = -\frac{\partial P}{\partial x_i} + \frac{\partial}{\partial x_j} \left[ (\mu + \mu_t) \frac{\partial U_i}{\partial x_j} \right] + f_b \quad (\text{eq. 1.7B})$$

Where, ( $U_i$ ) is the time average i-direction velocity, ( $\rho$ ) the density, ( $P$ ) the pressure, ( $\mu$ ) the viscosity, ( $\mu_t$ ) the turbulent viscosity and ( $f_b$ ) the buoyancy force.

#### Boussinesq approximation

The density variation is calculated according to the Boussinesq model in order to take into account the natural convection effects. The use of the Boussinesq model offers faster convergence than considering the density variable in all equations. In this model, the density is a constant value in all solved equations except from the buoyancy term calculation in the momentum equation:

$$f_b = (\rho - \rho_0)g \approx -\rho_0\beta (T - T_0) g \quad (\text{Eq. 1.8B})$$

This way the ( $\rho$ ) is eliminated from the buoyancy term using the Boussinesq approximation:

$$\rho = \rho_0(1 - \beta\Delta T) \quad (\text{Eq. 1.9B})$$

( $\beta$ ) the thermal expansion coefficient, ( $T$ ) the temperature, ( $\rho_0$ ) and ( $T_0$ ) the corresponding reference values for density and temperature and ( $g$ ) the gravity acceleration.

## Energy Treatment

$$\begin{aligned} \text{Energy Conservation:} \quad & \frac{\partial}{\partial x_i} (u_i(\rho E + P)) \\ & = \frac{\partial}{\partial x_i} \left[ k_{eff} \frac{\partial T}{\partial x_i} + u_i(\tau_{ij})_{eff} \right] + S_h \end{aligned} \quad (Eq. 1.10B)$$

Where ( $\varepsilon$ ) is specific energy (per unit mass), ( $k_{eff}$ ) the effective conductivity,  $(\tau_{ij})_{eff}$  the effective stress tensor and ( $S_h$ ) the source term, which adds the radiation contribution to the energy conservation equation. Auxiliary relationships for the calculations of quantities appearing in the energy equation are presented here. Specifically, relationships are given for the calculation of effective and turbulent conductivity as well as for the energy and enthalpy.

$$\begin{aligned} \text{Effective Conductivity:} \quad & k_{eff} = \gamma k_{feff} + (1 - \gamma)k_s \end{aligned} \quad (Eq. 1.11B)$$

Where, ( $\gamma$ ) the porosity, when  $\gamma = 1$  there is only fluid, ( $k_{feff}$ ) the fluid effective conductivity and  $k_s$  the solid conductivity. The fluid effective thermal is given as follows:

$$\text{Thermal Conductivity:} \quad k_{eff} = k_f + k_t \quad (Eq. 1.12B)$$

Where ( $k_f$ ) is the fluid conductivity and ( $k_t$ ) is the turbulent conductivity given by turbulent conductivity as:

$$\text{Turbulent Conductivity:} \quad k_t = \frac{C_p \mu_t}{Pr_t} \quad (Eq. 1.13B)$$

Where, ( $C_p$ ) is the specific heat capacity and ( $Pr_t$ ) the turbulent Prandtl number while the enthalpy ( $h$ ) is given by the following equation as:

$$\text{Enthalpy} \quad h = \int_{T_o}^T C_p dT \quad (Eq. 1.14B)$$

## Realizable k- $\varepsilon$ turbulence model

According to the Fluent help files (2006), this model was developed based on modifying the dissipation rate ( $\varepsilon$ ) equation to satisfy certain mathematical constraints on the normal stresses consistent with the physics of turbulent flows. This is not satisfied by either the standard or the RNG  $k$ - $\varepsilon$  models, which makes the realizable model more

precise than both models at predicting flows such as separated flows and flows with complex secondary flow features. In terms of the improved changes by Shih (1995), the transport equations for ( $k$ ) and ( $\varepsilon$ ) become:

$$\frac{\partial}{\partial t}(\rho k) + \frac{\partial}{\partial x_j}(\rho k u_j) = \frac{\partial}{\partial x_j} \left[ \left( \mu + \frac{\mu_t}{\sigma_k} \right) \frac{\partial k}{\partial x_j} \right] + G_k + G_b - \rho \varepsilon - Y_M + S_K \quad (\text{Eq. } 1.15B)$$

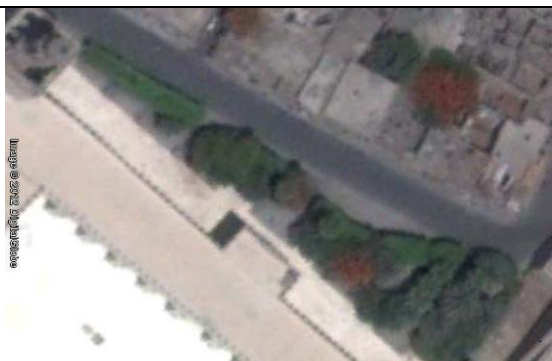
$$\frac{\partial}{\partial t}(\rho \varepsilon) + \frac{\partial}{\partial x_j}(\rho \varepsilon u_j) = \frac{\partial}{\partial x_j} \left[ \left( \mu + \frac{\mu_t}{\sigma_\varepsilon} \right) \frac{\partial \varepsilon}{\partial x_j} \right] + \rho C_1 S_\varepsilon - \rho C_2 \frac{\varepsilon^2}{k + \sqrt{\nu \varepsilon}} + C_{1\varepsilon} \frac{\varepsilon}{k} C_{3\varepsilon} G_b + S_\varepsilon \quad (\text{Eq. } 1.16B)$$

where ( $G_k$ ) represents the generation of turbulent kinetic energy that arises due to mean velocity gradients, ( $G_b$ ) is the generation of turbulent kinetic energy arising from buoyancy, and ( $Y_M$ ) represents the fluctuating dilation in compressible turbulence that contributes to the overall dissipation rate. ( $S_\varepsilon$ ) and ( $S_k$ ) are source terms defined by the user. ( $\alpha_k$ ) and ( $\alpha_\varepsilon$ ) are the turbulent Prandtl numbers for the turbulent kinetic energy and its dissipation.

## Appendix 'C'







**Can you explain why you find it comfortable or not in these zones, in terms of sun, wind, shade, rain protection, etc?**

**Appendix'D'****Basic ENVI-met 3.1 configuration file (Renovated part)**

```
% ---- Basic Configuration File for ENVI-met Version 3 -----
% ---- MAIN-DATA Block -----
Name for Simulation (Text):           =26-8-14
Input file Model Area                 =C:\envi-met\envimet31\26-8-14a\26-8b.in
Filebase name for Output (Text):     =26-8-14
Output Directory:                    =C:\envi-met\envimet31\26-8-14a\output
Start Simulation at Day (DD.MM.YYYY): =01.07.2012
Start Simulation at Time (HH:MM:SS):  =04:00:00
Total Simulation Time in Hours:      =20.00
Save Model State each ? min         =60
Wind Speed in 10 m ab. Ground [m/s]  =3.5
Wind Direction (0:N..90:E..180:S..270:W..) =315
Roughness Length z0 at Reference Point =0.15
Initial Temperature Atmosphere [K]    =302
Specific Humidity in 2500 m [g Water/kg air] =7
Relative Humidity in 2m [%]          =47
Database Plants                      =[input]\Plants.dat
```

( -- End of Basic Data --)

( -- Following: Optional data. The order of sections is free. --)

( -- Missing Sections will keep default data. --)

( Use "Add Section" in ConfigEditor to add more sections )

( Only use "=" in front of the final value, not in the description)

( This file is created for ENVI-met V3.0 or better )

[BUILDING]\_\_\_\_\_Building properties

```
Inside Temperature [K]                = 297.15
Heat Transmission Walls [W/m²K]       =0.35
Heat Transmission Roofs [W/m²K]      =0.41
Albedo Walls                          =0.4
```



Albedo Roofs =0.35

[SOURCES] \_\_\_\_\_ Type of emitted gas/particle

Name of component =PM10

Type of component =PM

Particle Diameter in [ $\mu\text{m}$ ] (0 for gas) =10

Particle Density [ $\text{g}/\text{cm}^3$ ] =1

Update interval for emission rate [s] =600

[SOILDATA] \_\_\_\_\_ Settings for Soil

Initial Temperature Upper Layer (0-20 cm) [K]=302

Initial Temperature Middle Layer (20-50 cm) [K]=302

Initial Temperature Deep Layer (below 50 cm)[K]=302

Relative Humidity Upper Layer (0-20 cm) =50

Relative Humidity Middle Layer (20-50 cm) =60

Relative Humidity Deep Layer (below 50 cm) =60

[SOLARADJUST] \_\_\_\_\_

Factor of shortwave adjustment (0.5 to 1.5) =1.0

[TIMING] \_\_\_\_\_ Update & Save Intervalls

Update Surface Data each ? sec =30.0

Update Wind field each ? sec =900

Update Radiation and Shadows each ? sec =600

Update Plant Data each ? sec =600

[TIMESTEPS] \_\_\_\_\_ Dynamical Timesteps

Sun height for switching dt(0) -> dt(1) =40

Sun height for switching dt(1) -> dt(2) =50

Time step (s) for interval 1 dt(0) =5.0

Time step (s) for interval 2 dt(1) =2.0

Time step (s) for interval 3 dt(2) =1.0

[TURBULENCE] \_\_\_\_\_ Options Turbulence Model

Turbulence Closure ABL (0:diagn.,1:prognos.) =1

Turbulence Closure 3D Modell (0:diag.,1:prog)=2

Upper Boundary for e-epsilon (0:clsd.,1:op.) =0

[LBC-TYPES] \_\_\_\_\_Types of lateral  
boundary conditions

LBC for T and q (1:open, 2:forced, 3:cyclic) =1

LBC for TKE (1:open, 2:forced, 3:cyclic) =2

[NESTINGAREA] \_\_\_\_\_Settings for nesting

Use aver. solar input in nesting area (0:n,1:y) =1

Include Nesting Grids in Output (0:n,1:y) =0

[PMV] \_\_\_\_\_Settings for PMV-Calculation

Walking Speed (m/s) =0.3

Energy-Exchange (Col. 2 M/A) =116

Mech. Factor =0.0

Heattransfer resistance cloths =0.5

[PLANTMODEL] \_\_\_\_\_Settings for plant  
model

Stomata res. approach (1=Deardorff, 2=A-gs) =2

Background CO2 concentration [ppm] =350

[RECEPTORS] \_\_\_\_\_

RECEPTOR 1 Co-ordinate =13,90

RECEPTOR 2 Co-ordinate =18,126

RECEPTOR 3 Co-ordinate =15,82

% --remove line above if your receptors are in the area input file--

Save Receptors each ? min =01.0

**Basic ENVI-met 3.1 configuration file (Non-Renovated part)**

```

% ---- Basic Configuration File for ENVI-met Version 3 -----
% ---- MAIN-DATA Block -----
Name for Simulation (Text):           =26-8-14
Input file Model Area                 =C:\envi-met\envimet31\26-8-14a\26-8b.in
Filebase name for Output (Text):     =26-8-14
Output Directory:                    =C:\envi-met\envimet31\26-8-14a\output
Start Simulation at Day (DD.MM.YYYY): =01.07.2012
Start Simulation at Time (HH:MM:SS): =04:00:00
Total Simulation Time in Hours:      =20.00
Save Model State each ? min         =60
Wind Speed in 10 m ab. Ground [m/s] =3.5
Wind Direction (0:N..90:E..180:S..270:W..) =315
Roughness Length z0 at Reference Point =0.15
Initial Temperature Atmosphere [K]   =302
Specific Humidity in 2500 m [g Water/kg air] =7
Relative Humidity in 2m [%]          =47
Database Plants                      =[input]\Plants.dat

```

( -- End of Basic Data --)

( -- Following: Optional data. The order of sections is free. --)

( -- Missing Sections will keep default data. --)

( Use "Add Section" in ConfigEditor to add more sections )

( Only use "=" in front of the final value, not in the description)

( This file is created for ENVI-met V3.0 or better )

[BUILDING]\_\_\_\_\_Building properties

```

Inside Temperature [K]                = 297.15
Heat Transmission Walls [W/m²K]       =0.35
Heat Transmission Roofs [W/m²K]      =0.41
Albedo Walls                          =0.4
Albedo Roofs                          =0.35

```

[SOURCES] \_\_\_\_\_ Type of emitted  
gas/particle

Name of component =PM10

Type of component =PM

Particle Diameter in [ $\mu\text{m}$ ] (0 for gas) =10

Particle Density [ $\text{g}/\text{cm}^3$ ] =1

Update interval for emission rate [s] =600

[SOILDATA] \_\_\_\_\_ Settings for Soil

Initial Temperature Upper Layer (0-20 cm) [K]=302

Initial Temperature Middle Layer (20-50 cm) [K]=302

Initial Temperature Deep Layer (below 50 cm)[K]=302

Relative Humidity Upper Layer (0-20 cm) =50

Relative Humidity Middle Layer (20-50 cm) =60

Relative Humidity Deep Layer (below 50 cm) =60

[SOLARADJUST] \_\_\_\_\_

Factor of shortwave adjustment (0.5 to 1.5) =1.0

[TIMING] \_\_\_\_\_ Update & Save Intervalls

Update Surface Data each ? sec =30.0

Update Wind field each ? sec =900

Update Radiation and Shadows each ? sec =600

Update Plant Data each ? sec =600

[TIMESTEPS] \_\_\_\_\_ Dynamical Timesteps

Sun height for switching dt(0) -> dt(1) =40

Sun height for switching dt(1) -> dt(2) =50

Time step (s) for interval 1 dt(0) =5.0

Time step (s) for interval 2 dt(1) =2.0

Time step (s) for interval 3 dt(2) =1.0

[TURBULENCE] \_\_\_\_\_ Options Turbulence Model

Turbulence Closure ABL (0:diagn.,1:prognos.) =1

Turbulence Closure 3D Modell (0:diag.,1:prog)=2

Upper Boundary for e-epsilon (0:clsd.,1:op.) =0

[LBC-TYPES] \_\_\_\_\_ Types of lateral  
boundary conditions

LBC for T and q (1:open, 2:forced, 3:cyclic) =1  
 LBC for TKE (1:open, 2:forced, 3:cyclic) =2  
 [NESTINGAREA] \_\_\_\_\_ Settings for nesting  
 Use aver. solar input in nesting area (0:n,1:y) =1  
 Include Nesting Grids in Output (0:n,1:y) =0  
 [PMV] \_\_\_\_\_ Settings for PMV-Calculation  
 Walking Speed (m/s) =0.3  
 Energy-Exchange (Col. 2 M/A) =116  
 Mech. Factor =0.0  
 Heattransfer resistance cloths =0.5  
 [PLANTMODEL] \_\_\_\_\_ Settings for plant  
 model  
 Stomata res. approach (1=Deardorff, 2=A-gs) =2  
 Background CO2 concentration [ppm] =350  
 [RECEPTORS] \_\_\_\_\_  
 RECEPTOR 1 Co-ordinate =13,90  
 RECEPTOR 2 Co-ordinate =18,126  
 RECEPTOR 3 Co-ordinate =15,82  
 % --remove line above if your receptors are in the area input file--  
 Save Receptors each ? min =01.0

## Appendix 'E'

## Solar radiation calculator

University of Oregon  
Solar Radiation Monitoring Laboratory

Home page  
Sponsors  
Site map  
Search  
Contact us

Software tools  
Solar position calculator

### Solar position calculator results

(Using solar constant = 1367 W/m<sup>2</sup>)

Date: 7/1/2012      Time: 19:00:00      Zone: GMT + 2  
 Lat: 30.20°      Long: 31.21°      Aspect: 180°  
 Pressure: 1013.0 mB      Temp: 35.0° C

Declination	23.0418°
Solar zenith angle (no refraction)	90.6772°
Solar zenith angle (with refraction)	90.2286°
Julian day	56110.2083
Equation of time	-3.9869 min
Hour angle	105.2133°
Extraterrestrial global horizontal solar irradiance	0.00 W/m <sup>2</sup>
Extraterrestrial direct normal solar irradiance	0.00 W/m <sup>2</sup>
Daily global ETR	11397.5 W/m <sup>2</sup>
Daily direct normal ETR	18381.6 W/m <sup>2</sup>
Earth radius factor	0.9666
Sunrise	05:01:48
Sunset	18:56:28

Note: To return to the calculator entry page with your entered values still in place, use your Web browser's "Back" button or function.

[Top of page](#)

[Home page](#)

The Data regarding the solar radiation such as the Solar Zenith angle, Extraterrestrial global horizontal solar irradiance and Extraterrestrial direct normal solar irradiance used in the simulations and the equations 7.2, 7.3, 7.4 and 7.5 were extracted from Solar radiation calculator based upon University of Oregon (Solar Radiation Monitoring Laboratory)

<http://solardat.uoregon.edu/cgi-bin/SolarPositionCalculator.cgi>